# *The deep seismic structure of northern England and adjacent marine areas from the caledonian suture seismic project*

Anthony H. J. Lewis

# The Deep Seismic Structure of Northern England and Adjacent Marine Areas from the Caledonian Suture Seismic Project

Anthony H. J. Lewis

Volume 1

A Thesis submitted for the degree of Doctor of Philosophy at the University of Durham



Graduate Society
University of Durham

Dept. of Geological Sciences
February 1986

## DECLARATION

I declare that this thesis, which I submit for the degree of Doctor of Philosophy at the University of Durham, is my own work and is not substantially the same as any which has previously been submitted for a degree at this or another university.

Anthony H. J. Lewis

University of Durham

February, 1986

# The Deep Seismic Structure of Northern England and Adjacent Marine Areas from the Caledonian Suture Seismic Project

A.H.J. Lewis

## ABSTRACT

This thesis describes the interpretation of the deep seismic structure from the wide-angle reflection/refraction Caledonian Suture Seismic experiment which extends from the Mid North Sea High across Northern England, the Irish Sea to southwest Ireland. A new method of displaying the large number of travel times in the form of contoured composite plots for a particular phase has been developed. The interpretation methods used include analysis of the wide-angle reflection travel times, time-term analysis, gravity modelling, and, ray tracing and synthetic seismogram modelling.

A mid-crustal gradient which returns PcP occurs between depths of 15.0-18.5 km beneath the line and is overlain by an upper crust with an average velocity of 6.16-6.20 km/s excluding sediments. This mid-crustal gradient was not recognised previously in the Irish Sea. A lower-crustal boundary recognised from the PmP phase occurs at 25.0 km depth beneath the Irish Sea and at 30 km beneath the North Sea. The average crustal velocity is 6.49-6.54 km/s excluding sediments and for the lower crust is 6.75-6.77 km/s. The sub-Moho Pn velocity is estimated to be 8.19 km/s beneath the Irish Sea, 8.32 km/s beneath Northern England and 8.02 km/s beneath the North Sea. The PmP and Pn boundaries diverge beneath the Irish Sea and define a transitional Moho over a 5 km depth range with an average velocity of 7.8-7.9 km/s.

The PcP and Pn boundaries correspond approximately with the top and base respectively of the reflective deep crust observed beneath the Irish Sea on BIRPS WINCH. The transitional Moho beneath the Irish Sea has a reflective character similar to the lower crust. The coincident PmP and Pn boundaries beneath the North Sea define an abrupt increase in velocity from 6.75 to 8.0 km/s which approximately corresponds to the prominent reflections beneath the non-reflective lower crust observed on the BIRPS NEC line at 10.5 to 11.0 s.

The upper crust of velocity 6.15-6.20 km/s appears to lie below the suture beneath Northern England and the North Sea along the line but may also occur above it further west. The lower crust and deeper structures lie below the suture and represent crust of the Southern Caledonides. The anomalous structure of the Moho and upper mantle beneath the Irish Sea found from CSSP and BIRPS may be related to the post-Caledonian formation of the Irish Sea basins. The reflective lower crust and transitional Moho may result from crustal thinning produced by ductile stretching.

Acknowledgements

I would like to thank a number of people . Prof. Dewey for the use of the departmental facilities. Prof Bott for his supervision, help and encouragement especially over the sometimes hectic last four months. Dr. Long for discussions and advice over the three years. Special thanks to Andy Green for collecting such a good dataset and producing his thesis for me to use over the last year and a half. I was helped continually by the departmental experts Dave Stevenson (Computing), Mike Smith (Reflection Processing) and Adrian Bowen (Deconvolution). With all the tape mounts, modelling and plotting I'd like to especially thank the computer operators. Brian Lander and the rest of the programming advisory staff for their advice and technical support over the three and half years. George Ruth humoured me as I went nuts over the refraction fieldwork using quarry blasts as sources: not recommended for mental health! Thanks to Brian Jacobs for the plots he provided from the Irish CSSP. Thanks to Martin Sinha at Cambridge for passing over the SEIS83 and SYNSEI synthetic seismogram packages. I'd like to thank SHELL petroleum for looking after me and providing me with a SHELL postgraduate studentship and giving me a job. Thanks to the BIRPS team (S. Klemperer, S McGeary, D. Matthews and R. Hobbs(!)) for letting me view the NEC line brute stacks. Thanks to Neil Chrosten for the velocity values. Thanks to John, Gill, Sandra, Pete (T), Clarence for keeping me level at various times over the three years. Rat wanted a mention as did Pip, so there it is! Finally but by no means least thanks to Mum, Dad, Alex, Gillian, John, Veronica and Granny for their foodparcels, visits and encouragement.

CONTENTS

# VOL. I

1 INTRODUCTION, GEOLOGY AND GEOPHYSICS . . . . . 1

1.1 Introduction . . . . . 1

1.1.1 The Caledonian Suture Seismic Project . . . 2

1.2 Geology of Caledonides of the British Isles . . . 3

1.2.1 The Hebridean Craton . . . . . 4

1.2.2 The NW Highlands . . . . . 6

1.2.3 The Grampian Highlands . . . . . 6

1.2.4 The Midland Valley Belt . . . . . 9

1.2.5 The Southern Uplands Belt . . . . . 10

1.2.6 The Solway Line . . . . . 11

1.2.7 The Lake District Belt . . . . . 14

1.2.8 The Southern Margin . . . . . 15

1.3 Tectonic Models of the Caledonides of the British Isles . . . . . 16

1.4 Seismic Structure of the Caledonides of the British Isles . . . . . 21

1.4.1 Refraction Surveys . . . . . 22

1.4.2 Deep Reflection Surveys . . . . . 27

1.5 Nature of the Deep Crust . . . . . 29

1.5.1 Compressional Velocities and Rock Compositions . . . . . 29

1.5.2 The Lower Crust . . . . . 31

1.5.3 The Upper Mantle . . . . . 33

1.6 Aims of The Caledonian Suture Seismic Project . 34

2 DATA PROCESSING TECHNIQUES . . . . . 36
2.1 Data . . . . . 36
2.1.1 The Information Matrices . . . . . 38
2.2 Tape Handling . . . . . 40
2.2.1 The Caledonian Suture Seismic Project Tapes . . . . . 40
2.2.2 Calculation of Distances . . . . . 41
2.2.3 The *FS Tapes . . . . . 42
2.2.4 Edinburgh Data . . . . . 42
2.3 Plotting . . . . . 43
2.4 Filtering and Deconvolution of the Bubble Pulse 43
2.4.1 Predictive Deconvolution . . . . . 44
2.5 Travel-times . . . . . 48
2.5.1 Correlation of Observed Arrivals . . . . . 48
2.5.2 Correlation of the Phases Observed from The Caledonian Suture Seismic Project . . . . . 50
2.5.3 Travel-time Picking . . . . . 50
2.5.4 The Travel-time Matrices . . . . . 51
2.6 Amplitudes . . . . . 52
2.7 Summary . . . . . 53

3 INTERPRETATION METHODS . . . . . 56
3.1 Interpretation of the travel-time matrices . . . 58
3.1.1 Reduction of the Travel-time Matrices . . 58
3.1.2 Travel-time Matrices for Wide-angle Reflections . . . . . 59
3.1.3 Travel-time Matrices for Refractions . . . 60
3.2 Travel-time Regression . . . . . 61
3.3 The Time-term Method . . . . . 61
3.3.1 The Assumptions in the Time-term Method . 64

3.4 The Analysis of Wide-angle Reflection Travel-times . . . . . 67
3.4.1 Corrections to a Datum . . . . . 69
3.4.2 Inversion of the Wide-angle Travel-times . 70
3.4.3 Assumptions of the Wide-angle Reflection Method . . . . . 72
3.5 Modelling . . . . . 73
3.5.1 SEIS83 . . . . . 73
3.5.2 Reflectivity Method . . . . . 75
3.5.3 Modelling of the Caledonian Suture Seismic Project Data . . . . . 75

4 RESULTS . . . . . 77
4.1 Introduction . . . . . 77
4.2 Interpretation of the Travel-time Matrices . . . 78
4.2.1 The Travel-time Matrix for PcP for the Irish Sea Shots . . . . . 78
4.2.2 The Travel-time Matrix for PcP for the North Sea Shots . . . . . 79
4.2.3 The Travel-time Matrix for PmP in the Irish Sea . . . . . 81
4.2.4 The Travel-time Matrix for PmP in the North Sea . . . . . 82
4.2.5 The Travel-time Matrix for Pn in the Irish Sea . . . . . 83
4.2.6 The Travel-time Matrix for Pn in the North Sea . . . . . 84
4.3 Wide-angle Reflection Results . . . . . 85
4.3.1 Wide-angle Reflection Results for the PcP phase . . . . . 86

4.3.2 Wide-angle Reflection Results for the phase PmP . . . . . 87
4.3.3 Discussion . . . . . 88
4.4 Time-term Results for Pn . . . . . 89
4.4.1 Time-term Analysis for Northern England Using all Pn Travel-times . . . . . 91
4.4.2 Time-term Analysis for the Irish Sea . . . 91
4.4.3 Time-term Analysis for the North Sea . . . 93
4.4.4 Discussion of the Time-term Analysis of Pn 95
4.5 Comparison of the PmP and Pn Results . . . . . 96

5 INTERPRETATION AND MODELLING OF THE DEEP STRUCTURE . . 97
5.1 Gravity Modelling . . . . . 98
5.2 Synthetic Seismogram Modelling . . . . . 104
5.2.1 Main Amplitude Variations . . . . . 104
5.2.2 1-D Synthetic Seismogram Modelling . . . . 106
5.2.3 2-D Synthetic Seismogram Modelling . . . . 111
5.3 Comparison of the CSSP Results with BIRPS . . . 118
5.4 Comparisons to Previous Geophysical Investigations in the Region . . . . . 122
5.5 Geological Interpretation . . . . . 124
5.5.1 Relationship to the Caledonides . . . . . 125
5.5.2 Nature of the Lower Crust . . . . . 126
5.5.3 Nature of the Transitional Moho . . . . . 130
5.5.4 Nature of the Upper Mantle . . . . . 132
5.5.5 Conclusion . . . . . 133

6 SUMMARY AND CONCLUDING REMARKS . . . . . 134

6.1 Further Work on the CSSP Data . . . . . 138

6.2 Further Work . . . . . 139

References . . . . . 141

VOL II

Appendix A : COMMON STATION SECTION PLOTS WITH TRAVEL-TIME PICKS . . . . . .

Appendix B : COMMON SHOT SECTION PLOTS WITH TRAVEL-TIME PICKS . . . . . .

Appendix C : COMMON DISTANCE SECTIONS AND MISCELLANEOUS PLOTS . . . . . .

Appendix D : PROGRAMME LISTINGS . . . . . .

Appendix E : CSSP NATURE PAPER - BOTT ET AL 1985 . . . .

LIST OF FIGURES


| FIGURE | TITLE | FOLLOWING PAGE |
|---|---|---|
| 1.1 | Location of CSSP profile | 2 |
| 1.2 | (a) Speculative cross-section perpendicularly crossing the CSSP profile from the Midland Valley to the Northern Pennines. Midland Valley structure taken from LISPB, Bamford etal (1979). Northern Pennine structure taken from Bott et al (1984). (b) Geological interpretation of the crustal structure under the Southern Uplands taken from Needham and Knipe (1986). (c) Shallow crustal structure along the CSSP profile | 4 |
| 1.3 | Tectonic framework of the North Sea area (from Glennie 1984). | 5 |
| 1.4 | Map of the main structural blocks of the British Caledonides. | 5 |
| 1.5 | Three plate model for the closure of the Iapetus Ocean proposed by Soper and Hutton (1984). | 20 |
| 1.6 | Diagrams illustrating models proposed for parts of the British Caledonides | 20 |
| 1.7 | (a) Schematic cartoons of the tectonic evolution of the British Isles (b) Two plate model of the closure of the Iapetus Ocean proposed by Leggett et al (1983). | 21 |
| 1.8 | Location of seismic surveys performed in the British Isles. | 23 |
| 1.9 | Summary of P-wave velocity structure of the crust from the surveys shown in Fig. 1.5. | 23 |
| 1.10 | (a) Results of the LISPB experiment across the British Caledonides (Bamford et al 1977) (b) Results of a refraction experiment across the Newfoundland Appalachians (Haworth 1981) | 24 |
| 1.11 | Results of the Irish CSSP (Jacob et al 1985) | 26 |
| 1.12 | Results of the WINCH BIRPS line (Brewer et al (1983)). | 28 |
| 2.1 | Diagram illustrating the different types of section that can be plotted using the CSSP data | 37 |
| 2.2 | Frequency diagram for the number of traces with station/shot offsets within +/- 1km of all possible common distances. | 38 |
| 2.3 | (a) A sketch diagram illustrating how a travel-time matrix for the North Sea is related to the CSSP profile. (b) A travel-time matrix for the Irish Sea displaying the directions of the four different types of | |

sections that can be plotted using the CSSP data. 40

2.4 Common station section for the Eskdalemuir Array station R5 for the Irish sea shots. 43

2.5 Common shot section N2 for selected stations
Filtered - amplitudes equalized - vred=6.0
(a) No deconvolution applied
(b) Predicted deconvolution performed 46

2.6 Common shot section N2 for selected stations
Predicted deconvolution performed
Bubble pulse period = 0.31 s 46

2.7 Common shot section N2 for selected stations
Predicted deconvolution performed
Bubble pulse period = 0.31 s 46

2.8 Common shot section N2 for selected stations
Predicted deconvolution performed
Bubble pulse period = 0.31 s 47

2.9 Common shot section N2 for complete section
(a) No deconvolution performed
(b) Predicted deconvolution performed
Bubble pulse period = 0.31 s 47

2.10 Common shot section N5
(a) No deconvolution performed
(b) Predicted deconvolution performed
Bubble pulse period = 0.26 s 47

2.11 Common shot section N6
(a) No deconvolution performed
(b) Predicted deconvolution performed
Bubble pulse period = 0.23 s 47

2.12 Common shot section N20
(a) No deconvolution performed
(b) Predicted deconvolution performed
Bubble pulse period = 0.28 s 47

2.13 Common shot section M17
(a) No deconvolution performed
(b) Predicted deconvolution performed
Bubble pulse frequency = 0.36 s 47

2.14 Common shot section N14 amplitudes corrected to common gain 53

3.1 Sketch diagrams illustrating the interpretation of the travel-time matrices. 60

3.2 Sketch diagram illustrating the variables used to correct for the shallow structure. The average sediment cover velocities were derived from Green (1984). 70

4.1 The travel-time matrices for the Irish and North Sea drawn with representative common mid-point and common distance lines. 78

4.2a Travel-time matrix for the phase Pg in the Irish Sea uncorrected for shallow structure 78

4.2b Travel-time matrix for the phase Pg in the North Sea uncorrected for shallow structure 78

4.3a Travel-time matrix for the phase PcP in the Irish Sea uncorrected for shallow structure 79

4.3b Travel-time matrix for the phase PcP in the Irish Sea uncorrected for shallow structure 79

4.3c Travel-time matrix for the phase PcP in the Irish Sea corrected for shallow structure 79

4.4a Travel-time matrix for the phase PcP in the North Sea uncorrected for shallow structure 80

4.4b Travel-time matrix for the phase PcP in the North Sea uncorrected for shallow structure 80

4.4c Travel-time matrix for the phase PcP in the North Sea corrected for shallow structure 80

4.5a Travel-time matrix for the phase PmP in the Irish Sea uncorrected for shallow structure 82

4.5b Travel-time matrix for the phase PmP in the Irish Sea uncorrected for shallow structure 82

4.5c Travel-time matrix for the phase PmP in the Irish Sea corrected for shallow structure 82

4.6a Travel-time matrix for the phase PmP in the North Sea uncorrected for shallow structure 83

4.6b Travel-time matrix for the phase PmP in the North Sea uncorrected for shallow structure 83

4.6c Travel-time matrix for the phase PmP in the North Sea corrected for shallow structure 83

4.7a Travel-time matrix for the phase Pn in the Irish Sea uncorrected for shallow structure 84

4.7b Travel-time matrix for the phase Pn in the Irish Sea corrected for shallow structure 84

4.8a Travel-time matrix for the phase Pn in the North Sea uncorrected for shallow structure 85

4.8b Travel-time matrix for the phase Pn in the North Sea corrected for shallow structure 85

4.9 Wide-angle reflection results for PcP in the North and Irish Seas 87

4.10 Wide-angle reflection results for PcP in the North Sea 87

4.11 Wide-angle reflection results for PcP in the Irish Sea 87

4.12 Wide-angle reflection results for PmP in the North and Irish Seas 88

4.13 Wide-angle reflection results for PmP in the North and Irish Seas corrected and uncorrected for the shallow structure 88

4.14 Wide-angle reflection results for PmP in the Irish Sea 88

4.15 Wide-angle reflection results for PmP in the North Sea 88

4.16 (a) Summary of the PcP wide-angle reflection results
(b) Summary of the PmP wide-angle reflection results 89

4.17 Pn time-term results for Northern England using the Irish and North Sea shots. 90

4.18 A sketch of a cross-section through the hyperspace region for a time-term analysis for one time-term. 91

4.19 Analysis of variance of the Pn time-term analysis for Northern England. 92

4.20 Pn time-term results for the Irish Sea using only the Irish Sea shots. 93

4.21 Pn time-term results for the Irish Sea using only the Irish Sea shots and the Irish station L15. 93

4.22 Analysis of variance of the Pn time-term analysis for the Irish Sea. 93

4.23 Pn time-term results all Pn travel-times observed from the Irish and North Sea shots and at the Irish station L15. 93

4.24 Analysis of variance of the Pn time-term analysis using all the travel-times. 94

4.25 Pn time-term results for the North Sea using only the North Sea shots 94

4.26 Analysis of variance of the Pn time-term analysis for the North Sea. 94

4.27 Pn time-term results for the North Sea constraining the velocity to 8.0, 8.1, 8.2 and 8.3 km/s. 94

4.28 Pn time-term results for all shots. The travel-times are corrected for shallow structure before calculating the time-terms 96

4.29 Pn time-term results for shots N1-N29. The travel-times are corrected for shallow structure before calculating the time-terms. 96

4.30 Residuals plotted against site position for the runs corresponding to the reference numbers given in Table 4.2. 96

4.31 (a) Summary of the wide-angle results. Velocity values are average velocities calculated for each layer.
(b) Summary of the Pn time-term results. Velocity values are average velocities calculated for each layer in km/s 97

5.1 (a) Bouguer anomaly contour map over Northern England and adjacent marine areas (from Green 1984)
(b) Bouguer anomaly contour map across Ireland (taken from Jacob et al 1985) 100

5.2 Bouguer gravity anomaly along the complete CSSP line from the Shannon Estuary to the North Sea. 100

5.3 Nafe-Drake curve displaying the locations of the results from CSSP 101

5.4 (a) Gravity variations due to the seismic model along the main CSSP line
(b) Gravity variations due to the seismic model along the CSSP line incorporating the Carlisle intrusion identified by Laving (1971) 102

5.5 Aeromagnetic anomaly map just north of Carlisle 102

5.6 Gravity variations due to the seismic model without the Pn boundary. 102

5.7 Gravity variations calculated using the seismic model with the PmP and Pn boundaries replaced by a single interface along the 7.9 km/s isovelocity line. 102

5.8 (a) Common station section for station 32 displaying the travel times calculated from ray tracing through the model illustrated
(b) Ray diagram for station 32 for the North Sea shots. The model is a 1-D approximation to the structure beneath the North Sea. 108

5.9 (a) Common station section for station 32 displaying the travel times calculated from ray tracing through the model illustrated.
(b) Synthetic seismogram computed using the reflectivity method for station 32 for the North Sea shots. 109

5.10 (a) Common station section for station 32 displaying the travel times calculated from ray tracing through a model sketched in (b).
(b) Ray diagram for station 32 for the Irish Sea shots. The model is a 1-D approximation to the structure beneath the Irish Sea. 109

5.11 Common station sections for the Irish Sea shots corrected to common gain for: a) Station 2, b) Station 15, c) Station 32 110

5.12 (a) Synthetic seismogram computed using the reflectivity method for a transitional Moho consisting of a linear velocity gradient. 110

5.13 Synthetic seismogram computed using the reflectivity method for a transitional Moho consisting of a linear velocity

gradient with thin low velocity layers. 110

5.14 Synthetic seismogram computed using the reflectivity method for a transitional Moho consisting of an abrupt velocity increase at its top surface from 6.75 to 7.9 km/s and a slight velocity gradient down to its bottom surface. 111

5.15 Synthetic seismogram computed using the reflectivity method for a transitional Moho consisting of an abrupt velocity increase across its top surface from 6.75 to 7.5 km/s and a gentle velocity gradient down to its bottom surface. 111

5.16 Final laterally varying velocity model used to compute the 2-D synthetic seismograms. Contours are iso-velocity lines. Contour interval is 0.2 km/s. 114

5.17 (a) Raypaths through the upper crust computed for station 8
(b) Raypaths through the lower crust computed for station 8
(c) Raypaths of non reflected rays computed for station 8
(d) 2-D synthetic seismogram for station 8 for the Irish Sea shots computed using SEIS83
(e) Observed seismogram for station 8 for the Irish Sea shots with amplitudes corrected to common gain.
(f) Observed seismogram for station 8 for the Irish Sea shots with amplitudes equalised.
(g) 2-D synthetic seismogram for station 8 for the North Sea shots computed using SEIS83.
(h) Observed seismogram for station 8 for the North Sea shots with amplitudes corrected to common gain.
(i) Observed seismogram for station 8 for the North Sea shots with amplitudes equalised. 116

5.18 (a) Raypaths through the upper crust computed for station 32
(b) Raypaths through the lower crust computed for station 32
(c) Raypaths of non reflected rays computed for station 32
(d) 2-D synthetic seismogram for station 32 for the Irish Sea shots computed using SEIS83.
(e) Observed seismogram for station 32 for the Irish Sea shots with amplitudes corrected to common gain
(f) Observed seismogram for station 32 for the Irish Sea shots with amplitudes equalised.
(g) 2-D synthetic seismogram for station 32 for the North Sea shots computed using SEIS83.
(h) Observed seismogram for station 32 for the North Sea shots with amplitudes corrected to common gain.
(i) Observed seismogram for station 32 for the North Sea shots with amplitudes equalised. 117

5.19 (a) Raypaths through the upper crust computed for station 50
(b) Raypaths through the lower crust computed for station 50
(c) Raypaths of non reflected rays computed for station 50
(d) 2-D synthetic seismogram for station 50 for the Irish Sea shots computed using SEIS83.
(e) Observed seismogram for station 50 for the Irish Sea shots with amplitudes corrected to common gain.
(f) Observed seismogram for station 50 for the Irish Sea shots with amplitudes equalised.
(g) 2-D synthetic seismogram for station 50 for the North Sea shots computed using SEIS83.
(h) Observed seismogram for station 50 for the North Sea shots

with amplitudes corrected to common gain.
(i) Observed seismogram for station 50 for the North Sea shots with amplitudes equalised. 117

5.20 (a) Raypaths through the upper crust computed for shot M17
(b) Raypaths through the lower crust computed for shot M17
(c) Raypaths of non reflected rays computed for shot M17
(d) 2-D synthetic seismogram for station 50 for shot M17 shots computed using SEIS83.
(e) Observed seismogram for shot M17 with amplitudes equalized. 117

5.21 (a) Raypaths through the upper crust computed for shot N1
(b) Raypaths through the lower crust computed for shot N1
(c) 2-D synthetic seismogram for station 50 for shot N1 shots computed using SEIS83
(d) Observed seismogram for shot N1 with amplitudes equalized 117

5.22 (a) Raypaths through the upper crust computed for station 32 using a velocity model with a linear velocity gradient between the PmP and Pn boundaries.
(b) 2-D synthetic seismogram for station 32 for the Irish Sea shots computed using SEIS83 118

5.23 Location of BIRPS WINCH Lines in the area of the northern Irish Sea with line drawings of the main reflections compiled by Brewer et al (1983) 119

5.24 BIRPS WINCH LINE-HG deep reflection profile which ran along the Caledonian Suture Seismic Project Line between shots 13 and 11. The two way travel times to the PcP, PmP and Pn boundaries found from CSSP are drawn. Note the change in horizontal scale. 120

5.25 (a) Results of BIRPS deep reflection profile WINCH-BC.
(b) Reduced refraction section across the Hebridean Craton (Taken from Armour 1975)
(c) Location map for the seismic profiles 121

5.26 (a) Results of BIRPS deep reflection profile SWAT-4.
(b) Reduced refraction section from SW Ireland to Land's End. (Taken from Holder 1969)
(c) Location map for the seismic profiles 122

5.27 (a) Results of BIRPS deep reflection profile SWAT-6/7.
(b) Reduced refraction section west of Land's End. (Taken from Holder 1969).
(c) Location map for the seismic profiles 122

5.28 (a) Results of BIRPS deep reflection profile SWAT-6/7
(b) Reduced refraction section south of Land's End. (Taken from Holder 1969).
(c) Location map for the seismic profiles 122

5.29 Preliminary results of LISPB taken from Bamford et al (1976). 123

5.30 Gravity variations due the combined Irish and mainline CSSP refraction results. 124

5.31 Gravity variations due the combined Irish and mainline CSSP refraction results with the depth of the mid crustal interface across Ireland decreased by 3 km. 124

6.1 Common station section for station 36 for the North Sea shots to show the large amplitude S-wave arrivals. 139

## LIST OF TABLES

| TABLE | TITLE | FOLLOWING PAGE |
|---|---|---|
| 1.1 | Compressional wave velocities in rocks. | 31 |
| 2.1 | Reverberation and bubble pulse frequencies for the CSSP shots (taken from Green 1984). | 45 |
| 4.1 | Travel-time regression results for selected stations and shots for PcP, PmP and Pn arrivals. | 86 |
| 4.2 | Summary of time-term results for Pn. | 90 |
| 5.1 | Parameters used in gravity modelling. | 100 |

# CHAPTER ONE

## INTRODUCTION, GEOLOGY AND GEOPHYSICS

### 1.1 INTRODUCTION

The Caledonian Suture Seismic Project (CSSP) aimed to obtain a better understanding of the variations of crustal seismic velocity with depth using data collected from a large refraction experiment running from SW to NE across Northern England than has hitherto been possible from similar surveys in the past. Difficulties in the interpretation of previous refraction surveys such as LISPB (Bamford 1979) were encountered mainly due to problems in distinguishing between the effects of lateral as opposed to vertical changes in velocity, as both may produce similar effects on refraction seismograms. The unique configuration of the Caledonian Suture Seismic Project with use of both closely spaced stations (mainly on land) and closely spaced shots (mainly at sea) should enable lateral variations to be resolved. In addition the line was also chosen to run along as near uniform crustal structure considered possible striking parallel to the Caledonian trend (SW to NE) and just south of the inferred surface trace of the Iapetus Suture in Northern England. The Caledonian Suture Seismic Project line does not cross any known major geological discontinuities except for the inferred trace of the Iapetus Suture under the Irish Sea. An extension of the approach used for the Caledonian Suture Seismic Project of shooting a series of along strike refraction profiles within each Caledonian structural zone has been suggested by

Figure 1.1 Location of CSSP profile showing LISPB line and the inferred surface trace of the Iapetus Suture.

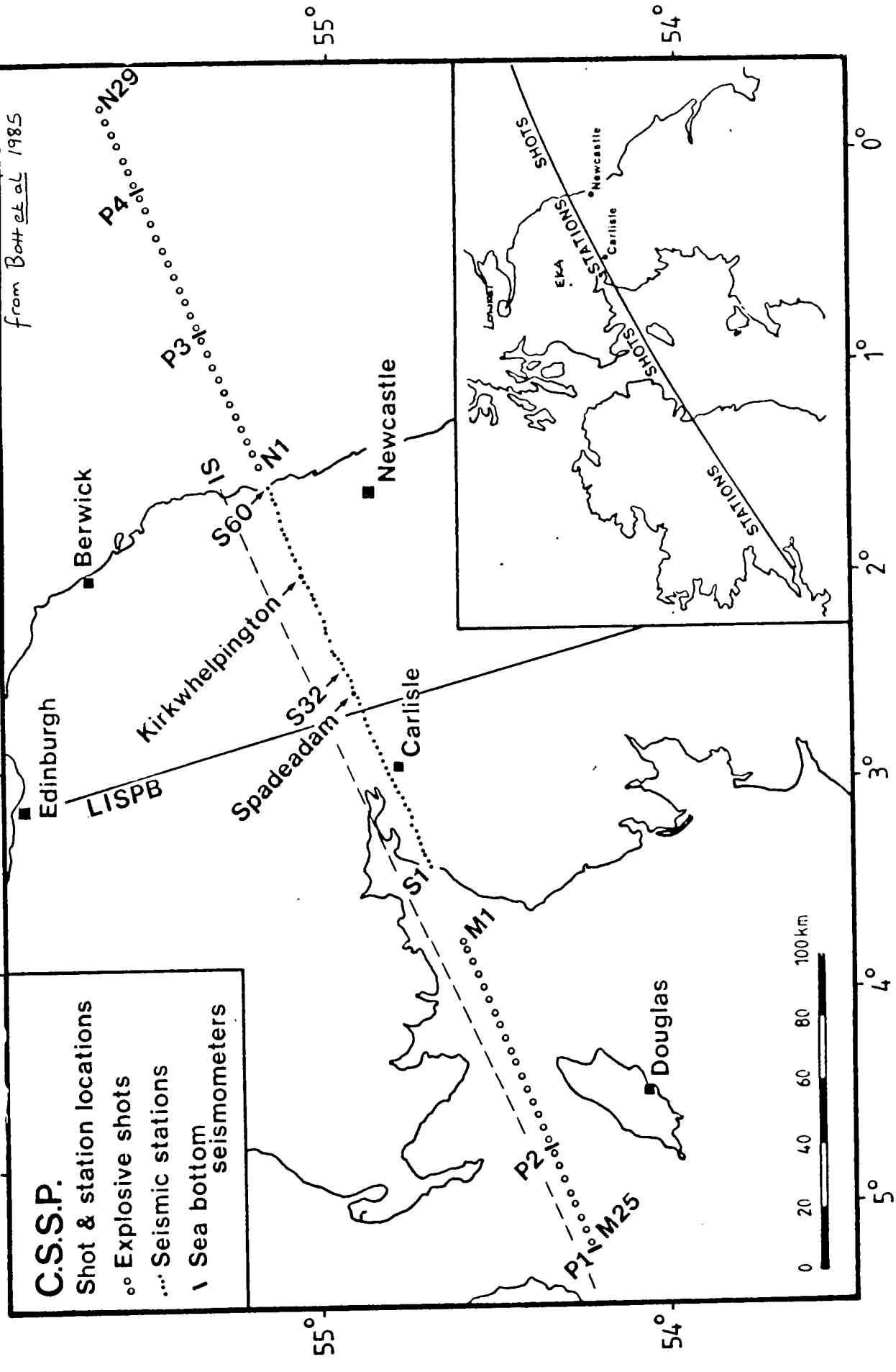

Haworth (1981) to identify the variations in deep structures not resolved by existing transverse lines such as LISPB.

The fieldwork and full details of the data acquisition are described in full by Green (1984) : below is a brief description of the main features of the experiment and the main data sets that are now held at Durham resulting from the survey.

### 1.1.1 The Caledonian Suture Seismic Project

The Caledonian Suture Seismic Project set out to investigate the deep crustal structure under northern England by arranging the shots and stations in a manner that could produce the best wide-angle reflection coverage avoiding the problems of shallow lateral variations encountered in previous seismic surveys. Approximately 60 stations were deployed across northern England at 2 km intervals with 57 shots in the Irish and North Seas at 4 km spacing (Fig. 1.1). Additional data was obtained from two land shots, the use of airguns, the deployment of Cambridge University Pull-Up Seabottom Seismometers (PUSS) and the establishment of "out-stations" in northern England, the Isle of Man and Southern Scotland. A line length of 390 km was obtained. This was extended across Ireland by the Dublin Institute for Advanced Studies in collaboration with Karlsruhe University (Jacob et al 1985) to provide a further 51 stations, 3 more shots in the Shannon Estuary and a further 10 shots in the Irish Sea to produce a total line length from the Shannon Estuary to the North Sea of 755 km.

In addition to the data recorded by stations set up specifically during the project by Durham, data has also been acquired from the UKAEA array at Eskdalemuir and the BGS nationwide network (including the Lownet Array). The Durham data was digitized at Durham using the facilities of the seismic processing laboratory (SPL) whilst the UKAEA and BGS data were digitized at Edinburgh using the facilities of the Global Seismology Unit of the BGS.

Green (1984) has described the data acquisition and field-work, the digitization of the data, the interpretation of the shallow crustal structure under the Caledonian Suture Seismic Project line and has presented simple preliminary models for the deeper structure. This thesis contains the main results obtained on the deep seismic structure beneath the main Caledonian Suture Seismic Project line. The shallow seismic structure is illustrated in Fig 1.2c (Bott et al 1985).

## 1.2 GEOLOGY OF CALEDONIDES OF THE BRITISH ISLES

Green (1984) has given a detailed description of the surface geology along the the Caledonian Suture Seismic Project profile and immediate surrounding regions. This description will not be repeated. Instead, taking into account that this study is concerned primarily with the deep structure, a summary of the Caledonian geology is presented in this section which highlights the contrasting geology and structural history of the crustal belts of the Caledonides. The Iapetus Suture divides these belts into the Northern

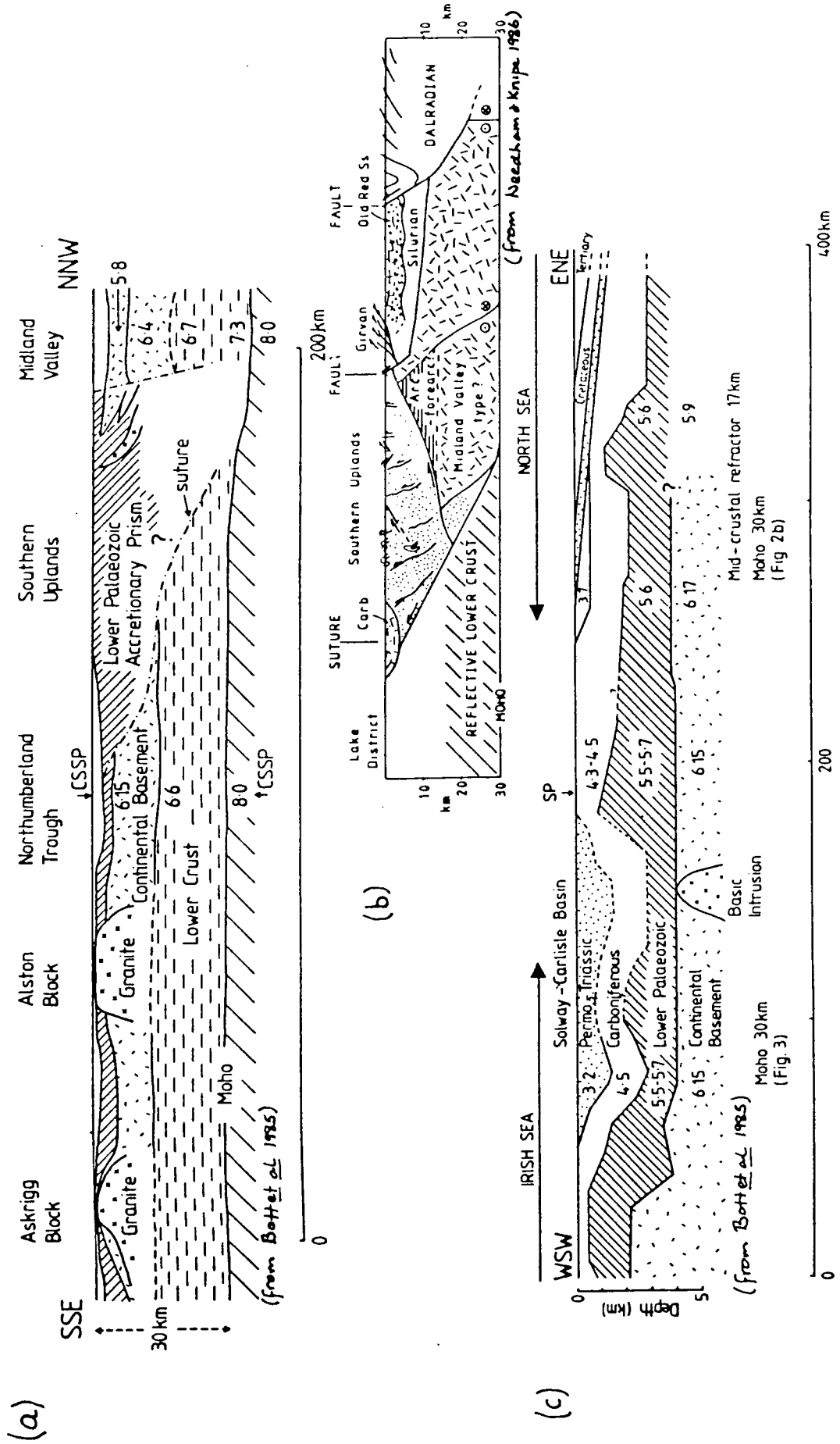


Figure 1.2 (a) Speculative cross-section perpendicularly crossing the CSSP profile from the Midland Valley to the Northern Pennines. Midland Valley structure taken from LISPB, Bamford etal (1979). Northern Pennine structure taken from Bott et al (1984).
(b) Geological interpretation of the crustal structure under the Southern Uplands taken from Needham and Knipe (1986).
(c) Shallow crustal structure along the CSSP profile.
SP = Spadeadam

Caledonides which comprise the southern margin of Laurentia together with accretions and the Southern Caledonides which comprise the northern margin of Cadomia. The exact location of the suture cannot be pinpointed but its surface trace as shown in Figs. 1.3 and 1.4 is based on interpretations of palaeontological (Cocks and Fortey 1982), geological (Anderton et al 1979) and geophysical evidence (Brewer et al 1983, Banks et al 1983). The Northern Caledonides consist of five main belts each about 40 to 50 km wide which cross Britain and Ireland from northeast to southwest. They are the Hebridean Craton, the NW Highlands, the Grampian Highlands, the Midland Valley Belt, and the Southern Uplands Belt. The Southern Caledonides comprise the Solway Line which consists of basins formed along the Iapetus Suture, the Lake District Belt of uplifted Lower Palaeozoic outcrops and the Southern Margin region.

Anderton et al (1979) give a useful summary of the stratigraphy of the British Isles and Glennie (1984) presents a recent succint summary of the most important events in the geological evolution of NW Europe. Much of the geological and tectonic description following is summarized from these sources supplemented by more recent reviews (Watson 1984 & 1985, Dewey and Shackleton 1984, Soper and Hutton 1984).

### 1.2.1 The Hebridean Craton

The oldest rocks in the British Isles lie within the Lewisian Complex of the Hebridean Craton west of the Moine Thrust. These rocks have locally suffered extensive reworking

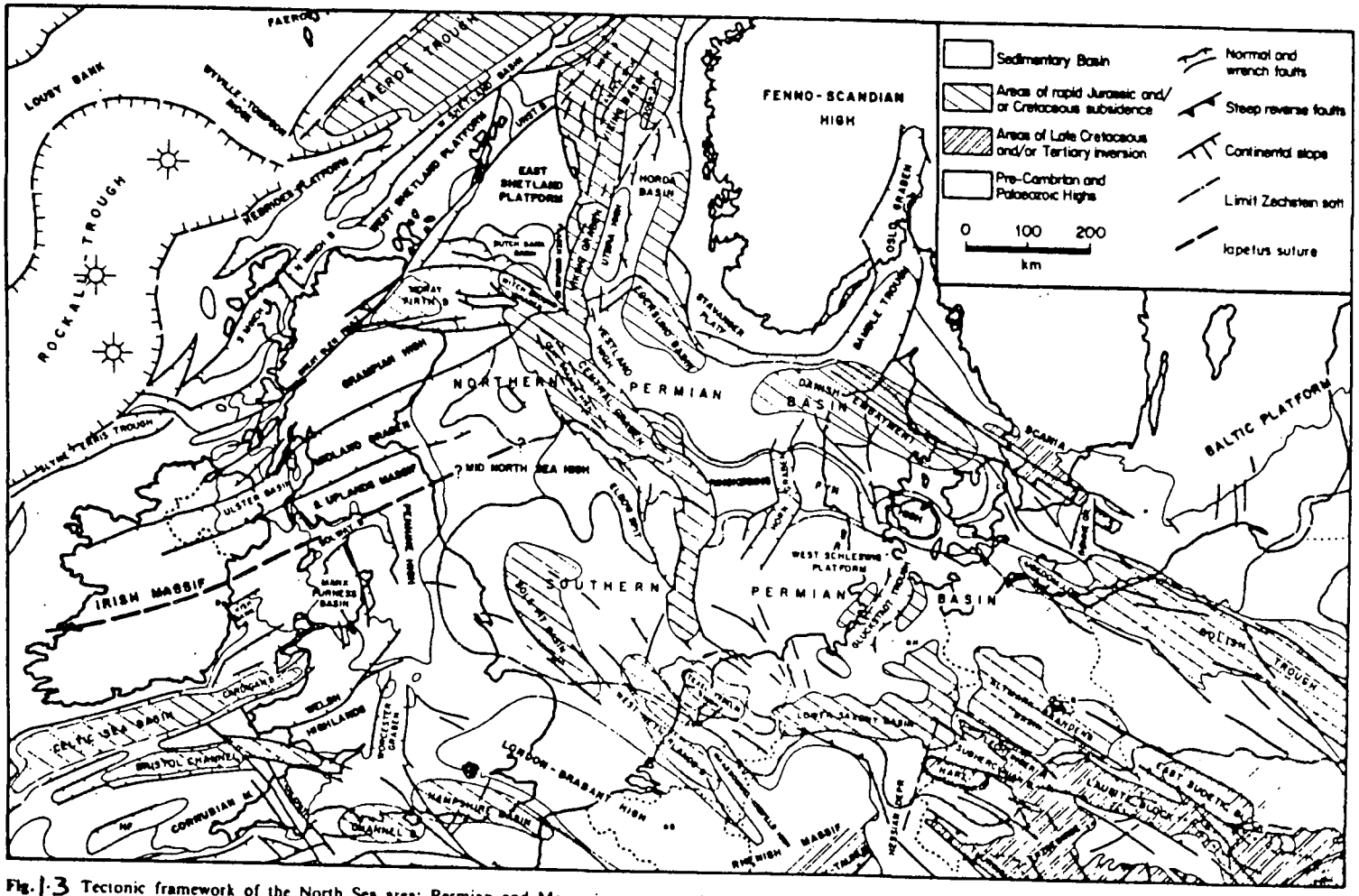


**Fig. 1.3** Tectonic framework of the North Sea area: Permian and Mesozoic tectonic units (simplified from Ziegler, 1982a, and Iapetus suture added).

(From Glennie 1984)

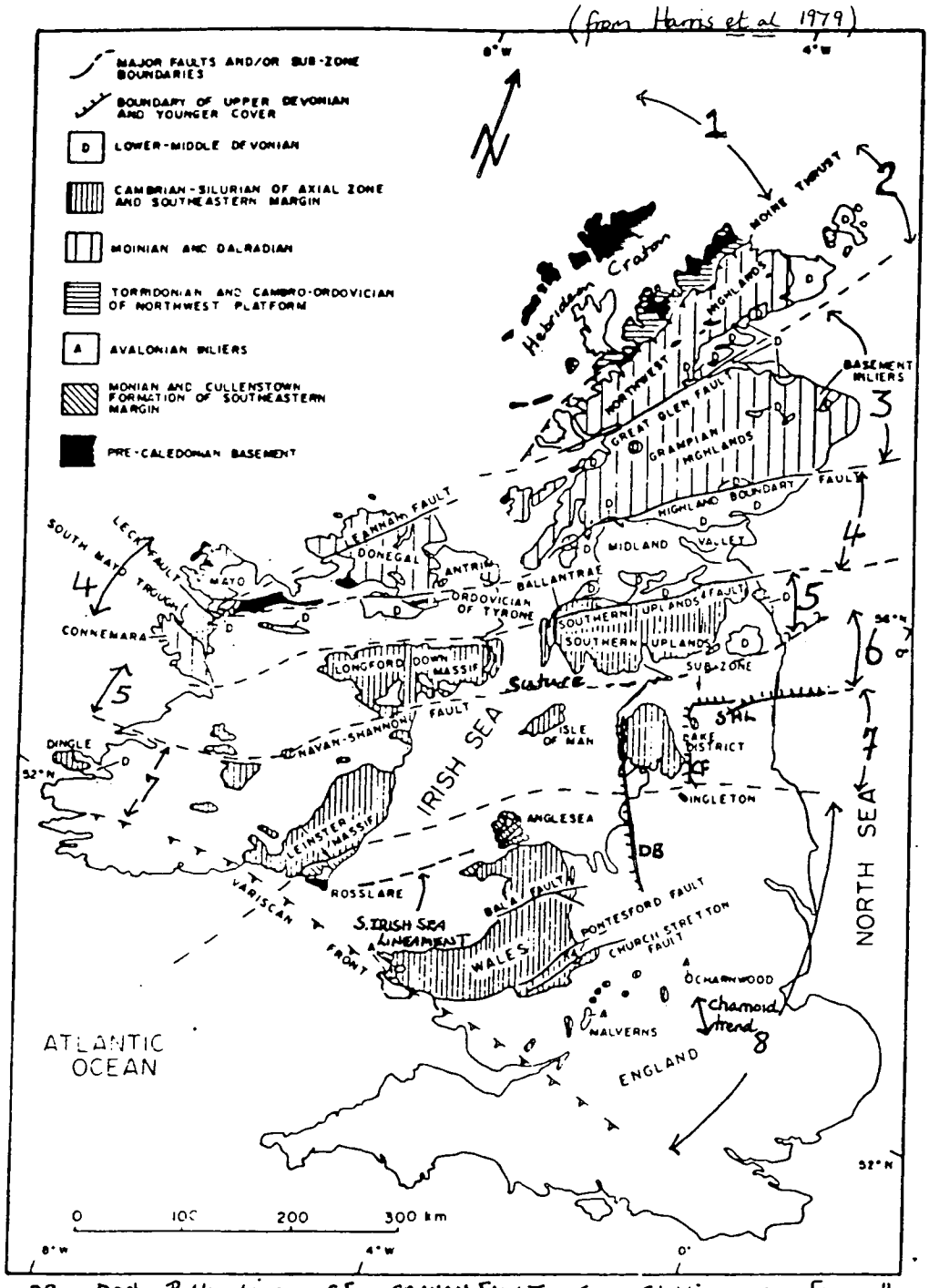


Figure 1.4 Map of the main structural blocks of the British Caledonides.
(See text for explanation of numbering)

in the Laxfordian, Grenvillian and Caledonian orogenies. The earliest unreworked rocks are the Scourian Gneisses which formed during the Archaean and consist of a thick series of coarsely banded acidic to intermediate gneisses interbanded with metasediments, basic, ultra-basic and anothositic rocks. The Scourian suffered amphibolite to granulite metamorphism (2900 to 2700 Ma) during the Badcallian metamorphic event (Harris 1983). The Scourian gneisses in general have a chaotic appearance on small to large scales but display a weak NW to SE grain.

Subsequent to these metamorphic events a suite of NW to SE trending dolerite dykes with tholeiitic composition ranging from a few centimetres to over 100 m wide were intruded cutting across the original Scourian metamorphic fabrics. These dykes, together with large tracts of Scourian gneisses and small volumes of sediments were deformed and metamorphised to amphibolite facies during the Laxfordian metamorphic event (1900 to 1700 Ma). Intrusion of granite sheets and pegmatitic veining occurred within the most deformed areas of the Laxfordian. This was followed by uplift, cooling and erosion.

The thick unmetamorphosed continental red clastic sediment sequences of the Stoer (~968 Ma) and Torridonian (~777 Ma) Groups were deposited in NNE trending rifts (Stewart 1982). Cambro-Ordovician shallow shelf limestones and sandstones unconformably overlie the Torridonian indicating a break in the geological record from ~777 Ma to ~510 Ma. The Moine sediments in the Northern Highlands have been thrust over the Torridonian and Hebridean Craton on the Moine Thrust. Butler

and Coward (1984) proposed a total westward movement of 54 km for the Moine Thrust and small displacements on the Outer Isles Thrust.

### 1.2.2 The NW Highlands

The Northwest Highlands lie between the Moine Thrust and the Great Glen Fault. They are formed of mainly Moine metasediments and are locally intruded by Caledonian granites and associated migmatites.

The Moine Series were deposited mainly as sands and muds with great lateral persistence. They unconformably overlie the Lewisian basement of the NW Highlands. The deformation and metamorphism of these rocks and of the underlying Lewisian basement yields radiometric dates around 1024 Ma and 740 Ma (Barr et al 1985). The first event is interpreted as the Grenvillian orogeny. The later event at 740 Ma is attributed to the Morarian metamorphism which produced the pegmatites visible in the Moines.

### 1.2.3 The Grampian Highlands

The Grampian Highlands are bounded to the north by the Great Glen Fault and to the south by the Highland Boundary Fault. Moine metasediments comparable to those in the NW Highlands are interfolded with the rocks of the Dalradian Supergroup which consist of a 20 km thick pile of mainly diachronous interbedded quartzites, slates and schists which generally young to the southeast, and were probably deposited

in a shallow shelf environment.

By the late Cambrian the deformation and metamorphism related to the Grampian Orogeny had produced the first SW to NE trending series of folds and faults. The crust was initially thickened and shortened by up to 70% with the formation of high pressure metamorphic assemblages. These were later overprinted by the diachronous metamorphic events which followed 20 to 35 Ma after the period of deepest burial. This peaked at 490 Ma in the Dalradian and at 460 Ma further towards the northwest in the Moines. There are two main suites of granitic intrusions. The first suite of syntectonic "Older Granites" were intruded between 490 Ma and 440 Ma and were accompanied by extensive migmatisation. The Older Granites are interpreted as products of regional anatexis related to crustal heating during the Grampian Orogeny (Watson 1984). The more voluminous and widespread "Newer Granites", formed between 435 Ma to 400 Ma, postdate the regional Grampian metamorphic events. They are not found west of the Grampian orogenic front which is marked by the Moine Thrust. This abrupt decline of the late magmatic activity towards the stable foreland may indicate that the partial melting and subsequent rise of the magmas have been controlled by tectonism above the melting zone related to the change from ductile to brittle deformation caused by the cooling and unroofing of the main Grampian Orogen (Watson 1984). The Newer Granites appear not to be directly related to the Grampian Orogeny.

The Great Glen and Highland Boundary Faults have suffered repeated movement since late Caledonian times. The amount of sinistral displacement along the Great Glen Fault is in dispute with estimates varying from 2000 km (Van der Voo 1981) to only 100 to 200 km (Irving and Strong 1984). Brewer et al (1983) showed that the Flannan Thrust identified on the WINCH deep reflection profiles and interpreted as a Caledonian thrust in the upper mantle is offset across the Great Glen Fault by 100 to 150 km. This and other recent results indicate strike slip movements along the Great Glen Fault of only 100 to 200 km during the Devonian and early Carboniferous.

The Highland Boundary Fault also had a complicated history of movement. Soper and Hutton (1984) and Dewey and Shackleton (1984) suggested that there may be sinistral displacements on the Highland Boundary Fault in addition to the well documented vertical movements. These movements included rapid uplift to the north during the final phase of the Caledonian Orogeny (415 to 408 Ma) and movements during the Devonian and Carboniferous. Movements on the Highland Boundary Fault had ended by the late Carboniferous (Watson 1985).

Since the end of the Caledonian Orogeny, of which the Grampian Orogeny is a part, the Grampian Highlands have remained a stable uplifted block. Post Caledonian sedimentation in the region was limited to the basins which formed adjacent to the Great Glen and Highland Boundary fault zones. For example the Orcadian Basin is filled by up to 5 km of Old Red Sandstone deposits eroded from the uplifted

Grampian and NW Highlands.

### 1.2.4 The Midland Valley Belt

The Midland Valley belt lies between the Highland Boundary and Southern Uplands Faults. No metamorphic basement is exposed but studies of inclusions in volcanic rocks (Upton et al 1983) indicate that a high grade granulite facies felspathic basement underlies the Caledonides north of the Iapetus Suture including the Midland Valley. Watson (1985) and Dewey and Shackleton (1984) interpreted this basement to be a southward continuation of the Grenvillian basement observed within the Hebridean Craton.

The early Ordovician Ballantrae Ophiolite suite of rocks are the earliest rocks exposed in the Midland Valley. This ophiolite is similar in age to the ophiolites of the Highland Boundary Complex. Several Silurian inliers of non-marine clastics derived from the south crop out just east of the Ballantrae Ophiolite. The earlier conglomerates comprise plutonic, volcanic and quartzitic clasts derived from a metamorphic basement to the south interpreted by Hall et al (1983) as the Pre-Caledonian basement underlying the Southern Uplands. The later conglomerates contain greywacke clasts interpreted by Leggett et al (1983) to be deposits of a forearc basin to the north of the Southern Uplands accretionary prism.

The Midland Valley subsided during the Lower Devonian and was filled by fluvial Old Red Sandstone deposits and by calc

alkaline volcanism. Thick lagoonal and deltaic sediments from the uplifted areas to the north of the Highland Boundary Fault were deposited during the Carboniferous. Tholeitic dykes and sills were intruded at about 300 to 295 Ma. The dykes cut across the Caledonian trend in an approximate east west direction. The Highland Boundary Fault has no detectable Mesozoic or Tertiary offsets and the Midland Valley Belt had a post-Palaeozoic history linked to that of the Grampian Highlands to the north (Watson 1985).

### 1.2.5 The Southern Uplands Belt

The Southern Uplands Belt lies south of the Southern Uplands Fault and north of the Iapetus Suture. It consists of thick sequences of imbricated and highly folded mid Ordovician to late Silurian deep water greywackes and shales. Early Ordovician basalts with mudstones, cherts and graptolitic shales occur along zones of intense imbrication on major reverse faults. These formations have been interpreted as ocean floor sediments accreted northwards onto the front of a late Ordovician to Silurian accretionary complex (Needham and Knipe 1986). Ordovician rocks up to 5 km thick dominate to the north of the complex and there is a general younging to the southeast where deposition ended during the late Silurian. Locally however the sediments young to the north within each imbricate sequence.

Early Devonian "Newer Granites" were intruded in the western parts of the Southern Uplands as the Criffel, Loch Dee, Loch Doon and Cheviot plutons. Recent isotopic work by

Halliday (1984) highlights the low concentrations of inherited zircons in the granite plutons south of, in comparison to those north of, the Southern Uplands Fault. In addition, the compositions of xenoliths found in Upper Palaeozoic and Mesozoic volcanic rocks indicate that shallow crystalline felspathic granulite basement underlies the Caledonides in Northern Britain including the Midland Valley and Southern Uplands. Anorthositic xenoliths found from the Southern Uplands imply a high anorthositic composition in the basement of the Southern Uplands.

Early Devonian calc alkaline volcanics surround the outcrop of the late Caledonian Cheviot granite. Up to 600 m of locally derived fluvial red felspathic sandstones and conglomerates were deposited onto the topography of the uplifted and eroded Silurian. The Devonian ended with the extrusion of the Birrenswark-Kelso lavas along the southern edge of the Southern Uplands Belt.

### 1.2.6 The Solway Line

The Solway Line marks the approximate position of the Iapetus Suture across the Irish Sea and Northern England. It is characterized by an absence of granites in contrast to the adjacent belts to the north and south and by the line of Carboniferous and Mesozoic basins. A detailed description of the geology of the basins and troughs has been given by Green (1984). Only the main features of the subsidence and depositional history are described below.

Deposition during the Carboniferous along the Solway line was dominated by differential subsidence of the Northumberland trough and the formation of the Peel Basin. The subsidence in the Northumberland Trough was initiated in the early Tournaisian and the resulting deposition of sediments was predominantly cyclic. Sedimentation rates kept pace with subsidence so that deposition remained at approximately sea level throughout the Carboniferous. By the late Visean the adjacent blocks subsided but differential subsidence continued. During the Namurian, differential subsidence ceased and was replaced by a broad regional subsidence of basins and blocks alike (Bott et al 1984, Leeder 1982). The estuarine marine sedimentation of the Dinantian changed progressively towards the freshwater and brackish deltaic sequences of the Westphalian coal measures.

At the end of the Carboniferous the quartz-dolerite Whin Sill complex was emplaced accompanied by the intrusion of a series of east west trending dykes. Uplift and erosion then occurred to produce a renewed period of subaerial erosion similar to that of the Devonian.

Permo-Trias sediments are found on the northern peninsula of the Isle of Man, in the Solway and Carlisle Basins, in southern Scotland and in Durham. The Lower Permian was a time of sub-aerial erosion with the deposition of coarse water-lain breccias and in the deeper parts of the basins playa type muds and silts. In the upper Permian widespread transgression of the Zechstein and Bakevellia Seas in the North and Irish Sea areas deposited evaporites with, in the Bakevellia Sea,

interbedded continental clastic deposits. These evaporite deposits were produced only patchily on the raised Mid-North Sea High. In the Trias a more regional marine transgression deposited the waterlain St. Bees and Kirklington sandstones and the Stanwix shales in the Carlisle Basin.

A line of Permo-Trias basins extends from north to south across the Northern Caledonides. These include the Minch, Ulster, Solway, Carlisle and Manx Furness Basins. The Northern and Southern Permian Basins in the North Sea area also formed to the east. Many of these basins formed by tensional reactivation of earlier Caledonian thrusts and faults (Brewer et al 1983).

Further Mesozoic sediments along the CSSP profile occur mainly in the North Sea region. Approximately 45m of shallow Upper Jurassic marine sediments are overlain by about 500 - 600 m of Cretaceous and 500 m of Tertiary sediments on the Mid North Sea High beneath the eastern end of the CSSP line.

Extensive extrusion of basic magmas centred on NE Ireland and western Scotland in the early Tertiary was accompanied by the emplacement of plutonic complexes. NW to SE trending dykes were intruded from Scotland across Northern England along pre-existing crustal weaknesses e.g. the Cleveland Dyke (Kirton and Donato 1985). The formation of the Tertiary Basins to the west of Scotland and the early Tertiary volcanism were related to the opening of the North Atlantic.

### 1.2.7 The Lake District Belt

The Lake District Belt just south of the inferred surface trace of the Iapetus Suture is defined as the SW-NE to W-E line including the uplifted areas of the Leinster Massif, the Isle of Man, the Lake District and the Alston Block.

The Lake District is composed of Lower Palaeozoic sediments and volcanic intrusions of Ordovician to Lower Devonian age. At its northern margin the Lower Ordovician Skiddaw Group forms a 7.5 km thick sequence of alternating graptolitic greywackes, siltstones, and mudstones which have been folded and metamorphosed to lower greenschist facies during the later stages of the Caledonian Orogeny. They are overlain unconformably by 4 km of Borrowdale Volcanics comprising interbedded tuffs, agglomerates and rhyolitic to mainly andesitic volcanics. 4.5 km of Silurian mudstone, siltstones and grits overlie the volcanics.

The Alston Block basement consists of Lower Palaeozoic rocks intruded by the Weardale granite. This is covered by a thin sequence of up to 2 km of Carboniferous sediments deposited during the subsidence that began in the area from the Visean. The rocks outcropping on the Isle of Man are mainly the Lower Ordovician Manx Group comprising 7.5 km of interbedded greywackes, siltstones and mudstones probably deposited in the same deep water basin as the Skiddaw Group in the Lake District. Carboniferous and Permo-Trias sediments of the Solway Basin outcrop in the northeast.

The granites of the Lake District yield ages from 450 to 390 Ma (O'Brien et al 1985). The Weardale Granite which underlies the Alston Block gives an age of 410 Ma (Dunham 1974). These dates are simiar to those of the Newer Granites of the Grampian Highlands and Southern Uplands. O'Brien et al (1985) concluded that these granites have sub-crustal origins probably related to a southward dipping subduction zone and that the Lake District Batholith has a similar mode of emplacement to the Caledonian Cairngorm granites.

The Manx Furness Basin formed between the Isle of Man and the Lake District in the early Permian and had an evolution similar to the Permo-Trias Solway Basin described in the previous section.

### 1.2.8 The Southern Margin

The only rocks similar in character and age to the Lewisian observed south of the Iapetus Suture in the British Isles outcrop within the gneissic terrain of the Rosslare Complex in southeast Ireland and display a different evolutionary history from the Pre-Cambrian to the north. The only other comparable Proterozoic basement to the south of the suture are exposed in the Baltic Shield area to the east.

The Pre-Cambrian of the Southern Caledonides outcrops as isolated inliers in five main areas which represent the visible exposures of the Pre-Cambrian Craton of England and Wales (Glennie 1984). These are the Monian sediments in Anglesey, the Uriconian and Longmyndian outcrops in

Shropshire, the Malvernian and Charnian rocks of the Midlands. The late Pre-Cambrian deformation and metamorphism observed in most of the inliers is attributed to a Celtic Orogenic event which preceeded the Caledonian orogeny.

After the Celtic Orogeny sedimentation during the Lower Palaeozoic was controlled by the presence of the Irish Sea shelf, the Midlands Platform and the subsidence of the Welsh Basin. The Midland Platform was flooded at times due to a slow progressive subsidence throughout the Lower Palaeozoic and the eustatic rises in sea level which occurred in the Lower Cambrian and Llandovery. Up to 1000 m of muds and silts were deposited on the edges of the Platform.

The Welsh Basin had a complicated history of subsidence, sedimentation and slight uplift. The sediments consist mainly of turbidites, black shales, muds and silts interbedded on the basin margins with predominantly andesitic to rhyolitic late Tremadoc to Wenlock volcanic lavas and tuffs. The volcanic activity shifted from the Lake District towards the southwest during the Ordovician and ceased in the Welsh Basin by Lower Caradoc times.

## 1.3 TECTONIC MODELS OF THE CALEDONIDES OF THE BRITISH ISLES

The timing of the initial opening of the Iapetus Ocean is in dispute. Anderton (1982) interpreted the Tayvalliach Volcanics as magmatism associated with the initial rifting which accompanied the separation of the Laurentian and Baltic Shield areas in the late Pre-Cambrian. However, Watson (1984)

considered that the Moine and Dalradian were deposited in an oceanic environment and suggested the Iapetus Ocean existed from mid-Proterozoic times. Cocks and Fortey (1982) have shown from palaeontological evidence that the Iapetus Ocean and Tornquist Seas existed during the Cambrian. The Tornquist Sea closed in the late Ordovician followed by the closure of the Iapetus Ocean in the late Silurian (Fig. 1.5). The resulting continental collisions produced low grade metamorphism and deformation (Watson 1984).

The main observations that must be explained by any tectonic models proposed for the formation of the Caledonides are:

1. The diachronous deposition of the Moine and Dalradian north of the Highland Boundary Fault.
2. The northwestward progression of the structural and metamorphic events during the Grampian Orogeny in the early Ordovician.
3. The change to brittle deformation and progressive westward propagation of the Caledonian thrusts ending with the Moine and Outer Isles Thrusts in the west.
4. The emplacement of a wide variety of Ordovician and Silurian rocks along the Highland Boundary Fault.
5. The formation of the Southern Uplands accretionary prism.
6. The trend from early Ordovician tholeiitic to mainly calc-alkaline magmatism in the Lake District on the northern edge of Cadomia.
7. The emplacement of the late granites during the late Ordovician and early Devonian from the Lake District to the Grampian Highlands and the lack of inherited zircons

south of the Southern Uplands Fault. The emplacement of these granites in the NW Highlands, the Grampian Highlands, the Southern Uplands and the Lake District belts but not in the Midland Valley or the Solway Line belts.

8. The presence of a northwest dipping lower crust under the Southern Uplands interpreted from both deep seismic evidence (Brewer et al 1983) and magnetic variation anomalies (Banks et al 1983).
9. The absence of any oceanic crust under the entire British Isles Caledonian Orogen except for outcrops of small ophiolitic complexes along the Great Glen, Highland Boundary and Southern Uplands Faults.

Early plate tectonic models (Figs. 1.6 a to e & g) envisaged initial southeastwards subduction under the northern margin of Gondwanaland to create the island arc type magmatism of the Lake District. This later gave way to northwestward subduction under the southern margin of Laurentia to produce the Southern Uplands accretionary prism. The Grampian Orogeny was attributed to northwestwards subduction under the Laurentian margin followed by continental collision in the late Silurian. However, the early Ordovician ages found for the Grampian Orogeny are too early to be related directly to the final closure of the Iapetus Ocean.

Wright et al (1976) proposed that the Grampian Orogeny was the result of the collision of Laurentia with an island arc lying to the south of the subduction zone at the Laurentian continental margin (Fig. 1.6f). Both this model and the

others discussed above require oceanic crust beneath the Midland Valley and Southern Uplands, for which there is no geophysical or geological evidence.

Watson and Dunning (1979) suggested a variation of the model of Wright (1976) by proposing the impingement of a micro-continent represented by the Midland Valley and Southern Uplands onto the southern edge of the Laurentian landmass to produce the Grampian Orogeny. The subduction at the Highland Boundary Fault zone which brought the two landmasses together ceased and subduction began to occur to the south of the micro-continent to form the Southern Uplands accretionary prism (Fig. 1.6h). However, recent work has highlighted dextral and sinistral strike slip movements within the Caledonian belt (Phillips et al 1976, Soper and Hutton 1984, Dewey and Shackleton 1984). It is clear that models involving only movement perpendicular to the strike are gross oversimplifications.

The Caledonian Orogenic belt runs from north to south between Greenland and Norway and approximately southwest to northeast from Newfoundland to the British Isles. This change in direction requires sinistral strike slip between Laurentia and Baltica (Fig. 1.7, Soper and Hutton 1984). Similarly dextral strike slip would occur between Laurentia and Cadomia (Fig. 1.7, Phillips et al 1976). Recent models incorporate a combination of oblique subduction, collision and strike slip fault movements within the Caledonian Orogenic Belt. The sense of these strike slip movements is in dispute (Phillips et al 1976, Dewey and Shackleton 1984, Soper and Hutton 1984).

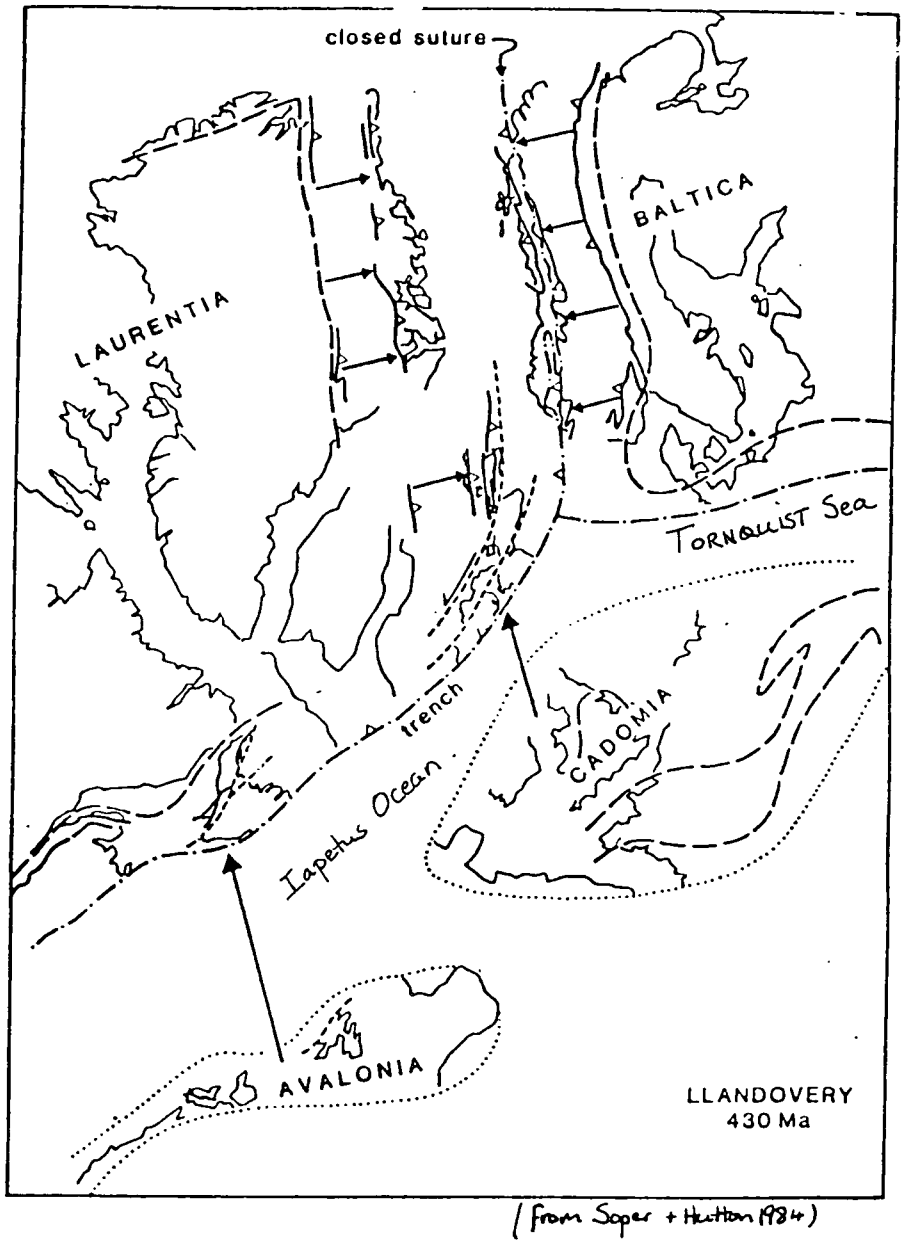


Figure 1.5 Three plate model for the closure of the Iapetus Ocean proposed by Soper and Hutton (1984)

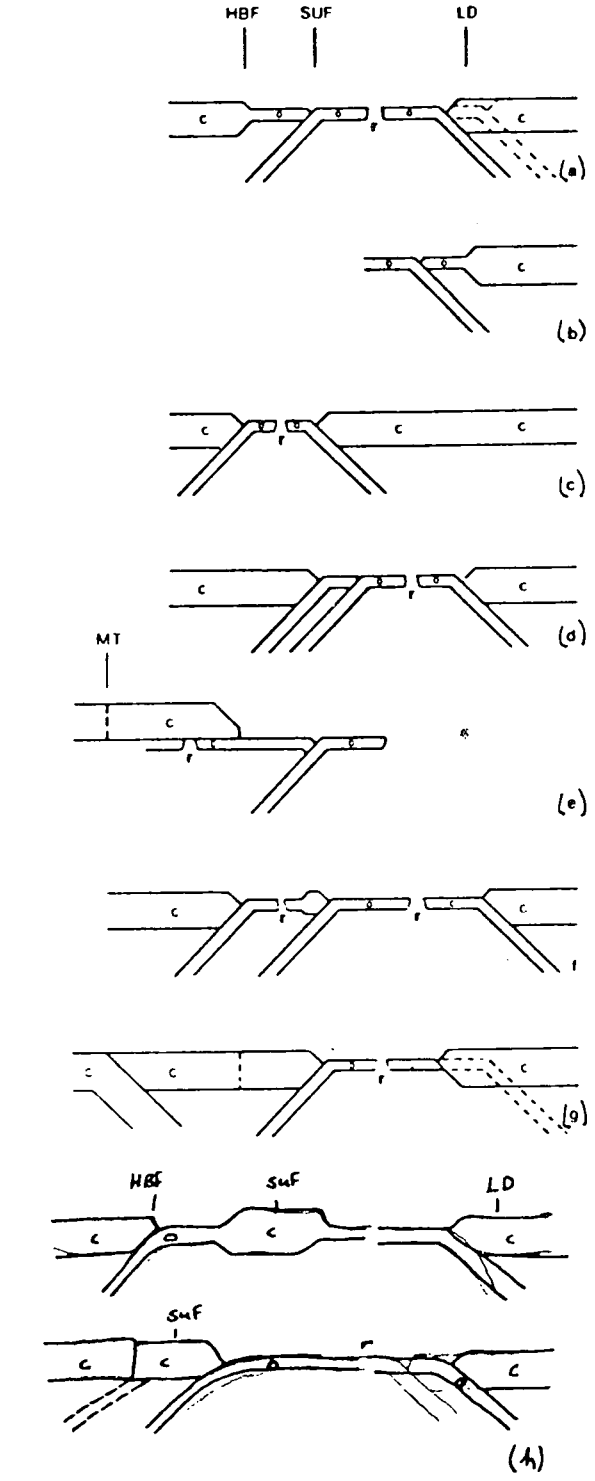


FIG 1-6 Diagrams illustrating models proposed for parts of the British Caledonides:
(a) after Dewey (1969),
(b) after Fitton & Hughes (1970),
(c) after Jeans (1973) and Gunn (1973),
(d) after Church & Gayer (1973),
(e) after Lambert & McKerrow (1976),
(f) after Wright (1976),
(g) after Phillips, Stillman & Murphy (1976).
Letters are used as follows:
HBF Highland Boundary Fault,
SUF South Uplands Fault,
LD Lake District,
MT Moine Thrust,

c continental crust,
o oceanic crust,
r spreading ridge.
Dashed lines indicate early positions of subduction zones.
(h) WATSON & Dunning (1979)
(i) Dewey & Shackleton (1984)

(Diagrams taken from Harris et al 1979)

(from Dewey & Shackleton (1984))

Sinistral strike slip probably predominated immediately after the closure of the Iapetus Suture during the early Devonian but dextral strike slip movements may have occurred along the Iapetus Suture during Ordovician to Silurian subduction under the Southern Uplands.

Dewey and Shackleton (1984) proposed that the Grampian Orogeny resulted from the conversion of a mid-oceanic ridge fracture system into a subduction zone and consequent obduction of a giant ophiolitic nappe onto the Laurentian margin (Fig. 1.6i). The resulting crustal thickening. deformation and metamorphism might account for the early Ordovician orogeny which took place long before continental collision in the late Silurian.

To summarize, the Caledonian Orogenic Belt probably suffered complicated strike slip movements which were possibly dextral during the closure of the Iapetus Ocean but subsequently became sinistral. The timing of the Grampian Orogeny well before continental collision in the late Silurian can be explained by the collision of micro-continents onto the Laurentian margin or by obduction of ophiolitic nappes. The Iapetus Ocean closed between the Lake District and the Southern Uplands. Northward and southward subduction had occurred along the line of the Iapetus suture. The late granites may be related to the partial melting of the remnant subducted slabs (Watson 1984).

These Caledonian features have been reactivated since the early Devonian first by tension related to Hercynian

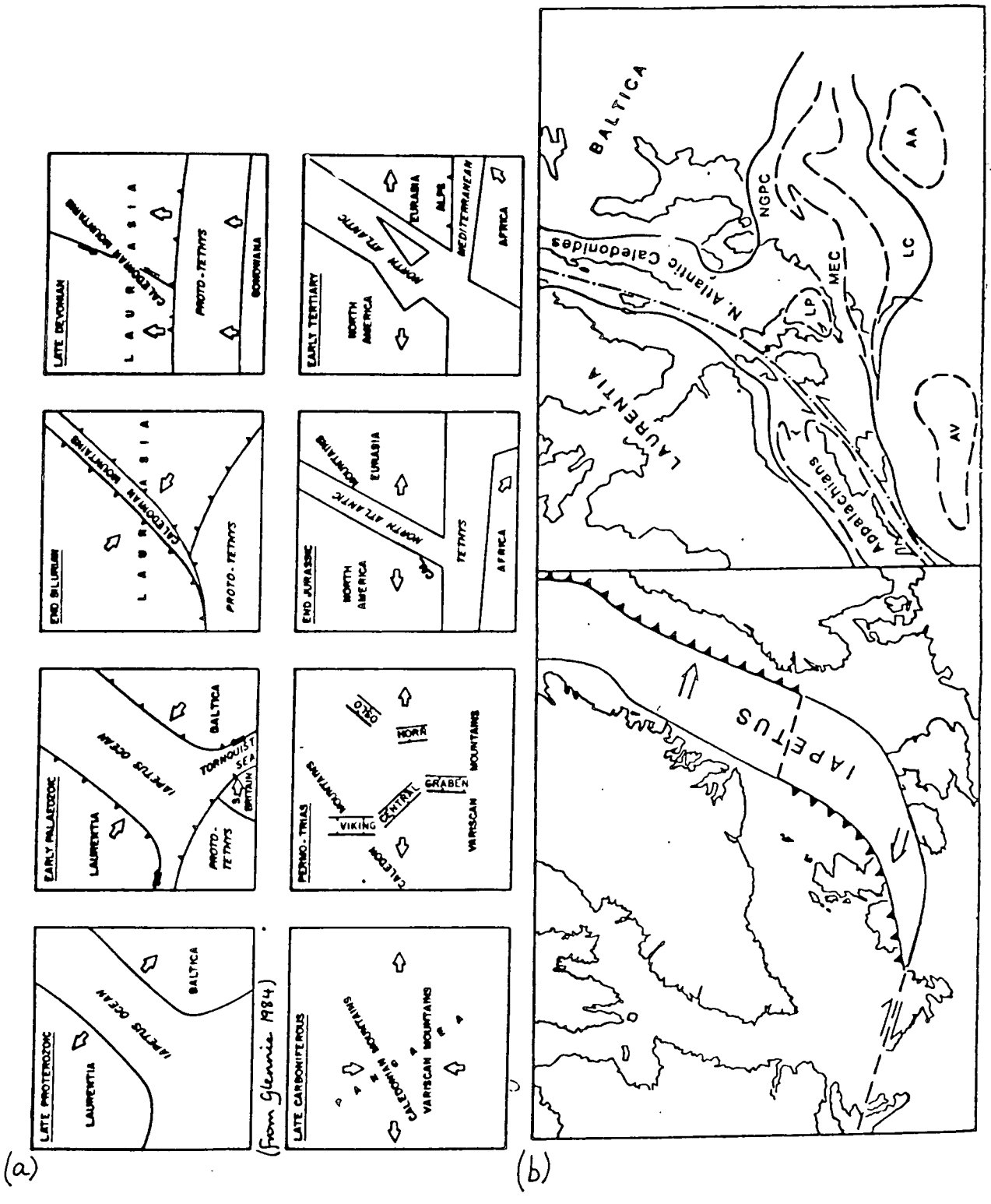


Figure 1.7 (a) Schematic cartoons of the tectonic evolution of the British Isles. Note scales vary.
(b) Two plate model of the closure of the Iapetus Ocean proposed by Leggett et al (1983).

subduction (Bott et al 1984) and compression caused by continental collision and closure of the Rheic Ocean (Glennie 1984). Subsequent doming and volcanism in the North Sea and formation of numerous Permo-Trias basins in NW Europe was probably produced either by partial melting of the Hercynian subducted slab under the British Isles or related to heating events which eventually led to the rifting and opening of the mid Atlantic by the late Jurassic. Other heating events occurred in the late Jurassic and early Tertiary related to the formation of the Rockall Trough and the opening of the Northern Atlantic respectively. East west tension predominated although compression occurred at the end of the Cretaceous during the Alpine Orogeny.

## 1.4 SEISMIC STRUCTURE OF THE CALEDONIDES OF THE BRITISH ISLES

The LISPB refraction survey and BIRPS WINCH deep reflection survey have been the largest and most detailed experiments that have crossed the Caledonides in the British Isles. The LISPB line crosses the Caledonian Suture Seismic Project profile at about station 25 near Spadeadam on the Northumberland/Cumbria border. The WINCH line crosses at approximately shot M22 in the Irish Sea and a short segment ran along the Caledonian Suture Seismic Project profile. The other important surveys are summarized in Figs. 1.8 and 1.9.

### 1.4.1 Refraction Surveys

The Lithospheric Seismic Profile in Britain (LISPB) of 1974 (Fig.1.10) indicated contrasting crustal structures beneath the Caledonides of Northern Britain and beneath the region south of the Southern Uplands Fault (Bamford et al 1976, 1977, 1978 & 1979, Faber and Bamford 1979, 1981). To the north, the upper crust is characterised by velocities of 6.1 to 6.2 km/s interpreted as Caledonian belt metamorphics of the Moine and Dalradian. The underlying middle crust at depths of 10 to 20 km yields velocities between 6.4 and 6.5 km/s which are interpreted as granulite facies Lewisian basement (Smith and Bott 1979, Hall 1978). The velocity of the lower crust is about 7.0 km/s. The Moho deepens from 24 km under Northern Scotland to 34 km under the Midland Valley. The sub Moho velocity is constant at 8.0 km/s.

To the south of the Southern Uplands Fault the LISPB results are at variance with the results of other surveys in the area (Swinburne 1975, Bott et al 1984 & 1985, Green 1984 and Hall et al 1983). The upper crust as suggested by LISPB consists of a maximum of 15 km of Lower Palaeozoic rocks of velocities 5.8 to 6.0 km/s beneath a thin local veneer of Upper Palaeozoic and Mesozoic sediments. Underlying the Lower Palaeozoic a layer of velocity 6.28 km/s, significantly lower than the 6.4 km/s layer found to the north, is interpreted as Pre-Caledonian basement similar to the Pentevrian basement of Brittany (Bamford 1977). The LISPB structure of the lower crust and Moho south of the Southern Uplands Fault is otherwise uncertain because of the absence of prominent

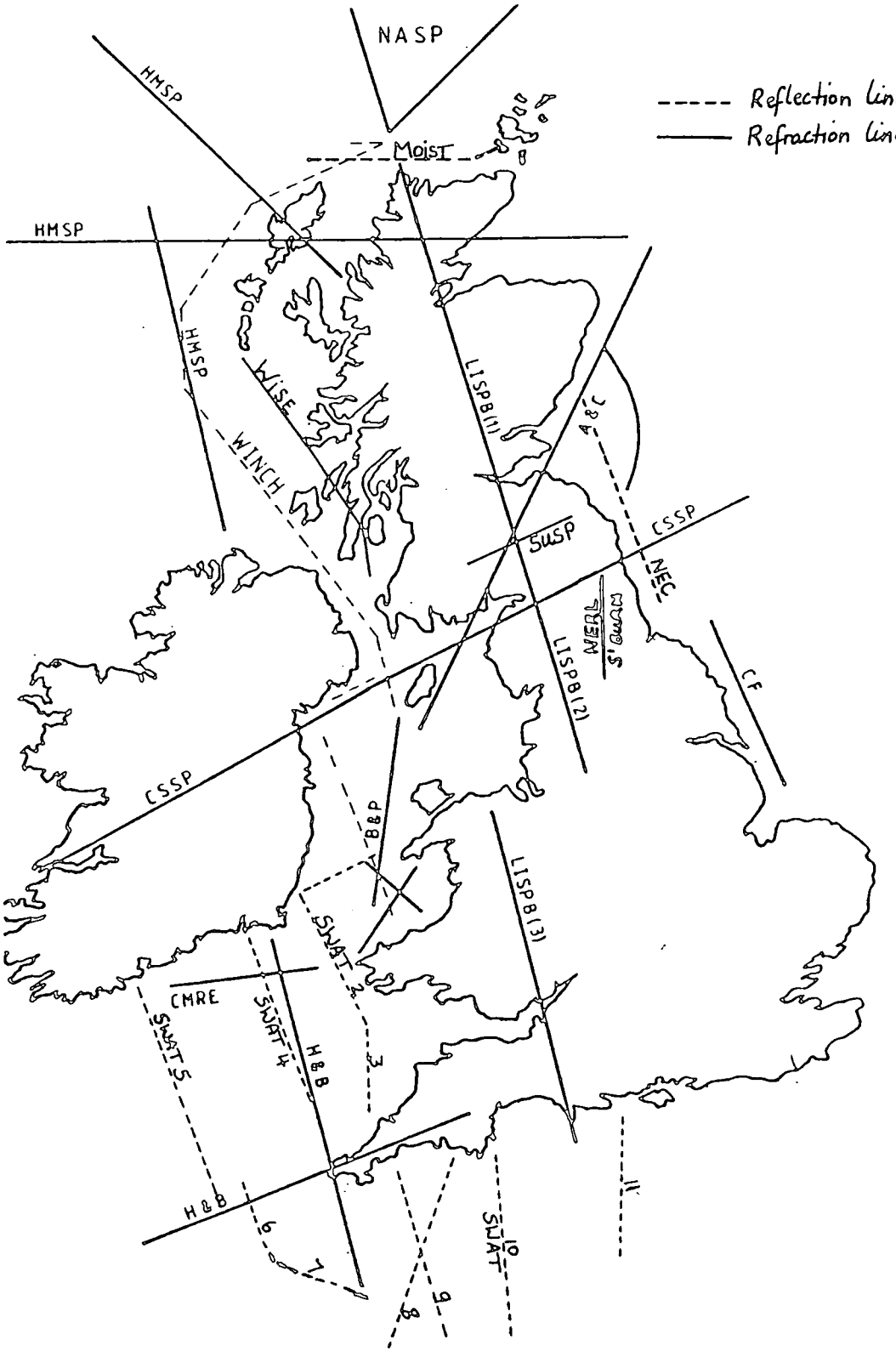


Fig 1.8 Location of seismic surveys performed in the British Isles. A & C = Agger and Carpenter (1964), CF = Collette et al. (1967,1970), LISPB = Bamford et al. (1976, 1977 & 1978), CMRE = Bamford (1971,1972), Bamford and Blundell (1970), B & P = Blundell and Parks (1969), H & B = Holder and Bott (1971), S'BURN = Swinburn (1975), HMSP = Armour (1978), NASP = Bott et al. (1974,1976), Smith and Bott (1975) (From Green, 1984) WISE = Summers et al (1982), WINCH = Brewer et al (1983), SWAT = Cheadle et al (1986), SUSP = Hall et al (1983).

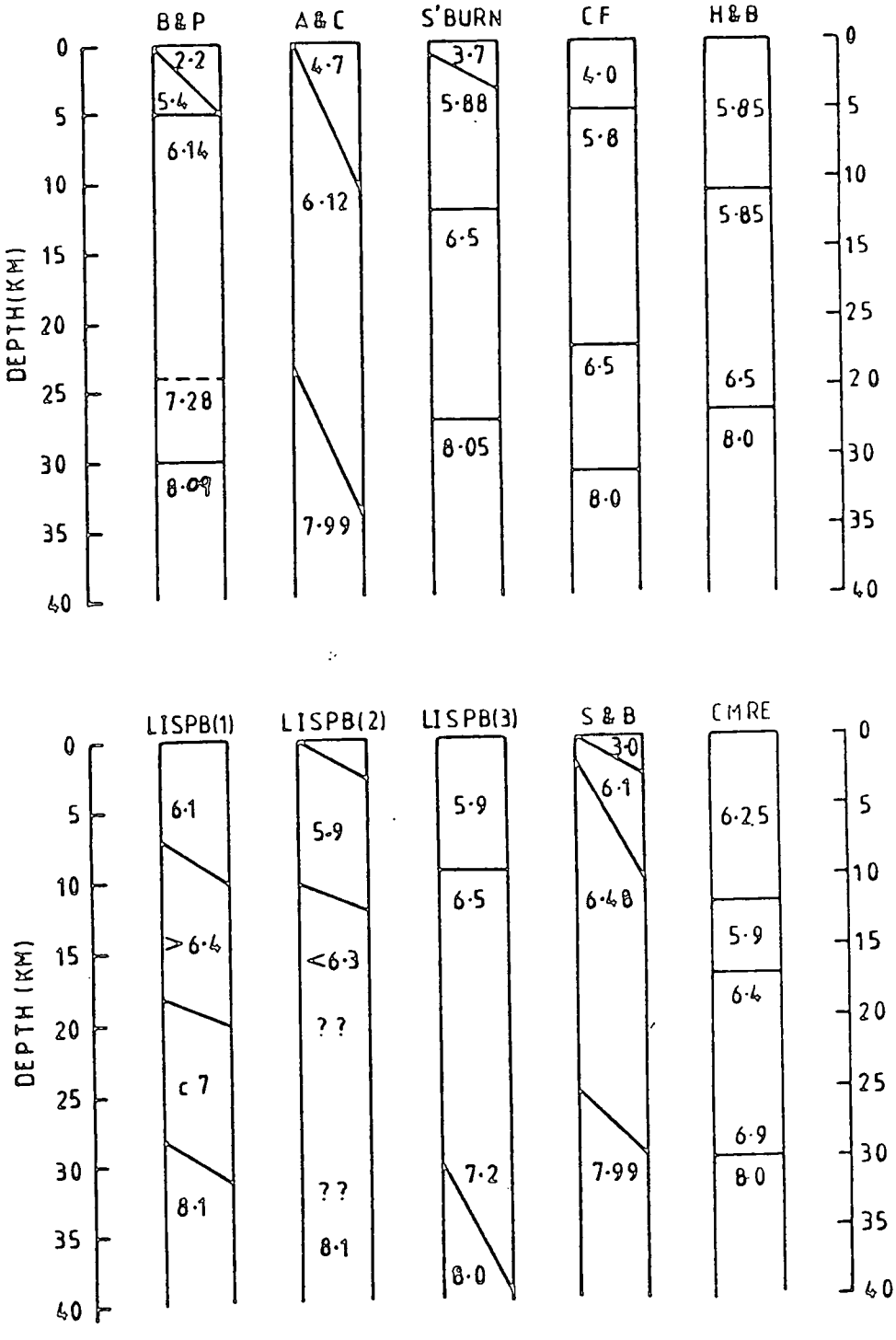


Fig 1.9 Summary of P-wave velocity structure of the crust from the surveys shown in fig 1.5 (from Green, 1984)

arrivals.

The NERL line (Bott et al 1984, Fig. 1.2a) ran north to south east of the LISPB line and used the LISPB shots. This indicated an upper crustal velocity of 5.88 km/s which agrees with the LISPB results. In contrast to the LISPB results, good Moho reflections were observed which indicated a sharp Moho at a constant depth of 27 km under Northern England with an underlying sub-Moho velocity of 8.05 km/s. A lower crustal velocity of 6.5 km/s was found below a mid crustal interface at 12 km depth. Two earlier surveys (Fig. 1.8) yielded upper crustal velocities of 6.14 km/s in the southern Irish Sea (Blundell and Parks 1969) and 6.12 km/s in the northern Irish Sea (Agger and Carpenter 1964). Neither indicated a mid-crustal interface although Blundell and Parks (1969) found a layer of velocity 7.3 km/s at 25 km depth beneath the southern Irish Sea. Agger and Carpenter (1964) quoted an unreversed sub-Moho velocity of 7.99 km/s under the northern Irish Sea.

An interpretation of the shallow structure underlying the Caledonian Suture Seismic Project (Bott et al 1985) (Fig. 1.2c) indicated Upper Palaeozoic and Mesozoic sequences underlain by Lower Palaeozoic rocks of velocities between 5.5 and 5.7 km/s at depths of 0.5 to 3.0 km. A seismic basement with a velocity of 6.15 km/s at 4 km depth underlies the entire line except in the northeast where it remained undetected. This has been interpreted as Pre-Caledonian metamorphic basement at shallow depth south of, or underlying, the Iapetus Suture (Bott et al 1985). The preliminary results

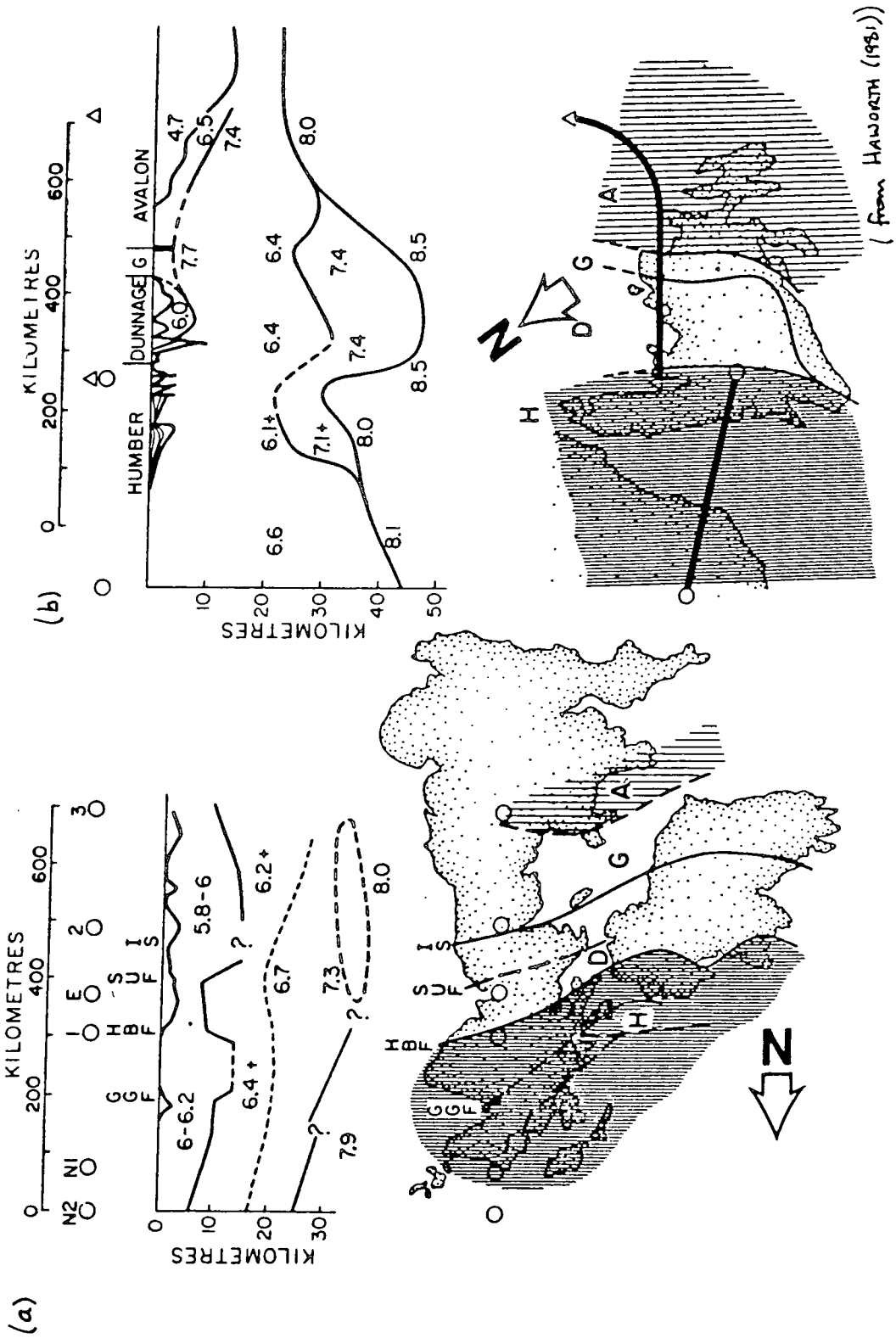


Figure 1.10 (a) Results of the LISPB experiment across the British Caledonides
(b) Results of a refraction experiment across the Newfoundland Appalachians.

indicated a mid crust of velocity 6.5 km/s at about 18 to 20 km under the Northumberand Trough and North Sea. This was not recognised under the Irish Sea. The results under the entire line yielded a uniform crustal thickness of 30 km with an average crustal velocity of 6.3 to 6.4 km/s. This interpretation is grossly at variance with the LISPB interpretations of the crust beneath the Spadeadam region where the two lines cross (Fig. 1.2 and Fig. 1.10a).

The SUSP refraction experiment (Hall et al 1983) ran along strike WSW to ENE across the northern part of the Southern Uplands. A shallow near surface refractor with a high velocity of 6.0 km/s was identified. This is in contrast to the north/south LISPB experiment which found a velocity of 5.88 km/s beneath the Southern Uplands. The SUSP results were combined with a re-interpretation of the LISPB refraction data for the Southern Uplands. Three main belts 15 to 20 km wide of high velocity (6.0 km/s) which strike parallel to the Caledonian trend (SW to NE) were proposed separated by areas of lower velocity (5.6 km/s). These anomalous ridges which have no magnetic signature are interpreted as metamorphic rocks of granodioritic to dioritic composition.

These conflicting geophysical results, taken with the geological observations, described earlier indicate a complicated and not fully understood crust between the Midland Valley and the Lake District. Such lateral and vertical heterogeneities cannot be resolved by surveys such as LISPB which cross the main strike of the Caledonian structures. Needham and Knipe (1986) recently attempted to reconcile the

differing results by proposing that the Southern Uplands accretionary prism has been obducted to the north onto the Pre-Caledonian basement of the Midland Valley and has been underthrust by the Pre-Caledonian basement of the Southern Caledonides identified from the shallow results of the Caledonian Suture Seismic Project (Bott et al 1985) (Fig. 1.2). However, the shallow block-like structures found by Hall et al (1983) beneath the Southern Uplands have still not been adequately explained by any tectonic model.

The extension of the Caledonian Suture Seismic Project across Ireland (Jacob et al 1985, Fig. 1.11) identified basement at 3.0 to 4.0 km depth with velocity increasing from 6.0 - 6.3 km/s beneath southwest Ireland to 6.3 - 6.5 km/s beneath northeast Ireland. This basement has been interpreted as Precambrian metamorphics overlain by lower Ordovician volcanics and Carboniferous sediments (Brown and Williams 1985). Two lens-shaped low velocity zones are inferred under the southwestern and northeastern ends of the line. These separate the upper crust from a mid-crust with a uniform velocity of 6.4 km/s. A mid-crustal interface is identified at about 20 km depth beneath which the lower crust has an average velocity of about 6.8 km/s. The Moho is deduced from the wide-angle reflections. Beneath the centre of the profile the Moho reaches a maximium depth of 32 km shallowing towards the southwest and northeast. The Moho beneath the southwest end of the line is a sharp interface but it progressively grades into a 3 to 4 km thick transition zone towards the northeastern end. The inferred top of this Moho gradient zone lies at a depth of about 28 km under the western edge of the

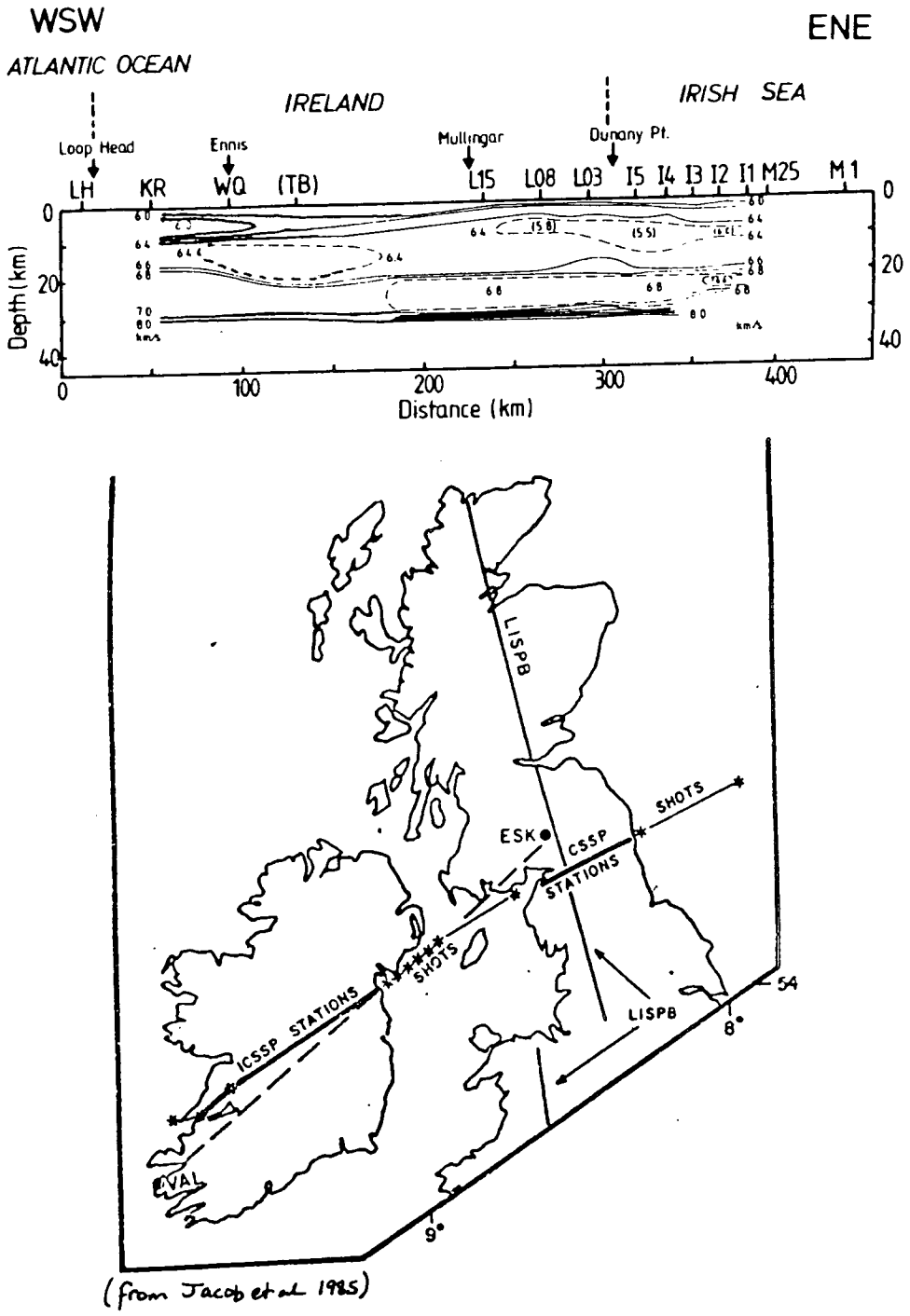


Figure 1.11 Results of the Irish CSSP.

Irish Sea. No results from analysis of Pn have been reported. These results are uncorrected for the shallow sediment delays and probably represent the crustal structure just to the north of the inferred surface trace of the Iapetus Suture (Fig. 1.11).

The existence of a low velocity layer beneath southwest Ireland has also been reported by Bamford (1972) but few other examples of low velocity zones have been identified in the British Isles. The nature of the refraction method makes the positive identification of such a layer difficult. Presence or absence of a low velocity layer may be mainly a matter of personal taste (Healey 1971, Jacob et al 1985 & Ansorge et al 1982).

A large refraction experiment, similar to LISPB, crossed the westward extension of the Caledonian Orogen of the Newfoundland Appalachians (Fig. 1.10b). The results show little resemblance to those of LISPB (Haworth 1981). The near surface velocities vary from 4.7 km/s in the southeast to 6.0 km/s in the northeast. In particular the high velocities of 7.4-7.7 km/s at shallow depths beneath the Dunnage and Avalon Zones are correlated with the subsurface extensions of the southeasterly dipping ophiolitic gabbro sheets observed at the surface. The upper crust yields velocities between 6.1 to 6.4 km/s. A lower crustal layer at about 25 km depth with a velocity of about 7.1-7.4 km/s defines a lens-shaped feature below the centre of the orogen. The sub-Moho velocity increases from 8.1 km/s under the Humber Zone, which is the equivalent of the Caledonides north of the Highland Boundary

Fault, to 8.5 km/s under the centre of the orogen and decreases to 8.0 km/s southeastwards under the Avalon Zone, which corresponds to the Southern Caledonides of the British Isles. The depth to the Moho decreases from 44 km to 30 km southwards across the Humber Zone, then increases to over 45 km beneath the centre of the orogen and decreases further south beneath the Avalon Zone to 24 km in the southeast.

### 1.4.2 Deep Reflection Surveys

The most important Caledonian structures observed on the WINCH deep reflection sections are the Outer Isles Thrust, the Great Glen Fault, the Iapetus Suture and the South Irish Sea Lineament (Fig. 1.12) (Brewer et al 1983). The Iapetus Suture is identified as a northwards dipping interface which forms the top surface of a wedge of reflective lower crust underlying the southern part of the westward extension of the Southern Uplands. The whole crust is transparent under the rest of the Southern Uplands Belt. North of the Southern Uplands Fault some lower crustal reflections are observed although these are not as prominent as those further to the south. A possible change in the nature of the deep crust across the suture may be indicated (Needham and Knipe 1986). The Iapetus Suture is identified only in the lower crust, but it probably surfaces in the vicinity of the Peel Basin.

Sedimentary basins such as the Peel Basin are the most clearly imaged shallow structures on WINCH. Most of these appear to lie in the hanging walls of thrusts produced by the tensional reactivation of earlier compressional features such

Figure 1.12 Results of the WINCH BIRPS line

(Brewer et al (1983)).

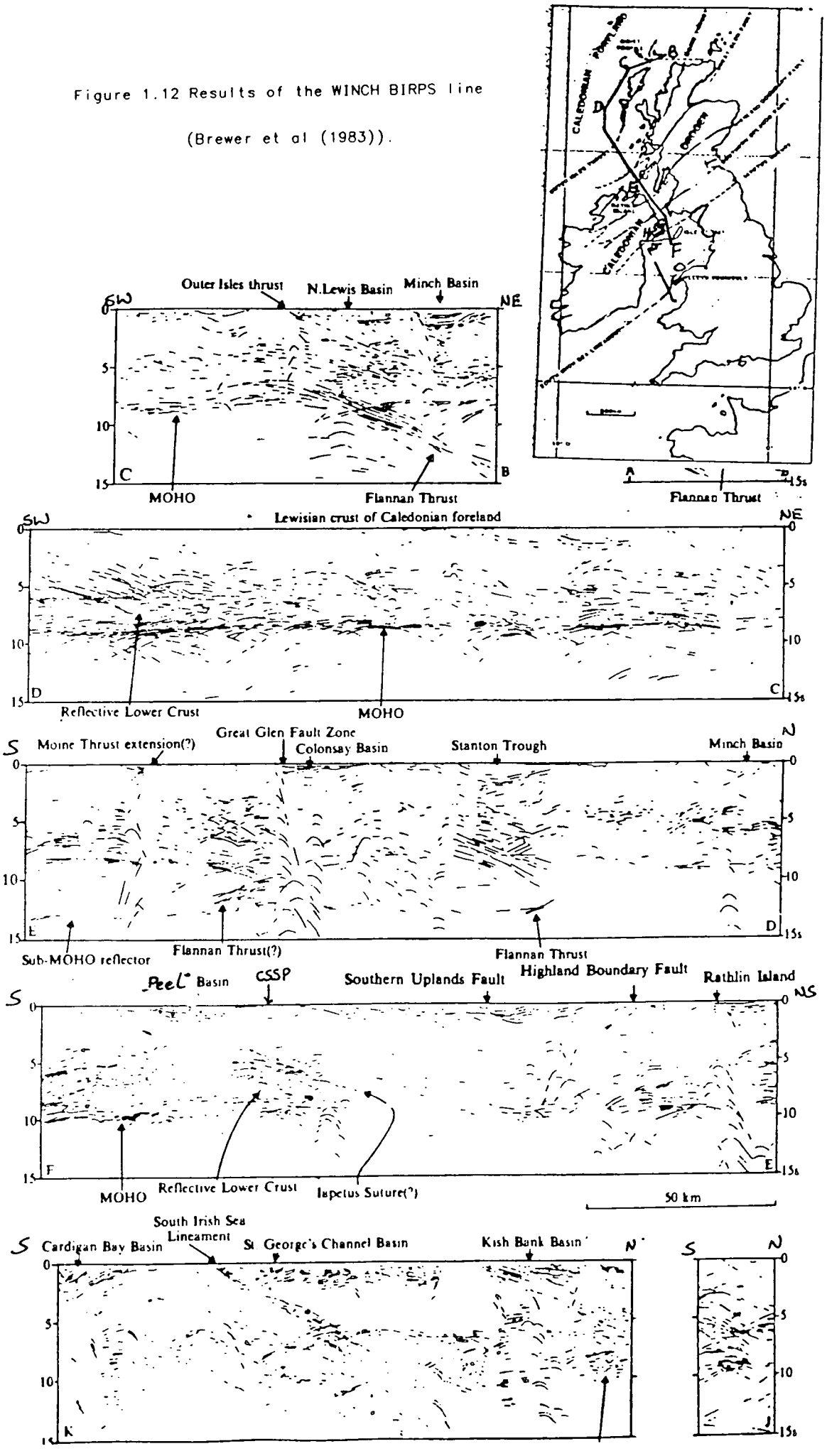

as the Iapetus Suture and the Outer Isles Thrust (Brewer et al 1983). The variations in the nature of the reflective lower crust, observed on all BIRPS profiles so far, show little correlation with the surface geology except in the vicinity of the Iapetus Suture. The character of the Moho is highly variable. It has been interpreted as the bottom of the reflective lower crust under the WINCH profile across the Irish Sea but under the Caledonian Foreland it appears as a narrow band of strong and fairly continuous reflectors (Fig. 1.12) (Brewer et al 1983). The gravity variations due to the Moho observed on the BIRPS WINCH and SWAT deep reflection profiles do not correlate with the observed gravity along the lines. Goldfinch (1985) concluded that the Moho as represented by the base of the reflective lower crust does not represent an abrupt density contrast.

The BIRPS North England Coast (NEC) line was shot in Sept 1985 and crosses the Caledonian Suture Seismic Project line at about shot N8 in the North Sea and runs northwards over the eastward extension of the Southern Uplands (Fig. 1.8). A northward dipping feature observed in the lower crust north of the Caledonian Suture Seismic Project line is tentatively interpreted as the Iapetus Suture (pers. inspect., Klemperer pers. comm.). Its position is further south than proposed by Banks et al (1983) from magnetic variation anomalies and by most geological interpretations. The Moho consists of a narrow band of prominent reflections between 10.5 to 11.0 s. There does not appear to be a well developed reflective midcrust to the south of the suture. To the north numerous diffractions and complicated reflections are observed between

6.0 to 10.5 s. These observations were made from a brute stack of the NEC profile and are preliminary. They are not publishable without the permission of BIRPS.

## 1.5 NATURE OF THE DEEP CRUST

The seismic refraction method as applied to the crust typically uses signal wavelengths of about a kilometre. The BIRPS reflection surveys use frequencies of 10 to 40 Hz which for a velocity of 6.0 km/s and a frequency of 20 Hz gives signal wavelengths of about 300 m and a horizontal Fresnel zone of approximately 3.5 km (Matthews and Cheadle 1986). The resulting limits to the vertical and horizontal resolving power of both methods limits the possibility of obtaining short wavelength details of the deep continental crust (Smithson and Decker 1974, Smithson and Brown 1977). The reflection method is used to detect lateral variations and reflection interfaces whereas the refraction method can yield velocity variation with depth within uniform blocks of crust of sufficient size. However, to obtain well constrained velocity structures down to the Moho for crust 30 km thick laterally uniform regions at least 130 km long are required to obtain reliable Pn arrivals.

### 1.5.1 Compressional Velocities and Rock Compositions

Interpretation of velocities obtained from refraction experiments in terms of rock compositions is problematical. The compressional velocities of minerals show an increase from 5.5 km/s for pure quartz through increasingly mafic minerals

such as amphiboles, pyroxenes and olivines to over 8.8 km/s for garnet (Christensen 1982). The velocity of a particular composition depends on the weighted mean of the constituent minerals. In general the more mafic the composition of a rock the higher its velocity. Temperature, pressure, porosity, permeabililty, fabric and the presence and nature of fluid filled fractures and cracks also have important effects on the velocity of a rock (Pratt et al 1977).

Table 1.1 gives a few examples of typical velocities for rocks of varying composition. Rocks from the upper crust with velocities of 5.8 to 6.3 km/s are generally regarded as either low grade metasediments, acidic to intermediate igneous rocks, or quartzo-felspathic gneisses (Hall 1978). Velocities of 6.4 to 6.5 km/s down to depths of 20 km in NW Scotland have been interpreted as Lewisian granulites (Smith and Bott 1975). Laboratory measurements at room temperature of the velocity of granulites from the Seiland Province in Norway yield values between 6.41 and 6.97 km/s at 6 kb which occurs at 20 km depth (Chroston and Evans 1983). The mean velocity is 6.7 km/s which would decrease to 6.5 km/s at the average temperature expected at 20 km depth. Such a velocity is typically observed in the lower crust in refraction surveys (Mueller 1977). Intermediate granulites and pyroxene granulites have velocities of 6.6 to 7.0 km/s and >7.0 km/s respectively at 6 kb (20 km depth). Amphibolites generally have high velocities >7.0 km/s and dunites have velocities greater than 7.7 km/s (Press 1966).

TABLE 1.1

COMPRESSIONAL WAVE VELOCITIES IN ROCKS
(see also Table 5.1)

| Material | Density ($g/cm^3$) | Velocity (km/s) | | |
|---|---|---|---|---|
| | | 100 MPa | 400 MPa | 1000 Mpa |
| greywacke | 2.692 | 5.84 | - | 6.20 |
| slate | 2.734 | 5.79 | - | 6.22 |
| granite | 2.643 | 6.13 | 6.29 | 6.45 |
| granodiorite | 2.705 | 6.27 | 6.30 | 6.56 |
| granitic gneiss | - | - | 6.30 | - |
| quartz diorite | 2.852 | 6.44 | - | 6.71 |
| diorite | - | - | 6.59 | - |
| acid granulites | - | - | 6.49 | - |
| dioritic granulite | - | - | 6.55 | - |
| pyroxene granulite | - | - | 6.86 | - |
| garnet granulite | - | - | 7.73 | - |
| anorthosites | - | - | 6·80 | 7·40 |
| amphibolite | 3.120 | 7.17 | - | 7.35 |
| gabbro and norite | 2.988 | 7.02 | - | 7.24 |
| dunite | 3.277 | 7.87 | - | 8.15 |
| eclogite | 3.383 | 7.52 | - | 7.87 |

400 MPa Taken from Chrosten (pers. comm)
100 & 1000 MPa Taken from Bott (1982)

### 1.5.2 The Lower Crust

The nature of the Lower Crust is controversial. It is observed to be electrically conductive in many areas (Hutton et al 1980, Banks et al 1983) and to be represented by a zone of numerous discontinuous reflections between 15 to 30 km depth on many deep reflection profiles in the UK and abroad. Typical velocities at such depths calculated from refraction surveys lie between 6.4 and 6.8 km/s. This indicates an intermediate granulitic composition if dry, but complicated variations from acidic to intermediate gneisses to amphibolites if wet. The presence of a free fluid phase in the lower crust has been suggested to explain the high electrical conductivity but Yardley (1985) indicated that such a free fluid phase would react rapidly with the surrounding "dry" granulite rocks to produce amphibolites. He concluded that free fluid phases cannot exist in a granulitic lower crust.

The reflective lower crust has been observed in Australia (Finlayson et al 1984), in the Basin and Range of North America (Brown et al 1986), in the Variscides of France (Bois et al 1986) and in SW Germany (Bortfeld et al 1985) as well as in the British Isles. Several geological explanations have been proposed:

1. Compositional layering which can be due to metamorphic banding (Mueller 1977 , Hale and Thompson 1982) or underplating by basic magmatic activity (McKenzie 1983). The reflective lower crust is observed under the Hebridean Craton where Lewisian basement rocks lie at shallow depth.

These rocks were formed at temperatures and pressures expected in the lower crust. They are interpreted to lie up to 20 km beneath the Caledonian foreland (Smith and Bott 1975). A reflective lower crust is observed beneath the Caledonian foreland (Fig. 1.12). There is no compositional banding observed in the rocks at the surface which could produce these reflections. Other causes other than compositional banding are indicated (Blundell and Raynaud 1986).

2. Deformation foliation caused by ductile stretching (Bott et al 1984, Blundell and Raynaud 1986). Bott et al (1984) proposed that tension may preferentially stretch the lower crust by ductile shearing to create a horizontal foliation which might produce the observed reflections. Such tensional stresses occurred in NW Europe during the Hercynian Orogeny and during the rift phase preceding the opening of the Atlantic in the Mesozoic (Blundell and Raynaud 1986).

3. Anisotropic effects caused by the preferred orientation of anisotropic minerals such as olivine (Hall 1985). Anisotropic effects have occasionally been observed within the continental crust and have been found in the upper mantle beneath SW Germany (Bortfeld et al 1985). They are commonly observed in the oceanic lithosphere (Crampin 1984).

4. The presence of shear zones or fluid filled cracks and fractures.

5. Blundell and Raynauld (1986) showed that an apparent reflective lower crust can be caused by offline reflections from only a few undulating reflective

surfaces.

The nature of the lower crust has been interpreted, from the composition of xenoliths found in volcanic vents and lavas, to be a complicated mixture of granulites and amphibolites (Upton et al 1983). These represent the composition of the crust and mantle at the time of the Upper Palaeozoic volcanism and not at the present day. In contrast geophysical results indicate the present state of the crust. The detailed composition and nature of the deep crust are in dispute.

### 1.5.3 The Upper Mantle

The topmost mantle generally has a uniform velocity beneath Britain within the range 7.8 to 8.1 km/s. Lower and higher values are observed elsewhere (Gajewski and Prodehl 1985. Finlayson et al 1984). Barton et al (1984) have shown that beneath the Central North Sea the Moho as interpreted from refraction and reflection is identical. Berkenheimer (1969) has proposed that the Ivrea body in Northern Italy which is composed of a complex sequence of lenticular basic and ultramafic bodies represents a section from the lower crust into the upper mantle. The BIRPS profiles show that the Moho consists of a band of reflections in some areas such as beneath the Caledonian foreland. However in other areas such as the northern Irish Sea the Moho represents the base to the reflective lower crust and no prominent reflections are observed. These changes in the reflective character of the Moho probably represent variations in the nature of the transition at the base of the crust from rocks with predominantly lower crustal compositions to those with mainly

an upper mantle composition (Brewer et al 1983).

## 1.6 AIMS OF THE CALEDONIAN SUTURE SEISMIC PROJECT

Geological and geophysical observations indicate that the crust and upper mantle across the Caledonides are heterogeneous. The results of one along strike refraction experiment such as the Caledonian Suture Seismic Project can only provide details of broad variations and are unlikely to prove or disprove detailed tectonic models. A series of along strike refraction profiles such as the Caledonian Suture Seismic Project within each Caledonian Belt is probably the best method to obtain comparable details of the velocity structures across the Caledonides of the British Isles.

The primary aim of the Caledonian Suture Seismic Project was to determine the velocity structure of the mid and lower crust along the Iapetus Suture. Within this broad aim it was hoped to answer some of the following questions:

1. Is the mid crust absent in the Irish Sea? Are the preliminary interpretations made by Green (1984) of lateral changes in the mid and lower crust between the Irish Sea and North Sea regions observed when all the sections are studied? If so where does the lateral change occur?
2. Is the sub-Moho velocity constant? Or as suggested by Green (1984) is it higher under the Irish Sea? Where does the lateral change occur?
3. How does the velocity depth profiles calculated under the North and Irish Seas compare with the WINCH and NEC BIRPS

lines?

4. Does the seismic model fit the gravity variations along the line?
5. How do the results of the Caledonian Suture Seismic Project compare with those of Jacob et al (1985) across Ireland?
6. Can the laterally varying results be interpreted in terms of the position of the Iapetus Suture?

# CHAPTER TWO

## DATA PROCESSING TECHNIQUES

The Caledonian Suture Seismic Project has produced an unprecedented amount of high quality refraction data due to the innovative arrangement of both closely spaced shots and stations. In this chapter the main features of the experimental design will be discussed; these include the practical problems encountered during the processing and the methods used to display the data set which exploit the unique configuration of the Caledonian Suture Seismic Project. The programmes developed to process and display the data will also be described.

### 2.1 DATA

The configuration of the Caledonian Suture Seismic Project described in the introduction and in Green (1984) enables the data to be presented in four different types of seismic refraction sections (Fig.2.1). These are:

1. Common station sections. This type of section displays all the shots recorded by a particular station and highlights any variations under the shots. A common station section will be referred to as CST60N which is an abbreviation for the common station section of station 60 for the North Sea shots N1-N29.
2. Common shot sections. This type of section displays all the stations which received a particular shot and highlights any variations under the stations. A common

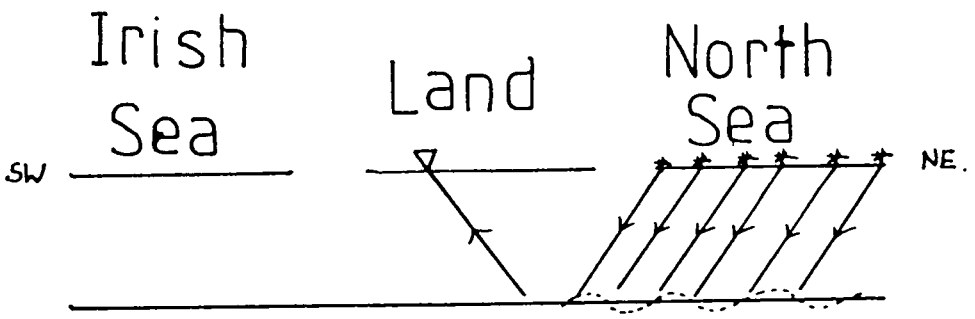


Common Station

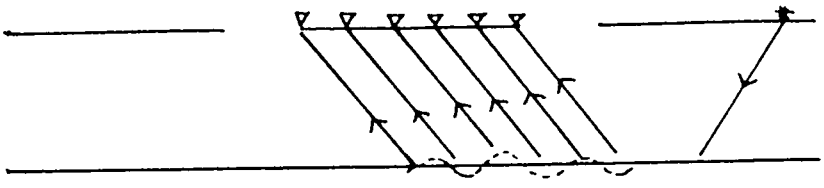

Common Shot

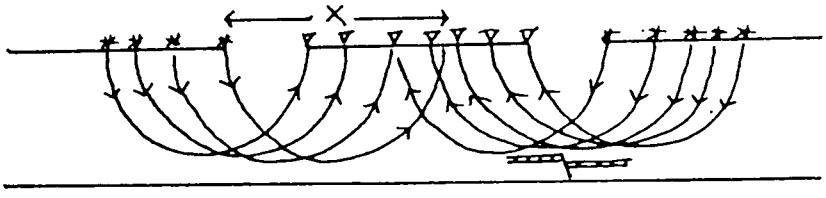


Common Distance

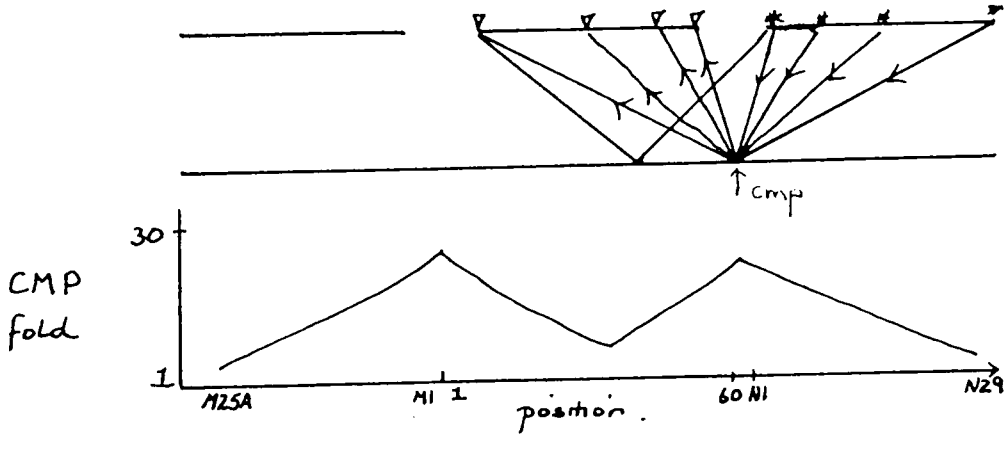


Common Midpoint

Figure(2.1) Diagram illustrating the different types of section that can be plotted using the CSSP data

shot section will be referred to as CSH/N20 which is an abbreviation for the common shot section of shot N20 for the mainline stations 1-60.

3. Common mid-point sections. This type of section displays all the traces given by (ST,SH) (where ST represents the station and SH the shot) which have a common mid-point. The closest station/shot pair defines the common mid-point and all the station/shot pairs (ST,SH) which have a midpoint which lies within +/- 1 km of the mid-point of the closest station/shot pair are plotted on the same common mid-point section e.g. the common mid-point defined by the trace (60,N1) is 262.56 km from M25B and the trace (46,N8) has a common mid-point position of 262.59 km and as this lies within +/- 1 km this trace will be plotted on the section for CMP60/N1. Using this method to locate traces with the same common mid-point avoids any assumptions about the stations having a spacing of exactly 2 km and the shots of 4 km. The +/- 1 km window is the smallest possible given the 2 km station spacing and the need to have enough traces to produce a useful section. This means that slight errors will be introduced as the traces associated with a particular common mid-point section will not all possess exactly the same common mid-point.

4. Common distance sections. This type of section displays all the traces (ST,SH) which have offsets within +/- 1 km of the distance chosen. Fig. 2.2 is a frequency diagram of the Caledonian Suture Seismic Project station to shot offsets. It can be seen that there are peaks at certain of the distances and that there is a general high between

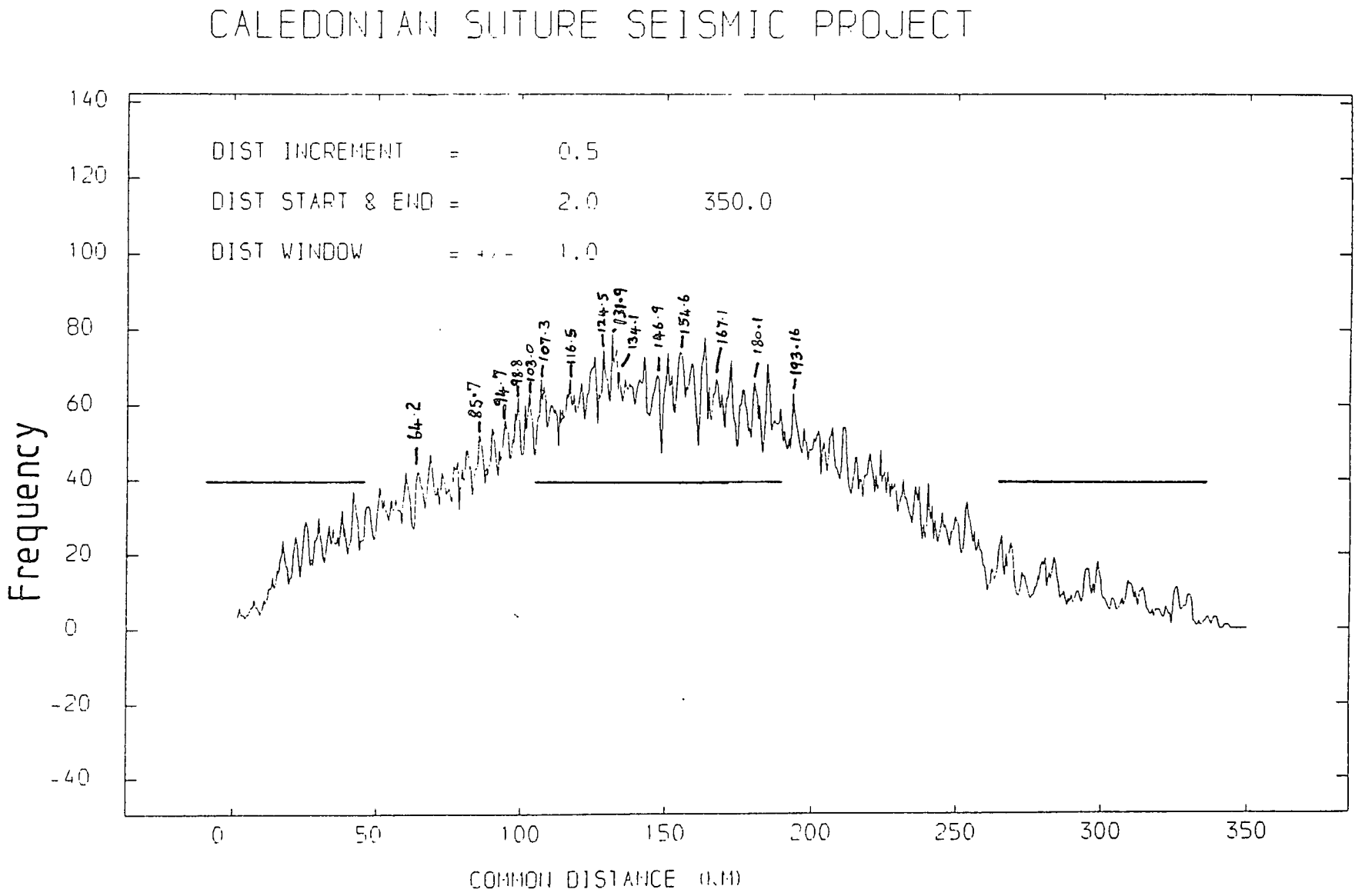


Figure(2.2) Frequency diagram for the number of traces with station/shot offsets within +/- 1km of all possible common distances.

50 km and 250 km. This is expected given that most stations lie close to the planned 2 km spacing and most shots the planned 4 km spacing and that the stations lie centred between the Irish Sea and North Sea shots. Only selected common distance sections have been plotted and those chosen are annotated on the frequency diagram. A common distance section is referred to as CDS/98.84 which is an abbreviation for the common distance section for the traces with station/shot offsets of 98.84 +/- 1 km.

All four types of section have been used (Appendices A, B and C): the common shot and common station sections were used predominantly to pick the travel times; the common mid-point sections were used mainly in the interpretation of the wide-angle reflections from the mid-crust (PcP) and from the Moho (PmP) whilst the common distance sections provided a means of assessing the extent of lateral variations, although, due to the few traces available to each common distance and the lack of sufficient density of traces, greater use of these sections in interpretating the data was limited in its usefulness.

### 2.1.1 The Information Matrices

As work proceeded in plotting the data it became clear that it was going to be important to minimise the amount of information on details of the experiment that had to be input from the terminal, not only to save time, but also to minimise the opportunities for error. For example it took six months to plot all the data in the form of common shot and common

station sections for the first time. A suite of programmes has been written to hold permanently much of the routine Caledonian Suture Seismic Project information on NUMAC in the form of information matrices with each location representing a particular trace. (see Section 2.5.4 and Appendix D for a complete description of the matrices).

Initially these matrices were used to hold the routine project information such as the location of a particular trace amid the 26 tapes held on NUMAC or the station to shot distances but as picking of the arrival times of the various phases proceeded (upto 3500 picks) a method of displaying all the data at once was needed to give an overview and also to check for errors. This was accomplished by plotting a travel time for a particular phase and shot/station pair (ST,SH) at locations with co-ordinates given by the respective distances of the station ST and shot SH from M25B along the edges of a matrix (as illustrated in Fig. 2.3). All the travel times for a particular phase can then be presented in one diagram by reducing these travel times to a particular velocity using the distances held in the distance matrix and the travel times in the travel time matrix and contouring the results. The amplitudes of each arrival can also be presented on similar contoured plots.

These matrices, once contoured graphically, display the main features of the data for each phase and present together in one diagram the four types of section described earlier. Fig. 2.3a displays how each type of section appears in the matrices. Fig. 2.3b illustrates how these matrices can be

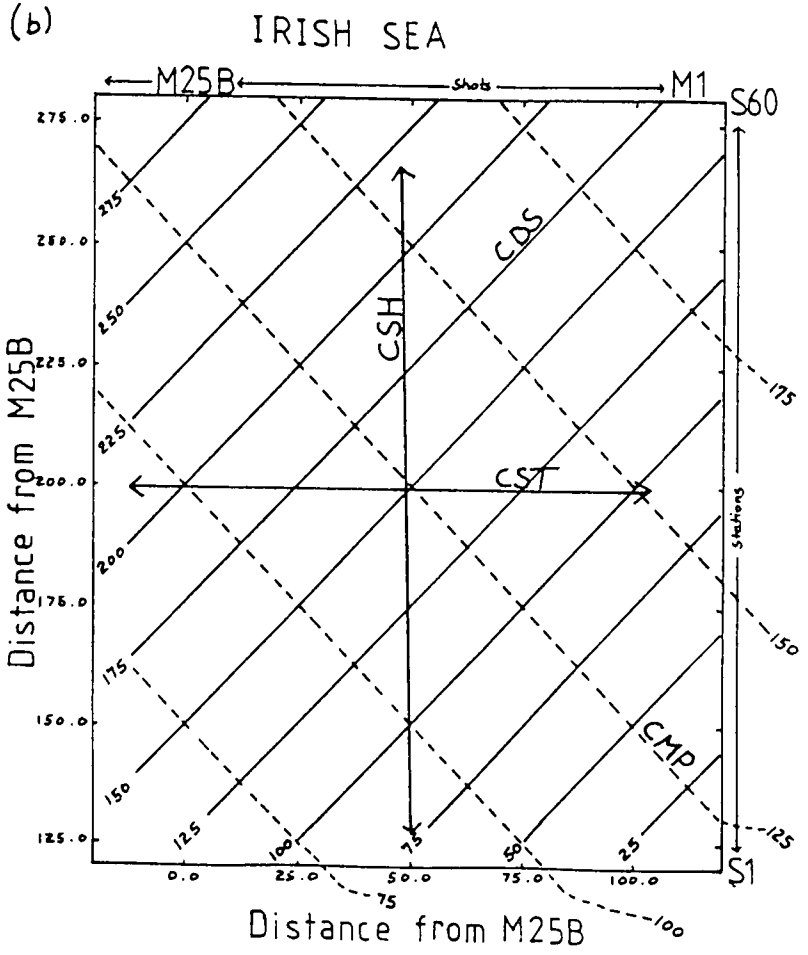


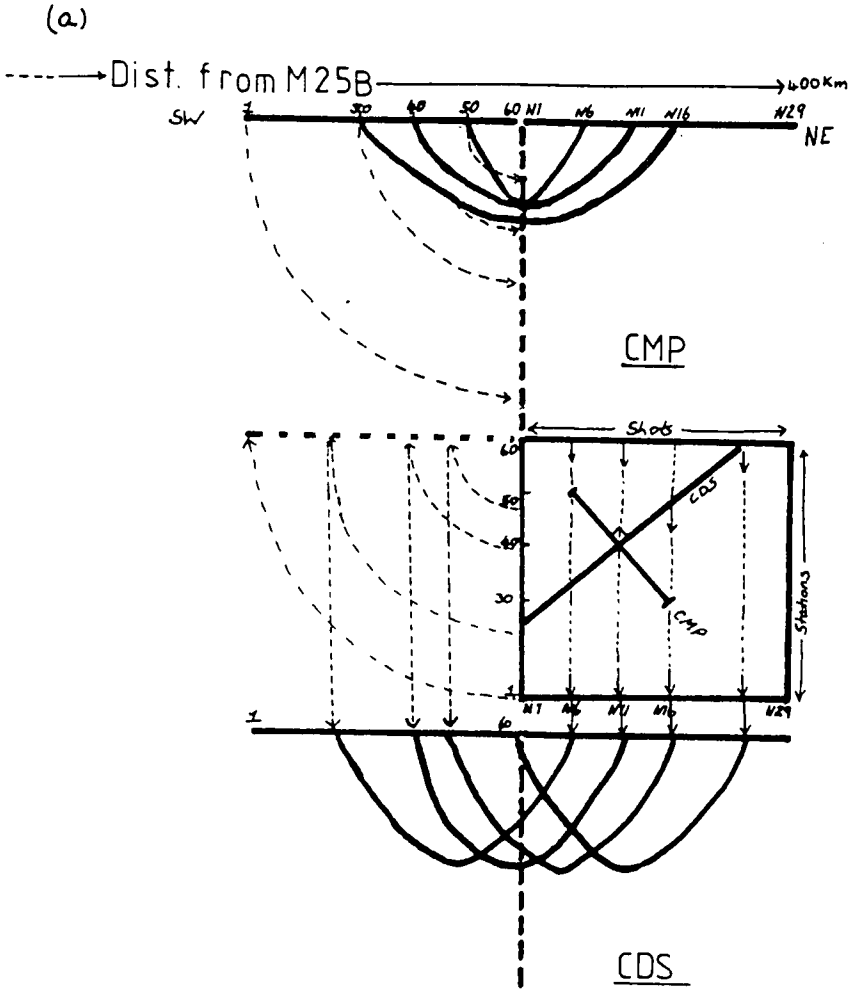


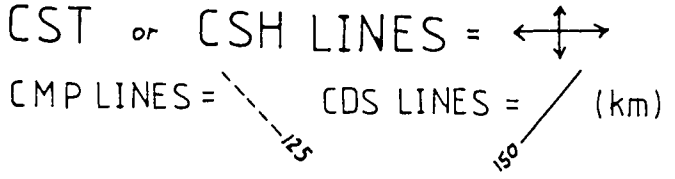


Figure(2.3) (a) A sketch diagram illustrating how a travel-time matrix for the North Sea is related to the CSSP profile.
(b) A travel-time matrix for the Irish Sea displaying the directions of the four different types of sections that can be plotted using the CSSP data.

considered conceptually as the Caledonian Suture Seismic Project line bent to a right-angle so that the shots and stations correspond to their position in the matrices. It is the spatial separation of stations and shots in the Caledonian Suture Seismic Project that causes there to be a simple relationship between the four different types of section and the matrices. The common distance and common mid-point lines in the matrices are drawn by using the equations :

$$XSHM25 = XSTM25 + XCDS \qquad (2.1)$$

$$XSHM25 = -XSTM25 + 2 \times XCMP \qquad (2.2)$$

where

XSHM25 - distance from M25B to the shot SH

XSTM25 - distance from M25B to the station ST

XCDS - the common distance required

XCMP - the distance of the common midpoint from M25B

The common mid-point lines run at right-angles to the common distance lines as XSTM25 is multiplied by (-1) in the equation for the common mid-point case and (+1) in the common distance equation.

## 2.2 TAPE HANDLING

### 2.2.1 The Caledonian Suture Seismic Project Tapes

26 Caledonian Suture Seismic Project digital data tapes are held in the operators room at Durham. 22 of these contain the original digitized traces in the Durham Self-Defining Tape Format (DSDTF) and the traces can be read from tape to disc using the two programmes TR-INPUT and TR-CSP. TR-INPUT reads

the matrix file TR-TAPES, which contains the tapename and file number for every trace on the DSDTF tapes, and, produces as output two files: a source file which will mount the relevant tapes and run TR-CSP, and an input file for TR-CSP which contains the details of the traces to copy from tape.

TR-CSP reads the required traces off tape and corrects the relevent traces for the tape-head misalignment of the playback tapedecks used in the digitizing process compared to the recording tapedecks used in the field (full details are given by Green 1984). The corrections are read from a file called TT-TCORRECT which must be available to run TR-CSP. Each trace is copied to two lines on disc: the first contains the relevant header information needed to plot the trace whilst the second contains the actual trace values in unformatted binary format.

### 2.2.2 Calculation of Distances

The station/shot distances are calculated by TR-CSP using the routine DISTAZ which calculates the distances to an accuracy of 1 part in $10^7$ using the latitudes and longitudes in the DSDTF header block and the formula of Robbins (1962). The distances for the common distance sections have to be changed from the station/shot offsets to the distance of the common mid-point of each trace from M25B. This is performed by the programme CDIST which reads the header line for each trace copied to disc and alters the distance calculated by DISTAZ to the corresponding common mid-point distance. The common mid-point distance is calculated easily from the distances of

the shots and stations from M25B which are all held in the distance matrix XMAT-M25B.

### 2.2.3 The *FS Tapes

The task of sorting the DSDTF tapes into separate common station and common shot sections and a selection of common distance and common mid-point sections has been completed. A number of errors were uncovered in latitudes and longitudes on the original tapes and these have been corrected on the tidied data stored on the remaining 4 tapes (one for each type of section). These tapes are accessed using the system tape-utility programme *FS (Appendix D). Each file on the *FS tapes contains one section and the files are named on the tapes in the same format as described in section 2.1 e.g. file CST60N contains the data of common station 60 for the North Sea shots.

### 2.2.4 Edinburgh Data

A programme TR-IGS has been written to demultiplex, decode the time and copy from tape to disc the data digitized at the BGS facility in Edinburgh. Each trace is copied to disc in the same format as that produced by TR-CSP so that the sections can be plotted using the project plotting programme CSSPLOT. TR-IGS was used to taperead the section in Fig. 2.4 but it is recommended that the time decoding routines are made more robust before any large-scale processing is attempted on this data. Problems were encountered especially where the time-code was poor.

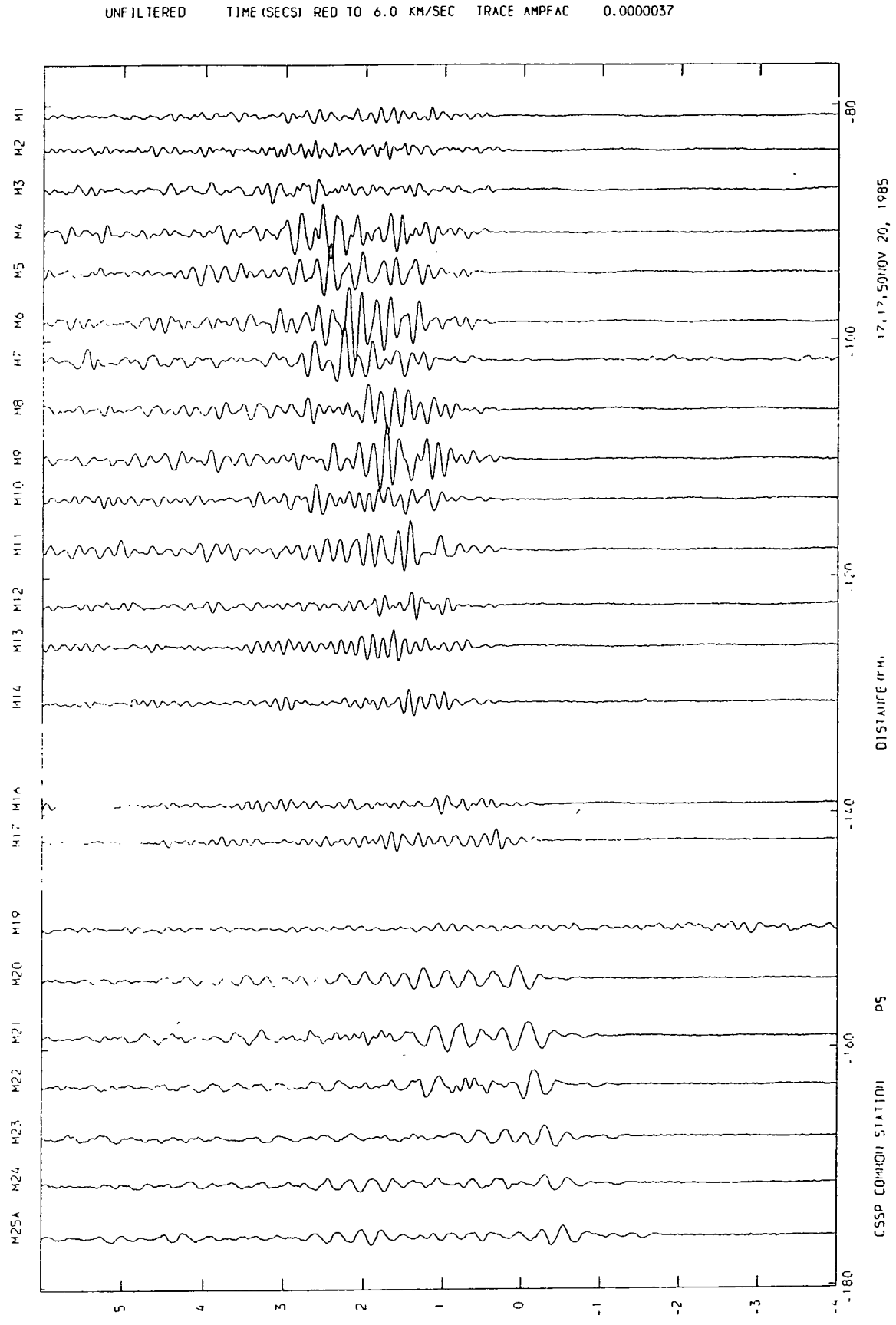


Figure(2.4) Common station section for the Eskdalemuir Array station R5 for the Irish sea shots.

## 2.3 PLOTTING

The programme CSSPLOT plots the data read from tape either by TR-CSP ,by TR-IGS or obtained from the *FS tapes. The programme can be run from the terminal and will request the user for input. Options are provided for:

1. Filtering
2. Demultiplexing the bubble pulse or any given periodicity in the data
3. Plotting the picked travel-times held in the travel time matrices
4. Plotting the trace amplitudes either corrected to common gain, equalised or uncorrected.

## 2.4 FILTERING AND DECONVOLUTION OF THE BUBBLE PULSE

Green (1984) showed that the frequency characteristics of the sections depend mainly on the frequency variation at the shots due to the depth of detonation and the size of the explosives used. It is now clear that all the different phases display a ghost arrival which appears on the sections at the period given by the formula of Burkhardt and Rees (1975) for the bubble oscillation. Attempts were made to remove these by using the methods of predictive deconvolution developed for reflection seismology (Robinson 1980) and the results are presented and discussed below.

### 2.4.1 Predictive Deconvolution

Predictive deconvolution is a standard technique used in reflection seismology for the removal of multiple reverberations from the seismogram where they overlap with later primaries. With a knowledge of the shape of the autocorrelation function of the source wavelet it is possible to design a filter to predict the position of the multiples in the seismogram and remove them leaving only the first occurrence of the waveform. The main problem with the method is to estimate the autocorrelation of the waveform. In reflection seismology the assumption is made that a reasonable estimate can be obtained from the autocorrelation function of each complete trace on the seismogram:

$$x(t) = s(t) * r(t) + n(t)$$

where
- x - seismogram trace
- s - source wavelet
- n - noise
- r - impulse response of the Earth assumed to be white, random and stationary

Provided r(t) is a spike series and the source wavelet is minimum delay an effective prediction error filter can be designed from the normal equations, and provided the multiple shape is the same as the primary, there is no alteration to the seismogram except multiple suppression. The filter is of the form:

$$P = (1,0,0,0.....,0,-P1.-P2.-P3.....,-PN)$$

($0$ at $t=a$)

a = periodicity in sample numbers

Reverberation frequency and bubble pulse frequency for the North Sea shots

| Shot | Depth(m) | Reverberation Frequency (Hz) | Bubble Pulse Frequency (Hz) |
|---|---|---|---|
| N1 | 51 | 7.3 | 2.8 |
| N2 | 61 | 6.1 | 3.1 |
| N3 | 64 | 5.8 | 3.2 |
| N4 | 74 | 5.0 | 3.6 |
| N5 | 81 | 4.6 | 3.8 |
| N6 | 97 | 3.8 | 4.4 |
| N7 | 100 | 3.7 | 4.5 |
| N8 | 100 | 3.7 | 4.5 |
| N9 | 105 | 3.6 | 4.7 |
| N10 | 105 | 3.6 | 4.7 |
| N11 | 100 | 3.7 | 4.5 |
| N12 | 100 | 3.7 | 4.5 |
| N13 | 98 | 3.8 | 4.4 |
| N14 | 93 | 4.0 | 4.3 |
| N15 | 75 | 4.9 | 3.6 |
| N16 | 73 | 5.1 | 3.6 |
| N17 | 68 | 5.5 | 3.3 |
| N18 | 69 | 5.4 | 3.3 |
| N19 | 74 | 5.0 | 3.6 |
| N20 | 76 | 4.9 | 3.6 |
| N21 | 84 | 4.4 | 4.0 |
| N22 | 82 | 4.5 | 3.9 |
| N23A | 82 | 4.5 | 3.9 |
| N24 | 79 | 4.7 | 3.8 |
| N25 | 72 | 5.2 | 3.5 |
| N26 | 72 | 5.2 | 3.5 |
| N27 | 74 | 5.0 | 3.6 |
| N28 | 81 | 4.6 | 3.9 |
| N29 | 85 | 4.4 | 4.0 |
| N23B | 85 | 4.4 | 2.8 |

Reverberation frequency and bubble pulse frequency for the Irish Sea shots.

| Shot | Depth(m) | Reverberation Frequency (Hz) | Bubble Pulse Frequency (Hz) |
|---|---|---|---|
| M1 | 33 | 11.3 | 2.1 |
| M2 | 36 | 10.3 | 2.2 |
| M3 | 42 | 8.8 | 2.4 |
| M4 | 47 | 7.9 | 2.6 |
| M5 | 55 | 6.8 | 2.9 |
| M6 | 60 | 6.2 | 3.1 |
| M7 | 64 | 5.8 | 3.2 |
| M8 | 65 | 5.7 | 3.2 |
| M9 | 63 | 5.9 | 3.2 |
| M10 | 56 | 6.7 | 2.9 |
| M11 | 67 | 5.6 | 3.3 |
| M12 | 47 | 7.9 | 2.6 |
| M13 | 55 | 6.8 | 2.9 |
| M14 | 55 | 6.8 | 2.9 |
| M15 | 63 | 5.9 | 3.2 |
| M16 | 59 | 6.3 | 3.1 |
| M17 | 53 | 7.0 | 2.8 |
| M18 | 70 | 5.3 | 3.5 |
| M19 | 61 | 6.1 | 3.1 |
| M20 | 95 | 3.9 | 4.3 |
| M21 | 139 | 2.7 | 5.8 |
| M22 | 134 | 2.8 | 6.3 |
| M23 | 134 | 2.8 | 6.3 |
| M24 | 133 | 2.8 | 6.3 |
| M25A | 97 | 3.8 | 4.4 |
| M25B | 96 | 3.9 | 3.0 |
| I1A | 57 | 6.5 | 2.9 |
| I2A | 37 | 10.1 | 2.2 |
| I3A | 34 | 11.0 | 2.1 |
| I4A | 36 | 10.3 | 2.2 |
| I5A | 31 | 12.0 | 2.0 |
| I1B | 57 | 6.5 | 2.9 |
| I2B | 38 | 9.8 | 2.2 |
| I3B | 33 | 11.3 | 2.1 |
| I4B | 35 | 10.7 | 2.1 |
| I5B | 30 | 12.4 | 1.9 |

Table 2.1 (from Green 1984)

Summers (1982) has discussed the applicability of predictive deconvolution to the enhancement of arrivals on poor quality refraction seismograms and concluded that such an approach fails due to the assumptions inherent in the method. A refraction seismogram, unlike a reflection seismogram, represents the addition of several different signals to coloured noise and not to the convolution of a minimum delay wavelet with a white random stationary impulse response.

The suppression of the bubble pulse in the Caledonian Suture Seismic Project for the first arrivals Pg and Pn should be possible as both are contaminated only with noise. The bandwidth of the arrivals on the Caledonian Suture Seismic Project data is from 4-12 Hz and commonly the traces appear almost monochromatic with frequencies centred on 4-5Hz (Green 1984). Attempts were made to deconvolve the bubble pulse on CSH/N2 for selected stations and Figs. 2.5 - 2.13 display the results of varying the filter parameters. A number of points can be made:

1. If the filter is designed using a narrow autocorrelation window, which includes only the primary and the first bubble pulse of Pg, the bubble pulses of both PmP and Pg are removed (Figs. 2.5 - 2.7). This illustrates that to the prediction error filter the PmP and Pg waveforms are similar which is not expected from wave theory: this effect must be due to the limited bandwidth of the data. The filter also appears to act as an inverse over the part of the trace within a narrow autocorrelation window. An autocorrelation window which covers the complete time window over which reverberations are to be removed was

2.5 (a)

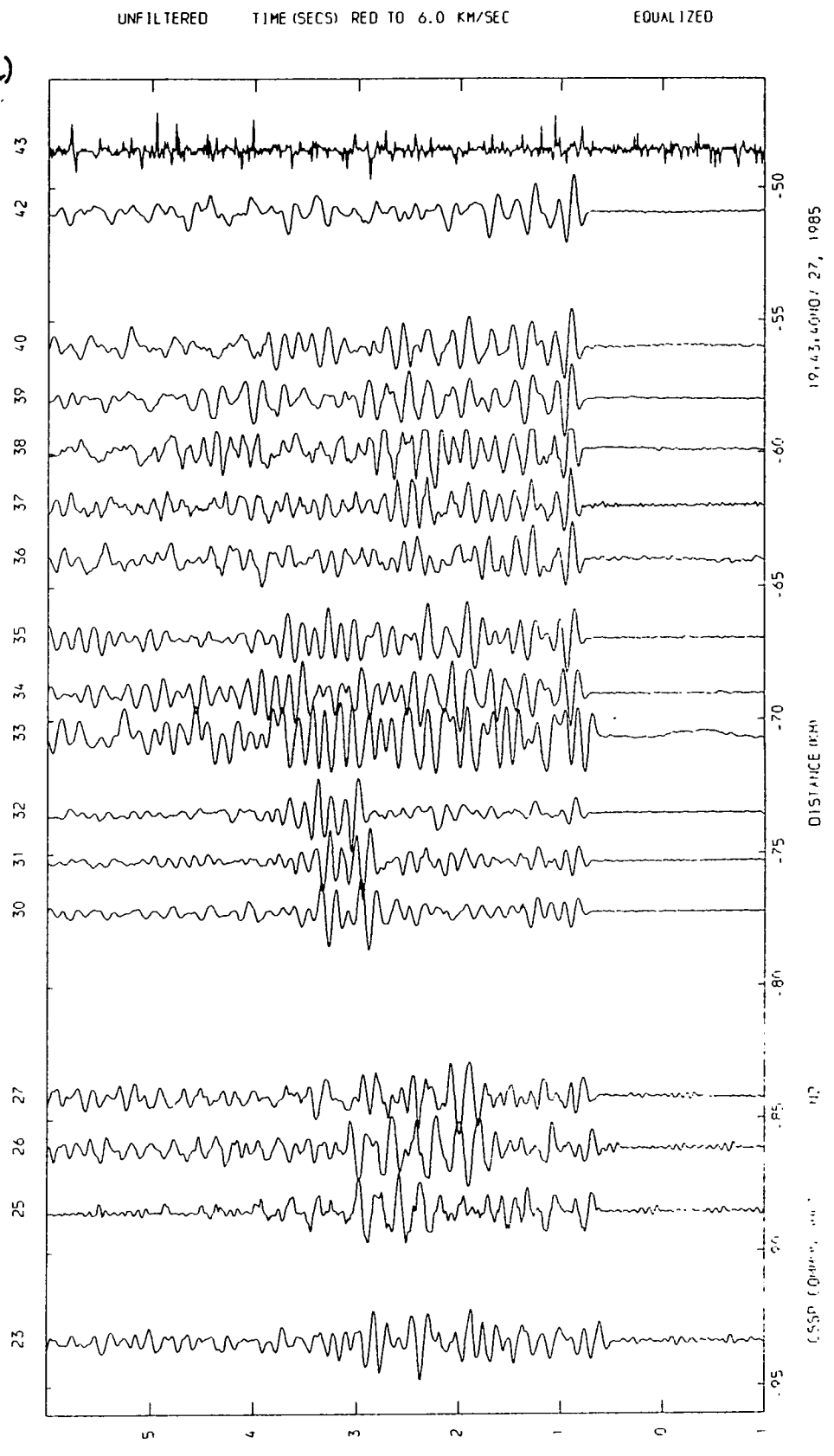


Figure(2 5) Common shot section N2 for selected stations
Filtered – amplitudes equalized – vred=6.0
(a) No deconvolution applied
(b) Predicted deconvolution performed
Autocorrelation window = 0 3 – 1.62 s (132 samples)
Filter length = 132 samples
Prediction gap = 32 samples
Bubble pulse period = 0.31 s

2.5 (b)

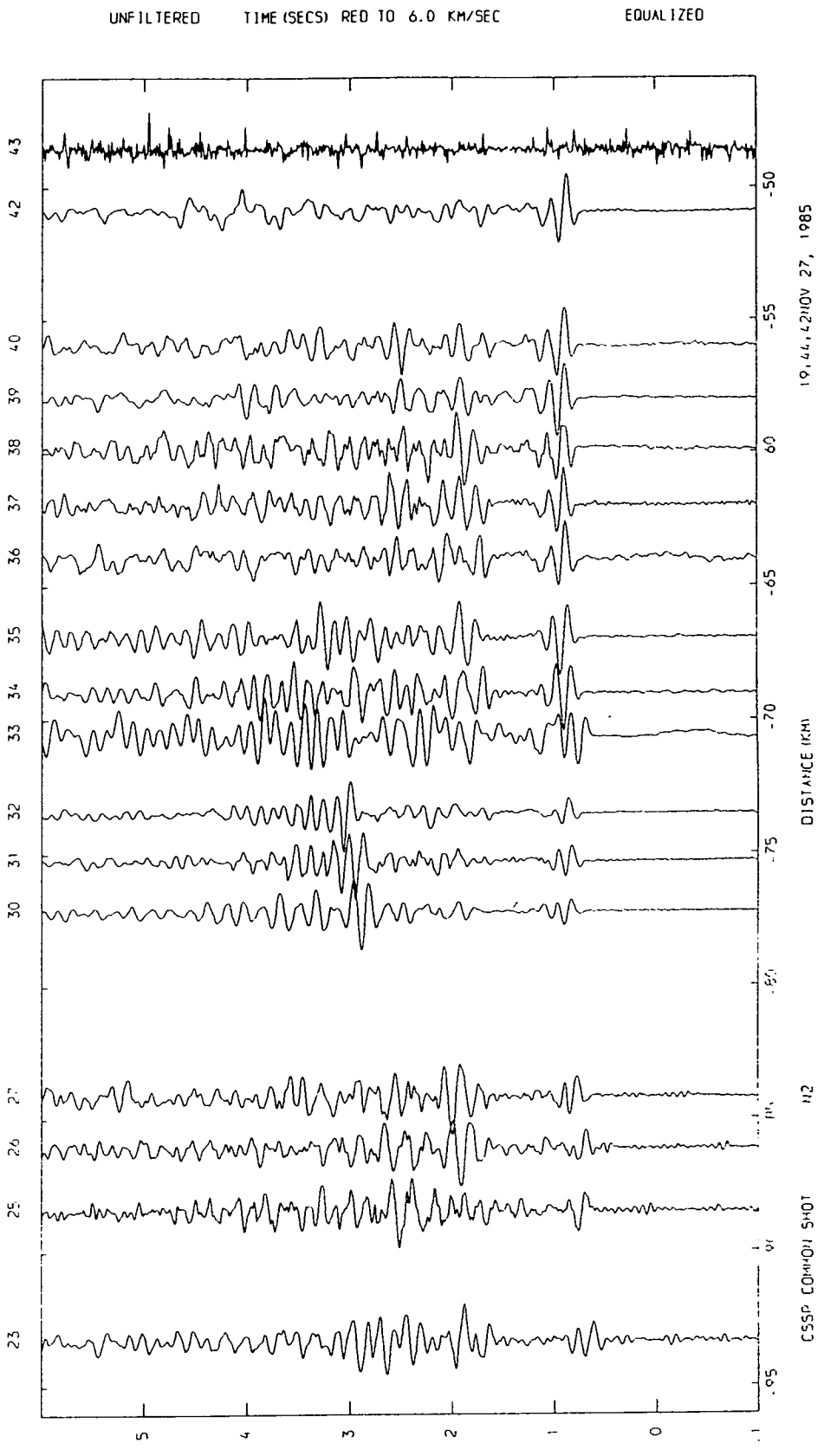
UNFILTERED
TIME (SECS) RED TO 6.0 KM/SEC
EQUALIZED
43
42
40
39
38
37
36
35
34
33
32
31
30
27
26
25
23
-50
-55
-60
-65
-70
-75
-80
-85
5
4
3
2
1
0
19,44,42NOV 27, 1985
DISTANCE (KM)
CSSP COMMON SHOT

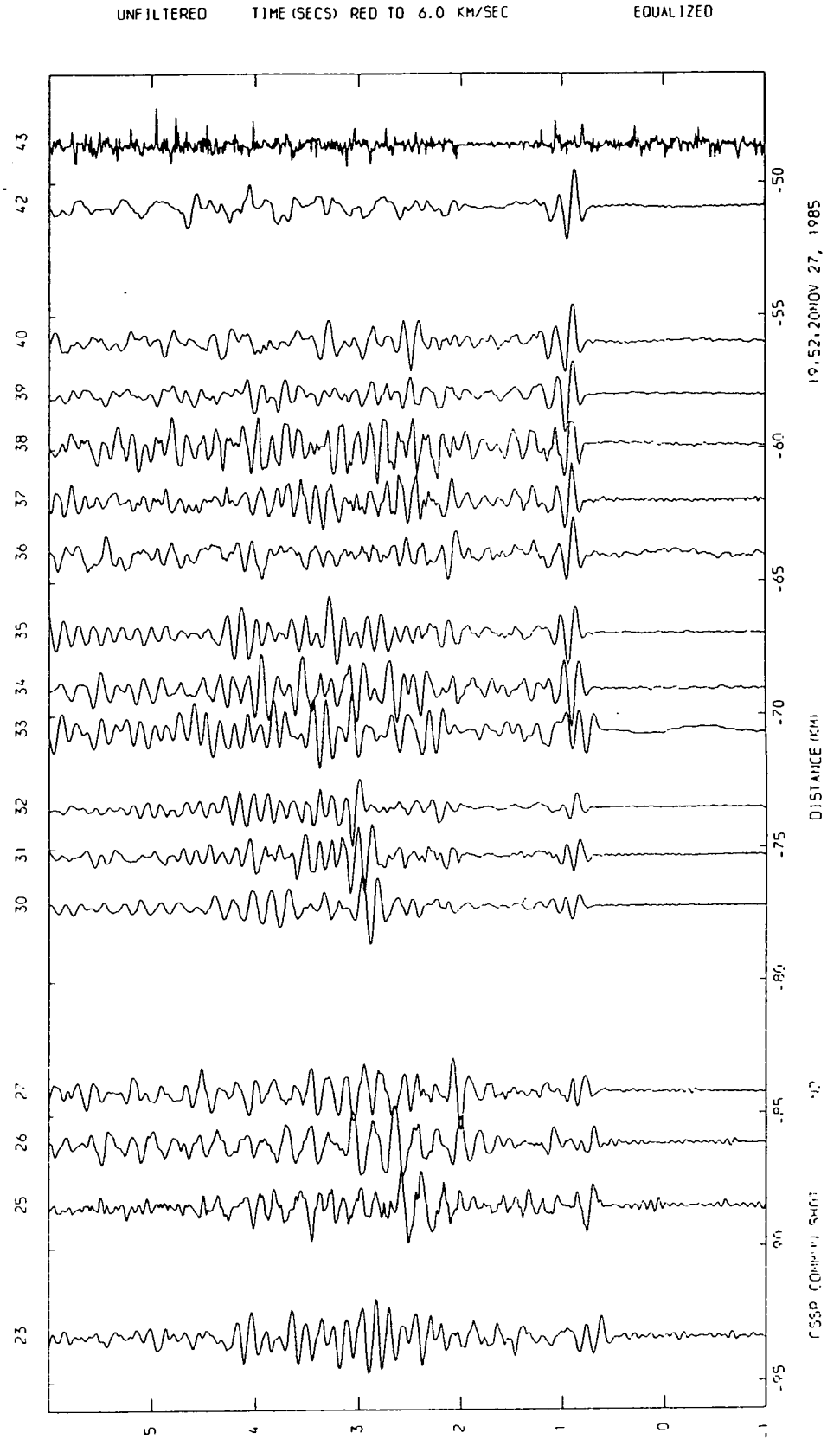


Figure(2.6) Common shot section N2 for selected stations
Filtered - amplitudes equalized - vred=6 0
Predicted deconvolution performed
Autocorrelation window = 0.3 - 2.0 s (170 samples)
Filter length = 132 samples
Prediction gap = 32 samples
Bubble pulse period = 0.31 s

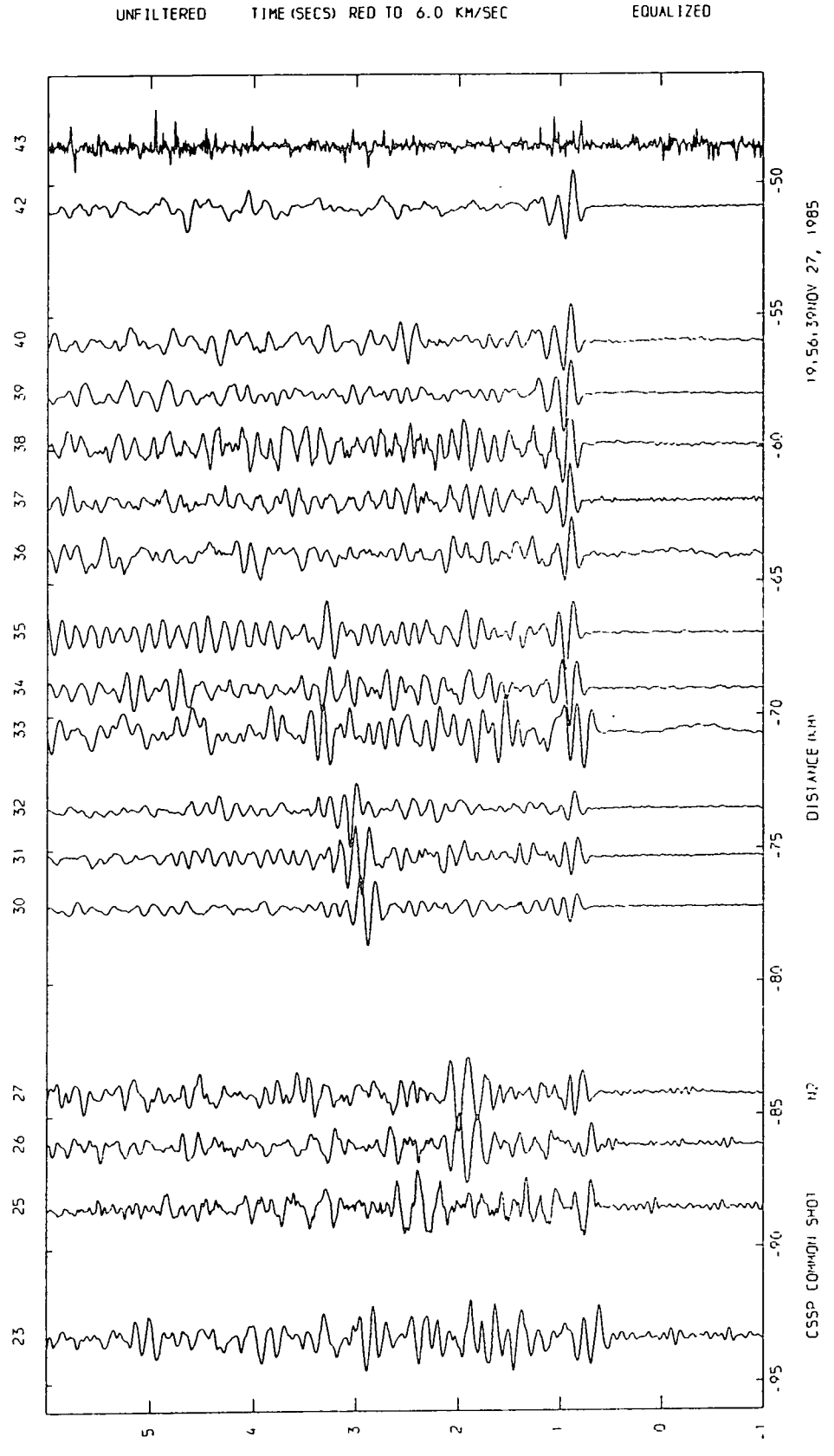


Figure(2.7) Common shot section N2 for selected stations
Filtered – amplitudes equalized – vred=6.0
Predicted deconvolution performed
Autocorrelation window = 0.3 – 4.3 s (400 samples)
Filter length = 132 samples
Prediction gap = 32 samples
Bubble pulse period = 0.31 s

found to produce the most satisfactory results (Fig. 2.7).

2. If the autocorrelation window includes only PmP and not Pg the resulting filter removes the bubble pulse on Pg and PmP but does not appear to suppress the reverberations as efficiently as the filter designed with a window which includes both phases. The PmP phase is contaminated with reverberations from Pg and so any filter designed from PmP would not be expected to be as efficient as one designed on the Pg phase.

3. It was found that the filter length and addition of small percentages of white noise had little effect. If the wrong bubble pulse frequency was used to calculate the predictive gap in the filter some suppression of the bubble pulses did occur although the action of the filter was unpredictable elsewhere on the traces.

4. Fig. 2.8 illustrates the effect of a prediction filter which was designed using the trace for station 32 and applying the same filter to the other traces. Efficient removal of the bubble pulses occurred only on stations near to 32 which must indicate a changing waveform due to either wave theory , attenuation or local surface effects near the stations.

5. Fig. 2.9 illustrates that the method works only for traces where either PmP or Pg have amplitudes well above the noise.

Using the parameters found to be most efficient on CSH/N2 to design the prediction error filter the method was applied to a number of different shots. Figs. 2.10 - 2.11 show that the bubble pulses are removed for CSH/N6 and CSH/N5 which both have different bubble pulse frequencies than shot N2. In the

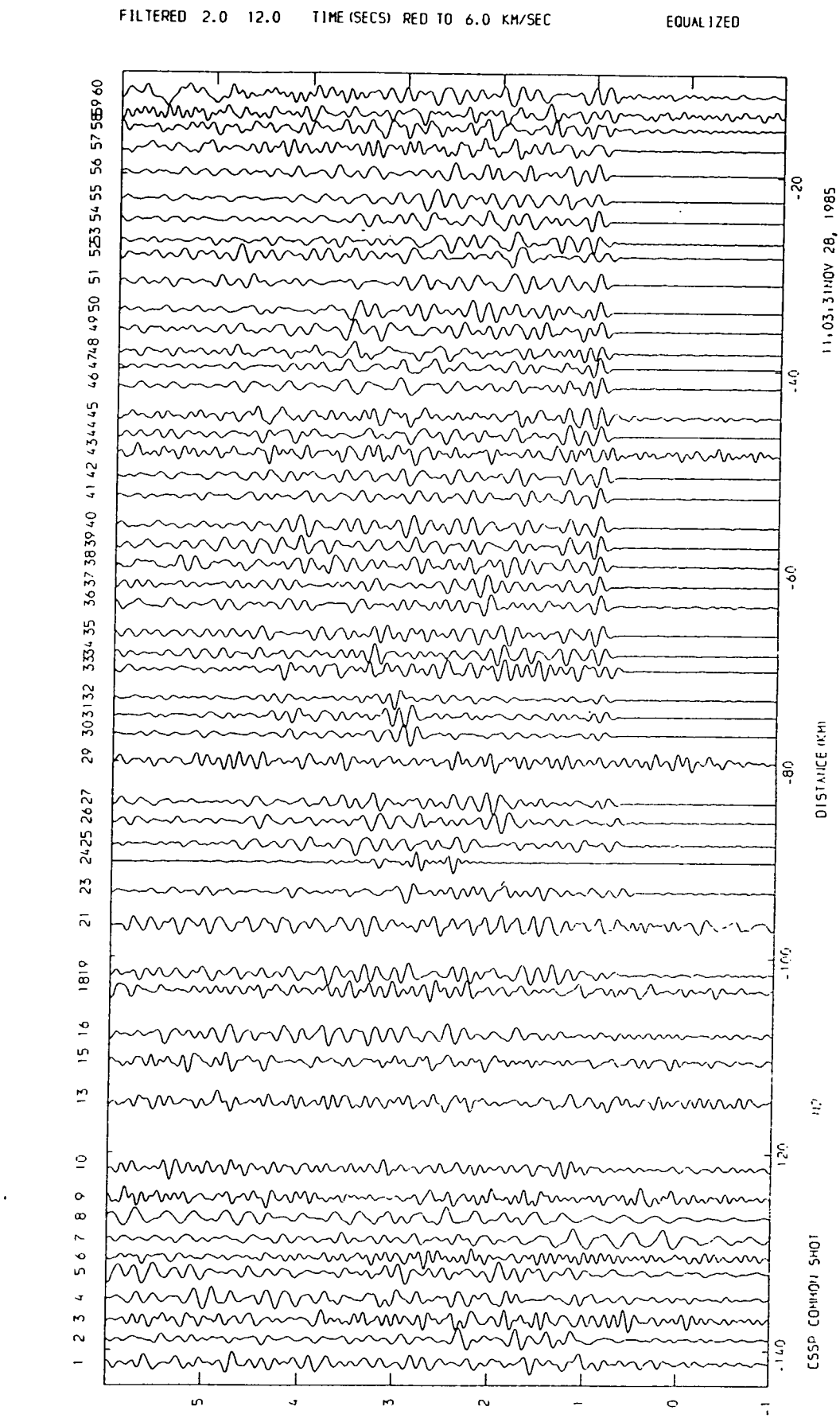


Figure(2.8) Common shot section N2 for selected stations
Filtered – amplitudes equalized – vred=6.0
Predicted deconvolution performed
Filter designed on station 32 only
Autocorrelation window = 0.3 – 4.3 s (400 samples)
Filter length = 132 samples
Prediction gap = 32 samples
Bubble pulse period = 0.31 s

2.9 (a)

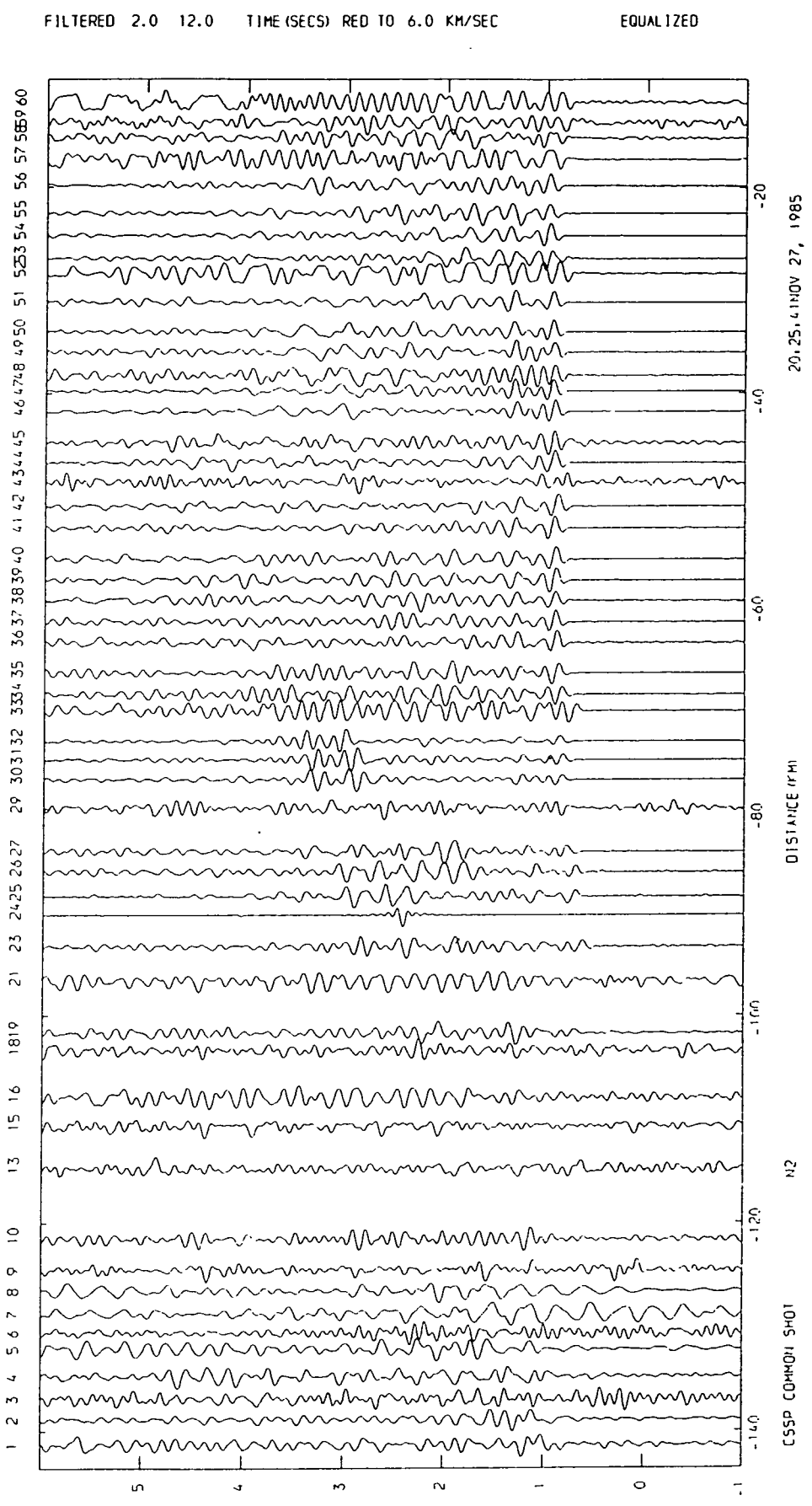


Figure(2.9) Common shot section N2 for complete section
Filtered - amplitudes equalized - vred=6.0
(a) No deconvolution performed
(b) Predicted deconvolution performed
Autocorrelation window = 0.3 - 4.3 s (400 samples)
Autocorrelation window = 0 - 4 s
Filter length = 132 samples
Prediction gap = 32 samples
Bubble pulse period = 0 31 s

2.9 (b)

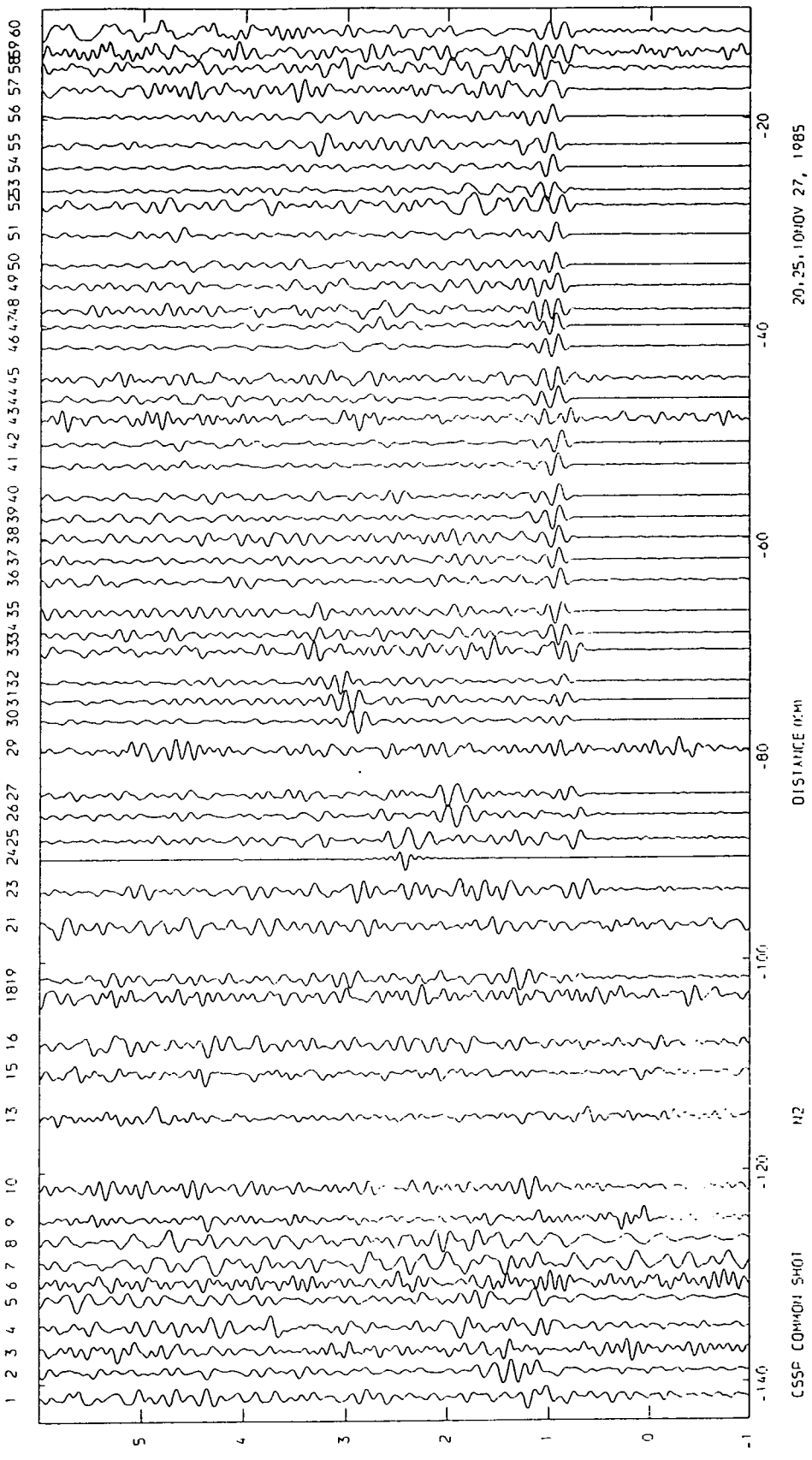
FILTERED 2.0 12.0 TIME (SECS) RED TO 6.0 KM/SEC EQUALIZED
1 2 3 4 5 6 7 8 9 10 13 15 16 18 19 21 23 24 25 26 27 29 30 31 32 33 34 35 36 37 38 39 40 41 42 43 44 45 46 47 48 49 50 51 52 53 54 55 56 57 58 59 60
-20
-40
-60
-80
-100
-120
-140
5
4
3
2
1
0
-1
20.25.10 NOV 27, 1985
DISTANCE (KM)
CSSP COMMON SHOT N2

2.10 (a)

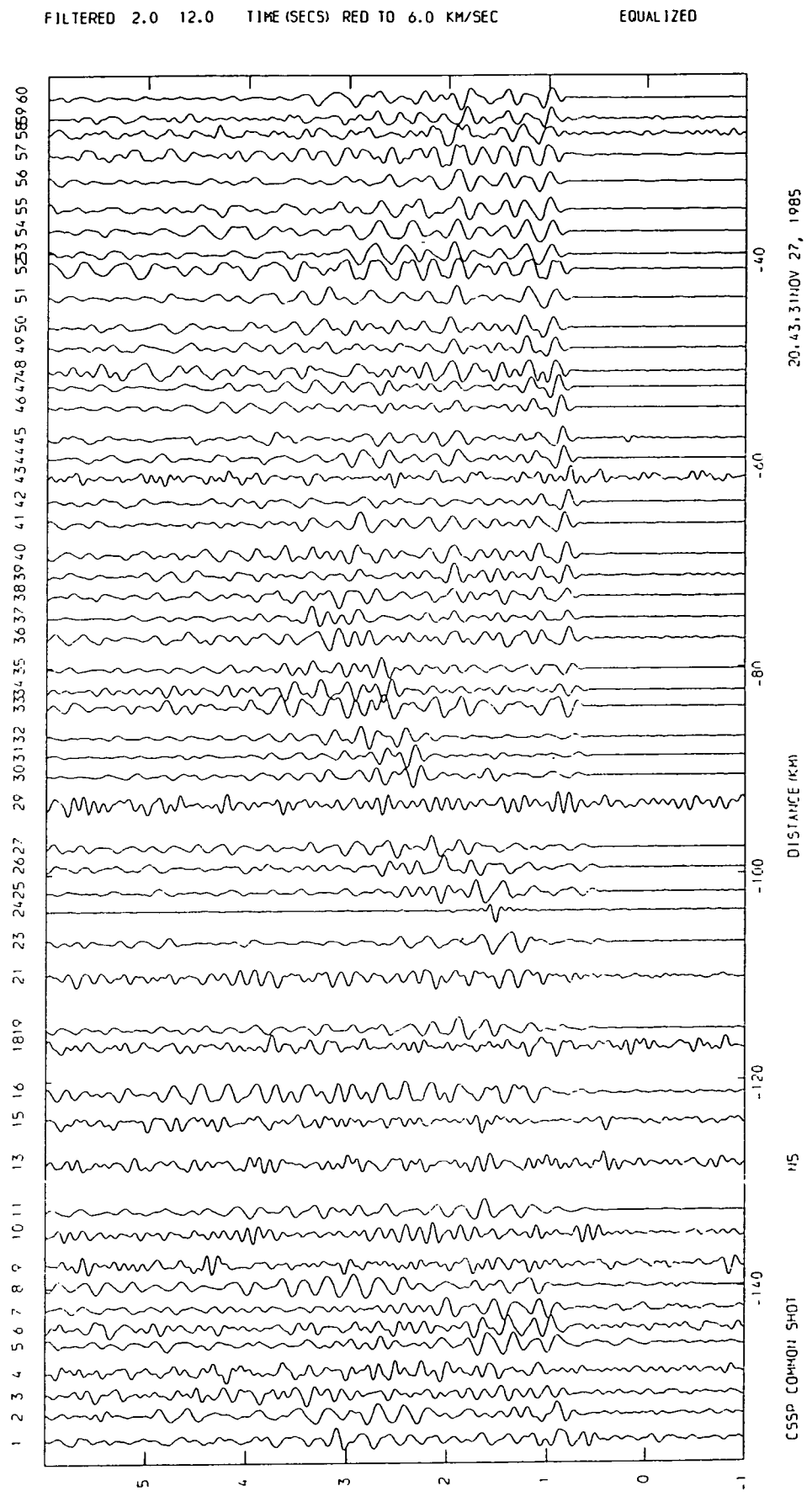


Figure(2.10) Common shot section N5
Filtered – amplitudes equalized – vred=6.0
(a) No deconvolution performed
(b) Predicted deconvolution performed
Autocorrelation window = 0.3 – 4.3 s (400 samples)
Filter length = 132 samples
Prediction gap = 32 samples
Bubble pulse period = 0.26 s

2.10 (b)

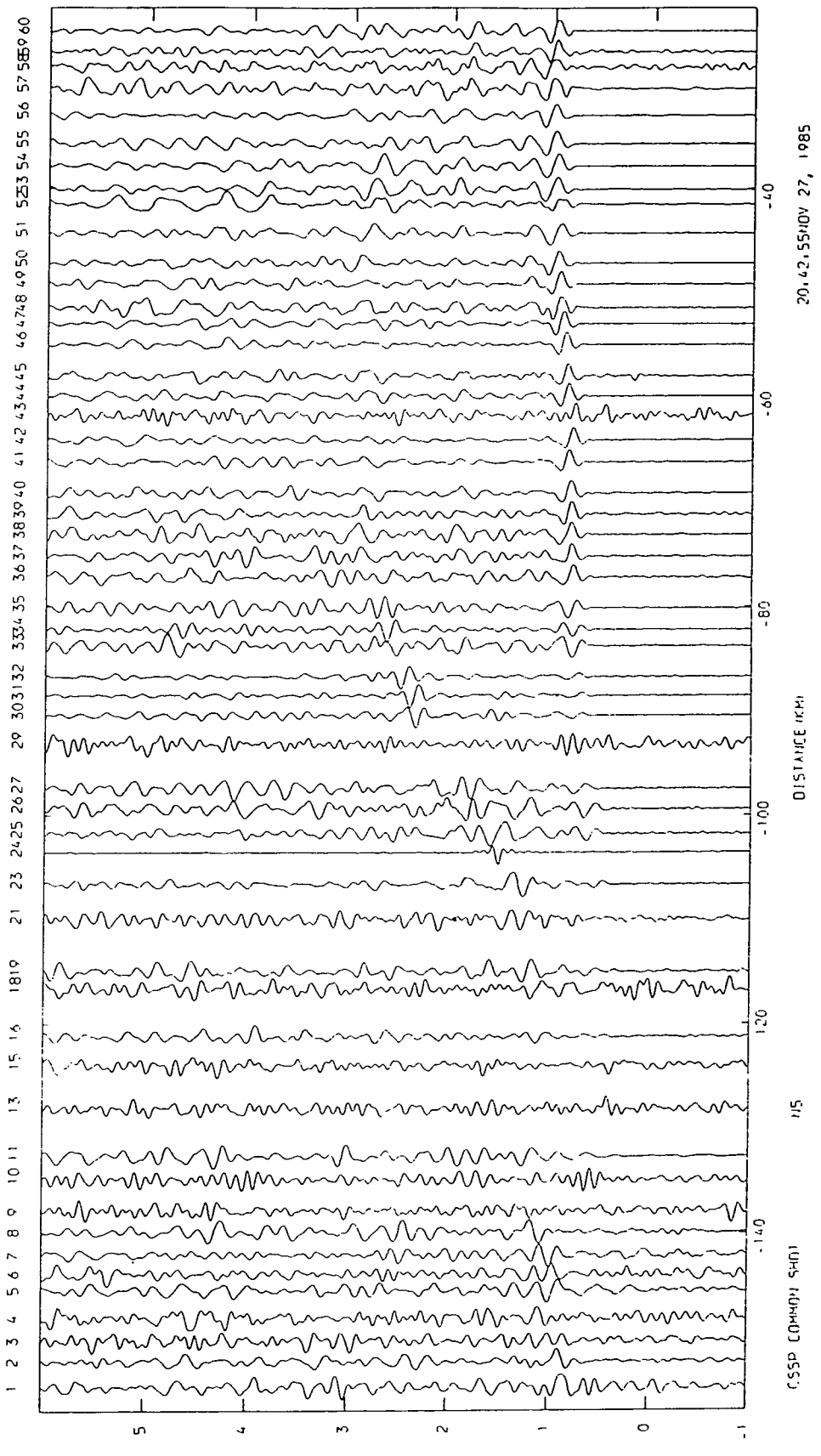
FILTERED 2.0 12.0 TIME (SECS) RED TO 6.0 KM/SEC EQUALIZED
1 2 3 4 5 6 7 8 9 10 11 13 15 16 18 19 21 23 24 25 26 27 29 30 31 32 33 34 35 36 37 38 39 40 41 42 43 44 45 46 47 48 49 50 51 52 53 54 55 56 57 58 59 60
-40
-60
-80
-100
-120
-140
DISTANCE (KM)
20:42:55:00 NOV 27, 1985
CSSP COMMON SHOT
5 4 3 2 1 0 -1

2.11 (a)

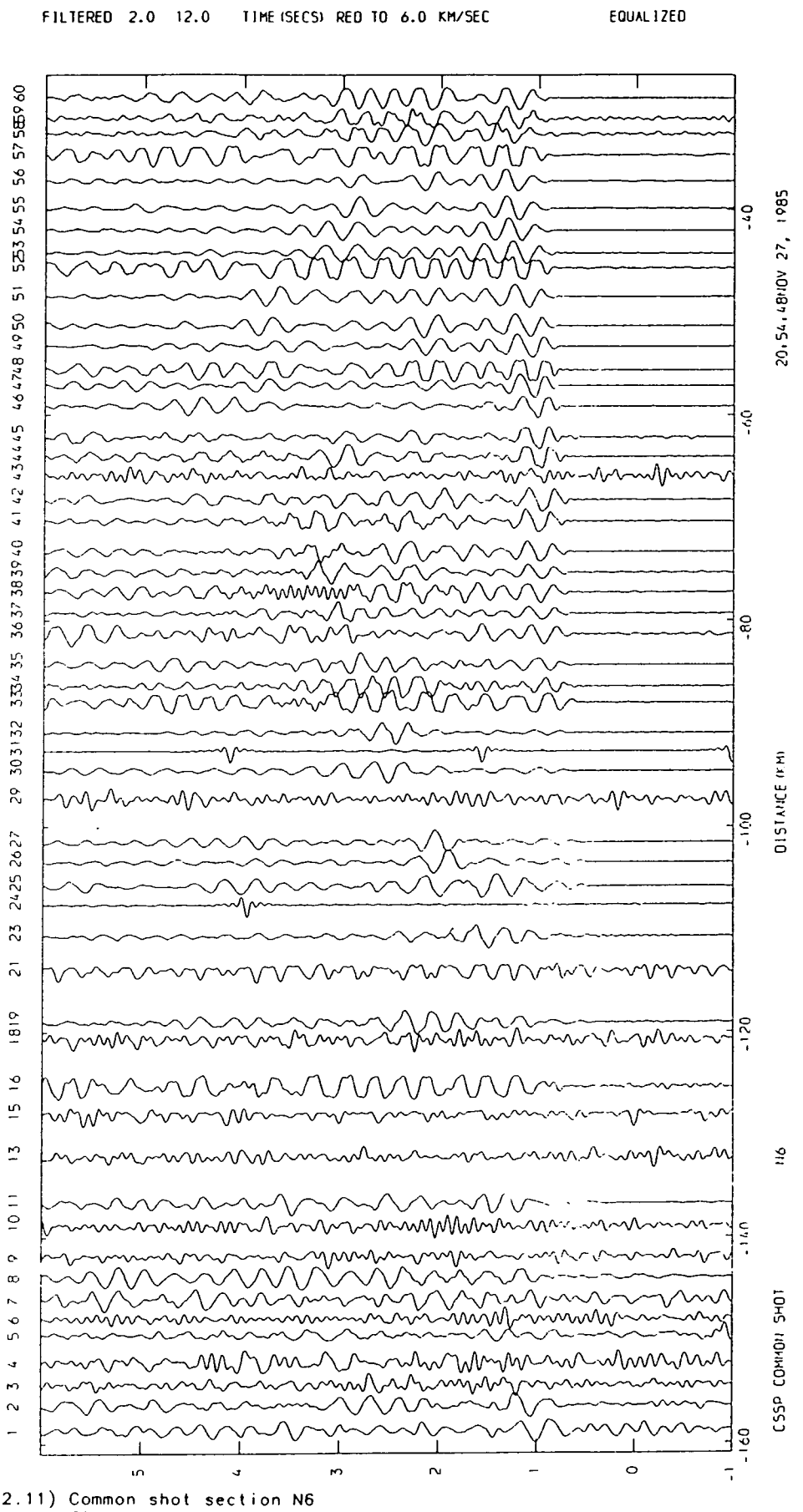


Figure(2.11) Common shot section N6
Filtered – amplitudes equalized – vred=6.0
(a) No deconvolution performed
(b) Predicted deconvolution performed
Autocorrelation window = 0.3 – 4.3 s (400 samples)
Filter length = 132 samples
Prediction gap = 32 samples
Bubble pulse period = 0.23 s

2.11 (b)

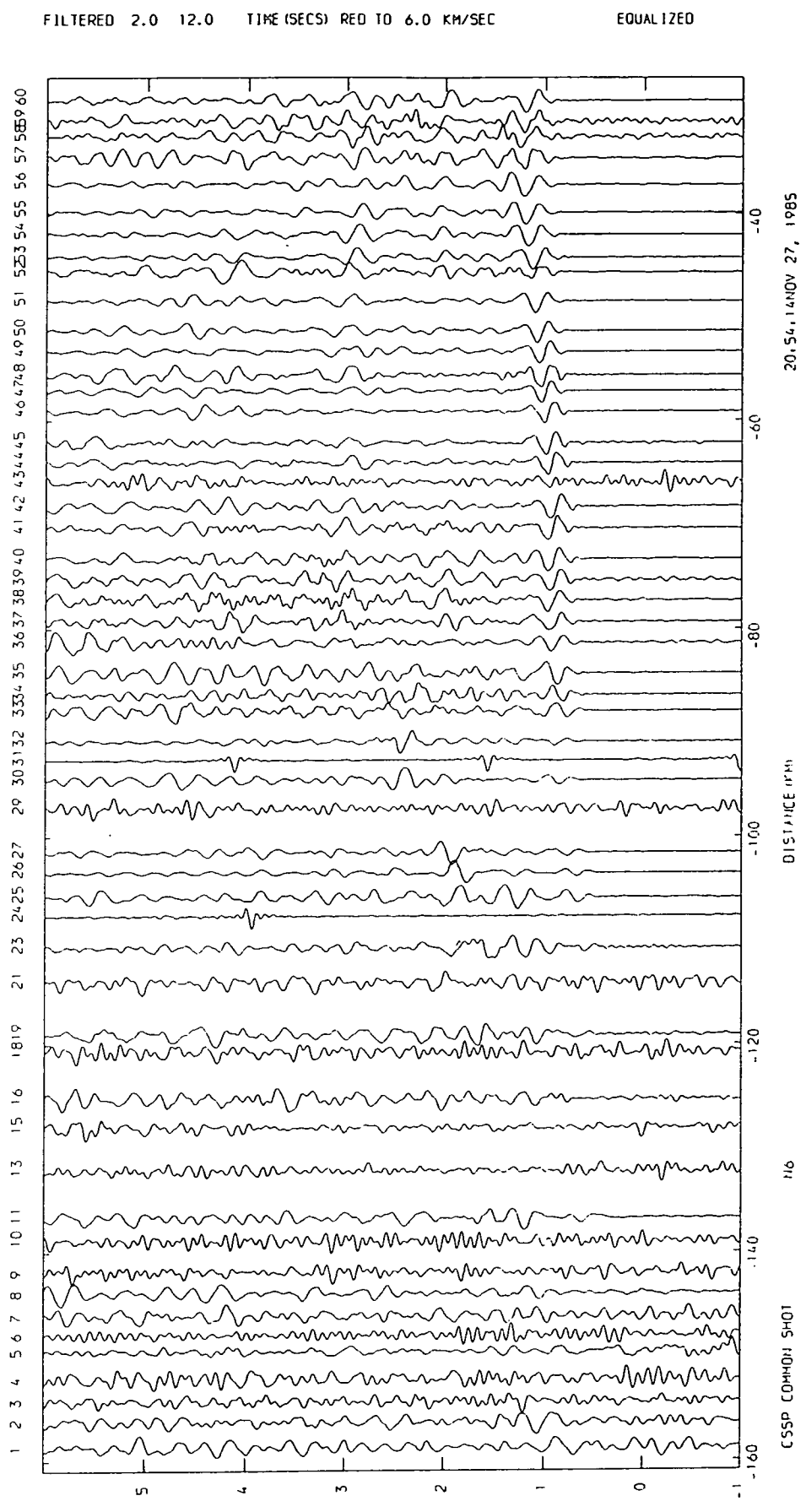
FILTERED 2.0 12.0 TIME (SECS) RED TO 6.0 KM/SEC EQUALIZED
1 2 3 4 5 6 7 8 9 10 11 13 15 16 18 19 21 23 24 25 26 27 29 30 31 32 33 34 35 36 37 38 39 40 41 42 43 44 45 46 47 48 49 50 51 52 53 54 55 56 57 58 59 60
-40
-60
-80
-100
-120
-140
-160
5
4
3
2
1
0
-1
20:54:14 NOV 27, 1985
DISTANCE (KM)
CSSP COMMON SHOT

2.12 (a)

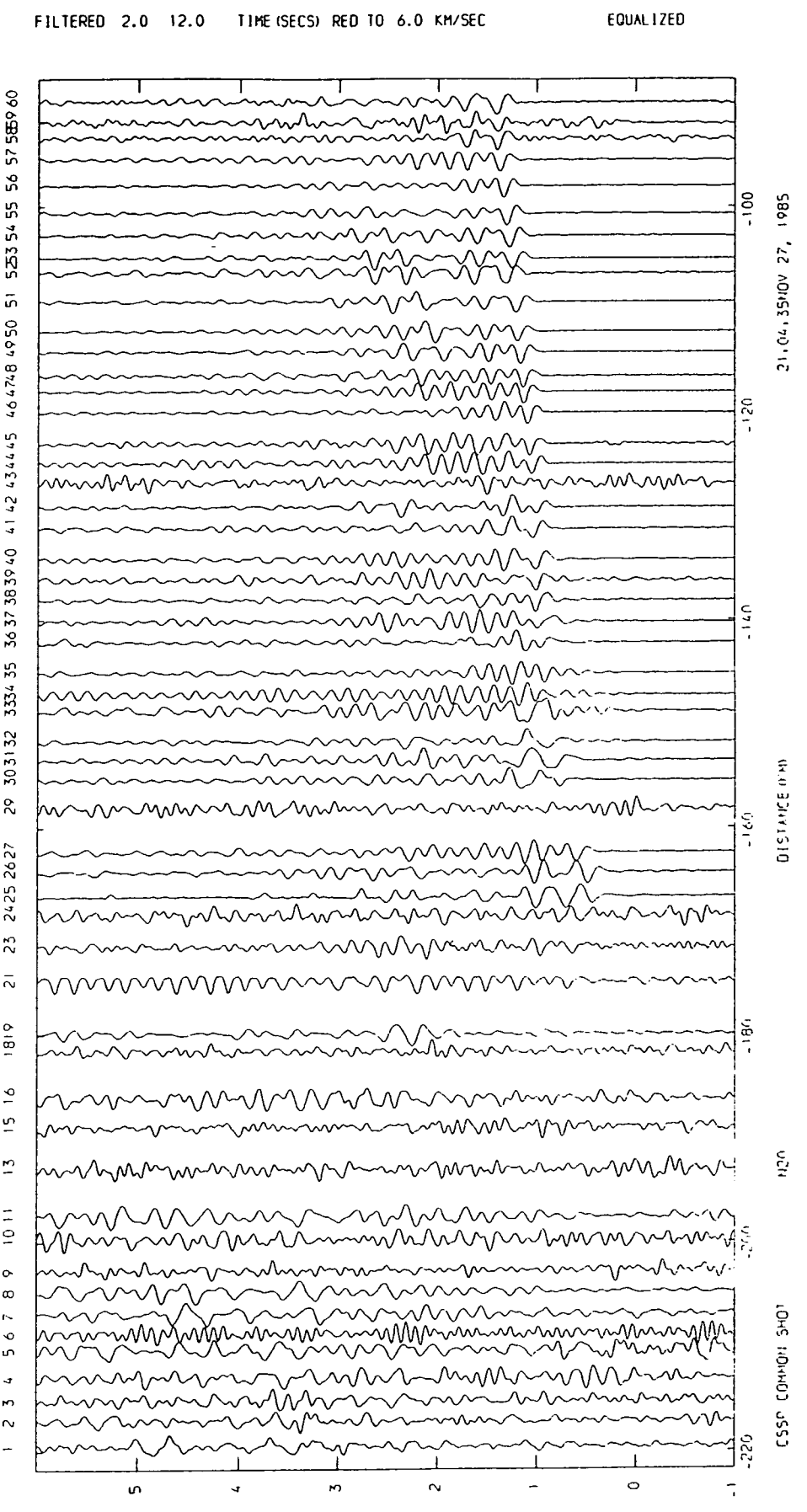


Figure(2.12) Common shot section N20
Filtered – amplitudes equalized – vred=6.0
(a) No deconvolution performed
(b) Predicted deconvolution performed
Autocorrelation window = 0.3 – 4.3 s (400 samples)
Filter length = 132 samples
Prediction gap = 32 samples

2·12 (b)

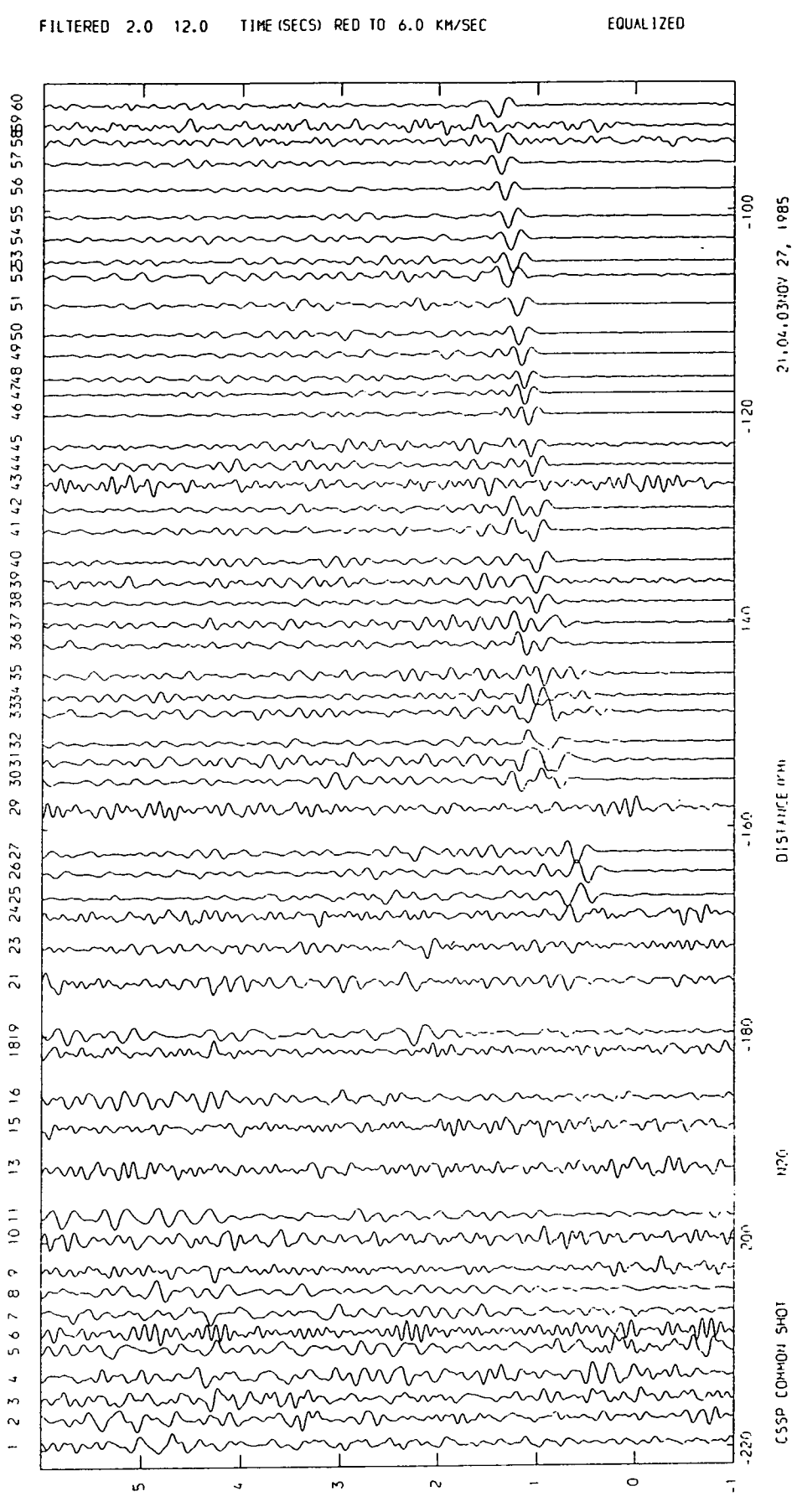
FILTERED 2.0 12.0 TIME (SECS) RED TO 6.0 KM/SEC
EQUALIZED
1 2 3 4 5 6 7 8 9 10 11 13 15 16 18 19 21 23 24 25 26 27 29 30 31 32 33 34 35 36 37 38 39 40 41 42 43 44 45 46 47 48 49 50 51 52 53 54 55 56 57 58 59 60
-100
-120
-140
-160
-180
-200
-220
5 4 3 2 1 0 -1
21-04-03-NOV 27, 1985
DISTANCE (KM)
CSSP COMMON SHOT

2.13 (a)

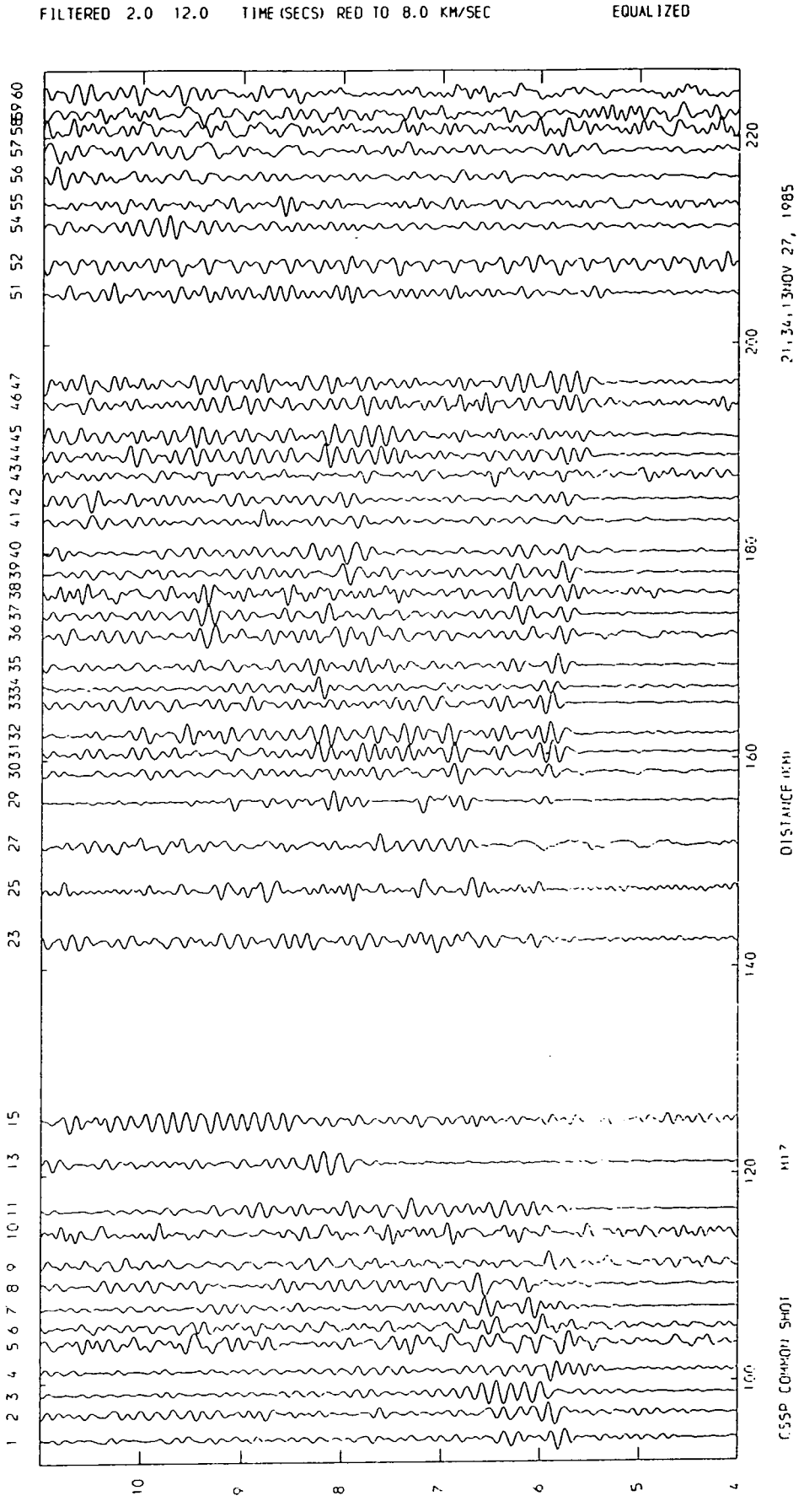


Figure(2.13) Common shot section M17
Filtered – amplitudes equalized – vred=8.0
(a) No deconvolution performed
(b) Predicted deconvolution performed
Autocorrelation window = 4.3 – 8.3 s (400 samples)
Filter length = 132 samples
Prediction gap = 32 samples
Bubble pulse period = 0.36 s

2·13 (b)

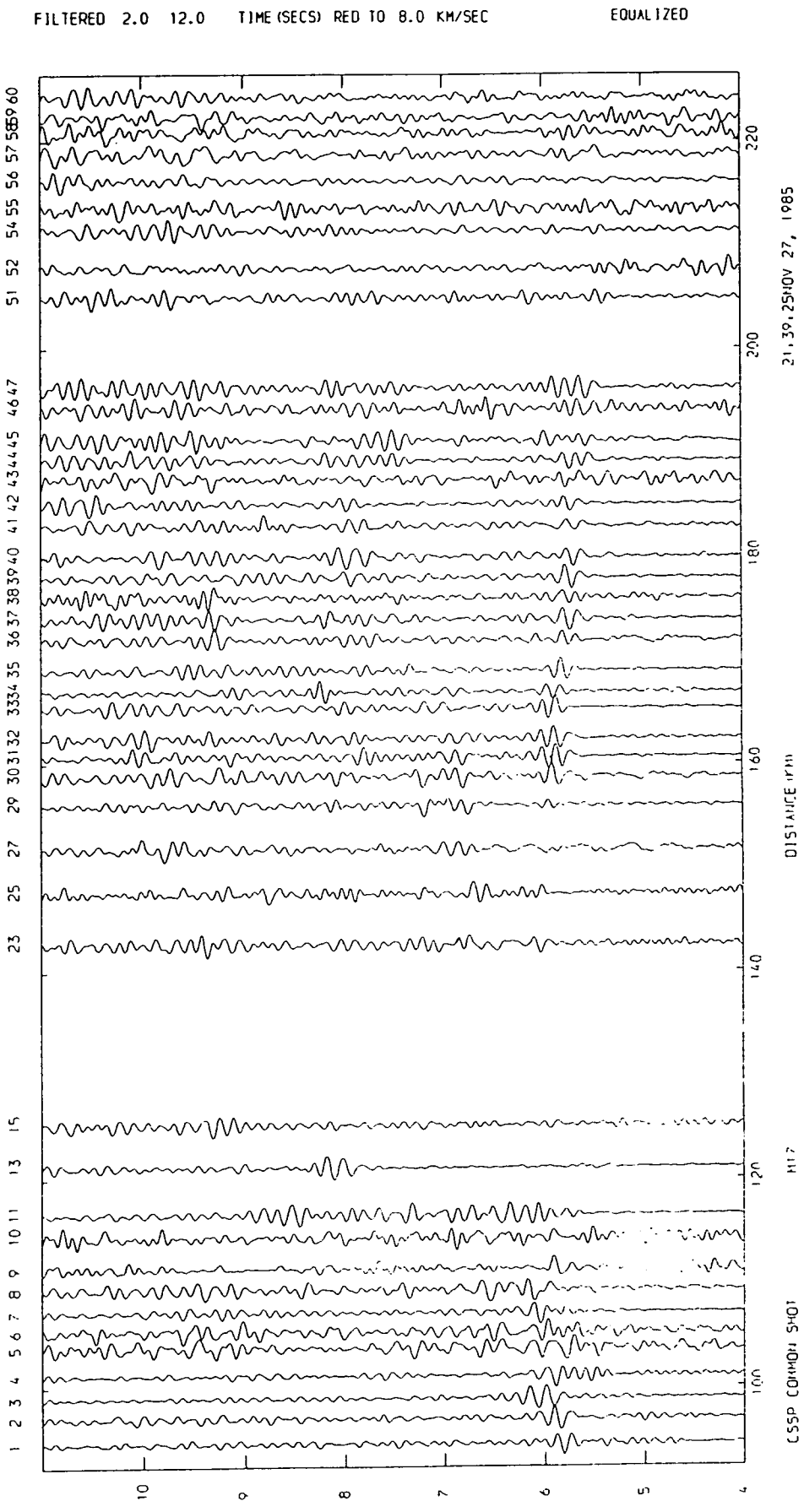
FILTERED 2.0 12.0 TIME (SECS) RED TO 8.0 KM/SEC
EQUALIZED
1 2 3 4 5 6 7 8 9 10 11 13 15
23 25 27 29 30 31 32 33 34 35 36 37 38 39 40 41 42 43 44 45 46 47
51 52 54 55 56 57 58 59 60
100 120 140 160 180 200 220
10 9 8 7 6 5 4
CSSP COMMON SHOT
DISTANCE (KM)
21:39:25 NOV 27, 1985

North Sea for shots N9-N29 no Pg phase is observed (Green 1984) and so the filter is designed over a window which includes only PcP and PmP for CSH/N20. Fig. 2.12 illustrates that the PmP phase has been removed where it has an arrival time after PcP which approximately equals the predicted gap used in the filter. Fig. 2.13 shows that the suppression of the bubble pulse for Pn is also possible using a prediction error filter on CSH/M17.

Barrodale et al (1984) have shown that the bubble pulse wavelets are not minimum delay and suggest an alternative method of estimating the bubble pulse wavelets using the l1 algorithm rather than the usual method involving the minimum phase assumption. The method used to deconvolve the Caledonian Suture Seismic Project sections does satisfactorily remove the bubble pulse reverberations but routine deconvolution was not performed due to the observation that where an arrival lies at about the predicted time of the bubble pulse behind another arrival it is suppressed and removed. This means that in cases where the arrival times of one phase are similar to a later phase the method of predicted deconvolution will not separate the phases and so will not aid picking: instead the later arrival is suppressed.

## 2.5 TRAVEL-TIMES

The errors in the location of the stations and shots are +/- 10m and +/- 100m respectively and the shot timing errors are estimated to be about +/- 20 ms (Green 1984). Combining all these errors a minimum error for any travel-time measured will be about 40-60 ms. The picking errors for the second arrivals and the Moho refractor (Pn) are estimated to be at least 100 ms and can be as high as 250 ms although because of the subjective nature of the picking process it is difficult to quantify these errors precisely.

### 2.5.1 Correlation of Observed Arrivals

Giese (1976) discussed the problems encountered in the picking process in refraction work and concluded that a phase must

1. have amplitudes greater than the background noise
2. have apparent velocities that are within reasonable limits
3. be observable over a reasonable distance range

Ansorge et al (1982) concluded from a comparative study of the different models obtained by different workers from the same data set during the workshop of the Commission on Controlled Source Seismology at Karlsruhe in 1977 that

1. Most workers identified the same main phases and as a result the main features of all the resulting models showed broad agreement in depths to and velocities of the main interfaces.
2. Differences in the models were on the whole due to differing interpretations given to low amplitude and

laterally discontinuous phases which decayed rapidly over short distances into the background noise.

3. Low velocity layers in some models were required because velocity gradients where none existed had been introduced and so lower velocities were needed underneath these gradients to obtain consistent travel-times.
4. Synthetic seismograms were found to be useful in distinguishing between some of the models.

Three main recommendations were made:

1. Better criteria were needed for more objective and reliable correlation of phases.
2. Improved quality and higher density data with true amplitude recovery were needed.
3. Inversion methods for laterally varying media needed to be developed.

Jacob et al (1985) also highlighted the problems of correlating arrivals on refraction seismograms and noted that any final models depend on the subjective bias of the seismologist during the initial picking of the phases observed. Finlayson et al (1984) have emphasized that picking the second arrivals on refraction seismograms is difficult due to the complex nature of the wavetrain which must to a large degree be attributable to scattering from local near surface inhomogeneities. It is the approach described by Finlayson et al (1984) that has been adopted to correlate the phases observed on the Caledonian Suture Seismic Project refraction sections.

### 2.5.2 Correlation of the Phases Observed from The Caledonian Suture Seismic Project

During the correlation of the arrivals observed on the Caledonian Suture Seismic Project sections the main aim was to identify only those phases which were seen consistently on adjacent common station and adjacent common shot sections. There are many bursts of energy and pickable arrivals visible on the sections but most of these appear on only a few sections. Because of the large amount of data it was considered at this stage to leave these ambiguous phases and to concentrate on the four most easily identifiable and consistent arrivals. These are:

1. The basement refractor Pg. (Green 1984)
2. The wide-angle reflections from the mid-crust PcP which were also observed in the NERL experiment in the same area by Swinburn (1975).
3. The wide-angle reflections from the Moho (PmP) which are commonly observed on refraction seismograms as the arrival with the largest amplitude.
4. The Moho refractor (Pn).

### 2.5.3 Travel-time Picking

The picking of the arrival times of the 4 phases was made as objective as possible by using both common station and common shot sections and continually repicking and replotting the sections with the travel-time picks displayed until a consistent travel-time data set was obtained. On quite a few sections the presence of the bubble pulse aided picking

whilst on others where the bubble pulse of an earlier arrival interfered with the first arrival of a later phase it was found difficult to make any pick for the later arrival with any allowable accuracy.

The travel-times were picked initially using the PERQ digitizing facilty on NUMAC and thereafter any alterations were measured from paper playouts plotted at a scale of 4.4 cms/s. The programme TMATCOPY was used to write the travel-times picked into the travel-time matrices. TMATCOPY accepts raw data from the PERQ or travel-times in seconds or travel-time corrections measured off the seismograms in units of distance and will prompt the user for any input required. The programme TMATREAD reads the travel-times in the travel-time matrices and outputs them to a file as a list and again prompts the user for any input required.

### 2.5.4 The Travel-time Matrices

One travel-time matrix was created for each phase and these are called TMAT-PG, TMAT-PCP, TMAT-PMP and TMAT-PN for phases Pg, PcP, PmP and Pn respectively. Each travel-time matrix consists of three lines of header information and 110 lines of formatted travel-time and travel-time error data. The first line contains the phase name in the first four locations (A4) and a title whilst the second and third lines consist of lists of the stations and shots respectively. A total of 110 stations and shots can be dealt with by the programmes which use the matrices. The travel-time for a particular trace and phase is then stored in the matrix corresponding to that phase

at the locations in the matrix given by the position of the station and shot in the lists in the second two lines of the matrix. For example if station ST is the second station listed on the second line and the shot SH is the third shot listed on the third line then the travel-time and error for this trace (ST,SH) will be inputted to the second line and third travel-time column in the mainbody of the matrix. Each "location" has the format 2F10.3 : which contains the travel-time pick and its error respectively so that the travel-time and error for trace (ST,SH) would be put into the location on the second line given by (40X,2F10.3,2140X).

The *SURFACE2 contouring package available on NUMAC was used to plot the travel-time matrices. The subroutine MATCOR in programme TTCORR arranges the travel-time data in the format required for the *SURFACE2 package by reading the travel-times from the travel-time matrices. TTCORR also corrects for the known shallow structure down to a datum using the apparent surface velocities calculated as described in Section 3.4.1.

## 2.6 AMPLITUDES

Once the travel-times of the 4 phases had been picked the amplitudes of the wave envelopes associated with each arrival could have been measured off the common station sections corrected to common gain which could then have been inputted to amplitude matrices, one for each phase, and, plotted in the form of contour diagrams. However it was found that even though the plotting programme CSSPLOT corrects the trace

2·14 (a) FILTERED 2.0 12.0 TIME(SECS) RED TO 6.0 KM/SEC TRACE AMPFAC 0.0013445

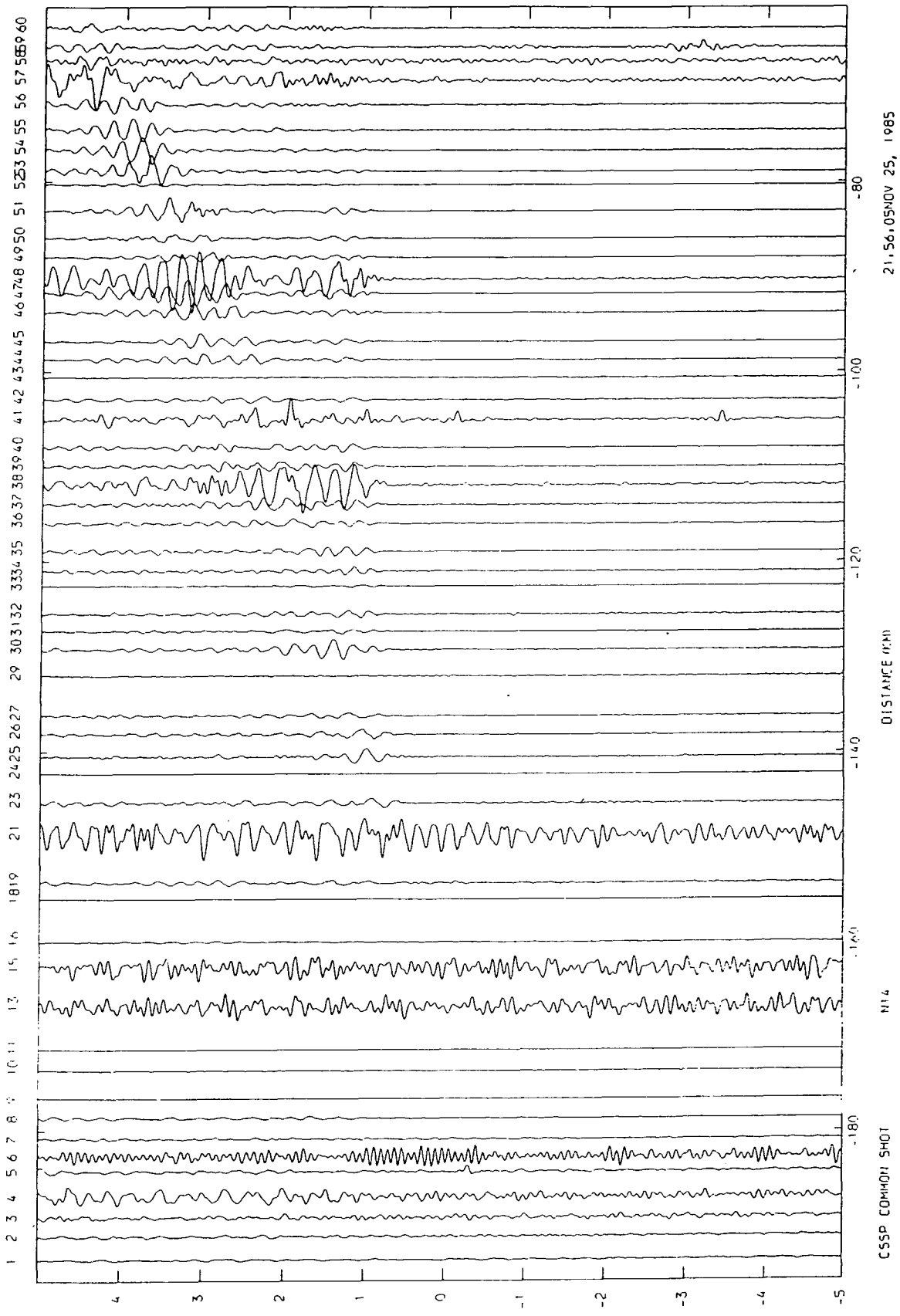


Figure(2.14) Common shot section N14 amplitudes corrected to common gain
(a) Stations 38, 48 & 57 have amplitudes that are too high. Stations 16, 33 & 52 (the silver box sites) have amplitudes that are too low.
(b) The traces with unexpected large amplitudes and the noisy stations have been removed: stations 31, 49 & 50 now appear to have amplitudes too small compared to adjacent stations.

2·14 (b) FILTERED 2.0 12.0 TIME (SECS) RED TO 6.0 KM/SEC TRACE AMPFAC 0.0017079

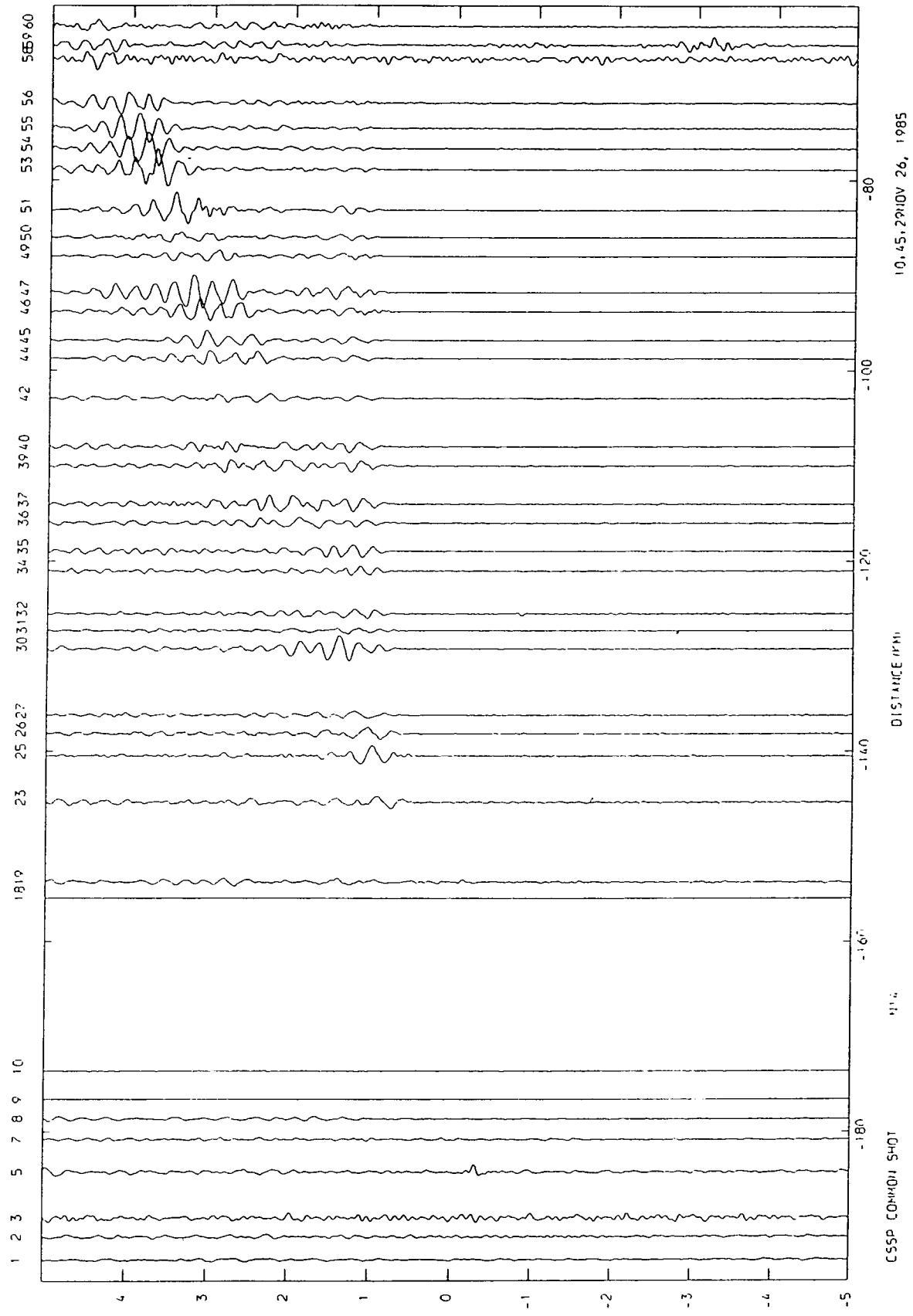

amplitudes to a common gain unexpected variations were found to occur between the amplitudes of adjacent stations on a common shot section plotted with the amplitudes corrected to common gain e.g. Fig. 2.14 . There did not appear to be any simple error in the field procedures that could have accounted for these anomalies. One possibility considered was the incorrect setting of the ampmods but the correcting of the anomalous amplitudes by factors of 2 did not remove the problem as the correction to the higher amplitude stations varied with distance to the shots. It was found after the experiment that some seismometers had bent spokes (Green pers.comm.) which may have affected both the amplitude and frequency responses of the seismometers. Other causes could be variations in ground to seismometer coupling or the effects of near surface features such as the Whin Sill which may focus the incoming seismic energy quite markedly.

It is concluded that this rapid variation in amplitudes is due to either shallow near surface effects or unknown instrumentation errors and that the production of amplitude matrices would not provide more information than available on the common station sections corrected to common gain.

## 2.7 SUMMARY

During the interpretation of any experimental data the limitations and advantages offered by the particular experimental design must be taken into account as must the subsequent parameters used to process and display the data. In this chapter most of the problems encountered have been

outlined that affect the interpretation process. In summary these are :

1. The variation in depth of detonation of the explosive shots has produced varying source amplitudes and frequencies;
   (a) Only those shots fired at a depth of 90m were fired at the optimum depth for the weight of charge used (150kg). It is these shots which have produced the largest amplitudes on the sections e.g. shots N4-N10 in the North Sea for common station sections corrected to common gain (Appendix A).
   (b) The bubble pulse oscillations of the shots are also clearly visible on the seismograms and must be taken into account during the correlation of the phases especially where two have similar arrival times.

(b) The rapid variation in amplitudes between adjacent stations on CSH sections can only be attributed to near surface focussing effects or unknown instrumentational problems.

Taking into account the large-scale nature of the experiment and the practical problems of running over 60 seismic stations and setting off 66 large explosive shots at sea, two recommendations can be made for future projects:

1. Each seismometer and ampmod at a station should be calibrated and tested before and after field use. Any amplitude variations between traces for a common shot section which have been corrected to common gain can then be attributed to geological effects or coupling problems of the seismometer to the ground once the possibilities of

malfunction of the ampmods or seismometers have been eliminated.

2. The weight of explosives used should be varied as the depth of detonation varies so that each shot is set off at approximately its optimum depth. The optimum depth equations are given by Burkhardt and Rees (1975) and Jacob (1975).

These recommendations are the minimum required if synthetic seismogram modelling of true amplitudes on common shot sections is to be meaningful.

# CHAPTER THREE

## INTERPRETATION METHODS

There are three main stages in the interpretation of refraction data: these are:

1. First the main arrivals observed on the reduced sections must be identified and the phases finally selected timed. These travel-times must then be displayed in suitable ways. Initial preliminary models are obtained by fitting the travel-times along common shot and common station directions in the matrices to the simple refraction and reflection equations using the linear least square method. These equations are :

$$T = X / V + a_i + a_j \qquad (3.1)$$

$$T^2 = X^2 / Vav^2 + 4 \times H^2 / Vav^2 \qquad (3.2)$$

$$(T^2 = X^2 / Vav^2 + \quad z^2 \quad )$$

where
- T - observed travel-time
- X - station shot offset
- V - velocity of the refracted phase
- a - delay time under the shot
- a - delay time under the station
- Vav - average velocity above H at the midpoint between the station and shot.
- H - Depth at the midpoint between the station and shot

The effects of the shallow structure can be assessed from these results. The travel-times can also be corrected for the known shallow structure above the basement to reveal the variations due to any deeper structures.

2. The second stage entails the processing of the travel-times using the time-term technique on the refracted phases and related methods on the wide-angle reflections to produce preliminary models of the deeper structure corrected for the known shallow structures above basement. Both these methods require certain assumptions to be made about the data and seismic structures. Problems may occur where these assumptions are invalid; these problems are discussed more fully in the preceding sections.

3. The final stage entails the construction of a model which includes the results from the first two stages and any other relevant geophysical information available. This model can then be tested and refined using the techniques of ray-tracing and synthetic seismogram modelling until the synthetic sections produced display the broad amplitude and travel-time features observed on the experimental sections.

The problems encountered in the initial phase correlations have been described in Section 2.5.1; the methods described in this chapter will assume a data set which includes all relevant reduced sections corrected to common gain and all the travel-times of the phases correlated.

## 3.1 INTERPRETATION OF THE TRAVEL-TIME MATRICES

The contoured plots of the travel-time matrices (Section 2.5.4) display the main variations along the common shot, common station, common mid-point and common distance directions and can be used as an aid to interpretation. Thus for a horizontal planar structure with no lateral velocity changes the travel-time contours would be parallel to the common distance lines. However, if the contours cross the common distance lines then lateral changes in velocity and/or variations in the depth structure are indicated.

### 3.1.1 Reduction of the Travel-time Matrices

The matrices which display the wide-angle reflections can be reduced to a velocity which represents the average velocity of the crust squared as given by the reflection equation 3.1: the reduced travel-times squared are given by the equation:

$$T^2(\text{reduced}) = T^2 - ( X / Vav )^2 \quad (3.3)$$

This is analogous to the reduction of the travel-times of a refracted phase by the equation:

$$T(\text{reduced}) = T - ( X / V ) \quad (3.4)$$

The values of H and Vav in the reflection equation 3.2 give the depth to and average velocity above the midpoint between the station shot pair. The values of $a_i$, $a_j$ and V in the refraction equation 3.1 correspond to the delay times at the station and shot respectively and the velocity of the refractor. The matrices for refracted and reflected phases must therefore be considered separately.

### 3.1.2 Travel-time Matrices for Wide-angle Reflections

The variations of the travel-times for wide-angle reflections along the common distance lines on a travel-time matrix (reduced to a reasonable average velocity and corrected for known shallow structures) are related to the lateral variation of the seismic structure across the range of common mid-point positions covered by the data. Any variations in the travel-times due to structures above the reflecting region also show up as travel-time variations on the matrix but would be associated with particular shot or station ranges. This effect, if observed on a matrix already corrected for shallow structure, may indicate the prescence of unknown near surface structures. The interpretation of any variations over the range of shots or stations where these anomalies are observed must be treated with caution.

The effects of any structures deduced for the mid-crust on the travel-times observed on a matrix displaying the wide-angle reflections from the Moho are similar to the effects of any unknown shallow structures. If the coverage of PcP is not as extensive as that for PmP, some effects observed in the PmP matrix that could be interpreted as being due to shallow structures may also be attributable to variations in the mid-crust (Fig.3.1).

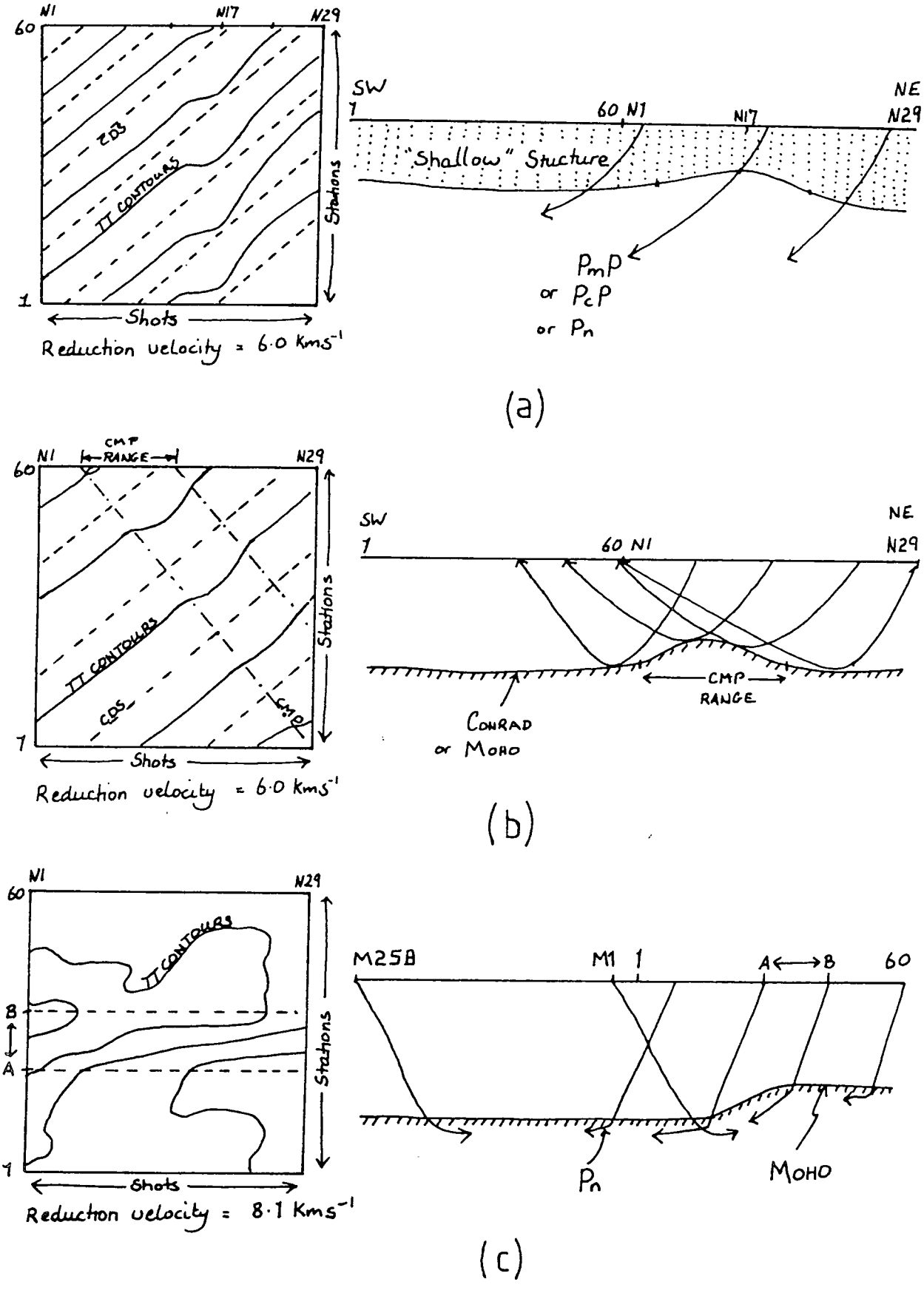


Figure(3.1) Sketch diagrams illustrating the
(a) Effect of varying shallow structure on the travel-time matrix for any "deep" phase (PcP, PmP, Pn)
(b) Effect of a rise in a reflecting interface on the travel-time matrix for the corresponding reflection (PcP, PmP)
(c) Effect of a rise in a refractor on the travel-time matrix for the corresponding refractor (Pn).

### 3.1.3 Travel-time Matrices for Refractions

It is more difficult in the case of a matrix displaying the travel-times for a refracted phase to distinguish between the effects of variations in the travel-times due to structures in the refractor as opposed to those due to unknown shallow structures; both show up over particular ranges of shots, or stations. However the effects of shallow structures are displayed on all matrices for any type of phase at the same range of shots or stations, and so, provided there is an overlap in the coverage between phases it should be possible to recognise the effects of any shallow structures where they occur.

By scanning along common shot or common station directions on a matrix displaying travel-times of a refracted phase e.g. Pn the gross variations in the delay times can be estimated. For example Fig. 3.1 illustrates how a steep slope in the Moho would show up on the travel-time matrix for the phase Pn. If the crust were homogeneous and planar the travel-time matrices for Pn (reduced to the Pn velocity) and the wide-angle reflections (reduced to the relevent average velocity squared) would have no contours displayed assuming zero observational errors.

## 3.2 TRAVEL-TIME REGRESSION

Preliminary models of the seismic structure can be obtained by fitting the two equations 3.1 and 3.2 to the wide-angle reflections and refractions respectively along common station and common shot directions in the matrices. The programme TT-REG performs this task. The effects of varying coverage along common shot, common station and common mid-point directions on a matrix in relation to the known shallow structural delays can produce rapid variations of the apparent velocities and therefore the depths to the interfaces. These anomalous areas where coverage is not good can be located and in the interpretation of the results obtained using the methods described in the following sections care can be taken to ensure that any anomalous results are not due to problems of data coverage with respect to the known shallow structure.

## 3.3 THE TIME-TERM METHOD

The time-term method was formulated by Scheidegger and Willmore (1957) and has been widely used in the interpretation of refraction data (Bamford 1973 & 1976, Berry and West 1966). The travel-time equation of a head wave can be represented by the equation 3.2 which can be altered to the form presented by Berry and West (1966):

$$t_{ij} = D_{ij} / V + a_i + a_j + d_{ij} \quad (3.5)$$

where $D_{ij}$ - is the distance between the normals to the refractor from the station i and shot j.

$V_i$ - is the velocity of the refractor

$a_i$ - is the delay time of the station

$a_j$ - is the delay time of the shot

The delay time represents the time taken for the refracted wave to pass through the lower velocity cover.

$d_{ij}$ - is the residual time not "explained" by the equation due to measurement errors or non-ideal behaviour of the refractor.

For n sites (shots or stations) there are a maximum of n(n-1) observations. If there are a minimum of (n+1) observations (m) the (n+1) unknowns can be found by solving the m resulting equations using the method of least squares. The computational methods are described by Swinburn (1975) and Summers (1982); the original time-term programme was changed to read the travel-times from the travel-time matrices and the erroneous errors highlighted by Green (1984) were removed from the calculations. The capability to select particular ranges of shots and stations to perform the calculations was also provided. One feature of the matrix solution to the m equations that has not been dealt with by Swinburn , Summers or Green needs to be described if the time-term programme is to

be understood and the short description of the matrix solution presented by Swinburn (1975) is repeated here in order to explain how the time-term programmes work.

The m observational equations can be written in matrix notation as:

$$[A][a] = [T] - [X]/v + [d]$$

where [A] - is the m x n coefficient matrix

[a] - is the column matrix (n x 1) of the site delay times

[T] - is the column matrix (m x 1) of the observed travel-times

v - is the scalar velocity of the refractor

Using standard least squares techniques by splitting the matrix [a] into two by the equation:

$$a_i = e_i - f_i / v \qquad (3.6)$$

the two equations below are obtained which are independent of the scalar v.

$$[A][e] = [T]$$

$$[A][f] = [X]$$

The least squares solutions for e and f are then given by

$$[e] = [A^T A]^{-1} [A^T][T]$$

$$[f] = [A^T A]^{-1} [A^T][X]$$

Defining

$$C_{ij} = T_{ij} - e_i - e_j$$

$$D_{ij} = X_{ij} - f_i - f_j$$

the residuals are given by

$$d_{ij} = C_{ij} - D_{ij} / v$$

the equation for the least squares velocity v can then be obtained by differentiating with respect to v the formula for d

$$v = \sum_{i=1}^{m} D_{ij}^2 \Big/ \sum_{i=1}^{m} C_{ij} D_{ij}$$

The coefficient matrix [A] contains mainly zeroes except for two ones in each row at the locations for the particular shot and station (i,j). This property can be exploited to formulate the square symmetric matrix $[A^TA]$ directly from the input without the need for matrix algebra. The total number of times station i and shot j are linked by a travel-time can be counted and input to the location $[A^TA](i,j)$ and $[A^TA](j,i)$. The total times a site(i) is used can also be input directly to the location $[A^TA](i,i)$ so that the diagonal in $[A^TA]$ represents the number of times any site is used.

### 3.3.1 The Assumptions in the Time-term Method

The assumptions used by Berry and West (1966) in deriving the time-term equation are

1. the velocity of the refracting interface is nearly constant
2. the range of dip of the refractor is slight (+/- 10 degrees)
3. the curvature of the refractor is slight
4. the velocity above the refractor beneath any site is a

function of only the depth to the refractor.

Bamford(1973) showed that iteration of the first solution to obtain better estimates of D using the calculated refractor topography, rather than using the station shot offset X, could improve the solution where assumption 2 is not thought to be valid. Swinburn (1975) found that iteration did not improve the time-term solutions for the NERL experiment and that the iteration process became unstable when badly constrained or poor data was used. Whitcombe and Maguire(1979) showed that for iteration to be stable the structure of the overburden must be accurately known.

Whitcombe and Rodgers (1981) and Whitcombe and Maguire (1979) have summarised the limitations of the time-term method due to the above four basic assumptions. In summary these limitations are:

1. Non-iterative travel-time solutions yield overestimates of the refractor velocity over anticlinal structures and underestimates over synclinal structures.
2. Synclines and velocity gradients below the refractor produce equivalent estimates: any solutions probably lie between the two extremes.
3. The relative length of the profile to any structural wavelengths of the refractor may affect the solutions obtained and still not show any signs of lack of fit. The effects vary depending on the station spacing, the profile length and the structural wavelengths of the refractor:
   a. If the structural wavelengths are greater than the survey length then any lack of fit may not show up

even if the solution is almost totally incorrect.

b. If the structural wavelengths are less than the survey length but greater than the critical distance any lack of fit of the solution will be correlated with the structural amplitudes of the refractor surface.

c. If the structural wavelength is less than the critical distance but greater than the station spacing no lack of fit will be observable even though the refractor topography is probably distorted.

d. If the structural wavelength is less than the station spacing the misfit of the solution will appear as noise in the residuals.

4. Non-iterative time-term results can produce apparent anisotropies due to undulating refractor topography (assumption 2). Even though the fit appears to be good the solution is non-unique.

Barton and Wood (1984) and many workers in the past have found a large scatter in the results for the structure of the Moho when using the time-term method to interpret Pn travel-times. This scatter is due to the varying near-surface effects and also the problems associated with the oversimplified assumptions inherent in the method. The solution time-terms can be corrected for the known shallow structure using the formula given by Swinburn (1975) or given in the programme TTERMC. The solution velocity calculated by the time-term method is affected by the shallow structure especially if there are any progressive delays varying laterally under the shots or stations. This effect can only be removed by correcting the travel-times down to a datum

below the shallow structure before using the time-term method. The resulting velocity calculated can not then be due to shallow structural variations although variations below the datum may still affect the solution velocities.

In conclusion the results from any time-term analysis of refractions must be interpreted with care and not treated as final. This is important for the processing of the Pn phase on surveys such as the Caledonian Suture Seismic Project where there is no true reversal on most of the refractor interface.

## 3.4 THE ANALYSIS OF WIDE-ANGLE REFLECTION TRAVEL-TIMES

Wide-angle reflections from the base of the crust are usually the most prominent arrivals observed on refraction seismograms and are seen more consistently than the corresponding head wave Pn. Bamford (1978) formulated a technique for the analysis of wide-angle reflections using a method similar to the time-term approach for refractions by solving the approximate $T^2/X^2$ relationship for reflections in a homogeneous one layered Earth. The use of the $T^2/X^2$ equation is a simplification: taking any realistic but still simple structure such as a multi-layered horizontally plane-layered structure the equations become very complicated: the parametric equations for such a model are given by Robinson (1970) and can be written:

$$X(n,\theta_1) = 2 \sin(\theta) \sum_{i=1}^{n} z_i \, v_i / S_i \quad (3.7)$$

$$T(n,\theta_1) = 2 v_1 \sum_{i=1}^{n} z_i / (v_i S_i)$$

where $$S = [ v_i^2 - ( v_i \sin\theta_i )^2 ]^{1/2}$$

$n$ - the subsurface is composed of n homogeneous layers

$v_i$ - the velocity of ith layer

$z_i$ - the depth of the ith layer

$\theta_1$ - the take off angle of the ray at the surface which reflects at the bottom of the nth layer

$X(n,\theta_1)$ - horizontal distance on the surface travelled by the ray

$T(n,\theta_1)$ - time taken by the ray to leave and return to the surface having been reflected from the bottomof the nth layer

T and X can be related by a series expansion given by Bamford (1978) which contains complicated velocity/layer depth relationships and so cannot be solved for the terms $z^2$ and $(1/v)^2$. In the $T^2/X^2$ equation these two terms are independent and so can be determined from a $T^2/X^2$ analysis. The effects of dips, refractions and inhomogeneities in the layers above a reflection zone can only be treated by ray tracing (Cerveny 1974).

Bamford (1978) corrected the wide-angle travel-times down to a datum within the layer immediately above the reflection zone using the known preliminary structure above the datum. However, it is probably only realistic to correct for the known shallow structure down to a datum just below the basement refractor; corrections to a deeper datum will propagate errors (due to inaccuracies in the preliminary structure between the deeper datum and the basement) into the

calculated reflecting interface.

### 3.4.1 Corrections to a Datum

Fig. 3.2 illustrates the variables used to correct to a datum below the varying shallow structure taken from Green (1984). The equations for the travel-time correction (dt) and the distance correction (dx) are:

$$dt = h_1 [\ 1/(v_1 \cos\theta_1) - 1/(v_2 \cos\theta_2)\ ] + h_d/(v_2 \cos\theta_2)]$$

$$dx = h_1(\tan\theta_1 - \tan\theta_2) + h_d \tan\theta_2 \qquad (3.8)$$

where

$$h_1 = a_g v_1 v_2 / (v_2^2 - v_1^2)^{1/2}$$

$$\cos\theta_1 = (1 - v_1^2/c^2)$$

$$\cos\theta_2 = (1 - v_2^2/c^2)$$

$$\tan\theta_1 = v /(c^2 - v_1^2)$$

$$\tan\theta_2 = v_2 /(c^2 - v_2^2)$$

where

$v_1$ - velocity of the sediment cover above the basement (Calculated from the results of Green (1984))

$v_2$ - refractor velocity of the basement (Green 1984)

$c$ - the apparent surface velocity over the shot or station

$h_1$ - depth to the basement

$a_g$ - time-term for the basement (Green 1984)

$h_d$ - datum depth

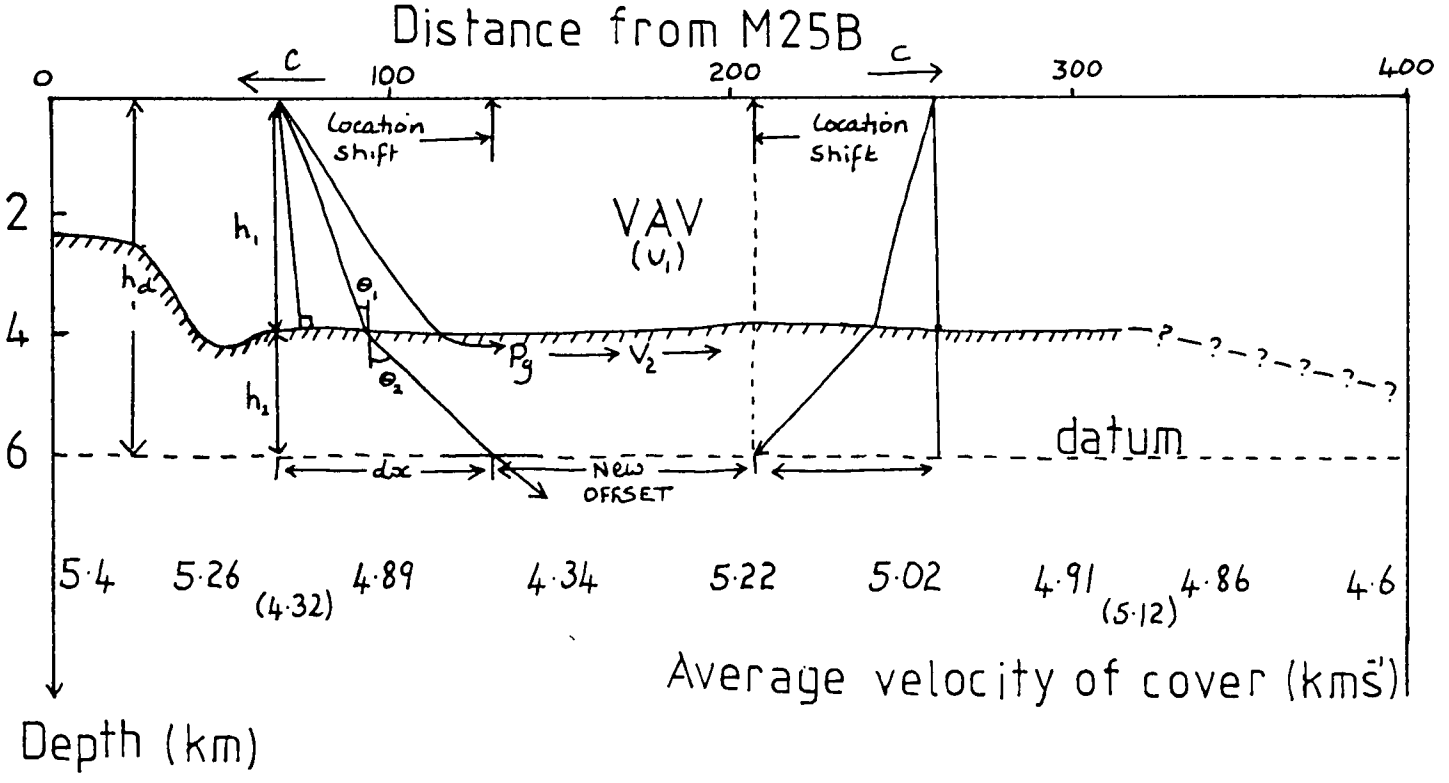


Figure(3.2) Sketch diagram illustrating the variables used to correct for the shallow structure. The average sediment cover velocities were derived from Green (1984).

The correction is applied to both the stations and the shots. The positions of each shot and station relative to M25B also change as well as the offsets and travel-times. This means that on the travel-time matrices the locations for each travel-time shifts appropriately as the positions of the shots and stations shift on the axes. The apparent surface velocities are calculated along common shot lines for the stations and common station lines for the shots.

### 3.4.2 Inversion of the Wide-angle Travel-times

To derive the equations needed to solve equation 3.1 for the terms $\tau^2$ and $1/v^2$ an approach similar to that used for the time-term method can be used. If there are m travel-time observations then the complete data set can be represented by the matrix equation

$$[A][\tau^2] = [T^2] - [X^2]/v^2$$

where

- M - is the number of common mid-points covered by the data
- $[T^2]$ - is an M x m travel-time matrix
- $[X^2]$ - is an M x m distance matrix
- $[\tau^2]$ - is an M x 1 matrix containing the two-way reflection travel-times squared
- [A] - is the M x m coefficient matrix

The coefficient matrix consists of m rows each containing a single 1 at the location corresponding to the common mid-point r for the particular shot/station pair used to measure the travel-time. The matrix $[A^TA]$ is a diagonal matrix where each value on the diagonal gives the number of travel-times

observed N(r) for each mid-point r=1...M. The inverse of a matrix such as $[A^TA]$ is a similar diagonal matrix with each value on the leading diagonal given by the inverse of the corresponding terms in the original matrix. Defining

$$[\tau^2] = [a] - [b]/v^2$$

then

$$[a] = [A^TA]^{-1}[A^T][T^2]$$

$$[b] = [A^TA]^{-1}[A^T][X^2]$$

The multiplication of $[A^T]$ with $[T^2]$ gives the sum of all squared travel-times for each common mid-point so that for common mid-point r

$$a_r = (1/N(r)) \sum_{n=1}^{N(r)} T_{rn}^2$$

$$b_r = (1/N(r)) \sum_{n=1}^{N(r)} X_{rn}^2$$

and

$$\tau_r = a_r - b_r/v^2$$

Substitution into the original equation

$$T_{rn}^2 = X_{rn}^2/v^2 + a_r - b_r/v^2 + d_r$$

defining

$$C_{rn} = T_{rn}^2 + a_r$$

$$D_{rn} = X_{rn}^2 - b_r$$

then the sum of the residuals I is given by

$$I = \sum_{r=1}^{M} \sum_{n=1}^{N(r)} ( C_{rn} - D_{rn}/v^2)$$

This equation is the same as that for the time-term method and the least squares velocity can be obtained using the equation

$$v^2 = \sum_{r=1}^{M} \sum_{n=1}^{N(r)} D_{rn}^2 \Big/ \sum_{r=1}^{M} \sum_{n=1}^{N(r)} C_{rn}.D_{rn}$$

and using this velocity the depth h can be found from the equation

$$h_r = 2\tau_r v$$

The equations for the solution uncertainties are similar to the formulae derived by Berry and West for the time-term method. The equations can be modified for lateral velocity changes and for slight velocity gradients above the reflector in the same way as is used for the time-term method.

### 3.4.3 Assumptions of the Wide-angle Reflection Method

The main assumptions in the method are:

1. the angle of incidence at the reflector is much greater than the dip of the reflecting interface. Bamford (1978) calculated that provided the dips of the reflector are less than +/-10 degrees the correction for the dip does not have to be applied.
2. the velocity structure above the reflecting region is homogeneous.
3. the station/shot offset X is a good estimate of the distance D between the normals to the interface from the station and shot.
4. the mid-point between the station and shot is a good estimate of the position of the reflecting point on the interface.

The theoretical fold for each common mid-point varies as illustrated in Fig.3.1. The actual fold will be less than these values as any phase is only observed over particular distance ranges. The actual fold for each mid-point can be estimated from the travel-time matrices with the data points displayed.

The main disadvantage of the method is that it preferentially weights the travel-time observations made at large offsets due to the distance squared term $X^2$. These are commonly the travel-times with the largest picking errors and these errors will be propagated into the calculated velocities and depths. To avoid this problem the equation 3.1 could be solved using non-linear optimisation techniques to obtain solutions for the two terms $\tau^2$ and $1/v^2$.

## 3.5 MODELLING

Modelling of the refraction sections was carried out using two synthetic seismogram packages. SYNSEI uses the reflectivity method formulated by Fuchs and Mueller (1971) as modified by Kennett (1975) to take into account shallow structural delays above the reflection zone. SEIS83 is based on generalized ray theory and was written by Cerveny and Psencik (1977). The programme RT01 was also used and is described by Green (1984).

### 3.5.1 SEIS83

The package SEIS83 calculates travel-times and amplitudes in a laterally varying structure and has the capability of dealing with vanishing layers and sharp lateral structures such as faults (Cerveny 1985). The complete package was obtained from Cambridge University and no major problems were encountered during its implementation onto the mainframe at Durham. The documentation attatched to the package is extensive and held in the file GPT9:SEI83.DOC: additional

documentation describing the implementation at Durham is presented in Appendix D. All the programmes in the package are suffixed by S83- and are held on GPT9.

There are five main steps involved to produce a synthetic model:

1. The initial 2-d velocity model is smoothed using the programme SMOOTH
2. The programme SEI83 uses the output from SMOOTH together with the input of the interfaces and station/shot positions to calculate travel-times and amplitudes of the rays requested.
3. The travel-times and model can be plotted using the programme RAYPLOT.
4. The synthetic seismograms are calculated using the output from SEIS83 and input of the source parameters by the programme SYNTPL which produces output in the format required by the project plotting programme CSSPLOT.

The main limitations of the ray theory method used by SEIS83 are

1. For crustal studies there is a shift of the singular (critical) points to nearer offsets by 10 or more km (Cerveny 1977, Gajewski and Prodehl 1985)
2. Only the rays requested in the input are calculated so that P-S conversions and full multiple reverberations are not produced.

### 3.5.2 Reflectivity Method

In contrast to methods using ray theory (which are time-domain techniques) the reflectivity method calculates the synthetic seismograms in the frequency domain: the integration of the reflectivity of a layered medium is carried out in the horizontal wavenumber (angle of incidence) domain. Multiplication of the reflectivity matrix with the source spectrum and inverse Fourier transformation yield the seismograms for the displacement components. The programme SYNSEI has been modified by Kennett (1975) to permit different upper surface structures above the reflection zone at shots and receivers: only elastic attenuation and time shifts are calculated for these layers. The main limitations of the method are

1. No lateral variations in the reflection zone are permitted.
2. There is a restriction to real angles so that surface waves are excluded. (Fuchs and Mueller 1971).

### 3.5.3 Modelling of the Caledonian Suture Seismic Project Data

The ray theory method must be used to model inhomogeneous structures. The reflectivity method should be used to study in more detail particular areas of the laterally varying structure deduced from SEIS83 modelling and to check the positions of critical points and frequency effects. The reflectivity method has been found to take about 30 percent longer than SEIS83 to produce final synthetic sections. Gajewski and Prodehl (1985) and Barton and Wood (1984) have

suggested that the synthetic seismogram modelling of the amplitudes on refraction seismograms should not be expected to yield exact agreement as much of the variations observable in the amplitudes depends on local near surface effects as much as on the deeper structure. To avoid this problem Gajewski and Prodehl (1985) have suggested that the amplitude ratios between Pg and PmP should be modelled. This type of modelling has not yet been tried on the Caledonian Suture Seismic Project data but such an approach may avoid the problems of the rapid variations in amplitudes observed on the common shot sections described in section 2.6.

# CHAPTER FOUR

# RESULTS

## 4.1 INTRODUCTION

This chapter presents the results obtained from the interpretation of the travel-time matrices and from the forward interpretation techniques using the time-term and related methods described in Chapter 3. 82 common station sections (Appendix A) and 58 common shot sections (Appendix B) were used to pick the 3414 travel-times for all phases; 558 for Pg, 698 for PcP, 1424 for PmP and 734 for Pn. All these travel-times are displayed on the sections in Appendices A and B. Appendix C contains all the common distance and common mid-point sections, and also, a representative selection of diagrams illustrating the typical fits of the various travel-time branches to equations 3.1 and 3.2 together with a set of summary plots of the complete regression analysis for each phase.

The description of the results follows the order used in Chapter 3. The variations in travel-times observed in the travel-time matrices are described and qualitative interpretations are made. The results from the wide-angle reflections are then presented followed by the time-term results. A final model is deduced which best fits the travel-times of the phases observed. This model is used as a starting point in the modelling stage of the interpretation process presented in Chapter 5.

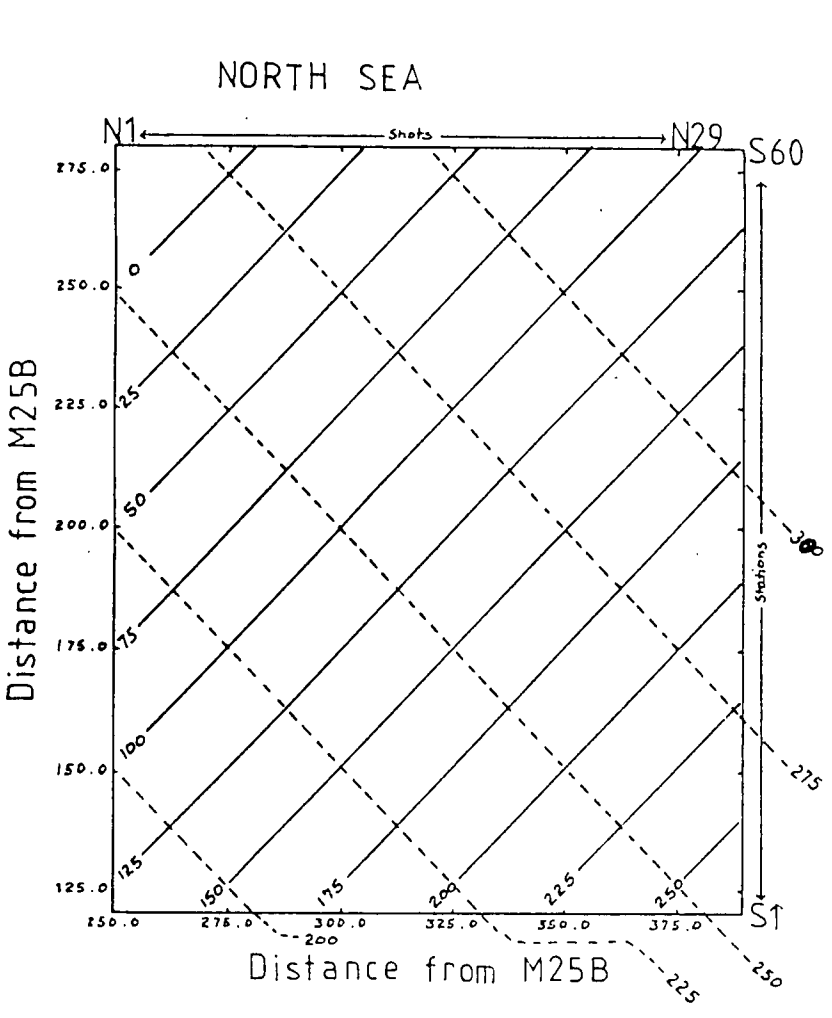


Figure(4.1) The travel-time matrices for the Irish and North Sea drawn with representative common mid-point and common distance lines.

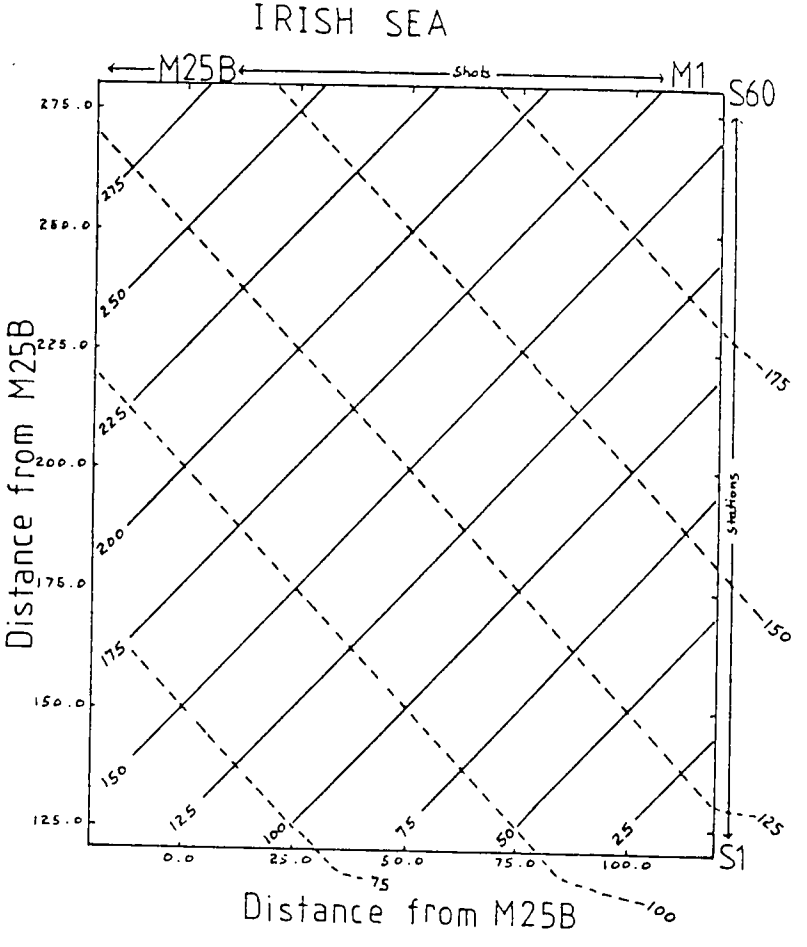

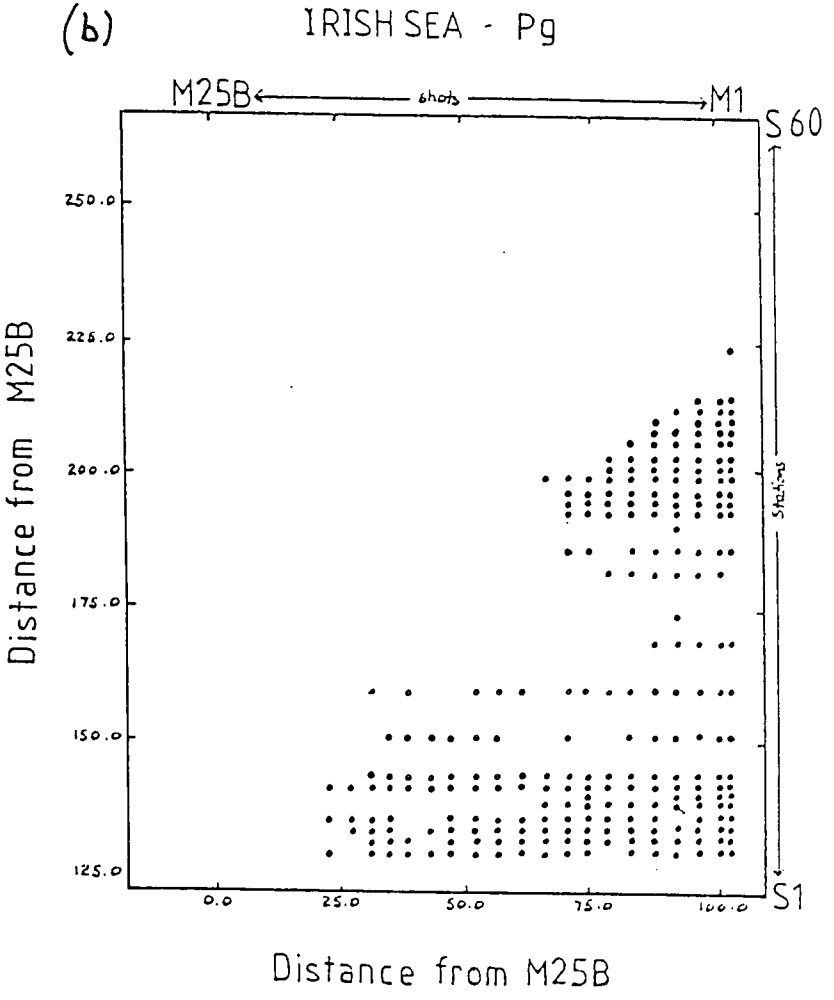


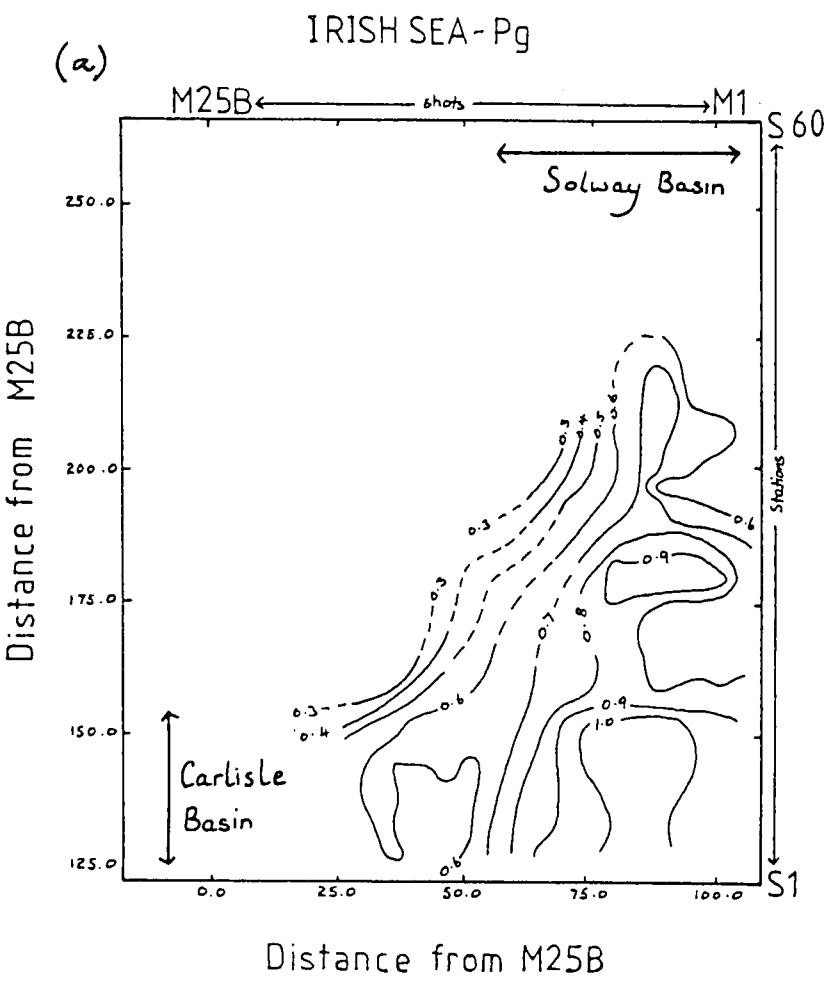


Figure(4.2a) Travel-time matrix for the phase Pg in the Irish Sea uncorrected for shallow structure
(a) reduced to a velocity of 6.0
(b) data points

Data Points = •

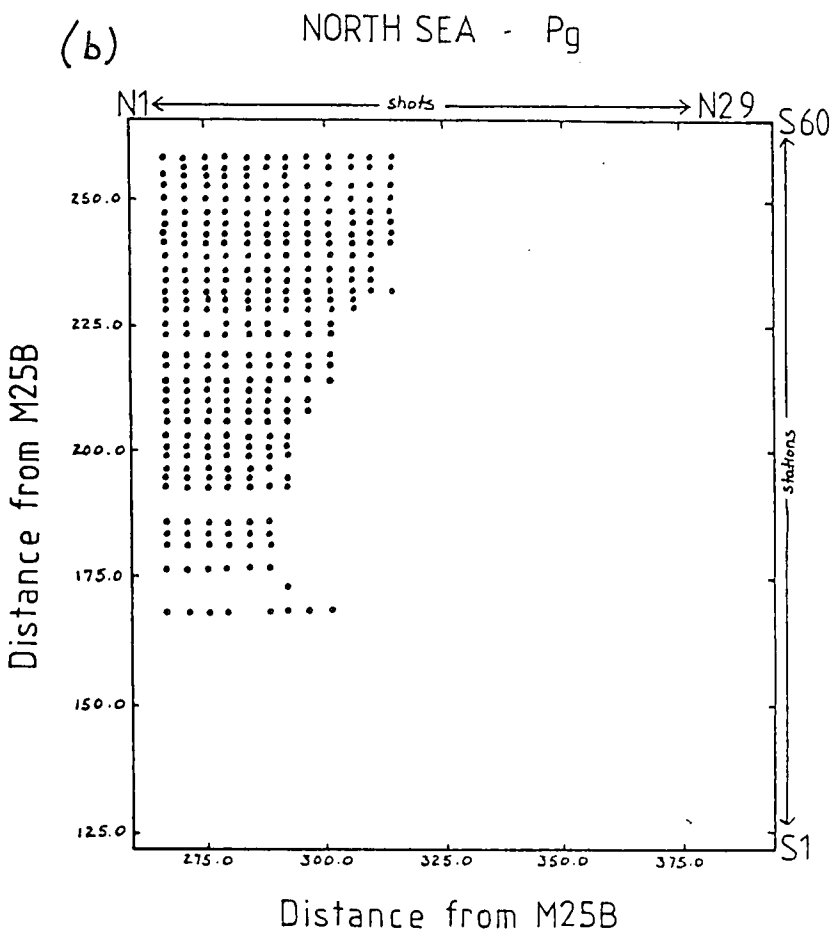


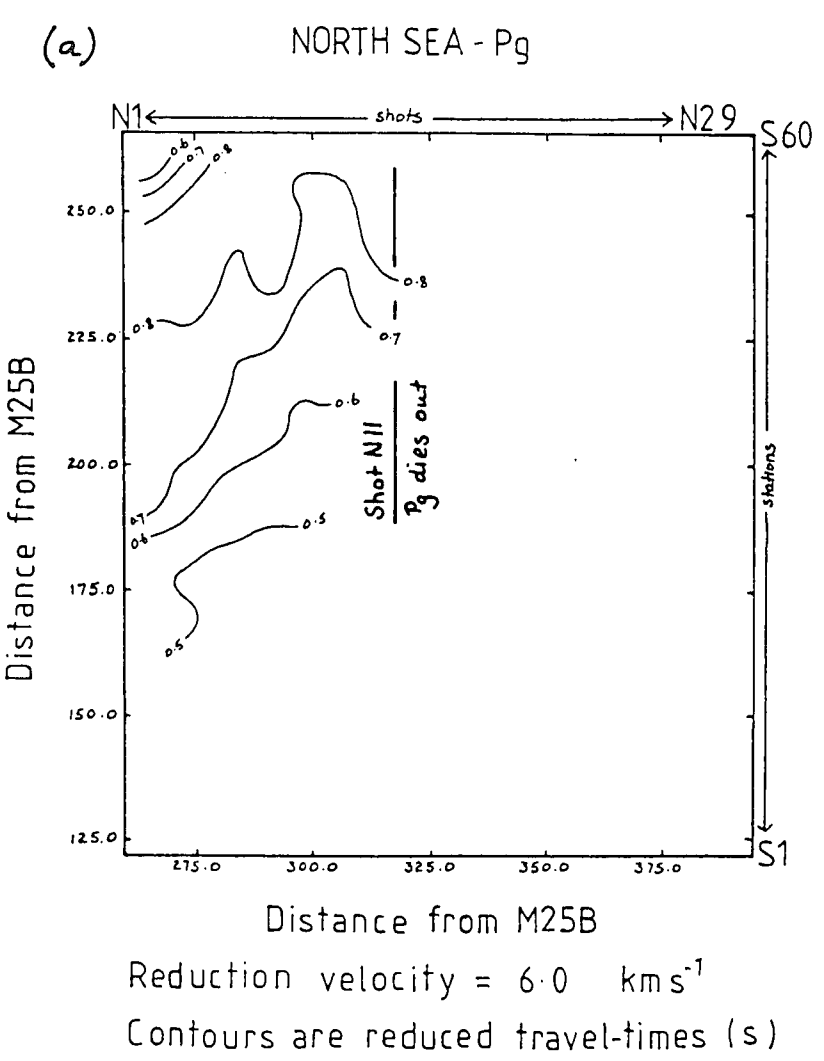


Data Points = •

Figure(4.2b) Travel-time matrix for the phase Pg in the North Sea
uncorrected for shallow structure
(a) reduced to a velocity of 6.0
(b) data points

## 4.2 INTERPRETATION OF THE TRAVEL-TIME MATRICES

Each phase is described in turn for the Irish Sea and North Sea respectively. All the matrices described in Section 3.1 are presented both uncorrected and corrected for the known shallow structure. Each corrected matrix has an overlay (Fig. 4.1) onto which is drawn representative common distance and common mid-point lines. The travel-time variations can be observed on the sections in Appendices A to C as well as on the travel-time matrices. The picking errors are estimated to be better than +/- 0.1 s for first arrivals and at least +/- 0.1 s for second arrivals.

The travel-time matrices for the phase Pg are displayed in Fig. 4.2. The delays due to the Solway Basin show up over the shot range M1 to M14 (102 to 47 km from M25b). The delays due to the Carlisle Basin show up over the station range 1 to 20 (129 to 170 km from M25B). These delays overlap in the travel-time matrix for Pg in the Irish Sea in the bottom right hand corner (Fig 4.2a). The disappearance of the phase Pg can be seen on Fig 4.2b at about the position of shot N11 in the North Sea. This phase has been treated in full by Green (1984).

### 4.2.1 The Travel-time Matrix for PcP for the Irish Sea Shots

This phase is difficult to observe on the sections due to the reverberations in the Solway Basin but is best seen on CST 8 M about 0.3 seconds behind Pg for shots M10-M16 (Appendix A). The contours in Fig. 4.3a are parallel to the common

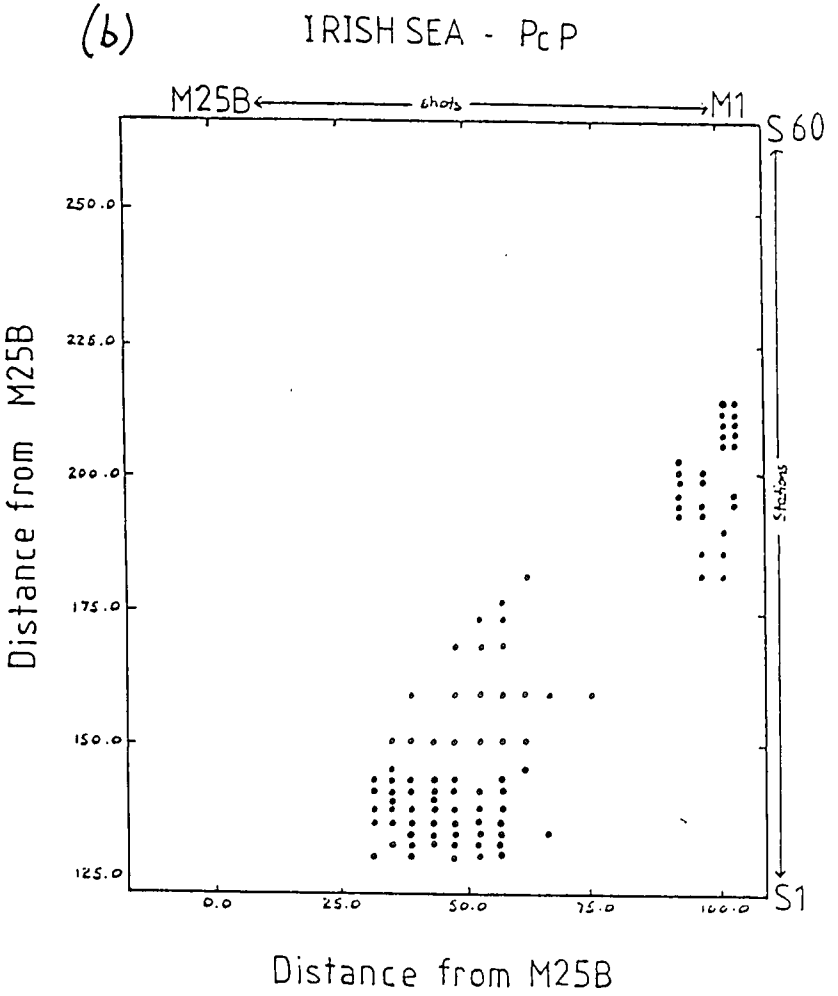


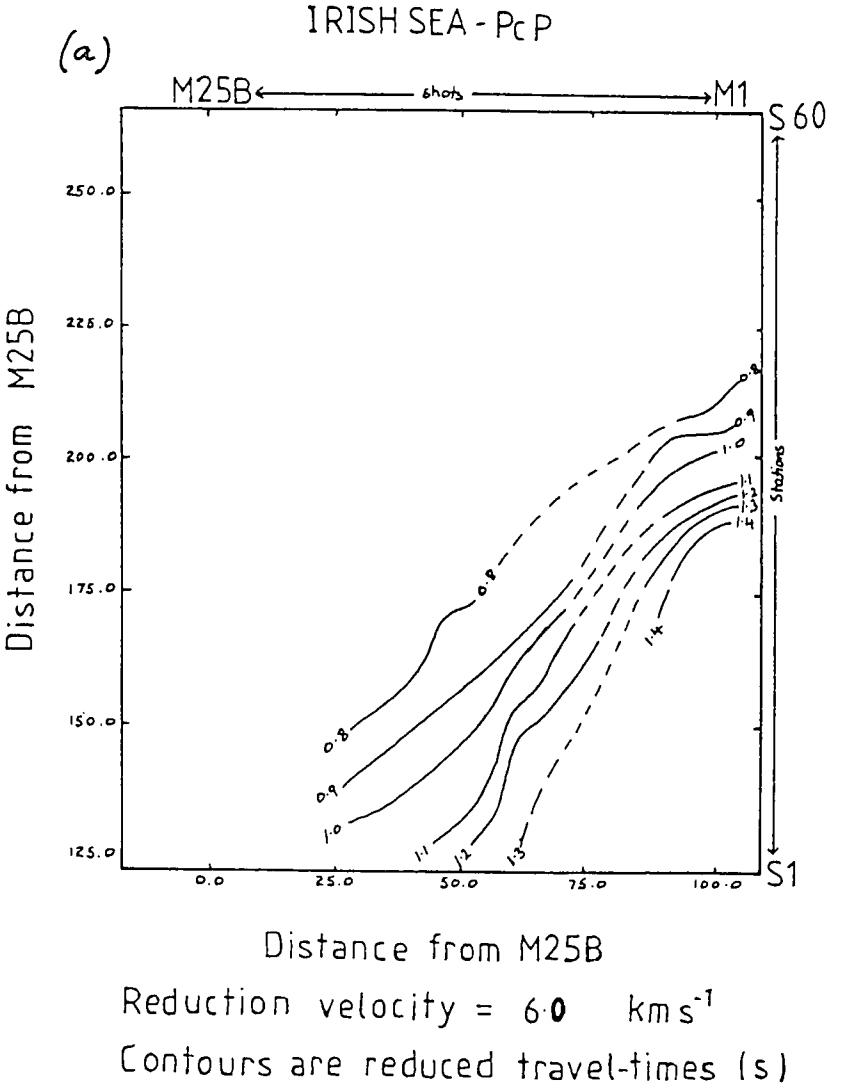


Figure(4.3a) Travel-time matrix for the phase PcP in the Irish Sea
(a) uncorrected for shallow structure
(b) reduced to a velocity of 6.0

Data Points = •

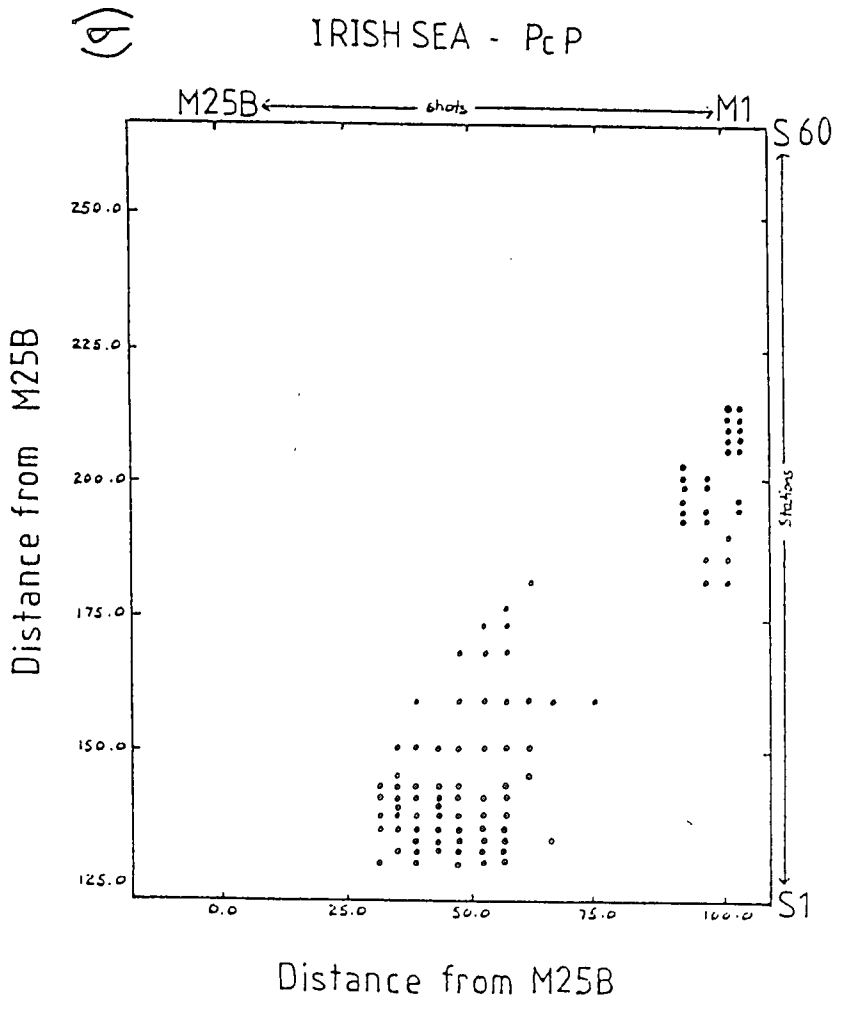


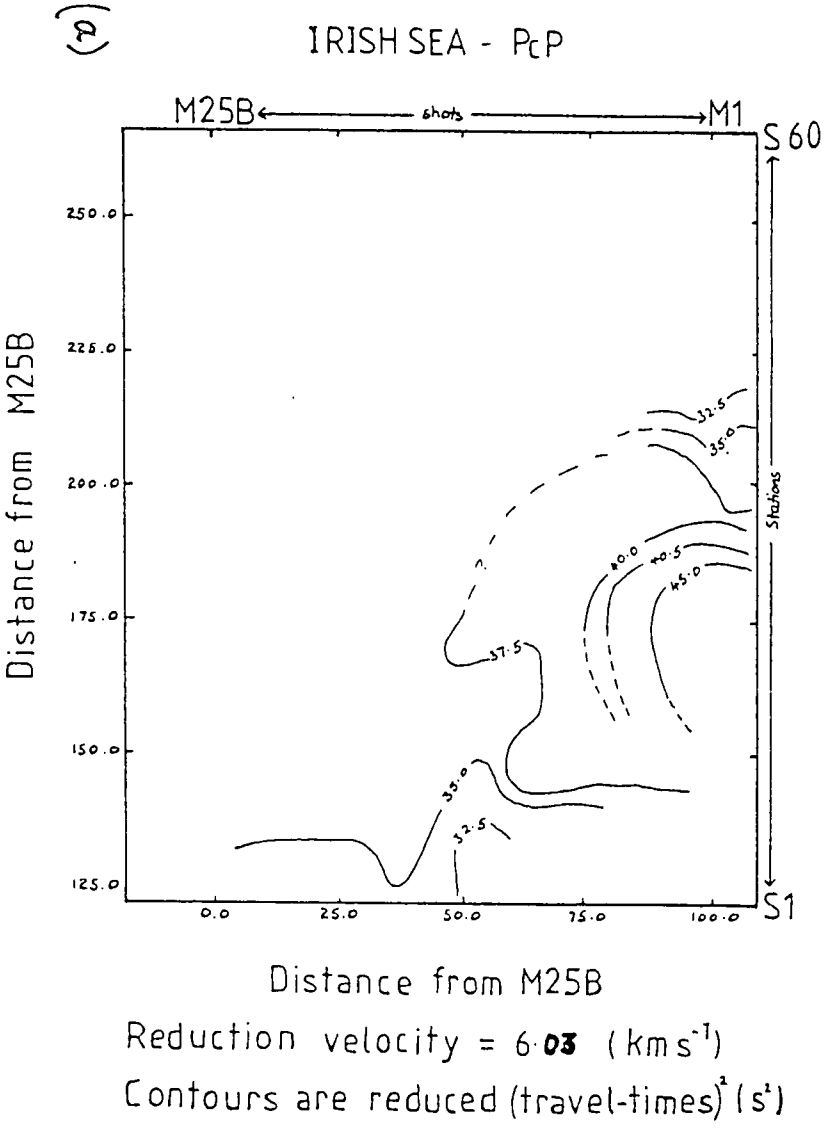


Figure(4.3b) Travel-time matrix for the phase PcP in the Irish Sea
uncorrected for shallow structure
(a) reduced to a velocity of 6.03 (km/s)
(b) data points

Data Points = •

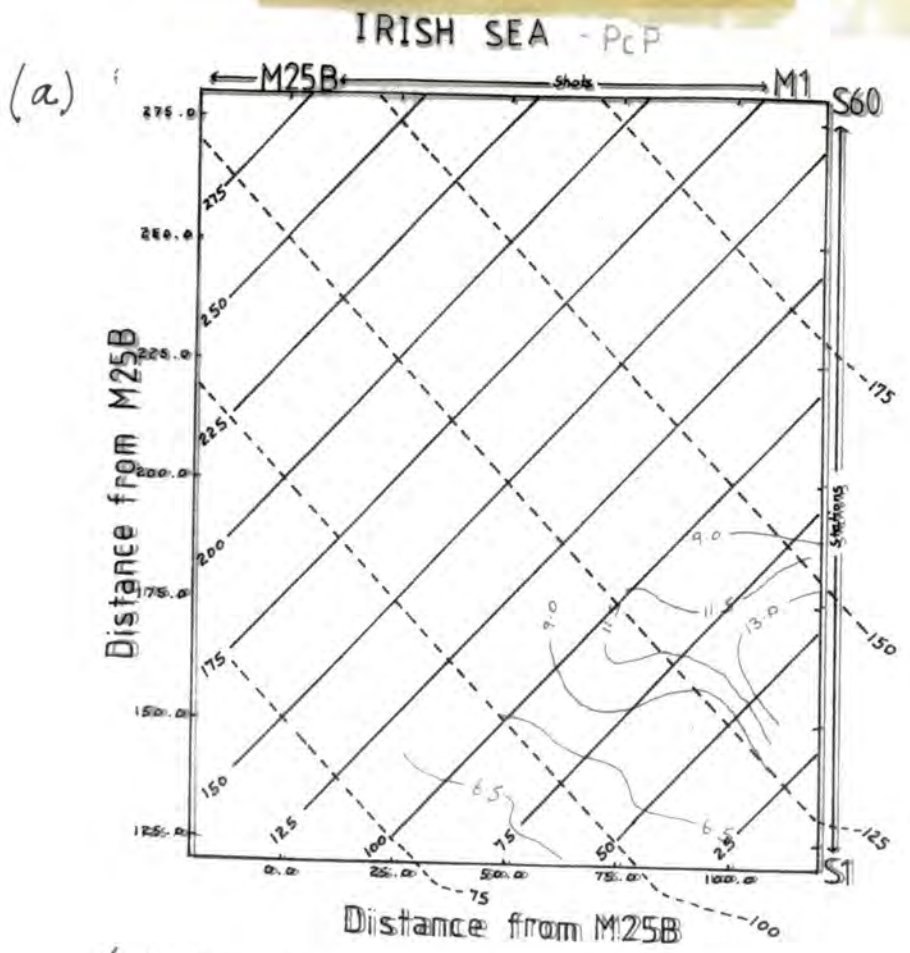


Figure(4.3c) Travel-time matrix for the phase PcP in the Irish Sea
corrected for shallow structure
(a) reduced to a velocity of 6.17 (km/s)
(b) data points
(c) overlay of the common distance
and common shot lines

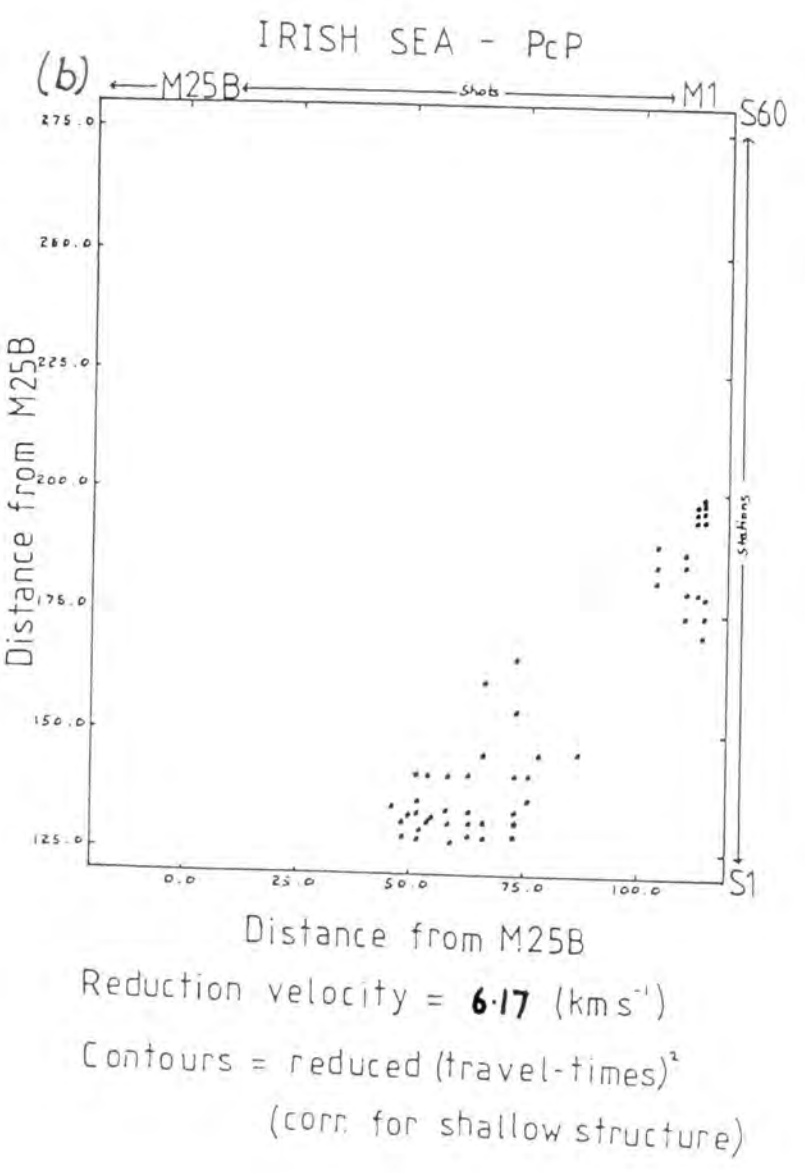

distance direction which indicates no major lateral variations in structure. The travel-time picking errors for PcP in the Irish Sea are 0.10 to 0.25 s which give errors from 4.0 to 10.0 $s^2$ for the travel-times squared for a travel-time of around 20.0 s. The contour interval used in the matrices displaying the travel-times squared is 2.50 $s^2$ which lies within the error range. To the degree of accuracy possible it appears that the PcP reflecting interface must be interpreted as nearly horizontal.

### 4.2.2 The Travel-time Matrix for PcP for the North Sea Shots

The PcP phase in the North Sea is observed over common mid-point positions from 200 to 365 km from M25B and at station to shot offsets from 30 to 125 km. It is a first arrival for shots N9 to N25 for most stations and so the travel-time picking errors are more accurate than for PcP in the Irish Sea. The contour interval used is 0.1 s in Fig. 4.4a and 2.5 $s^2$ in Figs. 4.4b and 4.4c. Three main features are observed on the travel-time matrix for PcP (Fig. 4.4b):

1. The feature labelled A represents a decrease of the travel-times east of the common mid-point position 250 km.
2. The feature labelled B on the matrices displaying the travel-times squared (Fig. 4.4b) is a delay over the shot range N20 to N25 (which lie 348 and 371 km from M25B).
3. The feature labelled C is a rapid increase in the travel-times from shot N14 to N20 (which lie 322 to 348 km from M25B).

All three features remain after correcting for the known shallow sediment delays down to a datum at 6.0 km depth (Fig.

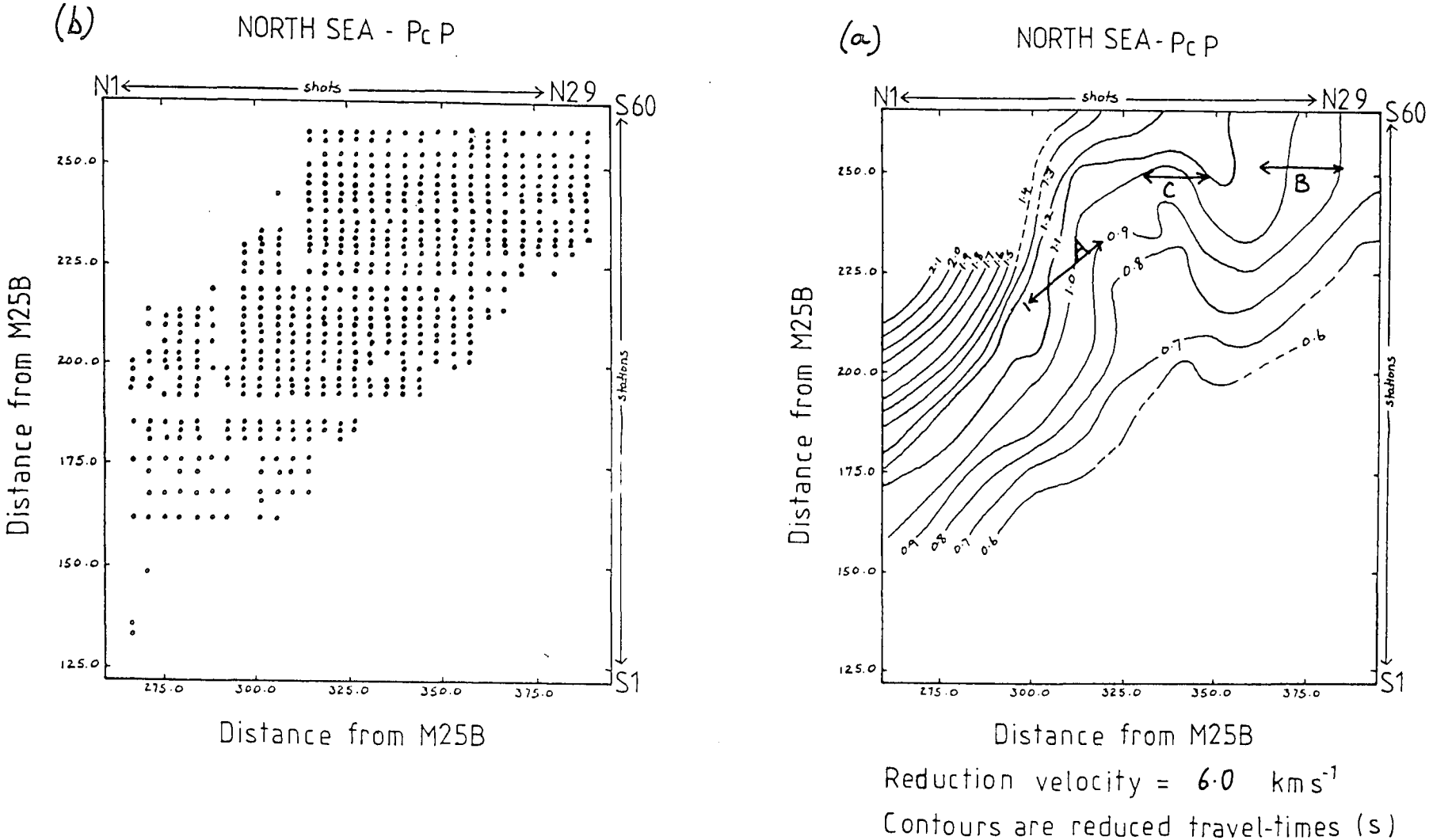


Figure(4.4a) Travel-time matrix for the phase PcP in the North Sea
uncorrected for shallow structure
(a) reduced to a velocity of 6.0
(b) data points

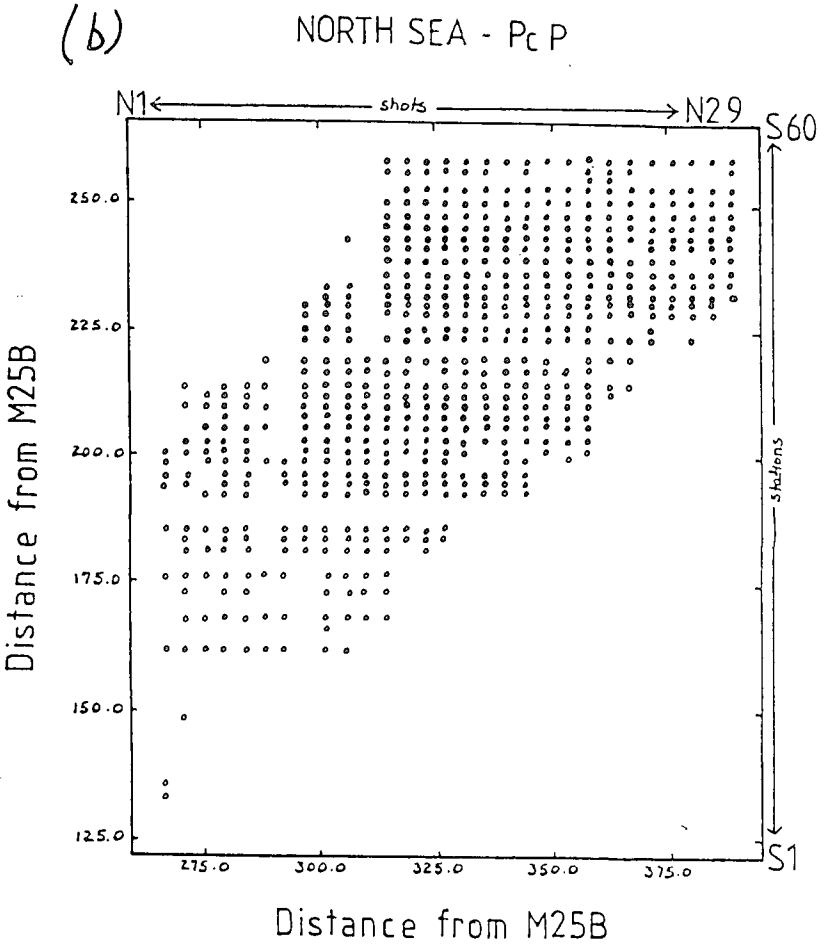


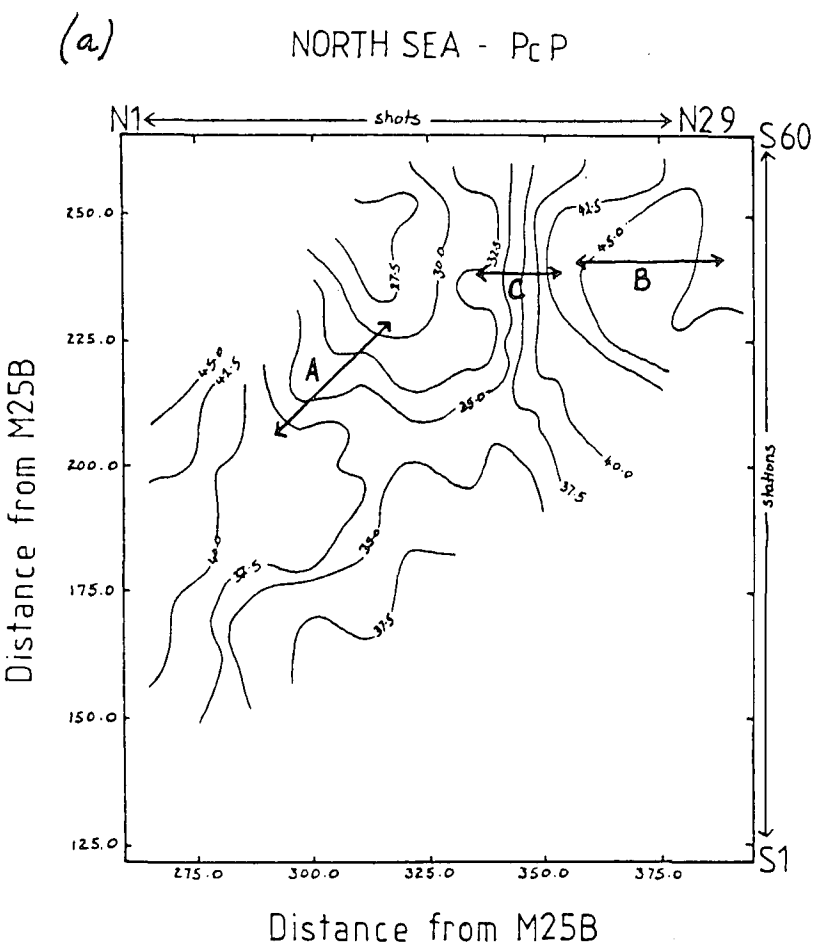


Data Points = ∘

Figure(4.4b) Travel-time matrix for the phase PcP in the North Sea
(a) uncorrected for shallow structure
(b) reduced to a velocity of 6.03 (km/s)
data points

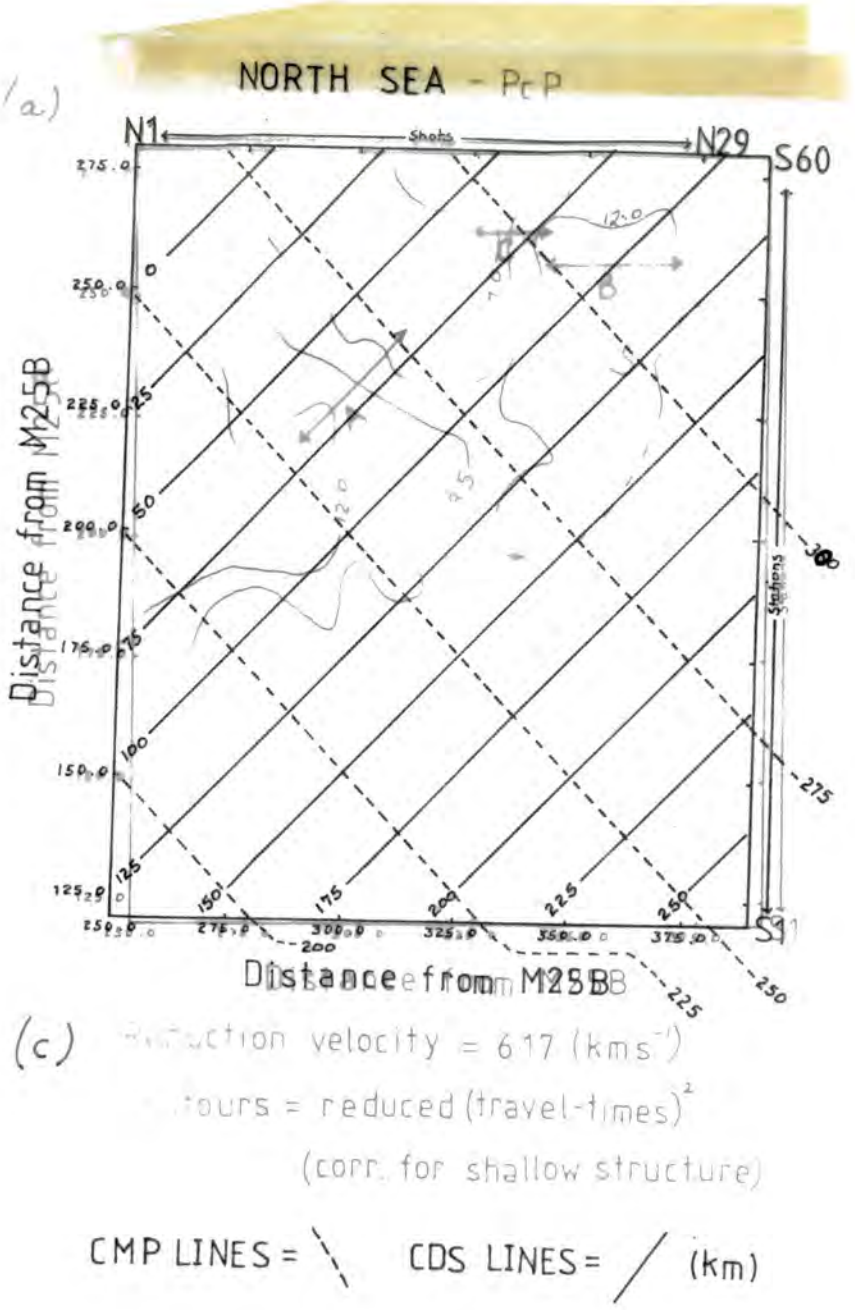


Figure(4.4c) Travel-time matrix for the phase PcP in the North Sea
(a) corrected for shallow structure
(b) reduced to a velocity of 6.17 (km/s)
(c) overlay of the common distance and common shot lines

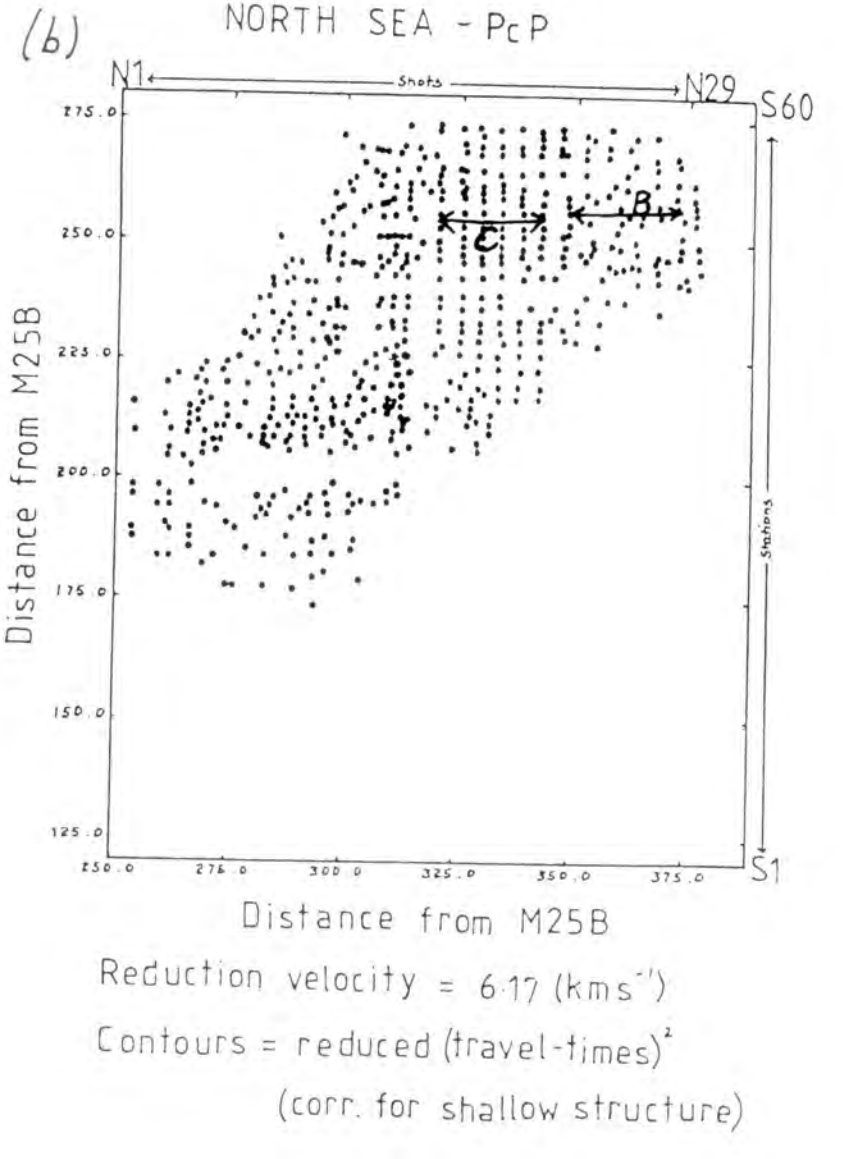

4.4c). It can be concluded that:

1. Feature A is an abrupt decrease in travel-times from the common mid-point positions of 250 to 275 km caused by either an increase in the average crustal velocity or a rise in the mid-crustal interface.
2. The area over which feature B is observed displays scattered travel-time points in Fig. 4.4c which indicates that the corrections for the known shallow structure have been applied adequately. This feature is possibly due to unknown near surface structures. The delays in the travel-times occur over a shot range which coincides with the position of the offline granite identified by Donato et al (1982) from a gravity interpretation of the area. Green (1984) also identified a lower velocity under the shots east of N11. It appears that this lower velocity is limited to the shot range N20 to N25.
3. Feature C is caused by the deepening of the 5.6 km/s layer identified by Green (1984) at a common mid-point position of about 310 km (Fig. 1.2). The apparent velocities above the feature are higher on its western side but lower on its eastern side at values less than 6.15 km/s (the basement refractor velocity). This means that the square root term in the equation used to correct for the shallow sediment delays (equation 3.8) becomes negative and the correction method breaks down. To avoid this problem the apparent velocity is set equal to the basement velocity plus a small increment of 0.1 km/s where it is less than the basement refractor velocity. The grid pattern of the positions of the travel-time data points displayed in Fig. 4.4c around feature C result from using

the same apparent velocities equal to the refractor velocity plus the increment of 0.1 km/s. The positions of the stations and shots all have similar distance corrections applied so that the original grid pattern observed in Fig. 4.4b is preserved in Fig. 4.4c. Feature C is not adequately removed by the correction routines over the shot range N14 to N20.

### 4.2.3 The Travel-time Matrix for PmP in the Irish Sea

PmP for the Irish Sea shots is observed over the common mid-point positions 60 to 180 km and at station to shot offsets from 75 to 225 km (Fig. 4.5). The coverage from station 8 to 30 is poor. The contour lines do not run exactly parallel to the common distance direction in Fig. 4.5a. For instance the travel-times along CDS/150.0 km decrease from CMP60/M1 to CMP1/M25B by about 0.35 s. This may indicate a rise in the Moho or an increase in the average crustal velocity towards the west. Two main features are visible in Fig. 4.5b:

1. The feature labelled A is an abrupt eastward increase in the travel-times which occurs for all stations in the vicinity of shot M14 (47 km from M25B). This marks the western edge of the Solway Basin and the feature is effectively removed by correcting for the known shallow structure (Fig. 4.5c).
2. The feature labelled B is a local increase in travel-times observed for arrivals from shots M10 to M14 which lie 47 to 65 km from M25B on the western side of the Solway Basin. This feature is accentuated by applying the

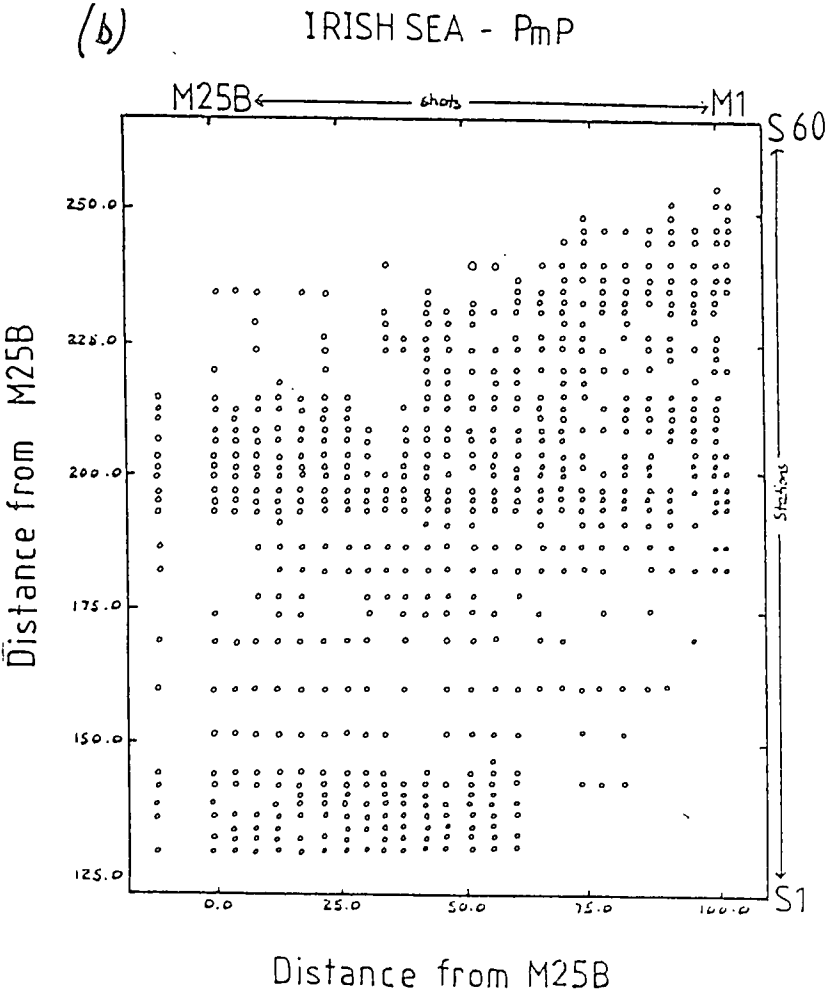


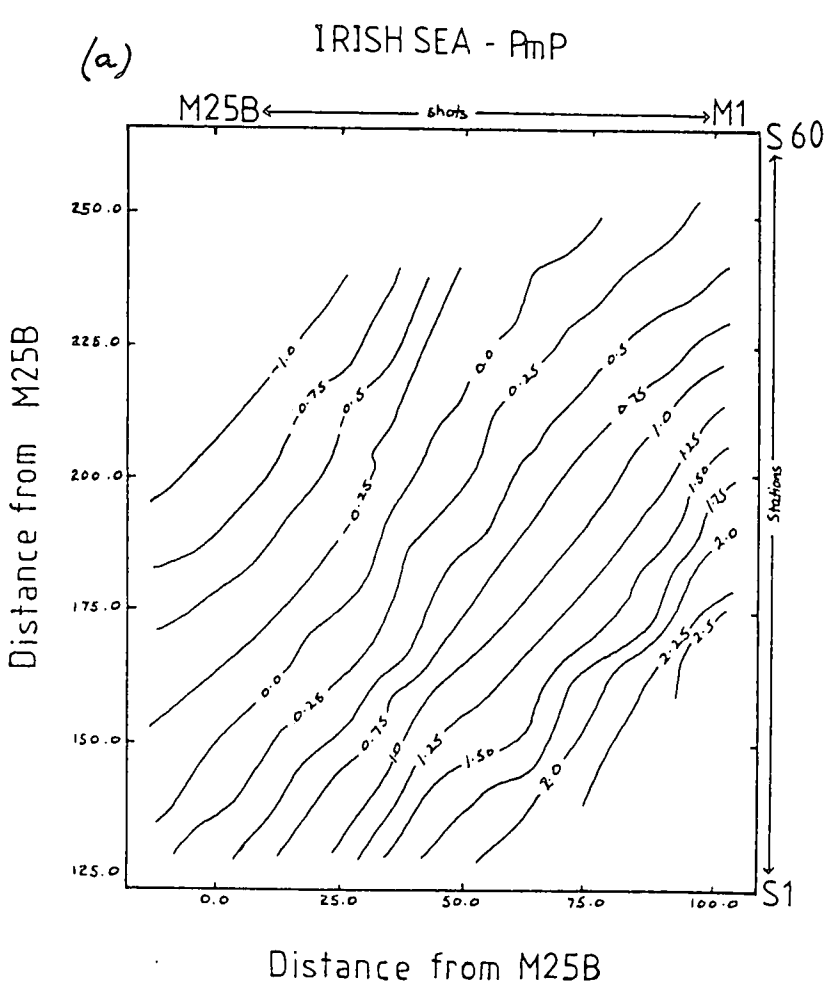


Figure(4.5a) Travel-time matrix for the phase PmP in the Irish Sea
(a) uncorrected for shallow structure
(b) reduced to a velocity of 6.0
data points

Data Points = ∘

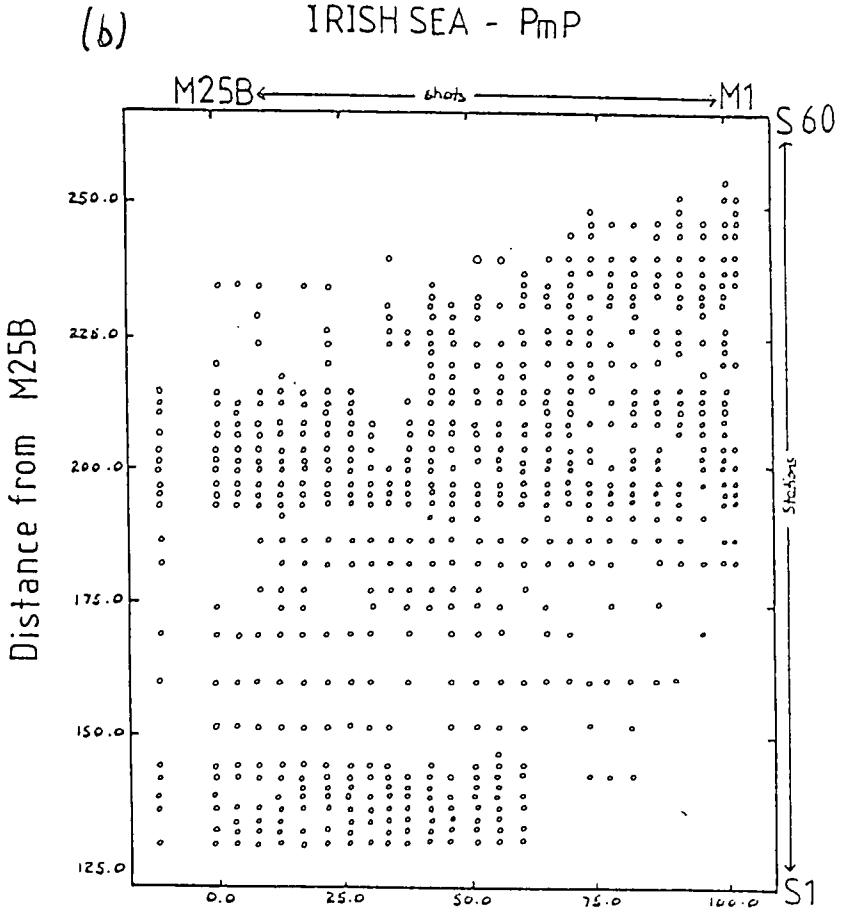


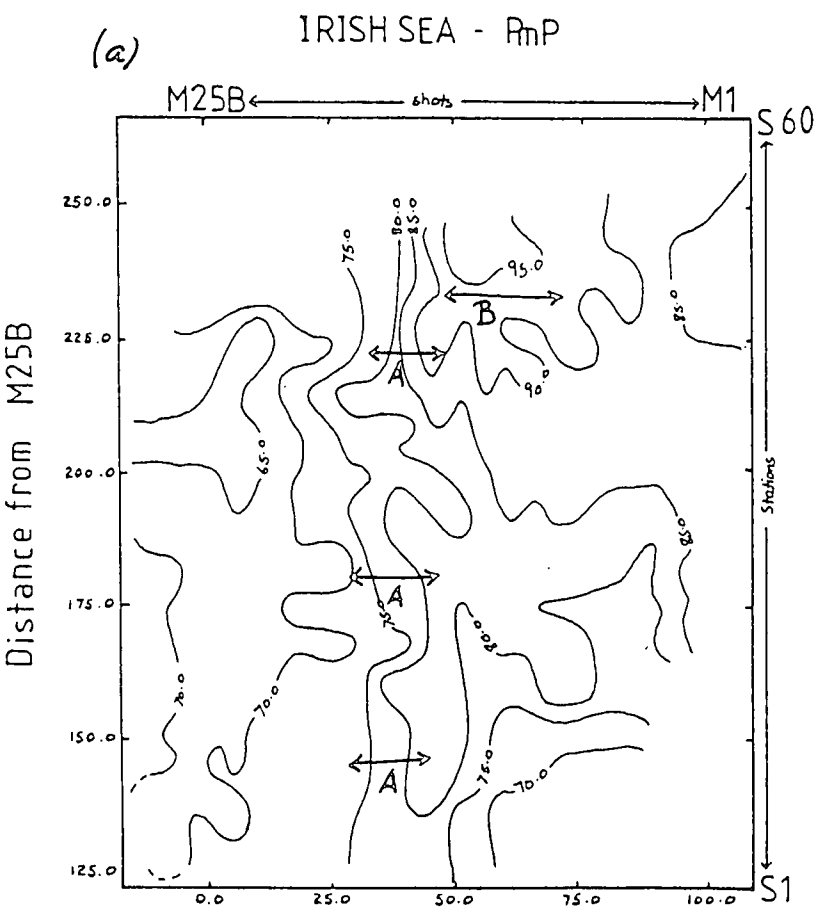


Figure(4.5b) Travel-time matrix for the phase PmP in the Irish Sea
(a) uncorrected for shallow structure
(b) reduced to a velocity of 6.37 (km/s)
data points

Data Points = ∘

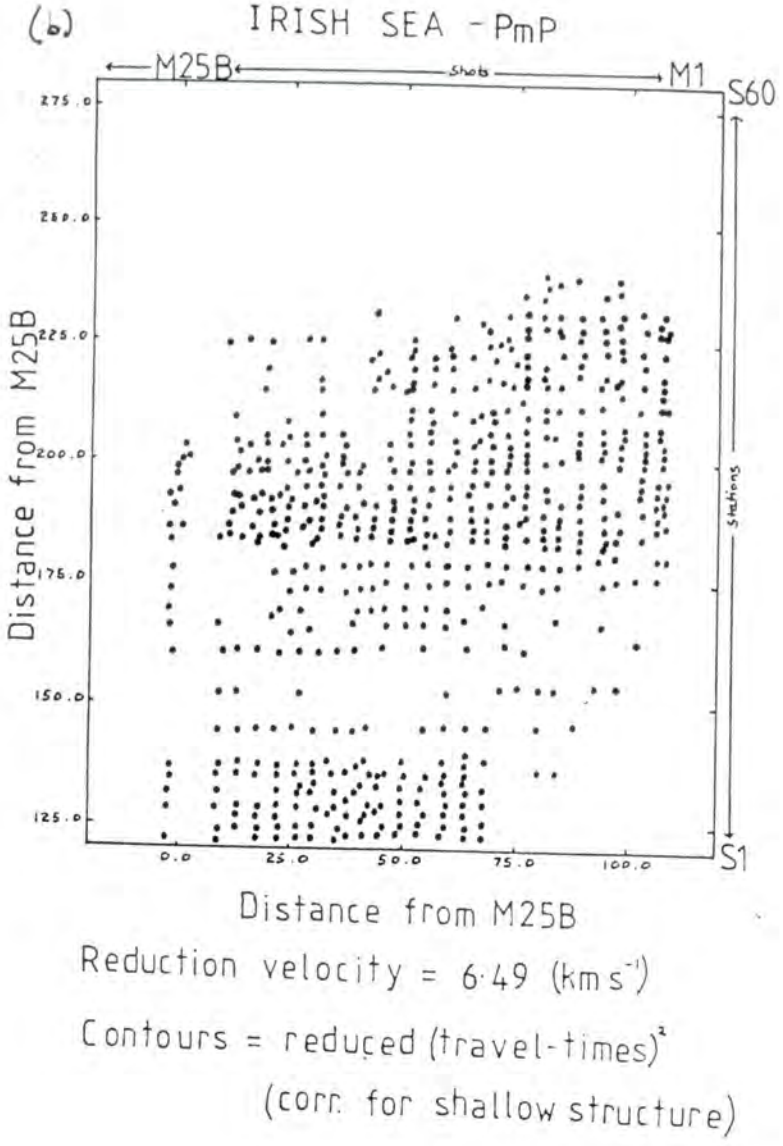


Figure(4.5c) Travel-time matrix for the phase PmP in the Irish Sea corrected for shallow structure
(a) reduced to a velocity of 6.49 (km/s)
(b) data points
(c) overlay of the common distance and common shot lines

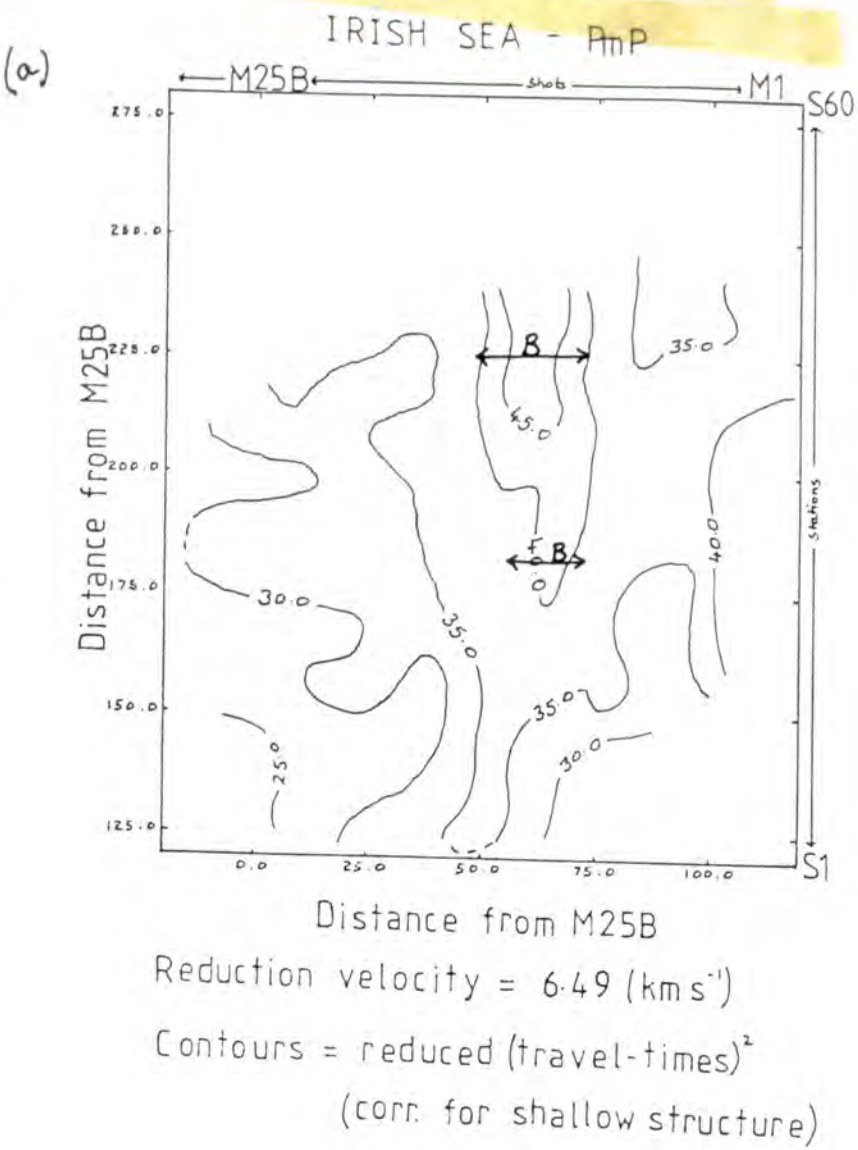

correction for the shallow structure (Fig. 4.5c). This feature is also observed on the corrected travel-time matrix for the phase Pn in the Irish Sea for the same shots (Fig. 4.7c). The PcP travel-times did not cover these shot ranges adequately but the PcP interface has been interpreted as being flat implying that the feature B originates below the mid-crustal interface or is due to an undetected structure on the mid-crustal interface or above it. The travel-times were difficult to pick for shots M1 to M14 because of the interference of the two wide-angle reflection phases PmP and PcP (see picks displayed on sections in Appendices A and B). In addition the amplitudes of all the phases are reduced for shots M11 to M14 possibly due to spurious interference and defocussing effects caused by the westwards shallowing of the Solway Basin (Appendix A).

### 4.2.4 The Travel-time Matrix for PmP in the North Sea

PmP in the North Sea is observed over common mid-point positions from 145 to 375 km and at station to shot offsets from 60 to 200 km. The problems encountered during the correction for the known shallow structure of the PcP phase in the North Sea over the rise in the 5.6 km/s layer (Section 4.2.2) are not encountered for PmP because of the higher apparent velocities which are all greater than the basement refractor velocity. The contour lines are slightly oblique to the common distance lines. The travel-times along the common distance directions decrease from CMP60/N29 to CMP60/N1 indicating either a westwards rise in the Moho or increase in

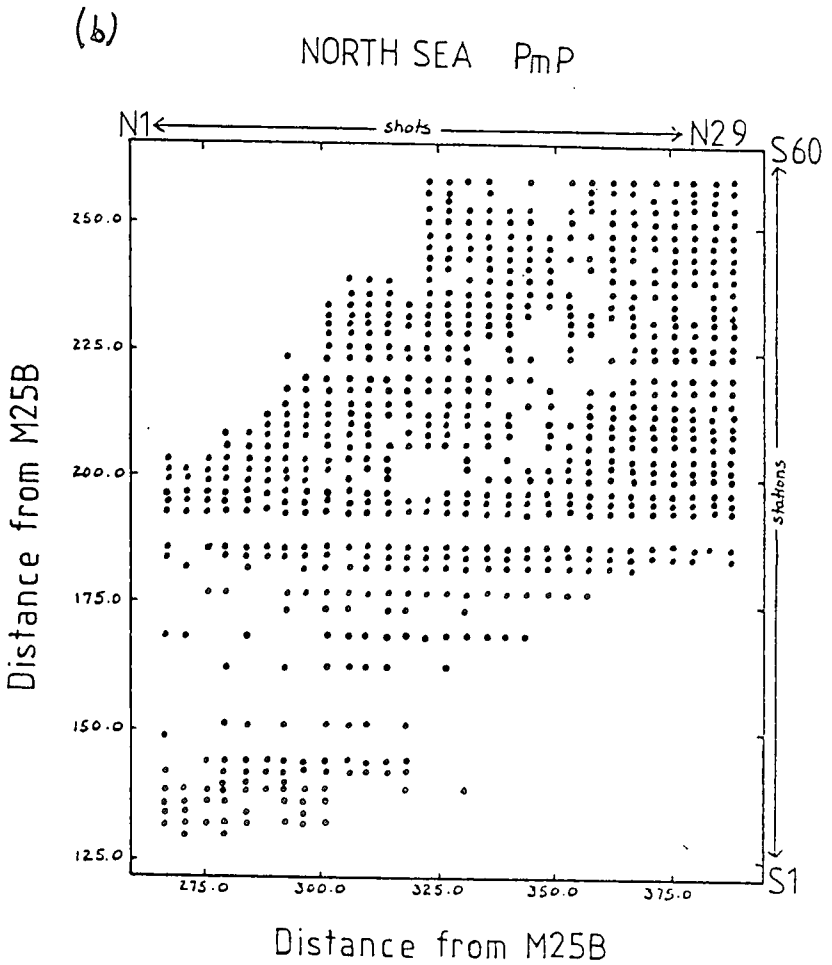


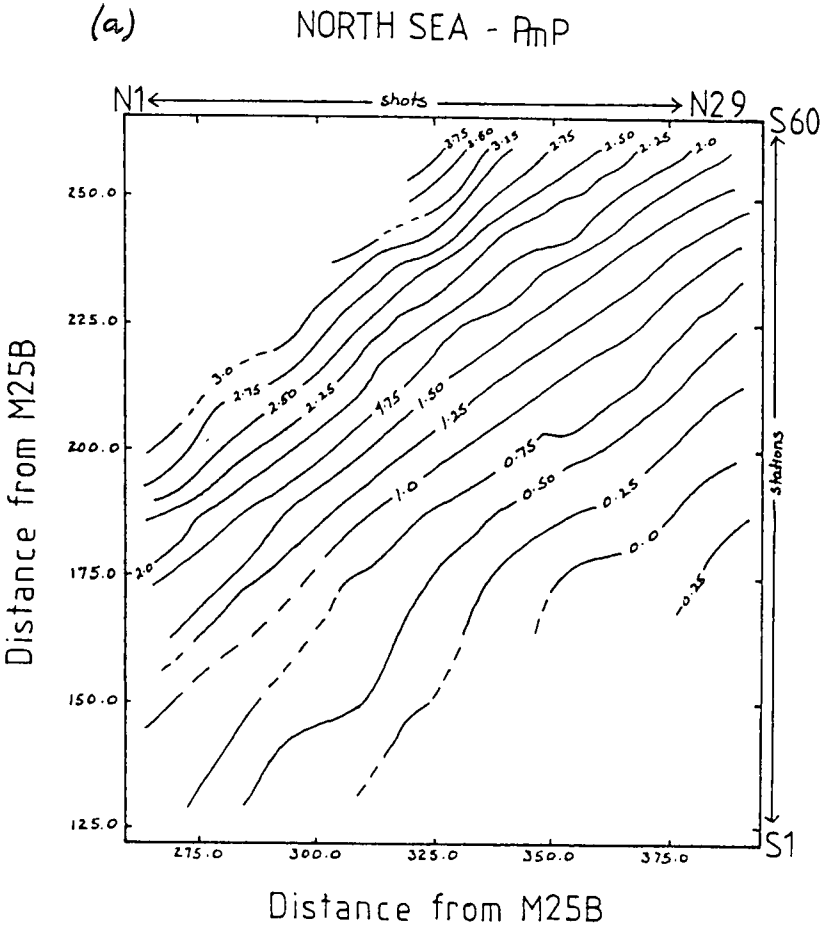


Figure(4.6a) Travel-time matrix for the phase PmP in the North Sea
(a) uncorrected for shallow structure
(b) reduced to a velocity of 6.0
data points

Data Points = •

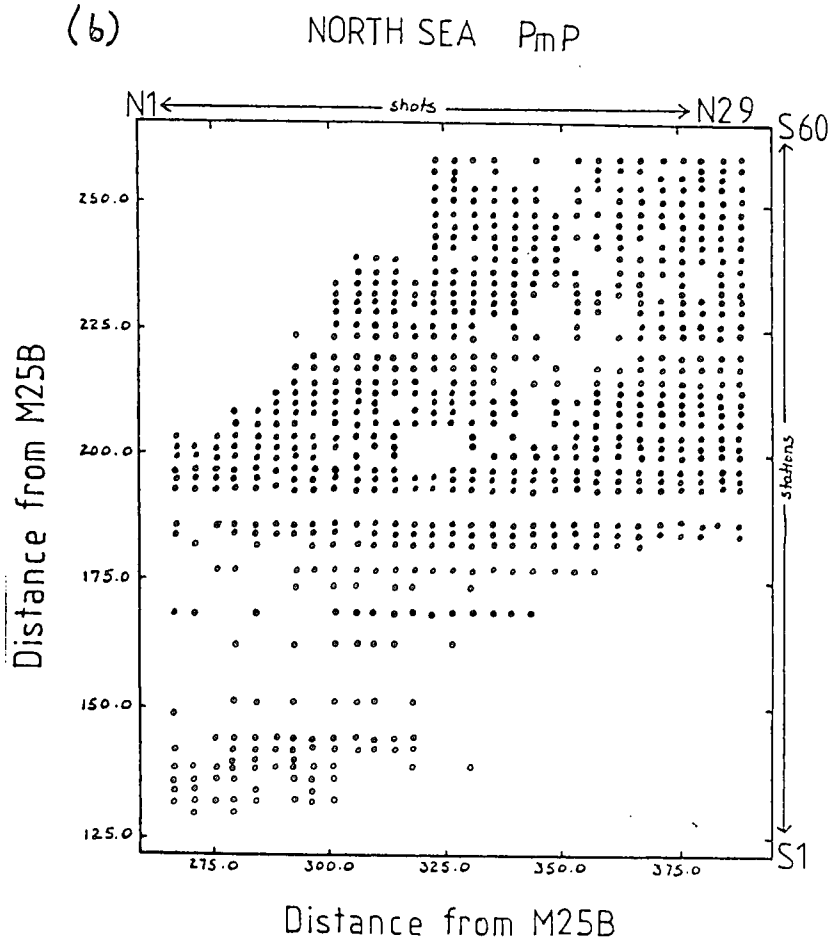


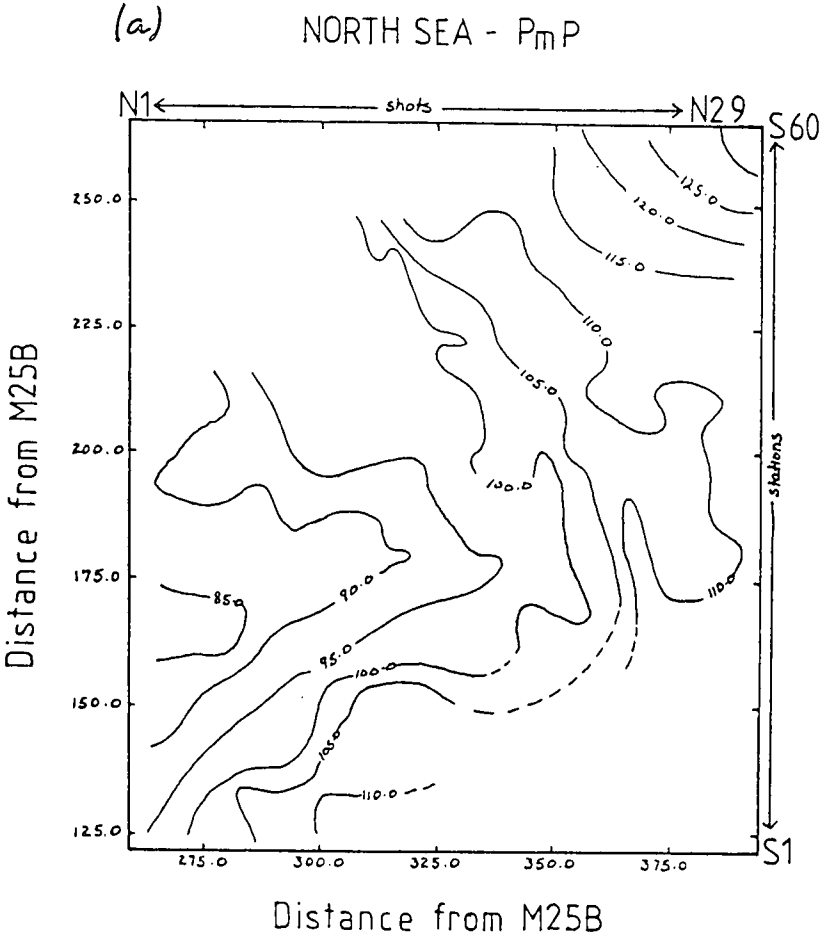


Data Points = •

Figure(4.6b) Travel-time matrix for the phase PmP in the North Sea
(a) uncorrected for shallow structure
(b) reduced to a velocity of 6.37 (km/s)
data points

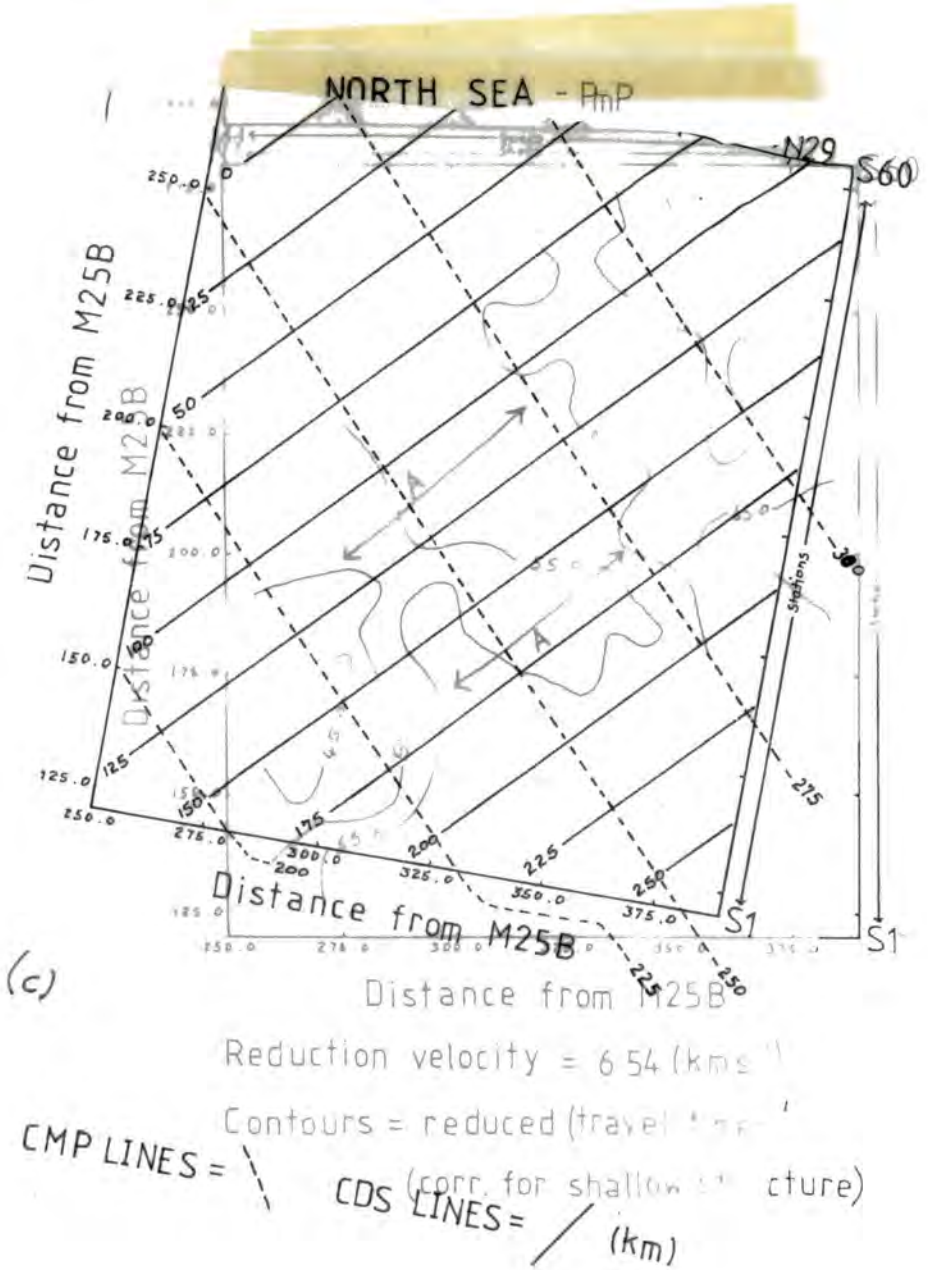


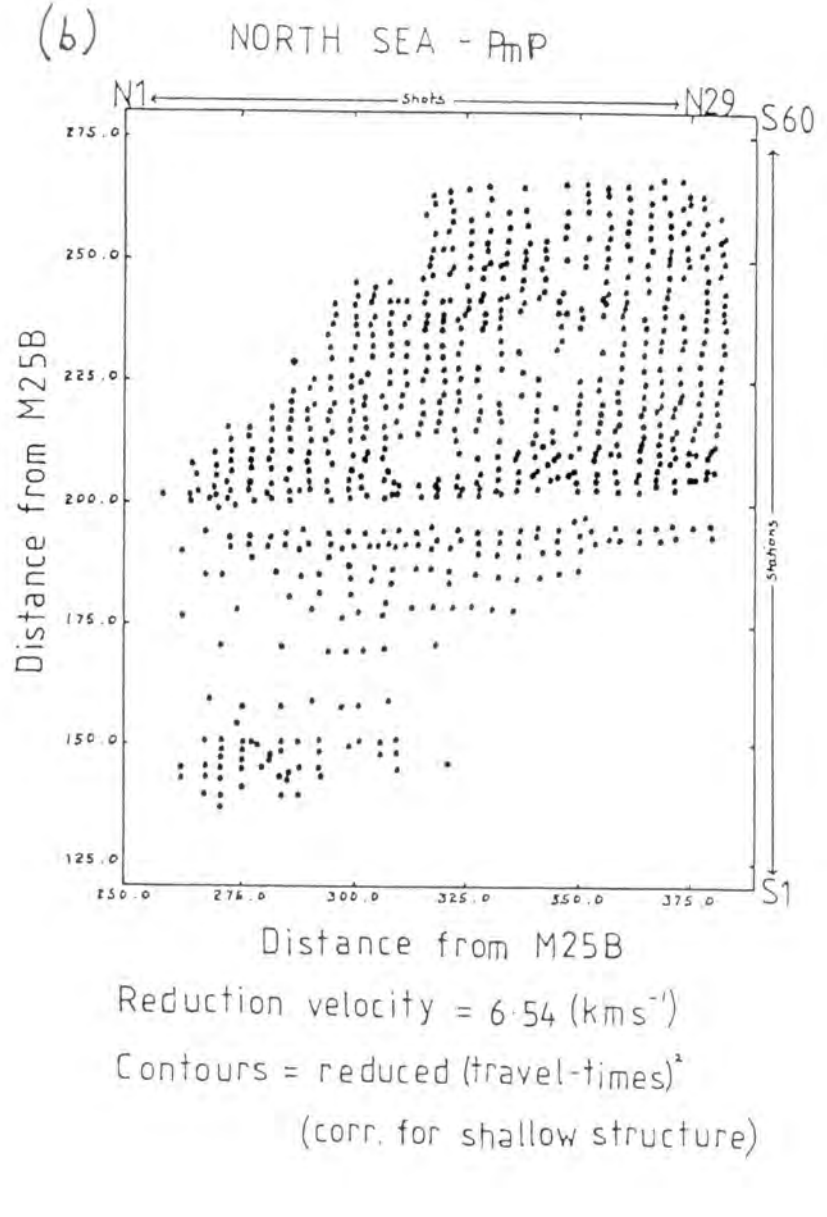


Figure(4.6c) Travel-time matrix for the phase PmP in the North Sea corrected for shallow structure
(a) reduced to a velocity of 6.54 (km/s)
(b) data points
(c) overlay of the common distance and common shot lines

the average crustal velocity. Comparable delays to that observed for shots N20 to N25 for PcP (labelled B in Fig. 4.4c) are not clearly visible in Fig. 4.6c due to the greater picking errors in the travel-times for PmP.

The feature labelled A on Fig. 4.6c is interpretated as the expression of the step in the mid-crust deduced from PcP (Fig. 4.4c). It is observed over the common mid-point range 250 to 225 km for PcP. For PmP it appears across the common mid-point positions from 235 to 260 km as a flat area within a general decrease in the travel-times across the common mid-point positions from 200 to 350 km. Any structures in a mid-crust at a depth of about 15 km would appear, assuming a crustal thickness of 30 km, in the travel-times for a PmP phase at common mid-point positions displaced laterally by 15 km. This corresponds to the 15 km offset observed between the effect of the step in the mid-crust in the PmP matrix compared to the PcP matrix.

### 4.2.5 The Travel-time Matrix for Pn in the Irish Sea

Pn in the Irish Sea is observed at station to shot offsets from 125 to 225 km. The coverage is poor for stations 1 to 19. The travel-times are reduced to a velocity of 8.0 km/s in Fig. 4.7a and 8.1 km/s in Fig. 4.7b. The feature labelled A in Fig. 4.7b is the delay also observed on the PmP matrix (Fig.4.5c) over the shot range M10 to M14 and is attributed to a delay above the base of the lower crust. Otherwise the travel-time contours are approximately parallel to the common station direction for most stations in the Pn matrix (Fig.

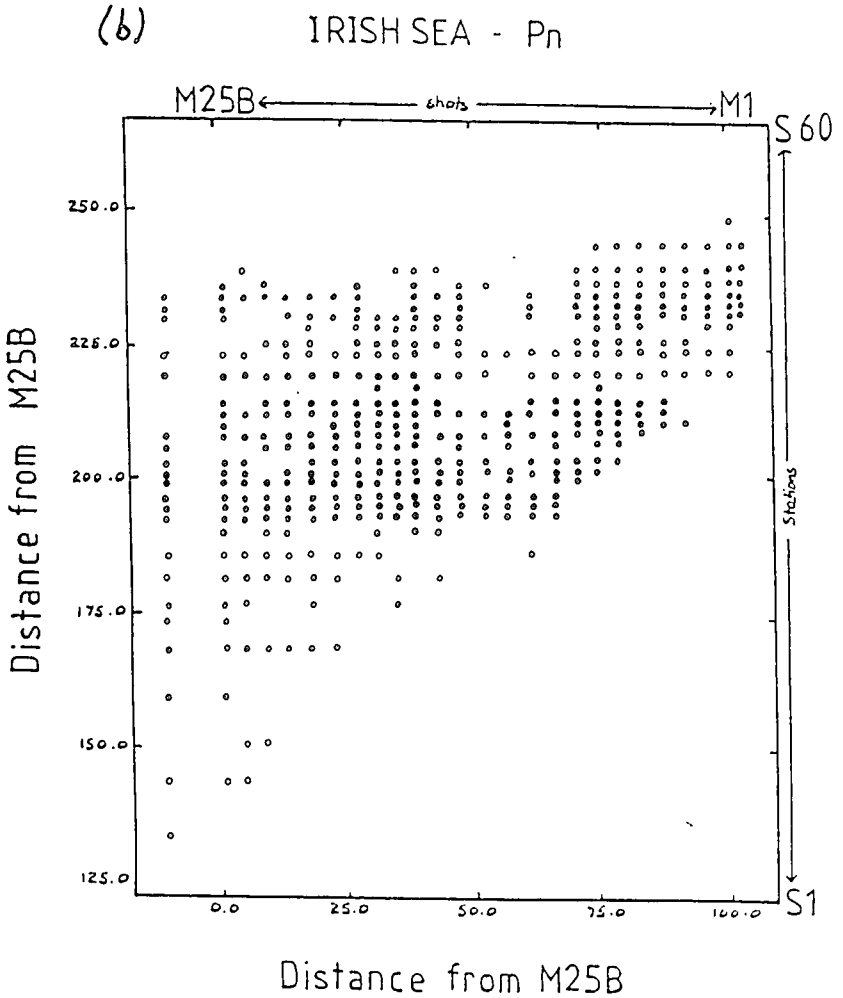


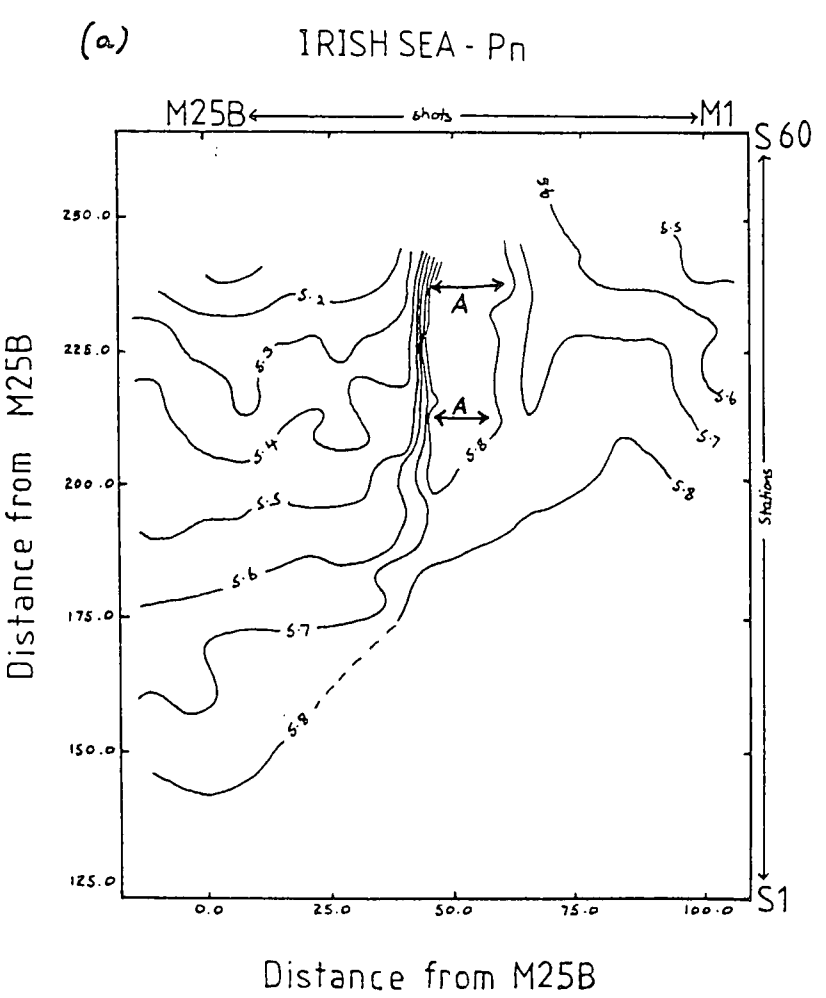


Figure(4.7a) Travel-time matrix for the phase Pn in the Irish Sea
(a) uncorrected for shallow structure
(b) reduced to a velocity of 8.0
data points

Data Points = •

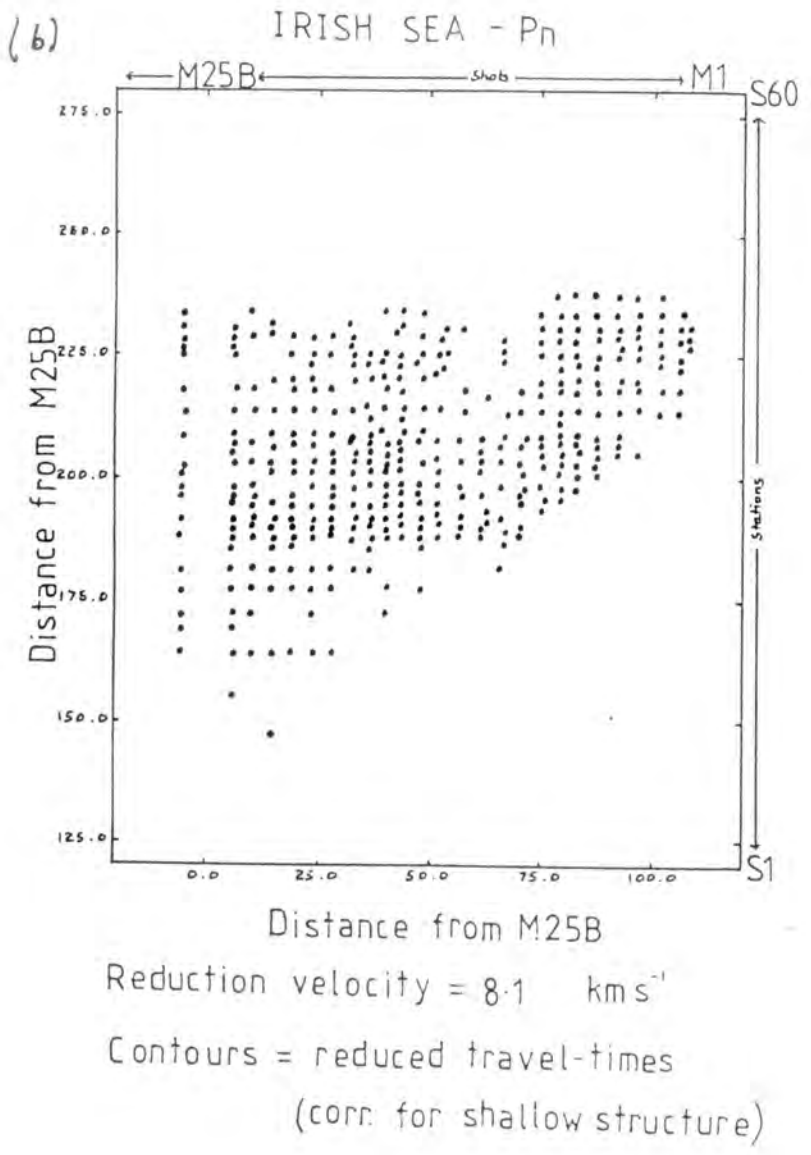


Figure(4.7b) Travel-time matrix for the phase Pn in the Irish Sea
(a) corrected for shallow structure
(b) reduced to a velocity of 8.1
(c) data points
overlay of the common distance
and common shot lines

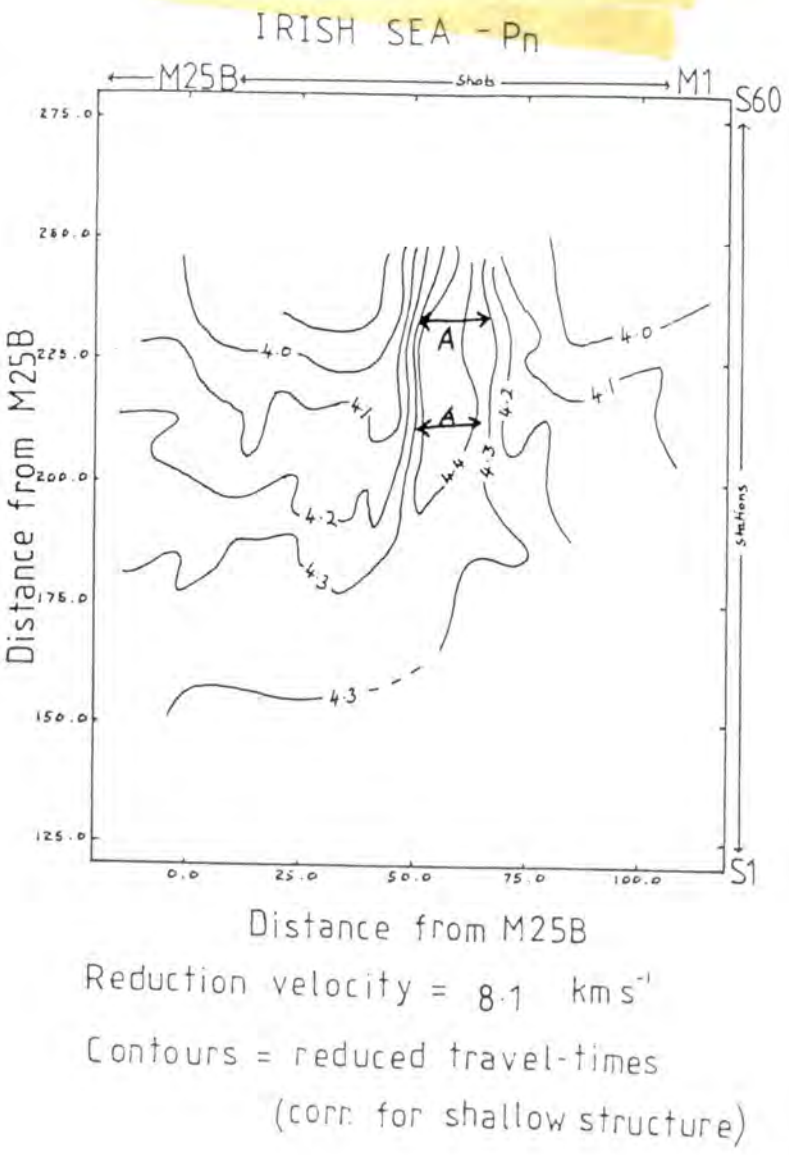

4.7b). This indicates that the delay times for all the shots are approximately the same. The delay times under the stations decrease from station 7 to 49 on the matrix corrected for the known shallow structure (Fig. 4.7b).

### 4.2.6 The Travel-time Matrix for Pn in the North Sea

Pn in the North Sea is observed over a range of station/shot offsets from 125 to 250 km. The coverage is poor for stations 1 to 29. The travel-times are reduced to velocities of 8.0 and 8.1 km/s in Figs. 4.8a and 4.8b respectively. The delay times appear to be flat for stations 23 to 60 (177 to 258 km from M25B) but increase from station 1 to station 23 (129 to 177 km from M25B). The feature labelled A in Fig. 4.8b is in an area of poor travel-time coverage from stations 20 to 29. Pn has larger amplitudes west of station 19 compared to Pn arrivals for the same offsets observed at stations east of station 30. For example compare the relative amplitudes of Pn on CST11N to that observed on CST30N in Appendix A. The data quality is good for these stations as the other phases are well displayed (refer to the stacked sections in Appendix A). The delay times under the shots appear to be constant west of station 19 although the contours change direction across feature A. They lie parallel to common station directions from stations 1 to 23 and to common shot directions from stations 23 to 60. A lateral change is interpreted, the effect of which is observed at the surface from stations 20 to 29 which corresponds to common mid-point positions on the Moho from 200 to 220 km. These common mid-point positions lie below stations 34 to 43.

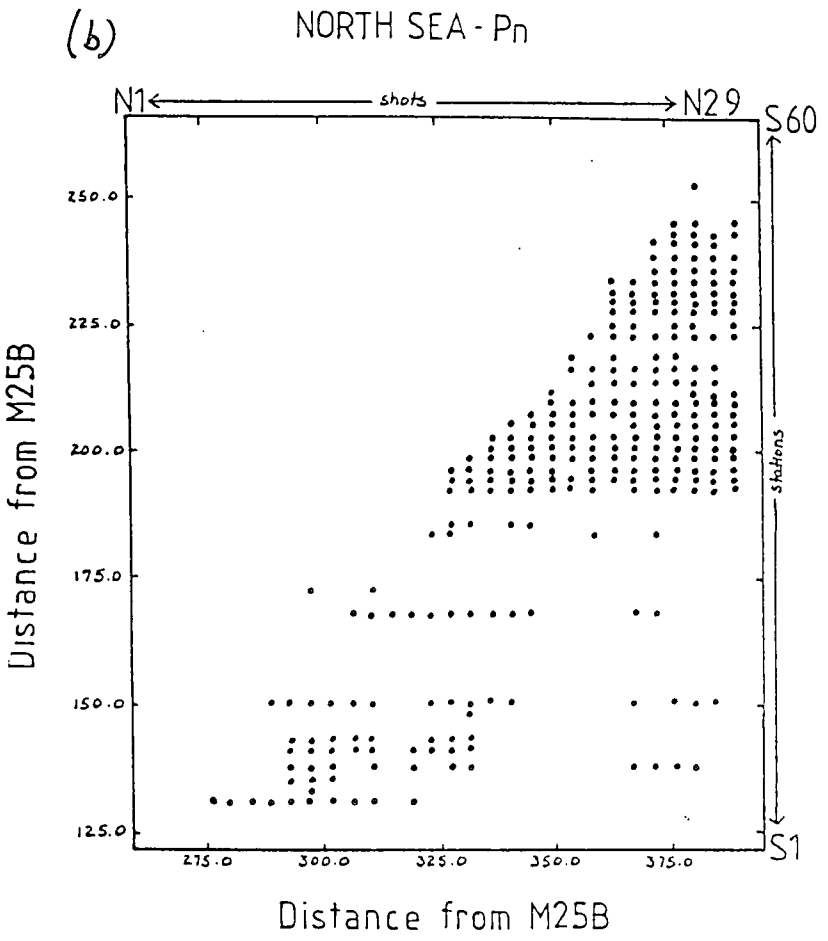


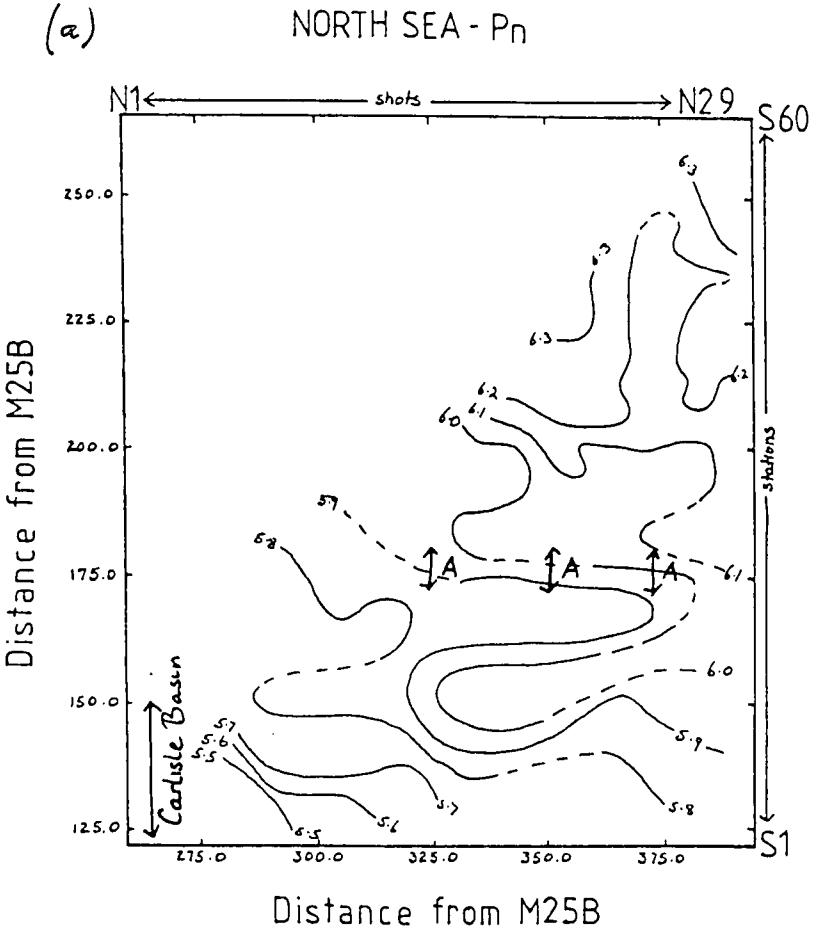


Figure(4.8a) Travel-time matrix for the phase Pn in the North Sea
uncorrected for shallow structure
(a) reduced to a velocity of 8.0
(b) data points

Data Points = •

(a)

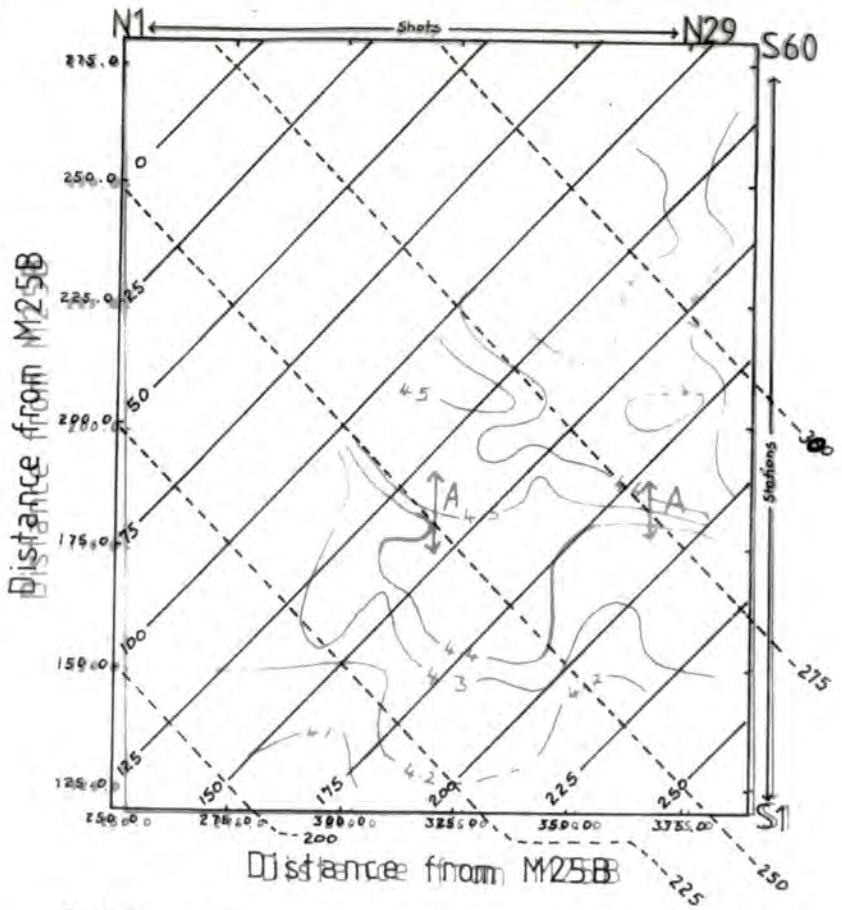


(c) Reduction velocity = 8.1 kms$^{-1}$

Contours = reduced travel-times

(corr. for shallow structure)

CMP LINES = \ CDS LINES = / (km)

Figure(4.8b) Travel-time matrix for the phase Pn in the North Sea corrected for shallow structure
(a) reduced to a velocity of 8.1
(b) data points
(c) overlay of the common distance and common shot lines

(b)

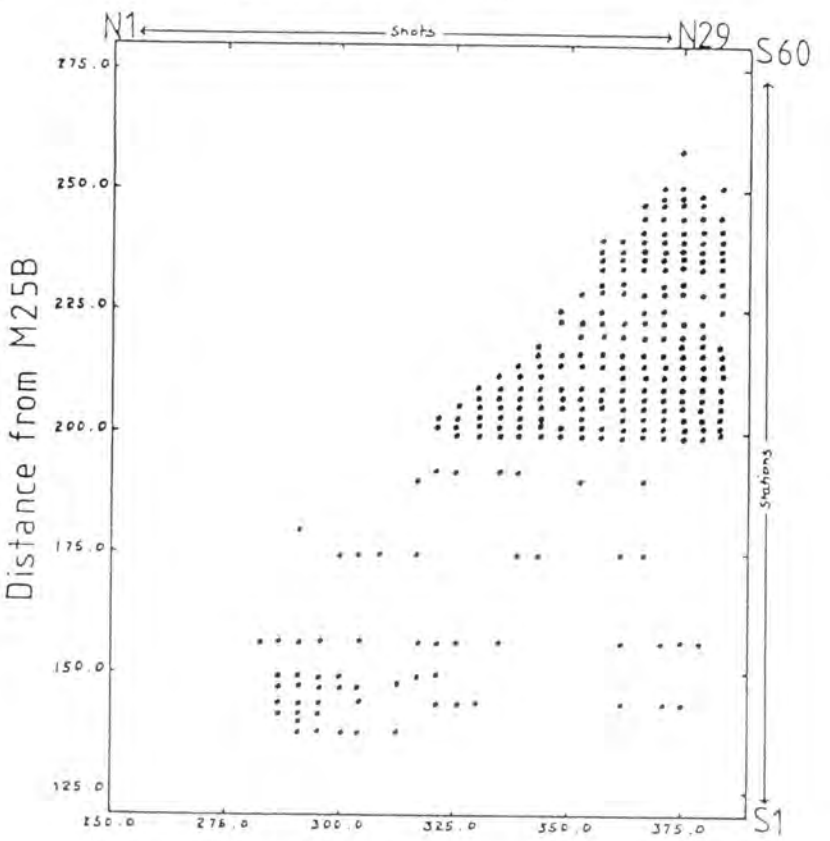


Distance from M25B

Reduction velocity = 8.1 kms$^{-1}$

Contours = reduced travel-times

(corr. for shallow structure)

## 4.3 WIDE-ANGLE REFLECTION RESULTS

The wide-angle reflection method formulated in Section 3.4 was used to obtain depths and average velocities from the PcP and PmP phases. By using common mid-point gathers the effects of topography on the reflecting interface are minimised. The unknown variations in the shallow structures and the difficulties of correcting for the known shallow structures where apparent surface velocities are less than the basement velocity will affect the results of the wide-angle reflection analyses. Where these effects are observed in the results they must be removed before proceeding to the modelling stage of the interpretation process.

The wide-angle reflection method also assumes that the wide-angle reflections observed are returned from a "sharp interface". The wavelengths of seismic waves with frequencies of about 4 Hz are about 1 to 2 km at mid to lower crustal depths. A sharp interface is therefore any gradient change in velocity which occurs over a depth range of up to 1 to 2 km. Table 4.1 displays the results of fitting the $T^2:X^2$ equation to the travel-time branches of PcP and PmP at near and far offsets. An estimate of the thickness of the gradient zone is given by the difference in depths calculated for near and far offsets labelled DH in Table 4.1. The values of DH are less than about 3 to 4 km. It can be concluded that to within the precision of the calculations the travel-time branches for the wide-angle reflections do not differ markedly from a simple hyperbolic curve and therefore approximate reflections from a sharp interface. Also the use of the Weichert-Herglotz

TABLE 4.1

Travel-time regression results for selected stations and shots:
(a) Using travel-times at near and far offsets. DH is the difference between the depths calculated at near and far offsets.
(b) Using all travel-times: dh is the 95% confidence limit on each depth.

(a)

| SITE | PmP | | | | | PcP | | | | |
|---|---|---|---|---|---|---|---|---|---|---|
| | V | | H | | DH | V | | H | | DH |
| 11A | 6.36 | 6.40 | 26.0 | 27.7 | 1.7 | - | - | - | - | - |
| M17 | 6.35 | 6.39 | 27.9 | 29.1 | 1.2 | - | - | - | - | - |
| M14 | 6.34 | 6.20 | 27.9 | 22.1 | -5.8 | - | - | - | - | - |
| M2 | 6.20 | 6.42 | 27.2 | 30.7 | 3.5 | - | - | - | - | - |
| 2 | - | 6.33 | - | 26.8 | - | - | - | - | - | - |
| 15 | 6.34 | 6.47 | 27.8 | 30.3 | 2.5 | - | - | - | - | - |
| 31 | 6.44 | 6.50 | 30.9 | 32.7 | 1.8 | - | - | - | - | - |
| 32 | 6.39 | 6.52 | 29.9 | 33.6 | 3.7 | - | - | - | - | - |
| 39 | 6.40 | 6.50 | 30.7 | 33.9 | 3.2 | - | - | - | - | - |
| 49 | 6.34 | 6.44 | 28.6 | 32.0 | 3.4 | - | - | - | - | - |
| 5 | - | - | - | - | - | - | - | - | - | - |
| 19 | 6.30 | 6.29 | 28.3 | 28.4 | 0.1 | - | - | - | - | - |
| 32 | 6.30 | 6.29 | 29.6 | 29.7 | 0.1 | 6.11 | 6.06 | 20.6 | 19.2 | -1.4 |
| 42 | 6.40 | 6.29 | 31.9 | 30.8 | -1.1 | 6.17 | 5.90 | 20.2 | 12.0 | -8.2 |
| 50 | 6.47 | 6.27 | 27.9 | 31.0 | 3.1 | 5.92 | 5.92 | 13.7 | 15.1 | 1.4 |
| 60 | - | 6.15 | - | 31.0 | - | 5.90 | 5.91 | 14.9 | 15.8 | 0.9 |
| N2 | - | 6.47 | - | 31.5 | - | 6.13 | 6.03 | 21.2 | 18.6 | -2.6 |
| N9 | 6.20 | 6.59 | 29.2 | 34.9 | 5.7 | 5.96 | 6.07 | 16.2 | 19.4 | 3.2 |
| N18 | 6.47 | 6.50 | 34.7 | 35.3 | 0.6 | 6.01 | 6.11 | 16.3 | 20.9 | 4.6 |
| N29 | 6.59 | 6.37 | 40.8 | 33.7 | -7.1 | 6.05 | - | 21.0 | - | - |

(b)

| | PcP | | | PmP | | | Pn | | |
|---|---|---|---|---|---|---|---|---|---|
| | V | H | dh | V | H | dh | V | H | dh |
| 11A | - | - | | 6.39 | 27.2 | 0.8 | 8.35 | 32.6 | 2.2 |
| M17 | 6.09 | 19.9 | 1.4 | 6.38 | 28.4 | 0.3 | 8.55 | 32.8 | 2.6 |
| M14 | 5.98 | 16.8 | 0.4 | 6.30 | 27.0 | 0.5 | 7.84 | 28.7 | 4.0 |
| M2 | 6.34 | 25.3 | 0.7 | 6.41 | 30.5 | 0.5 | 8.40 | 31.4 | 7.7 |
| 2 | 5.91 | 15.2 | 3.0 | 6.41 | 28.1 | 1.0 | - | - | - |
| 15 | 6.09 | 19.7 | 0.9 | 6.44 | 29.3 | 0.7 | 7.61 | 27.9 | 57. |
| 31 | 5.91 | 15.9 | 0.5 | 6.47 | 31.8 | 0.5 | 8.27 | 32.6 | 2.7 |
| 32 | - | - | - | 6.47 | 31.7 | 0.5 | 8.41 | 33.4 | 3.3 |
| 39 | - | - | - | 6.48 | 32.8 | 0.8 | 8.42 | 33.6 | 3.4 |
| 49 | - | - | - | 6.43 | 31.7 | 1.3 | 8.34 | 32.2 | 4.1 |
| 5 | - | - | - | 6.29 | 29.0 | 1.0 | 7.92 | 28.5 | 2.2 |
| 19 | 6.08 | 19.6 | 1.5 | 6.28 | 28.0 | 0.8 | 7.90 | 29.0 | 3.3 |
| 32 | 6.09 | 20.1 | 0.4 | 6.28 | 29.4 | 0.3 | 7.80 | 29.3 | 2.0 |
| 42 | 5.98 | 16.2 | 1.3 | 6.27 | 30.2 | 0.6 | 8.10 | 31.9 | 14. |
| 50 | 5.90 | 14.1 | 1.5 | 6.25 | 30.6 | 0.4 | 7.68 | 29.1 | 12. |
| 60 | 5.91 | 15.5 | 0.6 | 6.17 | 31.4 | 0.5 | - | - | - |
| N2 | 6.11 | 20.9 | 0.3 | 6.29 | 29.3 | 0.5 | - | - | - |
| N9 | 6.03 | 18.1 | 0.8 | 6.33 | 30.5 | 0.6 | 9.45 | 37.6 | 12. |
| N18 | 6.02 | 16.7 | 0.6 | 6.47 | 34.7 | 0.3 | 8.06 | 33.4 | 6.3 |
| N29 | 6.05 | 21.0 | 1.3 | 6.44 | 36.9 | 1.0 | 8.25 | 35.4 | 3.2 |

inversion method would not yield a better velocity depth model than the $T^2/X^2$ method given the effect of the shallow sediment delays on the apparent surface velocities and the interpretation of the interfaces as gradient zones less than about 3 to 4 km thick.

### 4.3.1 Wide-angle Reflection Results for the PcP phase

Fig. 4.9 illustrates the wide-angle reflection results for the PcP phase across the whole Caledonian Suture Seismic Project line. The travel-time residuals mostly lie within +/-0.1 s which is of the same order as the estimated picking errors for this phase. The calculated least squares average velocity for the upper crust between the datum at 6.0 depth km and the mid-crust is 6.16 km/s. Average velocities of 6.163 and 6.199 km/s are obtained from the PcP travel-times for the separate North and Irish Sea regions respectively (Figs. 4.10 and 4.11). The picking errors are larger for the Irish Sea (Section 4.2.1) than for the North Sea giving rise to the larger error of 0.005 km/s for the Irish Sea velocity in comparison to 0.001 km/s for the North Sea.

The mid-crustal gradient is interpreted, from the results displayed in Fig. 4.9, to be approximately horizontal at a depth of 15.5 km with a small step from 15.5 to 15.0 km at the common mid-point position of 260 km.

Figure(4.9) Wide-angle reflection results for PcP in the North and Irish Seas

(a)

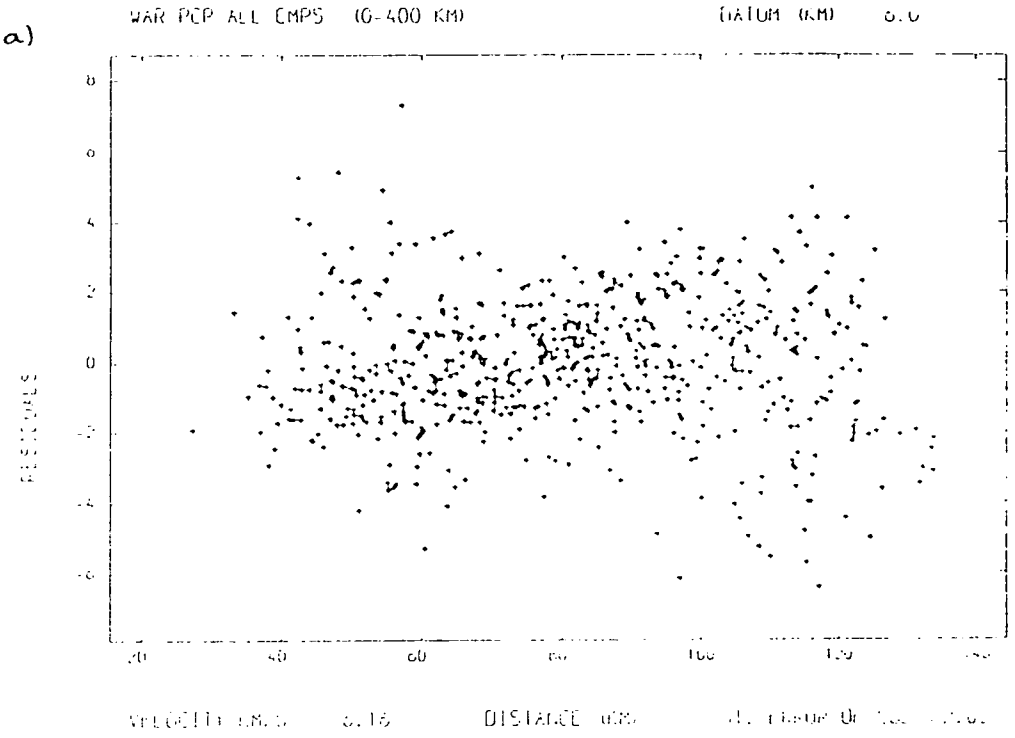


(b)

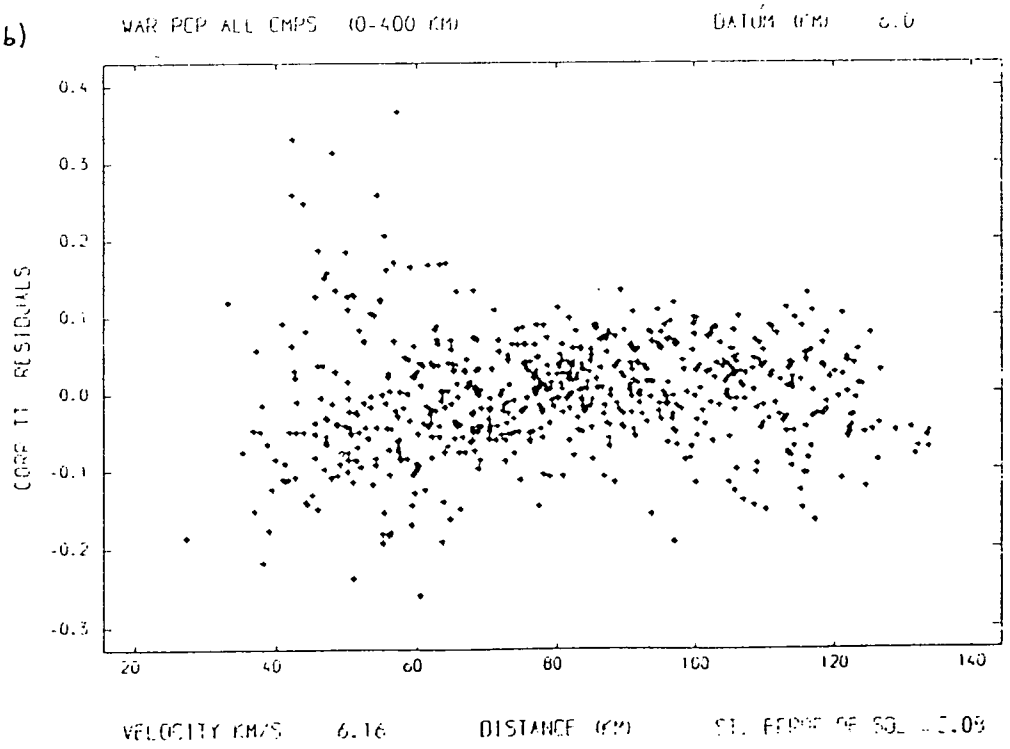

(c)

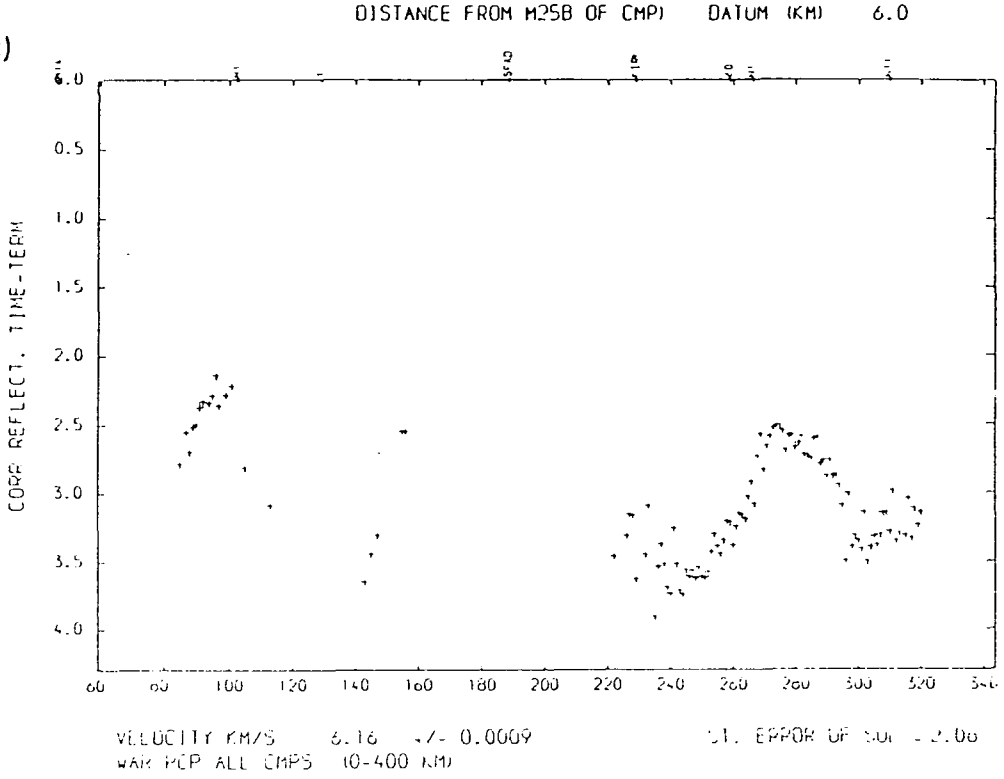
DISTANCE FROM M25B OF CMP)  DATUM (KM)  6.0
CORR REFLECT. TIME-TERM
0.0
0.5
1.0
1.5
2.0
2.5
3.0
3.5
4.0
60
80
100
120
140
160
180
200
220
240
260
280
300
320
VELOCITY KM/S  6.16  +/- 0.0009
WAR MCP ALL CMPS  (0-400 KM)

(d)

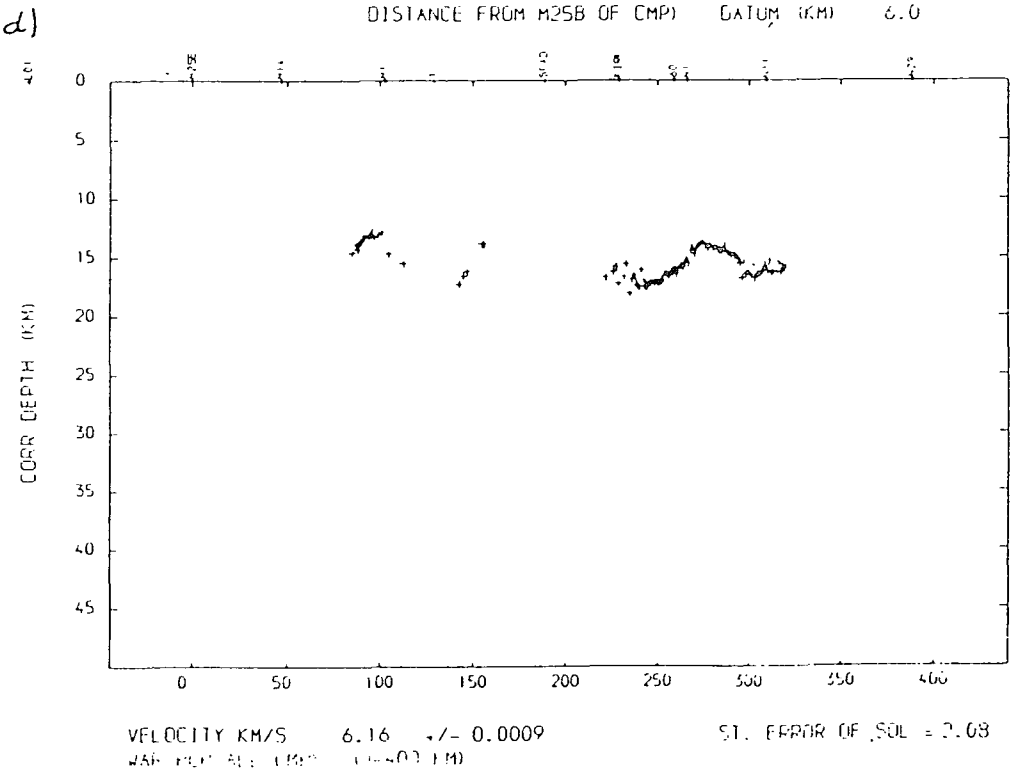
DISTANCE FROM M25B OF CMP)  DATUM (KM)  6.0
CORR DEPTH (KM)
0
5
10
15
20
25
30
35
40
45
0
50
100
150
200
250
300
350
400
VELOCITY KM/S  6.16  +/- 0.0009

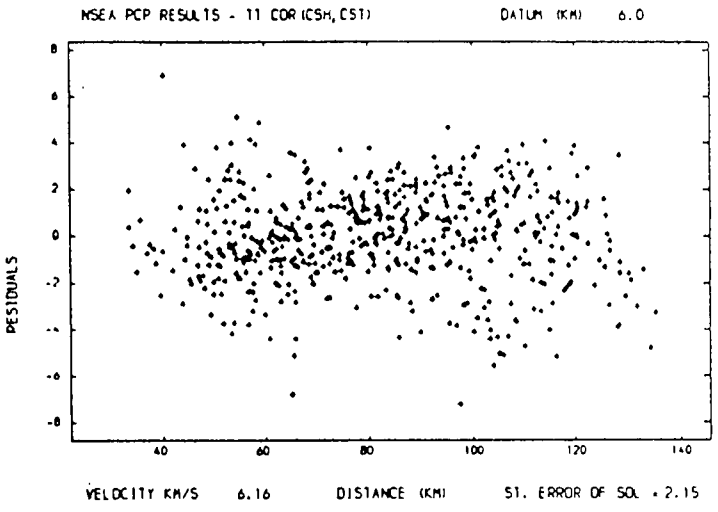


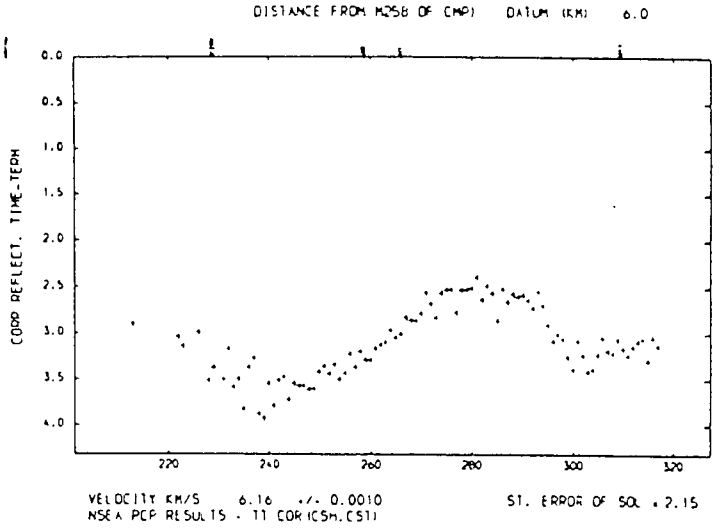


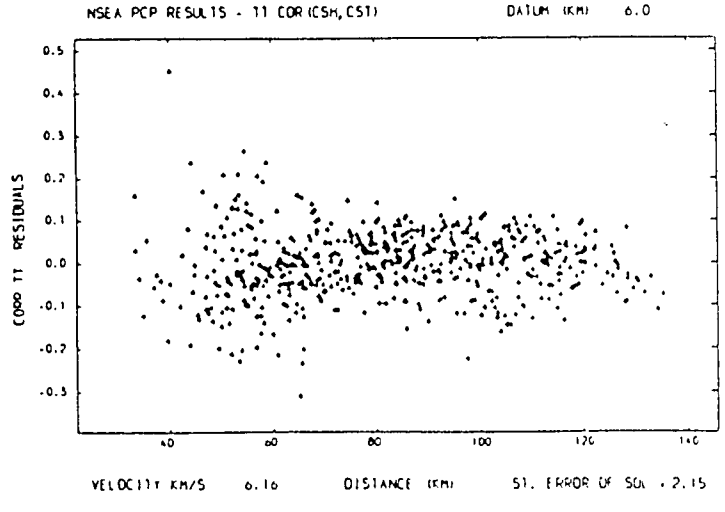


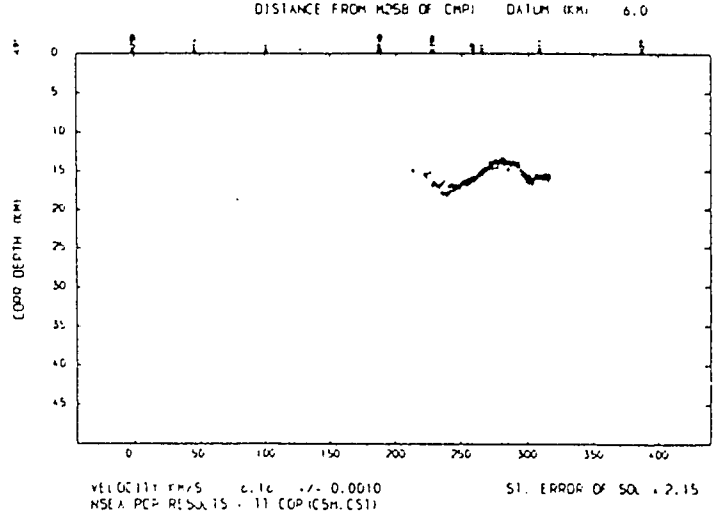


Figure(4.10) Wide-angle reflection results for PcP in the North Sea

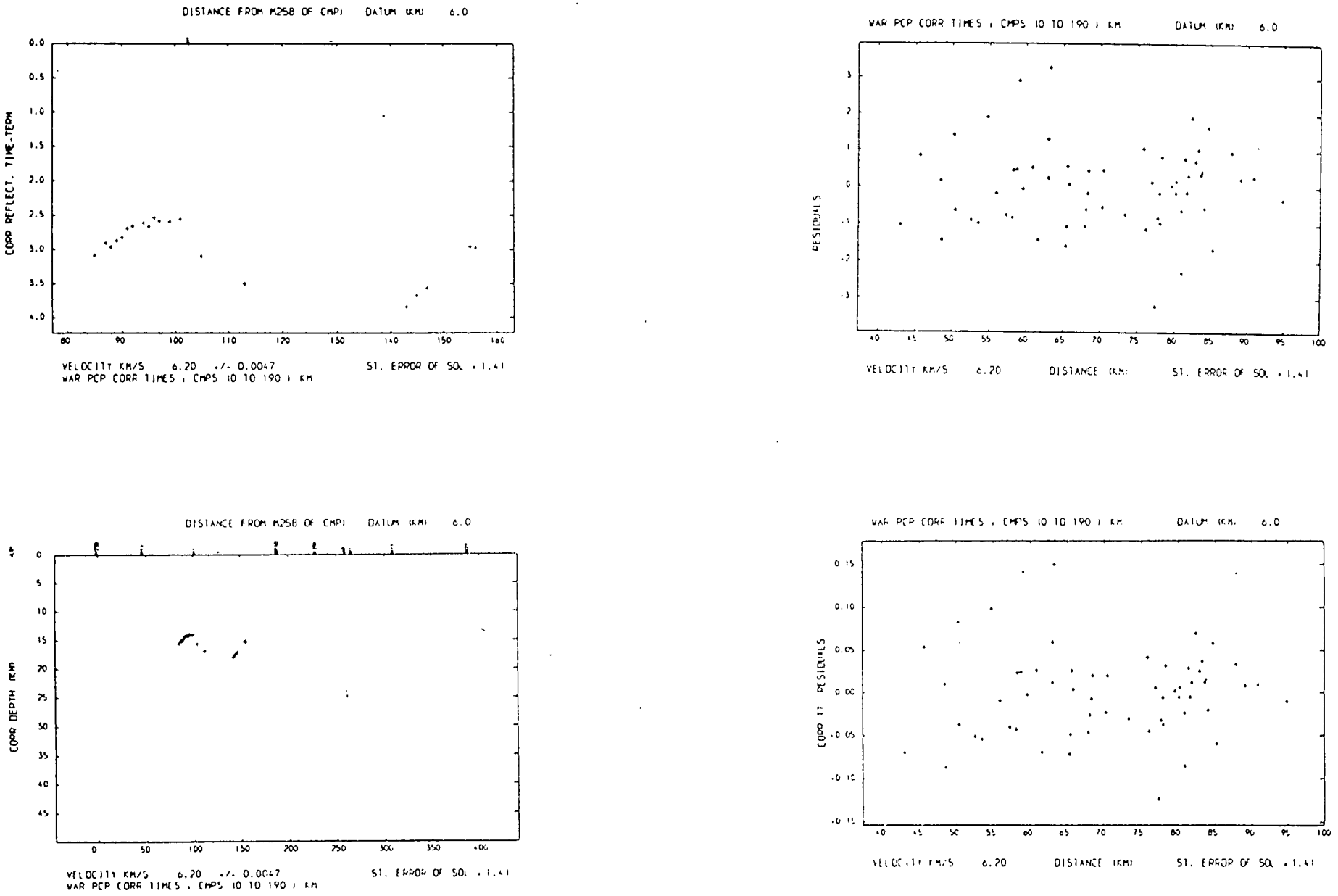


Figure(4.11) Wide-angle reflection results for PcP in the Irish Sea

### 4.3.2 Wide-angle Reflection Results for the phase PmP

Fig. 4.12 displays the results for the wide-angle reflection analysis of the PmP phase using all the PmP travel-times from the Caledonian Suture Seismic Project. The analysis is repeated for travel-times corrected and uncorrected for the known shallow structure in Fig. 4.13 to illustrate the effects of the shallow structure. The residuals are not improved by applying the corrections for the shallow structure. The velocities calculated are 6.38 km/s from the uncorrected travel-times and 6.51 km/s from the corrected travel-times. The 6.38 km/s velocity applies to the whole crust including sediments whilst the 6.51 km/s velocity applies to the crust between the datum at 6.0 km depth and the PmP reflecting interface. The depths calculated are improved by the correction of the travel-times for the shallow structure. In particular the rise in the uncorrected depths at a common mid-point position of 100 km is not observed for the corrected depths (Fig. 4.13). The average crustal velocities underneath the North and Irish Seas from the surface to the base of the lower crust are estimated as 6.39 and 6.34 km/s repectively. The average crustal velocities underneath the North and Irish Seas from the datum at 6.0 km depth to the base of the lower crust are 6.54 and 6.49 km/s repectively (Figs. 4.14 and 4.15).

Figure(4.12) Wide-angle reflection results for PmP in the North and Irish Seas

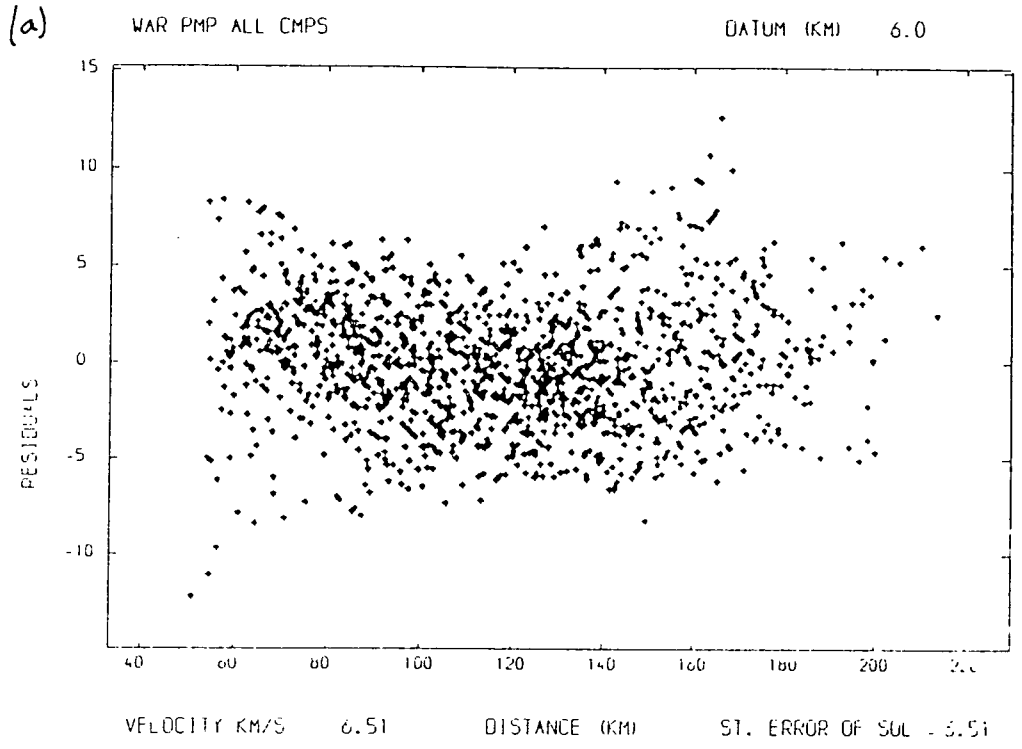


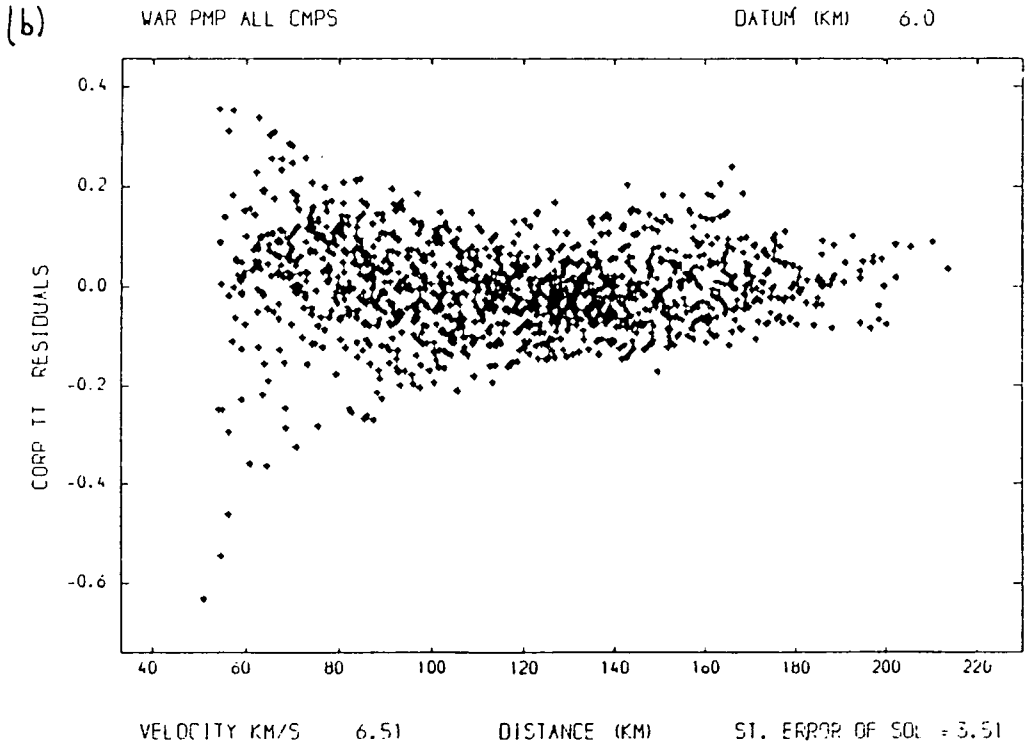

4·12 (c)

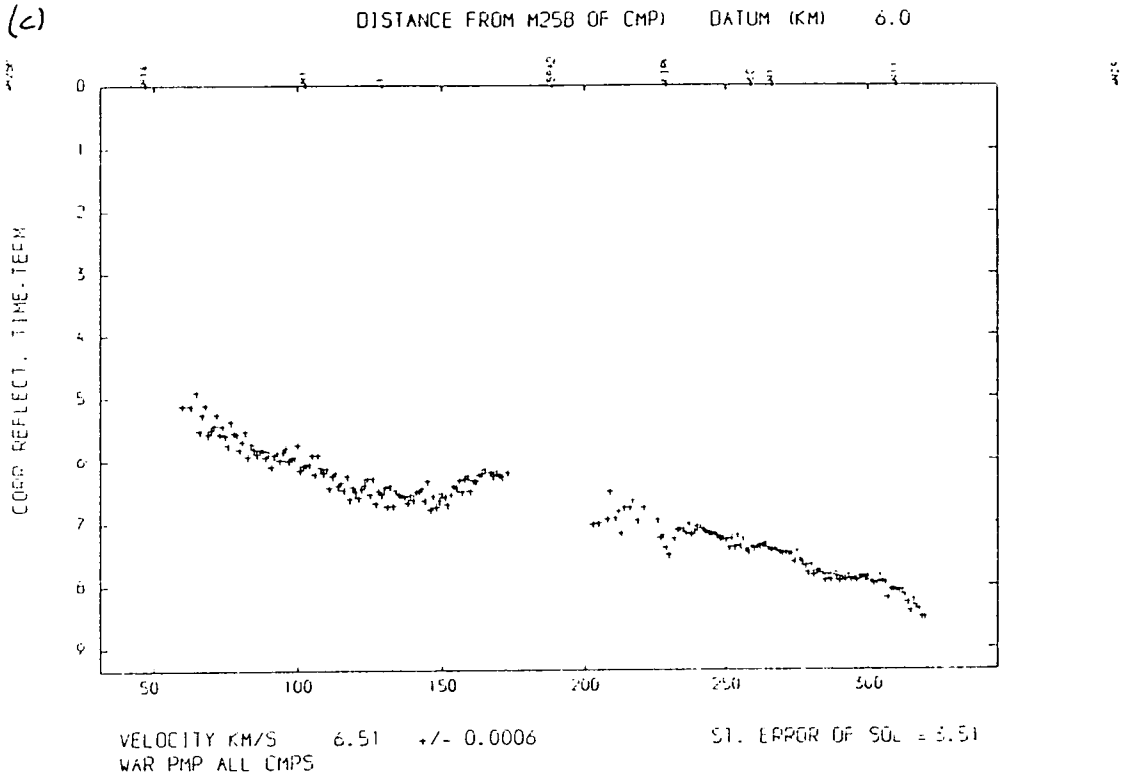
DISTANCE FROM M258 OF CMP)  DATUM (KM)  6.0
CORR REFLECT. TIME-TERM
0
1
2
3
4
5
6
7
8
9
50
100
150
200
250
300
VELOCITY KM/S  6.51  +/- 0.0006
ST. ERROR OF SOL = 0.51
WAR PMP ALL CMPS

(d)

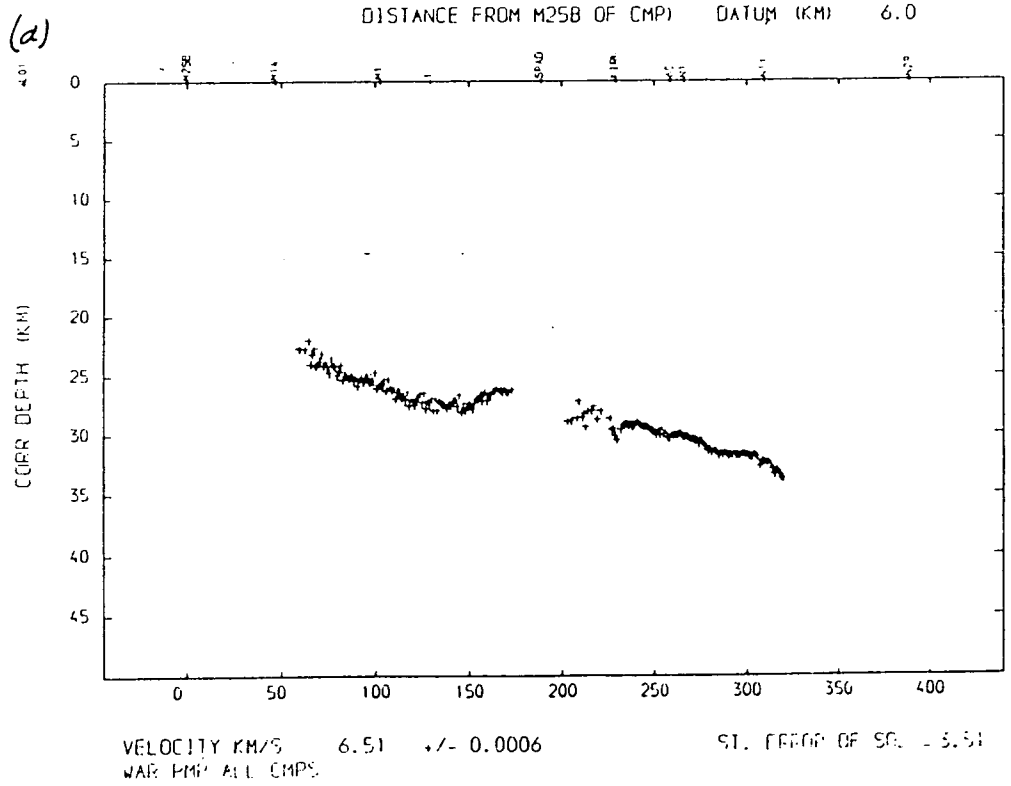
DISTANCE FROM M258 OF CMP)  DATUM (KM)  6.0
CORR DEPTH (KM)
0
5
10
15
20
25
30
35
40
45
0
50
100
150
200
250
300
350
400
VELOCITY KM/S  6.51  +/- 0.0006
ST. ERROR OF SOL = 0.51
WAR PMP ALL CMPS

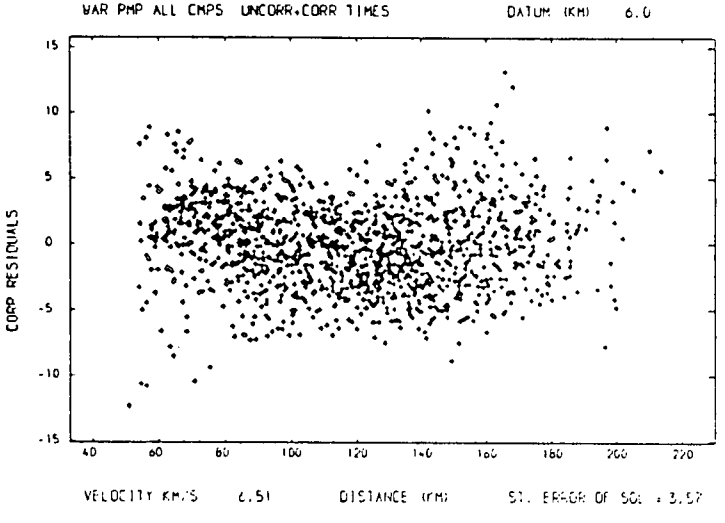


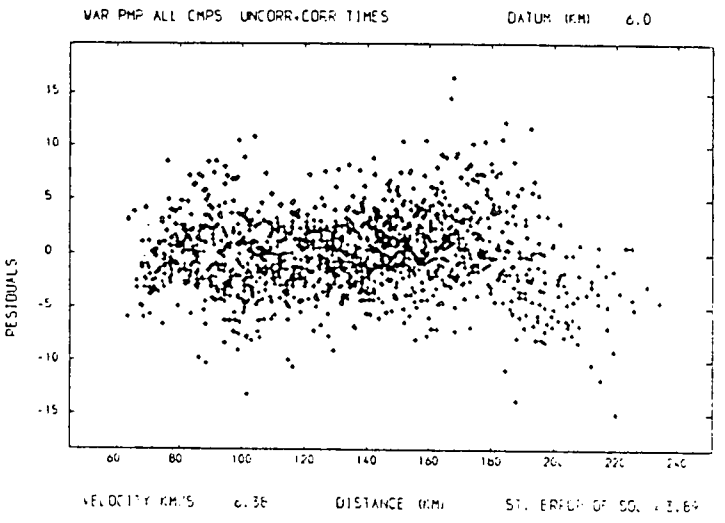


Figure(4.13) Wide-angle reflection results for PmP in the North and Irish Seas corrected and uncorrected for the shallow structure

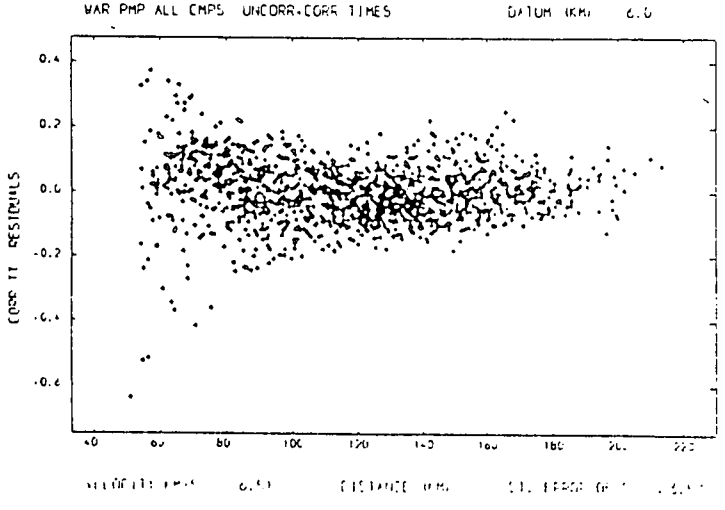


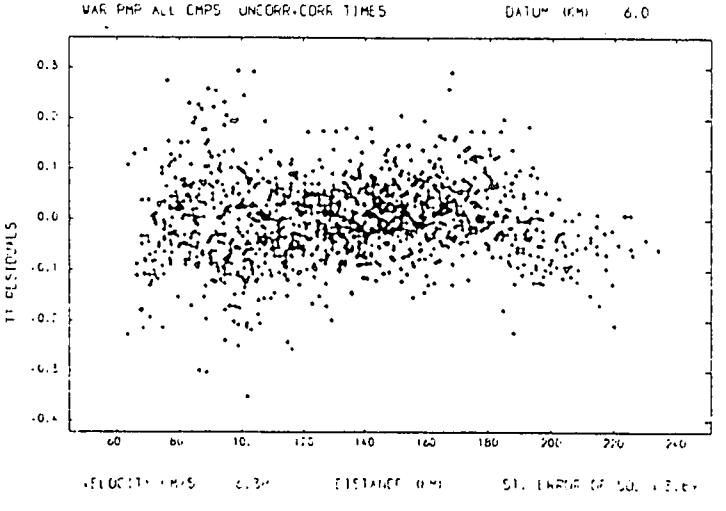

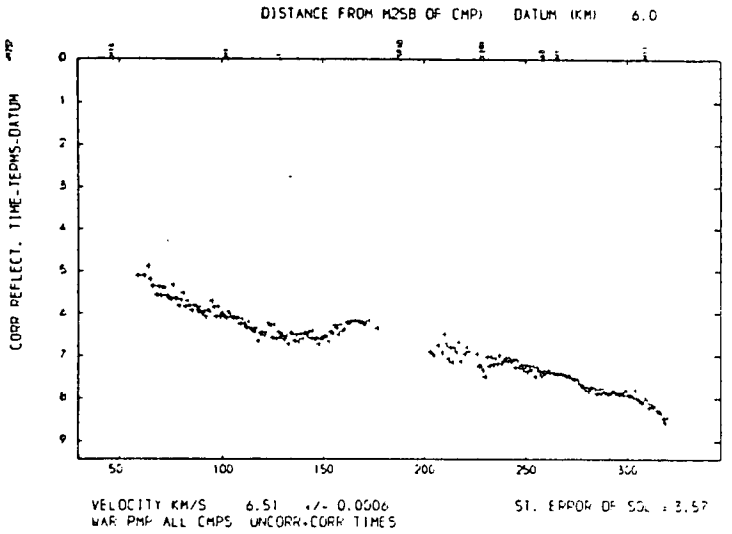


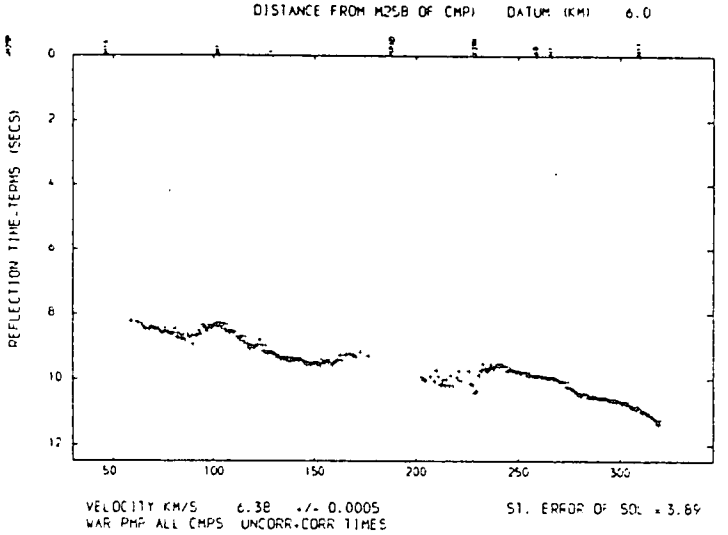


Fig 4·13 (continued)

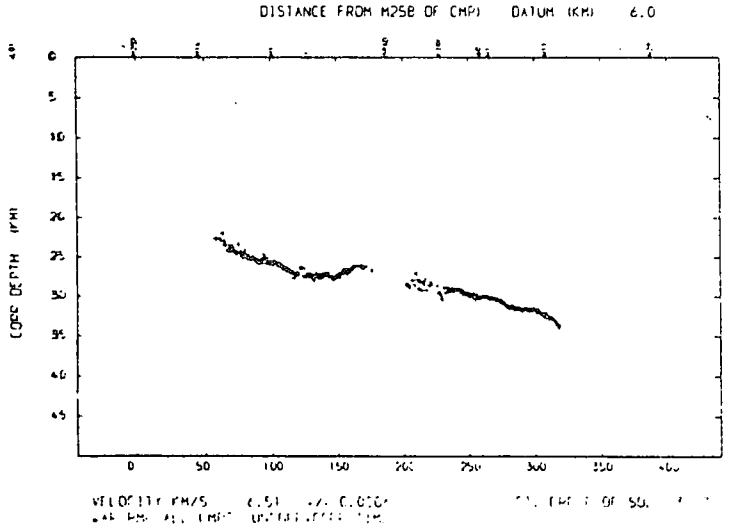


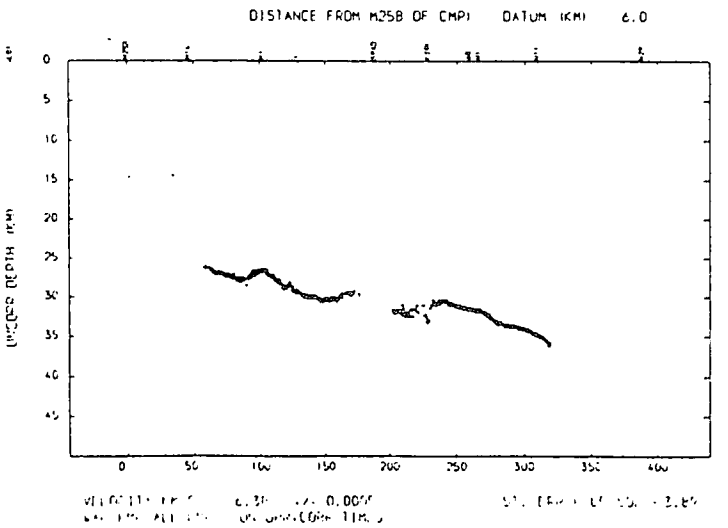

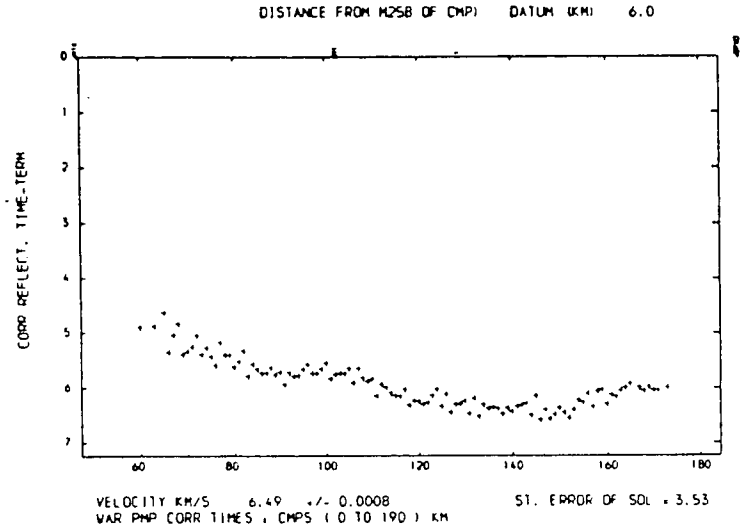


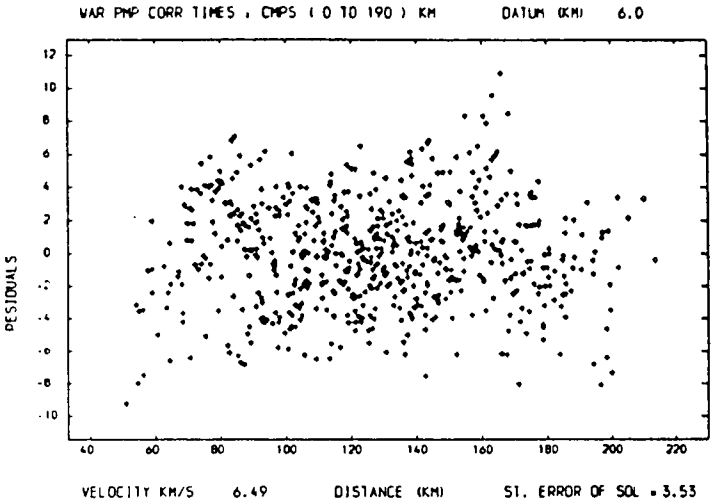


Figure(4.14) Wide-angle reflection results for PmP in the Irish Sea

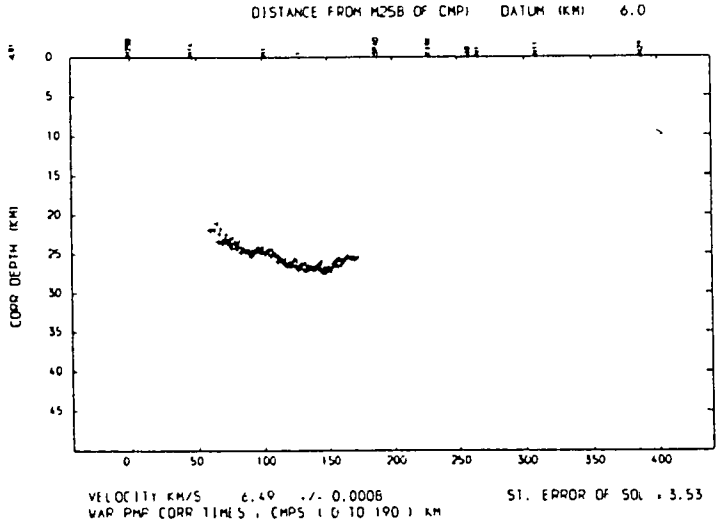


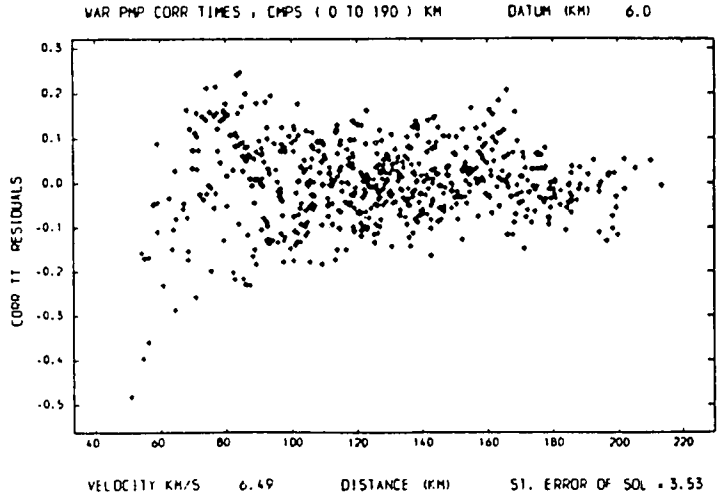

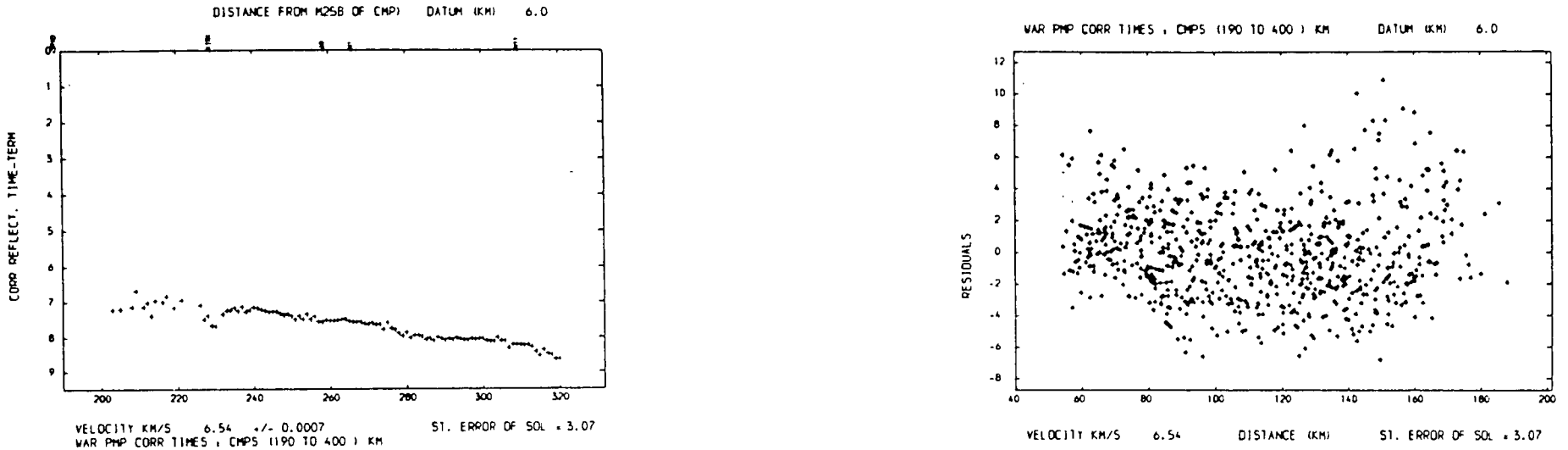


Figure(4.15) Wide-angle reflection results for PmP in the North Sea

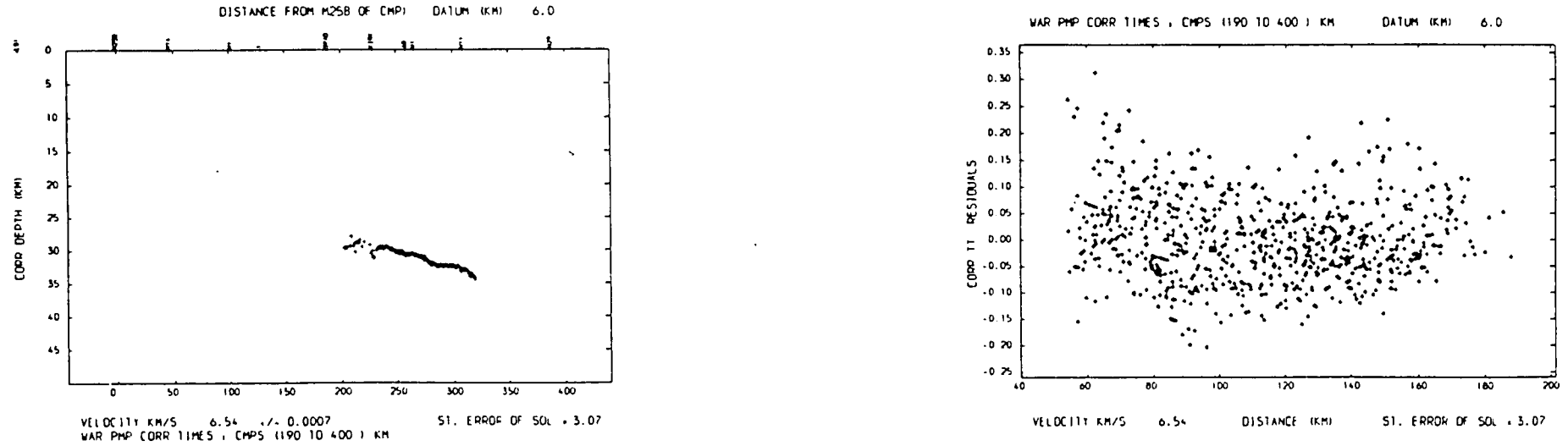

### 4.3.3 Discussion

Fig. 4.16 summarises the wide-angle reflection results for PcP and PmP. The figures written along the interfaces are the velocities in km/s calculated within a 20 km wide moving common mid-point window. The window width of 20 km was found to be the best compromise between the need to obtain an idea of the lateral variations and avoiding the problems which arise from limited data coverage. The coverage tends to be poor at the edges of the survey area which corresponds to the common mid-point positions 60 km and 320 km for PmP. and, 80 and 310 km for PcP. As a result there are only a few travel-time values available to each common mid-point in these areas which adversely affects the velocities and therefore the calculated depths.

The common mid-point positions greater than 300 km have PmP travel-time data observed only from shots N25 to N29 (Fig. 4.6). These shots lie on the edge of the delay discussed in Sections 4.2.2 and 4.2.4 and identified by Green (1984) which occurs under shots N20 to N25. The apparent velocities calculated over the common mid-point positions east of common mid-point 300 km are too large and as a result the depth to the interface appears spuriously to deepen (Fig. 4.16b).

An analysis of variance using the variance-ratio test (described in the next section) was performed on the average velocities obtained from the wide-angle reflections. The 95% confidence limits were estimated to be less than +/-0.02 km/s for all average velocities quoted in this chapter except for

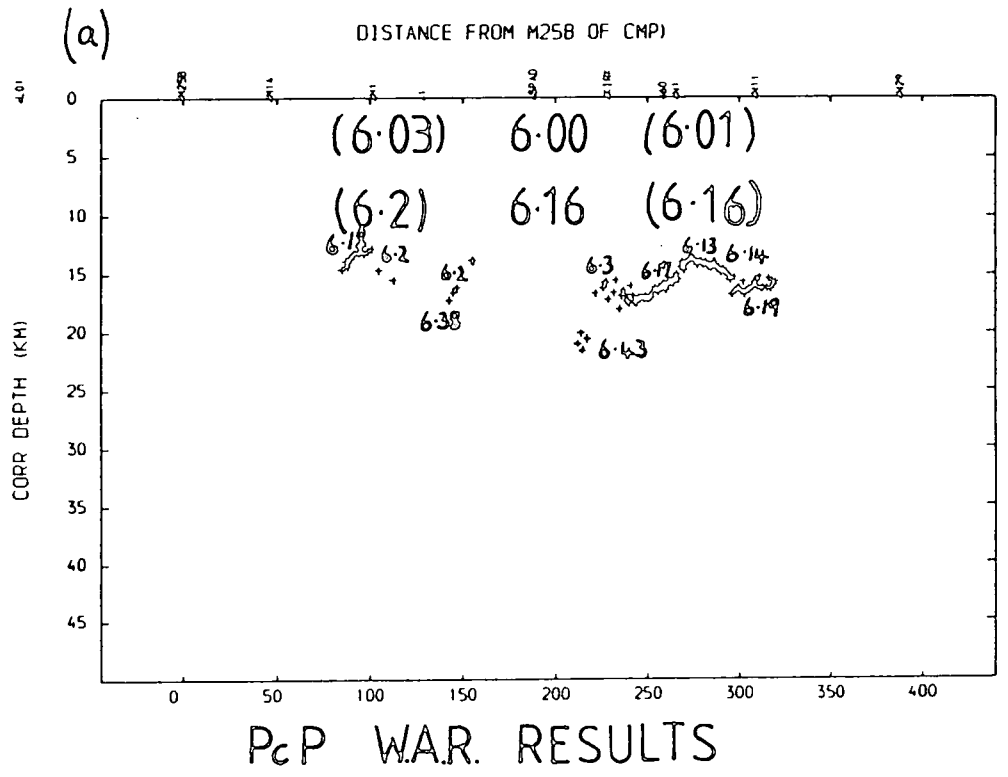


Figure(4.16) (a) Summary of the PcP wide-angle reflection results
(b) Summary of the PmP wide-angle reflection results

The velocities are in km/s. The top values are the average velocities between the interface and the surface. The bottom values are the average crustal velocities between the datum at 6.0 km and the interface. The velocities along the interface are calculated for 20 km wide common mid-point windows

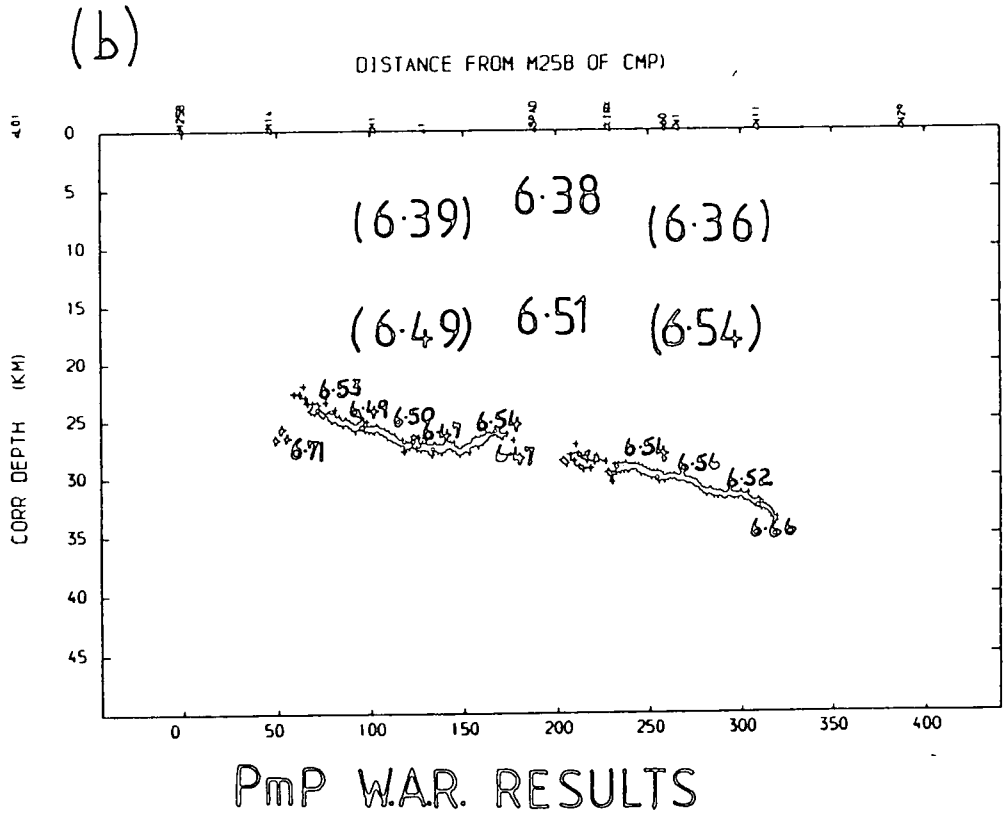

the 6.20 km/s velocity calculated from PcP for the Irish Sea shots which yielded a slightly higher 95% confidence error range of +/-0.06 km/s.

## 4.4 TIME-TERM RESULTS FOR PN

Table 4.2 summarises the time-term results from the analysis of the Pn travel-times. Each run is given a reference number. A representative selection of the runs are displayed in Figs. 4.17 to 4.30 and are discussed in detail below. There is reversal of the Pn refractor underneath the stations and between the adjacent ends of the shot and station lines for both the Irish and North Seas (Fig. 4.17). By incorporating the travel-times of Pn observed for station L15 in Ireland the Moho under the Irish Sea is also reversed (Fig. 4.18). In practise the limitations of the travel-time coverage somewhat reduces the areas where reversal occurs.

The Pn depths are calculated from the time-term values using the average velocities obtained from the wide-angle reflection analysis of the PmP phase. This calculation assumes that PmP and Pn are returned from about the same depths. If a velocity gradient zone separates PmP and Pn the average velocity calculated from PmP is smaller than the average velocity of the crust above Pn. The use of the PmP average velocity may therefore yield a slight underestimate of the Pn depths.

Two types of error estimate can be assigned to the solution velocities. The 95% confidence limits obtained using the

TABLE 4.2

Summary of time-term results for Pn. Constraint used is taken from Swinburn (1975). Nearest shot/station pairs at each end of line were used to tie shots and stations time-terms together

| REF Nº | Description | Velocity km/s | SITES | | | | |
|---|---|---|---|---|---|---|---|
| | | | STT | I1A - M15 | M14 - M7 | M6 - M1 | 1 - 49 - 60 | N1 - N29 |
| 1 | Check link-up between shots and stations | 8.32 | | | | M1 | 2 54 | N4 |
| 2 | | 8.32 | | | | M1 | 2-8 54 | N4 |
| 3 | | 8.32 | | | | M1 | 2 54 | N4 N5 |
| 4 | | 8.31 | | | | M1 | 2 54 | N4 N8 |
| 5 | | 8.32 | | | | | 54 | N4 |
| 6 | | 8.32 | | | | M1 | 2 | |
| 7 | Including L15 | 8.27 | | | | M1 | 2 54 | N4 |
| 8 | **North Sea** | 8.15 | | | | M1 | 2 54 | N4 |
| 9 | | 8.26 | | | | M1 | 2 54 | N4 |
| 10 | | **7.90** | | | | | 2.9 54 | N14 |
| 11 | 49=2.90 | 8.02 | | | | | 2.9 54 | |
| | 49=2.95 | 8.13 | | | | | 2.95 54 | N4 |
| | 49=3.00 | 8.13 | | | | | 3.0 54 | N4 |
| | 49=3.07 | 8.40 | | | | | 3.07 54 | N4 |
| 12 | Irish Sea | 8.35 | | | | M1 | 2 54 | N4 |
| 13 | | 8.36 | | | | | 54 | N4 |
| 14 | | - | | | | | 54 | N4 |
| 15 | | **8.25** | | | | M1 | 2 2.9 | |
| 16 | Including L15 | 8.19 | | | | M1 | 2 2.9 | |
| 17 | Irish Sea (no M7-M14) | - | | | | M1 | 2 2.9 | |
| 18 | | - | | | | | 2.9 | |
| 19 | | 8.28 | | | | M1 | 2 2.9 | |
| | **Summary** | | | | | | | |
| 20 | Time-terms | 8.03 | | | | | 2.9 54 | N4 |
| 21 | | 8.28 | | | | M1 | 2 2.9 | |
| 22 | Including L15 | 8.27 | | | | M1 | 2 54 | N4 |
| 23 | Travel-times corrected | 8.33 | | | | N | 2 2.9 54 | N4 |
| 24 | | 8.09 | | | | | 2.9 54 | N4 |
| 25 | | 8.19* | | | | N | 2 | |
| | | | US | I1A - M15 | M14 - M7 | M6 - M1 | 1 - 49 - 60 | N1 - N29 |

(49 used as constraint)

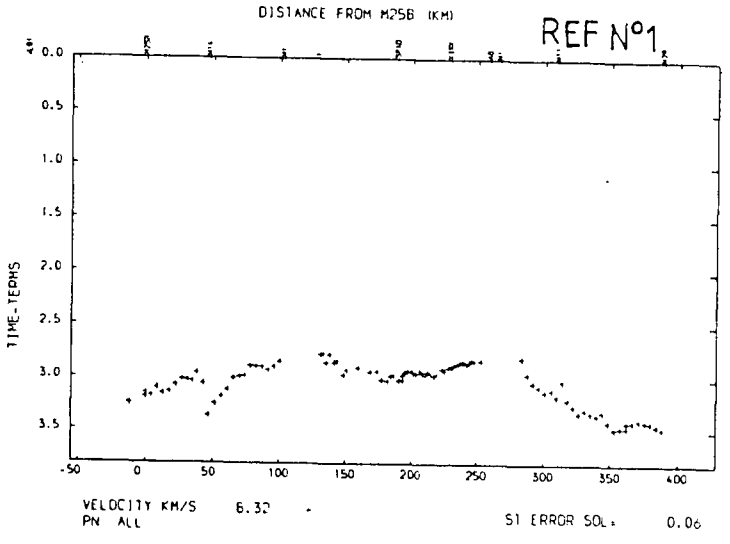


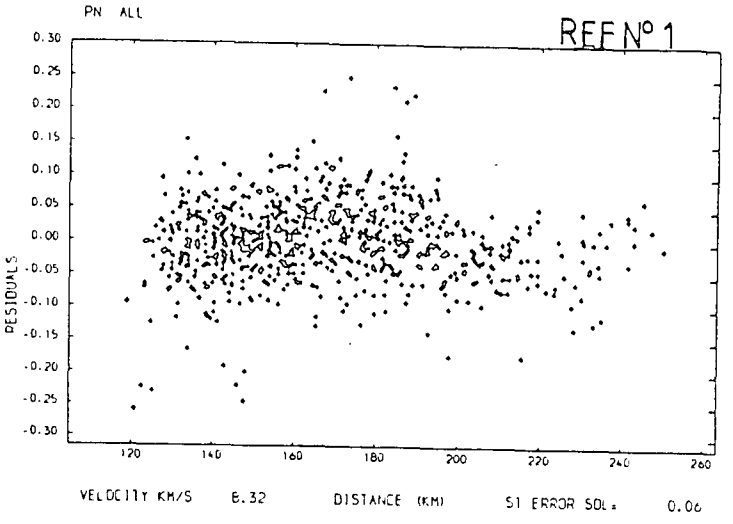


Figure(4.17) Pn time-term results for Northern England using the Irish and North Sea shots. The reference number corresponds to the numbers given in Table 4.2

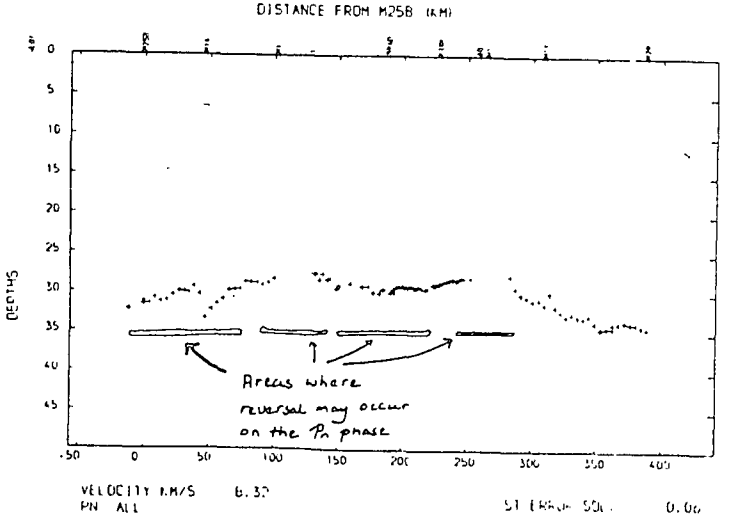


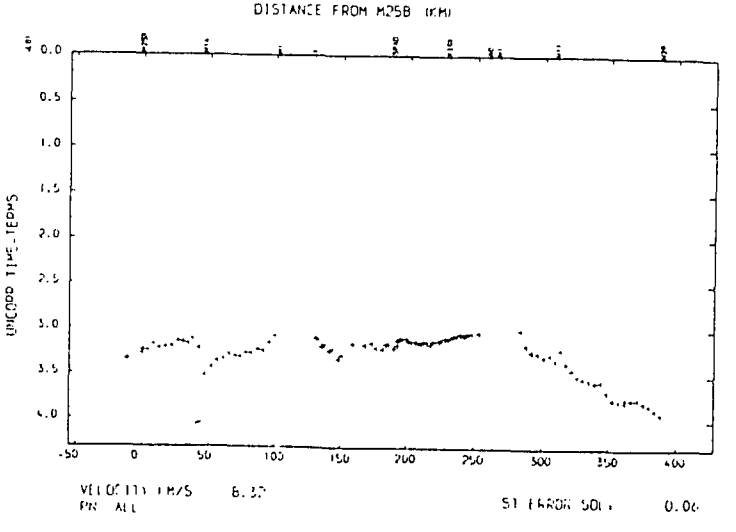

Berry and West (1966) formula take no account of the correlation between the velocity and the time-terms and may thus grossly underestimate the true uncertainty. An alternative approach is to use the variance-ratio test combined with time-term analyses carried out for a specified range of constrained velocities. Draper and Smith (1981), and, Ofoegbu and Bott (1985) give summaries of how to perform this analysis of variance. To illustrate this approach Fig. 4.18 is a sketch of a section of the hyperspace region for a time-term analysis. The contours are the values of the sum of the squares of the residuals between the observed and the predicted travel-times plotted as a function of velocity and one time-term. The time-term and the solution velocity are necessarily correlated as is indicated by equation 3.6. To obtain an estimate of the uncertainties, which takes into account the correlation with <u>all</u> the time-terms, the sum of residuals squared must be computed as a function of the velocity with the time-terms optimized for each specified velocity. The 95% confidence value of the function (Fc) can then be computed from the minimum sum of residuals squared (Fmin) using the equation

$$Fc = Fmin \left[ 1 + \left[ n / [m-n-1] \right] f_{n,m-n-1(1-a)} \right]$$

where $f_{n,m-n-1}$ is a fractile of the variance-ratio or F distribution, n is the number of variable parameters equal to the number of sites plus one and m is the number of observations. The values of velocity (labelled V1 and V2 in Fig. 4.18) which correspond to the 95% confidence level of the objective function can be obtained from a plot of F against the velocity (which corresponds to the line AA' in Fig. 4.18). These limits are clearly an overestimate of the true error but

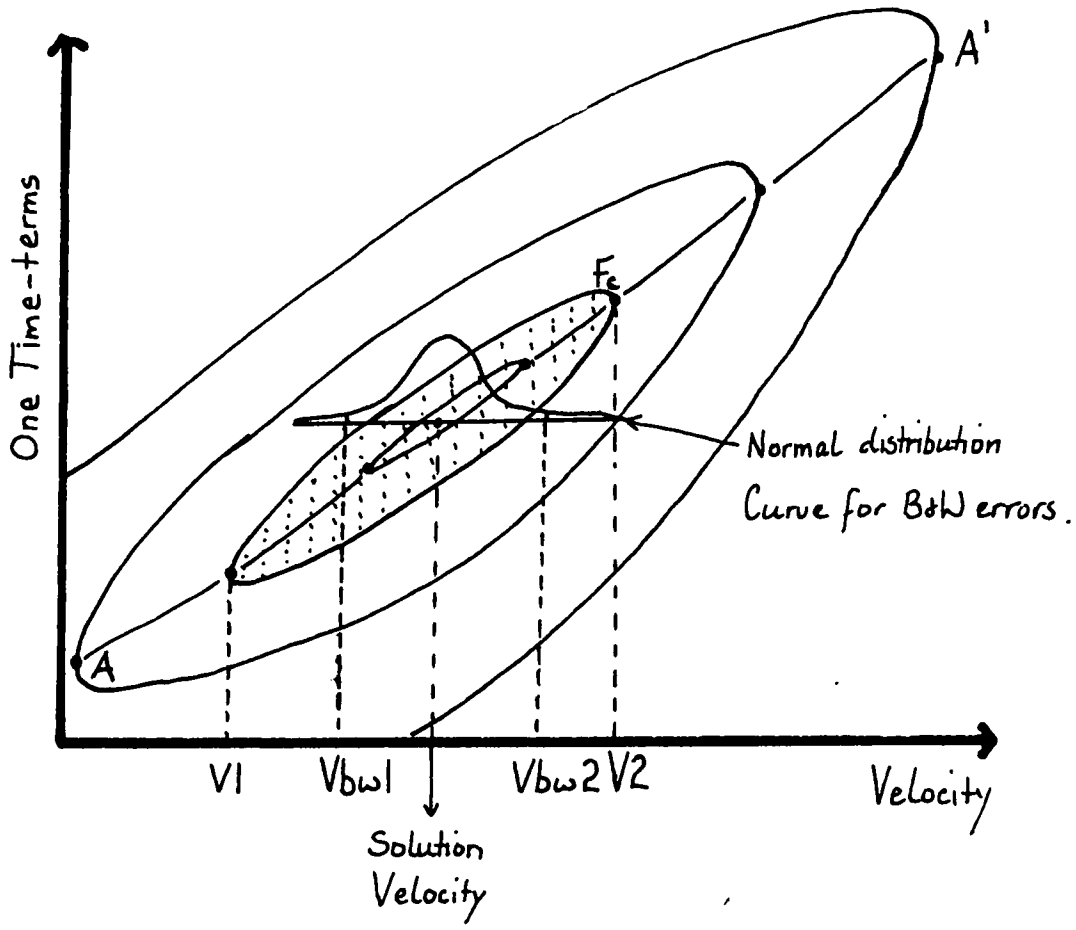


Figure(4.18) A sketch of a cross-section through the hyperspace region for a time-term analysis for one time-term. The contours are the values of the residuals squared between the observed and predicted travel-times plotted as a function of velocity and one time-term. See text for explanation of annotation.

are better than the Berry and West error (labelled Vbw1 and Vbw2 in Fig. 4.18) which can be a gross underestimate.

### 4.4.1 Time-term Analysis for Northern England Using all Pn Travel-times

The first six runs (Table 4.2) were performed to check that the time-term solutions are independent of the sites used to link the shots and stations together. The solutions are stable whether the link is achieved using the North Sea (as in run 5) or Irish Sea (as in run 6) ends of the line. The solution velocity using all the Pn travel-time data for Northern England is 8.32 km/s (Fig 4.17). Given the quantity of data and the well constrained reversal under the stations. this higher than expected velocity under Northern England appears to be real. The analysis of variance of this solution yields a 95% confidence range from 8.19 to 8.49 km/s (Fig. 4.19). On the other hand the Berry and West error analysis yield 95% confidence limits of +/- 0.01 km/s which is clearly an underestimate. The time-terms for shots M7 to M14 are anomalous (Section 4.2.3) probably because the travel-times are difficult to pick for these shots. These sites are removed for most subsequent runs.

### 4.4.2 Time-term Analysis for the Irish Sea

The time-term solutions using the travel-time data for Pn in the Irish Sea yield a solution velocity of 8.28 km/s (Fig. 4.20). Station 49 is constrained to 2.9 s. This value is taken from the results of Swinburn (1975). The solution

Figure(4.19) Analysis of variance of the Pn time-term analysis for Northern England. The bounds give the 95% confidence limits on the solution velocity. See text for details.

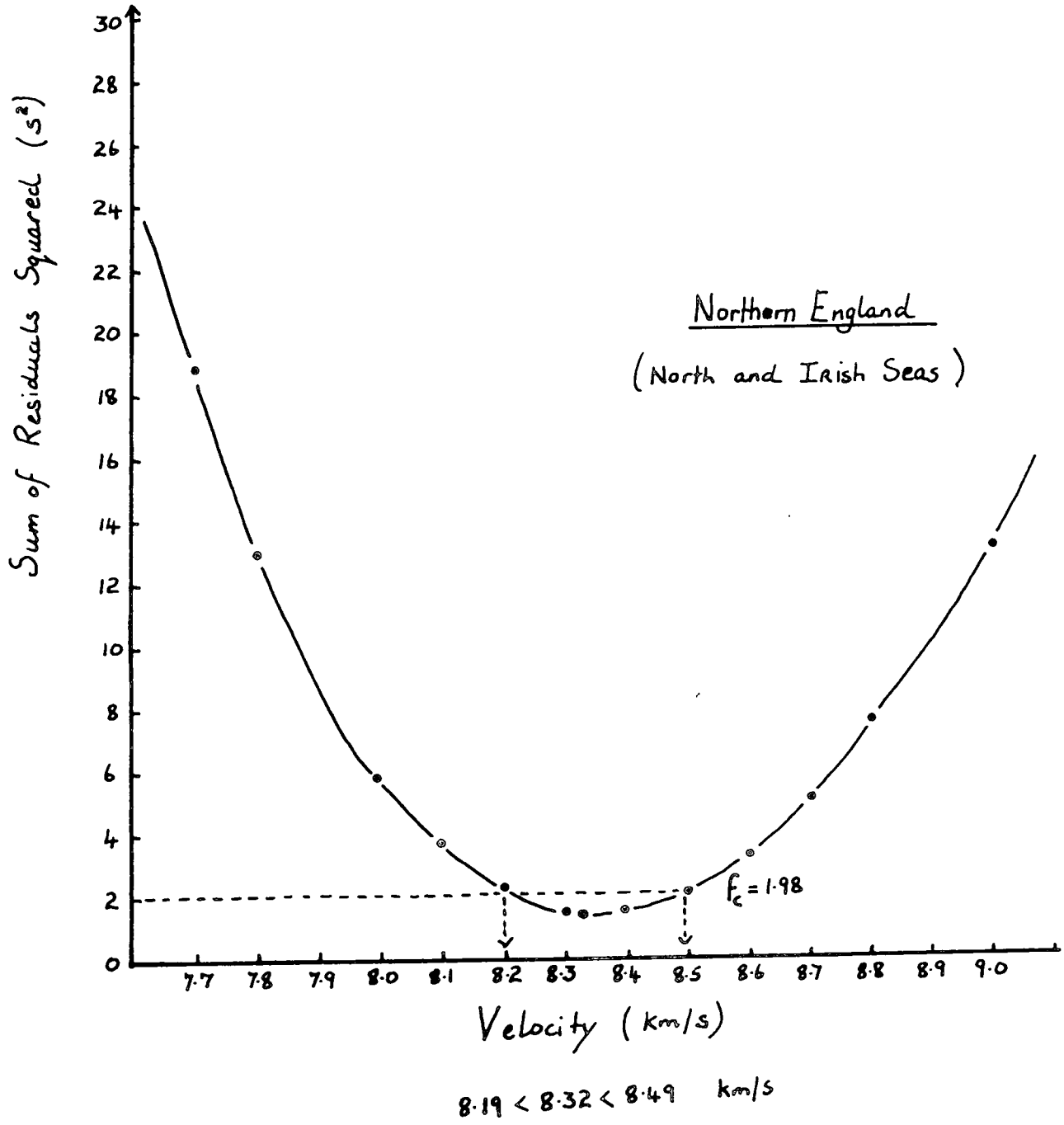

velocities vary from 8.21 to 8.28 km/s depending on which stations 42 to 52 are used to constrain the data (Fig. 4.20 and Table 4.2). However, including the Pn travel-time observations at the Irish station L15 yields a well constrained velocity of 8.19 km/s (Fig. 4.21). The solution is stabilized due to the reversal of the Irish Sea shots afforded by the use of station L15. The 95% confidence limits of 8.12 and 8.29 km/s are obtained for this velocity from an analysis of variance (Fig. 4.22) and the Berry and West method yields 95% confidence limits of +/- 0.02 km/s.

Including station L15 in Ireland and the North Sea shots a velocity of 8.27 km/s is obtained (Fig. 4.23). The analysis of variance of this solution yields a 95% confidence range from 8.16 to 8.39 km/s (Fig. 4.24). This velocity is obtained with reversed coverage under the Irish Sea and Northern England. The three 95% confidence limits obtained so far for the Pn refractor velocities 8.19 km/s, 8.27 km/s and 8.32 km/s are, 8.12 to 8.29 km/s, 8.16 to 8.39 km/s and 8.19 to 8.49 km/s respectively. These velocity differences are not significant within the estimated errors and it can be concluded that the Moho velocity under Northern England and the Irish Sea is greater than 8.12 km/s but less than 8.49 km/s. All three 95% confidence limits overlap in the velocity range 8.19 to 8.29 km/s. No rigorous statistical test can easily be applied to this range to check its significance. However it can be concluded that the best estimate possible of the Moho velocity under Northern England and Irish Sea regions to use in the initial synthetic seismogram model should be chosen from within the velocity range 8.19 to 8.29 km/s.

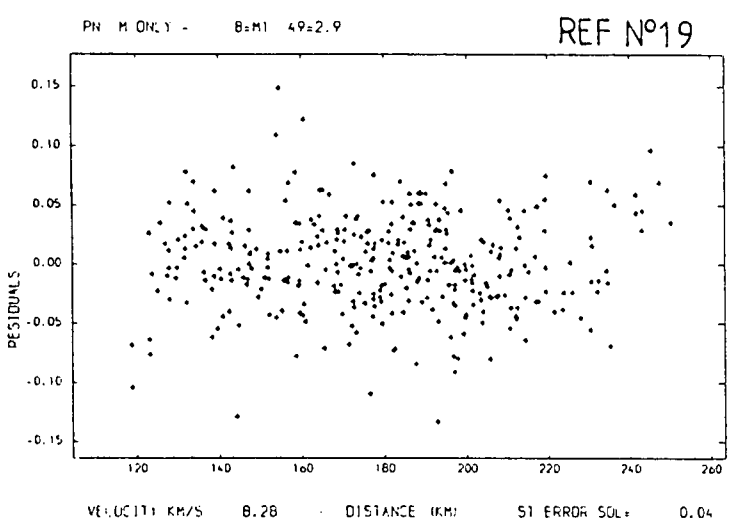


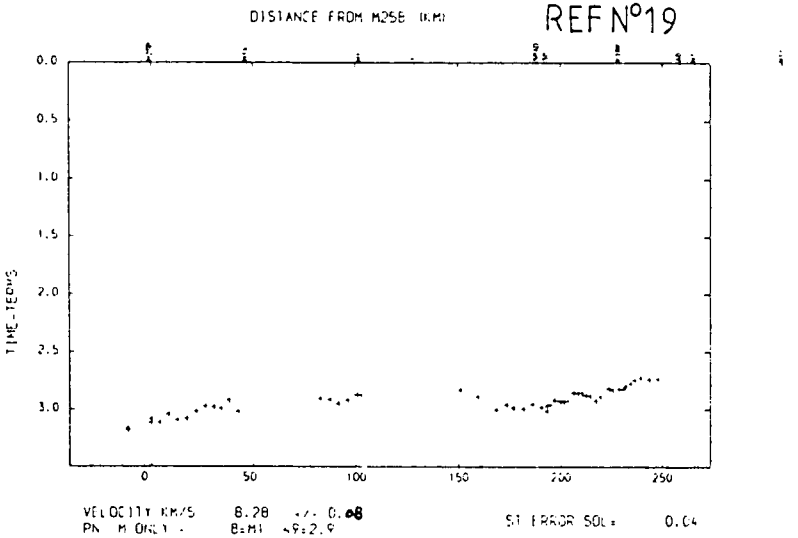


Figure(4.20) Pn time-term results for the Irish Sea using only the Irish Sea shots. The reference number corresponds to the numbers given in Table 4.2.

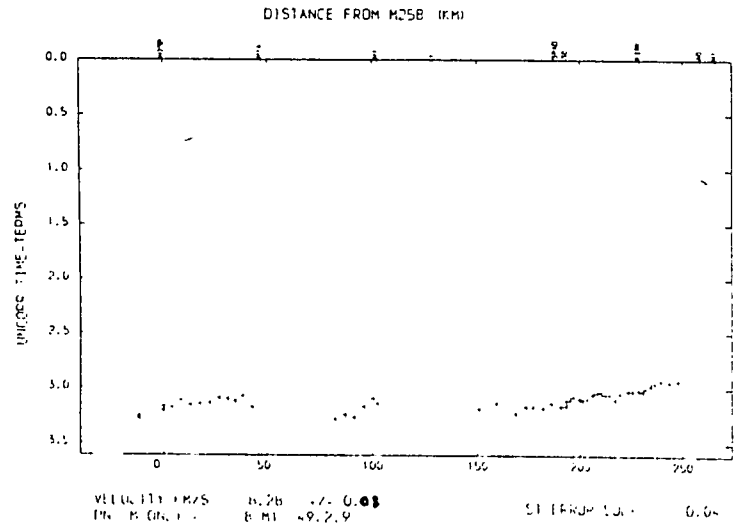


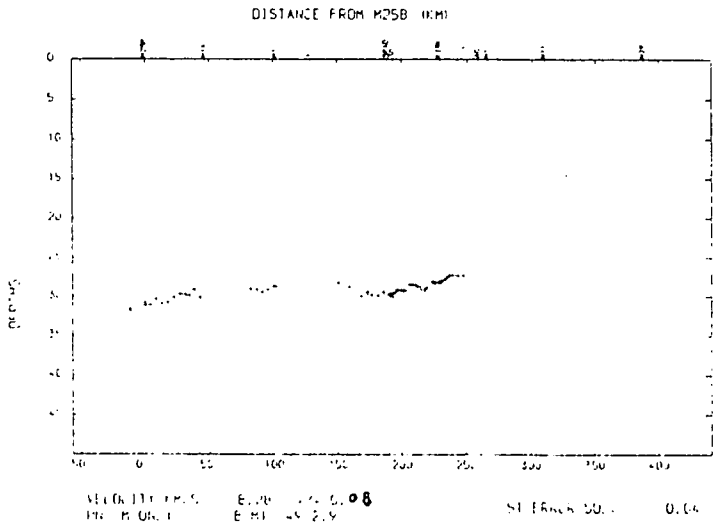

Figure(4.21) Pn time-term results for the Irish Sea using only the Irish Sea shots and the Irish station L15. The reference number corresponds to the numbers given in Table 4.2.

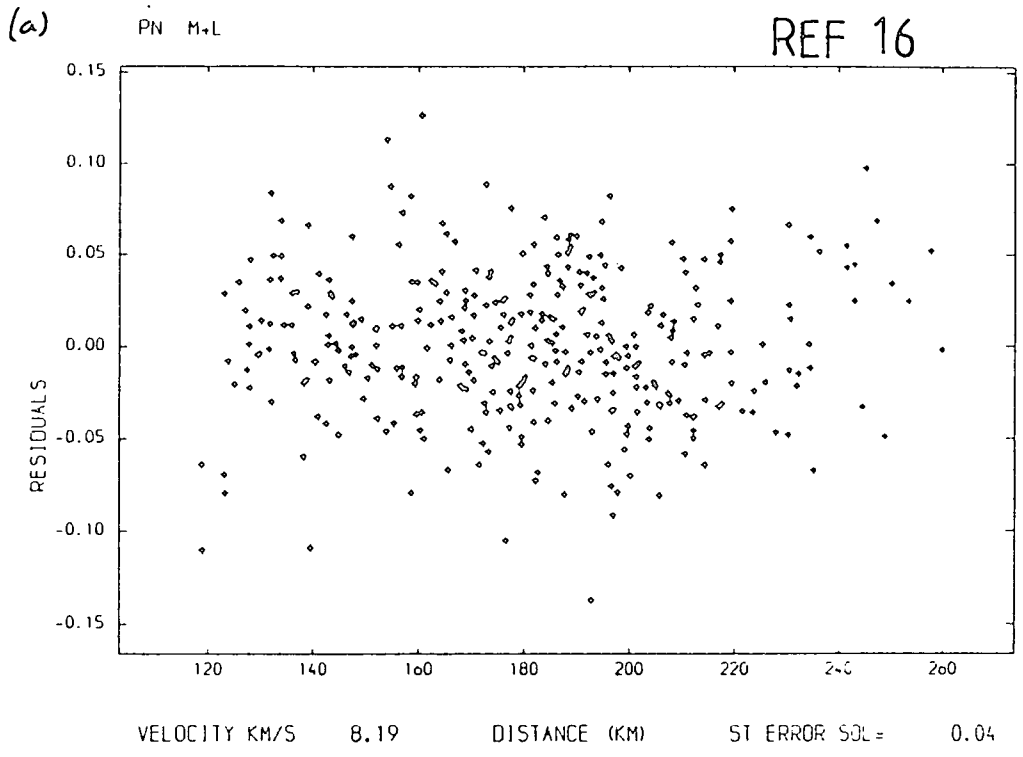


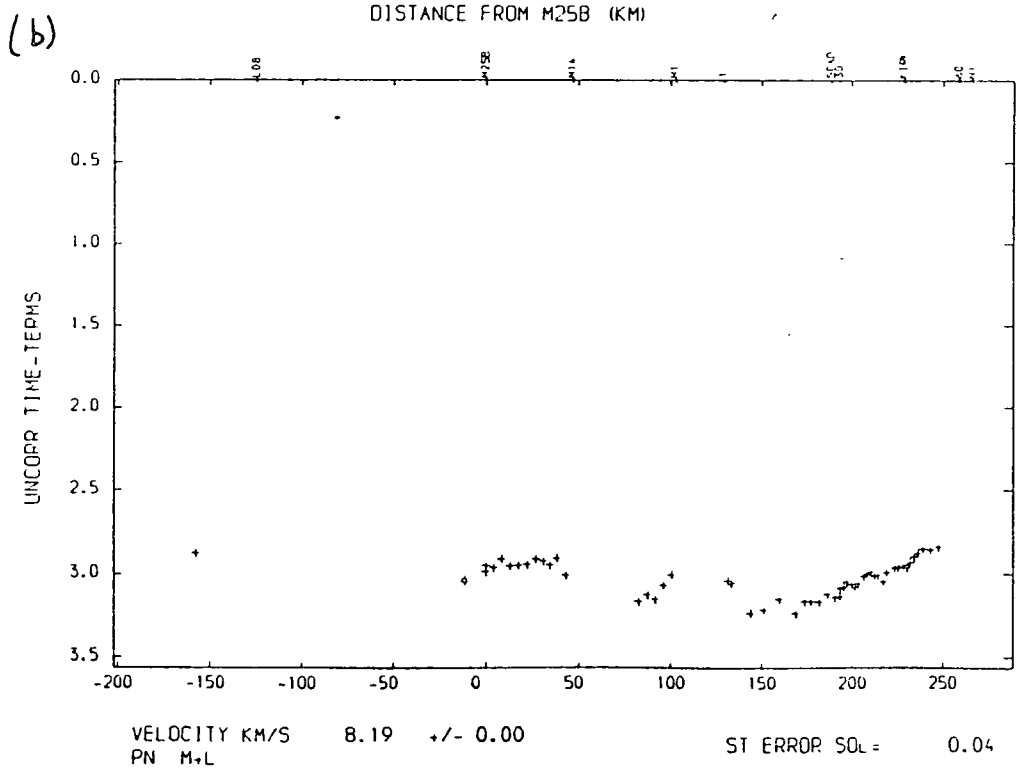

4.21 (c)

REF 16

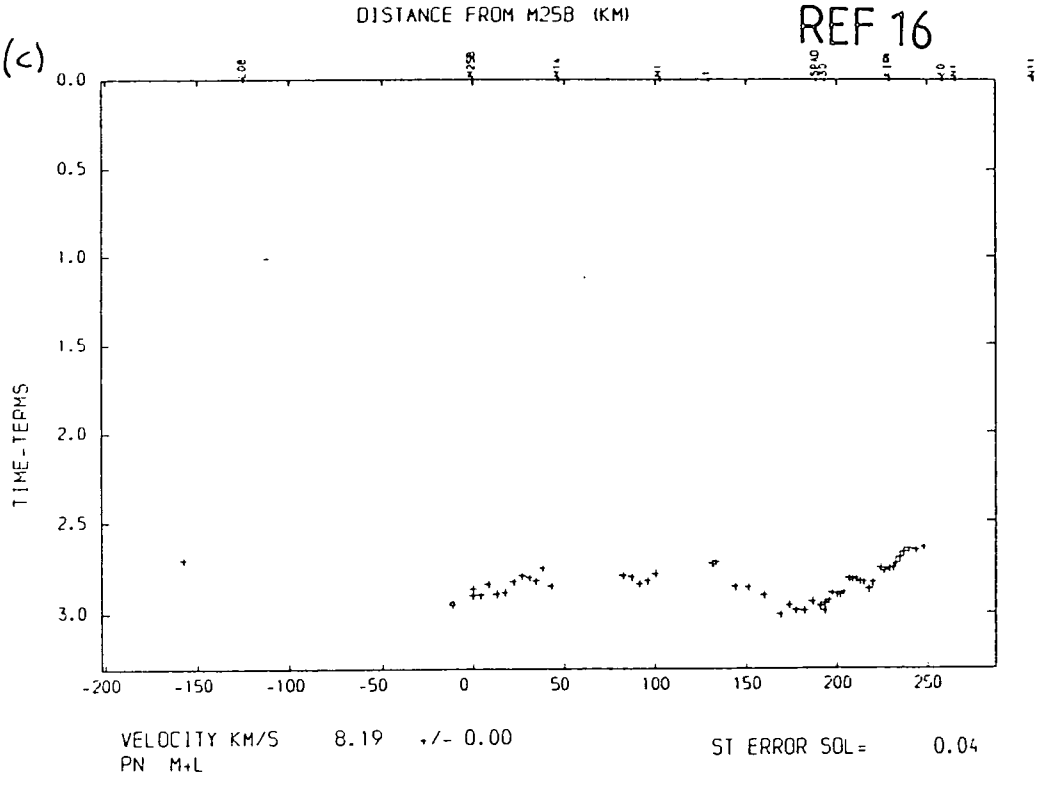


VELOCITY KM/S 8.19 +/- 0.00
PN M+L

ST ERROR SOL= 0.04

(d)

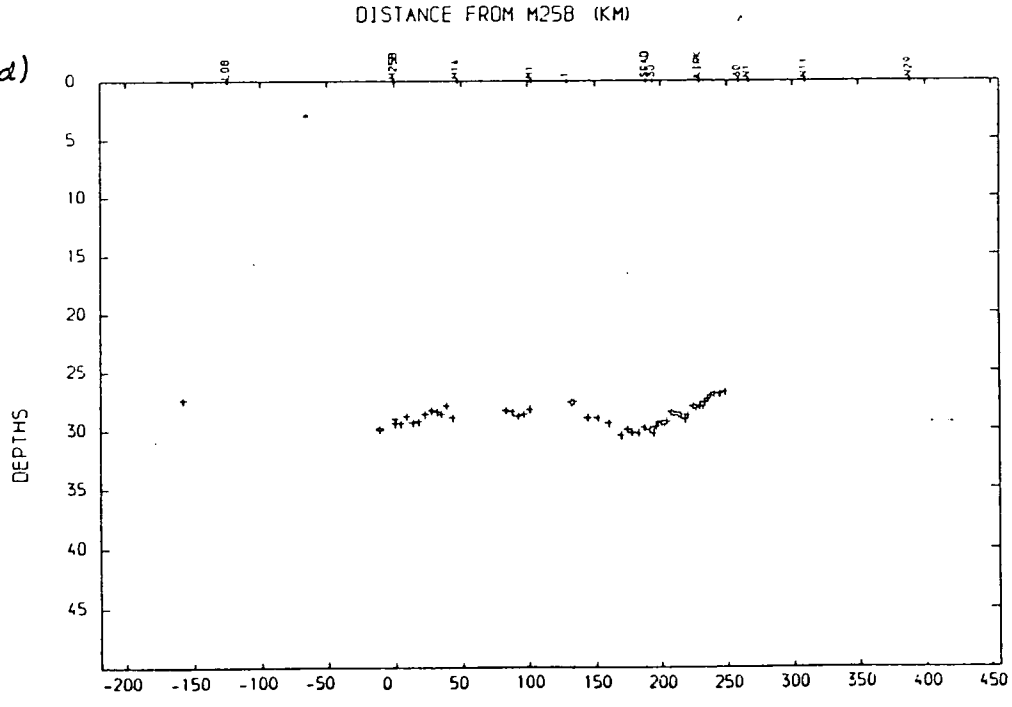


VELOCITY KM/S 8.19 +/- 0.00
PN M+L

ST ERROR SOL= 0.04

Figure(4.22) Analysis of variance of the Pn time-term analysis for the Irish Sea. The bounds give the 95% confidence limits on the solution velocity. See text for details.

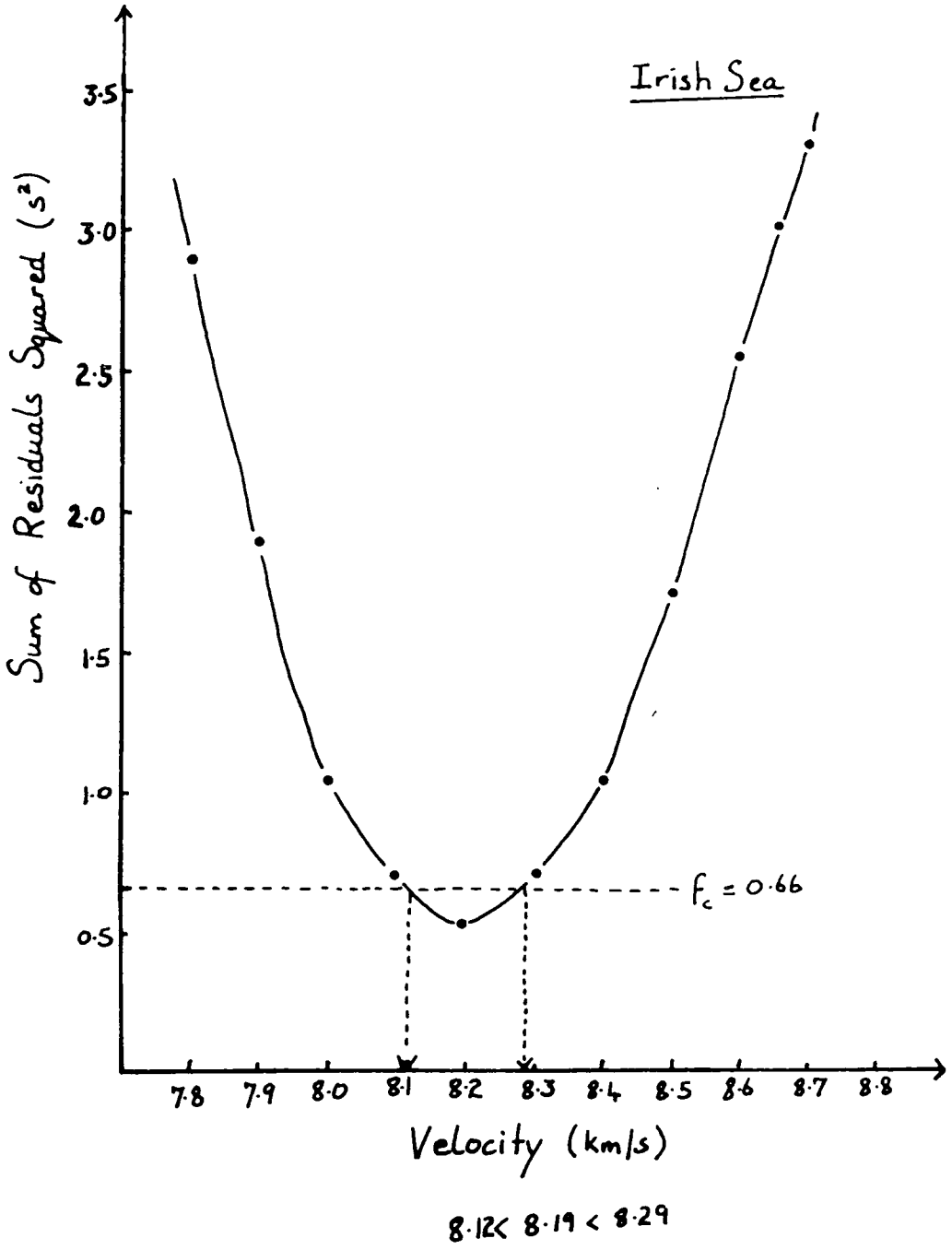


$8.12 < 8.19 < 8.29$

Figure(4.23) Pn time-term results all Pn travel-times observed from the Irish and North Sea shots and at the Irish station L15. The reference number corresponds to the numbers given in Table 4.2.

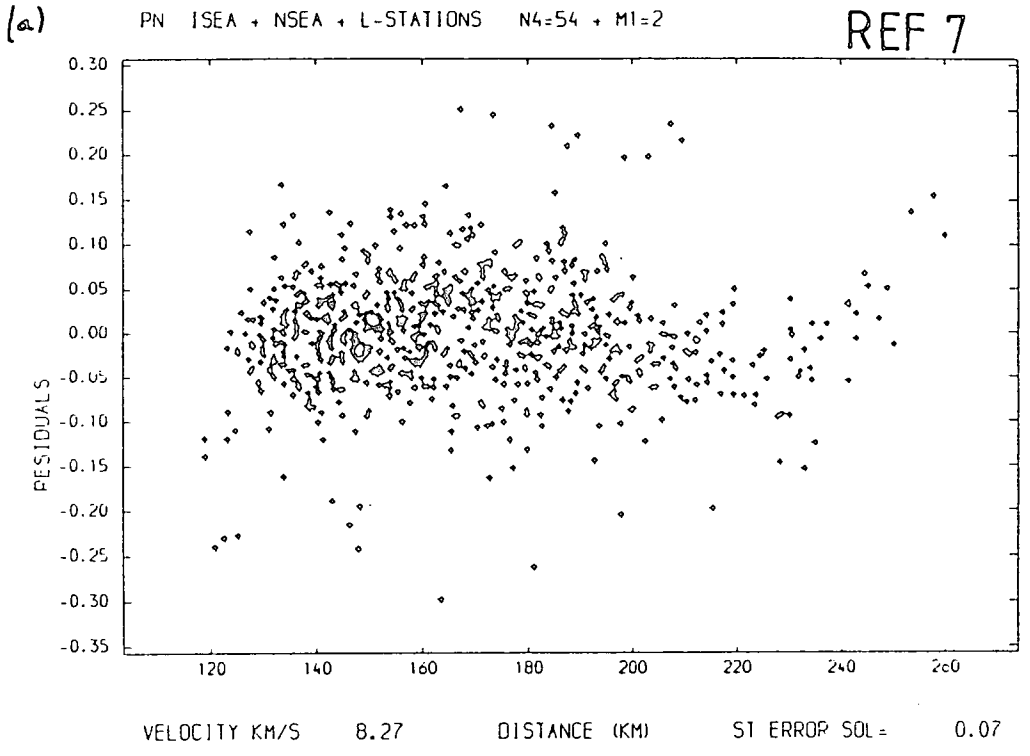


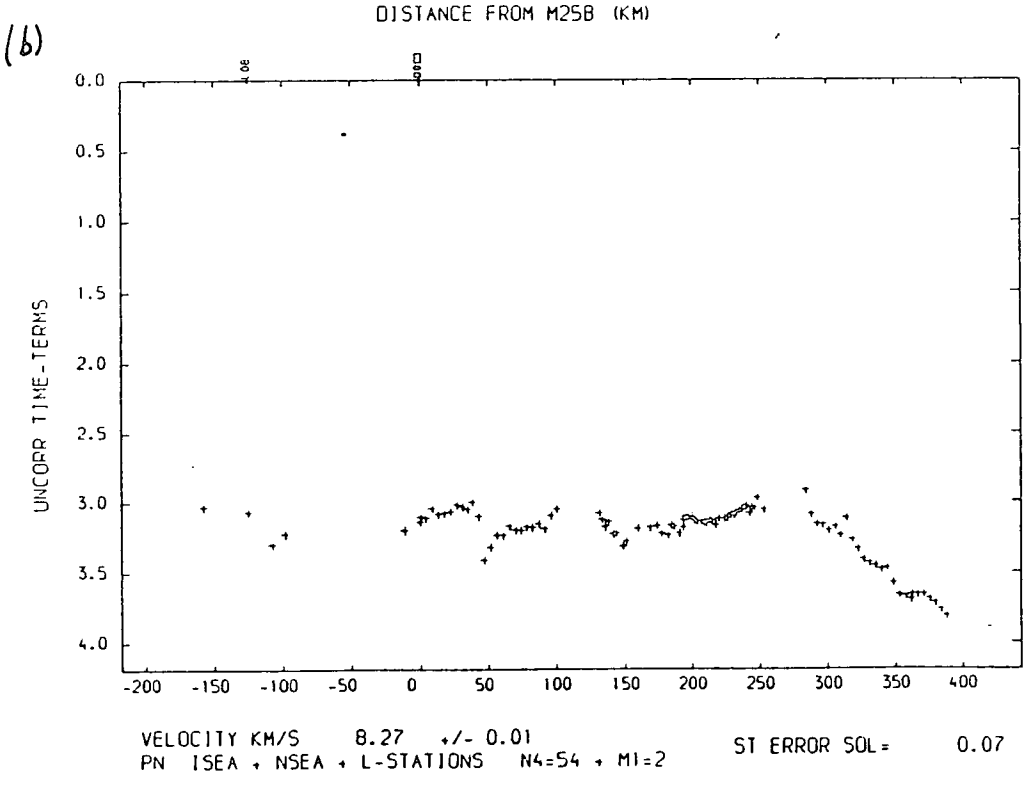

(c)

REF 7

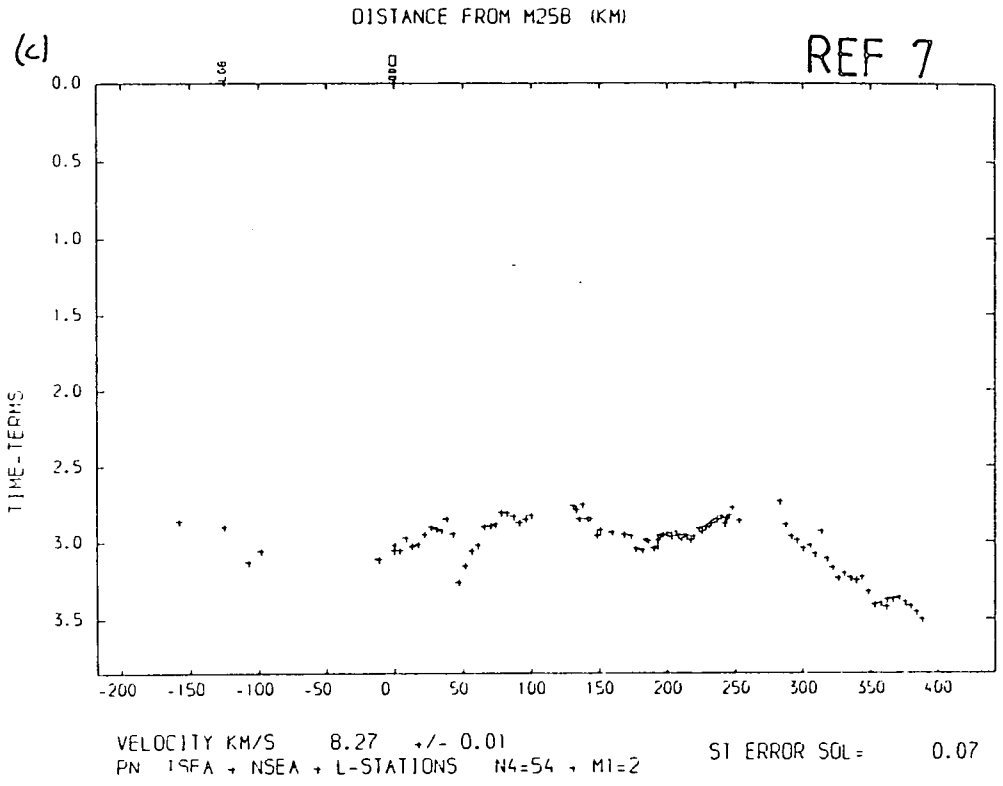


VELOCITY KM/S 8.27 +/- 0.01
PN ISEA + NSEA + L-STATIONS N4=54 + M1=2

ST ERROR SOL= 0.07

(a)

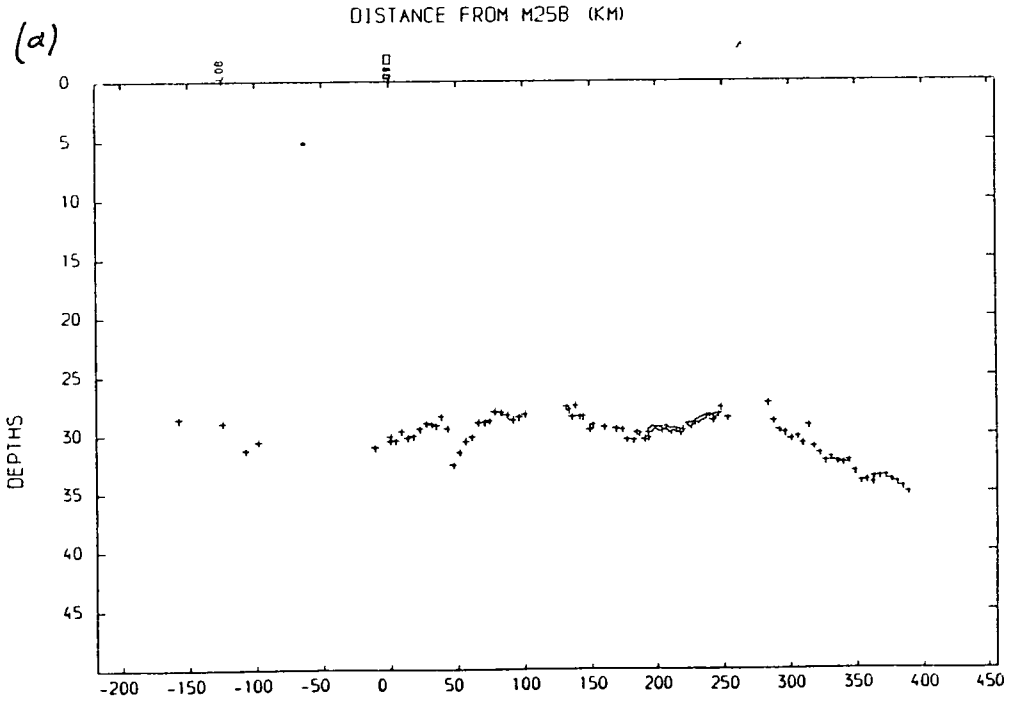


VELOCITY KM/S 8.27 +/- 0.01
PN ISEA + NSEA + L-STATIONS N4=54 + M1=2

ST ERROR SOL= 0.07

### 4.4.3 Time-term Analysis for the North Sea

Fig. 4.25 illustrates the time-term analysis using the North Sea Pn travel-times. Station 49 is constrained to a value of 2.9 s. The least squares velocity is 8.02 km/s. The analysis of variance of the solution yields very wide 95% confidence limits from 6.34 km/s to an undetermined upper limit greater than 10.0 km/s (Fig. 4.26) and the Berry and West method gives 95% confidence limits of 0.15 km/s. This solution for the North Sea is not well constrained. However, this result does agree with the 8.09 km/s found by Swinburn (1975). The time-terms and depths are also consistent with the results from the NERL experiment (Swinburn 1975, Bott *et al* 1985) and the structure of the base of the lower crust deduced from the PmP wide-angle reflection results (Fig. 4.16b, Section 4.5).

An attempt was made to control the results for the North Sea by including the LOWNET array station EBL in the analysis as this is offset from the shot line and should improve the velocity estimates. The travel-time picks of the first arrivals at distances greater than 130 km observed at EBL appear not to be compatible with the travel-times from the Caledonian Suture Seismic Project stations. These first arrivals have much larger amplitudes than Pn at the Caledonian Suture Seismic Project stations and the plotted arrivals have an apparent velocity of about 7.0 km/s. The picked phase at EBL thus appears not to be Pn, and these arrivals cannot be used to obtain a better estimate of the velocity of Pn beneath the North Sea.

Figure(4.24) Analysis of variance of the Pn time-term analysis using all the travel-times. The bounds give the 95% confidence limits on the solution velocity. See text for details.

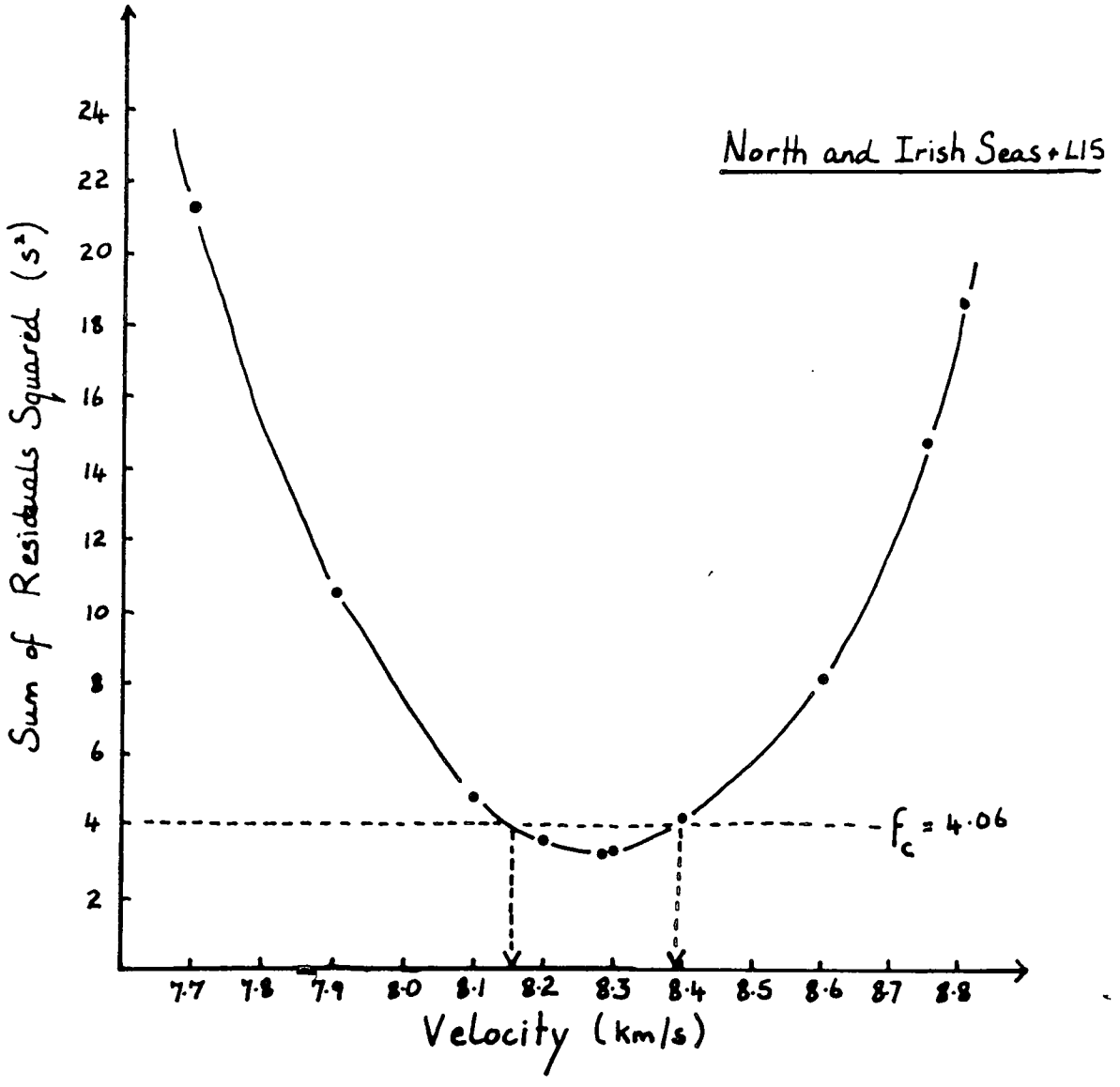


8·16 < 8·27 < 8·39

Figure(4.25) Pn time-term results for the North Sea using only the North Sea shots. The reference number corresponds to the numbers given in Table 4.2.

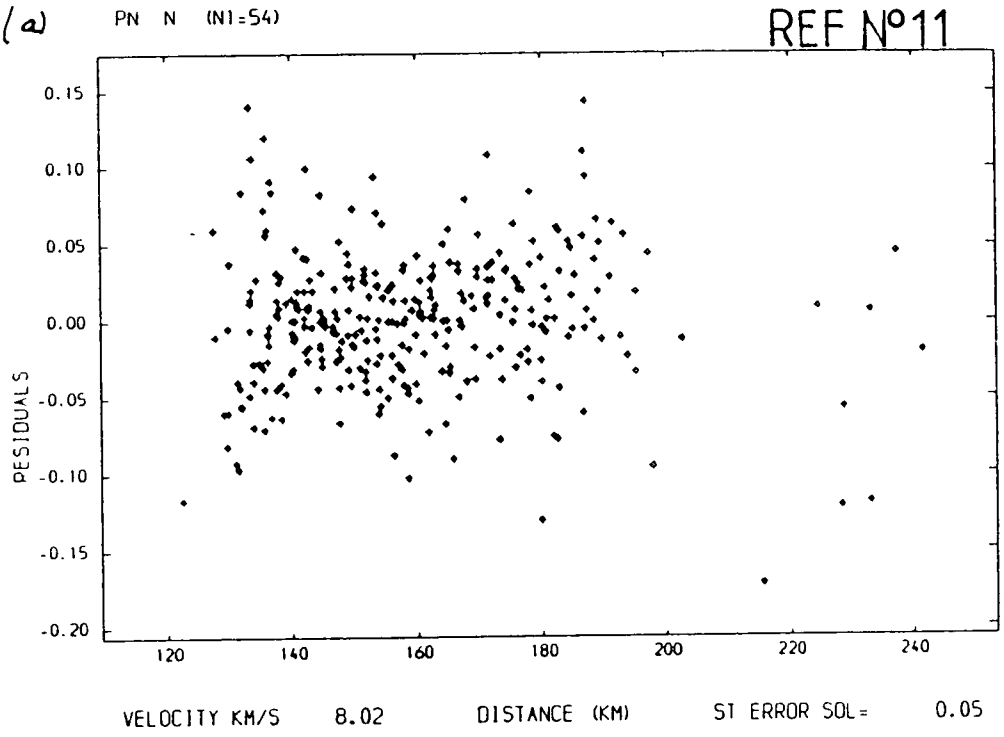


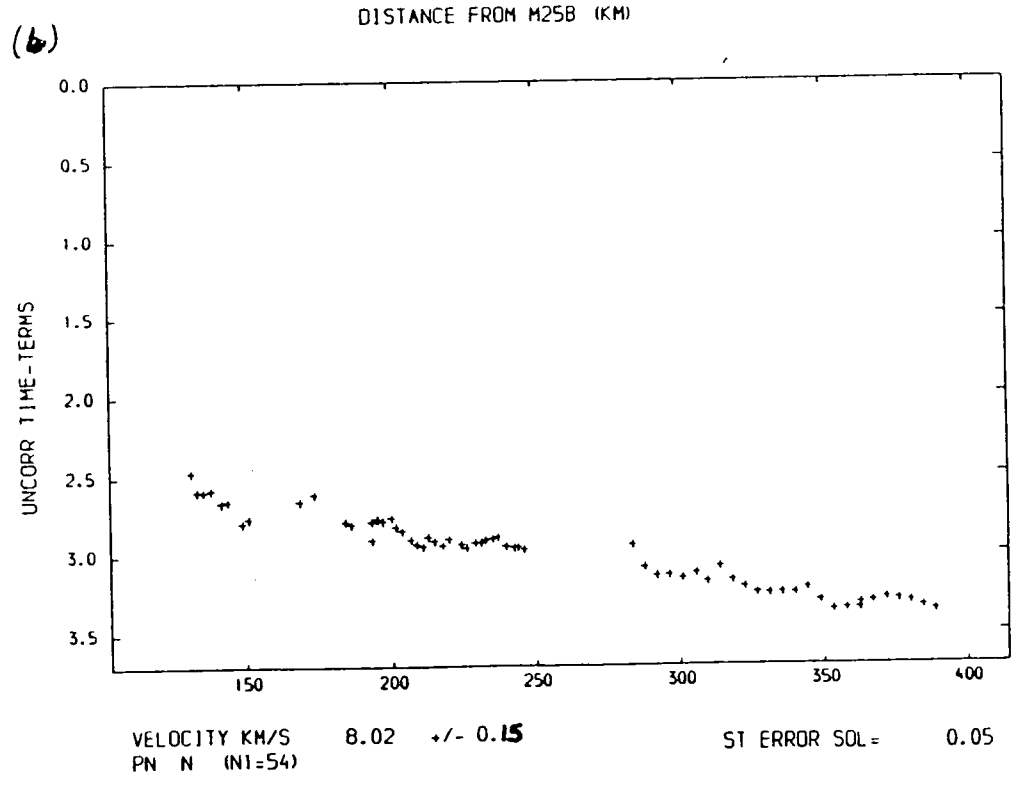

(c)

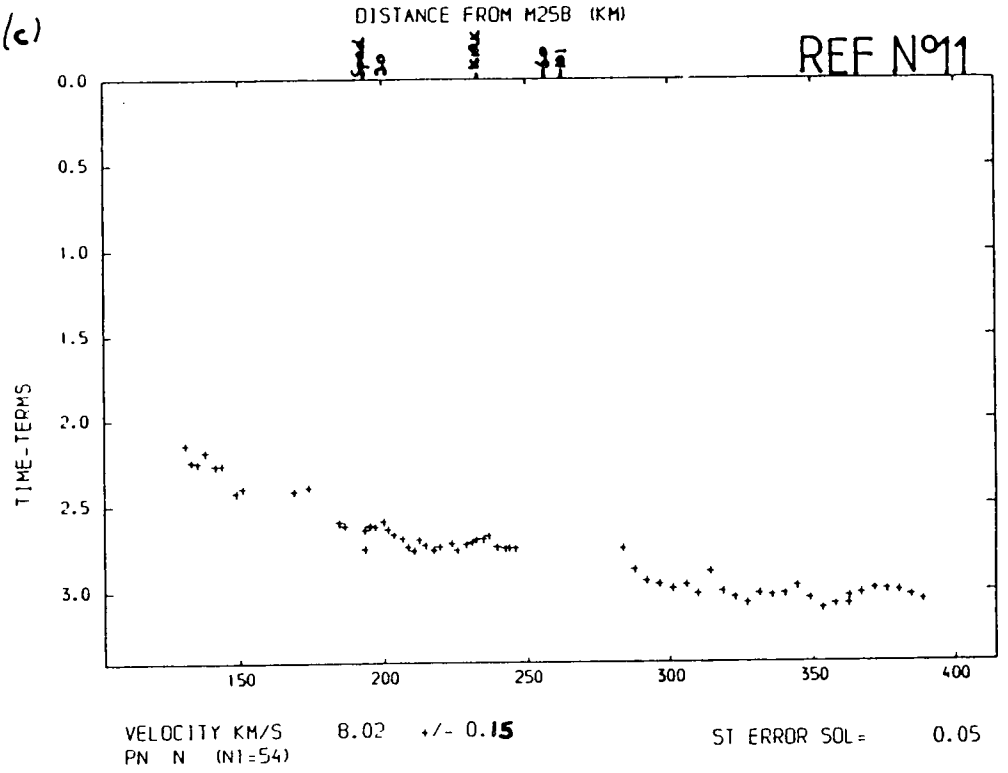


VELOCITY KM/S 8.02 +/- 0.15 ST ERROR SOL= 0.05
PN N (N1=54)

(d)

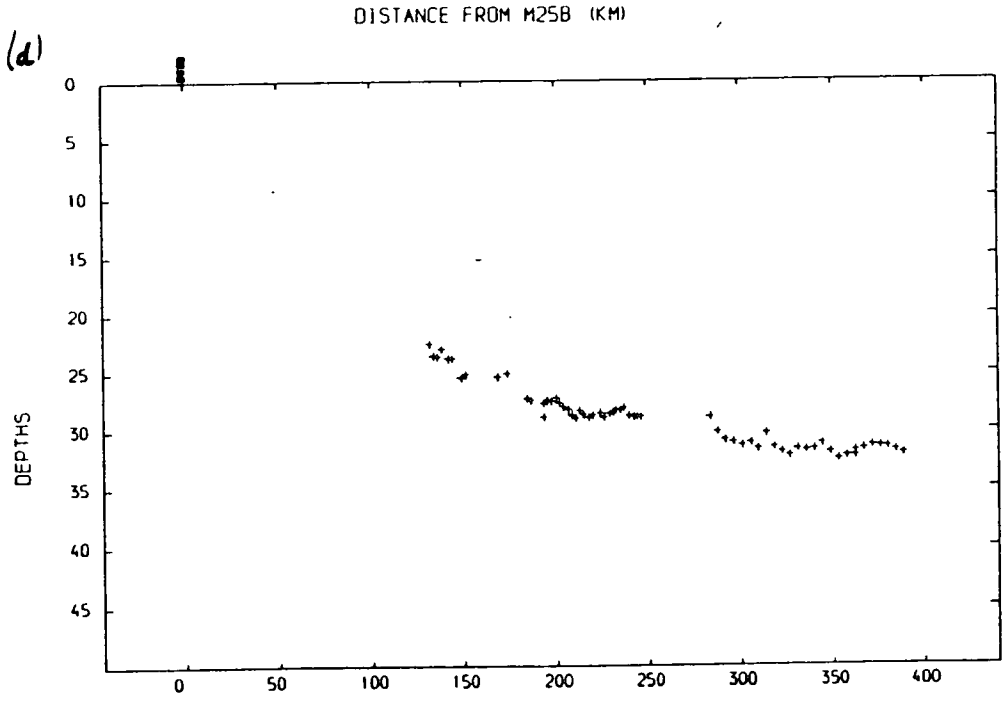


VELOCITY KM/S 8.02 +/- 0.16 ST ERROR SOL= 0.05
PN N (N1=54)

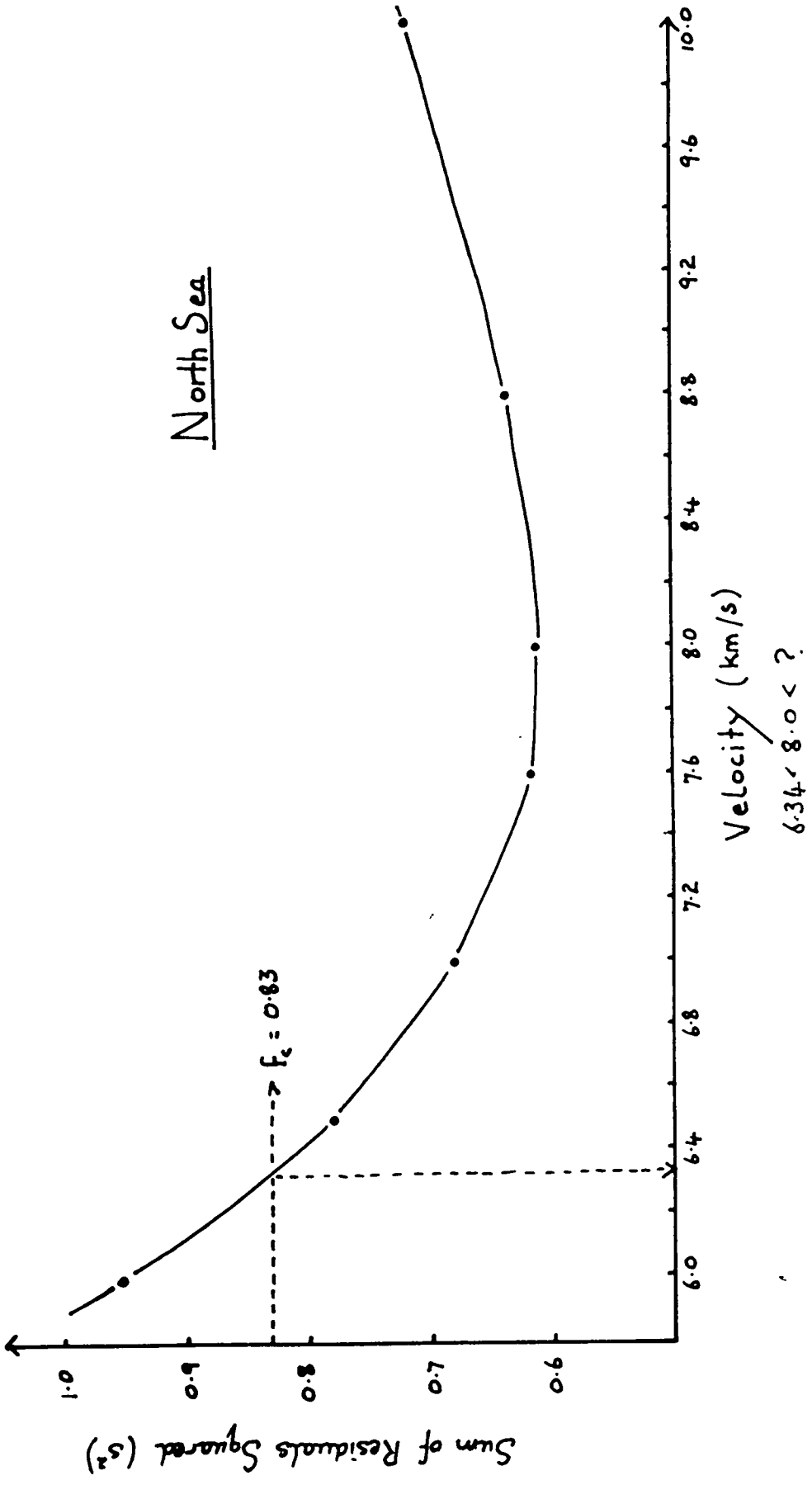


Figure(4.26) Analysis of variance of the Pn time-term analysis for the North Sea. The bounds give the 95% confidence limits on the solution velocity. See text for details.

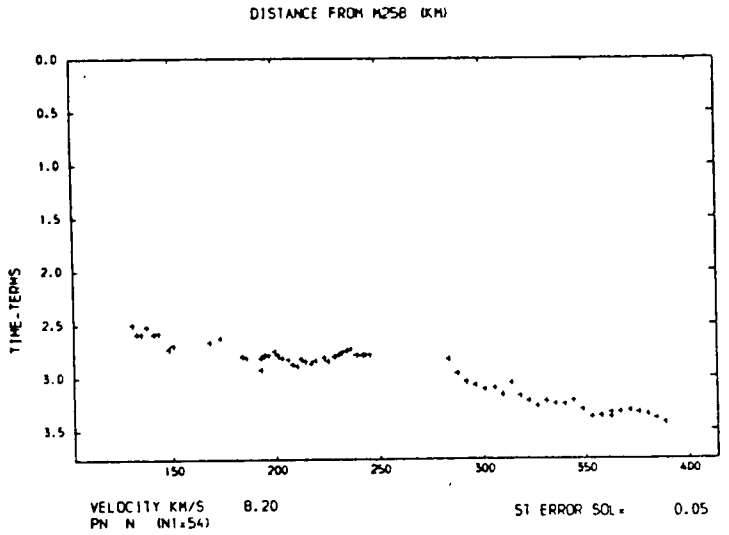


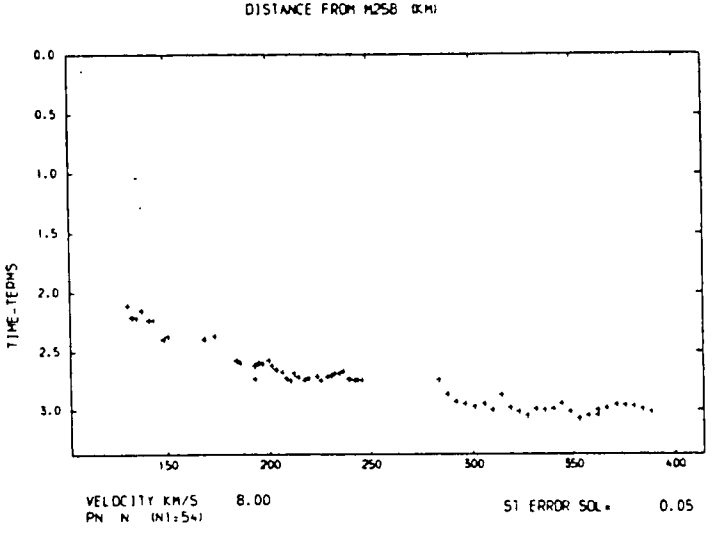


Figure(4.27) Pn time-term results for the North Sea constraining the velocity to 8.0, 8.1, 8.2 and 8.3 km/s.

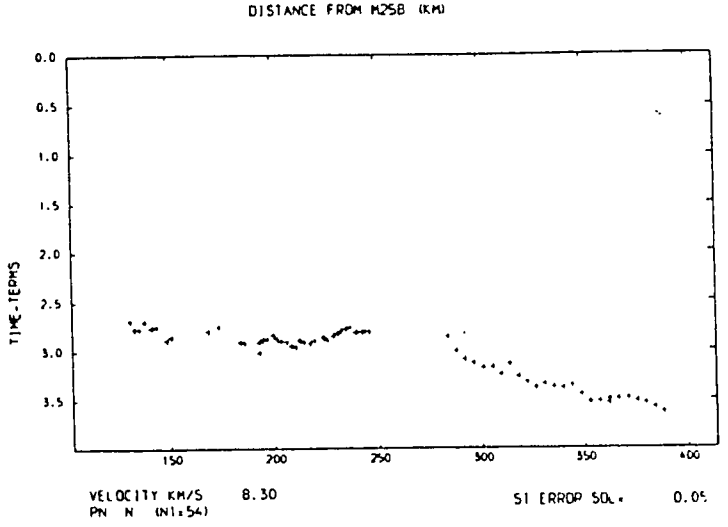


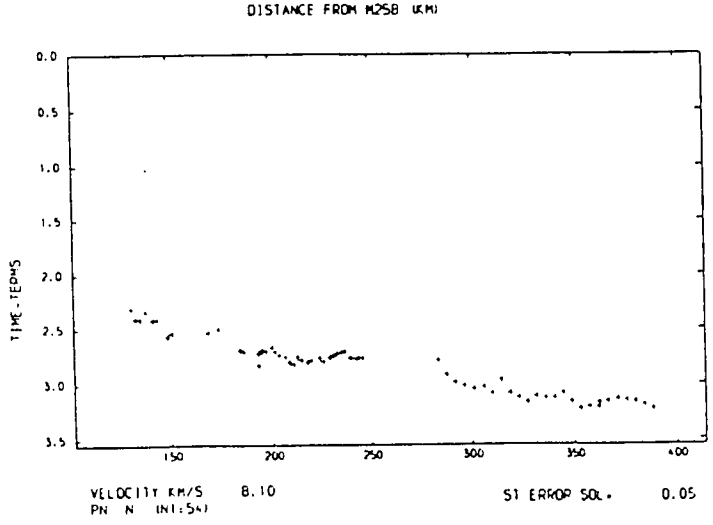

The solution is found to be sensitive to the constraint used on station 49. The estimated velocity increases to 8.4 km/s if the constraint on station 49 is increased from 2.9 s to 3.04 s. The effect of changing the constraint station from 49 to the stations 42 to 52 does not affect the time-term solutions.

The time-terms corrected for the shallow structure in Fig. 4.25 exhibit a break in slope at about station 34 (which lies 201 km from M25B) and decrease from 2.3 s to 3.0 from west to east from station 1 to shot N29. Possible causes could be either a higher Moho velocity west of station 34 or a westward rise in a Moho with a constant velocity of 8.0 km/s. A velocity between 8.19 to 8.49 km/s is estimated underneath Northern England from the analysis in section 4.4.1 and so a lateral change in the Moho velocity between the North Sea region and Northern England appears to be the best explanation. Fig. 4.27 illustrates that using higher velocities flattens the time-terms under the stations and causes the time-terms under the North Sea shots to increase with increasing distance. For example, for a velocity of 8.3 km/s the time-terms under the stations are constant at about 2.8 to 2.9 s whilst the time-terms for the shots increase eastwards from 2.8 s at N1 to about 3.6 s at N29. It is concluded that the velocity of 8.02 km/s is the best estimate of the Moho velocity under the North Sea given the instability of the solutions obtained when stations 1 to 34 are omitted (as in run 10) but that this result is preliminary. The depth to the Moho under the North Sea is further constrained using gravity data in chapter 5 before proceeding to synthetic

seismogram modelling.

### 4.4.4 Discussion of the Time-term Analysis of Pn

The Pn velocity is calculated to be 8.02 (6.34-10.0) km/s under the North Sea, 8.19 (8.12 - 8.29) km/s under the Irish Sea and 8.32 (8.19 - 8.49) km/s under Northern England. The Irish Sea and Northern England velocities do not differ significantly and both are estimated to exceed 8.12 km/s. No reliance can be placed on the estimate of the North Sea Pn velocity from the time-term analysis alone.

Fig. 4.28 and Fig. 4.29 illustrate the results of using travel-times corrected for shallow structure as input to the time-term programme (runs 23 to 25 in Table 4.2). This analysis was performed to check that the solution velocities are not due to spurious effects of the shallow sediment delays. The least squares velocity in the North Sea increases slightly to 8.09 km/s. For the Irish Sea the solutions were found to lie between 8.18 to 8.35 km/s. The residuals are plotted against the site positions in Fig. 4.30. The scatter is large and there appears to be no correlation of the residuals with the position of the sites. It is concluded that the solution velocities obtained are not due to any spurious effects of the shallow sediment cover.

The features observed on the travel-time matrices together with the Pn analysis may suggest that the velocity just below the Moho increases from about station 34 westward from 8.0 km/s to between 8.12 to 8.49 km/s. The Moho depths deduced

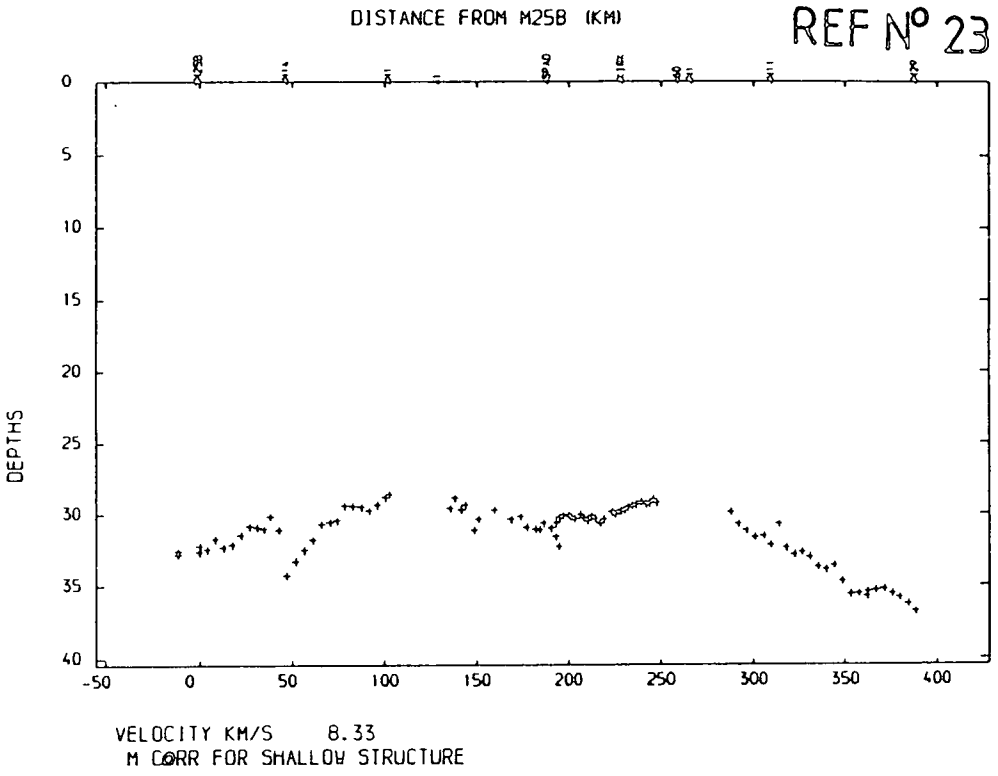


Figure(4.28) Pn time-term results for all shots. The travel-times are corrected for shallow structure before calculating the time-terms. The reference number corresponds to the numbers given in Table 4 2.

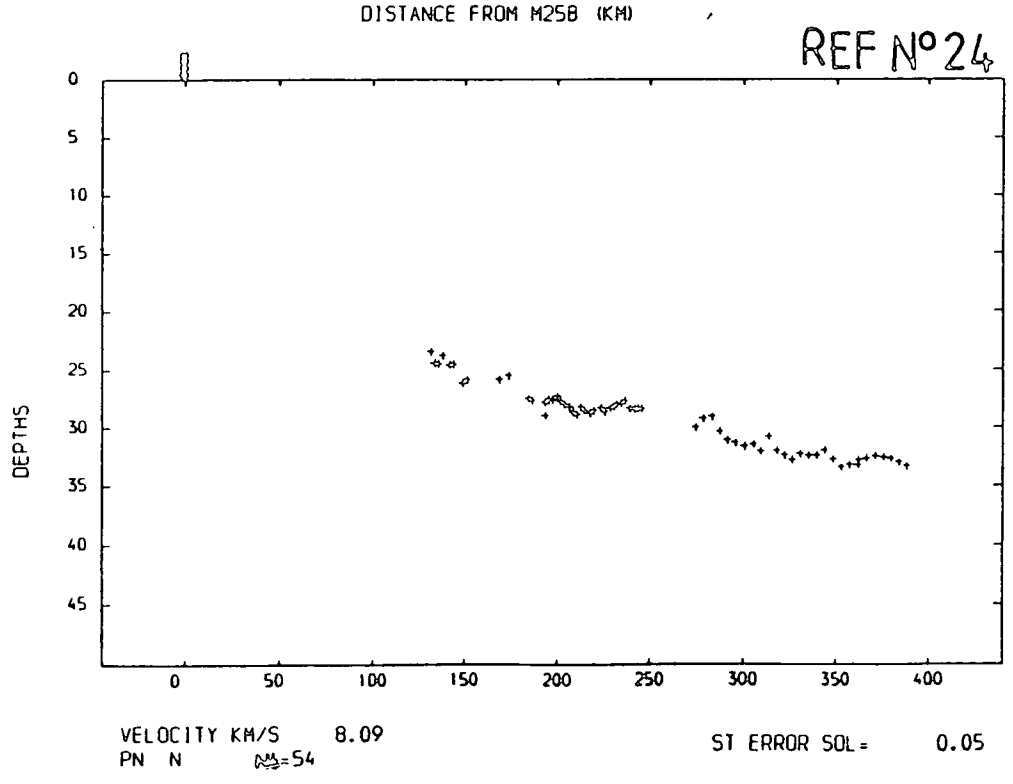


Figure(4.29) Pn time-term results for shots N1-N29 the travel-times are corrected for shallow structure before calculating the time-terms. The reference number corresponds to the numbers given in Table 4.2.

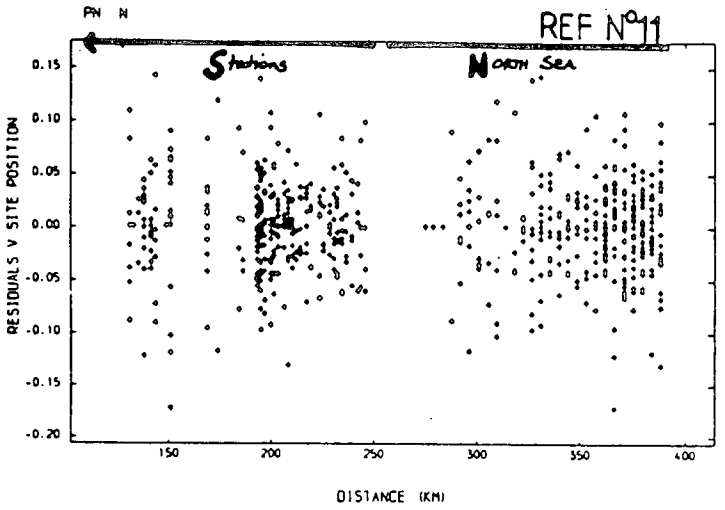


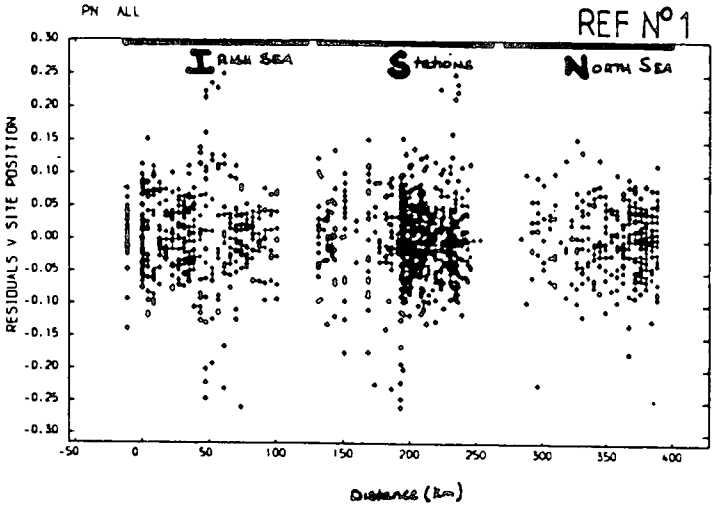


Figure(4.30) Residuals plotted against site position for the runs corresponding to the reference numbers given in Table 4.2.

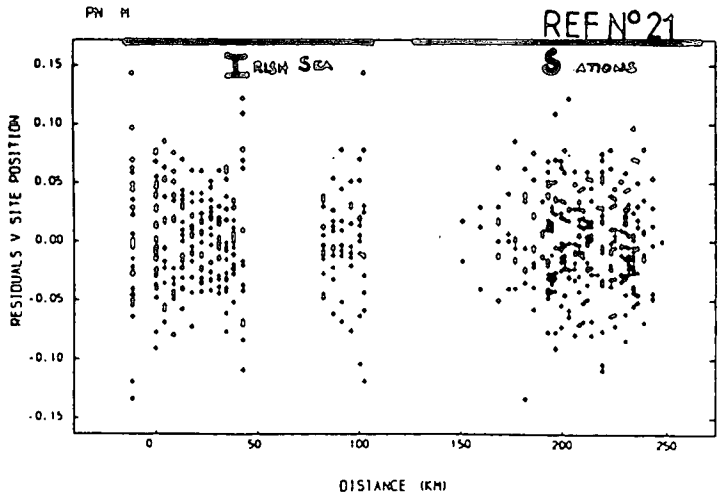


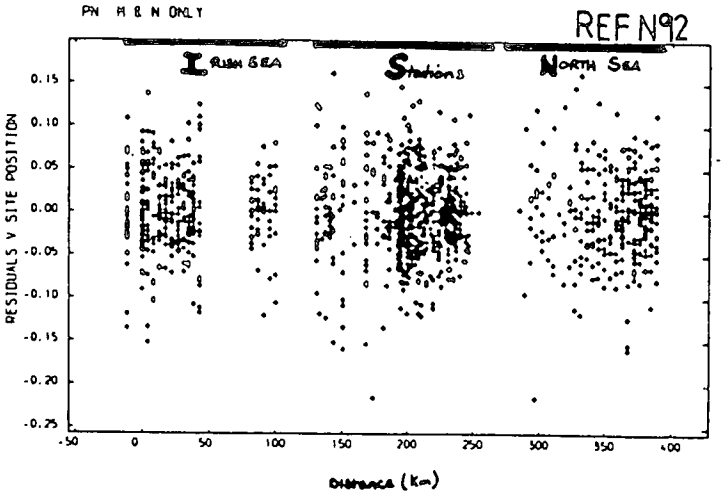

using these velocities are checked in Section 5.1 by comparing the gravity effect calculated using this seismic model to the observed gravity anomaly along the CSSP line.

## 4.5 COMPARISON OF THE PMP AND PN RESULTS

The qualitative interpretations made from the travel-time matrices together with the PmP and Pn results indicate that the PmP and Pn phases are returned from different depths under the Irish Sea in contrast to the results east of about station 34 where the calculated PmP and Pn depths are approximately the same. The separation of the two phases westwards beneath the Irish Sea can be explained by either an extended gradient zone or by a higher velocity layer between the PmP interface and the Pn refractor. Fig. 4.31 summarises the results from the analysis of the travel-times of PcP, PmP and Pn. The velocity and depths under the North Sea calculated from Pn are not well constrained but are consistent with previous work in the region and with the PmP results. The time-term solutions in the Irish Sea are well constrained.

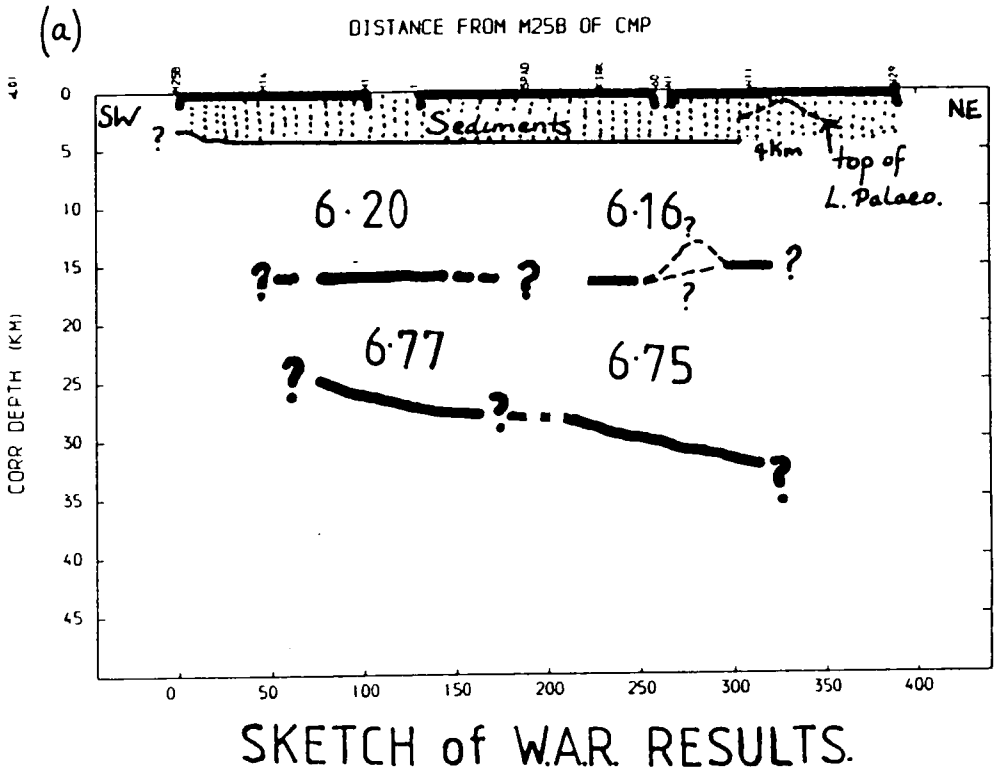


Figure(4.31) (a) Summary of the wide-angle results. Velocity values are the average velocities calculated for each layer.
(b) Summary of the Pn time-term results. Velocity values are the refractor velocities considered to be most probable.

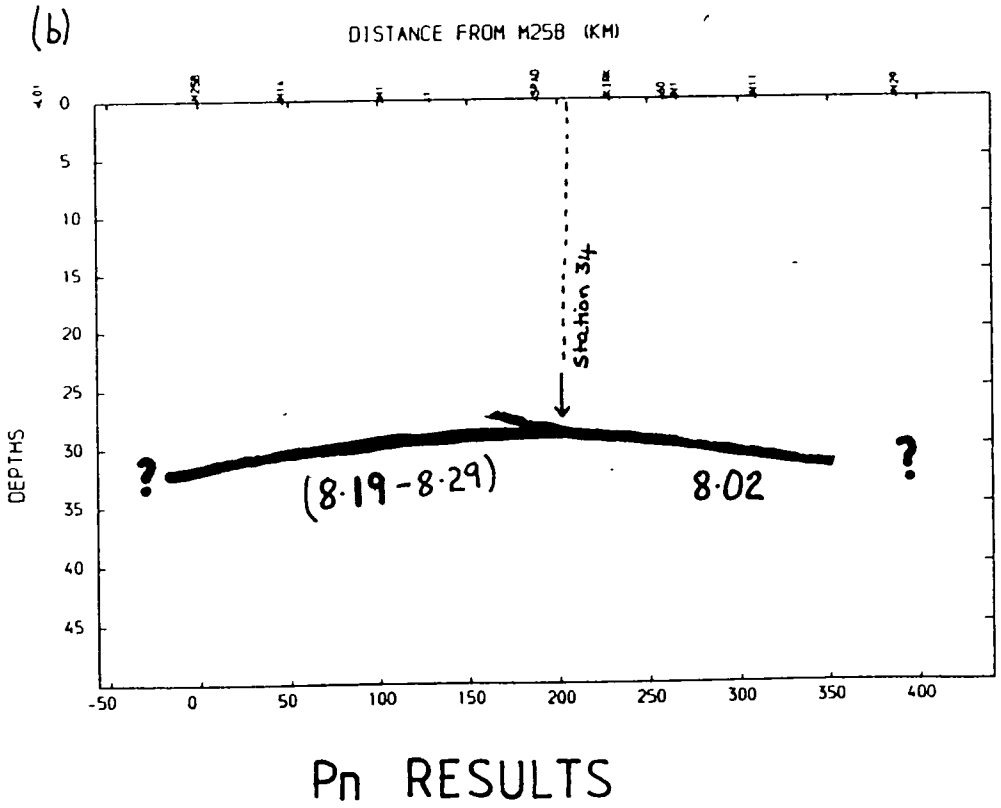

# CHAPTER FIVE

## INTERPRETATION AND MODELLING OF THE DEEP STRUCTURE

The preliminary model deduced from the forward intepretation methods presented in the previous chapter is used as a starting point for the gravity and synthetic seismogram modelling presented in this chapter. The model is first constrained using the gravity along the the Caledonian Suture Seismic Project line. Preliminary 1-D and 2-D synthetic seismogram modelling is then used to refine the model and to check that, to the degree of accuracy possible, the model produces synthetic seismograms that compare well to the observed sections. Discrepancies that still exist are highlighted and attempts are made to resolve any difficulties. Comparisons with the BIRPS WINCH profiles in the area are made to check the consistency of the model with the WINCH sections. Finally comparisons with previous geophysical investigations in the region are made and the geological implications of the results are discussed.

A number of terms need to be defined.

1. The velocity gradient at about 15.5 km identified from the PcP arrivals is referred to as the mid-crustal boundary.
2. The layer between the basement refractor identified by Green (1984) and Bott et al (1985) and the mid-crustal boundary is referred to as the upper crust.
3. The depths calculated from the PmP arrivals represent either an abrupt or gradational increase in velocity. If no interpretation of the velocity structure is implied the

PmP depths are referred to as the PmP boundary. If the PmP boundary is interpreted as an abrupt increase in velocity it is referred to as the PmP interface. If it is interpreted as a gradational increase in velocity it is referred to as the PmP gradient zone.

4. The layer between the mid-crustal boundary and the PmP boundary is referred to as the lower crust.
5. The depths calculated from the Pn time-term analysis are referred to as the Pn boundary.
6. If no interpretation of the internal velocity structure of the layer between the PmP and Pn boundaries is implied it is referred to as the transitional Moho. If a gradational increase in velocity with depth is interpreted the transitional Moho is referred to as a gradational Moho. The top surface of such a gradational Moho is defined by a PmP gradient zone. Alternatively, if only a gentle gradient is interpreted between the PmP and Pn boundaries the transitional Moho is referred to as a Moho layer. The top surface of the Moho layer can be defined either by a PmP interface or by a PmP gradient zone.

## 5.1 GRAVITY MODELLING

It is important to consider the Bouguer anomaly along the Caledonian Suture Seismic Project profile prior to detailed seismic modelling because of the control it gives on the depths to the Moho beneath the North Sea. These depths, found from the time term analyses of Pn presented in Section 4.4.3, were not well constrained. They are constrained by the Bouguer gravity anomaly.

The Bouguer gravity anomaly along the complete Caledonian Suture Seismic Project line decreases from 25 mgal at the Shannon Estuary to 5 mgal over central and eastern Ireland. It increases eastward across the Irish Sea to a peak of 35 mgal decreasing again east of the Carlisle Basin to remain relatively constant at about zero mgal north-eastwards onto the North Sea (Figs. 5.1 and 5.2). The line runs along the northern edges of the Peel Basin and Northumberland Trough and along the central line of the Solway and Carlisle Basins. The programme GRAV2D was used to model the gravity. The fit between the observed and calculated gravity values should not be expected to be better than about 5 mgal because of the three dimensional effects of the offline structures not modelled by GRAV2D.

The densities used are taken from Blundell et al (1985) and Green (1984) and are tabulated in Table 5.1. The upper crust was interpreted by Green (1984) to be Precambrian crystalline metamorphic basement which has a density of 2.74 $g/cm^3$ according to Blundell et al (1985). The basement is probably more basic at depth and so the density would be expected to increase slightly in the upper crust to about 2.80 $g/cm^3$. It was found that using 2.80 $g/cm^3$ as opposed to 2.74 $g/cm^3$ did not have a significant effect on the fit of the models. The lower crust has an average velocity of 6.75 - 6.77 km/s which lies within the range of lower crustal velocities given by Blundell et al (1985) of 6.45 km/s for pyroxene granulite gneiss and 7.00 km/s for garnet granulite gneiss (Table 5.1). By linear interpolation between these velocities the lower crust is assigned a density of 3.04 $g/cm^3$ which lies between the

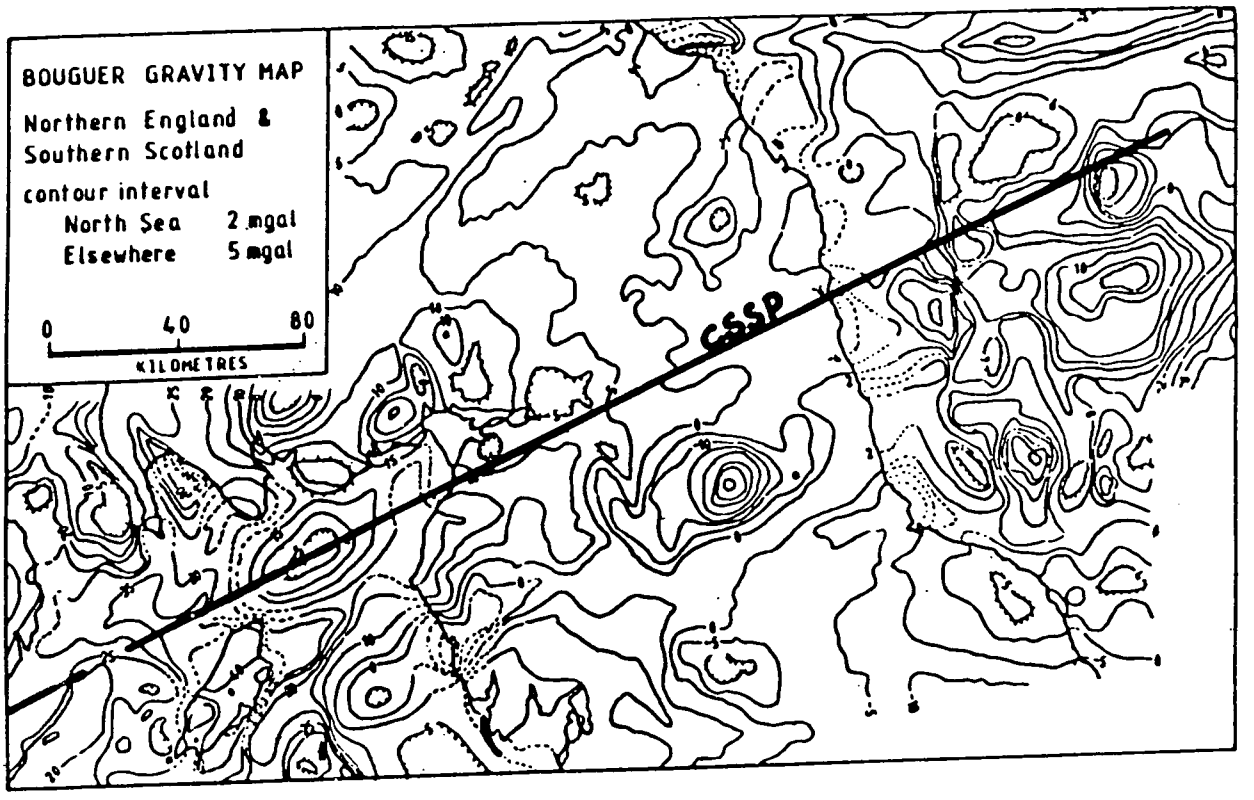


Figure(5.1) (a) Bouguer anomaly contour map over Northern England and adjacent marine areas.

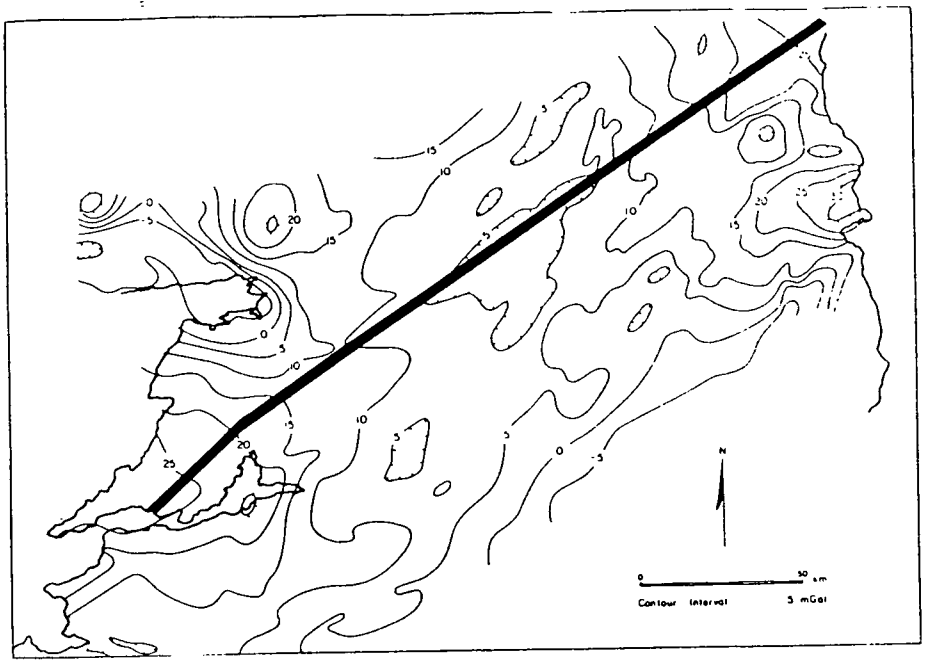


Figure(5.1) (b) Bouguer anomaly contour map across Ireland (taken from Jacob et al 1985)

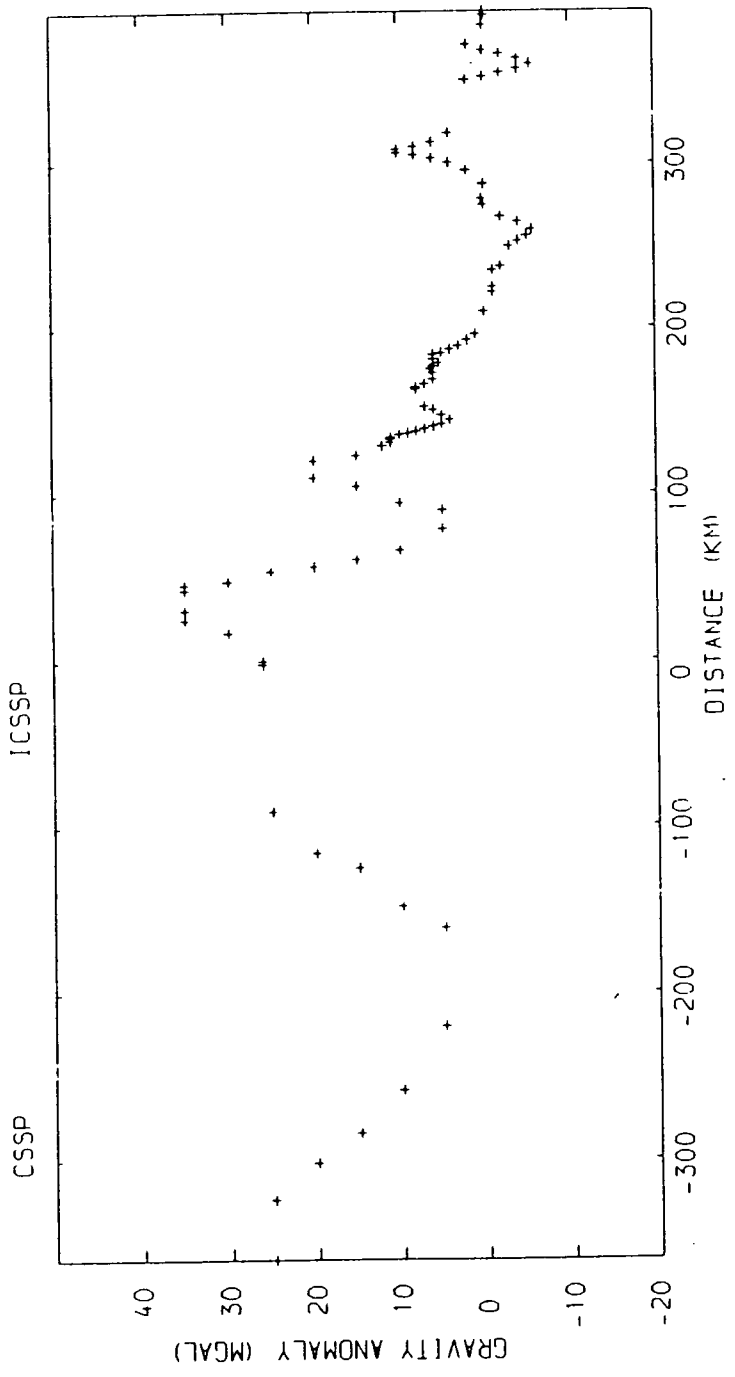


Figure(5.2) Bouguer gravity anomaly along the complete CSSP line from the Shannon Estuary to the North Sea.

TABLE 5.1

PARAMETERS USED IN GRAVITY MODELLING

| Material | Velocity (km/s) | Density ($g/cm^3$) |
|---|---|---|
| Permo-trias sediments | 3.2 | 2.35 |
| Carboniferous sediments | 4.5 | 2.60 |
| Lower Paleozoic sediments | 5.5-5.7 | 2.73 |
| Upper crust (felsp. to interm. gneiss) | 6.15-6.17 | 2.74-2.80 |
| North Sea granite | 5.8 | 2.58 |
| Carlisle basic intrusion | 6.15 | 2.89 |
| Lower crust | 6.75-6.77 | 3.04 |
| Moho Layer | 7.0-8.0 | 3.24 |
| Upper Mantle | >8.0 | 3.34 |
| From Blundell *et al* (1985) | | |
| Moine metamorphics and Lewisian amphibolite facies quatzo-felspathic gneiss | 6.15 | 2.74 |
| Pyroxene granulite gneiss | 6.45 | 2.86 |
| Garnet granulite gneiss | 7.00 | 3.10 |
| Moho Layer | 7.50 | 3.20 |
| Upper Mantle | 8.10 | 3.30 |

densities of 2.86 g/cm$^3$ and 3.10 g/cm$^3$ quoted by Blundell et al (1985) for these two rock types (Table 5.1). The upper mantle is assigned a density of 3.34 g/cm$^3$. The densities used in the gravity modelling are plotted against P-wave seismic velocity in Fig. 5.3. The points all lie within the scatter of the Nafe-Drake curve. Lateral density changes within the crustal and upper mantle layers are ignored.

The shallow seismic structure given by Bott et al (1985) beneath the Caledonian Suture Seismic Project was incorporated into the gravity model. No alteration was made to the depths and shapes of the interfaces except under the Irish Sea where the Solway and Carlisle Basins were separated into two distinct bodies. The densities used for the Permo-Trias, Carboniferous and Lower Palaeozoic sediments were taken from the model of the Solway Basin presented by Green (1984). These densities are given in Table 5.1. The deeper structure was taken from the results presented in the previous chapter illustrated in Fig. 4.31. The seismic model did not extend west of the position 50 km from M25B and east of the position 350 km from M25B. The interfaces beneath these areas were inferred from the adjacent seismic boundaries and adjusted slightly to produce a close fit to the observed gravity anomaly.

Fig. 5.4a illustrates that the complete model adequately fits the observed gravity anomaly to within 5 mgal except in the region of the Carlisle Basin. The major variations in the gravity anomaly are due to the sedimentary basins. However, the general increase in the gravity anomaly from about station

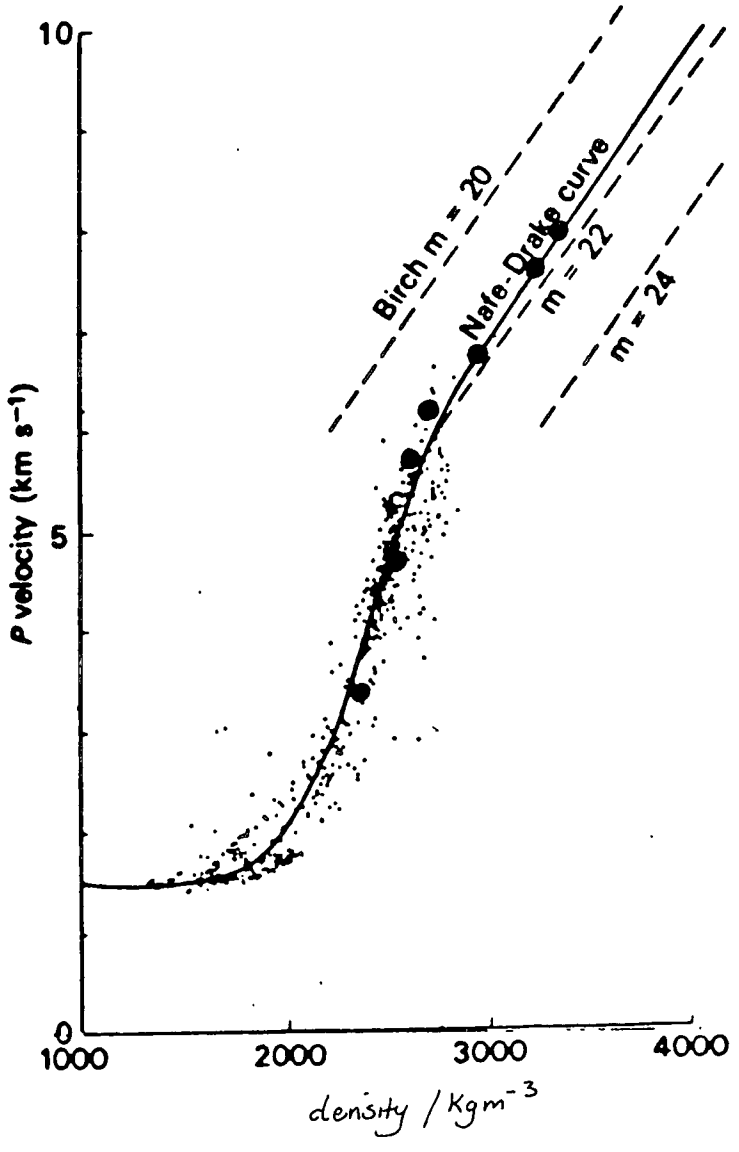


Figure(5.3) Nafe-Drake curve displaying the locations of the results from CSSP

Plot of *P* velocity against density observed for a wide selection of water-saturated sediments and sedimentary rocks, extended for hard rocks. BIRCH's (1961a) empirical relationship between density and *P* velocity as a function of mean atomic weight *m* is also shown on the diagram. Partly redrawn from NAFE and DRAKE (1963), *The sea*, Vol. 3, p. 807, Interscience Publishers. (After BOTT (1982))

34 westwards across the Irish Sea is explained by the shallowing of the PmP boundary. The eastern rise in the mid-crustal boundary at 260 km from M25B fits the rise in the gravity from 250 to 300 km from M25B. A Moho shallowing eastwards from 30 km to 29 km beneath shots N1 to N29 best fits the gravity anomaly over the North Sea. A number of points can be made:

1. After allowing for the effects of the sediments a residual positive gravity anomaly remains over the Carlisle Basin. Laving (1971) has interpreted the circular magnetic anomaly in this area as a dome-shaped basic intrusion underneath the Carlisle Basin (Fig. 5.5). The Caledonian Suture Seismic Project line does not cross the centre of this magnetic anomaly and so the dome-shaped intrusion proposed by Laving is incorporated into the seismic model allowing for this offset. The gravity due to the intrusion was calculated using the programme GRAVEND (Prof. Bott pers. comm.) which calculates the 3-D effect of a given body using end-corrections. Fig. 5.4b shows that the fit between the observed and calculated gravity is improved by the incorporation of the Carlisle intrusion into the model.

2. The granite interpreted by Donato et al (1983) in the vicinity of shots N20 to N25 is incorporated into the model as a 3-D body offset from the seismic line and is assigned a density contrast of -0.16 $g/cm^3$ with the surrounding metamorphic basement. The assumed granite density is slightly lower than that of Donato et al (1983) but is within the limits of precision of the modelling.

3. There is no evidence from the gravity to support the

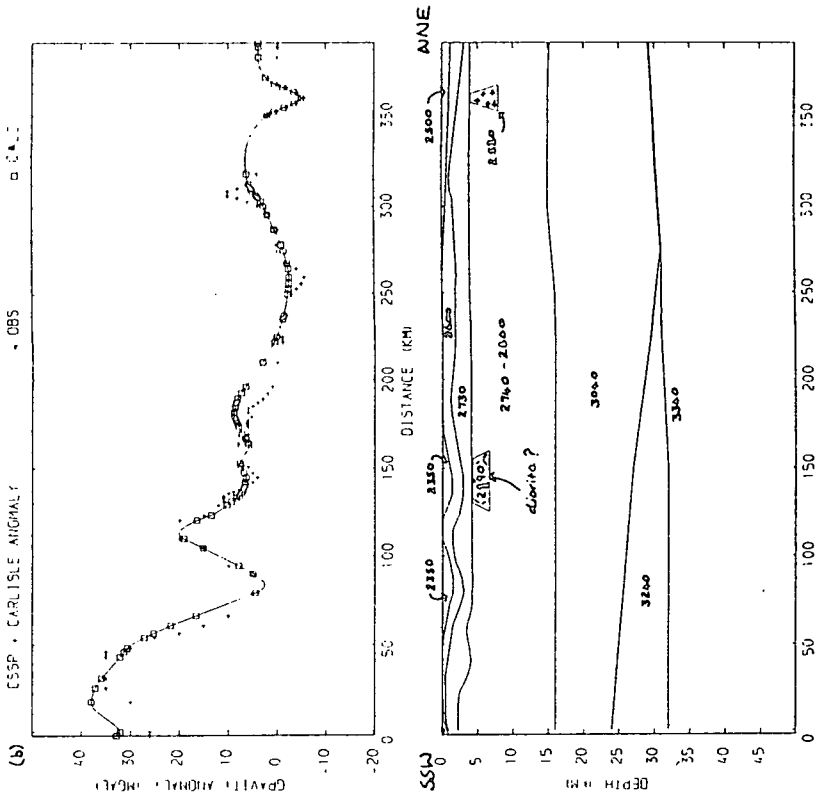


Figure(5.4) (a) Gravity variations due to the seismic model along the main CSSP line
(b) Gravity variations due to the seismic model along the CSSP line incorporating the Carlisle intrusion identified by Laving (1971).

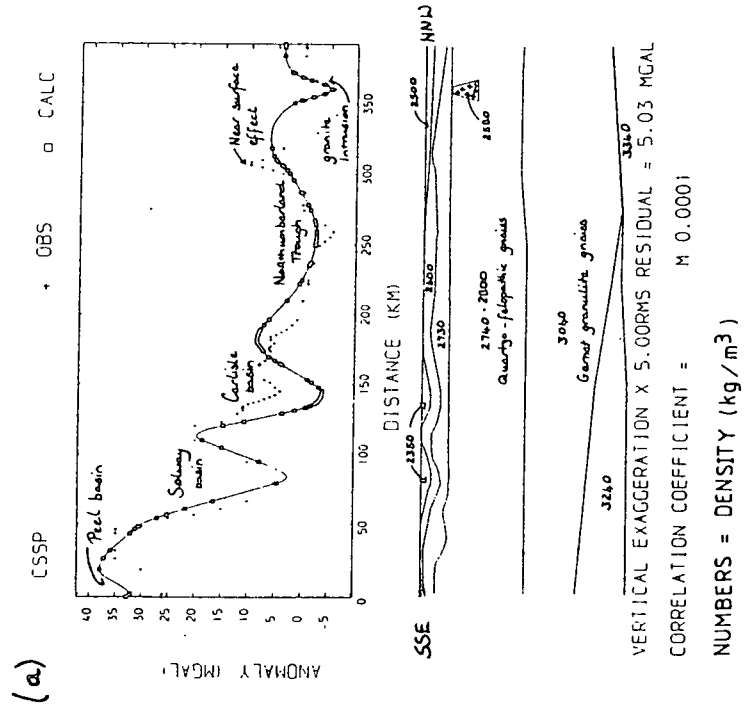

Figure 5 (a) Aeromagnetic anomaly map just north of Carlisle
(b) Model proposed by Lawing (1971).

(a)

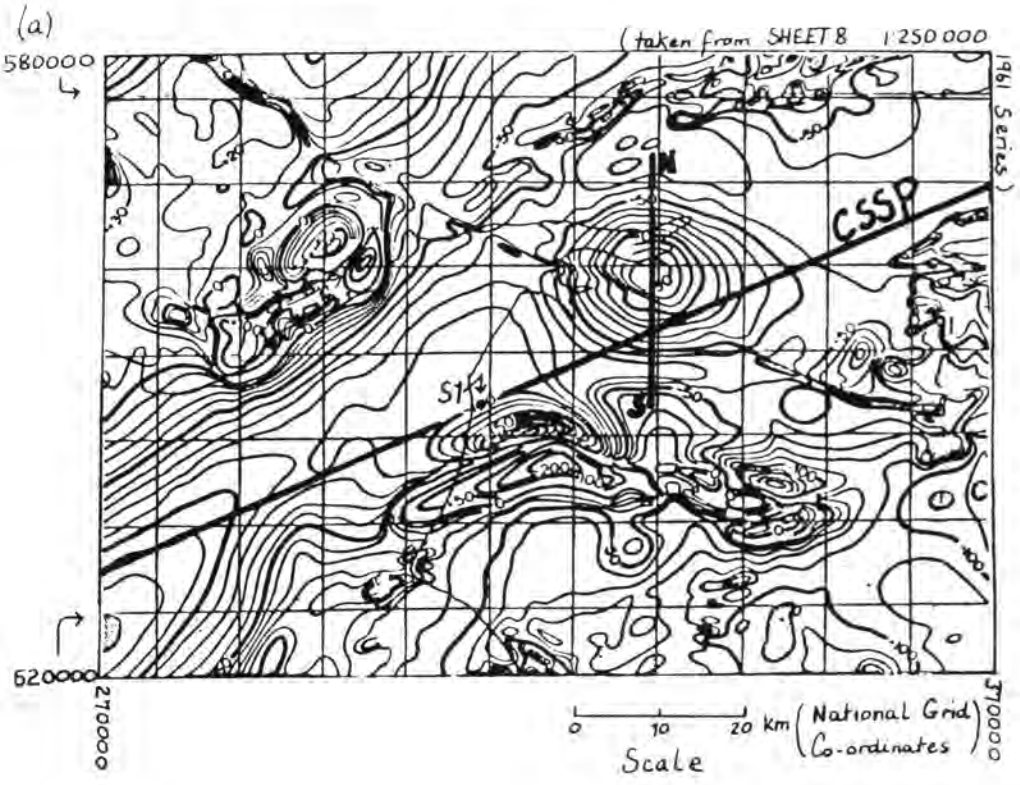


(b)

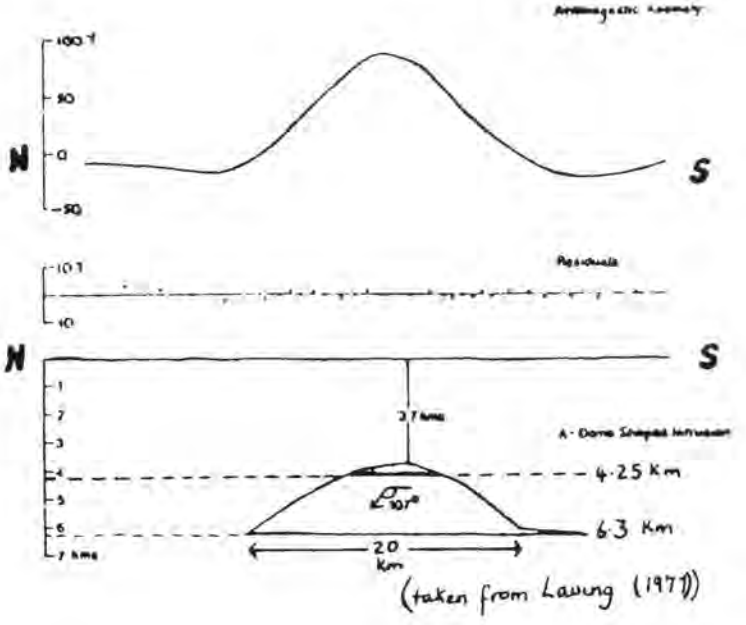


(taken from Lawing (1971))

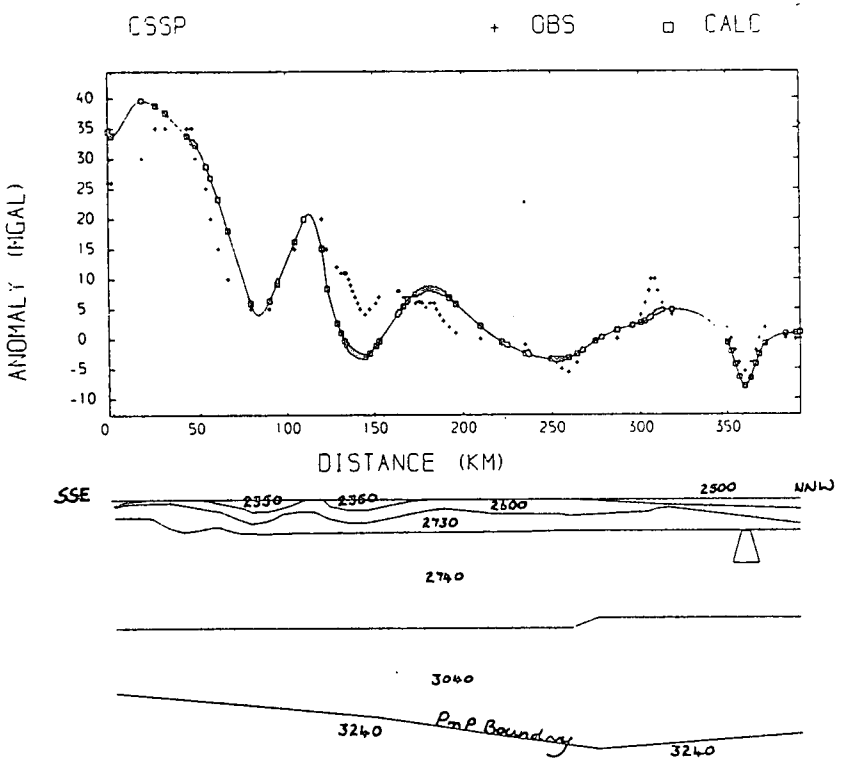


Figure(5.6) Gravity variations due to the seismic model without the Pn boundary.

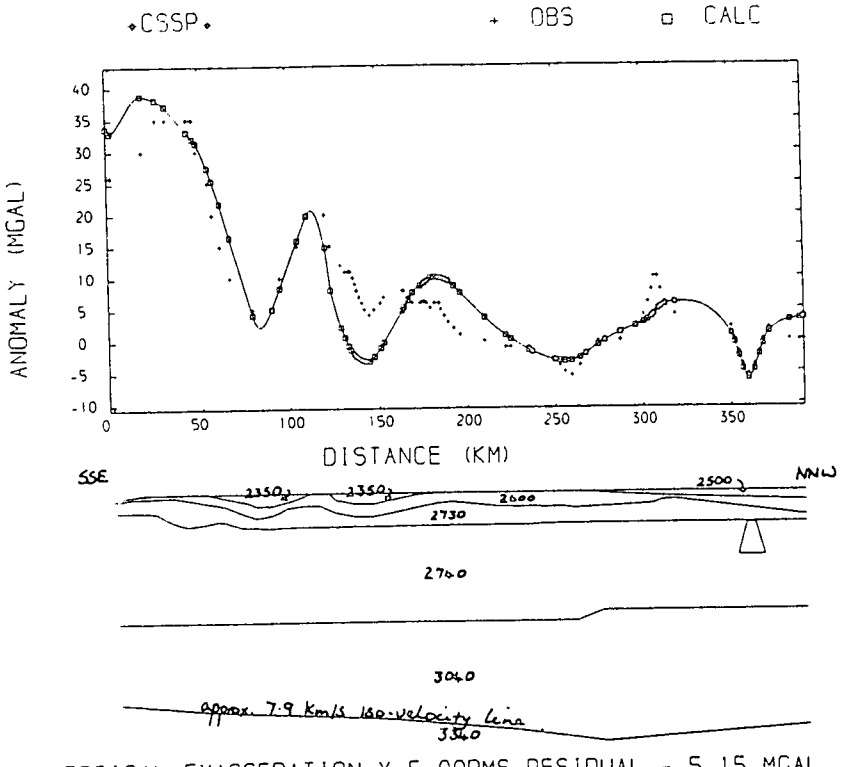


Figure(5.7) Gravity variations calculated using the seismic model with the PmP and Pn boundaries replaced by a single interface along the 7.9 km/s isovelocity line

tentative interpretation made from the travel-time matrices for Pn and PmP for the Irish Sea shots of a region of lower velocity, and therefore of lower density, between the mid-crustal and PmP boundaries, or at shallower depths (Sections 4.2.3 and 4.2.5). The relevant arrivals for shots M10 to M14 were difficult to pick due to their lower amplitudes possibly caused by spurious interference and defocussing effects due to the westwards shallowing of the sediments in the Solway Basin.

4. Fig. 5.6 shows the variations using a seismic model obtained from only the wide-angle reflections and Fig. 5.7 illustrates the variations in gravity using a seismic model in which the Moho is defined as the 7.9 km/s iso-velocity line. A close fit is obtained to within 5 mgal for both models. The increase in the gravity under the Irish Sea can be modelled by a sharp Moho (Fig. 5.6 and 5.7) but a gradient zone can also fit the data (Fig. 5.4b). The densities of 3.04 g/cm$^3$, 3.24 g/cm$^3$ and 3.34 g/cm$^3$ were used for the lower crust, the transitional Moho and the upper mantle respectively. The 35 mgal gravity high observed over the Irish Sea is explained by the combined gravity effect of the top and bottom of the transitional Moho. The greater density contrast is across the top of the transitional Moho as defined by the PmP boundary rather than across its base as defined by the Pn boundary.

5. There is no PmP coverage east of common mid-point position 300 km and the Pn results are not well constrained under the North Sea (Section 4.4.3). In the time-term analysis presented in Section 4.4.3 a Moho at a constant depth of

about 30 km is obtained if the sub-Moho velocity is constrained to 8.02 km/s. If a constraint velocity greater than 8.12 km/s is used the time-terms and depths to the Moho are observed to deepen by at least 6 km northeastwards from shots N1 to N29. A Moho that deepens by over 6 km beneath shots N1 to N29 is estimated to yield a regional gravity anomaly that is at least 10 mgal less than the observed anomaly over the North Sea. However, a Moho at an almost constant depth of 30 km shallowing slightly to a depth of 29 km under shot N29 yields a regional gravity anomaly that is within a few milligals of the observed anomaly. This means that the velocity of 8.02 (6.34 - >10.0) km/s calculated from the time-term analysis of Pn for the North Sea shots, despite the poor confidence limits, does give nearly constant time-terms under the North Sea which fit the gravity. The sub-Moho velocity beneath the North Sea is therefore probably about 8.0 km/s. Higher sub-Moho velocities of 8.19 (8.12 - 8.29) km/s and 8.32 (8.19 - 8.49) km/s were found beneath the Irish Sea and Northern England respectively (Sections 4.4.1 and 4.4.2).

From the combined results of the Pn time-term analyses and the gravity modelling it is therefore inferred that the sub-Moho velocity under the North Sea is significantly lower than the Moho velocity observed under the Irish Sea and Northern England. This lateral change in the sub-Moho velocity appears to occur in the vicinity of station 34.

## 5.2 SYNTHETIC SEISMOGRAM MODELLING

### 5.2.1 Main Amplitude Variations

The low frequency PcP and PmP phases are most conspicuously developed for the shots in deeper water in the North and Irish Seas which have significant energy in the 3 to 5 Hz band. Green (1984) showed that this may be due to scattering of energy with frequencies greater than 5 Hz by inhomogeneities with dimensions varying from a few tens of metres up to 200 metres. Recent work on scattering (Malin and Phinney 1985) has shown that random media can produce sensitive amplitude dependence with frequency for arrivals observed on refraction seismograms. Anelastic losses attenuate the higher frequencies with increasing range but cannot produce the abrupt lateral changes in the observed amplitudes. However, a further possibility is constructive interference at the source. The shots which have significant energy with frequencies less than 5 Hz are precisely those for which the bubble pulse frequency is greater than the reverberation frequency (Table 2.1).

It is important to understand the difference between the bubble pulse and reverberation frequencies. The reverberation frequency is produced by the constructive interference of multiples between the sea surface and the sea bed within the water column. The equations of Burkhardt and Rees (1975) give the frequency of these reverberations which produce the dominant frequency of the source energy. The expansion and contraction of the gas bubble produced by the explosion

generates the bubble pulse oscillations. Each expansion and contraction of the gas bubble produces a wavelet which has a dominant frequency equal to the reverberation frequency with the polarity reversing for each successive wavelet. The bubble pulse frequency gives the repeat period of the onset of each discrete bubble pulse. Constructive interference between the water column reverberation and bubble pulse oscillations occurs when the bubble pulse and reverberation frequencies are the same. These frequencies are equal at the optimum depth which is approximately 90 m for the Caledonian Suture Seismic Project shots (Green 1984). This resonance can produce very large amplitudes (Burkhardt and Rees 1975). If the bubble pulse frequency is just less than the reverberation frequency no individual bubble pulses are observed in the received signal. This is because successive bubble pulses combine at the shot to produce a single extended wavelet such as shots M20 to M25B in the Irish Sea. If the bubble pulse frequency is less than the reverberation frequency each bubble pulse is observed as a separate arrival as illustrated in Fig. 2.13 for shot M17.

Both constructive interference at source or scattering within the crust are possible explanations of the observed abrupt amplitude variations between the Caledonian Suture Seismic Project shots. These effects are referred to as "shot effects". The probable amplitude features produced by these shot effects are:

1. the large PcP, PmP and Pn amplitudes for shots N6 to N14 in the North Sea.
2. the large PmP amplitudes for shots M20 to M25B in the

Irish Sea.

Because of these problems no attempt has made to model the amplitudes in detail. The main amplitude features observed on the refraction sections corrected to common gain which are modelled using the synthetic packages are:

1. The disappearance of Pg beyond about shot N11
2. The prominent PmP arrivals observed in the North Sea and the weaker PmP development in the Irish Sea.
3. The larger Pn amplitudes observed in the Irish Sea than in the North Sea.

### 5.2.2 1-D Synthetic Seismogram Modelling

Green (1984) and Bott et al (1985) have presented preliminary one dimensional structures beneath the Irish and North Seas. The travel-time analysis presented in Chapter 4 has yielded a velocity structure beneath the North Sea that does not differ significantly from the published model of which the writer is a co-author (Bott et al 1985). The identification of PcP arrivals from the Irish Sea shots has yielded a mid-crustal boundary at 15.5 to 18.0 km beneath the Irish Sea which was not recognised previously. The original North Sea model is briefly described to illustrate that it produces synthetic seismograms that compare well with the observed sections. The original Irish Sea model is used to illustrate the effects of a gradational Moho. The internal velocity structure of the transitional Moho is then investigated in detail using the reflectivity method and a one-dimensional approximation to the two dimensional velocity

model beneath the Irish Sea (Fig. 4.31). The input wavelet used is a cosine tapered second derivative Gaussian wavelet with a maximum spectral amplitude at 4 Hz (Green 1984).

The seismic structure east of station 34 is approximately one dimensional. Fig. 5.8 illustrates a ray-traced model for a 1-D approximation to the structure beneath the North Sea in which the theoretical travel-times are displayed on the common station section for station 32 corrected to common gain. Fig. 5.9 is a 1-D synthetic seismogram calculated using the reflectivity method for the same model. This synthetic seismogram is the same as that presented by Bott et al (1985). Prominent PmP wide angle-reflections are obtained on the synthetic section although the amplitudes do not die away as abruptly as on the observed section. This observed rapid decay is attributed to the shot effects. The maximum amplitude of the PmP phase observed from the North Sea shots lies generally at ranges of about 95 to 105 km (Appendix A). Large amplitudes at this range are obtained on the synthetic section by introducing a slight velocity gradient just above the Moho. The amplitudes of the PcP reflections are larger on the synthetic section than on the observed seismogram. The main travel times and amplitude variations observed on this synthetic seismogram calculated using a 1-D approximation to the structure under the North Sea are consistent with the broad features of the arrivals observed at most of the Caledonian Suture Seismic Project stations east of about station 23.

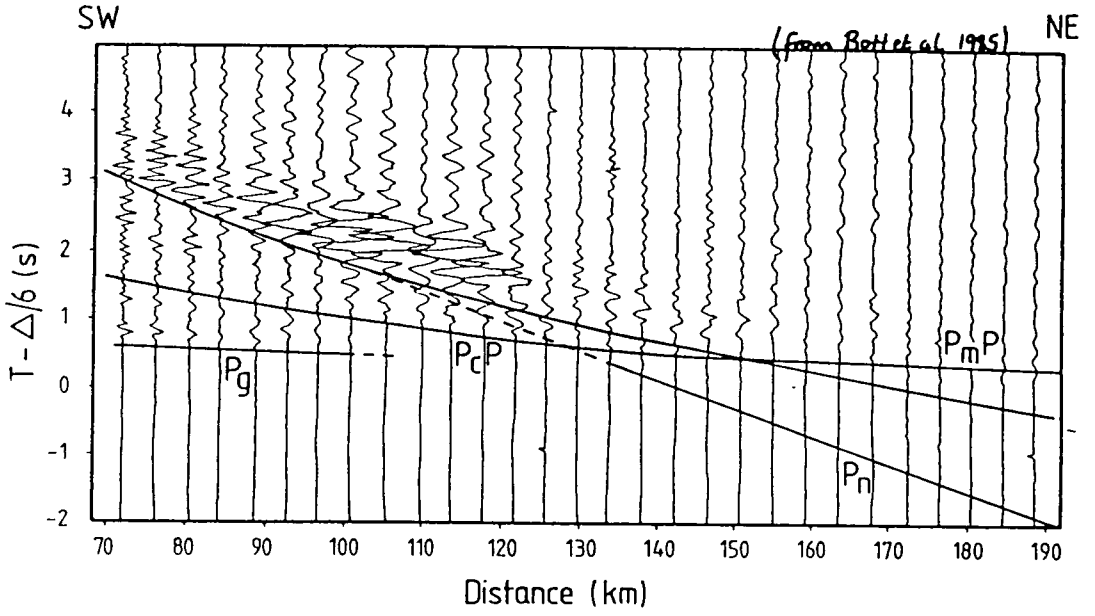


Figure(5.8) (a) Common station section for station 32 displaying the travel times calculated from ray tracing through the model illustrated

(b) Ray diagram for station 32 for the North Sea shots. The model is a 1-D approximation to the structure beneath the North Sea.

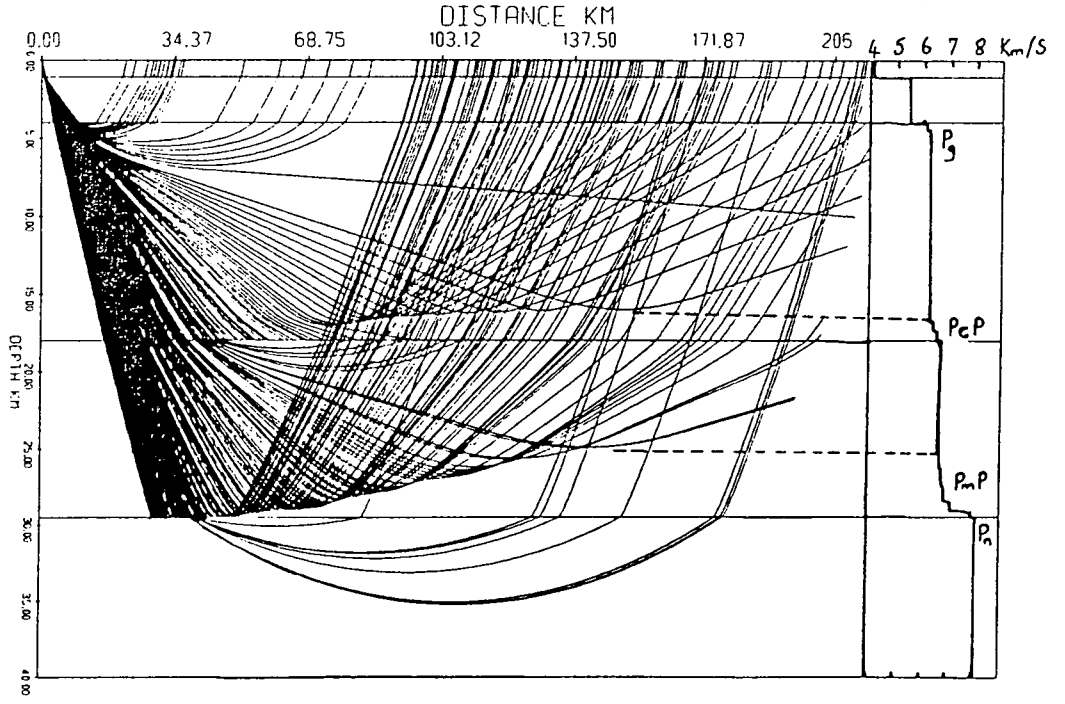


FINAL NSEA CST32/N 1-D

Fig. 5.10 illustrates a 1-D model of the Moho under the Irish Sea. The mid-crustal boundary is omitted in this model. The correct average crustal velocity is obtained by a gentle velocity gradient across the whole crust down to the top of a transitional Moho. This transitional Moho is defined by a velocity gradient zone seperating the PmP and Pn boundaries. The PmP wide-angle reflections for offsets greater than about 105 km are returned from the top of this gradational Moho (Fig. 5.10). The PmP arrivals between 95 to 105 km near the critical distance are returned from within the gradational Moho. It is clear that in general PmP arrivals are returned from the top of velocity gradients which define a gradational Moho. Only arrivals near to the critical distance penetrate significantly into the velocity gradient within such a gradational Moho. This indicates that not much detail of the velocity structure within a gradational Moho can be obtained from a travel time analysis. Consequently the velocity structure within the transitional Moho was investigated by amplitude modelling using the reflectivity method.

A selection of common station sections for the Irish Sea shots is displayed in Fig. 5.11. Only the common station sections for stations 1 to 25 have traces at ranges less than 80 km. PmP arrivals are observed on these sections at ranges greater than 80 km. No unambiguous PmP arrivals can be observed on the sections at ranges less than 80 km due to the shot effects and the poor data quality. The internal velocity structure within a transitional Moho can be defined by either a velocity gradient, a constant velocity or more complicated structures involving low velocity layers. Synthetic

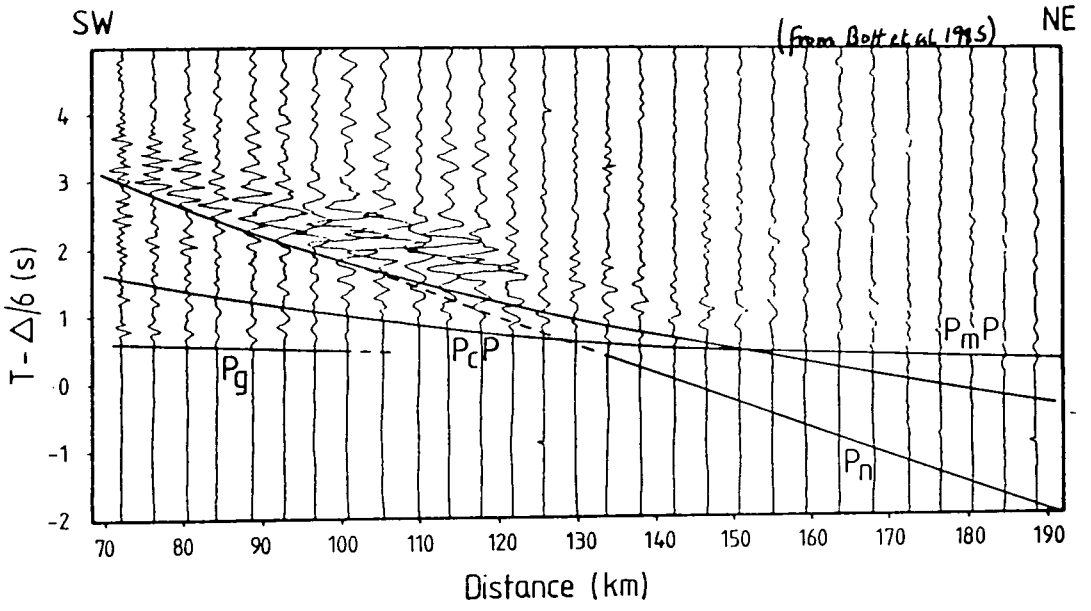


Figure(5.9) (a) Common station section for station 32 displaying the travel times calculated from ray tracing through the model illustrated.
(b) Synthetic seismogram computed using the reflectivity method for station 32 for the North Sea shots.

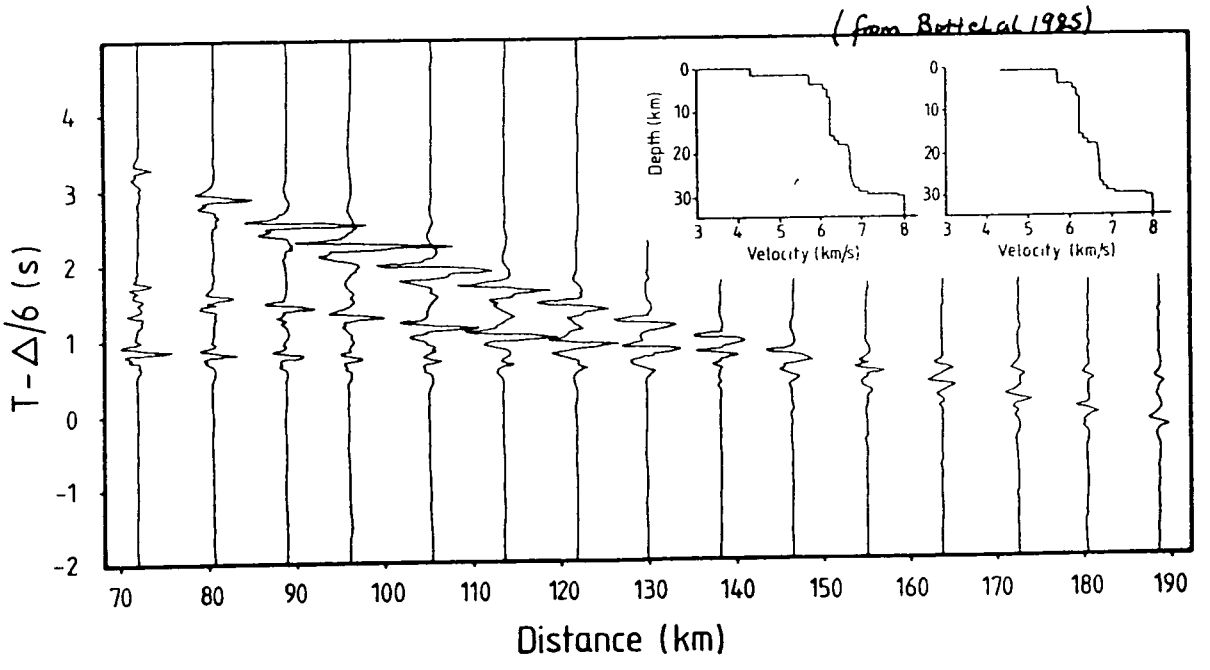

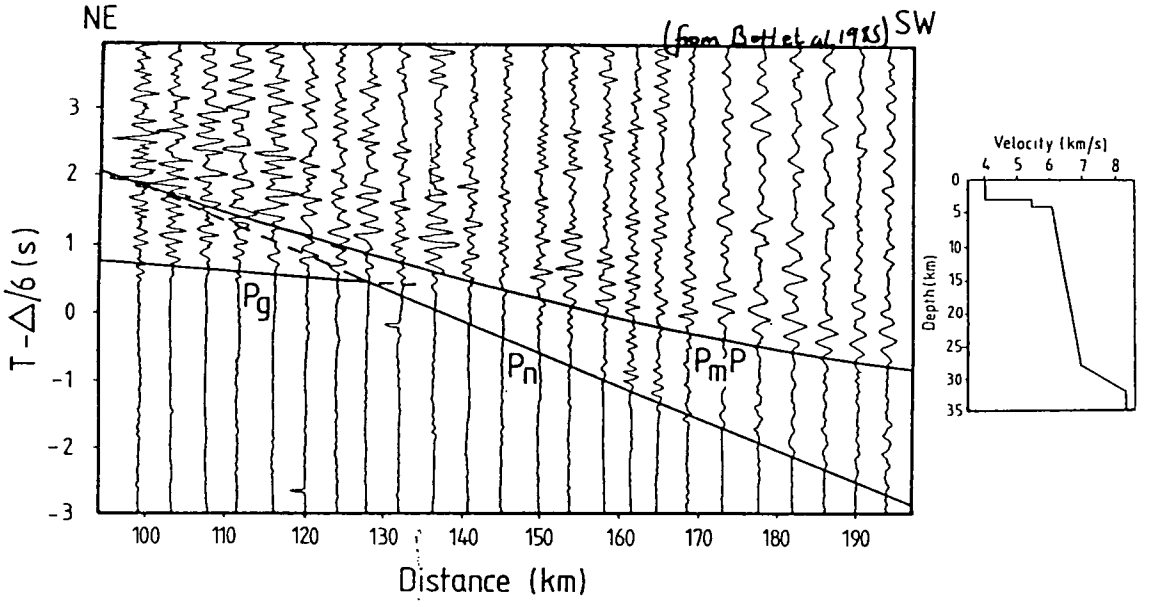


Figure(5.10) (a) Common station section for station 32 displaying the travel times calculated from ray tracing through a model sketched in (b).
(b) Ray diagram for station 32 for the Irish Sea shots. The model is a 1-D approximation to the structure beneath the Irish Sea.

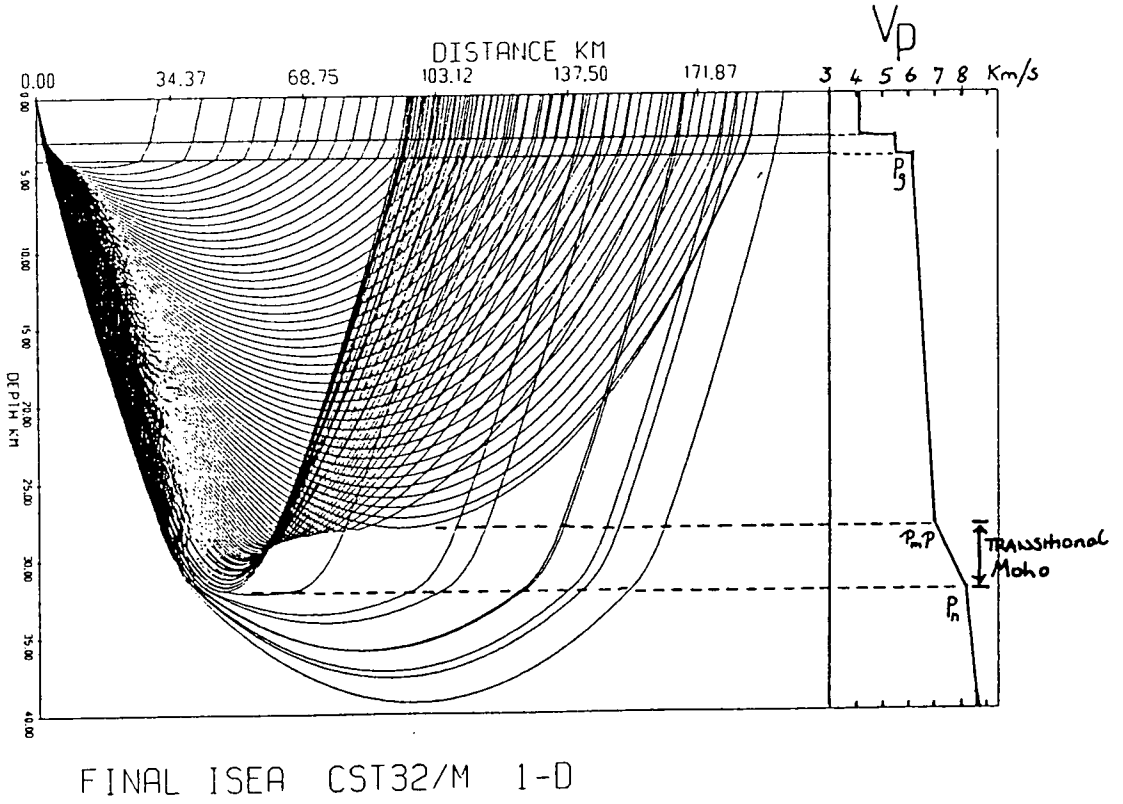


FINAL ISEA CST32/M 1-D

seismograms for four different velocity structures within a transitional Moho were produced using the reflectivity method. Figs. 5.12 to 5.15 display these synthetic seismograms and models. The velocity depth model used is a one dimensional approximation to the laterally varying velocity structure beneath the Irish Sea (Fig. 4.31). The programme SYNSEI allows only 45 velocity values and so the sub-Moho gradient is defined only down to 40 km on all models. These synthetic seismograms are not intended to fit a particular observed common station section but are used to discuss the effects on the PmP and Pn amplitudes of the velocity structure within the transitional Moho. A number of points can be made on the nature of the transitional Moho from an inspection of these synthetic sections:

1. A linear velocity gradient yields (Fig. 5.12) low amplitude PmP arrivals at ranges less than 90 km and large amplitudes at distances greater than 100 km. A velocity gradient within the transitional Moho cannot produce the observed PmP amplitudes at ranges between 80 to 90 km.
2. The PmP amplitudes can be increased at near offsets by the introduction of thin low velocity layers within the velocity gradient between the PmP and Pn interfaces (Fig. 5.13). On the synthetic seismogram the near offset PmP arrivals have higher frequencies than the arrivals at ranges greater than about 100 km. In the Irish Sea the shot effects produce a similar frequency variation but related to the water depth. The shot frequencies decrease from shot M1 to M25B (Table 2.1). For the mainline Caledonian Suture Seismic Project stations the ranges also increase from shot M1 to M25B. This means that the shot

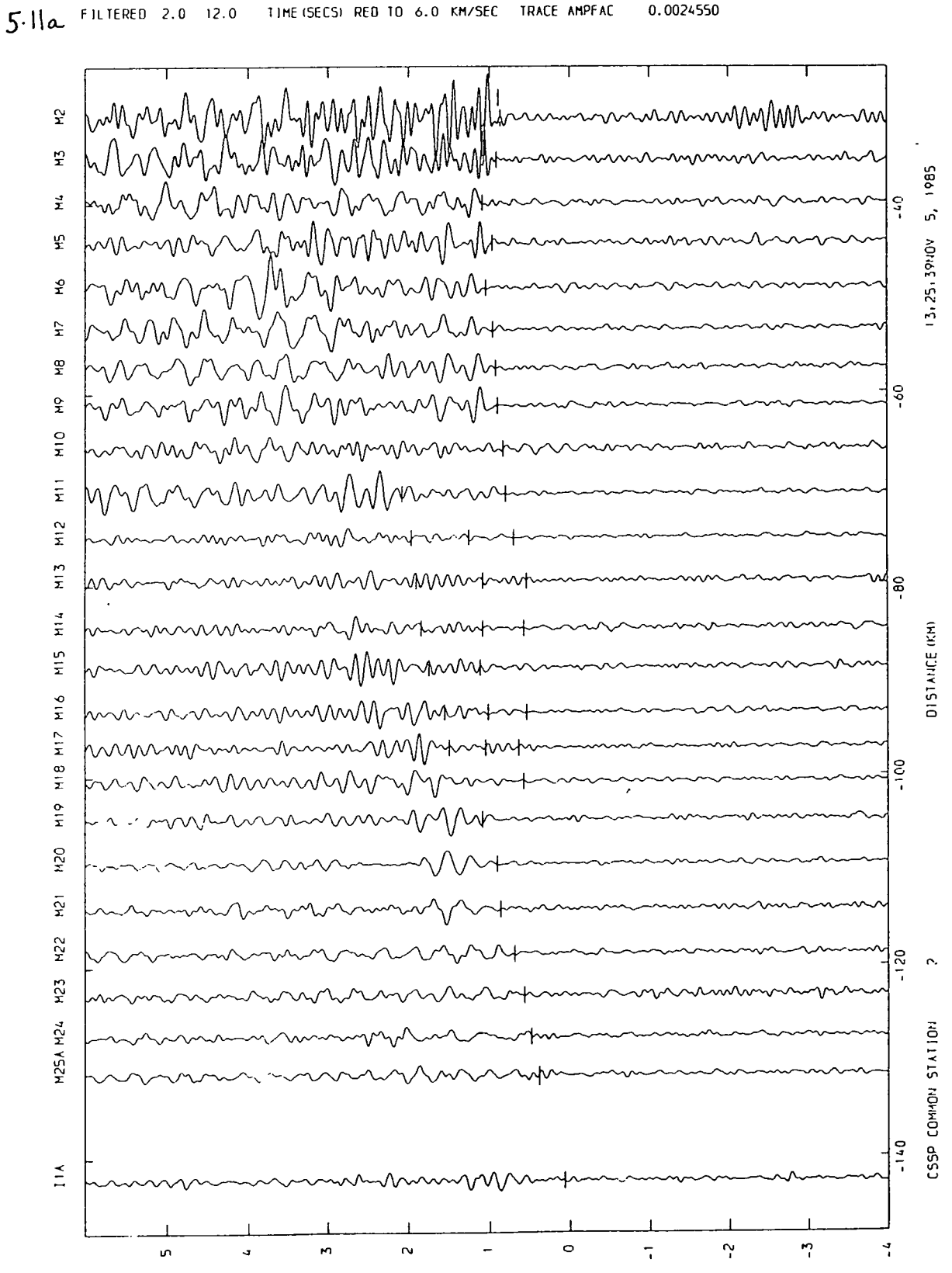


Figure(5.11) Common station sections for the Irish Sea shots corrected to common gain for (a) Station 2
(b) Station 15
(c) Station 30

5·11b

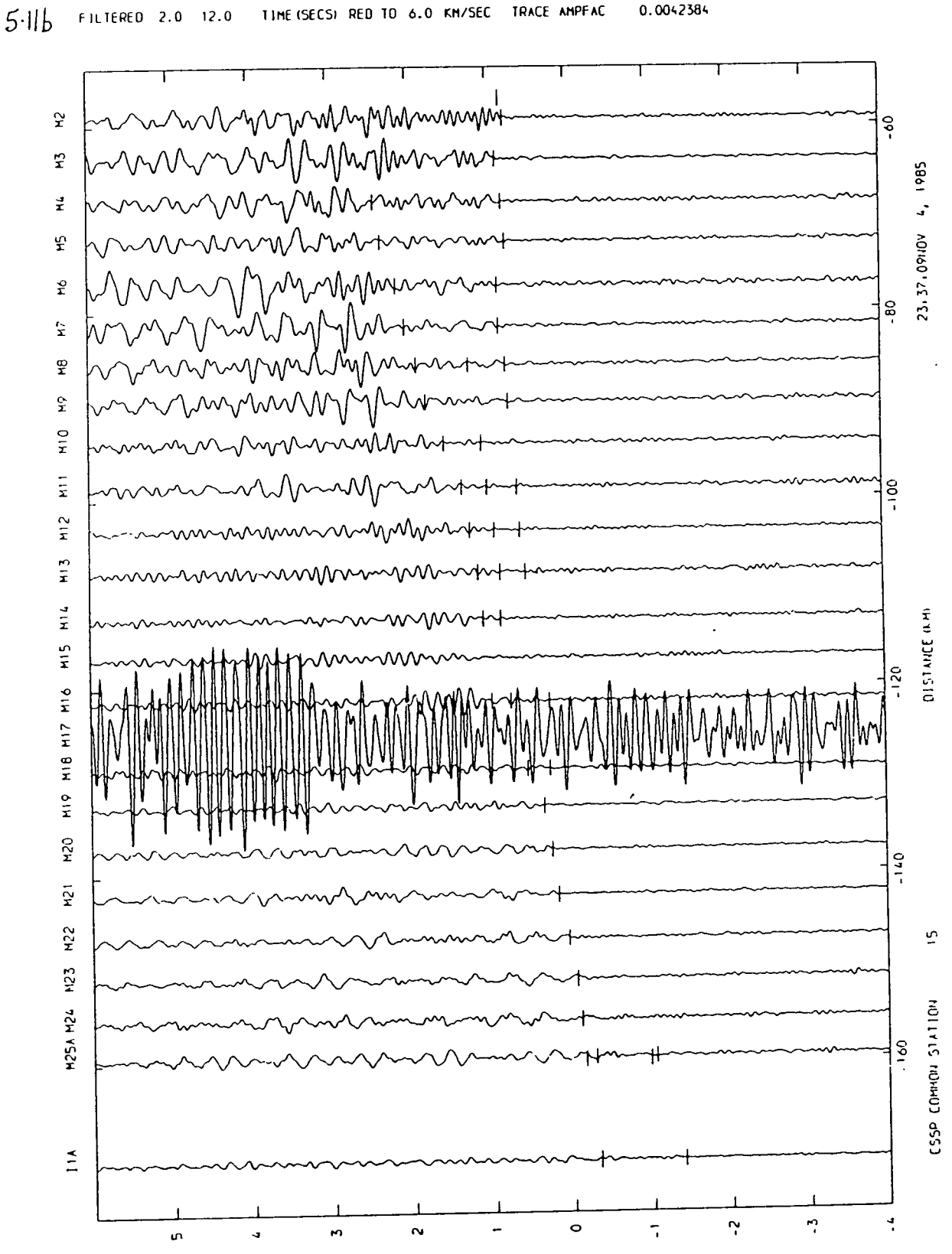
FILTERED 2.0 12.0 TIME (SECS) RED TO 6.0 KM/SEC TRACE AMPFAC 0.0042384
M2
M3
M4
M5
M6
M7
M8
M9
M10
M11
M12
M13
M14
M15
M16
M17
M18
M19
M20
M21
M22
M23
M24
M25A
11A
-60
-80
-100
-120
-140
-160
5
4
3
2
1
0
-1
-2
-3
-4
23.37.09NOV 4, 1985
DISTANCE (KM)
CSSP COMMON STATION 15

5·11c

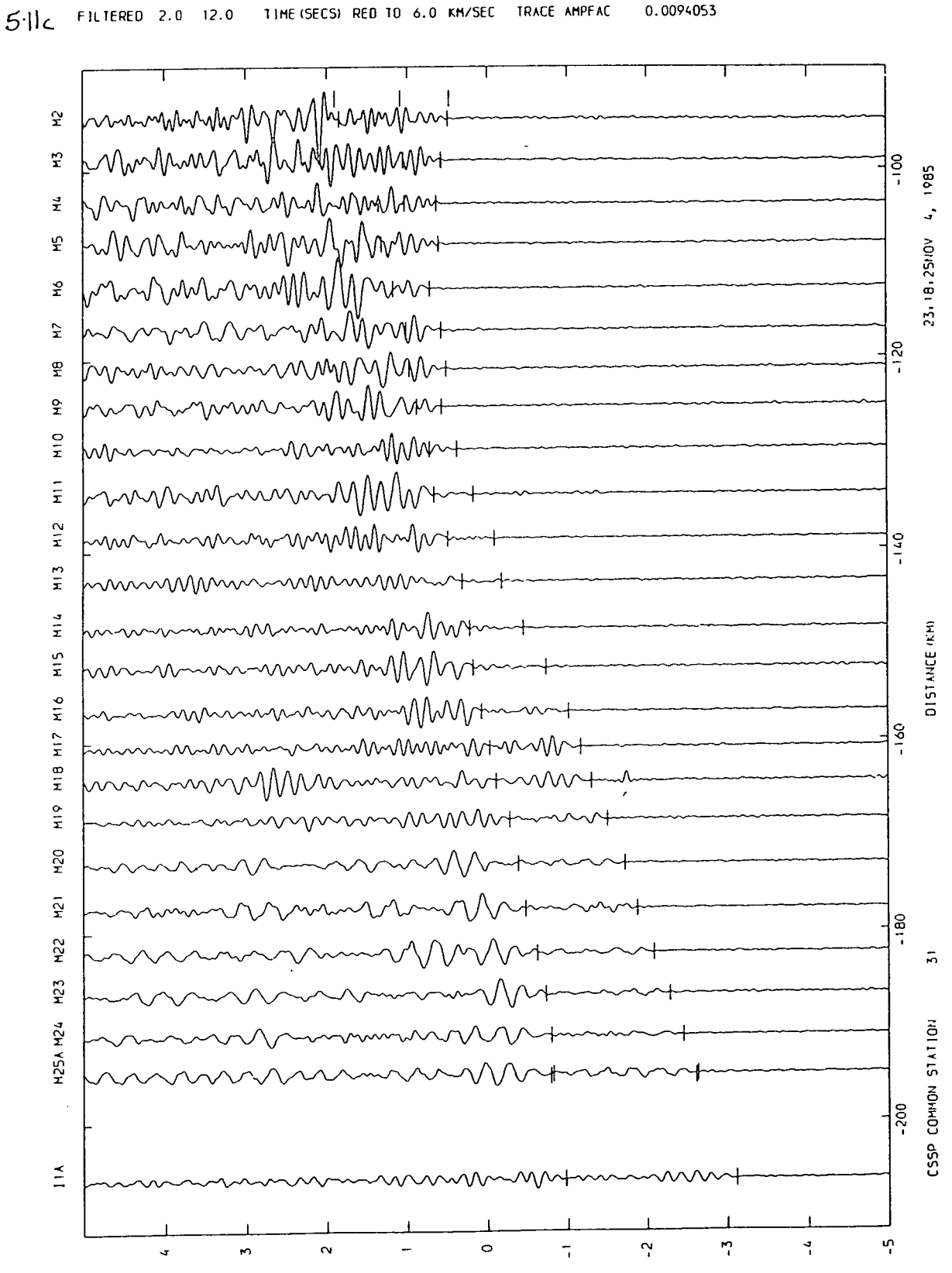
FILTERED 2.0 12.0 TIME (SECS) RED TO 6.0 KM/SEC TRACE AMPFAC 0.0094053
M2
M3
M4
M5
M6
M7
M8
M9
M10
M11
M12
M13
M14
M15
M16
M17
M18
M19
M20
M21
M22
M23
M24
M25A
11A
-100
-120
-140
-160
-180
-200
DISTANCE (KM)
23,18,25NOV 4, 1985
CSSP COMMON STATION 31
4
3
2
1
0
-1
-2
-3
-4
-5

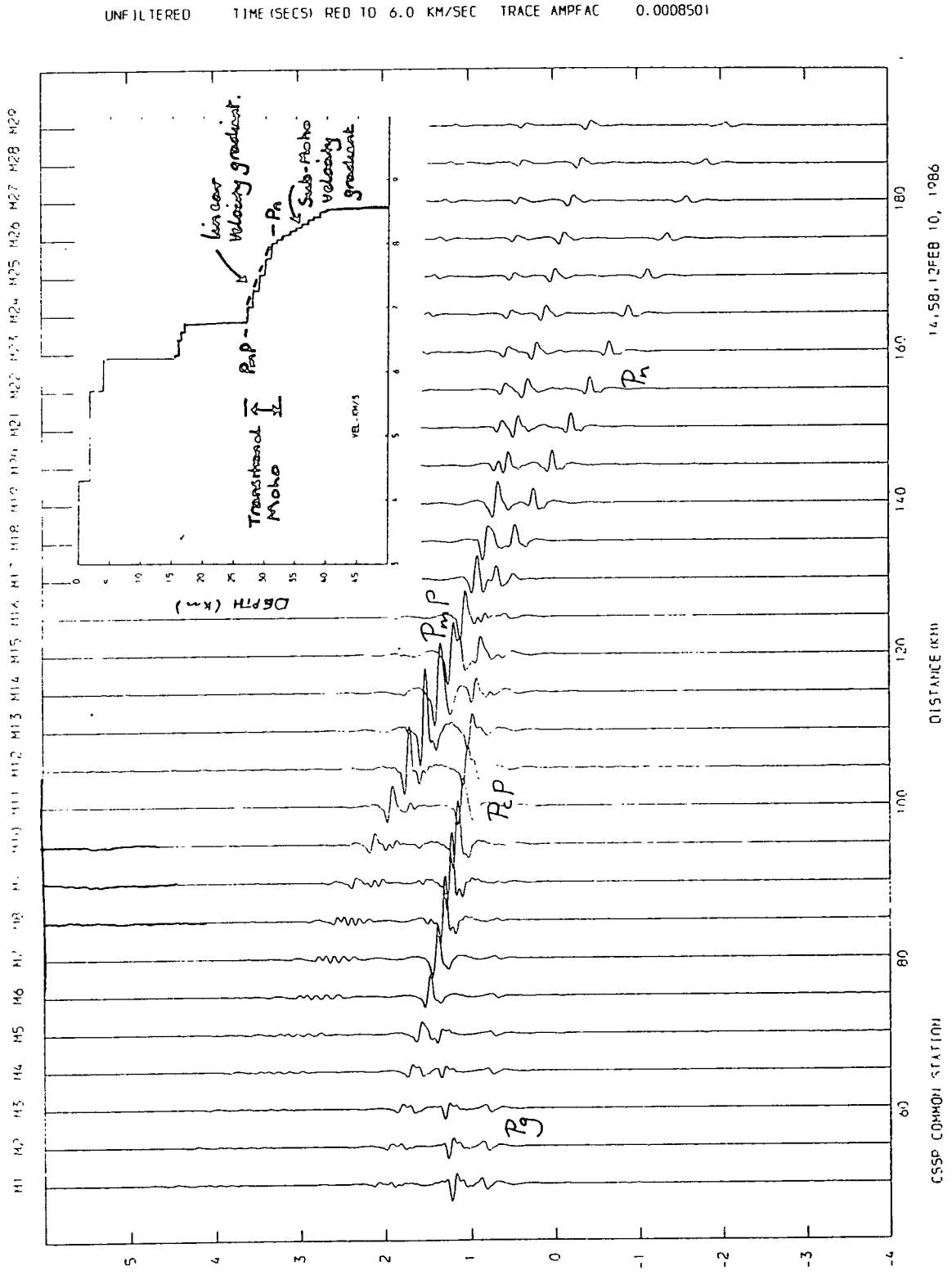


Figure(5.12a) Synthetic seismogram computed using the reflectivity method for a transitional Moho consisting of a linear velocity gradient.

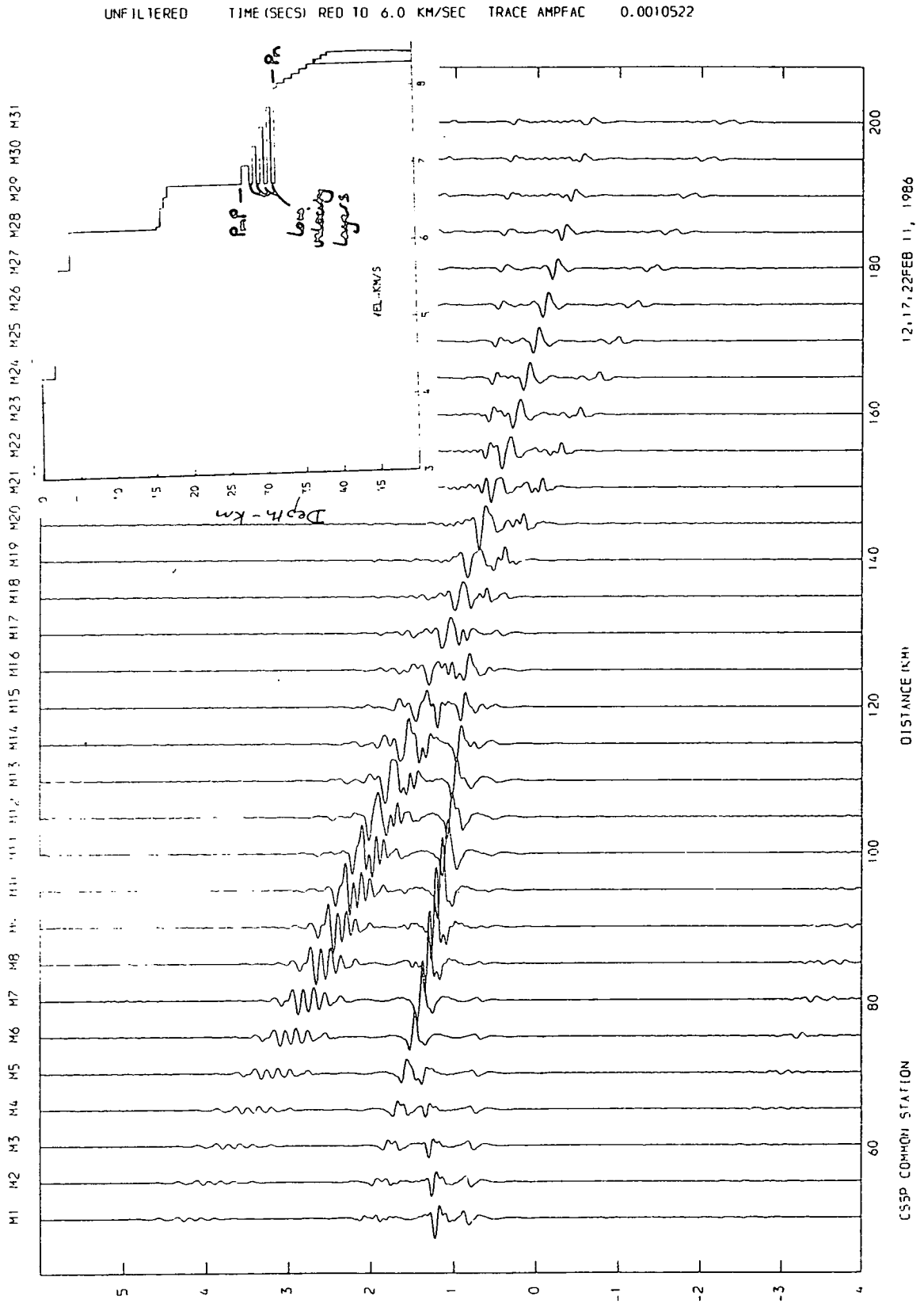


Figure(5.13) Synthetic seismogram computed using the reflectivity method for a transitional Moho consisting of a linear velocity gradient

effect produces an apparent decrease in frequency with range for receiving stations in Northern England. The frequency variations due to the shot effects may obscure any similar effects caused by possible thin low velocity layers in the transitional Moho. Comparing Figs. 5.12 and 5.13, it can be concluded that the amplitudes of the Pn arrivals are reduced by the introduction of thin low velocity layers within a gradational Moho.

3. A layer of shallow gradient between the PmP and Pn boundaries produces large amplitude PmP arrivals at ranges down to 80 km (Fig. 5.14). The low amplitude Pn arrivals between 120 and 180 km in the model represent a shadow zone due to the very small gradient between the PmP and Pn boundaries. Larger Pn amplitudes occur from 140 to 180 km. Such Pn amplitude variations would be expected to occur at these ranges on all observed sections. No such variations occur on the observed sections corrected to common gain (Appendices A and B). However, amplitude variations due to the shot effects may obscure such small amplitude variations.

4. Fig. 5.15 illustrates that a transitional Moho combining an abrupt velocity increase at the PmP interface and a velocity gradient below it can also produce large PmP amplitudes at ranges greater than 80 km.

Braile and Smith (1975) have concluded from synthetic seismogram modelling using the reflectivity method that the details of velocity structures within a transitional Moho cannot be obtained using the refraction method. However, from the discussion above it has been shown that a velocity gradient between the PmP and Pn interfaces cannot produce the

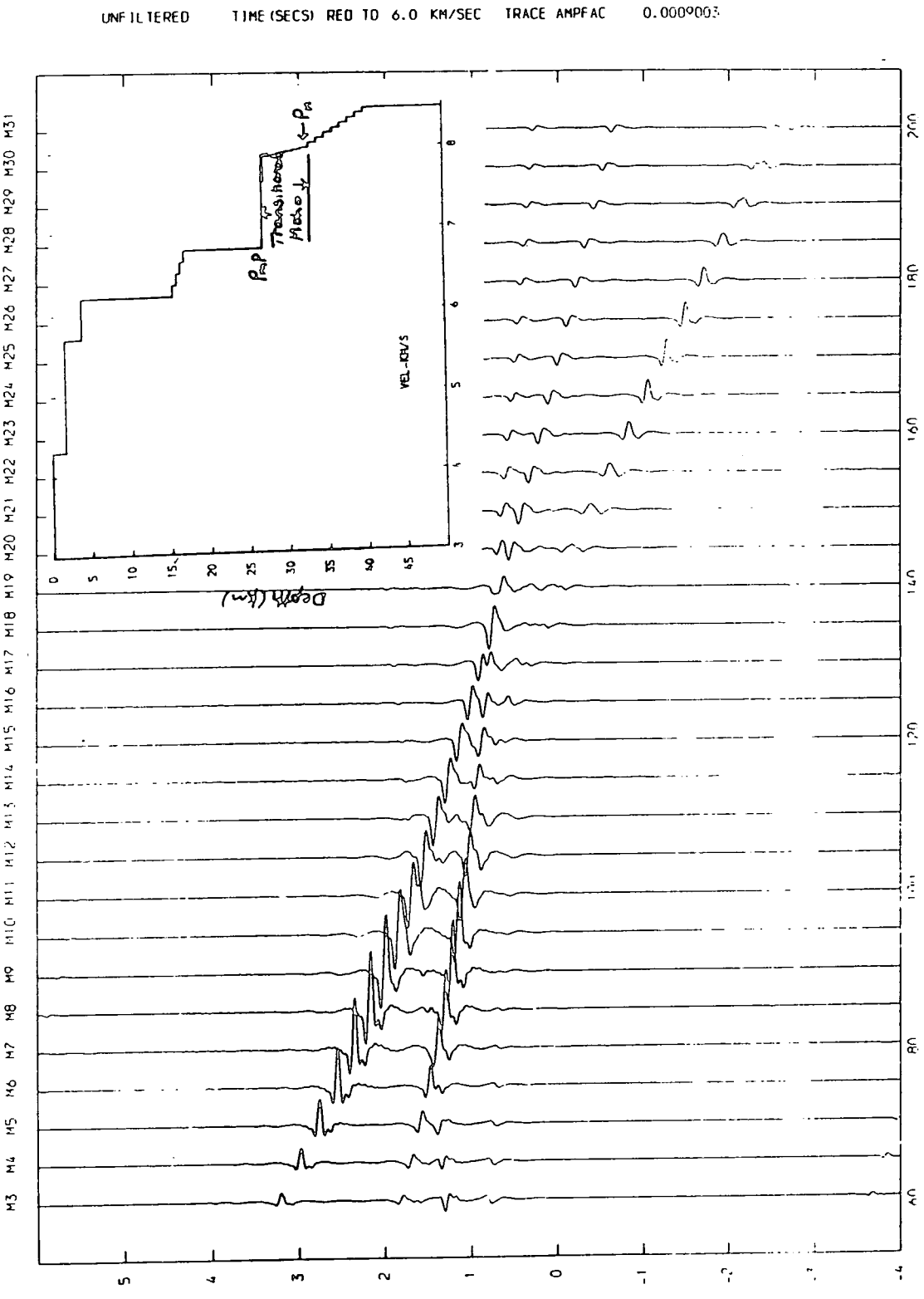


Figure(5.14) Synthetic seismogram computed using the reflectivity method for a transitional Moho consisting of an abrupt velocity increase at its top surface from 6.75 to 7.9 km/s and a slight velocity gradient down to its bottom surface.

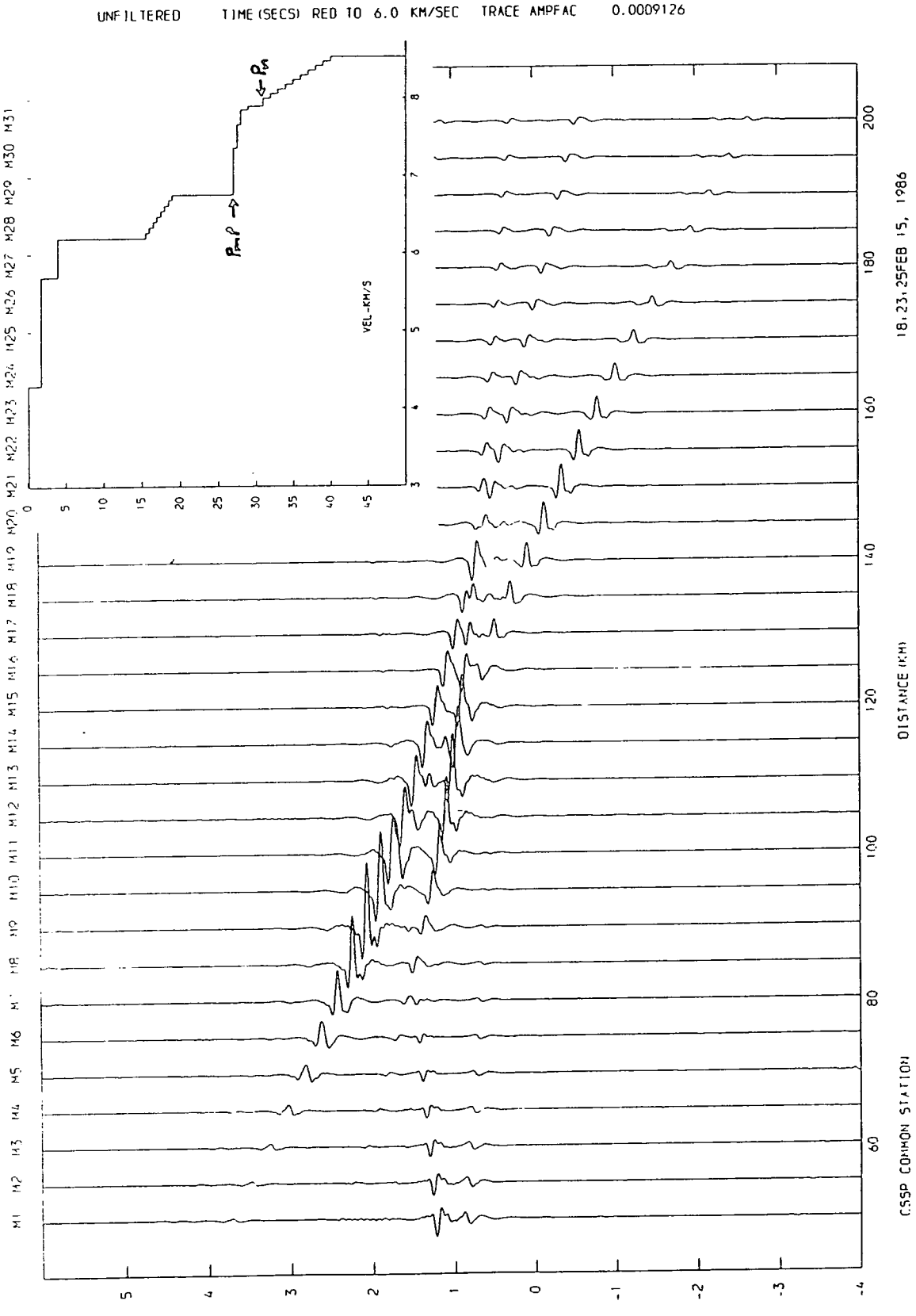


Figure(5.15) Synthetic seismogram computed using the reflectivity method for a transitional Moho consisting of an abrupt velocity increase across its top surface from 6.75 to 7.5 km/s and a gentle velocity gradient down to its bottom surface.

observed PmP arrivals at ranges less than 90 km. There are two main types of model proposed. Firstly, an abrupt velocity increase at the PmP interface underlain by a layer of gentle gradient down to the Pn boundary, and secondly, a complicated velocity gradient incorporating thin low velocity layers. Both models can produce PmP arrivals at ranges down to 80 km. However, the amplitude modelling using the reflectivity method indicates that a complicated velocity gradient incorporating thin low velocity layers yields low amplitude Pn arrivals in contrast to the Pn amplitudes on the observed sections. It must be concluded that an abrupt or sharp gradient increase in velocity at the PmP boundary best fits the broad PmP and Pn amplitude variations on the observed seismograms.

To conclude, the detailed nature of the region between the PmP and Pn interfaces under the Irish Sea cannot be deduced. However, 1-D synthetic seismogram modelling indicates that a transitional Moho with an abrupt increase in velocity at its top surface defined by the PmP boundary and a fairly uniform structure down to the Pn boundary can produce the observed amplitudes of the PmP and Pn arrivals from the Irish Sea shots.

### 5.2.3 2-D Synthetic Seismogram Modelling

Cerveny (1985) has highlighted the limitations of synthetic seismogram computations using generalized ray theory. Generalized ray theory gives inaccurate results at critical points and in regions of vanishing layers. The analyses of the arrival times of PmP and Pn presented in Sections 4.3 and

4.4 indicate that the PmP and Pn boundaries are at different depths beneath the Irish Sea in contrast to the results east of about station 34 where they appear to be at approximately the same depths (Fig. 4.31). These boundaries define the transitional Moho beneath the Irish Sea which represents an eastwardly vanishing layer beneath the Caledonian Suture Seismic Project profile. Preliminary modelling of the transitional Moho using interfaces to define both the PmP and Pn boundaries produced anomalous amplitudes for the synthetic PmP arrivals. This problem was probably caused by the coincident PmP and Pn boundaries beneath the North Sea. The Pn boundary was therefore removed and modelled by vertical velocity variations.

The input of the laterally varying velocity structure was the main problem encountered during the two-dimensional modelling using SEIS83. SEIS83 provides three methods of inputting the model but only two of these can be used for laterally varying structures. These are the bicubic spline and bilinear interpolation methods. The interpolation method produces spurious velocity gradients and uneven ray paths. Cerveny (1985) has recommended that this method should not be used for synthetic amplitude calculations. The spline method was therefore used. The spline method was found to produce small oscillations of the velocity structure which affected the raypaths. This problem has been reported by Cerveny (1985). Despite these problems the broad amplitude and travel-time variations have been successfully modelled. The wavelet used is a Gaussian envelope signal with a 4 Hz carrier frequency with a very narrow amplitude spectrum (Cerveny

1985).

A preliminary model combining the shallow structure presented by Green (1984) and Bott et al (1985) and the deeper structure deduced from the travel-time analyses presented in Chapter 4 constrained using the gravity anomaly was used as a starting point for the 2-D modelling using SEIS83. The first models incorporated the small variations observed in the depths to the PcP, PmP and Pn boundaries as observed in Figs. 4.16, 4.21 and 4.25. These boundaries were progressively smoothed by removal of all depth variations that did not produce calculated travel times which were consistent with the observed arrivals. For each model ray diagrams, travel time plots and synthetic seimograms were produced for stations 8, 32 and 50 for both the North and Irish Sea shots. Only two to three of these "runs" a week were possible before the installation of the AMDAHL 470 at Durham. Since about November 1985 almost one run per night has been possible.

The final velocity model is illustrated in Fig. 5.16. The PcP boundary was modelled as a velocity gradient zone with an increase in velocity from 6.2 to 6.75 - 6.77 km/s at depths of 15.5 to 18.5 km beneath the Irish Sea and 15.0 to 18.0 beneath the North Sea. The PmP boundary was modelled beneath the Irish Sea as an abrupt increase in velocity from 6.77 - 7.8 km/s underlain by a slight velocity gradient within the transitional Moho from 7.8 km/s to 8.0 km/s. Beneath the North Sea the PmP boundary was modelled as an abrupt increase in velocity from 6.75 to 8.0 km/s. The Pn boundary was modelled by vertical velocity variations beneath the Irish Sea

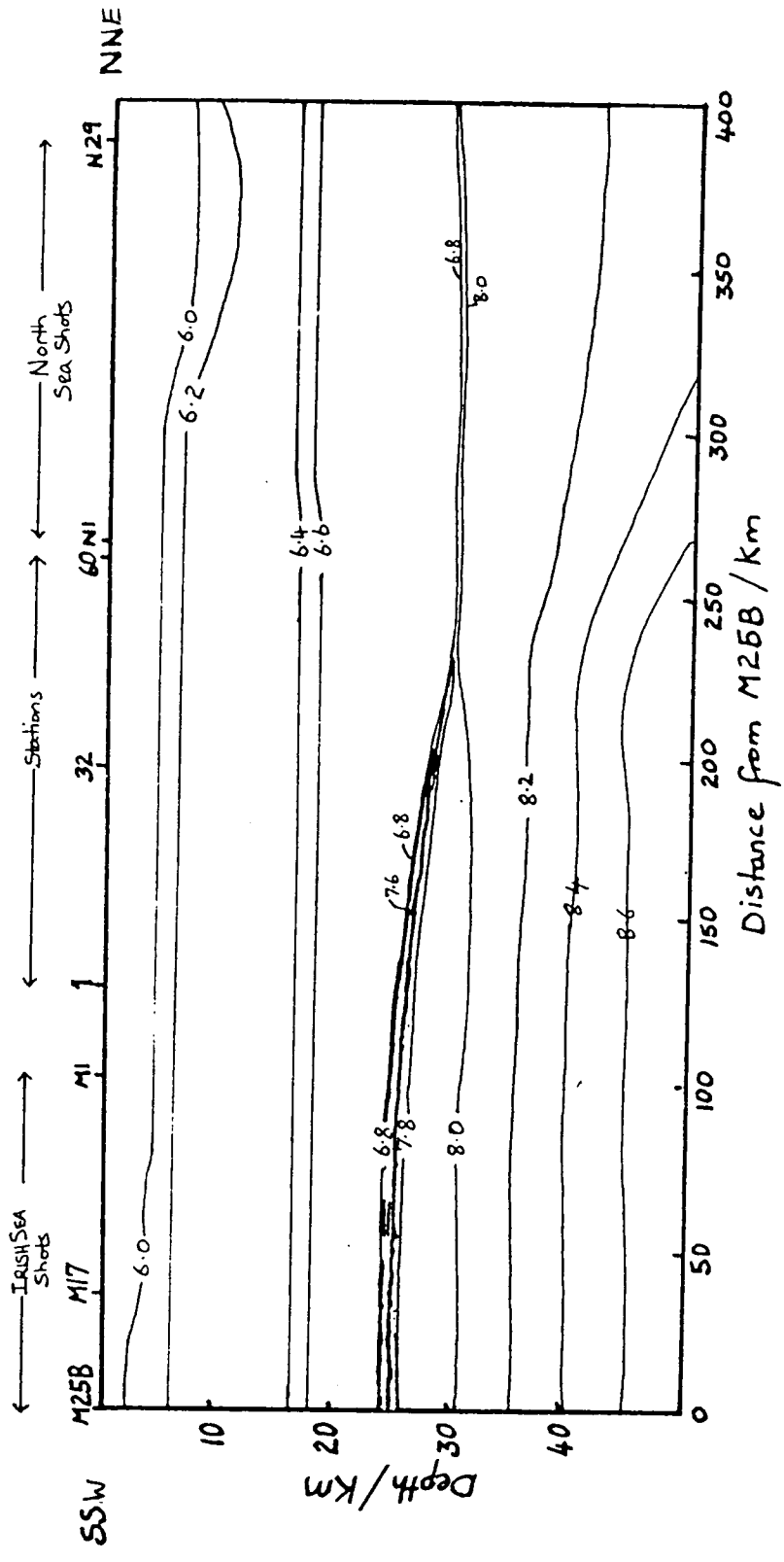


Figure(5.16) Final laterally varying velocity model used to compute the 2-D synthetic seismograms. Contours are iso-velocity lines. Contour interval is 0.2 km/s.

and as a sharp interface coincident with the PmP boundary beneath the North Sea. The sub-Moho velocities from the Pn boundary to a depth of 50 km increased from 8.0 to 8.8 km/s and 8.0 to 8.3 km/s beneath the Irish and North Seas respectively (Fig. 5.16).

The results for stations 8. 32 and 50 are presented in Figs. 5.17 to 5.19 respectively. Each figure contains 9 diagrams for a single receiving station labelled from (a) to (i) as follows:

(a) Raypaths through the upper crust.

(b) Raypaths through the lower crust.

(c) Raypaths of non reflected rays.

(d) 2-D synthetic seismogram for the Irish Sea shots computed using SEIS83.

(e) Observed seismogram for the Irish Sea shots with amplitudes corrected to common gain. The arrival times predicted by the laterally varying velocity model are drawn as a continuous line. Dashes denote the picked travel times.

(f) Observed seismogram for the Irish Sea shots with amplitudes equalized with picked and calculated arrival times as in (e).

(g) 2-D synthetic seismogram for the North Sea shots computed using SEIS83.

(h) Observed seismogram for the North Sea shots with amplitudes corrected to common gain with picked and calculated arrival times as in (e).

(i) Observed seismogram for the North Sea shots with amplitudes equalised with picked and calculated arrival

times as in (e).

Oscillations of the velocity structure created by the bicubic spline method used to smooth the velocity model mainly occurred in the upper crust where there are large velocity variations such as in Fig. 5.20(a).

In general the PcP arrivals are larger on the synthetic seismograms than on the observed sections. The synthetic seismogram modelling using the reflectivity method also produces PcP amplitudes that are too large. This may indicate that the interface is not a simple velocity gradient or an abrupt increase of velocity. A complicated laterally heterogeneous interface would produce scattering of the seismic energy to reduce the computed PcP amplitudes.

The following main points can be made about the fit of the travel times and amplitudes for each station:

1. Station 8 for the Irish Sea Shots (Fig. 5.17)

   The amplitudes of all arrivals are small between shots M10 to M17 on the observed section (Fig. 5.17e). This is probably due to the shot effects or other near surface causes. The fit of the calculated and observed travel-times is within the picking errors estimated to be about 0.25 s.

2. Station 8 for the North Sea Shots (Fig. 5.17)

   The fit between the calculated and observed travel-times is within the picking errors for the PcP and PmP phases. The correspondence between the calculated and observed Pn amplitudes is better than the fit between the calculated and picked travel-times. This misfit of the picked

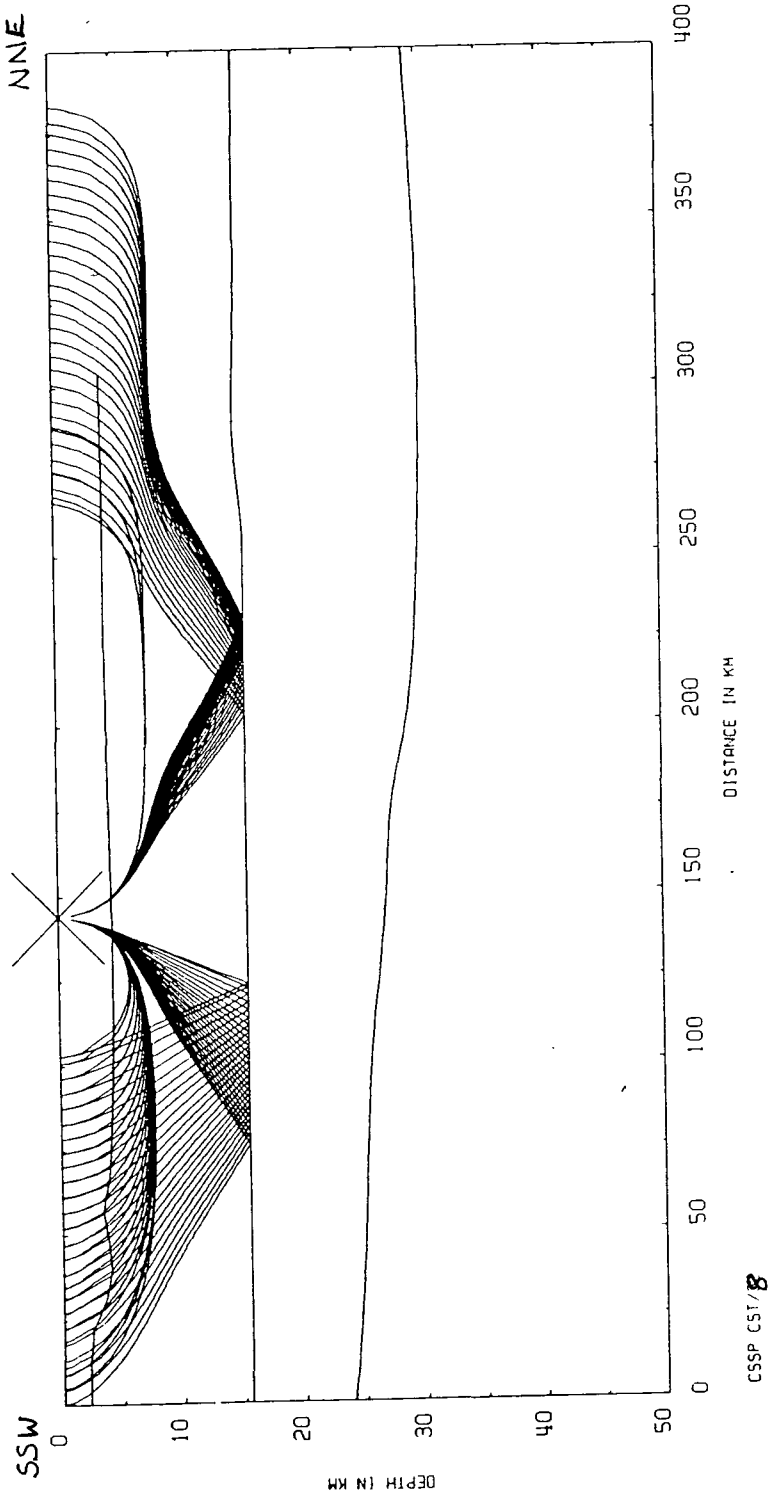


Figure(5.17) (a) Raypaths through the upper crust computed for station 8

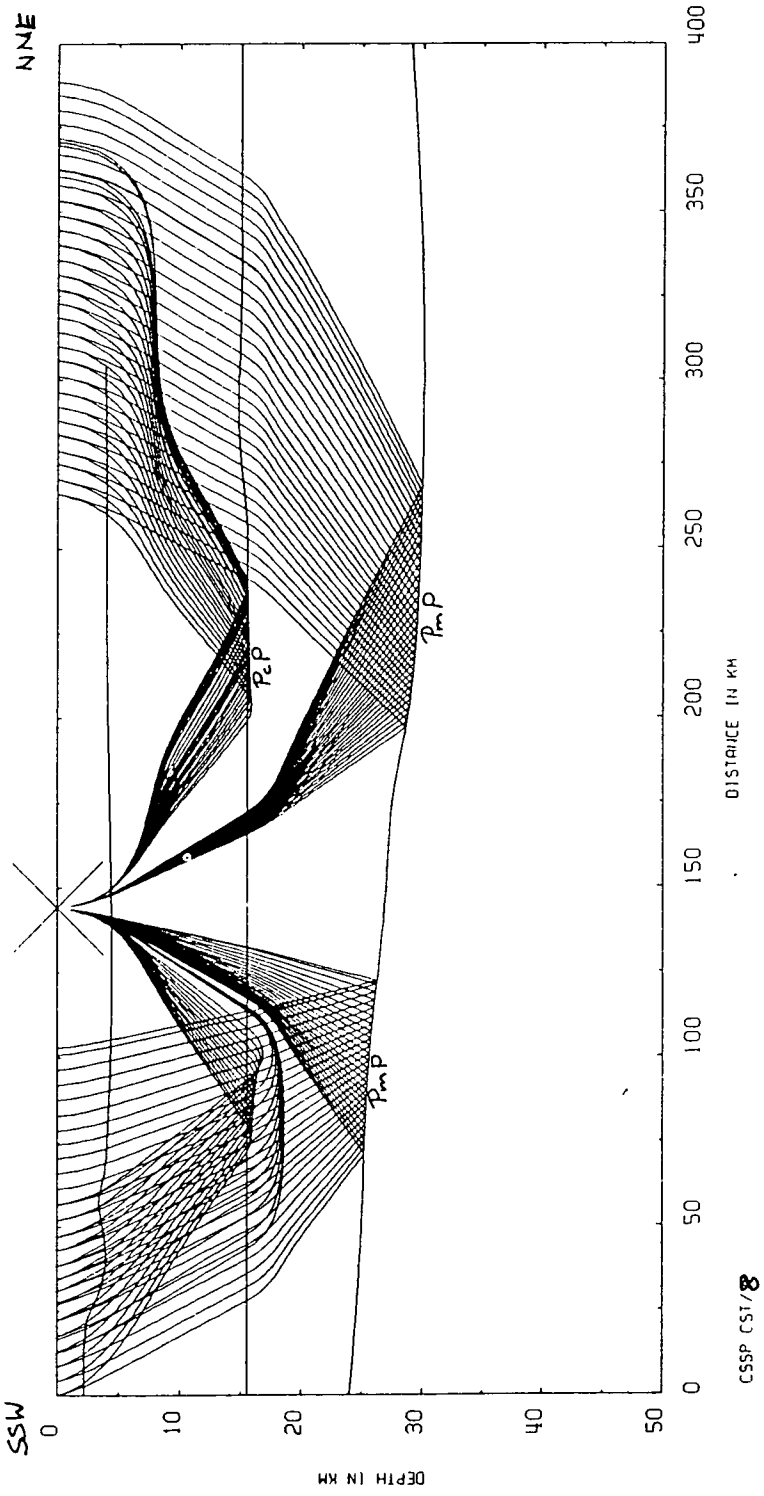


5·17 (b) Raypaths through the lower crust computed for station 8

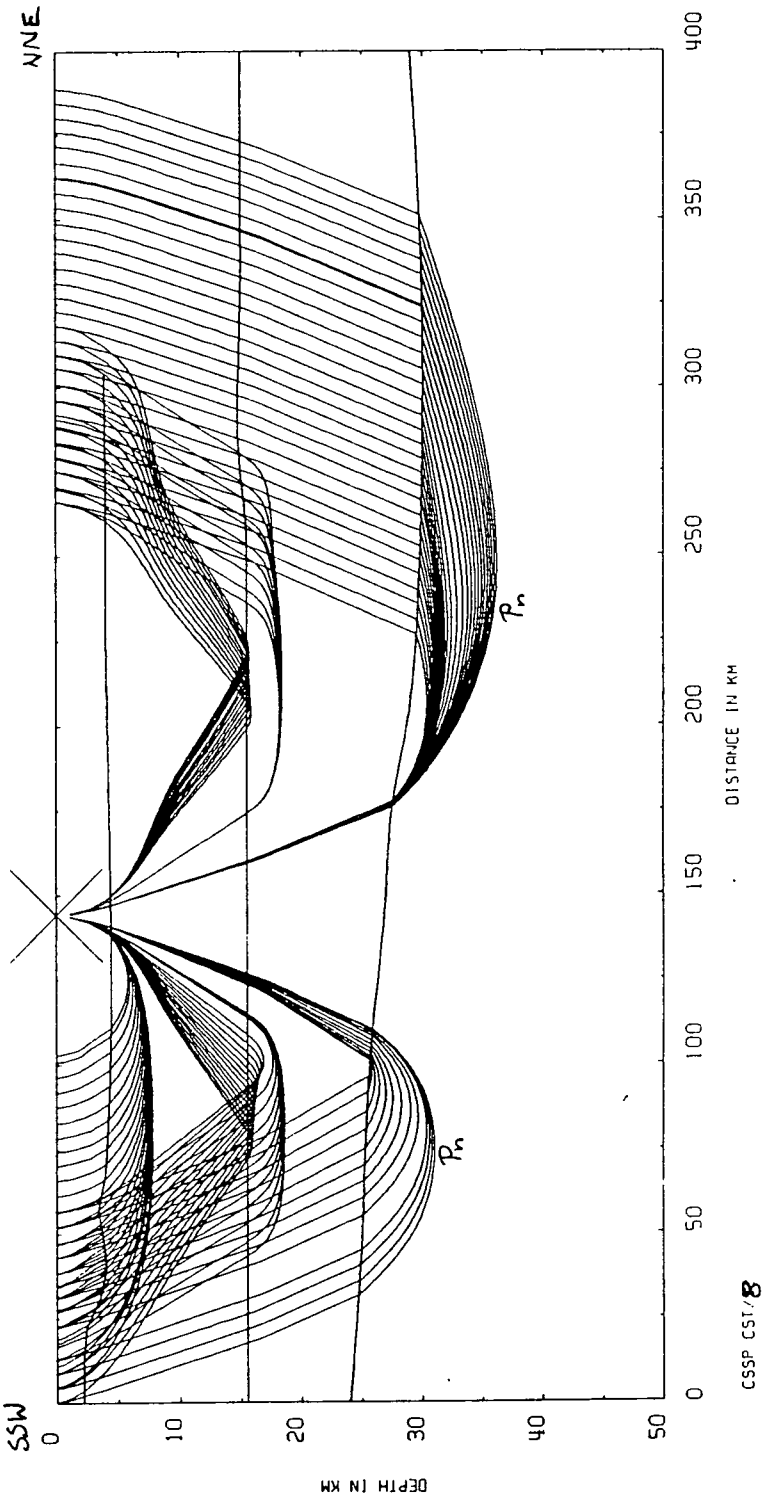


5-17 (c) Raypaths of non reflected rays computed for station 8

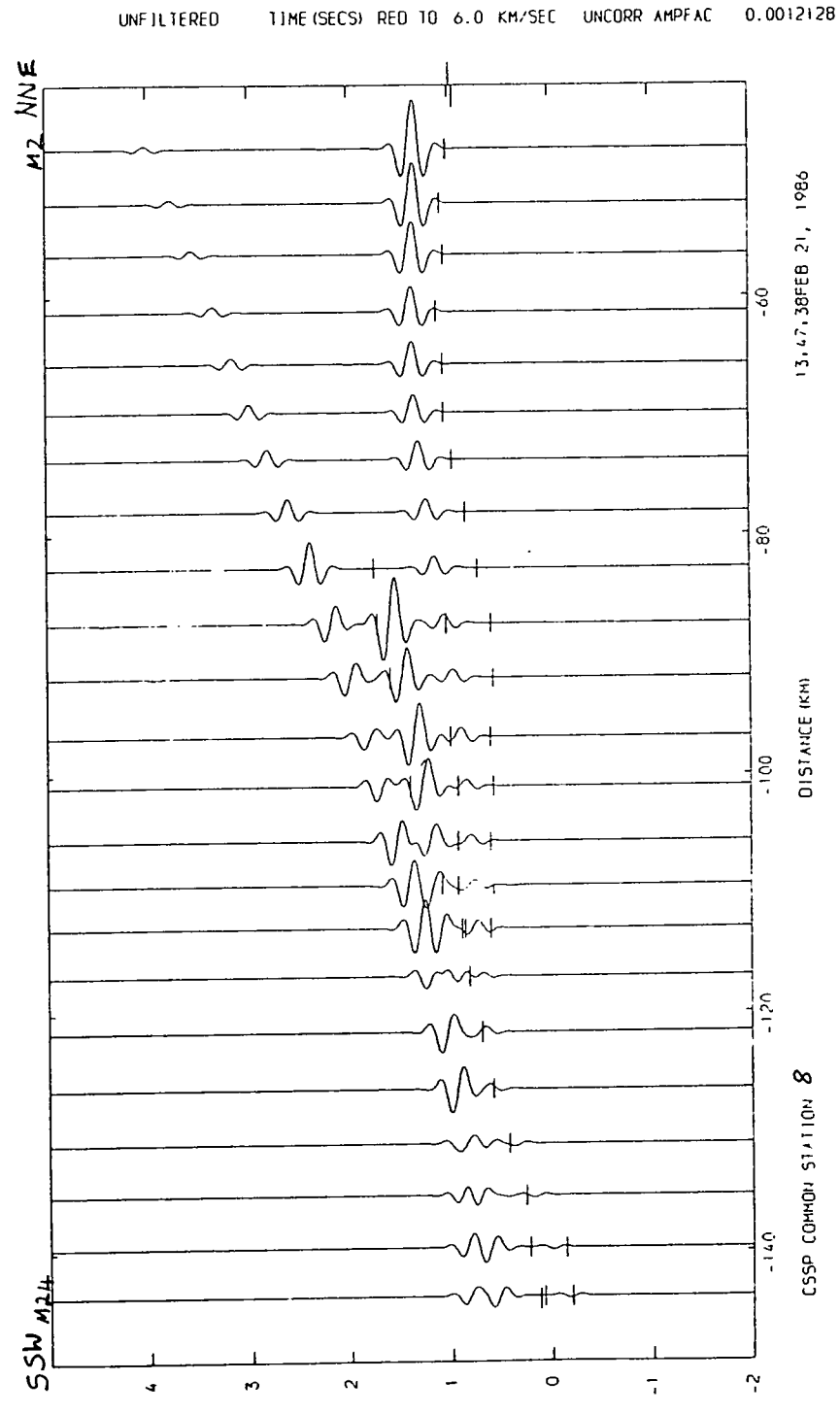


5·17(d) 2-D synthetic seismogram for station 8 for the Irish Sea shots computed using SEIS83.

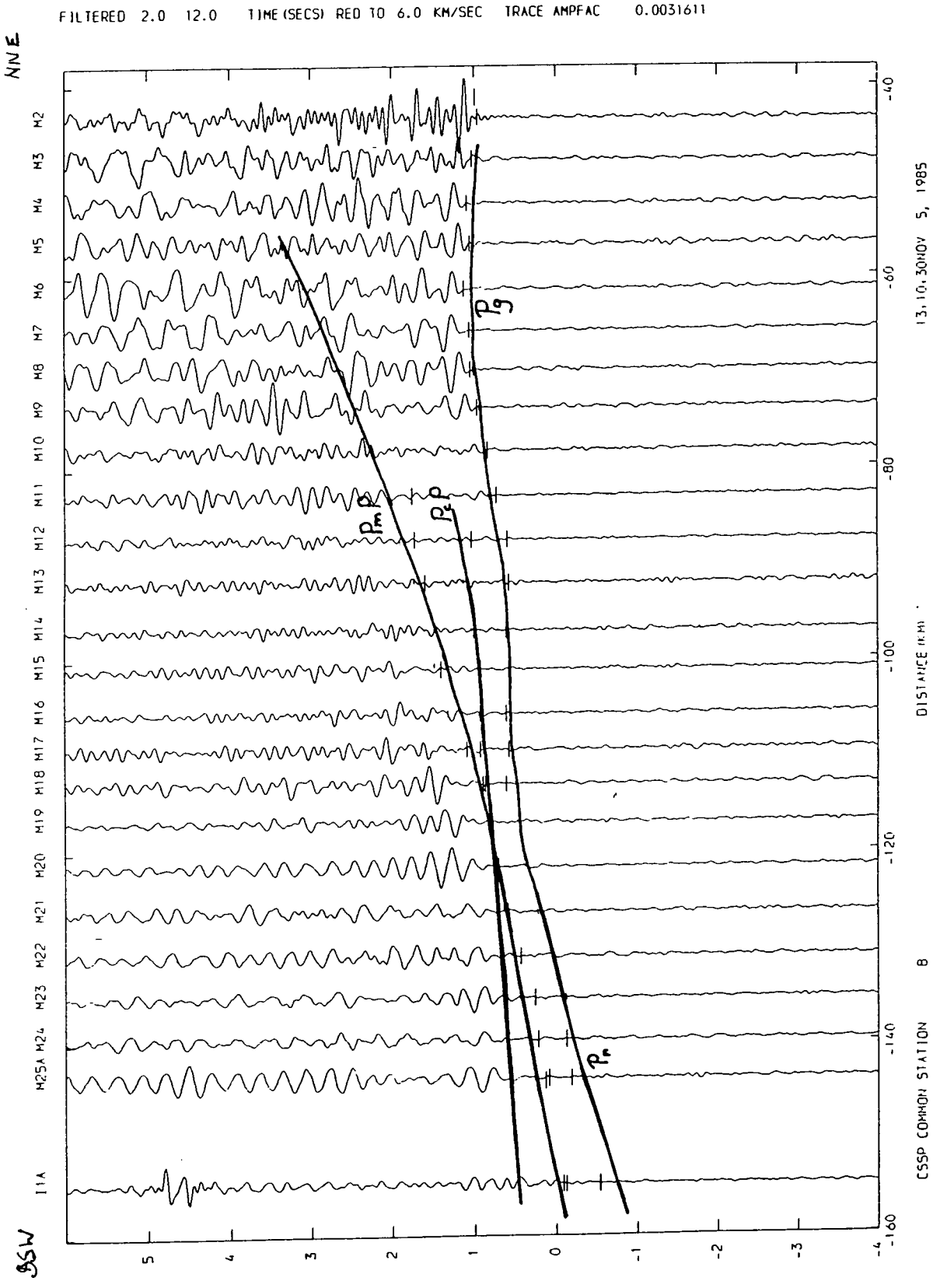


5·17(e) Observed seismogram for station 8 for the Irish Sea shots with amplitudes corrected to common gain. The arrival times predicted by the laterally varying velocity model are drawn as a continuous line. Dashes are the picked travel times.

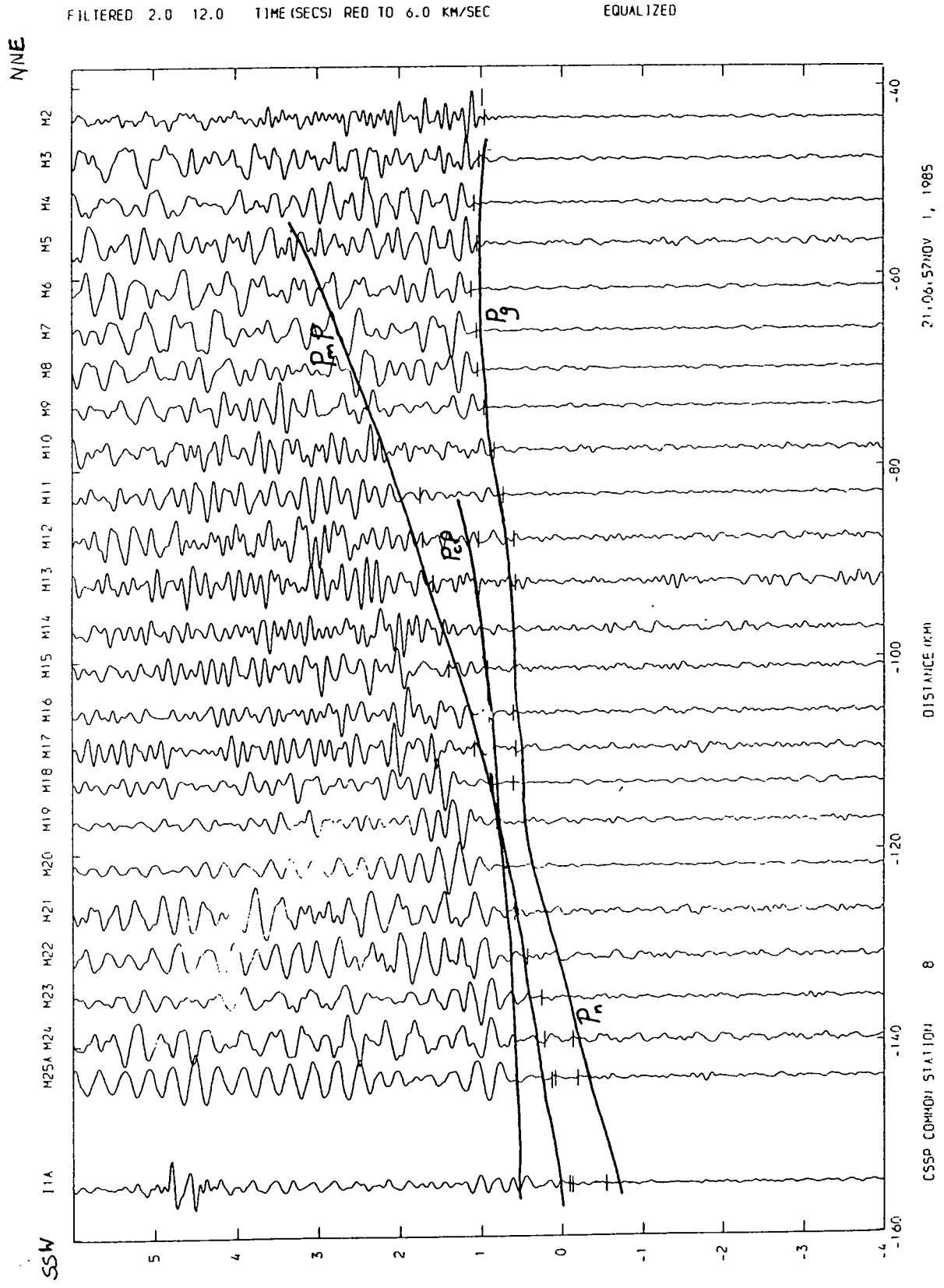


**5·17 (f)** Observed seismogram for station 8 for the Irish Sea shots with amplitudes equalised.
The arrival times predicted by the laterally varying velocity model are drawn as a continuous line.
Dashes are the picked travel times.

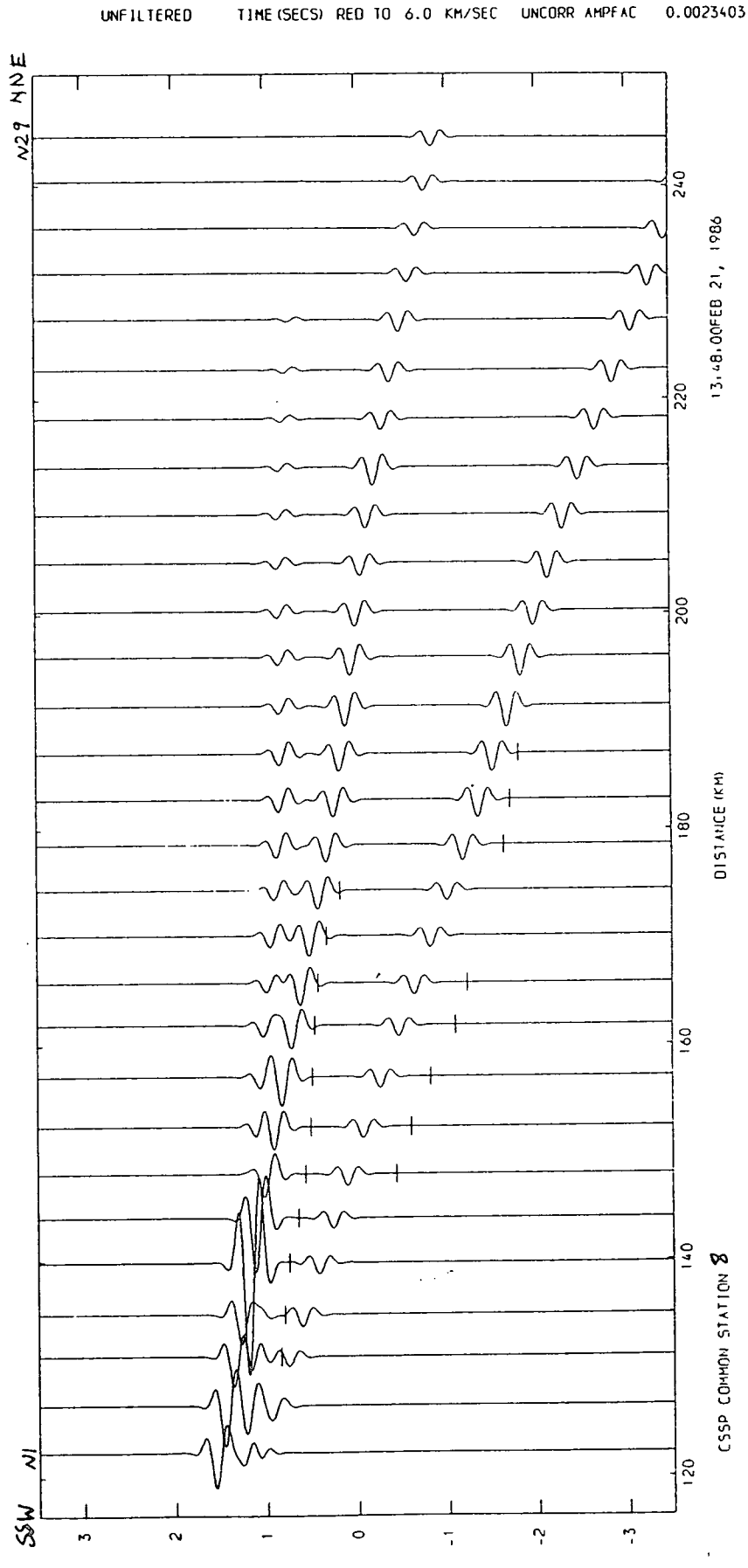


5.17(g) 2-D synthetic seismogram for station 8 for the North Sea shots computed using SEIS83.

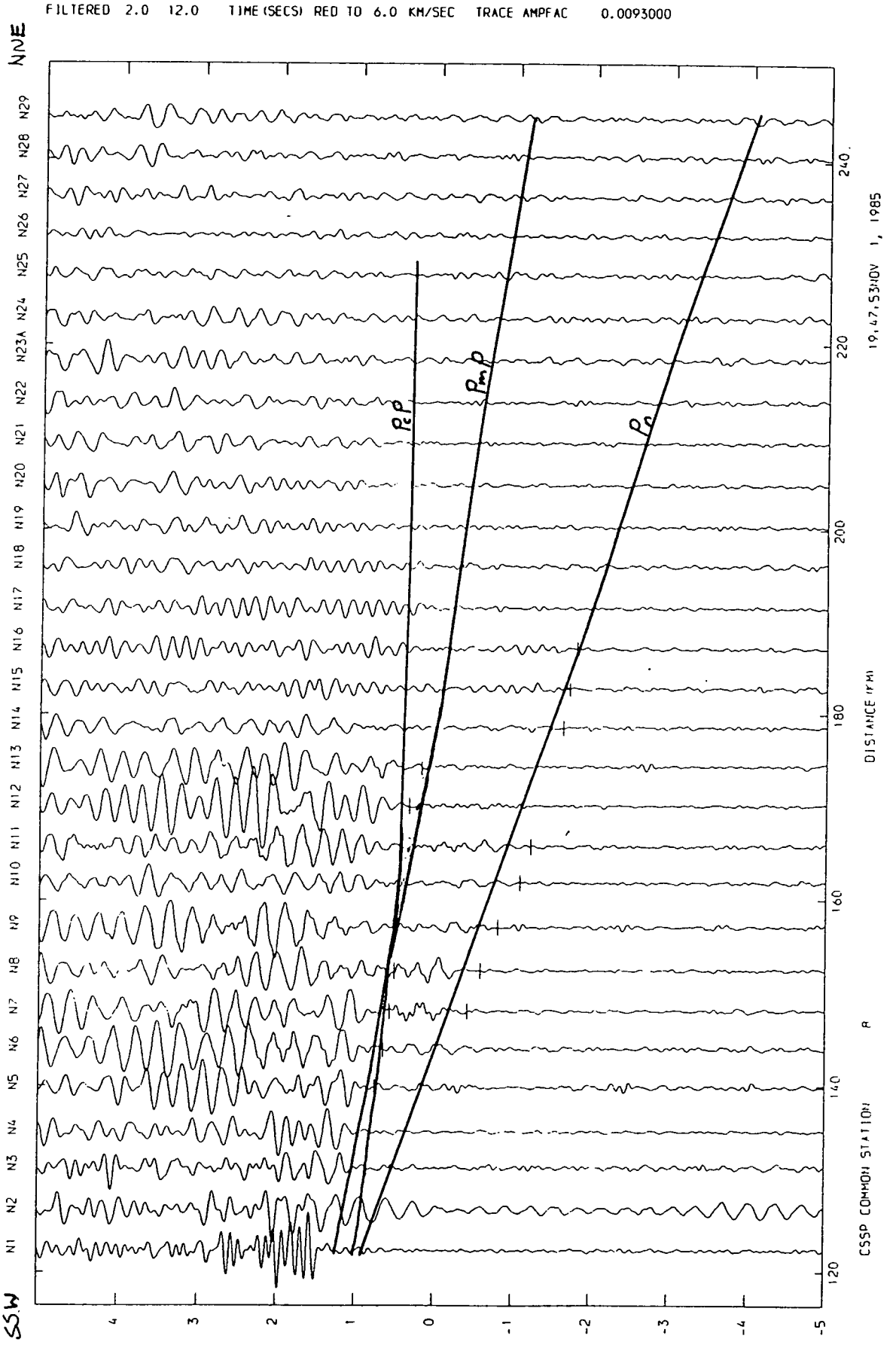


5.17 (h) Observed seismogram for station 8 for the North Sea shots with amplitudes corrected to common gain. The arrival times predicted by the laterally varying velocity model are drawn as a continuous line. Dashes are the picked travel times.

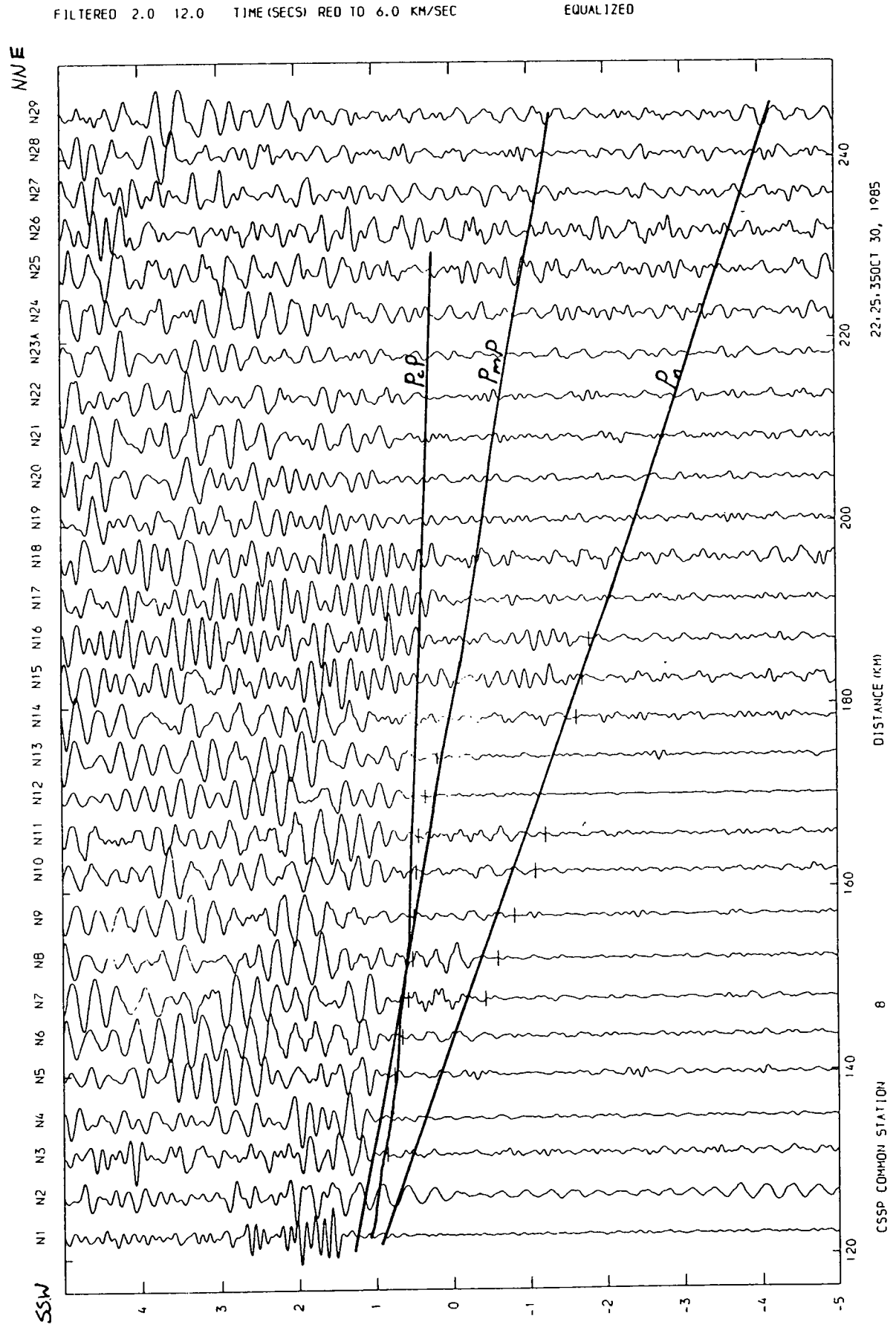


**5·17** (i) Observed seismogram for station 8 for the North Sea shots with amplitudes equalised.
The arrival times predicted by the laterally varying velocity model are drawn as a continuous line.
Dashes are the picked travel times.

travel-times is about 0.25 s which is equal to the estimated picking error. The travel times for Pn observed from shots N7 to N11 were probably picked too early.

3. Station 32 for the Irish and North Sea Shots (Fig. 5.18)
   The fit between the observed and calculated travel-times is good for all phases for station 32 in both the Irish and North Seas. The dying out of Pg is successfully modelled by the eastward lateral decrease in velocity in the basement beneath shots N11 to N25.

4. Station 50 for the Irish and North Sea Shots (Fig. 5.19)
   The calculated and observed travel times are consistent between the synthetic and observed seismograms for both the Irish and North Sea shots. Pg in the North Sea disappears more rapidly than actually observed. It was found that this disappearence of Pg was very sensitive to the lateral decrease in the velocities eastwards beneath shots N11 to N20 and also to the depth extent of this low velocity region. This sensitivity is probably an artifact of the velocity oscillations produced by the bicubic spline approximation of the velocity model. However, the synthetic seismograms do illustrate that a lateral decrease in velocity can produce the disappearance of Pg at about shot N11 for most stations.

5. Shots M17 and N1 (Figs. 5.20 and 5.21)
   The fit between the observed and calculated travel-times is good for all phases for shot M17. For shot N1 the fit is good for Pg and PcP. However, the correspondance between the calculated and observed PmP amplitudes is better than the fit between the calculated and picked PmP travel-times.

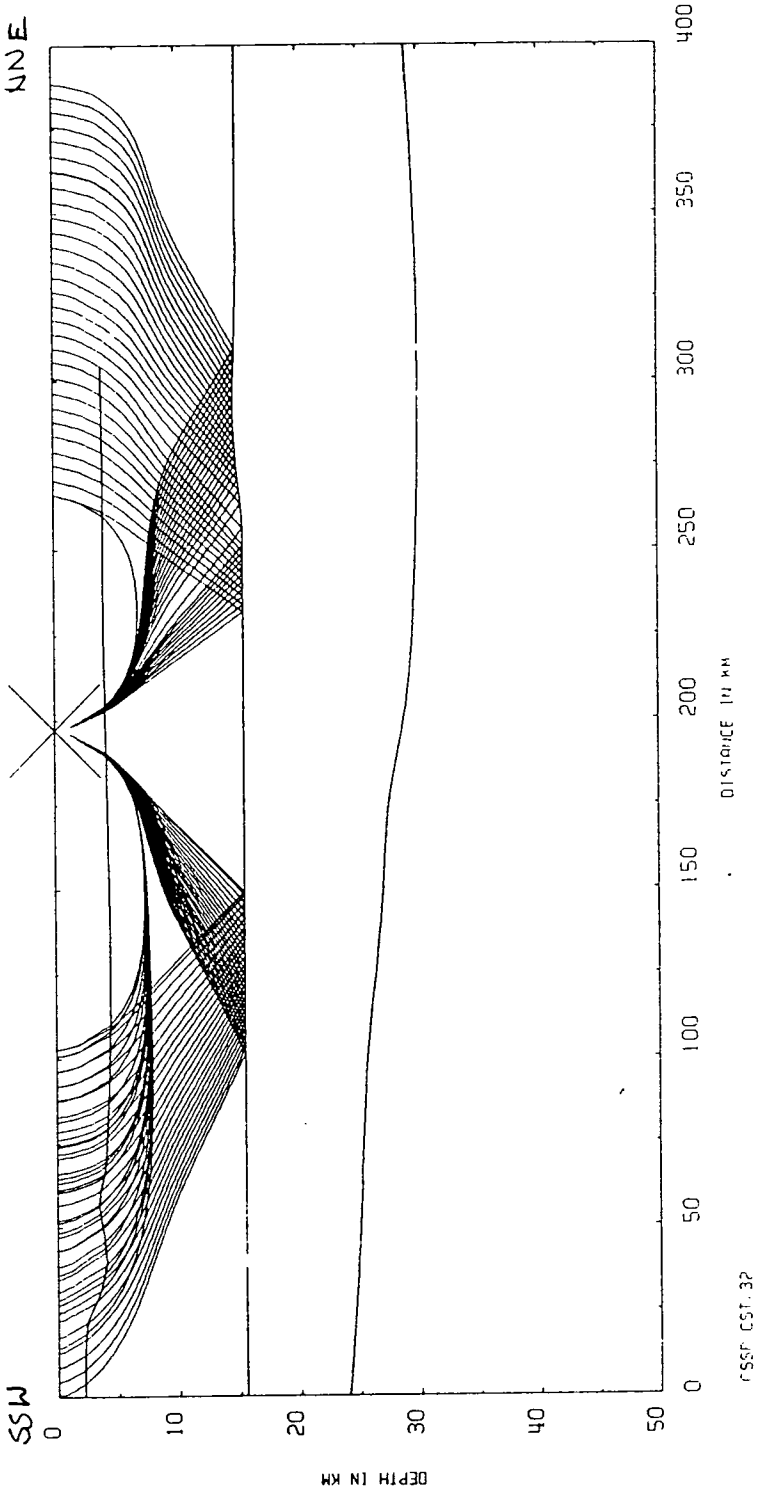


Figure(5.18) (a) Raypaths through the upper crust computed for station 32

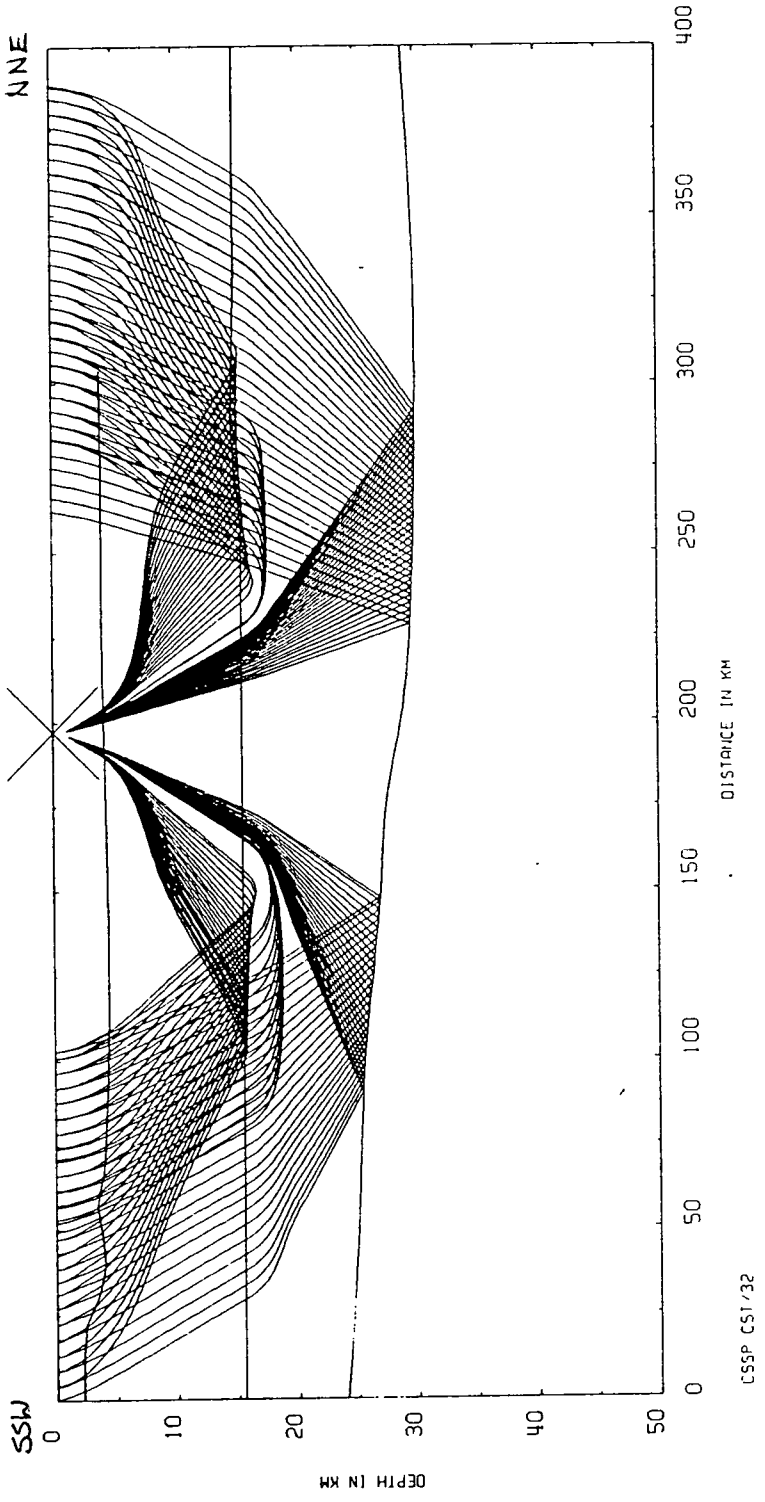


**5·18**(b) Raypaths through the lower crust computed for station 32

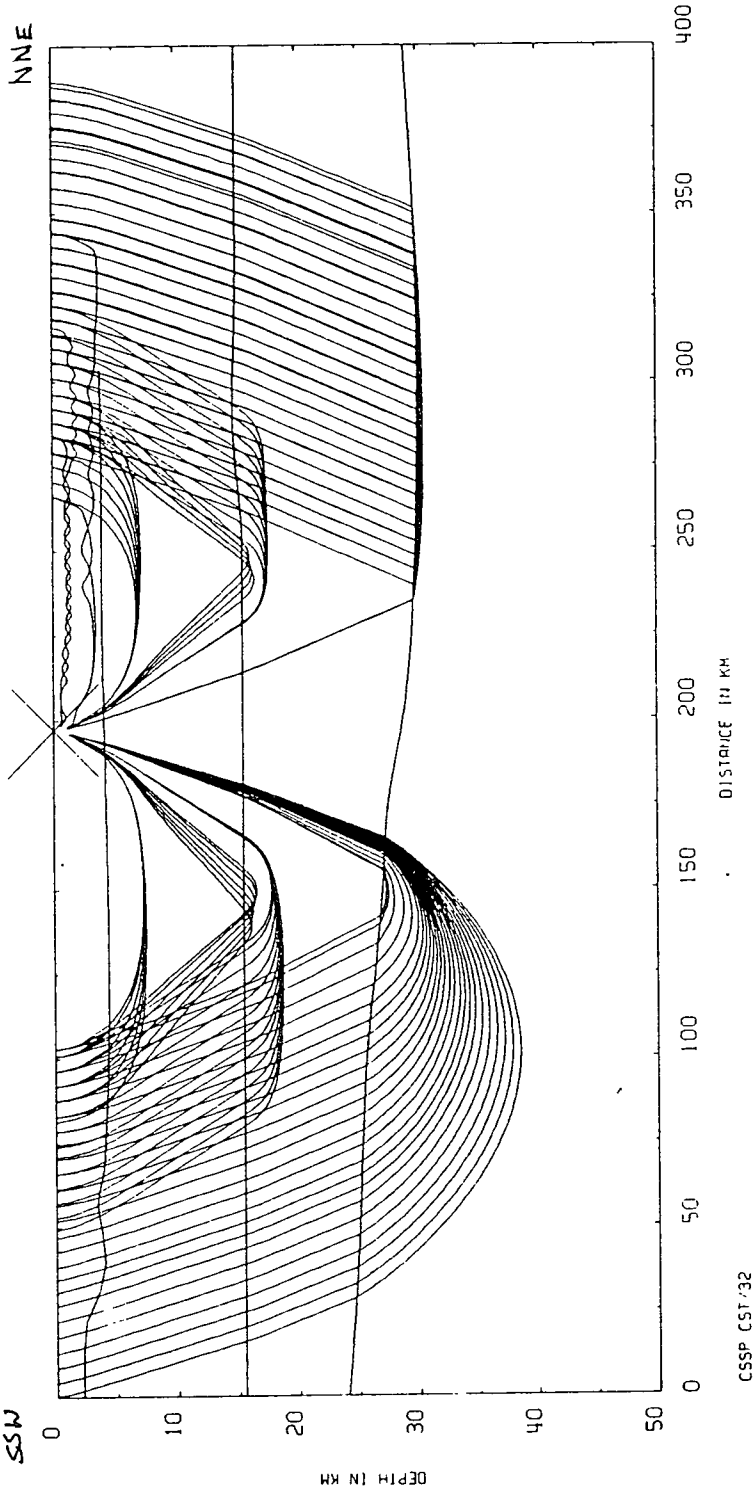


6.18 (c) Raypaths of non reflected rays computed for station 32

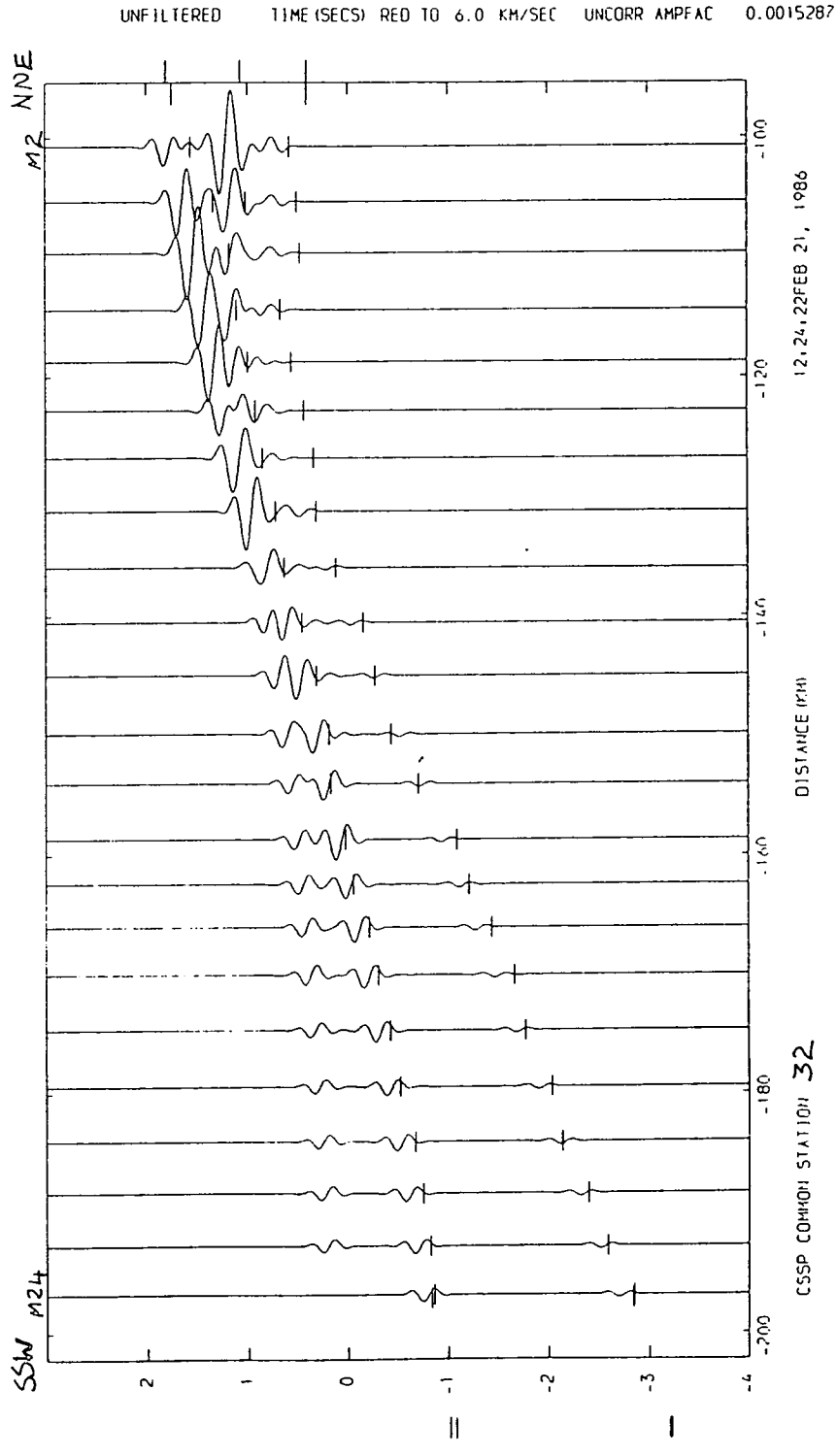


5.18 (d) 2-D synthetic seismogram for station 32 for the Irish Sea shots computed using SEIS83.

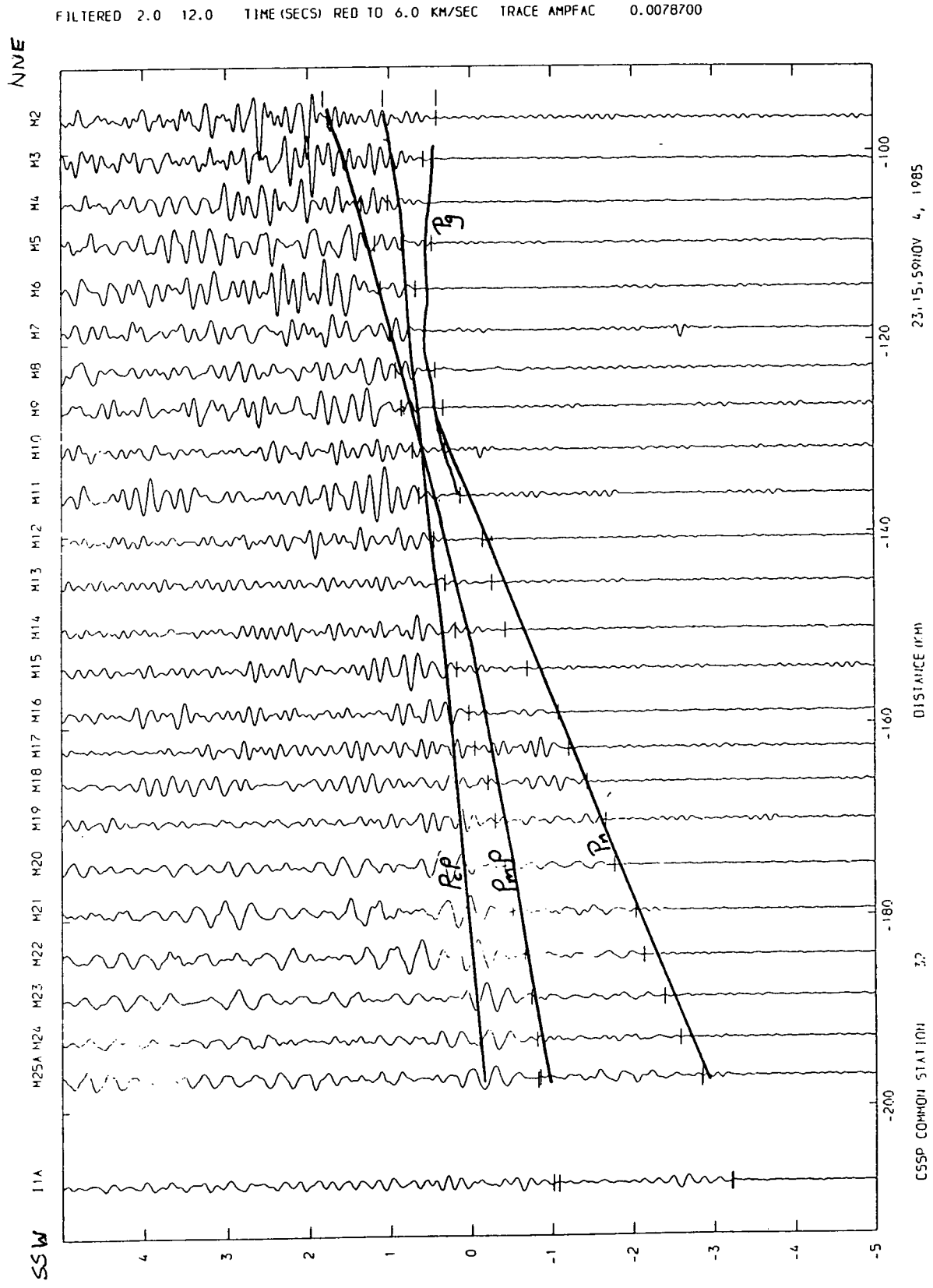


5-18 (e) Observed seismogram for station 32 for the Irish Sea shots with amplitudes corrected to common gain. The arrival times predicted by the laterally varying velocity model are drawn as a continuous line. Dashes are the picked travel times.

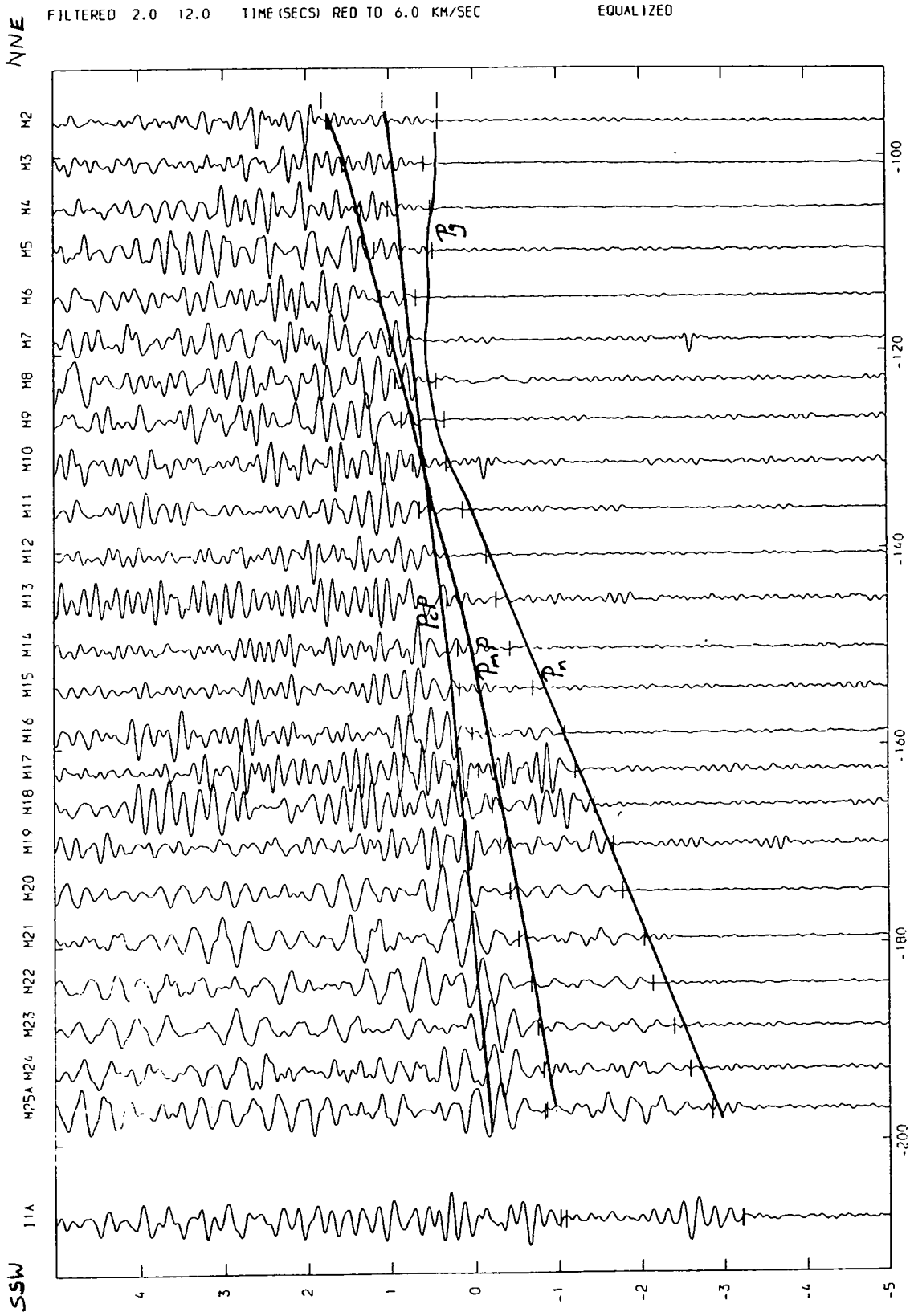


**5.18** (f) Observed seismogram for station 32 for the Irish Sea shots with amplitudes equalised.
The arrival times predicted by the laterally varying velocity model are drawn as a continuous line.
Dashes are the picked travel times.

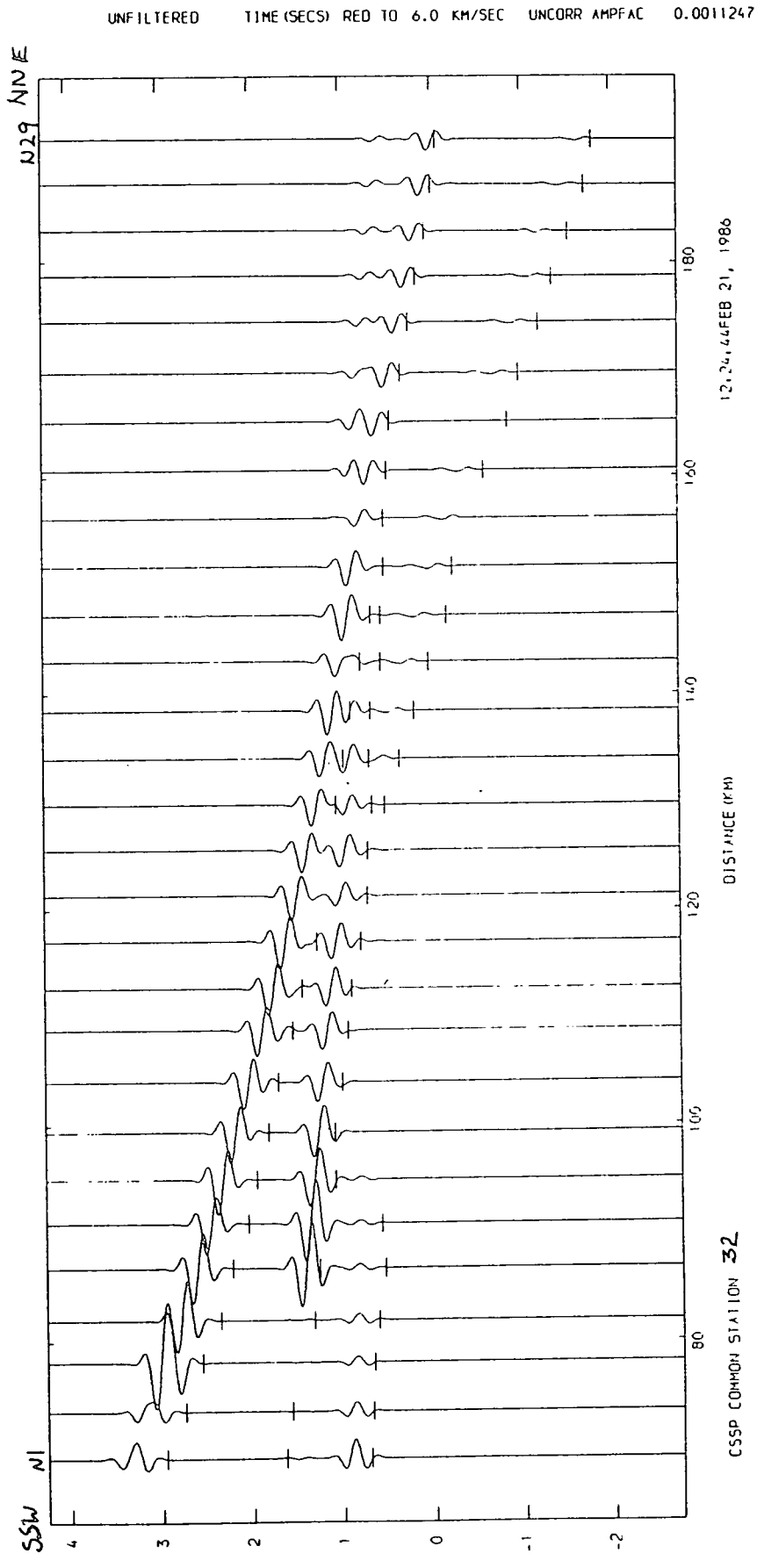


5.18 (g) 2-D synthetic seismogram for station 32 for the North Sea shots computed using SEIS83.

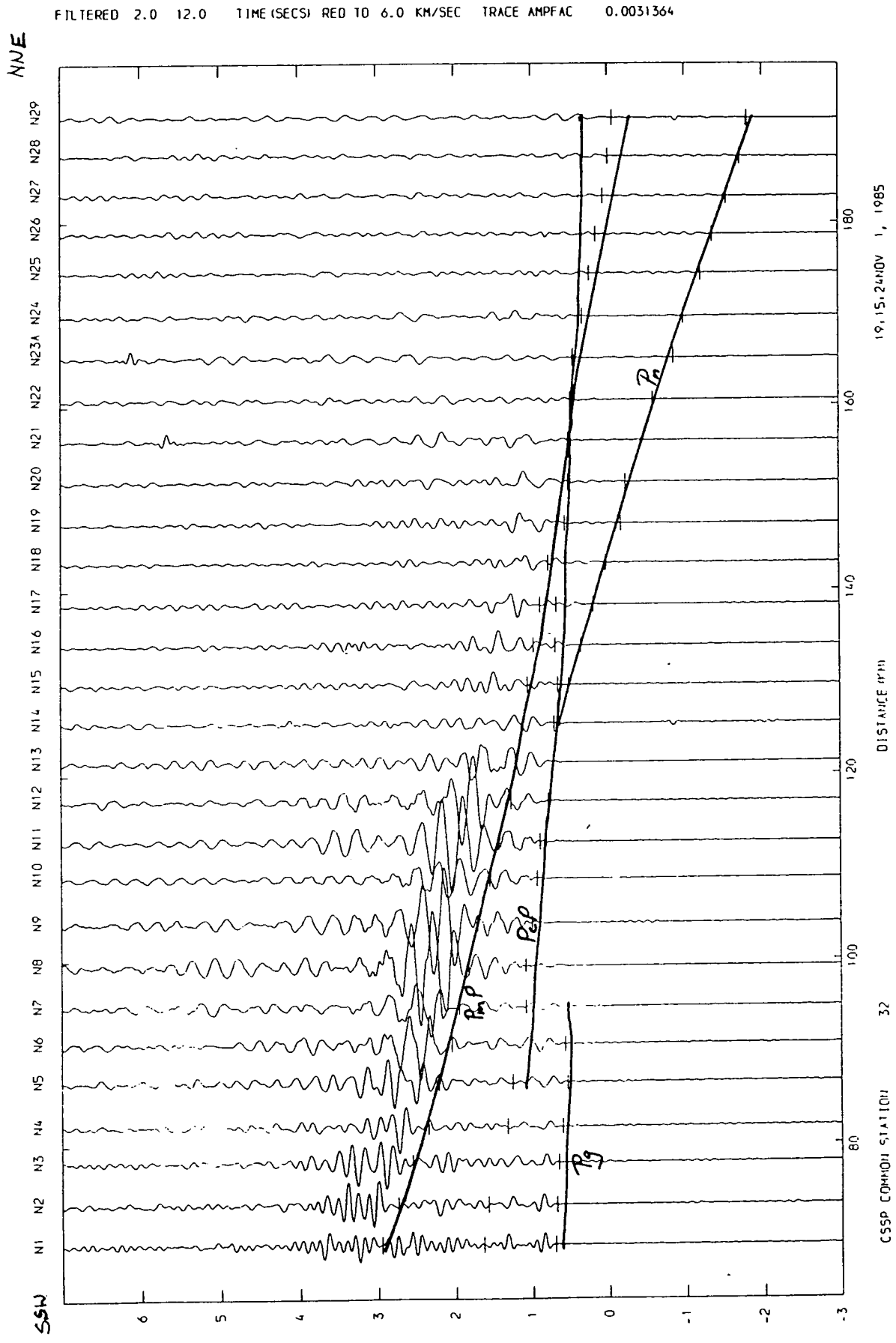


**5·18** (h) Observed seismogram for station 32 for the North Sea shots with amplitudes corrected to common gain. The arrival times predicted by the laterally varying velocity model are drawn as a continuous line. Dashes are the picked travel times.

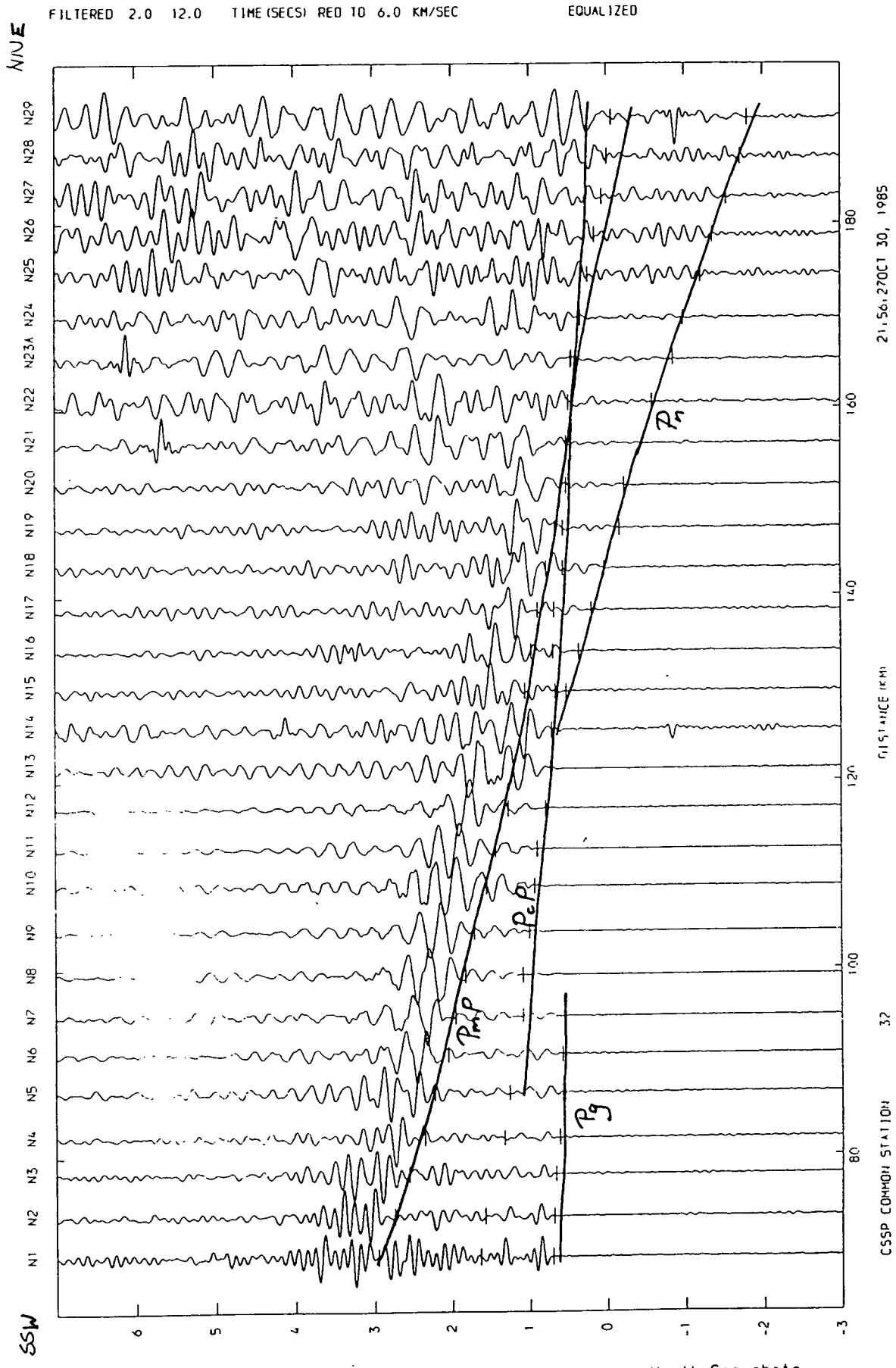


518 (i) Observed seismogram for station 32 for the North Sea shots with amplitudes equalised.
The arrival times predicted by the laterally varying velocity model are drawn as a continuous line.
Dashes are the picked travel times.

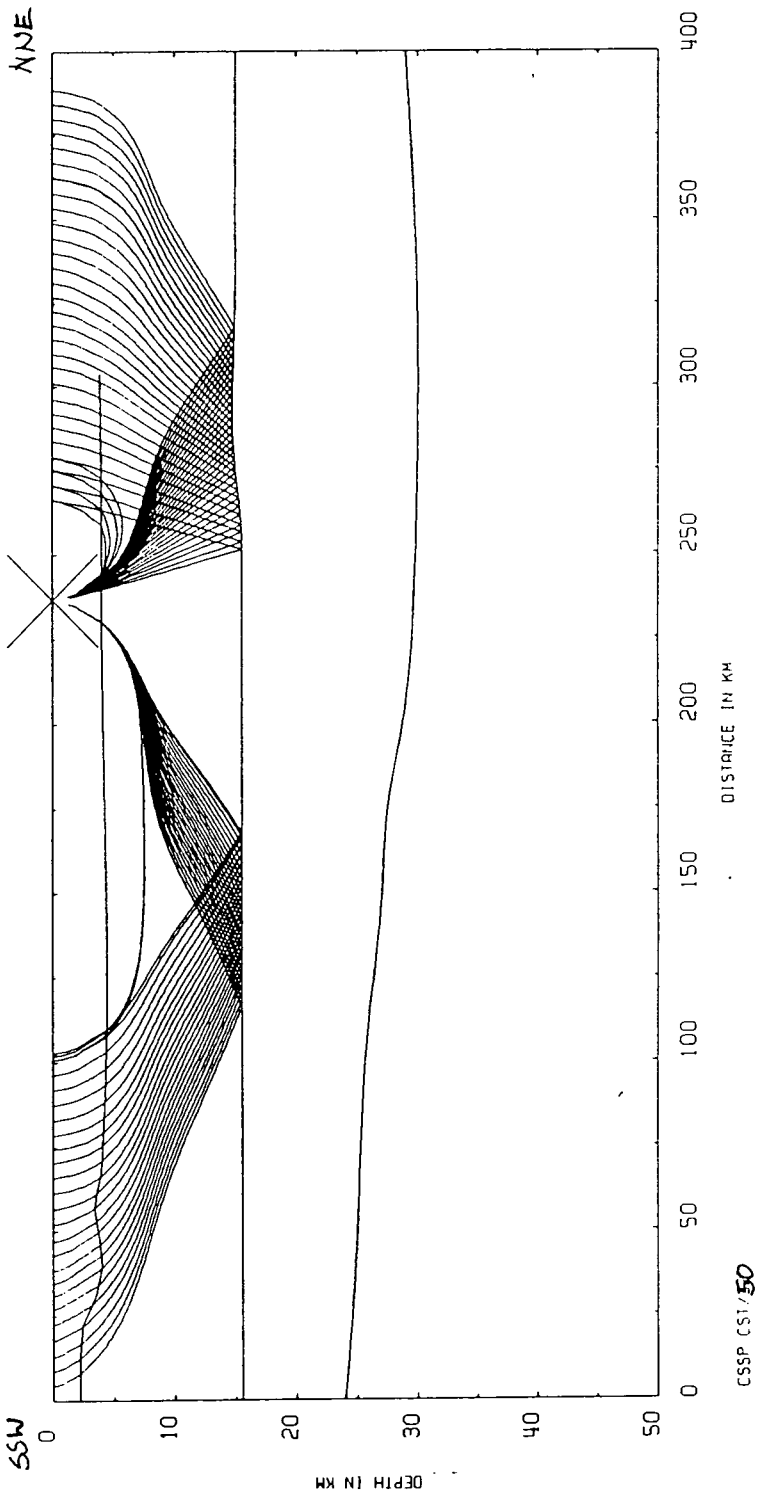


Figure(5.19) (a) Raypaths through the upper crust computed for station 50

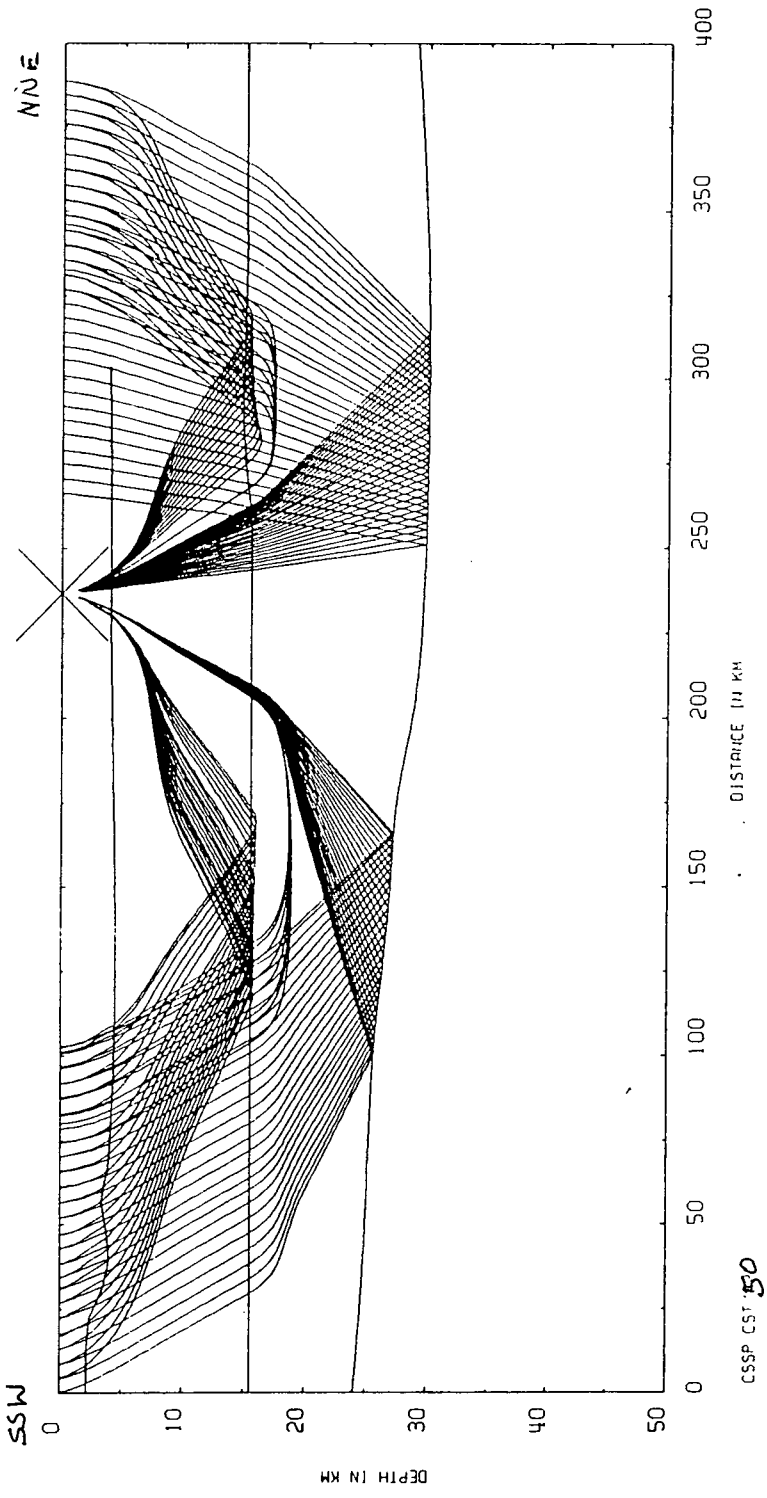


5.19 (b) Raypaths through the lower crust computed for station 50

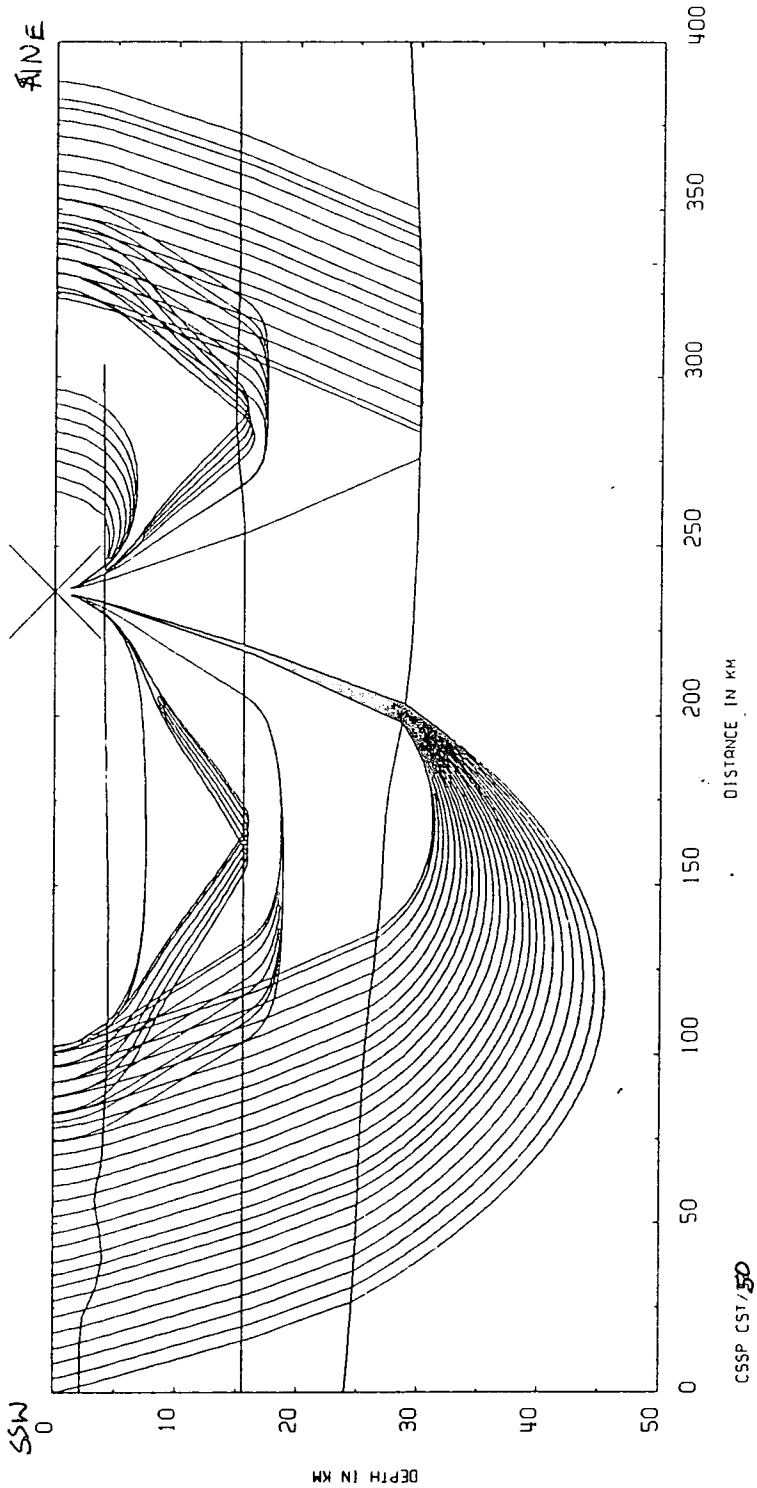


5.19 (c) Raypaths of non reflected rays computed for station 50

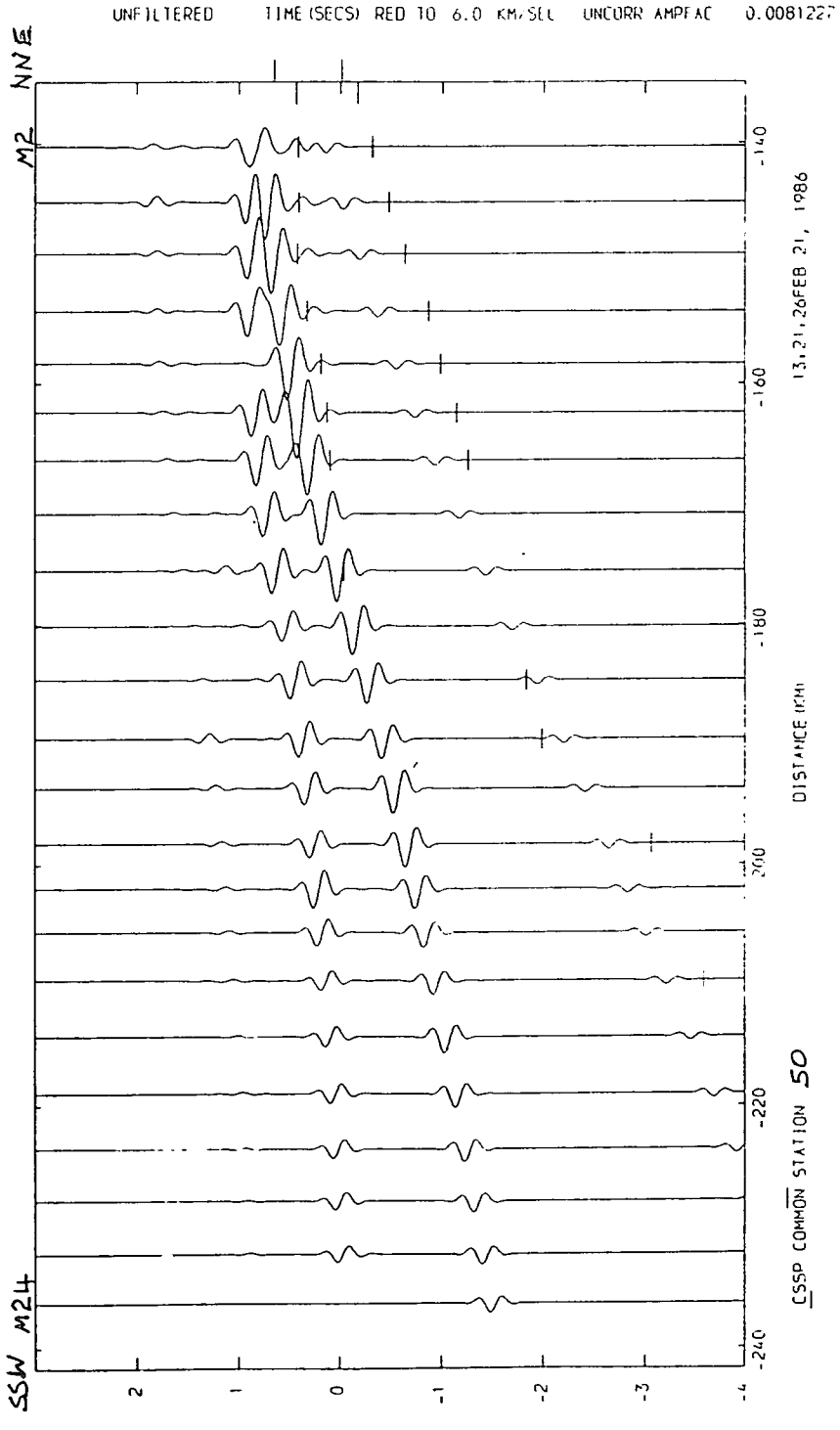


5.19 (d) 2-D synthetic seismogram for station 50 for the Irish Sea shots computed using SEIS83.

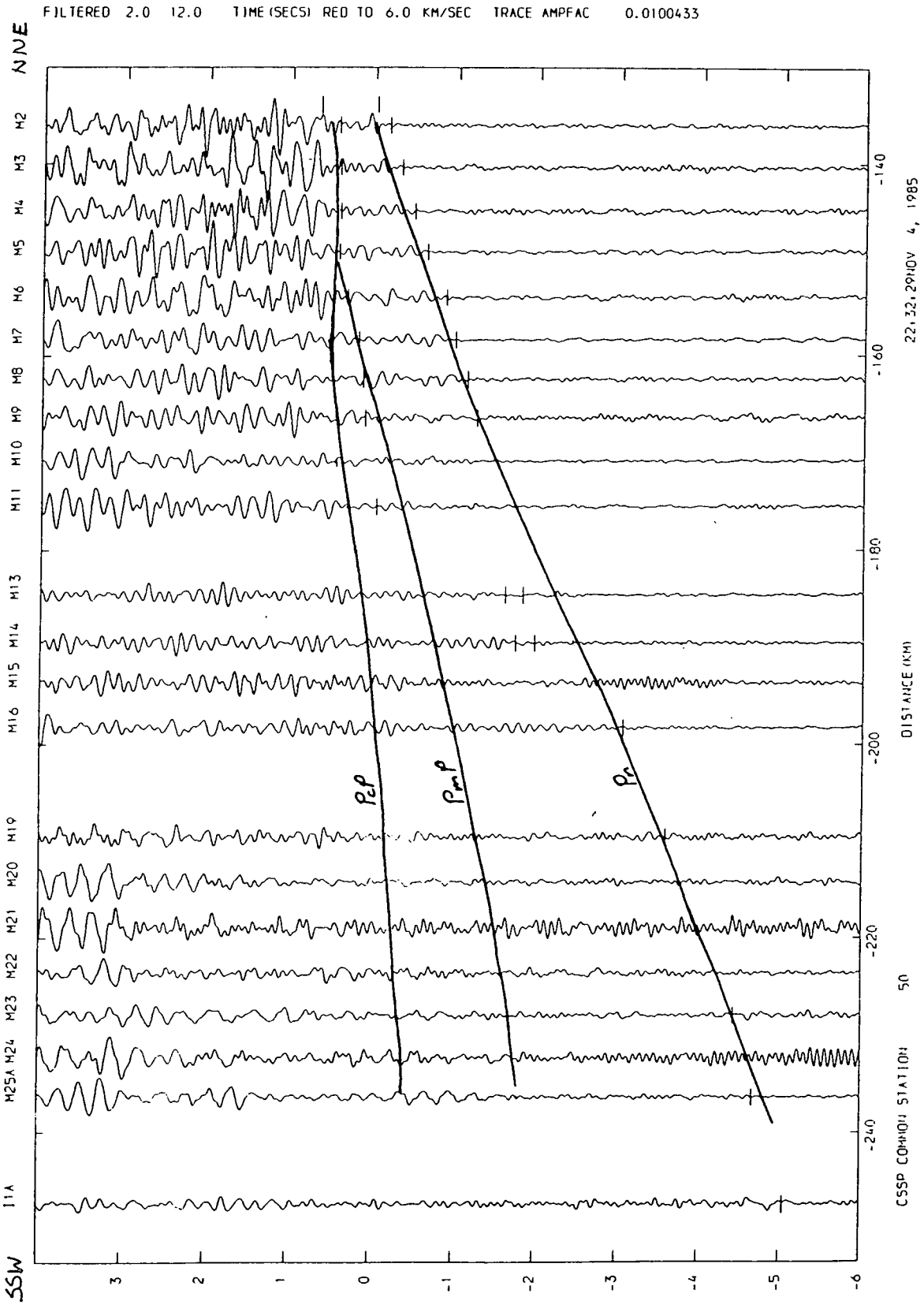


5-19(e) Observed seismogram for station 50 for the Irish Sea shots with amplitudes corrected to common gain. The arrival times predicted by the laterally varying velocity model are drawn as a continuous line. Dashes are the picked travel times

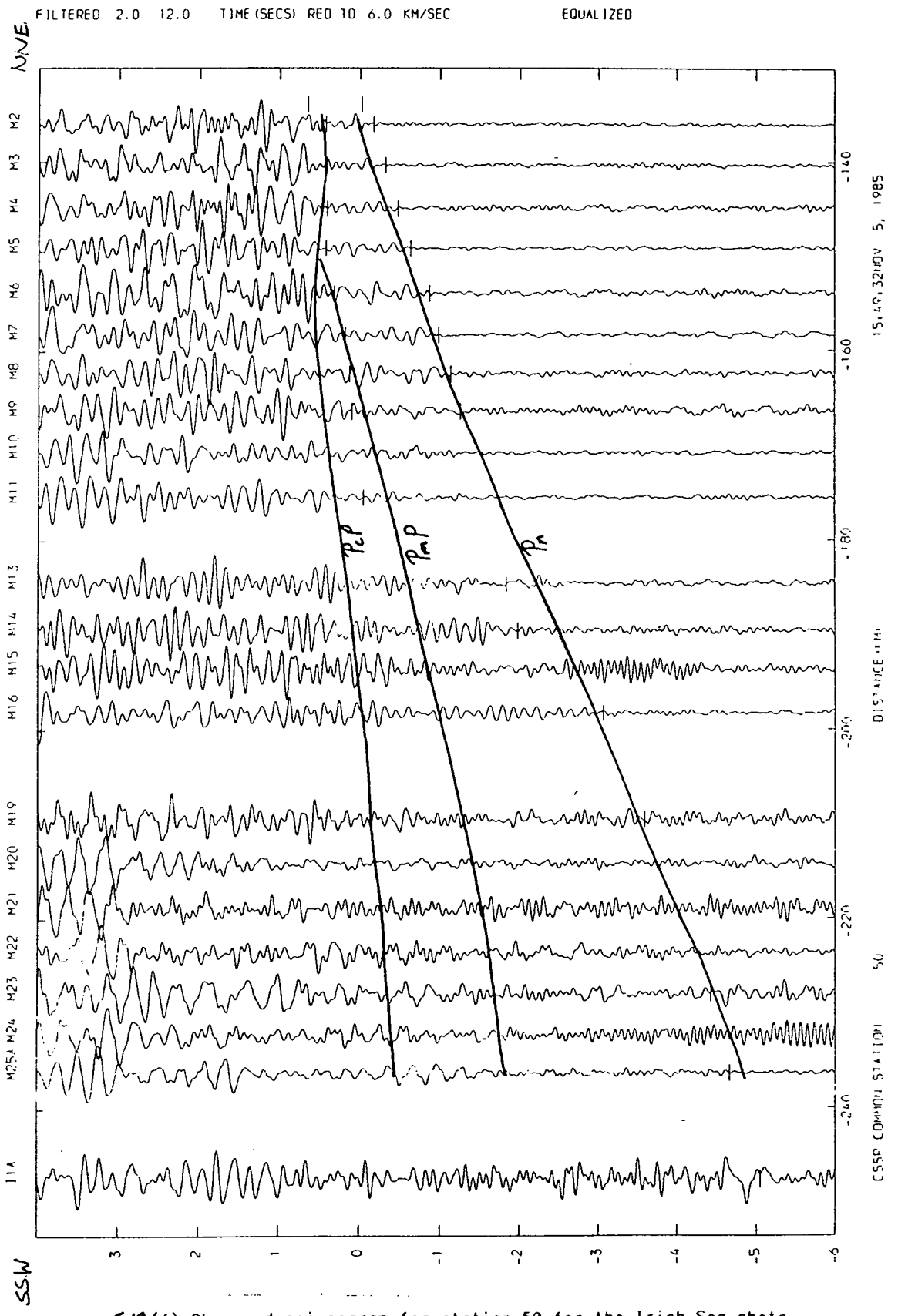


**5-19(f)** Observed seismogram for station 50 for the Irish Sea shots with amplitudes equalised.
The arrival times predicted by the laterally varying velocity model are drawn as a continuous line.
Dashes are the picked travel times.

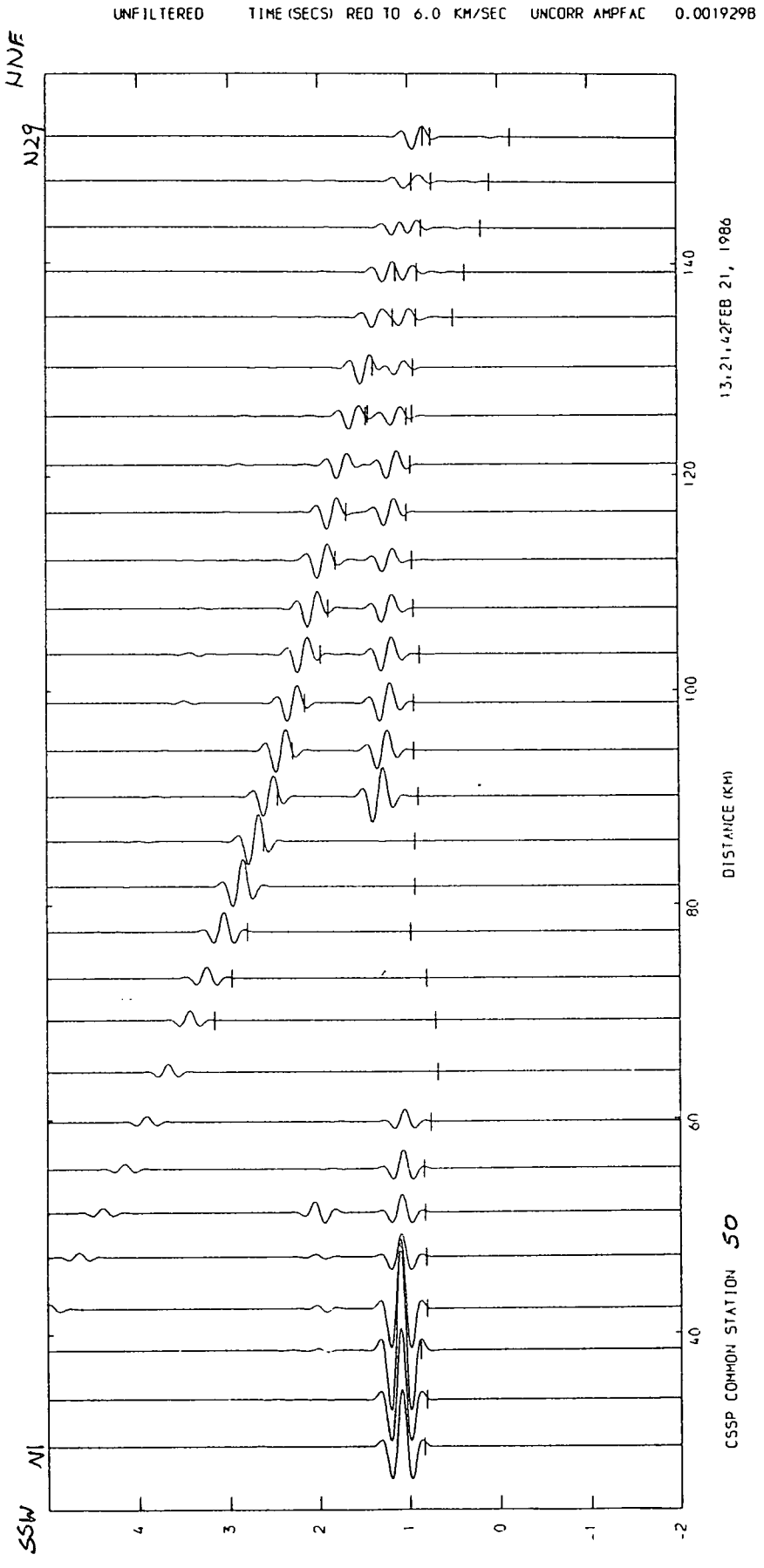


5.19 (g) 2-D synthetic seismogram for station 50 for the North Sea shots computed using SEIS83.

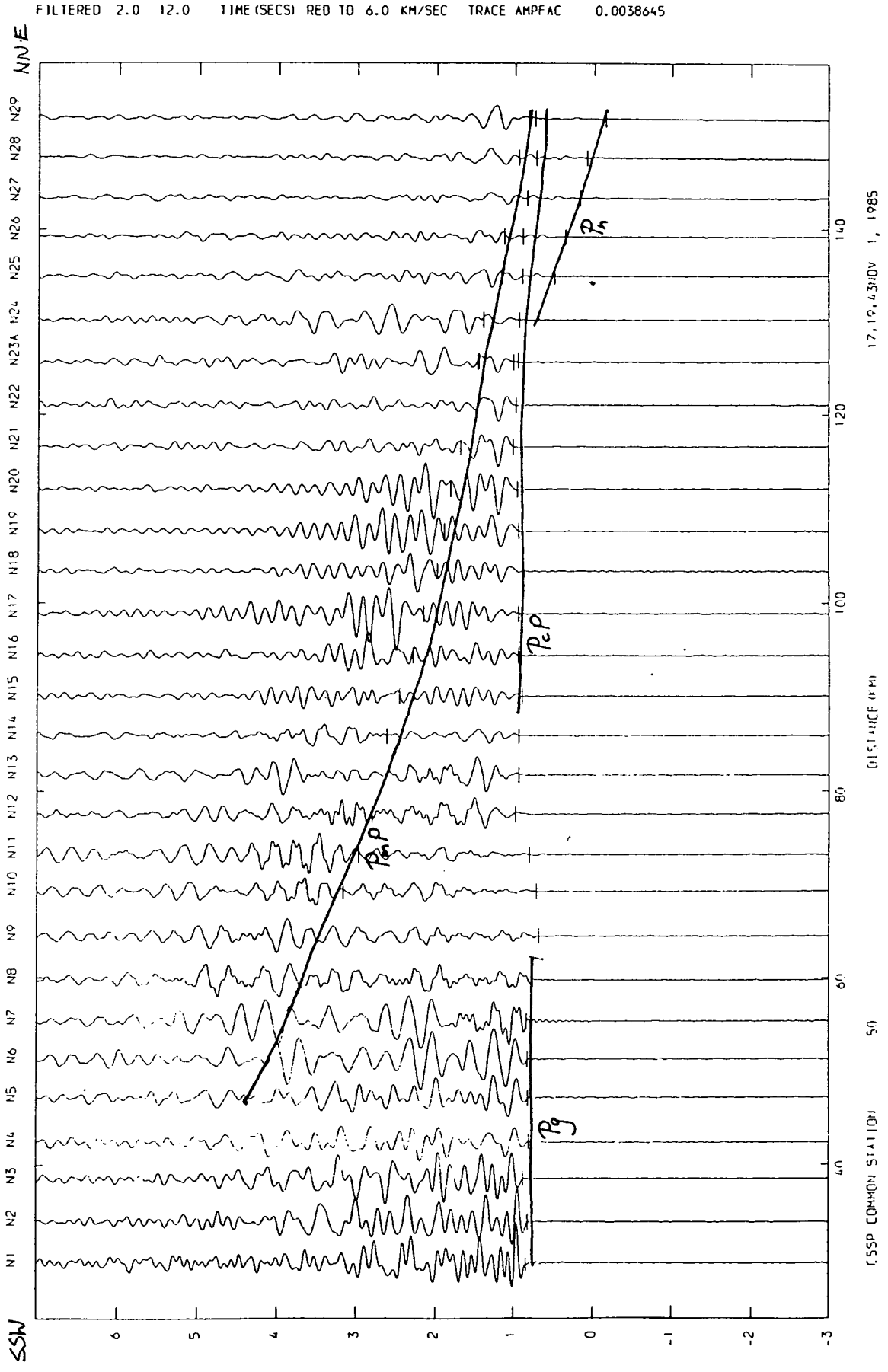


5-19 (h) Observed seismogram for station 50 for the North Sea shots with amplitudes corrected to common gain. The arrival times predicted by the laterally varying velocity model are drawn as a continuous line. Dashes are the picked travel times.

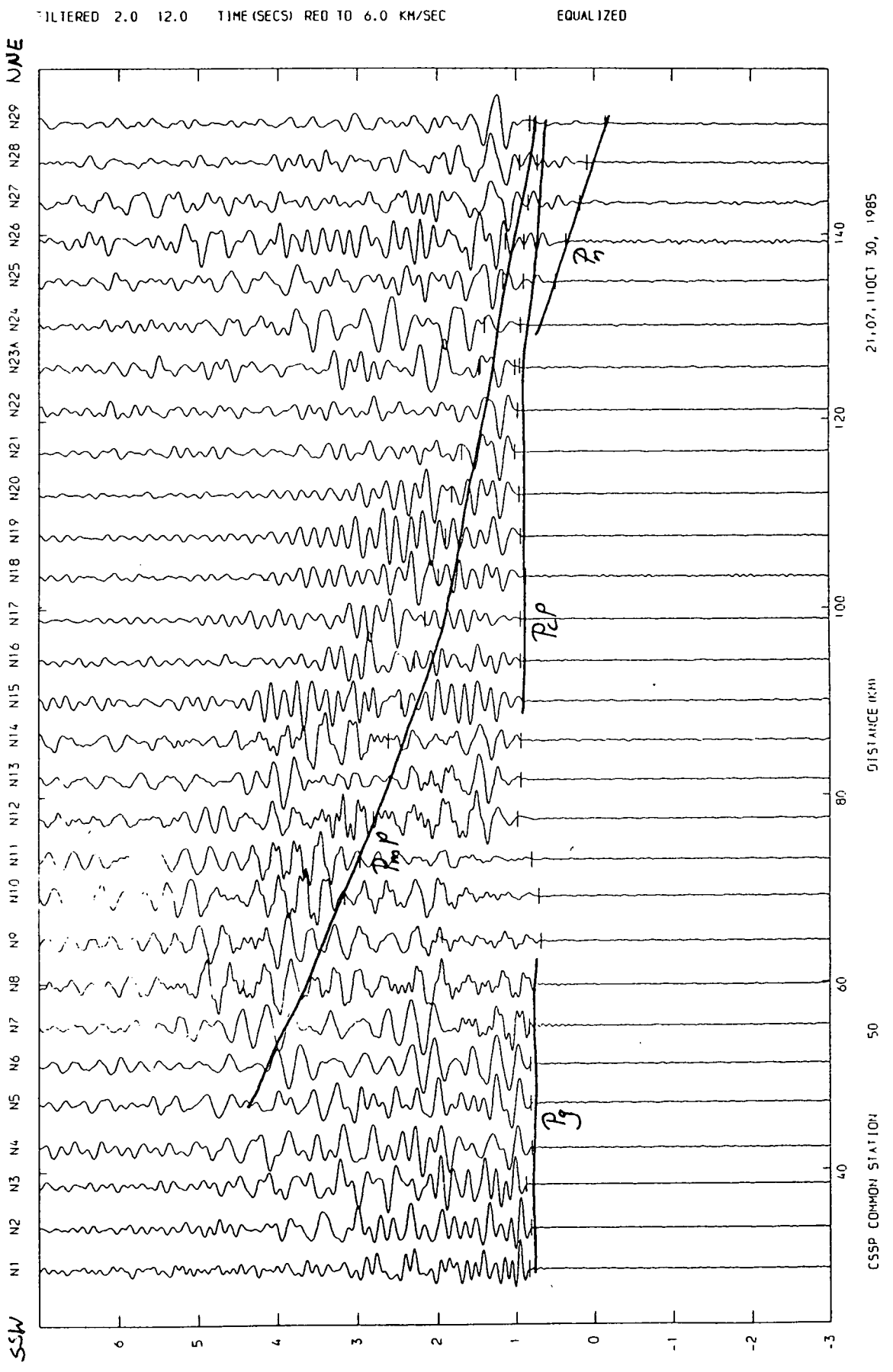


5.19 (i) Observed seismogram for station 50 for the North Sea shots with amplitudes equalised.
The arrival times predicted by the laterally varying velocity model are drawn as a continuous line.
Dashes are the picked travel times.

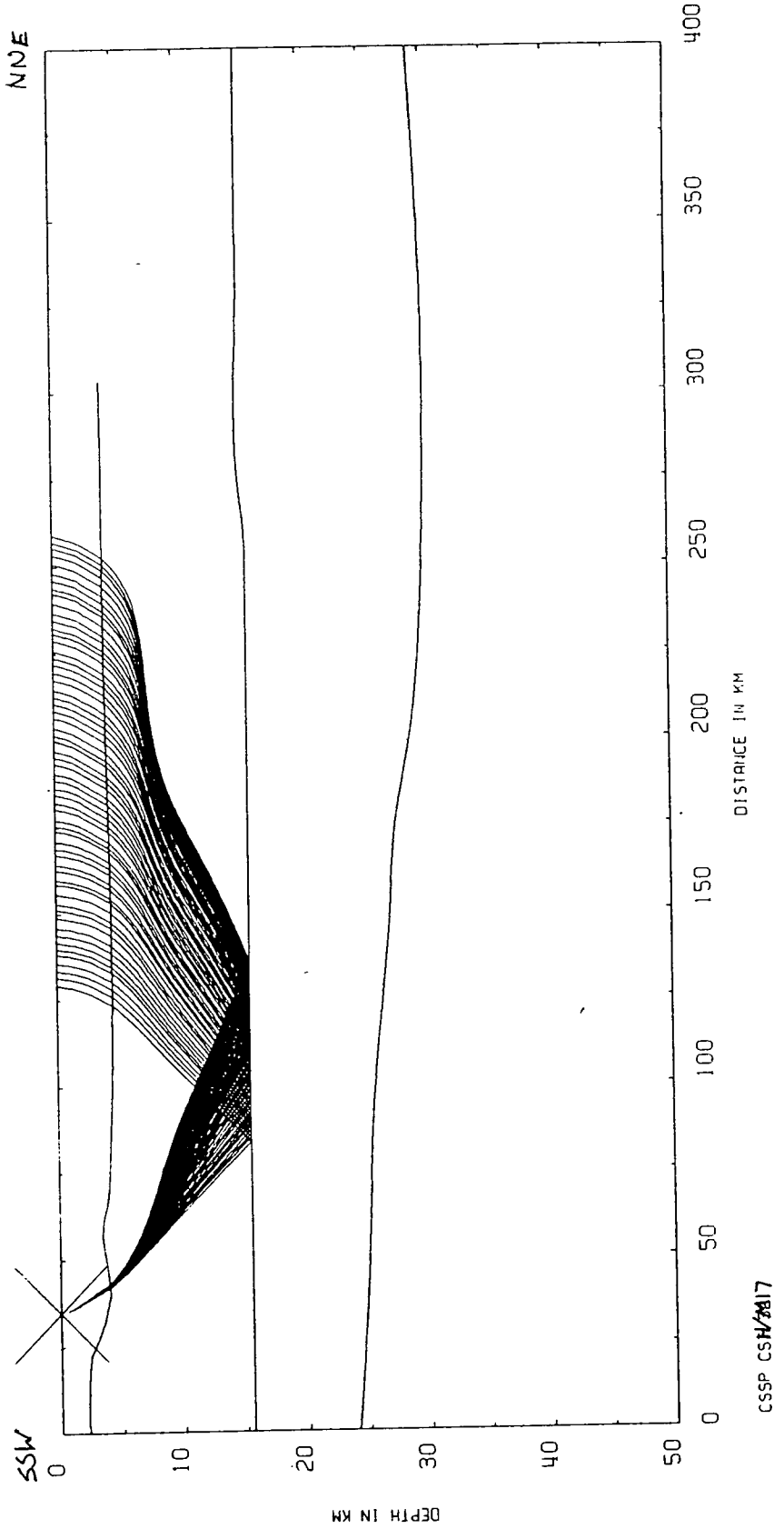


Figure(5.20) (a) Raypaths through the upper crust computed for shot M17

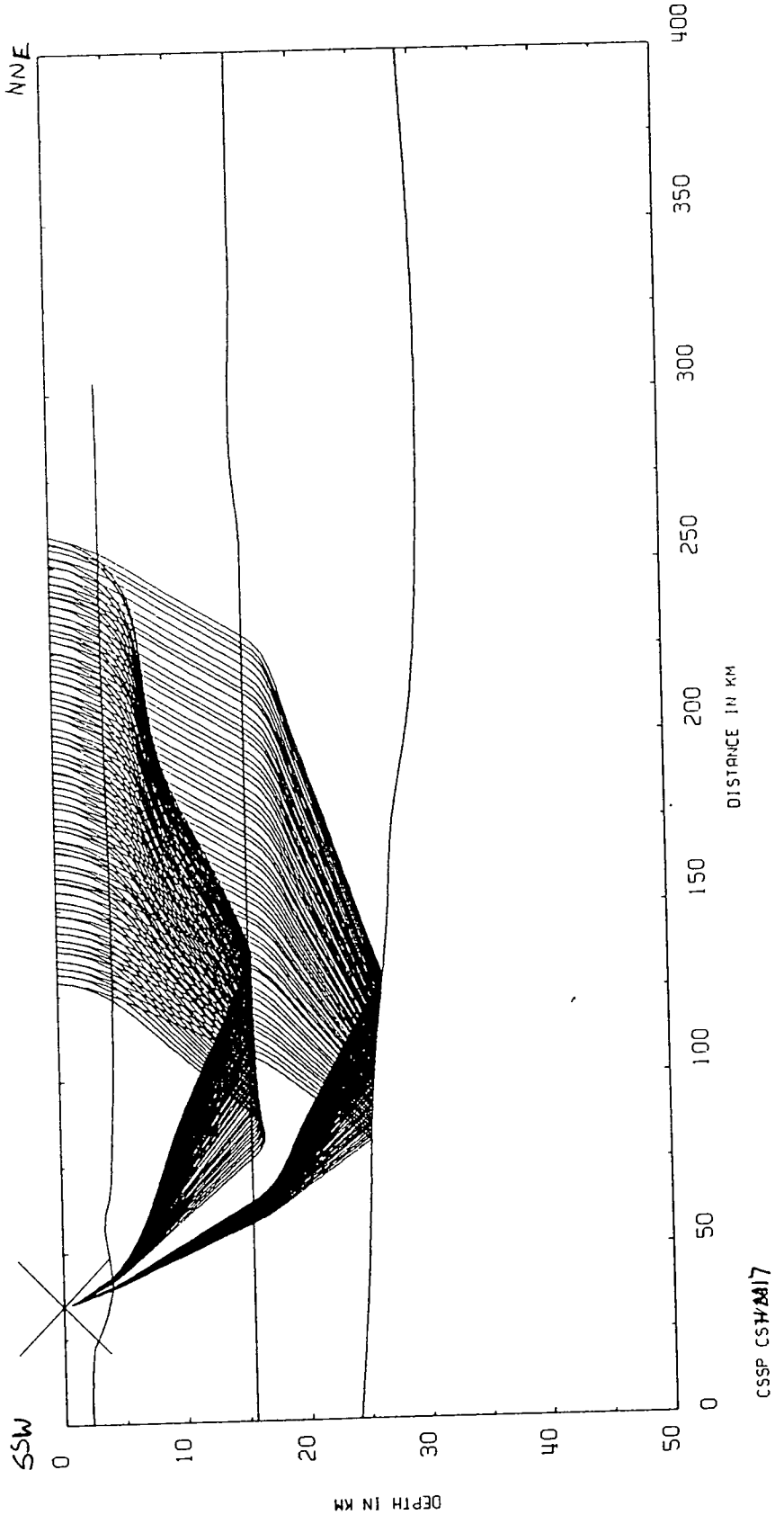


5.20 (b) Raypaths through the lower crust computed for shot M17

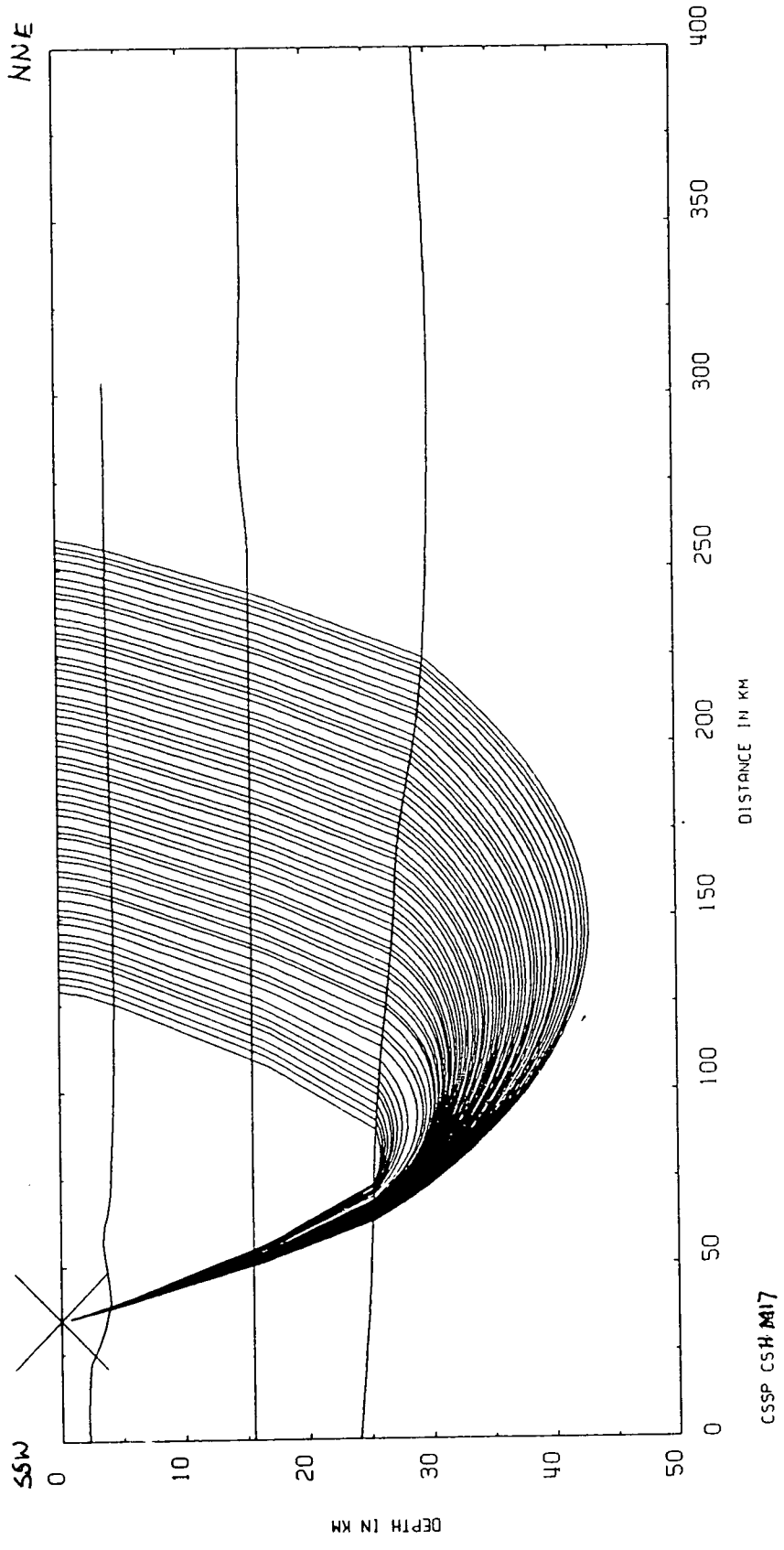


520(c) Raypaths of non reflected rays computed for shot M17

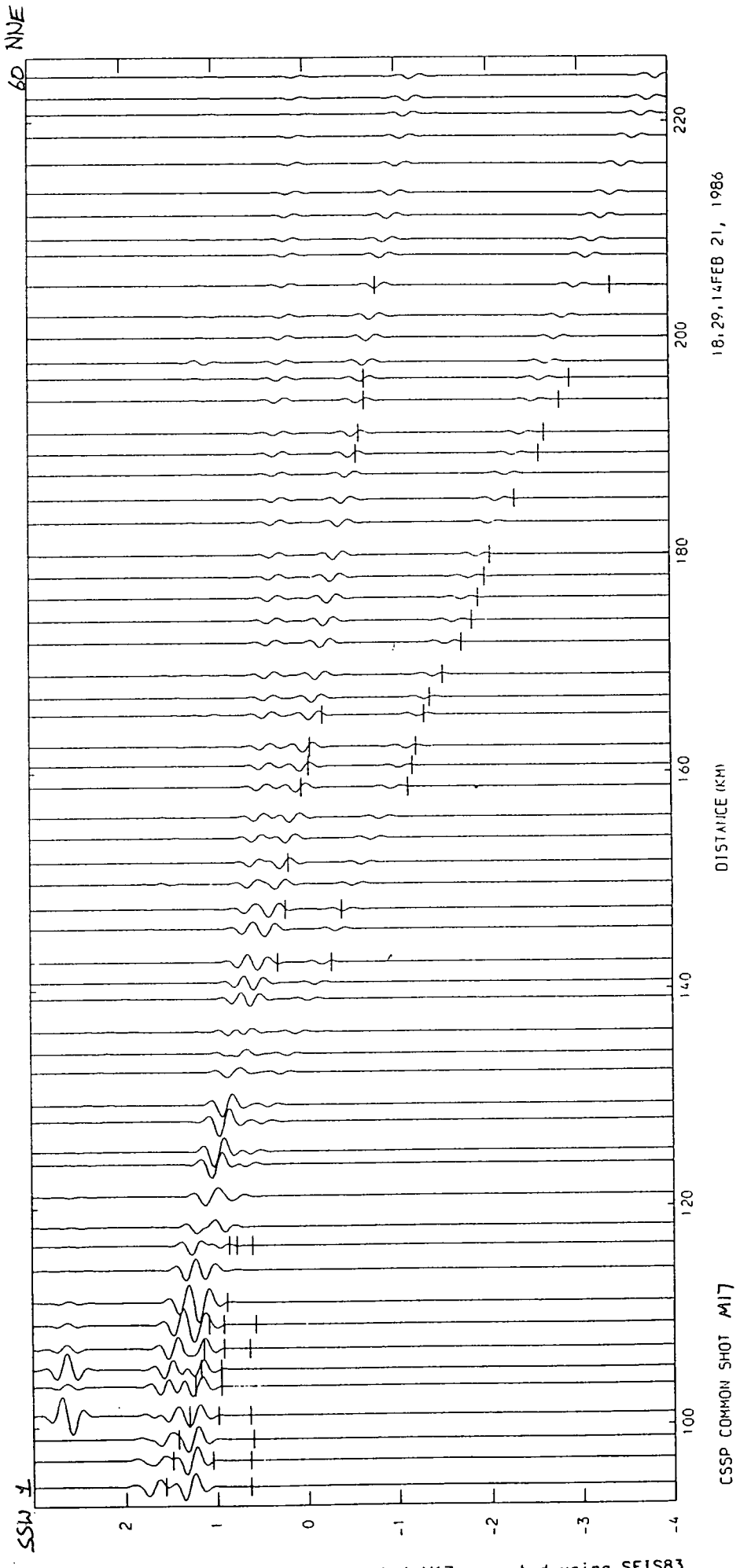


520 (d) 2-D synthetic seismogram for shot M17 computed using SEIS83.

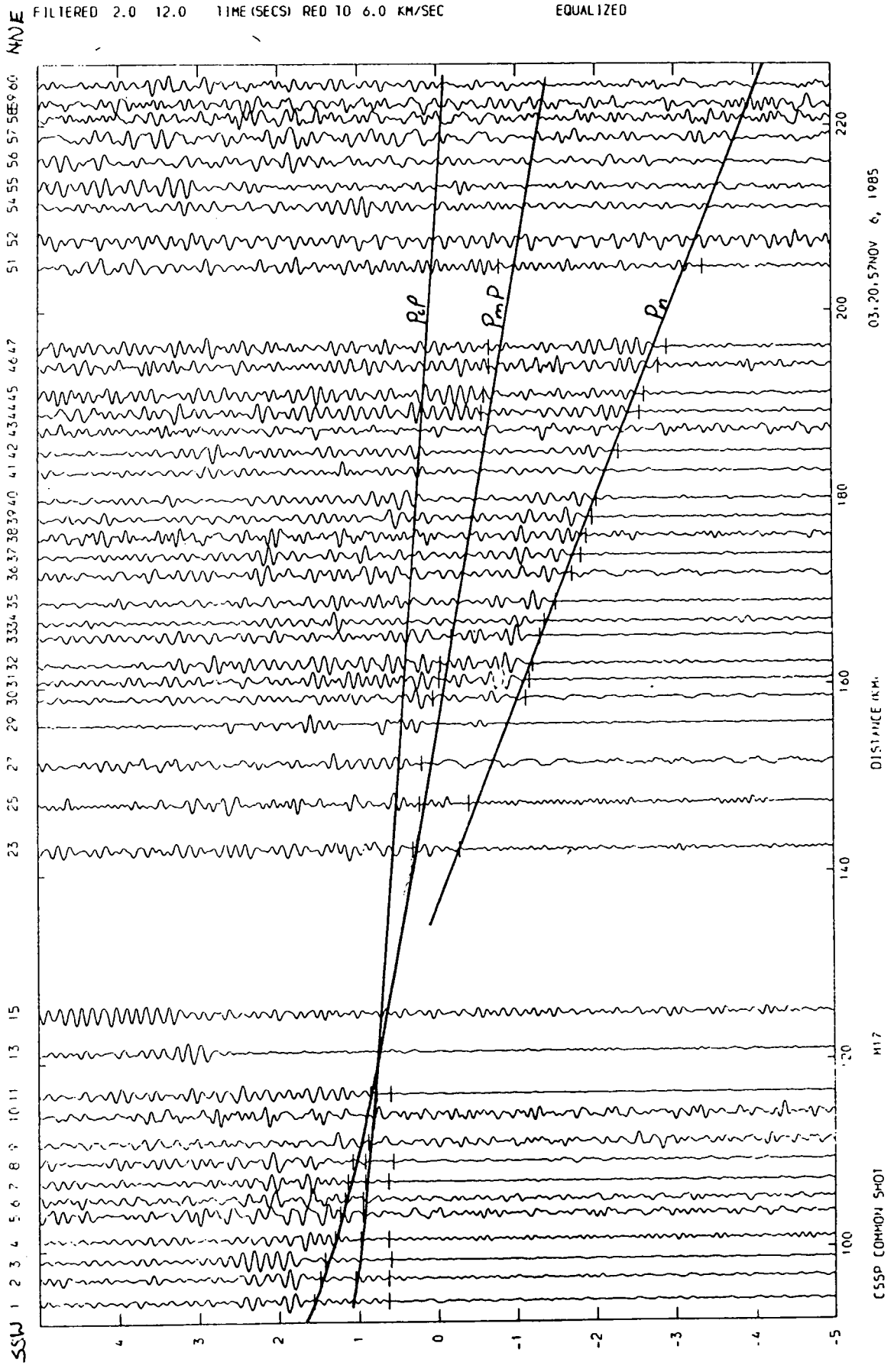


5.20 (c) Observed seismogram for shot M17
with amplitudes equalised.
The arrival times predicted by the laterally
varying velocity model are drawn as a continuous line.
Dashes are the picked travel times.

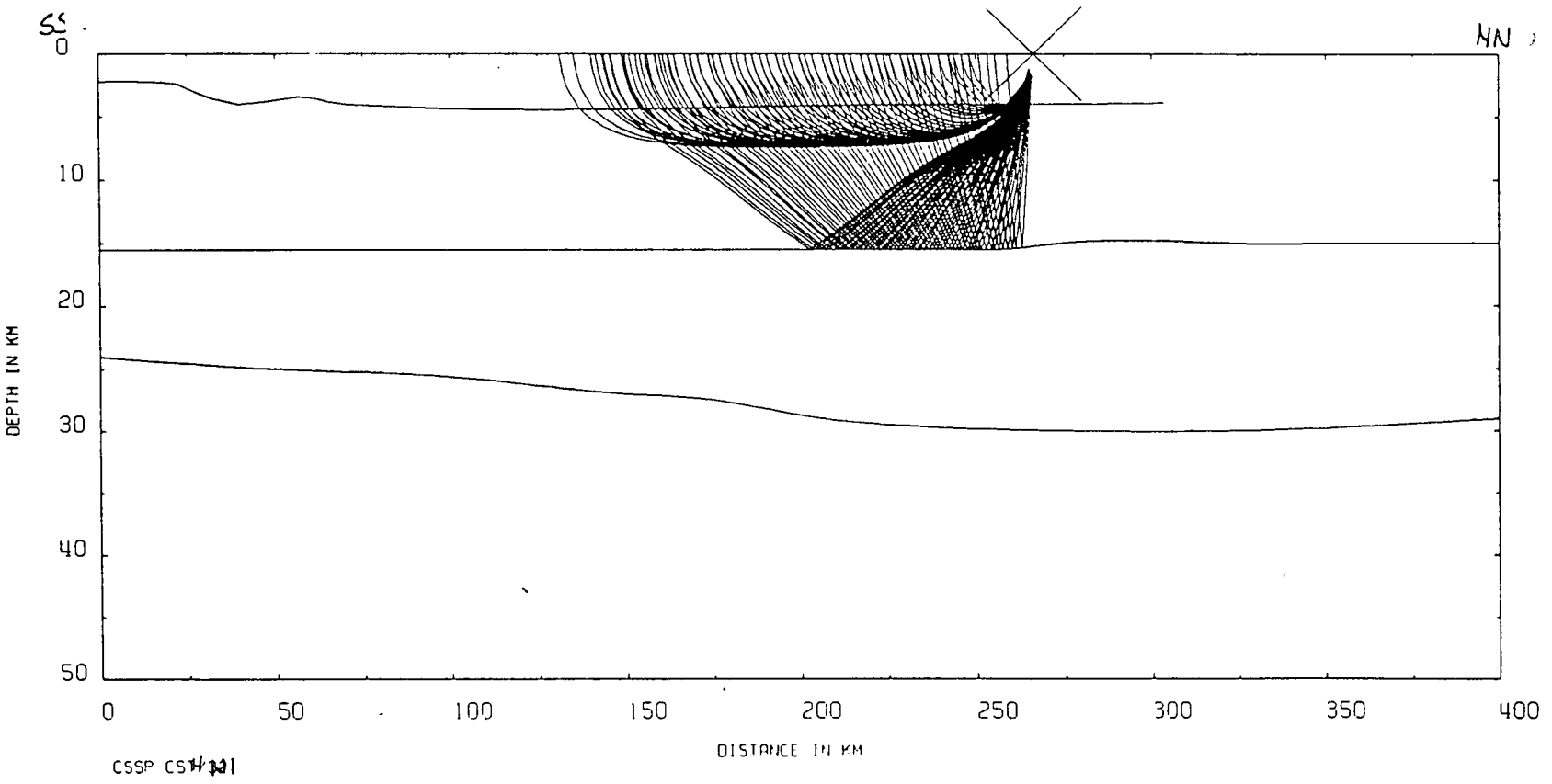


Figure(5.21) (a) Raypaths through the upper crust computed for shot N1

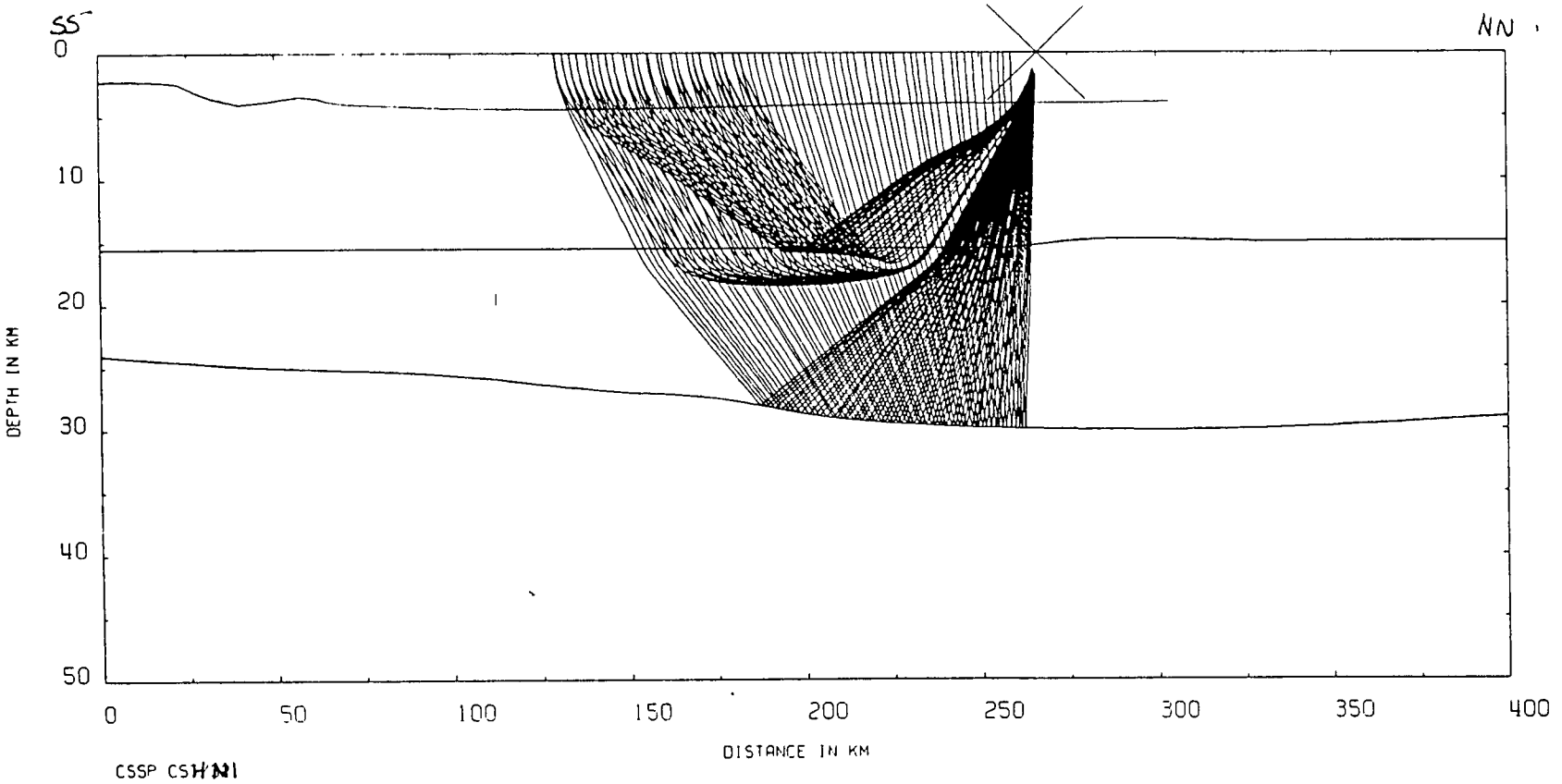


5.21 (b) Raypaths through the lower crust computed for shot N1

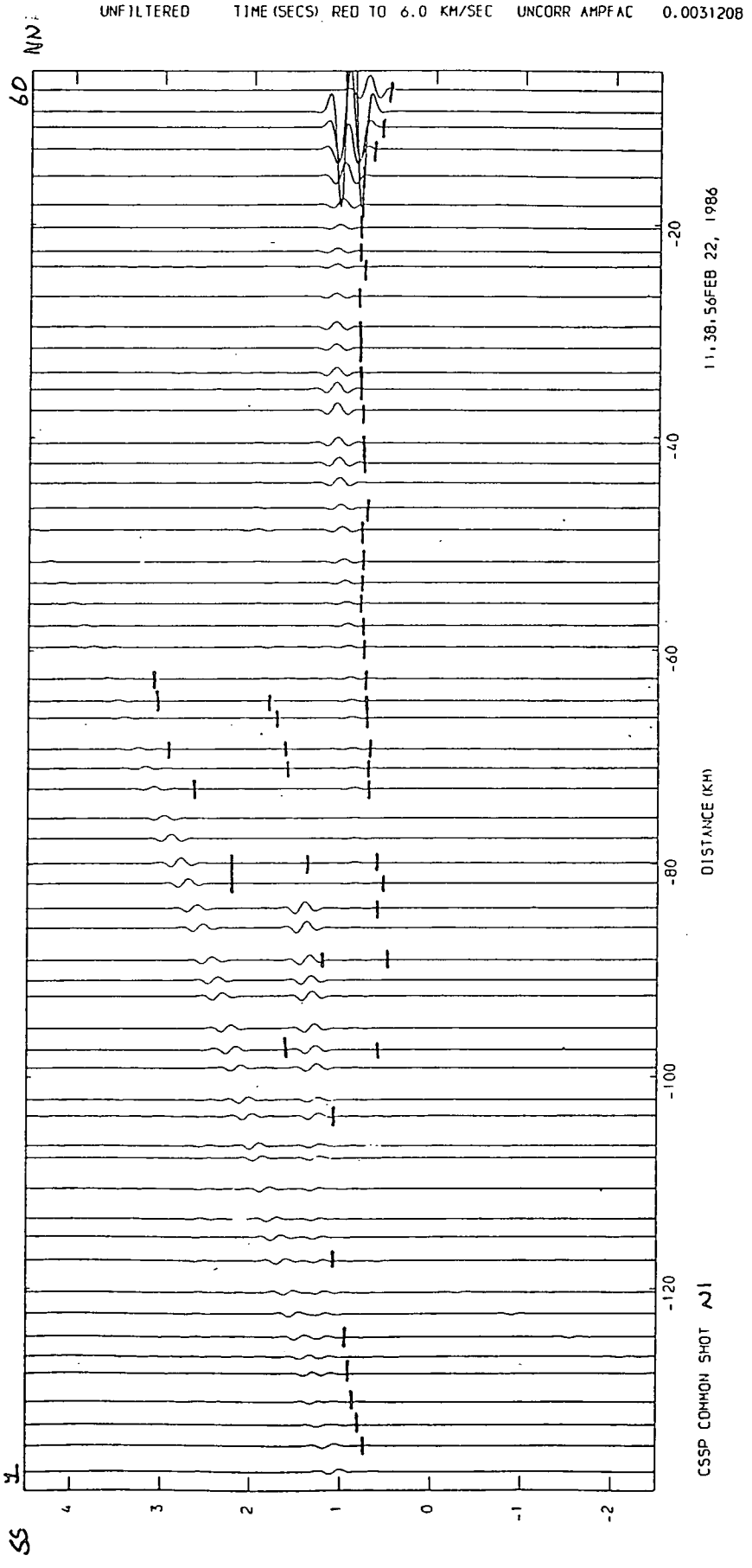


5.21 (c) 2-D synthetic seismogram for shot #1 computed using SEIS83.

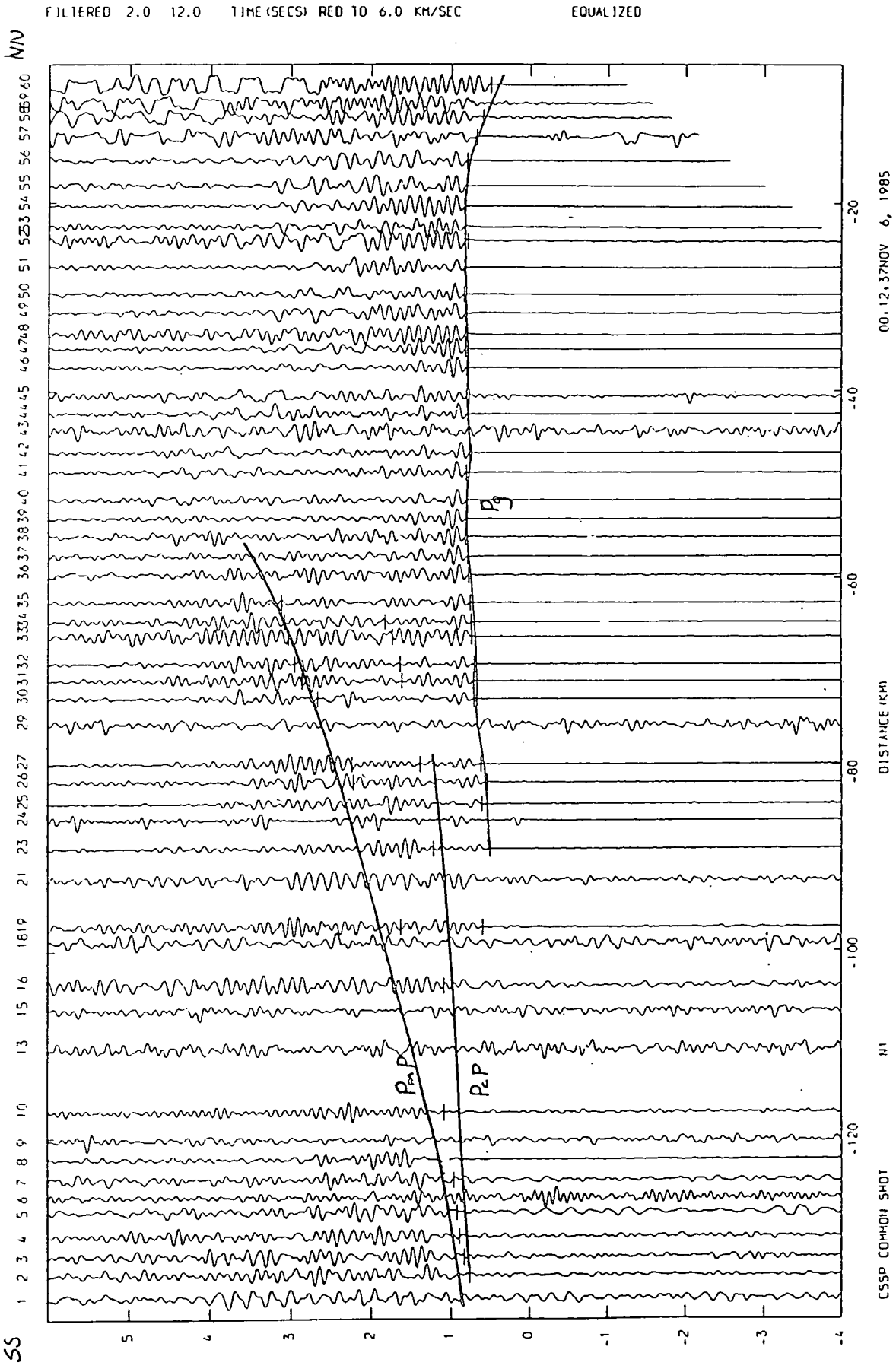


5.21 (d) Observed seismogram for shot M17
with amplitudes equalised.
The arrival times predicted by the laterally
varying velocity model are drawn as a continuous line.
Dashes are the picked travel times.

Some additional points can be made:

1. If a linear velocity gradient is inserted between the PmP and Pn boundaries the Pn amplitudes calculated from the Irish Sea shots are dramatically reduced. For example compare the Pn amplitudes on Fig. 5.22(b) to those on Fig. 5.13(d). The amplitudes calculated using the reflectivity method do not show such a dependence of Pn amplitudes on the structure of the overlying transitional Moho. The reflectivity method yields similar Pn amplitudes from a transitional Moho which incorporates either a velocity gradient between the PmP and Pn boundaries (Fig. 5.11) or a layer with only a slight gradient (Fig. 5.15). The decrease in Pn amplitudes for the 2-D model may be an artifact of the SEIS83 programme. However, if real it indicates that the transitional Moho cannot be a linear velocity gradient. Only a Moho layer with a slight velocity gradient will give the observed Pn amplitudes in the Irish Sea.
2. The reflectivity method indicates that the Pn arrivals are probably larger for the Irish Sea shots because of the larger sub-Moho velocity gradient. This effect is not as clearly observed on the 2-D synthetic seismograms calculated using SEIS83. This may be due to the presence of small velocity oscillations within the transitional Moho which may reduce the calculated amplitudes for the Pn arrivals.

To summarise, the main travel time and broad amplitude variations of the arrivals observed on the Caledonian Suture Seismic Project sections have been successfully modelled to within the estimated observational errors. The model proposed

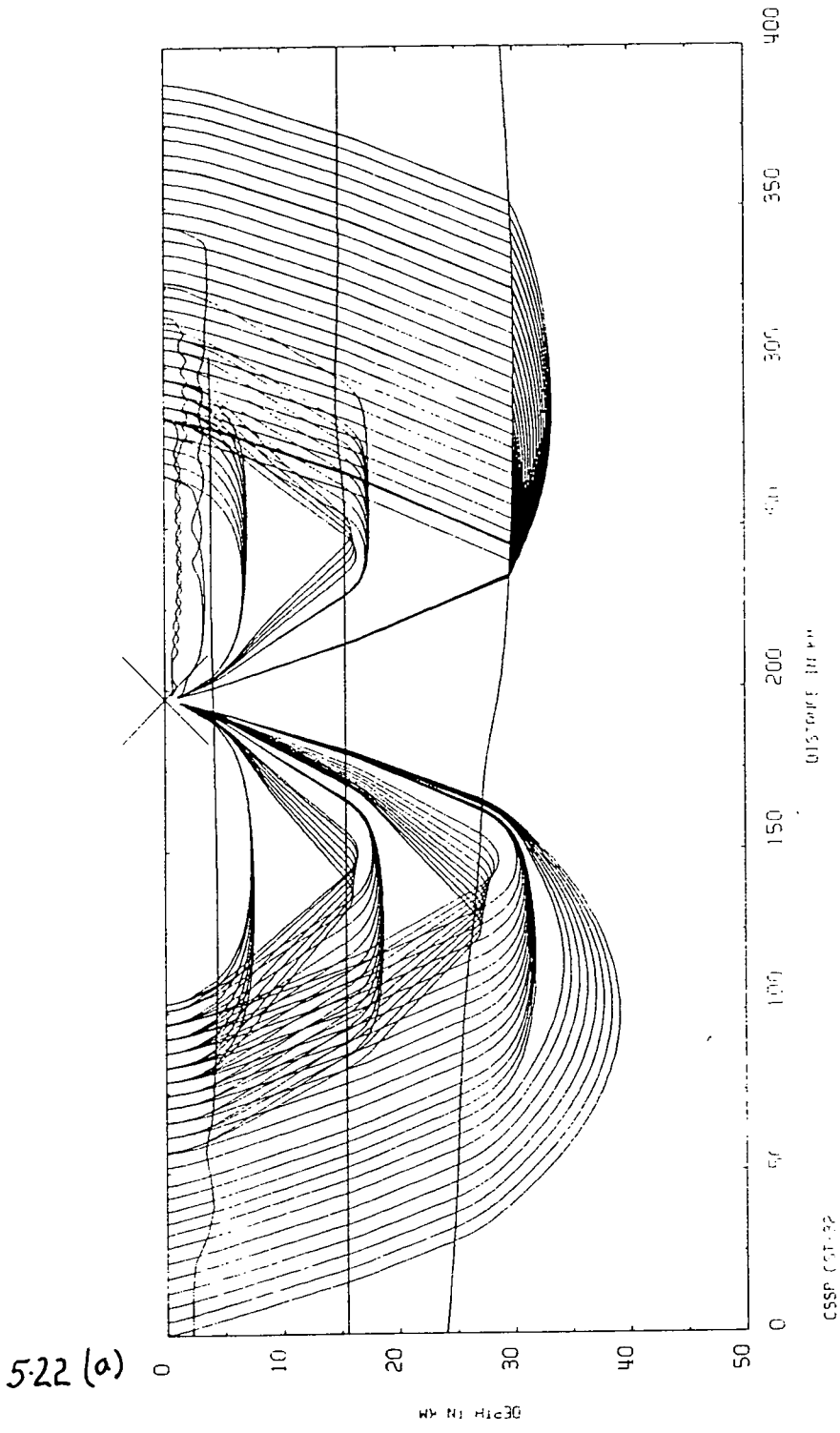


Figure(5.22) (a) Raypaths through the upper crust computed for station 32 using a velocity model with a linear velocity gradient between the PmP and Pn boundaries
(b) 2-D synthetic seismogram for station 32 for the Irish Sea shots computed using SEIS83.

UNFILTERED
TIME (SECS) REDUCED TO 6.0 KM/S
NW
M2
SS
124
Pn
low amplitude
180
32
2
1
0
-1
-2
II
I

5.22(b)

accounts for the disappearance of Pg and the larger Pn amplitudes in the Irish Sea than in the North Sea. The detailed nature of the Moho has not been deduced. It is clear that a velocity gradient cannot account for the observed PmP arrivals and, if the reduction in Pn amplitudes produced by SEIS83 are real, the observed Pn amplitudes from the Irish Sea shots. A velocity gradient with thin low velocity layers can account for the observed PmP arrivals but amplitude modelling using the reflectivity method indicates that such a gradational Moho yields low Pn amplitudes in contrast to the observed Pn arrivals from the Irish Sea shots. The preferred model is an abrupt increase in velocity at the PmP interface followed by a layer of uniform velocity or with a slight gradient. From this study it has become apparent that there is a need for a comparative investigation of the accuracies of the methods of computing synthetic seismograms. Only then can the details of the amplitude variations be modelled with confidence.

## 5.3 COMPARISON OF THE CSSP RESULTS WITH BIRPS

Fig. 5.23 illustrates the location of the BIRPS WINCH and NEC lines with respect to the Caledonian Suture Seismic Project profile. The two way travel-times in the Irish Sea calculated for the PcP, PmP and Pn interfaces are shown on line drawings which display the most prominent reflections observed on the WINCH sections (Brewer et al 1983). The two way travel-times across the whole CSSP line are illustrated in Fig. 5.24 together with the BIRPS reflection section WINCH-HG which was shot along the Caledonian Suture Seismic Project

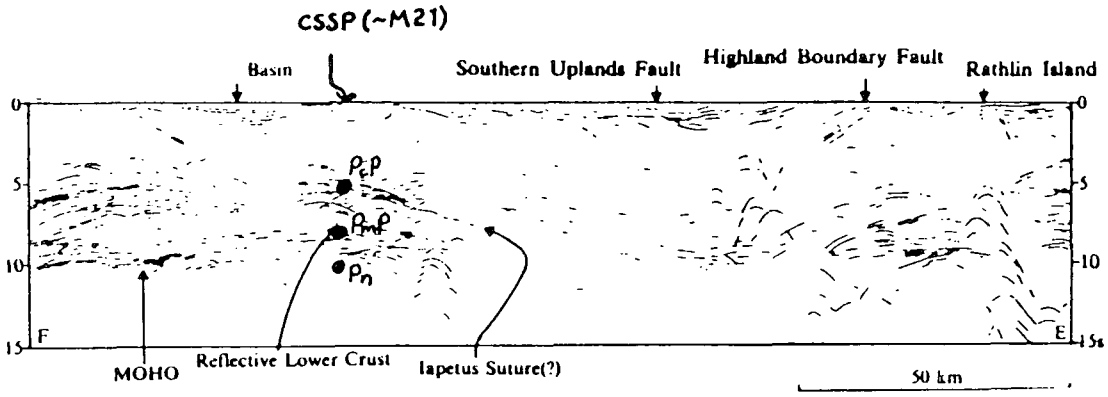


● = CSSP Results.

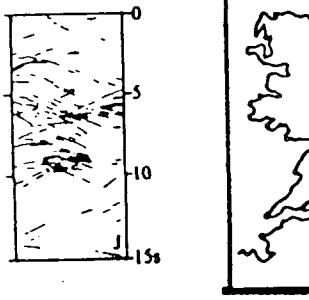


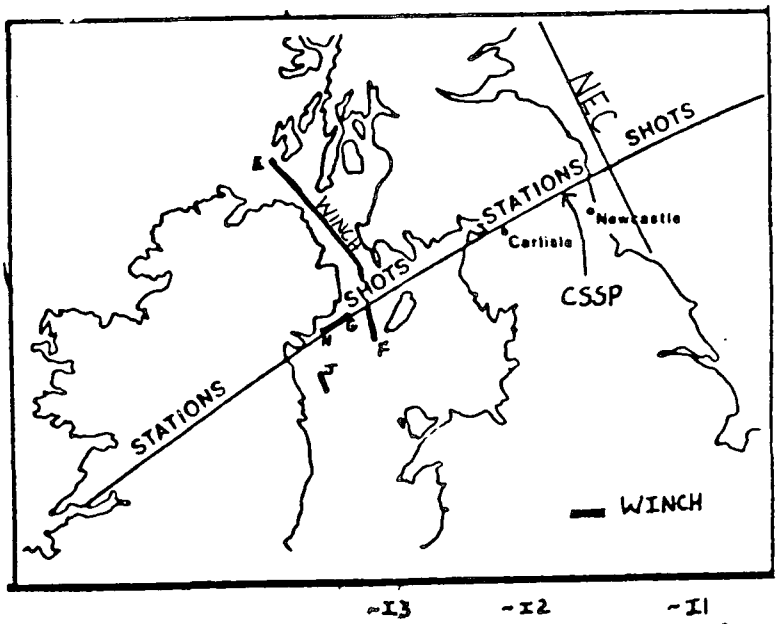


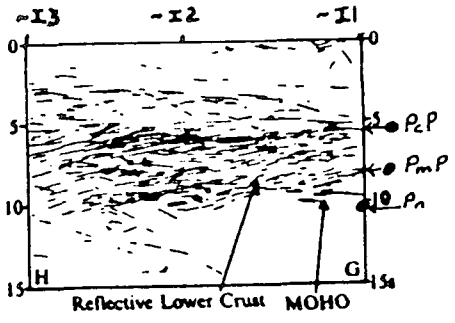


Line drawing of unmigrated WINCH data. This is a synthesis of independent efforts by the individual authors to make the drawing as objective as possible. To convert time to approximate depth in kilometres multiply seconds by 3 (in the crust) and by 4 (in the mantle). Letters beside segments refer to profile location in Fig (above) (from Brewer et al 1983)

Figure(5.23) Location of BIRPS WINCH Lines in the area of the northern Irish Sea with line drawings of the main reflections compiled by Brewer et al (1983).

profile between shots I1 and I3. The Pn two way travel-times were calculated under the Irish Sea assuming an average velocity between the PmP and Pn interfaces of 8.0 km/s.

A number of observations can be made for the Irish Sea:

1. The PcP interface appears to correspond approximately with the top of the reflective lower crust.
2. The PmP interface lies within the reflective lower crust. Two zones containing a greater density of reflections are observed in the mid and lower crust from 5 to 7 and 8 to 10 s respectively. The two zones can be observed on the WINCH-EF and WINCH-HG sections in Figs. 5.23 and 5.24. The PmP boundary approximately coincides with the top of the lower zone. The PcP boundary lies near the top of the upper zone. The synthetic seismogram and gravity modelling have indicated that the PmP interface represents the boundary across which both the velocity and density increase abruptly. This interface lies within the reflective lower crust.
3. The Pn interface coincides approximately with the base of the reflective lower crust. Goldfinch (1986) found that the modelled gravity effect produced by variations in the depth to the base of the reflective lower crust did not correspond to the observed gravity. This may now possibly be explained by the presence of the PmP boundary within the reflective lower crust across which the main crust/mantle density increase occurs.

In the North Sea the two way travel-times to the coincident PmP and Pn interfaces are estimated from CSSP results to be

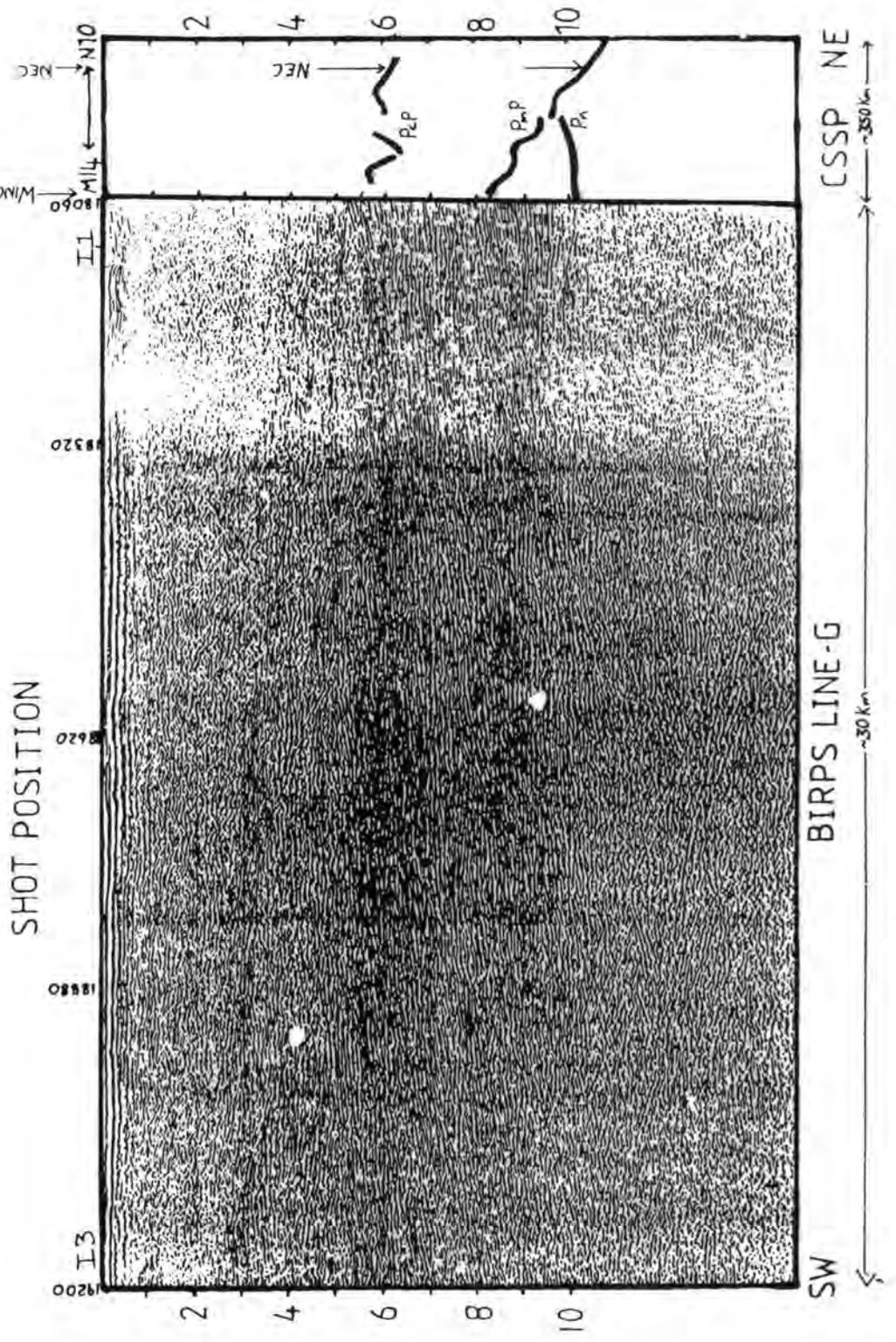


Figure(5.24) BIRPS WINCH LINE-HG deep reflection profile which ran along the Caledonian Suture Seismic Project Line between shots 13 and 11. The two way travel times to the PcP, PmP and Pn boundaries found from CSSP are drawn. Note the change in horizontal scale

about 10.4 s where the CSSP line is crossed by the NEC line (Fig. 4.13). Prominent reflections interpreted as the Moho were observed on the NEC line at about 10.5 to 11.0 s. No distinctive reflective lower crust was observed although the Caledonian Suture Seismic Project refraction results indicate a mid-crustal boundary at about 6.0 s two way travel-time.

The large amplitude PmP wide angle reflections observed at ranges greater than 60 km on the refraction sections in the North Sea indicate a sharp Moho which is recognised as a prominent narrow band of vertical reflections on the NEC profile. This implies that a sharp Moho produces both prominent vertical reflections and large amplitude wide angle reflections to near offsets. In the Irish Sea the Moho is more complicated and is interpreted as a transitional layer within which there is a constant velocity or slight velocity increase with depth. On the WINCH reflection sections its base marks the bottom to the reflective lower crust. The top of the transitional Moho appears to lie within the reflective lower crust. This implies that such a transitional Moho does not produce prominent vertical reflections from its top or bottom surface but has an internal character similar to the overlying reflective lower crust.

This correspondance of the character of the Moho as determined by wide-angle and vertical incident seismology appears to be more general:

1. In NW Scotland Armour (1977) observed prominent PmP wide angle reflections to near offsets from a sharp Moho (Fig. 5.25). The Moho appears on the WINCH-CD profile on the

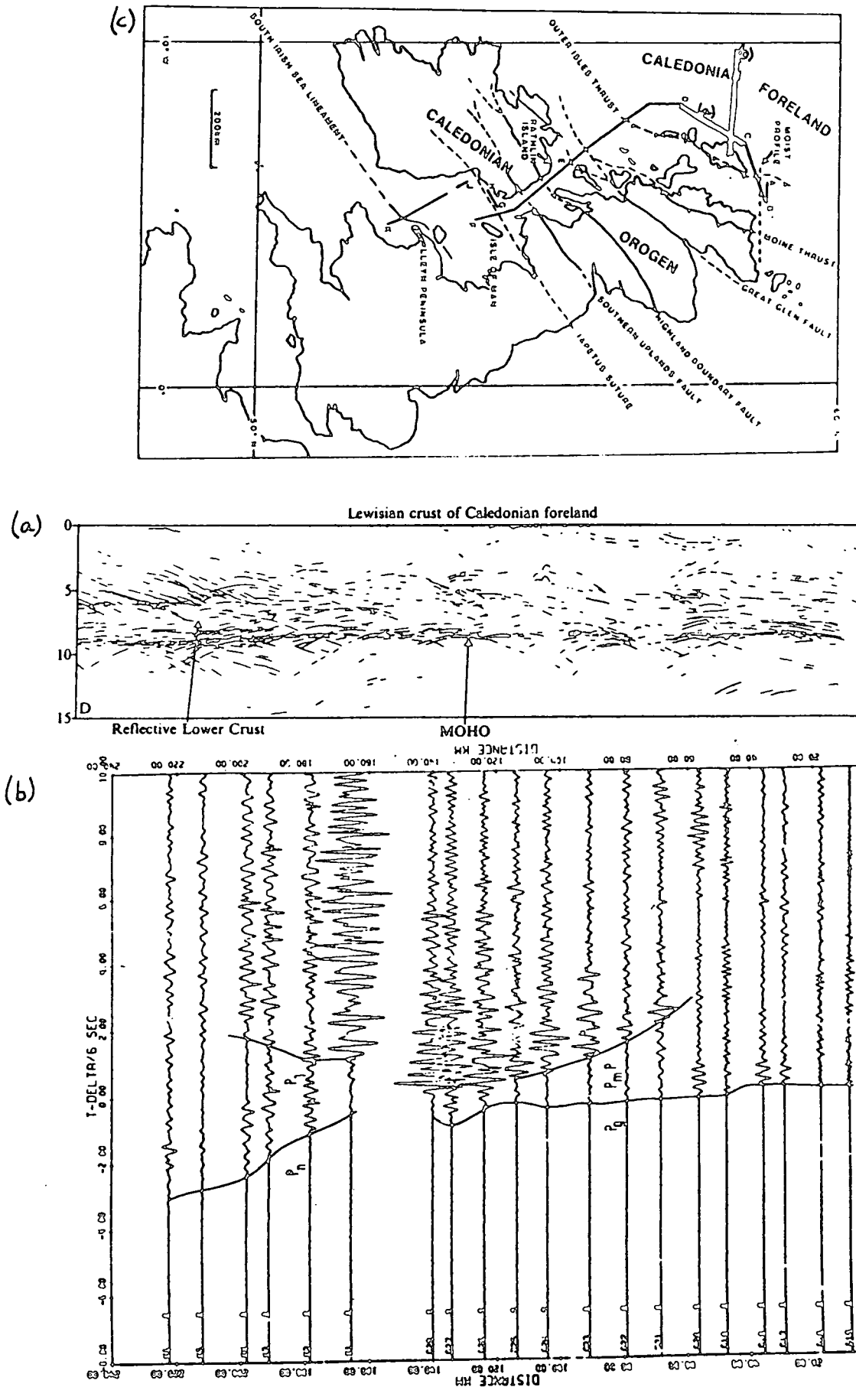


Figure(5.25) (a) Results of BIRPS deep reflection profile WINCH-BC.
(b) Reduced refraction section across the Hebridean Craton (Taken from Armour 1975).
(c) Location map for the seismic profiles

Hebridean Craton as a narrow band of prominent reflections at the base of a reflective lower crust (Brewer et al 1983) (Fig. 1.12).

2. Poor PmP arrivals were observed north of Cornwall in the southern Irish Sea by Holder and Bott (1971) (Fig. 5.26). A reflective lower crust was observed on SWAT-4 similar to that observed on the WINCH profiles further to the north. The Moho appears to represent the base of the reflective lower crust and is not marked by any prominent reflections.

3. In contrast, prominent PmP arrivals were observed on two further refraction lines to the west and south of Cornwall (Holder and Bott 1971). SWAT lines 6 to 10 in this area revealed a Moho consisting of a narrow band of prominent reflections (Figs. 5.27 and 5.28).

Generally a 30-40 mgal gravity high occurs over the Irish Sea. The BIRPS deep reflection profiles in the region indicate the regional development beneath the Irish Sea of the distinctive reflective lower crust. This reflective deep crust appears to disappear to the north across the Iapetus Suture, to the east somewhere between the WINCH line in the Irish Sea and the NEC line in the North Sea and to the south between SWAT lines 4 and 6. These observations suggest that the transitional Moho and shallowing of the PmP interface recognised beneath the Caledonian Suture Seismic Project profile may occur regionally beneath the Irish Sea.

To summarise, a sharp Moho produces a narrow band of prominent vertical reflections and large amplitude wide angle reflections. In areas where the Moho appears to represent the

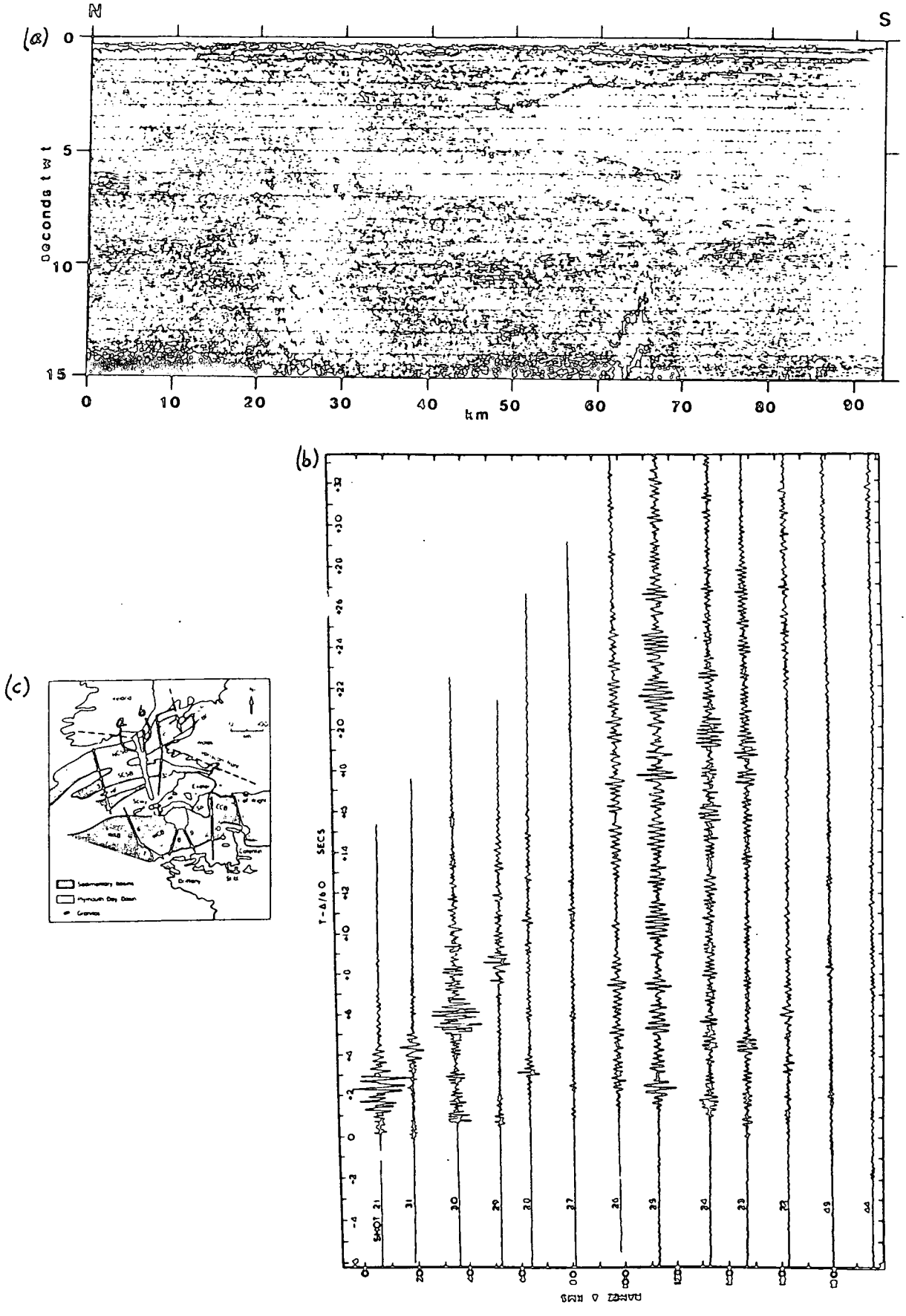


Figure(5.26) (a) Results of BIRPS deep reflection profile SWAT-4.
(b) Reduced refraction section from SW Ireland to Land's End. (Taken from Holder 1969).
(c) Location map for the seismic profiles

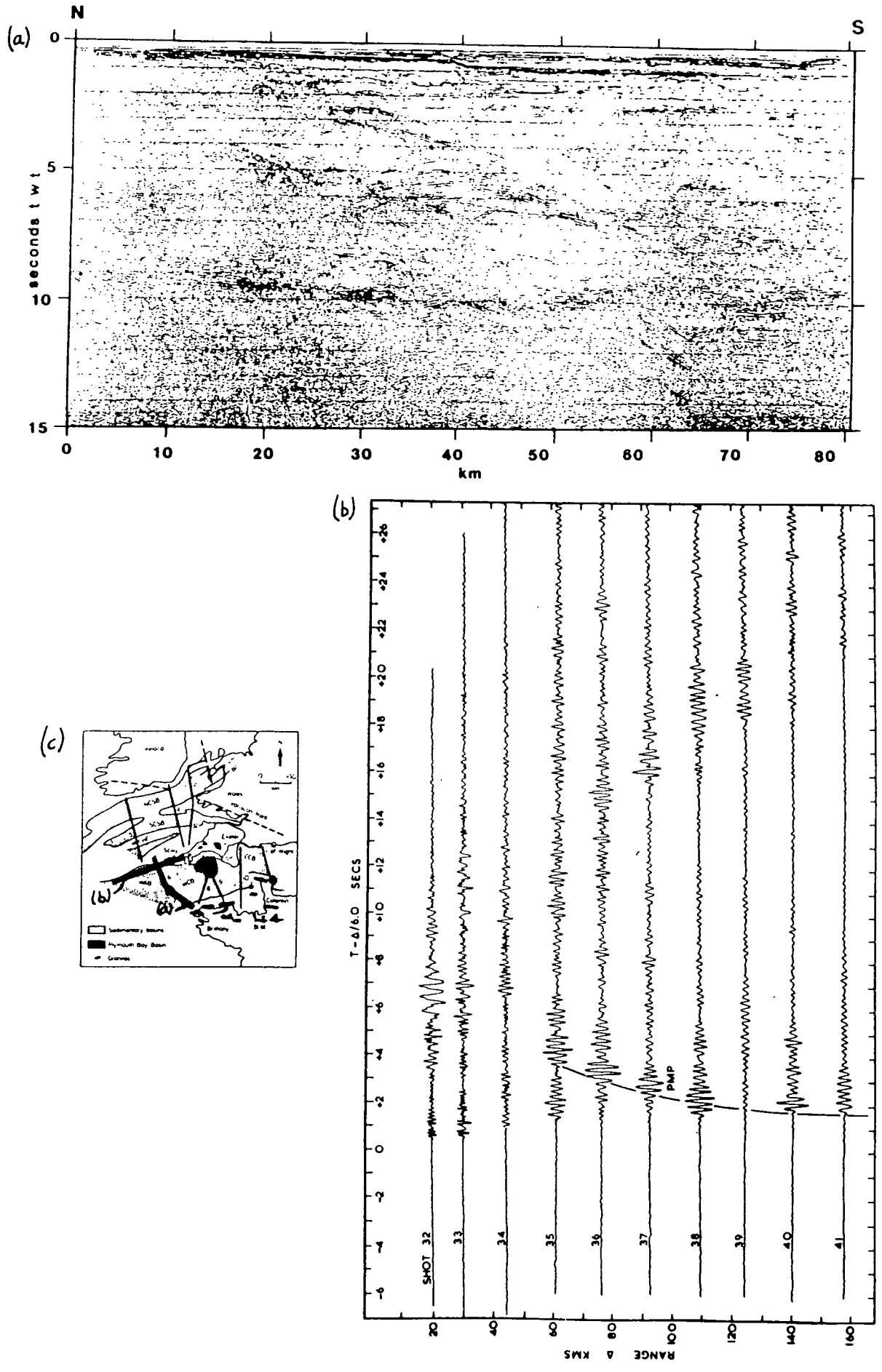


Figure(5.27) (a) Results of BIRPS deep reflection profile SWAT-6/7.
(b) Reduced refraction section west of Land's End.
(Taken from Holder 1969).
(c) Location map for the seismic profiles

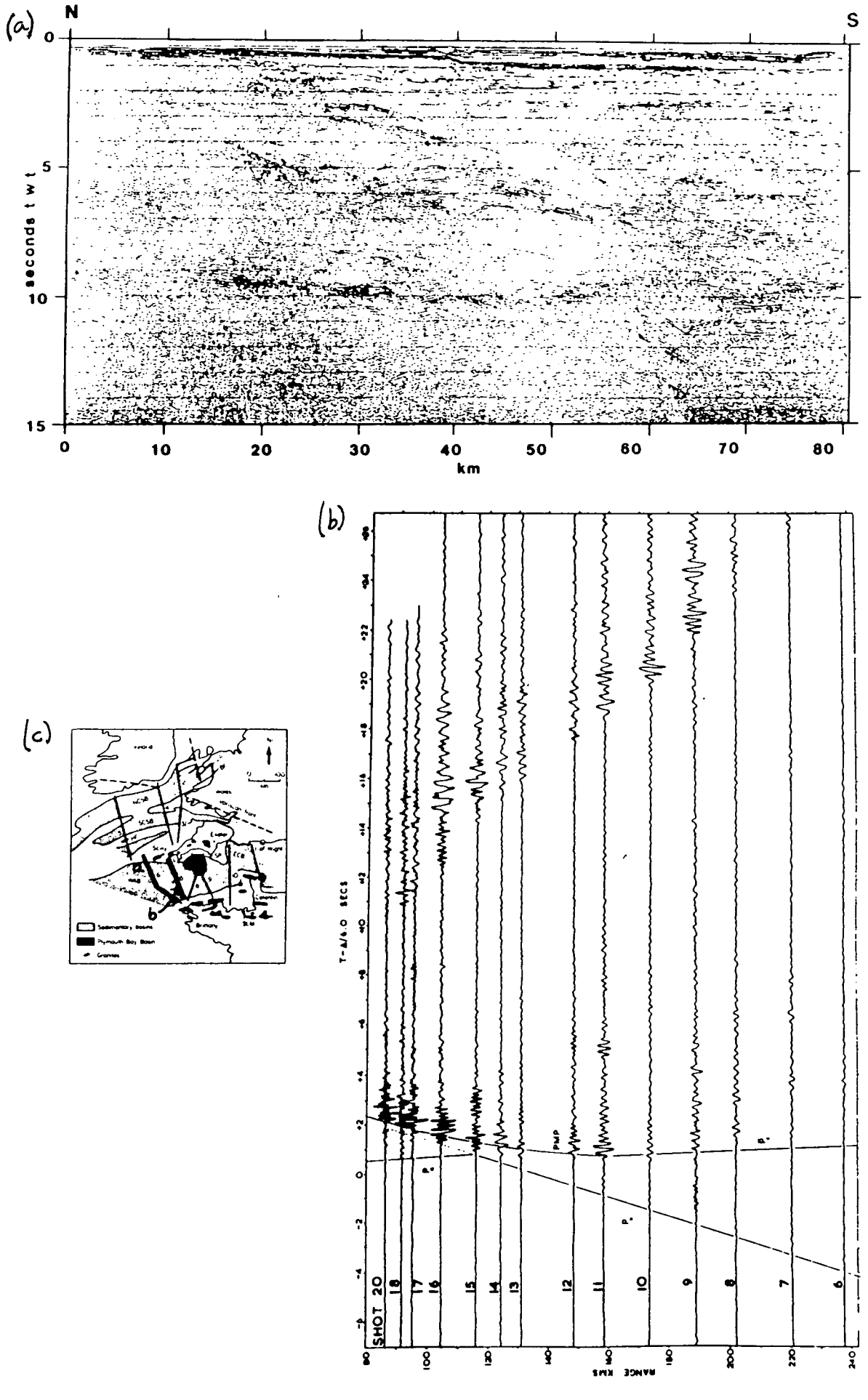


Figure(5.28) (a) Results of BIRPS deep reflection profile SWAT-6/7.
(b) Reduced refraction section south of Land's End.
(Taken from Holder 1969).
(c) Location map for the seismic profiles

base of the reflective lower crust no prominent vertical or wide angle reflections are observed. Such a Moho is recognised as a complicated transition zone between the lower crust and upper mantle in the northern Irish Sea and may be developed more regionally beneath the Irish Sea.

## 5.4 COMPARISONS TO PREVIOUS GEOPHYSICAL INVESTIGATIONS IN THE REGION

The preliminary results of LISPB (Bamford 1976) indicated apparent velocities of 8.15 km/s from northward travelling Pn and 8.20 km/s from southward travelling Pn just north of Carlisle (Fig. 5.29). These high velocities are consistent with the velocities of 8.19 (8.12 - 8.29) km/s and 8.32 (8.19 - 8.35) km/s found underneath the Irish Sea and Northern England respectively from the time-term analysis of Pn arrivals along the Caledonian Suture Seismic Project profile. Blundell and Parks (1969) recognised a layer of velocity 7.3 km/s at 24 km depth beneath the southern Irish Sea. This layer may represent the PmP boundary in the Southern Irish Sea. Agger and Carpenter (1964) obtained an unreversed velocity from northward travelling Pn arrivals at Eskdalemuir of 7.99 km/s. An analysis of the Irish Sea shots observed at LOWNET and Eskdalemuir should yield the structure north of the profile.

The NERL profile (Bott et al 1984) indicated a mid-crustal boundary at 12 km depth beneath the Pennine blocks. The Caledonian Suture Seismic Project indicated a mid-crustal interface at 15.0 to 15.5 km beneath the Northumberland

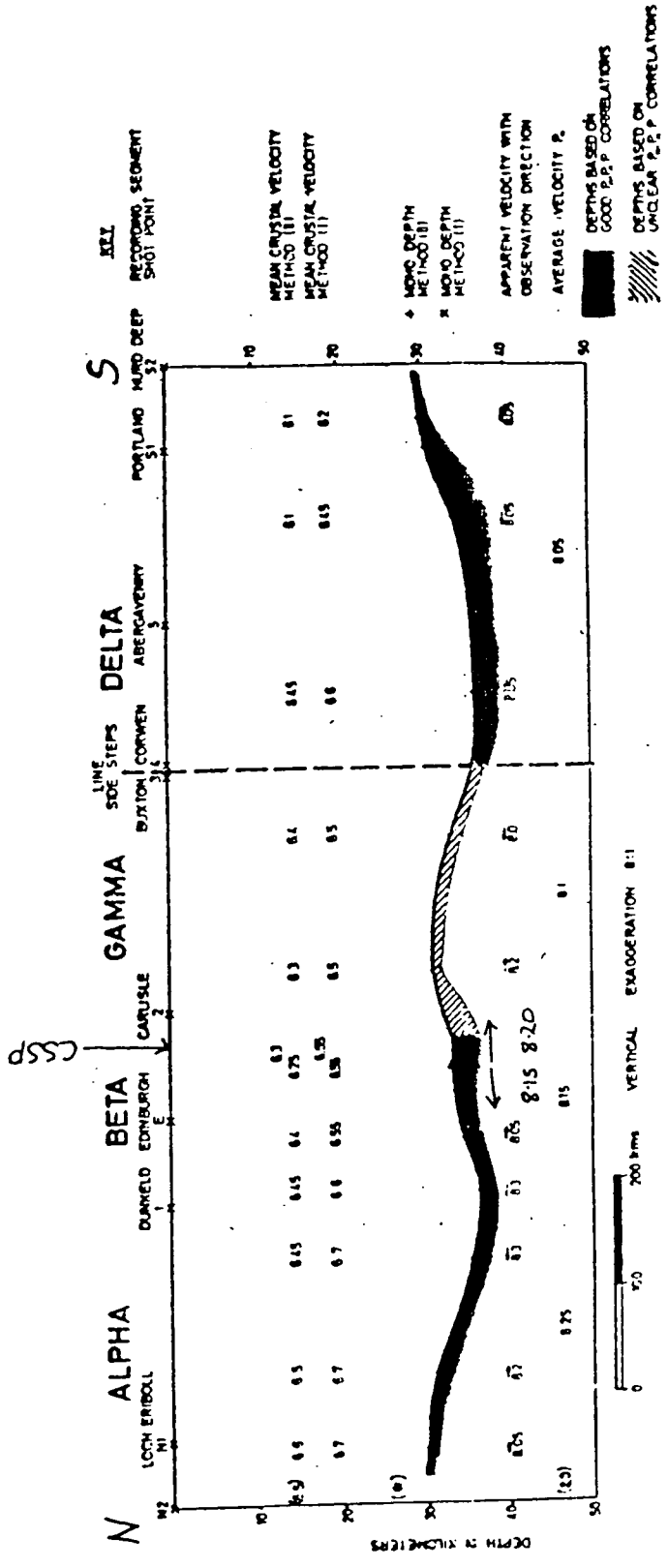


Figure(5.29) Preliminary results of LISPB taken from Bamford et al (1976).

Trough. The Moho is found at 29 km beneath the NERL profile. To within the errors of the depth estimates this is in excellent agreement with the 30 km depth to the Moho beneath eastern end of the Caledonian Suture Seismic Project line. These results indicate a relatively flat Moho at about 29 to 30 km beneath NE England.

Fig. 5.30 illustrates the gravity variations due to a model compiled from the Irish (Jacob et al 1985) and mainline CSSP results. The densities are taken from Table 5.1. The shallow structure across Ireland is taken from Brown and Williams (1985) and Jacob et al (1985). The PmP interface beneath Ireland is interpreted as the top of the Moho velocity gradient found by Jacob et al (1985). The Pn interface is extrapolated across Ireland and is made coincident with the PmP interface in SW Ireland to create a sharp Moho similar to that found under the North Sea. The calculated and observed gravity differ markedly across Ireland. These differences may be caused by lateral density variations. To remove this discrepency, the depth of the mid-crustal interface beneath Ireland was decreased by 3.5km with no alteration to its shape. The calculated gravity using this new model lies within 5 mgal of the observed gravity from SW Ireland to the North Sea (Fig. 5.31).

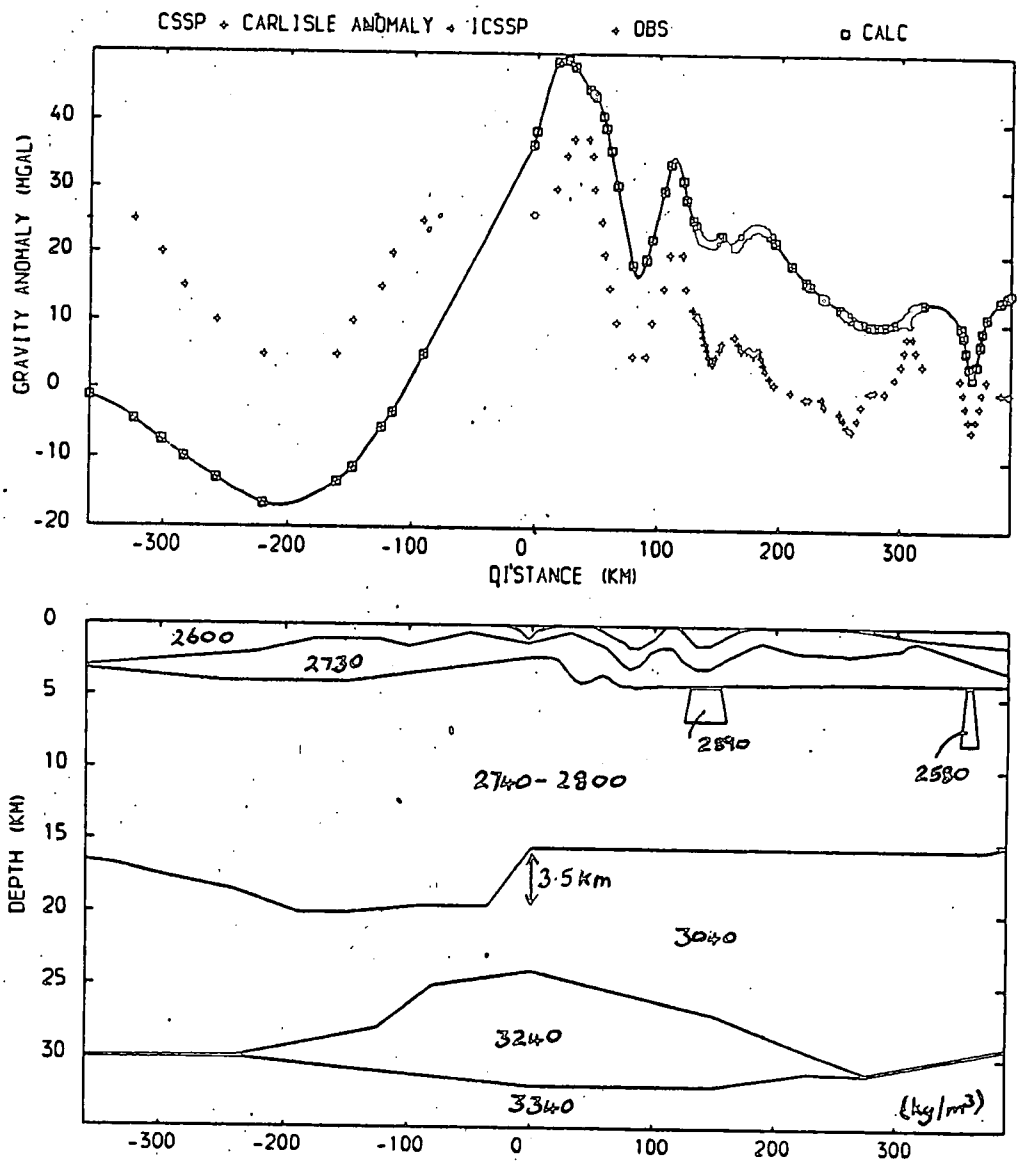


Figure(5.30) Gravity variations due to combined Irish and mainline CSSP refraction results.

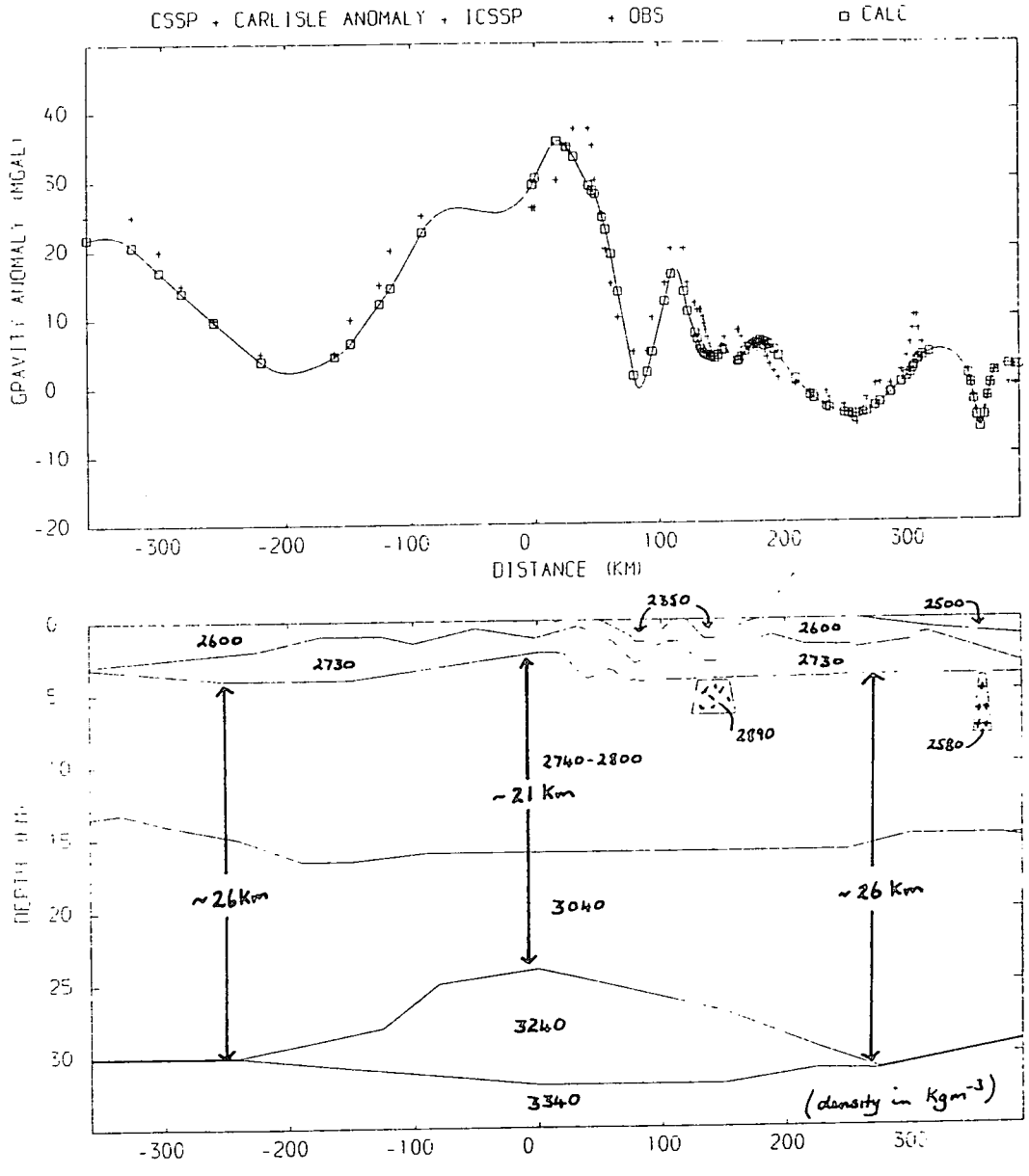


Figure(5.31) Gravity variations due the combined Irish and mainline CSSP refraction results with the depth of the mid crustal interface across Ireland decreased by 3 km.

## 5.5 GEOLOGICAL INTERPRETATION

The main observations that must be explained by a geological model of the crust beneath the Caledonian Suture Seismic Project profile are as follows:

1. The velocities of 6.15 - 6.2 km/s, 6.75-6.77 km/s and 8.0 to 8.3 km/s for the upper crust, lower crust and upper mantle respectively.
2. The transitional Moho beneath the Irish Sea and the lateral decrease in the sub-Moho velocity eastwards from 8.19 (8.12 - 8.29) km/s beneath the Irish Sea and 8.32 (8.19 - 8.49) km/s beneath Northern England to 8.02 (6.34 - >10.0) km/s under the North Sea.
3. The 5 km thinning of the crust (Fig. 5.29) by the westward shallowing of the PmP boundary beneath the Irish Sea to produce the observed 35 mgal gravity high.
4. The reflective lower crust observed on the WINCH EF, HG, J and KL lines and on SWAT lines 4 and 5 in the Irish Sea and its absence in adjacent regions.
5. The transitional Moho which produces vertical reflections similar to the those observed in the overlying reflective lower crust.
6. The base of the reflective deep crust which approximately coincides with the Pn boundary.
7. The narrow band of prominent reflections from the Moho observed on the BIRPS NEC line in the North Sea which correspond to the refractive Moho recognised from the Caledonian Suture Seismic Project results.

### 5.5.1 Relationship to the Caledonides

The Iapetus Suture is observed in the lower crust on the WINCH-EF line as the northwards dipping top surface to a wedge of reflective lower crust beneath the westward extension of the Southern Uplands north of the Caledonian Suture Seismic Project profile (Fig. 5.21). It is not obviously observed in the upper crust but is inferred to extend to the surface near the Peel Basin south of the Caledonian Suture Seismic Project line. Where the CSSP line is crossed by the WINCH profile the suture is approximately at the boundary between the lower and upper crust. Further east. the surface trace of the suture is interpreted to lie along the southern margin of the Solway Basin by Needham and Knipe (1986). A northward dipping reflector in the lower crust on the NEC profile in the North Sea is also interpreted as the Iapetus Suture. It cannot be traced through the upper crust (Klemperer pers.comm.). However, simple extrapolation suggests it probably surfaces close to the Caledonian Suture Seismic Project line in the North Sea.

The CSSP profile thus appears to lie close to the inferred surface trace of the Iapetus Suture from the North Sea to the east coast of the Irish Sea but west of the Solway Basin it probably lies significantly north of the suture. An average upper crustal velocity of 6.18-6.20 km/s was found beneath the mainline CSSP profile from an analysis of PcP arrivals in Chapter 4. This is interpreted as high velocity metamorphic basement which appears to lie below the suture in the upper crust along the line east of the central Irish Sea. However,

the results are not well constrained west of the Solway Basin where the upper crust of similar velocity probably lies above the suture.

The inferred location of the surface trace of the Iapetus suture along the CSSP line indicates that the lower crust and deeper structures from the North Sea to the Irish Sea lie below the suture. The deep structure beneath the CSSP profile from the North Sea to the Irish Sea inclusive therefore probably represents deep crust of the Southern Caledonides.

### 5.5.2 Nature of the Lower Crust

The Caledonian Suture Seismic Project results indicate that the lower crust has an unexpectedly high average velocity of 6.75 to 6.77 km/s beneath the suture which disagrees with the LISPB interpretation where the two lines cross. A mid-crustal layer of velocity 6.4 - 6.5 km/s was recognised from the LISPB experiment north of the Southern Uplands Fault. This is underlain by a lower crust of velocity 6.7 km/s (Bamford 1979). The deep structure beneath the Southern Uplands and Northern England was not accurately determined from LISPB. The CSSP results however, indicate that the structure of the deep crust beneath the Iapetus Suture differs somewhat from that north of the Southern Uplands Fault as indicated by LISPB. The reflective lower crust on the deep reflection profile WINCH-EF disappears northwards across the suture and beneath the Southern Uplands. This may indicate that the boundary between two different types of crust occurs across the suture. However, the lower crust beneath the Iapetus

Suture in the North Sea does not appear to be reflective. The reflective deep crust is developed regionally beneath the Irish Sea. These observations indicate that the anomalous deep crustal structure beneath the Irish Sea is probably related to the post-Caledonian formation of the Irish Sea depression (Bott 1968). Thus the lack of reflective lower crust beneath the Southern Uplands in contrast to the crust beneath the Irish Sea does not necessarily imply a change in type of crust across the Iapetus Suture. Comparison of the crust overlying the suture with that beneath and to the south of it must therefore await determination of the velocity/depth variations beneath the Southern Uplands. An analysis of the Eskdalemuir and LOWNET records of the Irish Sea shots may contribute to this although a CSSP type experiment along strike of the Southern Uplands is clearly required.

The average velocity of 6.75 - 6.77 km/s places constraints on the average composition of the lower crust. The following two compositional models were suggested by Ringwood and Green (1966):

1. If the lower crust is dry it must be composed of granulites of granodioritic (6.4-7.3 km/s) to dioritic (6.6-7.6 km/s) composition. This composition is similar to that of the upper crust. The mid-crustal boundary may therefore represent a metamorphic phase change. Such a boundary would be gradational. The mid-crustal boundary was modelled as a gradient zone 3 km thick which is consistent with this model. Rocks of basic composition would occur as eclogites in the lower crust. Eclogites have velocities greater than 7.8 km/s in the lower crust

and densities greater than 3.4 gm/cm (Christensen 1982). These velocities are too high and imply that a dry lower crust cannot have an average basic composition.

2. If the lower crust contains water, then the velocities of rocks of granodioritic to dioritic composition would be too low (Table 1.1). Basic rocks in a wet lower crust would occur as amphibolites which have velocities from 7.0 to 7.6 km/s. These velocities are higher than the observed average velocity of the lower crust. Incorporation of a proportion of lower velocity acidic and intermediate gneisses would decrease the average velocity to the observed values. Such a lower crust would have an average intermediate to basic composition. A lower crust comprising 50% amphibolites with 50% gneisses of average granodioritic composition would yield an average velocity of 6.70 to 7.45 km/s. This average velocity range is slightly too high. The lower crust beneath the CSSP line if wet must therefore have less than 50% of amphibolites.

The PcP and PmP boundaries define the lower crust. PcP lies to the top of an upper zone which contains a greater density of reflections in the reflective deep crust observed on the BIRPS WINCH-EF line (Fig. 5.21). PmP lies to the top of a similar lower zone which contains a greater density of reflections (Fig. 5.21). In Chapter 1 the various models proposed to explain this reflective character of the lower crust were described. These models propose either compositional variations or fracture planes which are probably water saturated to explain the reflectivity of the lower crust. Compositional variations could be original features of the crust (e.g. anorthositic banding) or could be produced

subsequently by igneous intrusion or by metamorphism associated with tectonism. Planes of weakness would be produced by the tectonism. This reflective character of the lower crust can be fitted into either of the above geological models as follows:

1. If the dry lower crust has an average granodioritic to dioritic composition, the heterogeneities needed to account for the reflective character can be produced by:
   (a) thin bands of eclogite representing basic intrusions into the lower crust
   (b) Anorthositic layering in the lower crust. Anorthosites have velocities between 6.8 to 7.4 km/s which are slightly higher than the observed 6.75 - 6.77 km/s average velocity in the lower crust. Upton et al (1983) suggested that anorthosites were common in the lower crust beneath the Southern Uplands from a study of volcanic inclusions.
   (c) Alteration along shear or fracture zones to produce acoustic impedance contrasts with the surrounding unaltered lower crustal rocks. Alternatively, metamorphism associated with ductile stretching may cause banding.
2. A mixture of amphibolites and more acidic gneisses in a wet lower crust could produce the observed reflective lower crust due to the impedance contrasts between the amphibolites and gneissic bodies or layers. These might occur either as a result of intrusion or ductile stretching. In addition shear zones and fluid filled fractures may occur and enhance the reflections from the lower crust.

The models proposed can explain both the observed average velocity and the reflective character of the lower crust beneath the Irish Sea. The proposed compositional variations can be explained by either intrusion of additional material or by alteration of an original homogeneous lower crust into a banded or sheared medium by tectonic processes such as ductile stretching and deformation. However, the association of the banded lower crust with the anomalous deep crustal structure beneath the Irish Sea in contrast to the North Sea supports a tectonic origin to the banding during thinning and stretching of the crust during the formation of the Irish Sea basins.

### 5.5.3 Nature of the Transitional Moho

The refraction results indicate that the top of the transitional Moho as defined by the PmP boundary beneath the Irish Sea lies within the deep reflective crust observed on the BIRPS WINCH-EF line. Its base as defined by the Pn boundary coincides with the bottom of this deep reflective crust. The average velocity within the transitional Moho is estimated to be approximately 7.8 to 7.9 km/s from ray tracing and amplitude modelling. This velocity indicates an ultra-basic or hybrid eclogitic average composition:

1. If the transitional Moho was originally lower crust it may have been converted to a near eclogite average composition by intrusion of basic magmas or by metamorphism of an original wet lower crust formed predominantly of amphibolites to a near eclogite average composition.

There are a number problems wth these models: first, eclogites are not commonly observed, if at all, as volcanic inclusions in volcanic rocks or in exposures anywhere in the British Isles and second, the crustal thickening accompanying the intrusion of basic magmas into the base of the lower crust and the present 5 km thinning requires an original anomalous thin crust in relation to adjacent areas.

2. Alternatively the transitional Moho can be interpreted as original mantle material which has been altered by shearing and deformation due to the stretching and thinning of the overlying crust

Both these processes could produce heterogeneities capable of accounting for the observed reflections. They can be related to basin formation and the thinning of the crust. Hypothesis for basin formation are controversial (Bott 1982). Both underplating and tectonic deformation of the mantle require thinning of the crust, and, underplating also requires a magma source. However, the crust beneath the Irish Sea is anomalous in contrast to the crust beneath the North Sea. This indicates that the original deep crustal structure beneath the Irish Sea has been altered possibly during the periods of basin formation during the Carboniferous or Permo-Trias. A model involving stretching appears to account for these changes without requiring heating and extrusion of magmas which are not observed in the Irish Sea.

### 5.5.4 Nature of the Upper Mantle

The time-term analysis of the Pn arrivals, ray tracing and amplitude modelling have indicated that the sub-Moho velocities are significantly higher beneath the Irish Sea than beneath the North Sea. Amplitude modelling indicates that the higher velocities and amplitudes of Pn beneath the Irish Sea and Northern England compared to the North Sea are caused by steeper velocity gradients in the upper mantle west of central Northern England (station 34). The anomalous upper mantle beneath the Irish Sea compared with that beneath the North Sea could be due to:

1. compositional effects in the peridotitic upper mantle (Ringwood 1975). This could be an original Caledonian feature. Such compositional differences, if due to alteration of the upper mantle beneath the Irish Sea, may be related to either metamorphism produced by hot spot activity or an influx of fluids or to magma emplacement associated with the formation of the transitional Moho by underplating. It may alternatively be related to stretching and thinning of the overlying crust.
2. The high velocities may be due to anisotropic effects. Such effects can be produced by the preferred orientation of olivine crystals along foliation or cleavage planes in peridotite (Bamford and Crampin 1984). Such an orientation of olivine may be produced by stresses caused by convective mantle upwelling or by the tectonic processes which also stretch and thin the overlying crust.

### 5.5.5 Conclusion

To conclude, the deep structure deduced from CSSP mainly represents the crust of the Southern Caledonides. Since continental collision in the late Silurian the crust in the region has undergone tension and compression related to the Hercynian Orogeny, the formation of the Permian Basins, the formation of the North Sea and the opening of the Atlantic. In particular the crust beneath the Irish Sea appears to have been dramatically altered to produce a marked contrast in crustal structure along the Caledonian strike below the Iapetus Suture. The detailed composition of the lower crust, transitional Moho and upper mantle are controversial. Various geological models have been described. Most of these can explain the observed properties of the crust. The structure beneath the North Sea under the eastern end of the CSSP profile may represent the best example of the original Cadomian crust. The association of the banded lower crust with the anomalous deep crustal structure beneath the Irish Sea in contrast to the North Sea supports a tectonic origin to the banding produced during thinning and stretching of the crust possibly during the formation of the Irish Sea basins. Any future studies of the contrasting crustal structures across the Iapetus Suture will need to take into account these significant lateral variations both parallel to and across the Caledonian trend.

# CHAPTER SIX

## SUMMARY AND CONCLUDING REMARKS

An outline of the current state of the understanding of the structure beneath Northern England and adjacent marine areas has been given in Chapter 1. Green (1984) and Bott et al (1985) present the shallow crustal structure and preliminary deeper structures beneath the CSSP profile which have improved upon this understanding. The more detailed investigation of the deep crustal structure beneath the CSSP profile presented in the preceding chapters also improves upon this understanding. The unique configuration of the CSSP has produced an unprecedented quantity of high quality refraction and wide-angle reflection data. A new method of displaying the large number of travel times in the form of contoured plots for a particular phase has been developed which exploits this innovative design. Each such composite travel time plot displays the main features of the data for each phase and presents in one diagram the four types of section which can be plotted using the CSSP data. A summary of the significant results obtained from the present study is as follows:

1. An analysis of the arrival times of PcP has yielded a mid-crustal gradient between depths of 15.5-18.5 km beneath the Irish Sea, which was not recognised previously, and between depths of 15.0-18.0 km beneath the North Sea. The average upper crustal velocity was estimated to be 6.03 km/s including sediments and 6.20 km/s excluding sediments beneath the Irish Sea, and, 6.01 including sediments and 6.16 km/s excluding sediments

beneath the North Sea.

2. Two-dimensional synthetic seismogram modelling indicates that the disappearance of Pg east of shot N11 can be explained by a lateral decrease in the basement velocity beneath shots N20 to N25 from 6.15 km/s to 5.8 km/s. No other lateral velocity variations within the upper crust have been identified.

3. An analysis of the arrival times of PmP has yielded a lower-crustal boundary which deepens from a depth of 25.0 km beneath the Irish Sea to 30 km beneath the North Sea. The average crustal velocity beneath the Irish Sea is estimated to be 6.39 km/s including sediments and 6.49 km/s excluding sediments. Beneath the North Sea it is 6.36 km/s including sediments and 6.54 km/s excluding sediments. The average velocity of the lower crust is calculated to be 6.77 km/s beneath the Irish Sea and 6.75 km/s beneath the North Sea. No other significant lateral variations in the lower crust have been identified.

4. Time-term analysis of the Pn arrivals indicate sub-Moho velocities of 8.19 (8.12 - 8.29) km/s beneath the Irish Sea, 8.32 (8.19 - 8.49) km/s beneath Northern England and 8.02 (6.34 - >10.0) km/s beneath the North Sea. Constraints imposed by the Bouguer gravity anomaly along the profile indicate a Pn velocity of 8.02 (+/- 0.1) km/s beneath the North Sea. The depths calculated define a Pn boundary which shallows from 32 km to 30 km from beneath the Irish Sea towards Northern England and is at a constant depth of about 30 km beneath the North Sea. Synthetic seismogram modelling using both the reflectivity and generalized ray theory methods indicate that the

sub-Moho gradient below the Pn boundary is steeper beneath the Irish Sea than beneath the North Sea. The lateral decrease in the sub-Moho velocity gradient occurs beneath the middle of Northern England below about station 34.

5. The contrasting depths calculated for the PmP and Pn boundaries define a transitional Moho beneath the Irish Sea. Synthetic seismogram modelling using both the reflectivity and generalized ray theory methods indicates that the PmP boundary is an abrupt increase in velocity from 6.75 to 7.8 km/s over a depth range of about 1 km. This is underlain by a gentle velocity gradient within the transitional Moho from 7.8 to 8.0 km/s. Beneath the North Sea the coincident PmP and Pn boundaries define an interface across which the velocity increases abruptly over about a km from 6.75 km/s to 8.0 km/s.

In Section 1.6 several specific questions were formulated which it was hoped would be answered by this study. Several of these questions have already been answered in the above summary. The remaining questions are discussed below.

1. A comparison of the CSSP results and BIRPS indicates that:
   (a) The PcP interface corresponds approximately with the top of the reflective lower crust observed beneath the Irish Sea. No distinctive lower crust was observed on the NEC line although the Caledonian Suture Seismic Project refraction results indicate a mid-crustal boundary at about 6.0 s two way travel-time.
   (b) The PmP boundary beneath the Irish Sea lies within the reflective lower crust.
   (c) The Pn boundary beneath the Irish Sea coincides approximately with the base of the reflective lower

crust. The coincident PmP and Pn interfaces beneath the North Sea almost exactly correspond to the prominent reflections observed on the NEC line at about 10.5 to 11.0 s two way travel time.

(d) The transitional Moho beneath the Irish Sea has a reflective character similar to the lower crust.

A comparison of refraction and BIRPS deep reflection profiles elsewhere in the British Isles indicates that a sharp Moho produces a narrow band of prominent vertical reflections and large amplitude wide-angle reflections. In areas where the Moho appears to represent the base of the reflective lower crust, no prominent vertical or wide angle reflections are observed. Such a Moho is recognised as a complicated transition zone between the lower crust and upper mantle in the northern Irish Sea and may be developed more regionally beneath the Irish Sea.

(d) A comparison of the Irish CSSP results with the mainline CSSP results indicate that the PmP boundary shallows from Ireland towards the centre of the Irish Sea. No results from an analysis of Pn have been reported for the Irish CSSP profile. The calculated gravity anomaly using the seismic structure beneath the entire CSSP profile indicates a possible 3·5km disparity between the depths of the mid-crustal boundary beneath Ireland and the mainline CSSP profile across Northern England. The calculated gravity along the entire CSSP line fits the observed gravity anomaly to within 5 mgal if the depth to the mid-crustal boundary beneath Ireland is reduced by 3·5km.

(d) The BIRPS WINCH and NEC line indicate that the CSSP line

appears to lie very close to the inferred surface trace of the Iapetus Suture from the North Sea to the Irish Sea except west of the Solway Basin where it lies significantly to the north. This means that the basement of velocity 6.15 km/s which increases to 6.20 km/s at depth in the upper crust lies both above and below the suture along the line. The lower crust and deeper structures from the North Sea to the Irish Sea lie below the suture and therefore represent crust of the Southern Caledonides. The anomalous structure of the Moho and upper mantle beneath the Irish Sea found from CSSP and BIRPS may be related to the post-Caledonian formation of the Irish Sea basins. The reflective lower crust and transitional Moho may result from crustal thinning produced by ductile stretching.

## 6.1 FURTHER WORK ON THE CSSP DATA

It has been possible to examine only a limited amount of the data collected during the Caledonian Suture Seismic Project. It is suggested that the following work needs to be carried out on the remaining data.

1. An analysis of the Eskdalemuir, LOWNET and BGS CSSP data should lead to a better understanding of the structure north of the CSSP line under the Southern Uplands and beneath the Irish Sea. The variations in velocity structure related to the disappearance of the reflective lower crust beneath the Southern Uplands could be investigated in detail.
2. An analysis of the excellent shear waves recorded from the

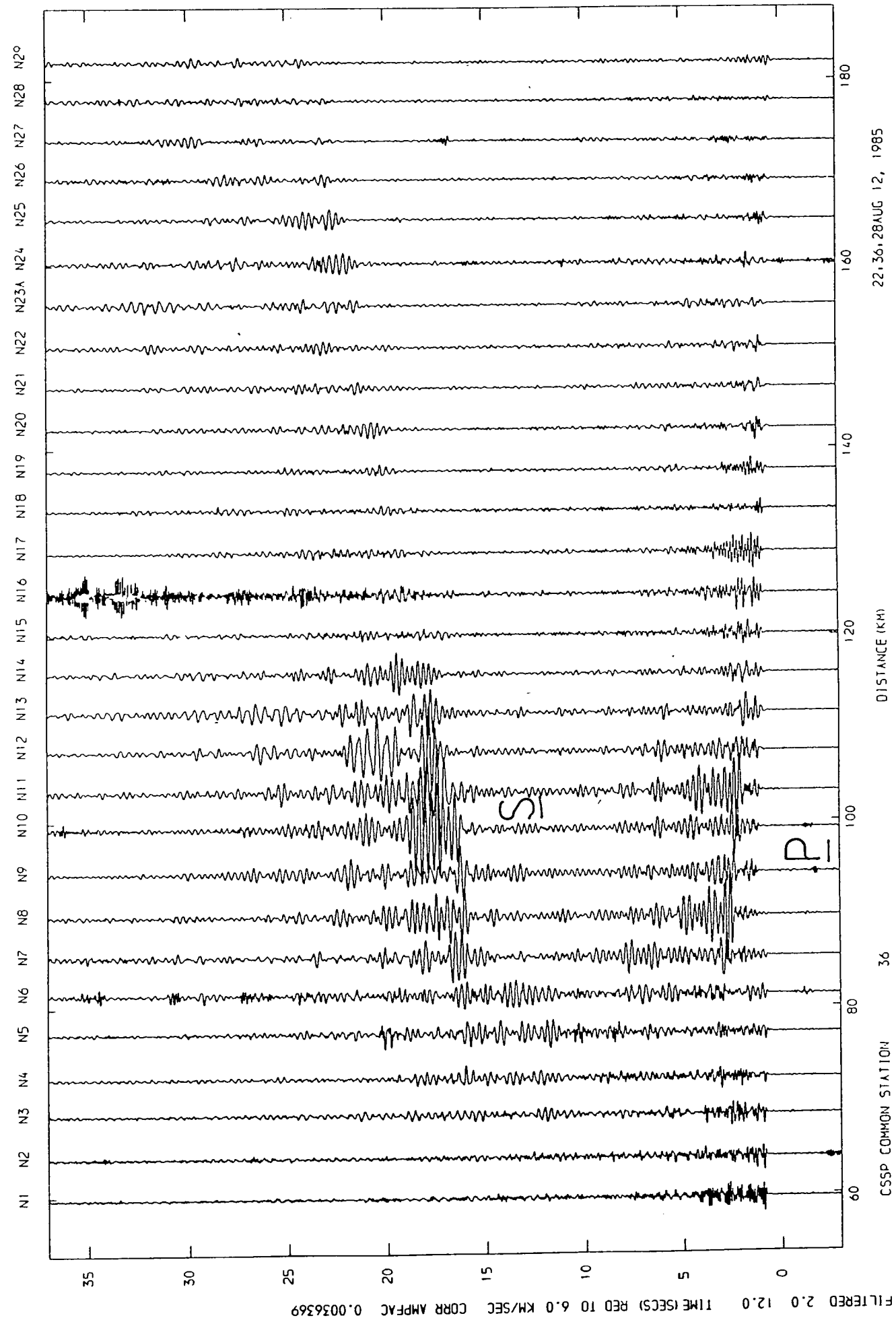


Fig 6.1 Common Station Section for Station 36

North Sea shots (Fig. 6.1) should lead to a better understanding of the composition of the crust.

## 6.2 FURTHER WORK

There is still a considerable amount of information to be gained from the CSSP data. This study, however, has posed some questions that are best answered by further surveys. The most interesting questions raised are

1. Is the transitional Moho developed regionally beneath the Irish Sea as indicated by the regional gravity high and the widespread occurrance of a reflective lower crust? In addition, the varying crustal structure beneath the westward extension of the Southern Uplands observed on WINCH may represent contrasting crustal structures across the Iapetus suture. Alternatively, the disappearance of the reflective lower crust may be related to the northward thinning of the transitional Moho. Green (1984) proposed a north-south reversed wide-angle reflection/refraction profile between the Isle of Man and the Mull of Kintyre with stations deployed on the Isle of Man and Stranraer Peninsula to investigate the northward extension of the 6.15 km/s basement refractor beneath the Southern Uplands. Such a profile might also confirm the inferred regional development of the transitional Moho beneath the Irish Sea and the variations northwards in its structure.
2. Given these major lateral contrasts in crustal structure beneath the Irish Sea along the Caledonian strike, the structure beneath the North Sea may be the best example of the original Cadomia crust. No detailed velocity

structures of the deep crust beneath the Southern Uplands are available. This means that the question of whether there are contrasts in the velocity structure of the deep crust across the Iapetus Suture remains unanswered. The results from CSSP have indicated the usefulness of shooting along strike refraction profiles with the use of both closely spaced stations and closely spaced shots. The deep crustal structure beneath the Southern Uplands can be investigated best by shooting a refraction profile similar to CSSP along strike from west to east. The resulting structures north and south of the Iapetus Suture beneath the adjacent along strike profiles can then be compared to deduce whether any contrasts represent remnant structural differences between the Southern and Northern Caledonides.

## REFERENCES


AGGER H.E., & CARPENTER, E.W.,1964 A crustal study in the vicinity of the Eskdalemuir seismological array

Geophys. Jour. Roy. Astr. Soc.. 9. 69-83

ANDERTON R., BRIDGES P.H., LEEDER M.R.,AND SELWOOD B.W., 1979 A dynamic stratigraphy of the British Isles.

George Allen and Unwin Ltd. London 301pp.

ANSORGE J., PRODEHL C., & BAMFORD D., 1982 Comparative interpretation of explosion seismic data.

J. Geophysics 51 69-84

ARMOUR A., 1978 A seismic refraction study of the crustal structure of north west Scotland and adjacent continental margin.

Unpublished Ph.D. Thesis, University of Durham

BAMFORD S.A.D., 1971 An interpretation of the first arrivals from the Continental Margin Refraction Experiment.

Geophys. Jour. Roy. Astr. Soc. 24 213-229

BAMFORD S.A.D., 1972 Evidence for a low velocity zone in the crust beneath the western British Isles.

Geophys. Jour. Roy. Astr. Soc. 30 101-105

BAMFORD S.A.D., 1973 An example of the iterative approach of time-term analysis.

Geophys. Jour. Roy. Astr. Soc. 31 365-372

BAMFORD S.A.D., 1976 MOZAIC time-term analysis.

Geophys. Jour. Roy. Astr. Soc. 44 433-446

BAMFORD S.A.D., 1978 Interpretation of wide angle reflection travel times in crust mantle structures.

J. Geophys. 44 219-230

BAMFORD S.A.D., 1979 Seismic constraints on the deep geology of the Caledonides of Northern Britain.

In The Caledonides of the British Isles - reviewed Geological Society of London 1979

BAMFORD S.A.D., & BLUNDEL D.J., 1970 South-west Britain continental margin experiment.

Rep. Inst. geol. Sci. London 70/14

BAMFORD S.A.D., FABER S., KAMINSKI K., PRODEHL C., FUCHS K., KING R., & WILLMORE P., 1976 A lithospheric seismic profile in Britain - I Preliminary results.

Geophys. Jour. Roy. Astr. Soc. 44 145-160

BAMFORD S.A.D., NUNN K., PRODEHL C., & JACOB B., 1977 LISPB - III Upper crustal structure of Northern Britain.

Journ. Geol. Soc. Lond. 133 481-488

BAMFORD S.A.D., NUNN K., PRODEHL C., & JACOB B., 1977 LISPB - IV Crustal structure of Northern Britain.

Geophys. Jour. Roy. Astr. Soc. 54 43-60

BAMFORD S.A.D., & CRAMPIN S., 1977 Seismic anisotropy - the state of the art

Geophys. Jour. Roy. Astr. Soc. 49 1-8

BAMFORD S.A.D., & PRODEHL C., 1977 Explosion seismology and the continental crust-mantle boundary.

J. geol. Soc. London. 134 139-151

BANKS R.J., BEAMISH D., & GEAKE M.J., 1983 Magnetic variation anomalies in Northern England and Southern Scotland.

Nature 303 June 9th 1983

BARR D., ROBERTS A.M., HUGHTON A.J., PARSON L.M. AND HARRIS A.L., 1985 Structural setting and geochronological significance of the west Highlands granitic gneiss, deformed early granite with Proterozoic Moine rocks of NW Scotland.

Journ. Geol. Soc. 142s(4) 663-676

BARROWDALE I., CHAPMAN N.R., & ZALA C.A., 1984 Estimation of bubble pulse wavelets for deconvolution of marine seismograms.

Geophys. Jour. Roy. Astr. Soc. 77 331-341

BARTON P., MATTHEWS D., HALL J., & WARNER M., 1984 Moho beneath the North Sea compared on normal incidence and wide-angle seismic records.

Nature 308 55-56

BARTON P., & WOOD R., 1984 Tectonic evolution of the North Sea basin: crustal stretching and subsidence.

Geophys. Jour. Roy. Astr. Soc. 79 987-1022

BELOUSSOV V.V., & PAVLENKOVA N.I., 1984 The types of the Earth's crust.

J. of Geodynamics. 1 167-183

BERKENHEIMER, 1969 Direct evidence for the compostion of the lower crust and the Moho

Tectonophysics 8(2) 97-105

BERRY M.J., & WEST G.F., 1966 An interpretation of the first arrival data of the Lake Superior experiment by the time-term method.

Bull. seismol. Soc. Am. 56 141-171

BIRCH F.,1960 The velocity of compressional waves in rocks to 10 Kilobars, Part 1.

J. Geophys. Res. 65 1083

BLUNDELL D.J. & PARKS R., 1969 A study of the crustal structure beneath the Irish Sea.

Geophys. Jour. Roy. Astr. Soc. 17 45-62

BLUNDELL D.J., HUPICH C.H., & SMITHSON S.B., 1985 A model for the MOIST seismic reflection profile, Northern Scotland.

J. Geol. Soc. 142 245-258

BLUNDELL D.J. AND RAYNAUD B., 1986 Modelling Lower Crustal Reflections Observed on BIRPS profiles

In Reflection Seismology: A Global Perspective. Eds. Barazangi M. and Brown L., A.G.U. 13 5-19

BOIS C., CAZES M., DAMOTTE B., GALDEANO A., HIRN A., MASCLE H., MATTI P., RACOULT J.F. & TORREILLES G., 1986 Deep seismic profiling of the crust in Northern France: the ECORS profile.

In Reflection Seismology: A Global Perspective. Eds. Barazangi M. and Brown L., A.G.U. 13 5-19

BORTFELD R.K., GOWIN J., STILLER M., BAIER B.,BEHR H.J., HEINRICHS T., DURBAUM H.J., HAHN A., REICHERT J., SCHMOLL J., DOHR G., MEISSNER R., BITTNER R., MILKEREIT B. AND GEBRANDE H., 1985 First results and preliminary interpretation of deep-reflection seismic recordings along profile DEKORP 2-South

J. Geophysics 57 137-163

BOTT M.H.P., 1961 A gravity survey off the NE coast of England.

Proc. York. geol. Soc. 33 1-20

BOTT M.H.P., 1967 Geophysical investigations of the Northern Pennine basement rocks.

Proc. Yorks. Geol. Soc. 36 part 2, 139-169

BOTT M.H.P., 1968 The geological structure of the Irish Sea basin.

In Geology of Shelf Seas Ed. D.T. Donovan, Oliver & Boyd, London

BOTT M.H.P., 1974 The geological interpretation of a gravity survey of the English Lake District and the Vale of Eden.

Journ. Geol. Soc. Lond. 130 309-331

BOTT M.H.P., 1982 The Interior of the Earth: its structure, constitution and evolution

Edward Arnold Publishing Ltd. pp403

BOTT M.H.P., & SMITH P.J., 1984 Crustal structure of the Faeroe-Shetland channel

Geophys. Jour. Roy. Astr. Soc. 76 363

BOTT M.H.P., SWINBURN P., & LONG R.E., 1984 Deep structure and Stainmore Troughs.

Proc. York. geol. Soc. 44 479-495

BOTT M.H.P., LONG R.E., GREEN A.S.P., LEWIS A.H.J., SINHA M.C. AND STEVENSON D.L., 1985 Crustal structure south of the Iapetus Suture beneath Northern England

Nature 314 724-727

BRAILE L.W., & SMITH R.B., 1975 Guide to the interpretation of crustal refraction profiles.

Geophys. Jour. Roy. Astr. Soc. 40 145-176

BREWER J.A., MATTHEWS D.H., WARNER M.R., HALL J., SMYTHE D.K., & WHITTINGTON R.J., 1983 BIRPS deep seismic reflection studies of the British Caledonides.

Nature., London. 305 206-210

BREWER J.A. AND SMYTHE D.K., 1984 MOIST and the continuity of crustal reflector geometry along the Caledonian-Appalachian Orogen.

Journ. Geol. Soc. Lond. 141

BRIDEN J.C., TURNELL H.B., WATTS D.R., McCLELLAND BROWN E. and EVERETT S., 1982 Palaeomagnetism of the Scottish Highlands and the question of the magnitude of displacement on the Great Glen Fault

Paper sub. at Symposium Geophys. Soc. and Euro. Seism. Comm. Leeds, UK

BROWN C. AND WILLIAMS B., 1985 A gravity and magnetic interpretation of the structure of the Irish Midlands and its relation to ore genesis.

Journ. Geol. Soc. Lond. 142(6) 1059

BROWN L., BARAZANGI M., KAUFMANN S. AND OLIVER J., 1986 The first decade of COCORP: 1974-1984

In Reflection Seismology: A Global Perspective. Eds. Barazangi M. and Brown L., A.G.U. 13 107-120

BURKHARDT H., & VEES R., 1975 Explosions in shallow water for deep seismic sounding experiments.

J. Geophys. 41 463-474

BUTLER R.W.H. and COWARD M.P., 1984 Geological constraints, structural evolution and deep geology of the NW Scottish Caledonides.

Tectonics 3 347-365

CERVENY V., 1966 On dynamic properties of reflected and head waves in the n-layered Earth's crust.

Geophys. Jour. Roy. Astr. Soc. 11 139-147

CERVENY V., MOLOTKOV I.A., & PSENCIK I. 1977 Ray methods in seismology

Univerzita Karlova, Prague

CERVENY V., 1985 Ray synthetic seismograms for complex 2-D and 3-D structures.

Journal Geophysics 58 2-26

CHEADLE M., MATTHEWS D., McGEARY S., WARNER M., MASCLE A., GARIEL O., MONTADERT L., LEFORT P., LeGALL J-C., CAZES M. AND SCHROEDER I.J., 1986 Deep seismic reflection profiling between England, France

Journ. Geol. Soc. Lond. 143 45-52

CHRISTENSEN N.I., 1982 Seismic velocities.

In handbook of physical properties of rocks Vol. II Ed. R.S. Carmichael, CRC Press.

CHRISTENSEN N.I., 1979 Compressional wave velocities in rocks at high temperature and pressure, critical thermal gradients, and crustal low velocity zones.

J Geophys. Res. 84 6849-6857

CHROSTEN P.N., & EVANS C.J., 1983 Seismic velocities of granulites from the Seiland petrological province, North Norway: Implications for Scandanavian lower crust.

J. Geophys. 52 14

COCKS L.R.M., & FORTEY R.A., 1982 Faunal evidence for oceanic separations in the Paleozoic of Britain.

J. Geol. Soc. London. 139 465-478

COLLETTE B.J., LAGAAY R.A., RITSEMA A.R., & SCHOUTEN J.A., 1970 Seismic investigations in the North Sea, 3 to 7.

Geophys. Jour. Roy. Astr. Soc. 19 183-199

CRAMPIN S., CHESNOKOV E.M., & HIPKIN R., 1984 Seismic anisotropy - the state of the art.

First break 2 9-18

DAVYDOVA N.I., 1975 Seismic properties of the Mohorovicic Discontinuity.

Keter publishing house, Jensalim Etd.

DIMITROPOULOS K., 1981 Caledonian granites on the course of uncertainty in LISPB interpretation in the Grampian Highlands area.

Geophys. J. 65 695

DEWEY J.F., 1971 A model for the Lower Paleozoic of the Southern margin of the early Caledonides of Scotland and Ireland.

Scott. J. Geol. 7 219

DEWEY J.F., 1982 Plate tectonics & the evolution of the British Isles.

J. Geol. Soc. London. 139 375-412

DEWEY J.F. & SHACKLETON R.M., 1984 A model for the evolution of the Grampian tract in the early Caledonides and Appalachians

Nature 312 115-121

DONATO J.A., MARTINDALE W., & TULLEY M.C., 1983 Buried granites within the Mid North Sea High.

J. Geol. Soc. London. 140 825-837

DUNHAM K.C., 1974 Granite beneath the Pennines in North Yorkshire

Proc. Yorkshire Geol. Soc. 40 191-194

FABER S., & BAMFORD S.A.D., 1979 Lithospheric structural contrasts across the Caledonides of Northern Britain.

Tectonophysics 56 17-30

FABER S., & BAMFORD S.A.D., 1981 Moho offset beneath North Scotland.

Geophys. Jour. Roy. Astr. Soc. 67 661-672

FINLAYSON D.M., COLLINS C.D.N., & LOCK J., 1984 P wave velocity features of the Lithosphere under the Eromanga basin Eastern Australia, including a prominent mid-crustal (Conrad?) discontinuity.

Tectonophysics 101 267-291

FITTON J.G., & HUGHES D.J., 1970 Volcanism and plate tectonics in the British Ordovician.

Earth Planet. Sci. Lett. 8 223-228

FOUNTAIN D.M., 1976 The Ivrea-Verbano and Strona-Ceneri zones, Northern Italy: A cross section of the continental crust - new evidence from seismic velocities of rock samples.

Tectonophysics 33 145-165

FUCHS K., & MUELLER S., 1971 Computations of synthetic seismograms by the reflectivity method and comparison with observations.

Geophys. Jour. Roy. Astr. Soc. 23 417-433

FUCHS K., 1979 Structure, physical properties and lateral heterogeneities of the subcrustal lithosphere from long-range deep seismic sounding observations on continents.

Tectonophysics 56 1-15

GAJEWSKI D., & PRODEHL C., 1985 Crustal structure beneath the Swabian Jura, S.W.Germany, from seismic refraction investigations.

J. Geophys. 56 69-80

GLENNIE K.W., 1984 Introduction to the petroleum geology of the North Sea

Blackwell Scientific Publishers pp236

GREEN A.S.P., 1984 The crustal structure beneath Northern England and adjacent sea areas

Unpublished PhD thesis, University of Durham

HALE L.D., & THOMPSON G.A., 1982 The seismic reflection character of the continental Mohrovic Discontinuity.

J. Geophys. Res. 87 4625-4635

HALL J., & Al-HADDAD F.M., 1976 Seismic velocities in the Lewisian metamorphic complex northwest britain - 'in situ measurements.

Scott. J. Geol. 12 305-314

HALL J., 1977 'LUST' - a seismic refractio survey of the Lewisian basement complex in N.W.Scotland.

J. Geol. Soc. 135 555-563

HALL J., 1978 Crustal evolution in northwestern britain and adjacent regions.

In Crustal structure of the Eastern North-Atlantic seaboard. Eds D.R. Bowes & B.E.Leake

HALL J., & SIMMONDS G., 1979 Seismic velocities of Lewisian metamorphic rocks at pressures to 8 kbar: relationship to crustal layering in Northern Britain.

Geophys. Jour. Roy. Astr. Soc. 58 337-347

HALL J., POWELL D.W. WARNER M.R., EL-ISA Z.H.M. ADESANYA O., & BLUCK B.J., 1983 Seismological evidence for shallow crystalline baesment in the Southern Uplands of Scotland.

Nature 305 418-420

Reply to Seismological evidence for shallow crystalline basement in Southern Uplands Scotland, by Oliver & McKerrow 1984.

Nature. 308 89-90

HALL J., 1985 Geophysical constraints in crustal structure in the Dalradian region of Scotland.

J. Geol. Soc. 142 149-155

HALL J., & MUBARIK A., 1985 Shear waves in a seismic survey of Lewisian basement: on extra control on lithological variation and porosity.

J. Geol. Soc. 142 677-688

HALL J., 1985 Seismic velocity and electrical conductivity in lower crustal rocks: lithology, fabric and fluids.

Abstract Conference on Origin of seismic reflections from the deep continental crust and upper mantle Joint meeting of the Metamorphic and Tectonic Studies Groups and the Joint Association for Geophysics, Keele Nov. 1985

HALLIDAY A.N., 1984 Coupled SM-Nd & U-Pd Systematics in late Caledonian granites and the basement under Northern Britain.

Nature 307 229-233

HARRIS A.L., 1979 The Caledonides of the British Isles-reviewed.

Scot. Acad. Press pp768

HARRIS A.L., 1983 The growth and structure of Scotland

In Geology of Scotland edited CRAIG G.Y. 2nd ed. Scot. Acad. Press

Geophys. 26 806-819

HAWORTH R.T., 1981 Geophysical expression of Appalachian-Caledonide structures on the continental margins of the North Atlantic.

Canadian Soc. Petrol. Geol. Memoir 7 429-446

HEALY J., 1971 A comment on the evidence for a worldwide zone of low seismic velocity at shallow depths in the Earth:s crust.

Monogr. Am. geophys. Union. 14

HENDERSON W.G. AND ROBERTSON A.H.F., 1982 Highland Border rocks and their relation to marginal developement in the Scottish Caledonides

Journ. Geol. Soc. 139 433-450

HOLDER A.P., 1969 A seismic refraction study of the Earth's crust beneath SW Britain

Unpublished Ph.D. Thesis, University of Durham

HOLDER A.P. AND BOTT M.H.P., 1971 Crustal Structure in the Vicinity of SW England

Geophys. Jour. Roy. Astr. Soc. 23 456-489

HUTTON V.R.S., INGHAM M.R. AND MBIPSOM E.W., 1980 AN electrical model of the crust and upper mantle in Scotland

Nature 289 30-33

IRVING E. AND STRONG D.F., 1984 Evidence against large-scale Carboniferous strike-slip faulting in the Appalachian-Caledonian orogen.

Nature 310 762-764

KENNETT B.L.N., 1975 Theoretical seismogram calculation for laterally varying crustal structures

Geophys. Jour. Roy. Astr. Soc. 42 579-589

KIRTON S.R. AND DONATO J.A., 1985 Some buried Tertiary dykes of Britain and surrounding waters deduced by magnetic modelling and seismic reflection methods

Journ. Geol. Soc. Lond. 142(6) 1047-1058

JACOB A.W.B., 1969 Crustal phase velocities observed at the Eskdalemuir seismic array.

Geophys. Jour. Roy. Astr. Soc. 18 189

JACOB A.W.B., 1975 Dispersed shots at optimum depth - an efficient seismic source for lithospheric studies.

J. Geophys. 41 63-70

JACOB A.W.B., KAMINSKI W., MURPHY T., PHILLIPS W.E.A., & PRODEHL C., 1985 A crustal model for a NE/SW profile through Ireland.

Tectonophysics 113 75-103

KARNER G.D., 1985 Continental tectonics - a quantative view of the thermal and mechanical properties of the continental lithosphere in compressional and extensional stress regimes.

In press. Centre National d'Etudes Spatials, Summer School of Space Physics, Toulouse, France. 53p.

LANDISMAN M., MUELLER S., & MITCHELL B.J., 1977 Physical properties of the continental crust. Review of evidence for velocity inversions in the continental crust.

In The structure and physical properties of the Earth's crust. Ed. J.Hancock, Am. Geophys. Union Monographs. 14

LAVING G.J., 1971 Automatic methods for the interpretation of gravity and magnetic field anomalies and their application to marine geophysical surveys.

Unpublished PhD thesis, University of Durham.

LEEDER M.R., 1982 Upper Paleozoic basins of the British Isles - Caledonide inheritance versus Hercynian plate margin processes.

J. geol. Soc. London. 139 479-491

LEGGETT J.K., McKERROW W.S., & SOPER N.J., 1983 A model for the crustal evolution of Southern Scotland.

Tectonics 2 187-210

MALIN P.E. AND PHINNEY R.A., 1985 On the relative scattering of P- and S-waves

Geophys. Jour. Roy. Astr. Soc. 80(3) 603-618

MATTHEWS D., & HIRN A., 1984 Crustal thickening in Himalayas and Caledonides.

Nature 308 497-498

MATTHEWS D. H. AND CHEADLE M. J., 1986 Deep reflections from the Caledonides and Varicides west of Britain and comparisons with the Himalayas.

In Reflection Seismology: A Global Perspective. Eds. Barazangi M. and Brown L., A.G.U. 13 5-19

McKERROW W.S., & COCKS L.R.M., 1976 Progressive faunal migration across the Iapetus Ocean.

Nature. London. 263 305

MEISSNER R., 1966 An interpretation of the wide angle measurements in Bavarian molasse basins.

Geophys. Prosp. 14 1-16

MEISSNER R., 1967 Exploring deep interfaces by seismic wide angle measurements.

Geophys. Prosp. 15 598-617

MUELLER S., 1977 A new model of the continental crust.

In The Earth's crust Ed. J.Hancock Monogr. Am. geophys. Union 20

NEEDHAM T. AND KNIPE, 1986 Accretion and collision related deformation in the Southern Uplands accretionary wedge, SW Scotland

Geology in press

O'BRIEN J.A., PLANT P.R. AND TARNEY J., 1985 The geochemistry, metasomatism and petrogenesis of the granites of the English Lake District.

Journ. Geol. Soc. 142 1139

OFOEGBU C. O. AND BOTT M. H. P., 1985 Interpretation of the Minch linear magnetic anomaly and of a similar feature on the shelf north of Lewis.

Journ. Geol. Soc. 142 1077

OLIVER G.J.H., & McKERROW W.S., 1984 Seismological evidence for shallow crystalline basement in Southern Uplands, Scotland.

Nature. London. 309 89

OITHMAN D.B., POLVE M., & ALLLEGRE C.J., 1984 Nd-Sr Isotopic composition of granites & constraints of the lower continental crust.

Nature 307

PRATT H.R., SWOLFS H.S., LINGLE R. AND NIELSEN R.R., 1977 In-
-situ and laboratory measurements of velocity and permeability

In The Earth's crust Ed. J.Hancock Monogr. Am. geophys. Union 20

PHILLIPS W.E.A., STILLMAN C.J., & MURPHY T., 1976 A Caledonian Plate tectonic model.

J. geol. Soc. London› 132 579-609

PRESS F., 1966 Seismic velocities.

In handbook of physical constraints Mem. geol. Soc. Am. 97 196

RINGWOOD & GREEN 1966 Petrological nature of the stable continental crust.

In The Earth beneath the continents, Ed Steinhurt & Smith AGU 611-619

RINGWOOD, 1975 Composition and ptrology of the Earth's mantle.

McGraw Hill, New York pp617

ROBBINS A.R., 1962 Long lines on the spheroid.

Emp. Svy. Rev. 125

ROBINSON A.E., 1981 Physical applications of stationary time series.

Griffon (NY) pp297

SCHEIDEGGER A.E., & WILLMORE P., 1957 The use of least squares method for the interpretation of data from seismic surveys.

Geophysics. 22 9-22

SMITH P.J., & BOTT M.H.P., 1975 Structure of the crust beneath the Caledonian foreland and Caledonian belt of the North Scottish shelf region.

Geophys. Jour. Roy. Astr. Soc. 40 187-205

SMITHSON S.B., & DECKER E., 1974 A continental crust model geothermal implications.

Earth planet. Sci. Lett. 22 215-225

SMITHSON S.B., & BROWN S.K., 1977 A model for the lower continental crust.

Earth planet. Sci Lett. 35 134-144

SOPER N.J., & HUTTON D.W., 1984 Late Caledonian displecements in Britain: implications for a 3-plate collision model.

Tectonphysics 3 781-794

STEWART A.D., 1982 Late Prtoerozoic rifting in NW Scotland: genesis of the Torridonian

Journ. Geol. Soc. Lond. 139 413-420

SUMMERS T. 1982 A seismic study of crustal structure in the region of the Western Isles of Scotland.

Unpublished PhD thesis. University of Durha.

SWINBURN P.M., 1975 The crustal structure of Northern England.

Unpublished PhD thesis, University of Durham

THIRLWALL M.F., 1981 Implications for the Caledonian Plate Tectonic models of chemical data from volcanic rocks of the British Old Red Sandstone.

J. geol. Soc. London. 138 123-138

THOMPSON A.S., 1984 A geophysical model of the Solway basin.

Unpublished MSc thesis, University of Durham

THORPE R.S., BECKINSALE R.D., PATCHETT P.J., PIPER G.R. AND EVANS J.A., 1984 Crustal growth and late Precambrian-early Palaeozoic plate tectonic evolution of England and Wales.

Journ. Geol. Soc. Lond. 141 520-536

UPTON B.J.G., ASPEN P., & CHAPMAN N.A., 1983 The upper mantle and deep crust beneath the British Isles evidence from inclusions in volcanic rocks.

J. geol. Soc. London.

VAN der VOO R. AND SCOTESE C.R., 1981 Palaeomagnetic evidence for a large (2000 km) sinistral offset along the Great Glen Fault during the Carboniferous

Geology 9 583-589

WARNER M.R., HIPKIN R.G., & BROWITT C.W., 1982 Southern Uplands seismic refraction profile - preliminary results.

Geophys. Jour. Roy. Astr. Soc. 69 279

WATSON J., 1984 The ending of the Caledonian orogeny in Scotland

Journ. Geol. Soc. Lond. 141 193-214

WATSON J., 1985 Northern Scotland as as Atlantic-North Sea divide

Journ. Geol. Soc. Lond. 142(2) 221-244

WATSON J. AND DUNNING F.W., 1979 Basement cover relations in the British Caledonides

In The Caledonides of the British Isles- reviewed Ed. Harris A.L. et al Geol. Soc. of Lond. 67-91

WHITCOMBE D.N., & MAGUIRE P.K.H., 1979 The response of the time-term method to simulated crystal structures.

Bull. seismol. Soc. Am. 69 1455-1473

WHITCOMBE D.N., & RODGERS, 1981 The efects of refractor topography and overburden anisotropy on time-term solutions of refractor anisotropy.

Geophys. Jour. Roy. Astr. Soc. 67 449-464

WILLMORE P.L., & BANCROFT A.M., 1960 The time-term approach to refraction seismology.

Geophys. Jour. Roy. Astr. Soc. 3 419-432

WINDLEY F., 1977 The crust-mantle boundary in Space and time.

J. Geol. Soc. London. 134 99-102

WOOD R., & BARTON P., 1983 Crystal thinning and subsidence in the North Sea

Nature. London. 302 134-136

YARDLEY B.W.D., NINE F.J., & BALDWIN C.T., 1982 The plate tectonic setting of NW. Britain & Ireland in late E. and early Ordivician times.

J. Geol. Soc. London. 139 445-463

YARDLEY B.W.D., 1985 Fluids in the continental crust

Abstract Conference on Origin of seismic reflections from the deep continental crust and upper mantle Joint meeting of the Metamorphic and Tectonic Studies Groups and the Joint Association for Geophysics, Keele Nov. 1985

ZUCCA J.J., 1984 The crustal structure of the S. Rhinegraben from reinterpretation of seismic refraction data.

J. Geophys. 55 13-22

ZIEGLER p.h., 1982 Geological atlas of Western and Central Europe

Elsevier, Shell Int. Pet. Maat. Dist. Amsterdam, 130pp

## Appendices in VOL II